

UNIVERSITY OF CALGARY

The Environmental Context of the Earliest Acheulean at Olduvai Gorge, Tanzania

by

Robert Vincent Patalano

A THESIS

SUBMITTED TO THE FACULTY OF GRADUATE STUDIES

IN PARTIAL FULFILMENT OF THE REQUIREMENTS FOR THE

DEGREE OF DOCTOR OF PHILOSOPHY

GRADUATE PROGRAM IN ARCHAEOLOGY

CALGARY, ALBERTA

MAY, 2019

© Robert Vincent Patalano 2019

ABSTRACT

Water, vegetation, and human habitats are tightly coupled, and Olduvai Gorge, Tanzania is an exceptional locality for examining evolutionary events that associate with water availability and environmental stability or change. This project investigates interactions between and among paleo-hydrology, habitat type, and the human response to changing environmental settings. The objective is to interpret the climate and environmental context of the oldest Acheulean stone tool industry at Olduvai Gorge using plant leaf wax lipid marker molecules, or biomarkers, as a source for carbon and hydrogen isotopes. The emphasis is on a roughly 200,000-year period (1.83 to 1.66 Ma), a timeframe that includes a key transition in stone tool technology from the Oldowan to the Acheulean, and the widespread distribution of the genus *Homo*.

To investigate the human-environment interactions for Olduvai's earliest Acheulean, terrestrial sediments from Beds I and II were systematically sampled and processed for normal (*n*-) alkanes and *n*-alkanoic acids. The focus is on the Frida Leakey Korongo North (FLK-N) and West (FLK-W) archaeological sites, which contain Oldowan and Acheulean tools, respectively, the geologic feature known as the Castle, and multiple landscape geological samples. From a methodological perspective, the innovation lies in the detailed environmental analyses using leaf wax biomarkers as a proxy record for paleo- hydrology and vegetation, and for the assessment of changes in precipitation, temperature, atmospheric CO₂, aridity/humidity and plant type.

The results indicate that both Oldowan and Acheulean assemblages were predominantly used within woodland settings with abundant freshwater nearby. The archaeological sites were situated within a mosaic environment of open grassland, closed riparian and groundwater-fed woodlands, lacustrine habitats, and ecotones. Both technological types were most likely used to process plant material such as hard-shelled nuts and fruits, but the Acheulean was also utilized for exploiting underground tubers as well as meat obtained in open settings.

ACKNOWLEDGMENTS

This dissertation would not have been completed without the help and assistance from colleagues, family, and friends, as countless individuals have significantly contributed to this project over the years. First, I want to thank my thesis committee; Dr. Mary Anne Katzenberg, Dr. Craig Gerlach, Dr. Casey Hubert, and Dr. Michael Richards. I am most grateful for your insightful knowledge and editorial feedback and for helping me accomplish this endeavor. All of you are exceptionally engaged in other academic affairs, and therefore your commitment to helping me achieve a PhD is extremely appreciated.

There have been a lot of additional people at the University of Calgary who have aided me in finishing this research. I am enormously thankful to the members of the Isotope Science Laboratory and the Petroleum Reservoir Group at the University of Calgary for allowing me to use their equipment and analytical instruments. I would specifically like to thank Veith Becker for processing my isotope samples and Kimberly Nightingale for allowing me access to laboratory equipment that was vital to completing my research.

I am incredibly obliged to the funding I received while finishing my degree. I would like to thank the Social Sciences and Humanities Research Council of Canada (SSHRC) for supporting the Stone Tools, Diet, and Sociality project. Beneficial funding for this study also came from the Ruggles-Gates Fund for Biological Anthropology and the Explorers Club Exploration Fund Grant. I would also like to thank the University of Calgary for awarding me the Dr. Murray Fraser Memorial Graduate Scholarship and multiple Eyes High International Doctoral Scholarships. Lastly, I would like to thank the Department of Anthropology and Archaeology at the University of Calgary for numerous graduate stipends, scholarships, and teaching opportunities.

I would like to thank the Tanzanian Commission of Science and Technology, The University of Dar es Salaam, and the National Museums of Tanzania for allowing me to conduct research in Tanzania and especially at Olduvai Gorge. Without any of these institutions, this dissertation would not be possible. I would also like to acknowledge members of The Olduvai Paleoanthropology and Paleoecology Project (TOPPP) who granted me access to some of their archaeological sites. Additionally, there are numerous Tanzanians who assisted me in fieldwork that would not have been completed without their help that I am greatly thankful to have worked with at Olduvai.

I could not ask for a better group of people to work alongside all these years than those members of the Stone Tools, Diet, and Sociality project. Through both good times and bad, we have conducted wonderful research together and constantly work as a remarkably unified research unit. I know there have been many people involved with the SDS project over the years from all levels of academia and I would like to thank all of you for your help throughout my dissertation. I would like to especially thank Robert William Bird, Pastory Bushozi, Siobhán Clarke, Julien Favreau, Jamie Inwood, Makarius Itambu, Fergus Larter, Patrick Lee, Aloyce Mwambwiga, María Soto, and Laura Tucker. It is going to be extremely difficult to move on from the University of Calgary and not see you guys every day. However, I know we will continue to work with each

other in the future I look forward to our further adventures. I am so fortunate to be involved with such an extraordinary class of intelligent and talented individuals, thank you all.

Without a doubt, I must thank my family. Alicia and Chris, I want you to know how thankful I am to have you as sister and brother. I do not say it often (or ever), but our conversations about movies, TV, comics, sports, or whatever have always been fantastic stress relievers and have helped me relax during the more-stressful periods of my PhD. I also want you to know how proud I am of both of you and all that you have accomplished. You guys constantly make me want to be a better older brother so that you look up to me as much as I look up to you. Thank you.

Mom and dad, I really cannot say thank you enough. You have supported everything I have ever wanted to accomplish in life, and it is impossible to show how appreciative I am of that. Without you, I would never have been able to do all the wonderful things I have been fortunate enough to do over the years, especially moving across the continent and to another country to complete a PhD. You guys have taught me so much about working hard, being a good person, and taking responsibility for my actions; traits that I intend to pass on to Owen. I hope that I have made you both proud and plan to continue to meet and exceed your expectations. I love you both.

Dr. Mercader, where do I even begin. You have been a mentor, advisor, teacher, and most importantly, a friend. You were the one to give me this incredible opportunity, have been the most supportive PhD advisor, and have gone above and beyond your responsibilities to make sure I succeed at every level. I am immensely indebted to all you have done for me since I began my degree including field and laboratory financial support, intellectual (and not so intellectual) discussions, introducing me to incredible colleagues from all over the world, reviewing every grant and job application, always having an open door policy, never being too busy to answer questions, hundreds of cups of coffee and tea, and other innumerable encouragements. You have taught me to be an academic, but more importantly, showed me what is truly important about working in foreign countries; that is, respecting local people and making them as important to research as anyone from an academic institution. If I am half as successful in my career as you have been, I will consider it a great accomplishment. I hope you know how thankful I am for all you have done for me, and even if I do not always act it, I feel incredibly privileged to have worked alongside you the past five years. Thank you.

Finally, I want to thank my wife, Kelly, who truly is the most incredible person in my life. Not only did you upend her life and move to Calgary with me, but you have supported me in more ways than I can possibly list since I started my degree. There is no way to thank you for everything you have done for us as a family over the years and I definitely do not tell you often enough how appreciative I am to have you in my life. To Ann, Pete, Tricia, and Kenny, I am sorry for selfishly keeping this wonderful individual in Canada these past six years. Kelly, you are amazing; you willingly moved away from your family even though you knew I would spend months away in Africa and leave you in Calgary. I do not know how I can ever repay you for that. Also, you have given me the greatest gift in our son, Owen. Coming home to you two is the highlight of my day and I cannot believe how lucky I am to have you two in my life. I cannot wait to start our next adventure together wherever that may be. I love you.

FOR KELLY

TABLE OF CONTENTS

Abstract	ii
Acknowledgments.....	iii
Dedication	v
Table of Contents	vi
List of Figures	xii
List of Tables	xvii
Chapter 1: Introduction	1
1.1 Introduction to the Research Problem.....	1
1.2 Identification of the Problem	3
This dissertation	4
1.3 Exploration of the Problem.....	5
1.4 Importance to Human Evolution Scholarship.....	11
1.5 Chapters Summaries	12
Chapter 2: Ecological Primers and Theoretical Foundations	19
2.1 An Introduction to African Phytochoria and Biomes	19
2.2 Flora and the African Continent	20
2.2.1 Microhabitats and Biomes	23
2.3 Extant Phytochoria and Biomes of Sub-Saharan Africa.....	28
2.3.1 Zambezi Regional Center of Endemism	28
2.3.2 Sudanian Regional Center of Endemism	31
2.3.3 Guineo-Congolian Regional Center of Endemism	32
2.3.4 Somalia-Masai Regional Center of Endemism.....	34
2.3.5 Karoo-Namib Regional Center of Endemism.....	36
2.3.6 Cape Regional Center of Endemism.....	38
2.3.7 Afrotropical Archipelago-like Centre of Endemism	39
2.3.8 Zanzibar-Inhambane Regional Mosaic	41
2.3.9 Other Criteria and Floristic Classifications.....	43
2.4 Overview of Present-day Climate and Vegetation.....	44
2.4.1 The Olduvai Gorge Region.....	44
2.4.2 Physiography of Olduvai Gorge	49
2.5 Referentials for Olduvai's Paleolandscape	51
2.6 Chapter 2 Summary	56

Chapter 3: Climate Change and Human Evolution.....	58
3.1 Introduction.....	58
3.2 Controlling Factors of Climate and Environment.....	60
3.2.1 Convention for Dating the Pleistocene	60
3.2.2 Orbital Forcing and Global Climate	64
3.2.3 Milankovitch Cycles	65
3.2.4 Glacial-Interglacial Intensification	67
3.2.5 Differing Controls on Regional Climate.....	68
3.2.6 East African Tectonic Uplift.....	69
3.2.7 East African Moisture-Aridity Cycles	71
3.2.8 Orbital Forcing and Paleo-Lake Olduvai.....	73
3.3 Environmental Hypotheses for Human Evolution.....	75
3.3.1 Habitat Specific Hypotheses	77
3.3.2 Variability Hypotheses.....	81
3.4 Chapter 3 Summary	85
Chapter 4: Olduvai Gorge.....	86
4.1 Introduction.....	86
4.2 Stratigraphic Summary of the Olduvai Beds	89
4.3 Chapter 4 Summary	95
Chapter 5: Plant Leaf Wax Lipid Marker Molecules.....	97
5.1 Leaf Wax Lipid Biomarkers	97
5.2 Lipid Biosynthesis	103
5.2.1 Fatty Acid Biosynthesis	103
5.2.2 Alkane Biosynthesis.....	106
5.3 Photosynthetic Pathways	109
5.4 Isotope Signatures from Lipid Biomarkers.....	113
5.5 Controls on $\delta^{13}\text{C}$ and δD of Lipid Compounds.....	115
5.5.1 Plant Type	115
5.5.2 Atmospheric CO_2	119
5.5.3 Plant Water-Use Efficiency	123
5.5.4 Temperature	125
5.5.5 Aridity/Humidity.....	130
5.5.6 Source Water.....	136
5.6 Isotope Fractionation	141

5.6.1 $\delta^{13}\text{C}$ Fractionation	142
5.6.2 δD Fractionation	143
5.7 Leaf Wax Diagenesis	145
5.7.1 Preservation.....	145
5.7.2 Diagenesis and Fractionation.....	147
5.7.3 Taphonomy	150
5.8 Chapter 5 Summary	151
Chapter 6: Paleo-reconstructions in East Africa.....	152
6.1 Stable Isotopes of Pedogenic Carbonates	152
6.1.1 Olduvai Gorge.....	154
6.1.2 Omo-Turkana Basin.....	160
6.2 Paleontological Proxies.....	165
6.2.1 The ‘Earliest’ Hominins.....	166
6.2.2 Olduvai Fauna.....	168
6.2.3 Omo-Turkana Basin.....	176
6.3 Macro- and Microbotanical Remains at Olduvai Gorge.....	178
6.4 Geology and Stratigraphy	179
6.5 Isotopes of Lipid Biomarkers.....	181
6.6 Chapter 6 Summary	187
Chapter 7: The Acheulean Stone Tool Industry	189
7.1 Introduction.....	189
7.2 Earliest Examples of the Acheulean	191
7.2.1 Kenya	192
7.2.2 Ethiopia.....	193
7.2.3 Tanzania.....	195
7.3 Emergence of the Acheulean	198
7.4 The Acheulean at Olduvai Gorge	200
7.5 Environmental Context of the Earliest Acheulean.....	204
7.6 Chapter 7 Summary	206
Chapter 8: Methods.....	207
8.1 Sample Collection.....	207
8.1.1 FLK-N.....	212
8.1.2 Clays Below Tuff IF	215
8.1.3 FLK-W.....	215

8.1.4 LAS	220
8.1.5 BPT	222
8.1.6 Castle Clays	223
8.2 Sample Preparation and Total Lipid Extraction.....	226
8.2.1 Sample Preparation	226
8.2.2 Soxhlet Extraction.....	226
8.2.3 Ultrasonic Extraction	228
8.3 Leaf Wax Lipid Compound Separation	230
8.3.1 Silica Gel Column Chromatography.....	230
8.3.2 Silver Nitrate Column Chromatography	232
8.3.3 Aminopropyl Column Chromatography	234
8.4 Technique Development	236
8.4.1 Lipid Extractions.....	236
8.4.2 Soxhlet vs. Ultrasonic Extraction	240
8.4.3 Silica Gel.....	242
8.4.4 Implementation of SiAgNO ₃	244
8.4.5 Fatty Acid Methyl Esters	253
8.5 Summary of Extraction Techniques.....	257
8.6 Gas Chromatography and Isotope Ratio Mass Spectrometry	260
8.6.1 Gas Chromatography Mass Spectrometry (GC-MS).....	260
8.6.2 Isotope Ratio Mass Spectrometry (IRMS) and the δ Notation	266
8.6.3 Standards.....	270
8.7 Data Analysis	271
8.7.1 CPI	271
8.7.2 ACL.....	272
8.7.3 Mixing.....	273
8.7.4 Quantification	277
8.7.5 Modern H-isotopes from Precipitation	279
8.7.6 FAME Corrections.....	280
8.8 Methods Summary	281
Chapter 9: Results	282
9.1 GC-MS Compound Quantitation	282
9.1.1 FLK-N.....	283
9.1.2 Clays Below Tuff IF	286

9.1.3 FLK-W	297
9.1.4 BPT	307
9.1.5 Castle Clays	312
9.1.6 LAS	319
9.2 $\delta^{13}\text{C}$ and δD	320
9.2.1 FLK-N.....	320
9.2.2 Clays Below Tuff IF	327
9.2.3 FLK-W.....	330
9.2.4 BPT	334
9.2.5 Castle Clays	335
Chapter 10: Discussion	343
10.1 Leaf Wax Lipid Preservation	343
10.1.1 Plant Wax Abundances	346
Castle Clays	348
FLK North.....	352
Clays Below Tuff IF	355
10.1.2 Taphonomy	360
10.2 Plant Landscape Coverage: C_3 and C_4 Proportions	366
10.2.1 FLK North.....	367
10.2.2 Castle Clays	371
10.2.3 FLK West.....	374
10.3 Environmental Factors Influencing $\delta^{13}\text{C}$ and δD	378
10.3.1 FLK North.....	379
10.3.2 Castle Clays	383
10.3.3 FLK West.....	389
10.3.4 The C_{22} n-Acid.....	391
10.4 Using the δD of Rainfall to Infer Paleo-Precipitation.....	393
10.4.1 Moisture Dynamics in East Africa.....	393
10.4.2 Meteoric Water Lines	398
10.4.3 C_{28} n-Acid and Paleo-precipitation.....	402
10.5 Implications for Human Evolution	407
10.5.1 Stone Tools and Woody Plant Abundance	407
10.5.2 FLK North Advantage	409
10.5.3 The Environmental Context of the Earliest Acheulean at Olduvai Gorge.....	411

Chapter 11: Conclusions	415
11.1 Leaf Wax Preservation.....	415
11.2 Water Availability and Plant Landscapes	416
11.3 Plant Ecosystems in Upper Bed I and Lower to Middle Bed II, Olduvai Gorge.....	418
11.4 Environments and Stone Tool Technology.....	420
11.5 Recommendations for Future Biomarker Research at Olduvai Gorge	421
References.....	424
Appendix A.....	468
Concentrations for individual <i>n</i> -alkanoic acids - $\mu\text{g/g}$ of dry sediment	468
Appendix B.....	474
Raw and Corrected $\delta^{13}\text{C}$ and δD Isotope Values	474
Appendix C	480
C ₃ percentages modeled using linear and sine-squared equations.....	480
Appendix D.....	483
Clays Below Tuff IF	483

LIST OF FIGURES

Figure 1-1. Overview of Olduvai Gorge.....	4
Figure 1-2. Archaeological and geological sampling location around Olduvai Gorge	9
Figure 2-1. Geographic, Regional Centers of Endemism, and average rainfall overview of the Africa continent	22
Figure 2-2. The Crater Highland of the Arusha Region of Northern Tanzania.....	44
Figure 2-3. Monthly precipitation and average temperatures throughout Tanzania.....	46
Figure 2-4. Elevation profiles of Olduvai Gorge and Ngorongoro Crater.....	48
Figure 2-5. Physiographic distinctions of Olduvai Gorge.	50
Figure 3-1. Average benthic foraminifera $\delta^{18}\text{O}$ record for the last 1.8 million years.....	62
Figure 4-1. Olduvai Gorge.....	87
Figure 4-2. Bed displacement due to faulting along the Second Fault.	94
Figure 5-1. Schematic of leaf anatomy and wax lipids.....	98
Figure 5-2. Typical GC-MS trace of <i>n</i> -alkane and <i>n</i> -alkanoic acid compounds.	100
Figure 5-3. Acetyl and Malonyl Coenzyme A.....	104
Figure 5-4. Proposed metabolic pathway for leaf wax biosynthesis.	107
Figure 5-5. Calvin-Benson Cycle.	109
Figure 5-6. Hatch-Slack Pathway.	110
Figure 5-7. Photosynthesis and Photorespiration.....	111
Figure 6-1. Proportions of species by body mass in Lower and Upper Bed II.....	174
Figure 7-1. The earliest known examples of the Acheulean in East Africa.	189
Figure 7-2. Acheulean cleaver and handaxe from Olduvai Gorge.	191
Figure 7-3. Partial crude handaxes from Kokiselei 4, Kenya.	192
Figure 7-4. Handaxes from Konso-Gardula, Ethiopia.....	194

Figure 7-5. Bifacially-flaked handaxe from Olduvai Gorge.....	195
Figure 7-6. Acheulean sites of Eastern and Southern Africa.....	197
Figure 8-1. Stratigraphic subsections of Olduvai Beds I and II.....	209
Figure 8-2. Archaeological and geological sampling locations around Olduvai Gorge.....	210
Figure 8-3. Stratigraphy of the FLK-N archaeological levels and column sampling from Geological Trench 7	214
Figure 8-4. Column sampling and stratigraphy of the FLK-W archaeological site.....	218
Figure 8-5. Geologically inferred braided stream channel reconstruction of the Lower Augitic Sandstone.	221
Figure 8-6. General stratigraphy of Olduvai’s Castle.....	225
Figure 8-7. Schematic of a Soxhlet extraction apparatus	227
Figure 8-8. Schematic of a silica gel column for chromatography.....	230
Figure 8-9. Schematic of a silver nitrate-infused silica gel column for chromatography.....	233
Figure 8-10. Schematic of an aminopropyl column.....	235
Figure 8-11. GC-MS chromatograms for contamination isolation tests	239
Figure 8-12. Chromatograms of the same sample extracted using different techniques	241
Figure 8-13. Unresolved Complex Mixture of a sample from FLK-W	243
Figure 8-14. Unresolved Complex Mixture of a “modern” sample from Olduvai Gorge.....	244
Figure 8-15. GC-MS chromatograms for a FAME standard eluted over different concentrations of silver nitrate	250
Figure 8-16. <i>n</i> -alkane GC trace with UCM interference compared to <i>n</i> -alkanoic acids without an UCM	253
Figure 8-17. Methylation of <i>n</i> -alkanoic acids to produce Fatty Acid Methyl Esters	255
Figure 8-18. Summary of lipid extraction techniques	258
Figure 8-19. Mass spectra for identifying compounds using GC-MS.....	261

Figure 8-20. National Institute of Standard and Technology library mass spectra	262
Figure 8-21. Mass spectra of the molecular ions representing the mass of the C ₂₉ -C ₃₃ <i>n</i> -alkanes	263
Figure 8-22. Histogram showing the distribution of <i>n</i> -alkane C ₂₉ and C ₃₁ δ ¹³ C values for C ₃ and C ₄ plants	275
Figure 8-23. Monthly precipitation data in relation to precipitation δD in East Africa	279
Figure 9-1. Homologue distribution and abundances (μg/gdw) of <i>n</i> -alkanoic acids from FLK-N Trench 7	285
Figure 9-2. Homologue distribution and abundances (μg/gdw) of <i>n</i> -alkanes and <i>n</i> -alkanoic acids from the clays below Tuff IF	290
Figure 9-3. Homologue distribution and abundances (μg/gdw) of <i>n</i> -alkanes and <i>n</i> -alkanoic acids from FLK-W	300
Figure 9-4. Homologue distribution and abundances (μg/gdw) of <i>n</i> -alkanes and <i>n</i> -alkanoic acids from the BPT.....	310
Figure 9-5. Homologue distribution and abundances (μg/gdw) of <i>n</i> -alkanes and <i>n</i> -alkanoic acids from the Castle Clays	315
Figure 9-6. LAS chromatogram of <i>n</i> -alkanes dominated by an Unresolved Complex Mixture.	319
Figure 9-7. Carbon isotope values (δ ¹³ C) from FLK-N Trench 7	324
Figure 9-8. Hydrogen isotope values (δD) from FLK-N Trench 7.....	326
Figure 9-9. Carbon isotope values (δ ¹³ C) from FLK-W for <i>n</i> -alkanes C ₂₅ -C ₃₃	333
Figure 9-10. Carbon isotope values (δ ¹³ C) from the Castle Clays for <i>n</i> -alkanoic acids C ₂₂ -C ₃₂	339
Figure 9-11. Hydrogen isotope values (δD) from the Castle Clays for <i>n</i> -alkanoic acids C ₂₂ -C ₃₂	341
Figure 10-1. Abundances for the C ₂₀ to C ₃₄ <i>n</i> -alkanoic acids from the Castle Clays.....	347
Figure 10-2. Abundances of Castle Clays <i>n</i> -alkanoic acids plotted against δD from the C ₂₈ <i>n</i> -acid	349
Figure 10-3. Abundances of Castle Clays <i>n</i> -alkanoic acids plotted against δ ¹³ C from the C ₂₈ <i>n</i> -acid	349

Figure 10-4. Abundances for the C ₂₀ to C ₃₄ <i>n</i> -alkanoic acids from FLK-N Trench 7.....	353
Figure 10-5. Abundances of FLK-N <i>n</i> -alkanoic acids plotted against δD from the C ₂₈ <i>n</i> -acid..	354
Figure 10-6. Abundances of FLK-N <i>n</i> -alkanoic acids plotted against δ ¹³ C from the C ₂₈ <i>n</i> -acids	354
Figure 10-7. Total abundance of <i>n</i> -alkanoic (µg/g of dry sediment) from the Clays below Tuff IF	356
Figure 10-8. Relative abundance of the C ₂₁ to C ₃₅ <i>n</i> -alkanes from FLK-W.....	361
Figure 10-9. Percentage of C ₃ and C ₄ plants based on <i>n</i> -alkanoic acid δ ¹³ C and specific end- member values for FLK-N Trench 7	368
Figure 10-10. Percentage of C ₃ and C ₄ plants based on <i>n</i> -alkanoic acid δ ¹³ C and specific end- member values for the Castle Clays.....	372
Figure 10-11. Percentage of C ₃ and C ₄ plants based on <i>n</i> -alkane δ ¹³ C and specific end-member values for FLK-W	375
Figure 10-12. Carbon (δ ¹³ C) and hydrogen (δD) isotope fluctuations for <i>n</i> -alkanoic acids C ₂₈ -C ₃₂ and C ₂₂ from FLK-N	380
Figure 10-13. Carbon (δ ¹³ C) and hydrogen (δD) isotope fluctuations for <i>n</i> -alkanoic acids C ₂₈ -C ₃₂ and C ₂₂ from the Castle Clays	384
Figure 10-14. Covarying and anti-phasing instances for the C ₂₈ <i>n</i> -alkanoic acid throughout the Castle Clays	386
Figure 10-15. Carbon isotope data and corresponding percentage of C ₄ grasses plotted against diatom abundance from FLK-W	390
Figure 10-16. Moisture dynamics of the major seasonal monsoons in Eastern Africa	395
Figure 10-17. Monthly variations in precipitation δD and δ ¹⁸ O for GNIP stations near Olduvai Gorge.....	397
Figure 10-18. Relationship between δD and δ ¹⁸ O in rainwater recorded at GNIP stations near Olduvai Gorge.....	400
Figure 10-19. Monthly δD and δ ¹⁸ O estimates from the OIPC for Olduvai Gorge.....	407
Figure 10-20. FLK-W δ ¹³ C data plotted against total number of lithics, fauna, and human modified bones at FLK-W	412

LIST OF TABLES

Table 4-1. Olduvai Gorge Geochronology with Sites	90
Table 5-1. Molecular and structural formulas of leaf wax lipid biomarkers	98
Table 5-2a. Saturated (normal) alkanolic acids	103
Table 5-2b. Saturated (normal) alkanolic acids	105
Table 5-3. Saturated (normal) alkanes	108
Table 8-1. FLK-N Trench 7 samples	213
Table 8-2. Clays below Tuff IF samples.....	216
Table 8-3. Summary of lithics recovered at FLK-W	217
Table 8-4. FLK-W samples.....	219
Table 8-5. Lower Augitic Sandstone samples	221
Table 8-6. Bird Print Tuff samples	223
Table 8-7. Castle Clays samples	224
Table 8-8. Summary of sample amounts used in lipid extraction.....	226
Table 8-9. Total concentration of FAME standards extracted using different silver nitrate concentrations	252
Table 8-10. GC-MS parameters.....	265
Table 8-11. Reference standards for hydrogen and carbon isotopes	267
Table 8-12. Monthly δD estimates for Olduvai Gorge	280
Table 9-1. CPI and ACL for FLK-N Trench 7	284
Table 9-2a. CPI and ACL for clays below Tuff IF <i>n</i> -alkanes.....	288
Table 9-2b. CPI and ACL for clays below Tuff IF <i>n</i> -alkanoic acids.....	289
Table 9-3. CPI and ACL for FLK-W	299
Table 9-4. CPI and ACL for the Bird Print Tuff.....	309

Table 9-5. CPI and ACL for the Castle Clays	314
Table 9-6. $\delta^{13}\text{C}$ values for FLK-N Trench 7	323
Table 9-7. $\delta^{13}\text{C}$ correlation (r^2) for $\text{C}_{22}\text{-C}_{32}$ <i>n</i> -acids from FLK-N Trench 7	323
Table 9-8. δD values for FLK-N Trench 7	325
Table 9-9. δD correlation (r^2) for $\text{C}_{22}\text{-C}_{32}$ <i>n</i> -acids from FLK-N Trench 7	325
Table 9-10. $\delta^{13}\text{C}$ values for the clays below Tuff IF	329
Table 9-11. $\delta^{13}\text{C}$ correlation (r^2) for $\text{C}_{22}\text{-C}_{32}$ <i>n</i> -acids from the clays below Tuff IF	329
Table 9-12. $\delta^{13}\text{C}$ values for FLK-W	332
Table 9-13. $\delta^{13}\text{C}$ correlation (r^2) for $\text{C}_{25}\text{-C}_{33}$ <i>n</i> -alkanes from the FLK-W	332
Table 9-14. $\delta^{13}\text{C}$ values for the Bird Print Tuff	334
Table 9-15. $\delta^{13}\text{C}$ values for the Castle Clays	338
Table 9-16. $\delta^{13}\text{C}$ correlation (r^2) for $\text{C}_{22}\text{-C}_{32}$ <i>n</i> -acids from the Castle Clays	338
Table 9-17. δD values for the Castle Clays	340
Table 9-18. δD correlation (r^2) for $\text{C}_{22}\text{-C}_{32}$ <i>n</i> -acids from the Castle Clays	340
Table 9-19. Results Summary	342
Table 10-1. Hydrogen isotope values of rainfall recorded at GNIP station near Olduvai	396
Table 10-2. Meteoric Water Line formulas	398
Table 10-3. Deuterium excess values	401
Table 10-4. Monthly δD and $\delta^{18}\text{O}$ estimates for Olduvai Gorge	401
Table 10-5. Estimated C_{28} δD values from eastern African GNIP stations	405

CHAPTER 1: INTRODUCTION

1.1 Introduction to the Research Problem

Effectively responding to environmental change and habitat variability is a defining characteristic of modern humans and our extinct ancestors. Throughout the Pleistocene, climate in East Africa oscillated between humid and arid periods (Potts, 2012a), and the ability to deal with “ecological shocks” required that early humans be mobile and have a flexible diet; a fundamental attribute to the development of the genus *Homo* (Hardy et al., 2015; Wells, 2012). In addition, these wet and dry environmental shifts fragmented local ecosystems into ‘oasis-like’ concentrations of plants (Ashley et al., 2010a; Ashley et al., 2014; Ashley et al., 2010b; Ashley et al., 2009), fracturing habitats into assorted patches of distinct landscape structure. Causal relationships between and among environmental change, habitat type and distribution, food resources, and cultural innovation has resulted in multiple hypotheses examining human-environment interactions (deMenocal, 2004; Potts, 1998a, b; Stanley, 1992; Vrba, 1985; Vrba et al., 1989), such as placing Pleistocene stone tool technologies and behavior in specific sedimentary, vegetational, and climatic contexts (Biberson, 1963; Bibi et al., 2018; de la Torre et al., 2017; Howell and Clark, 1963; Potts et al., 2018).

Often overlooked in human evolution research are the environmental conditions in which a significant technological shift occurred, such as the emergence of the Acheulean in East Africa between 1.7 and 1.8 million years ago (Mega annum - Ma). One central question, however, asks whether the adoption of the Acheulean in favor of the Oldowan was environmentally driven. Bibi et al. (2018) investigated the transition from Oldowan to Acheulean technologies at Olduvai Gorge in a framework of paleoecological and paleoenvironmental changes. Others have examined major

transitions in human evolution alongside major global climate changes (deMenocal, 2011; Potts, 1996; Vrba, 1985), or changes in eastern African faunal communities (Bibi and Kiessling, 2015; Bobe and Behrensmeyer, 2004; Bobe and Eck, 2001), while a minority focused on records of environmental variability with established links to specific terrestrial environments (Feakins et al., 2007; Feakins et al., 2013; Magill et al., 2013a, b).

The emergence of the Acheulean in East Africa ~1.75 Ma (Beyene et al., 2013; Diez-Martín et al., 2015; Lepre et al., 2011), was the first major transition in stone tool technology, coinciding with the widespread distribution of the genus *Homo* throughout Africa, Europe, and Asia. As the Acheulean signified early complex behavior through the repeated manufacture of large-sized, standardized tools (Diez-Martín et al., 2015), it is indicative of advance foresight requiring developments in spatial perception beyond those known for apes or earlier (>2.0 Ma) hominins. Therefore, multiple hypotheses have been advanced regarding the emergence of the Acheulean (Fitzhugh, 2001; Gallotti and Mussi, 2018b; Gamble et al., 2011; Kuhn, 2004; Shennan, 2011); nevertheless, environmental data for the earliest known Acheulean archaeological assemblages are lacking. While there are several lines of evidence for African climate change and ecological reconfiguration beginning around 1.8 Ma (Cerling, 1992; Cerling et al., 1993; deMenocal, 2004; Marlow et al., 2000; Schefuß et al., 2003), no strong correlation exists between remodeling of African landscapes and the origins of *Homo erectus* or development of the Acheulean. Furthermore, paleoclimate records do not support unidirectional shifts to permanently drier conditions in East or South Africa (deMenocal, 2004).

Although the Acheulean appears in the archaeological record by 1.7 Ma, coinciding with the expansion of *Homo erectus* into areas unoccupied by earlier hominins (Beyene, 2003; Semaw et al., 2008), high-resolution datasets for local and regional climate are missing for the earliest

Acheulean sites. Furthermore, the timing of the first Acheulean assemblages in Ethiopia and Kenya are poorly constrained geologically (Semaw et al., (2008): p. 87), while the environmental background for hominin technological adaptations in East Africa between 2.0 and 1.8 Ma is unclear.

1.2 Identification of the Problem

The earliest known examples of the Acheulean in East Africa, made up of handaxe and cleaver assemblages of proto-bifaces or bifaces, are found at Kokiselei 4, West Turkana, Kenya at an estimated age of 1.76 Ma (Lepre et al., 2011), and at Konso-Gardula, Ethiopia, $^{40}\text{Ar}/^{39}\text{Ar}$ dated to 1.74 ± 0.03 Ma (Beyene et al., 2013). Slightly younger, but chronologically well-bracketed material that is also more technologically and morphologically complex, is found at the Frida Leakey Korongo West (FLK-W) site, Olduvai Gorge, Tanzania, $^{40}\text{Ar}/^{39}\text{Ar}$ dated to 1.698 ± 0.015 Ma (Diez-Martín et al., 2015) (Fig. 1-1). Although the Acheulean does not become widespread until about 1.5 Ma, shortly thereafter, the technology disperses across Africa (Chazan et al., 2008; Gibbon et al., 2009; Kuman and Clarke, 2000), the Near East (Bar-Yosef and Goren-Inbar, 1993), India (Pappu et al., 2011), and then later in China (Hou et al., 2000; Zhu et al., 2004), and Indonesia (Simanjuntak et al., 2010).

Water, vegetation, and human habitats are tightly coupled (Magill et al., 2013b), yet 160 years after being first described by Gabriel de Mortillet in the French town of Saint-Acheul, the environmental context of the earliest Acheulean is still poorly understood. Was the transition from the Oldowan to the Acheulean driven by environmental changes? Did the Acheulean emerge as a response to the opening of African landscapes as has been suggested (de la Torre, 2016; Hay, 1976; Isaac, 1971; Isaac and McCown, 1976; Potts, 2013), although environmental data is scarce? And

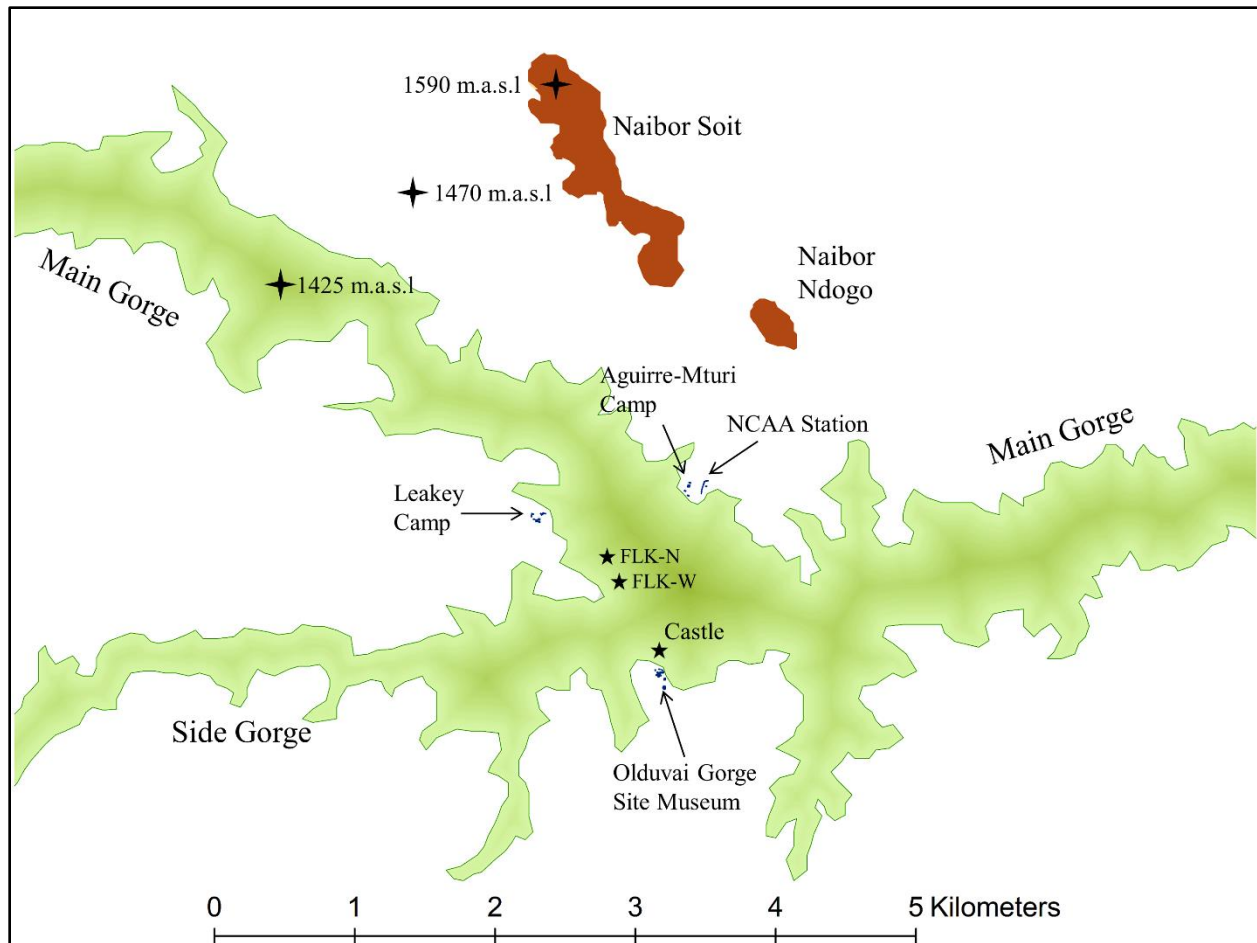


Figure 1-1. An overview of Olduvai Gorge, Tanzania highlighting the Main and Side gorges, metamorphic outcrops Naibor Soit and Naibor Ndogo, the main research stations, a general altitudinal profile, and the location of sites studied in this dissertation.

more specifically, what was the environmental context of the archaeological transition from the Oldowan to the Acheulean between Olduvai Beds I and II?

This dissertation advances research in the fields of human ecology, evolutionary anthropology, and ancient climate studies by examining human-environment interactions between water availability, plant landscapes, and stone tool technology at Olduvai Gorge, Tanzania through isotope geochemistry. The emphasis is on the environmental and archaeological transition between Olduvai Beds I and II, a nearly 200,000-year period (1.83 to 1.66 Ma), which includes a key shift in stone tool technology from the Oldowan to the Acheulean, and the widespread distribution of our genus, *Homo*. The principle goal is to investigate the dynamic human response to fluctuating

climates, ecological setting, and habitat choice, and to answer questions on how evolutionary outcomes correspond in time and space with specific environmental events by utilizing biologically specific marker molecules, or *biomarkers*, stable isotopes, and analytical chemistry to interpret water availability, vegetation type and abundance, precipitation vs. aridity, and relative temperatures.

1.3 Exploration of the Problem

Although a trend toward drier conditions in Africa over the Plio-Pleistocene is evident in marine (Feakins et al., 2007; Schefuß et al., 2003) and soil carbonate (Levin et al., 2004; Quade and Levin, 2013) records, it is difficult to associate specific landscape remodeling events at specific hominin-activity locales with gradual, continental-scale environmental changes. Moreover, abundant environmental data exist for Olduvai Gorge (Albert et al., 2009; Albert et al., 2006; Barboni et al., 2010; Bibi et al., 2018; Prassack et al., 2018), but very few studies have used isotope compositions of plant biomarkers from terrestrial sources (Magill et al., 2013a, b). This research is adding to the environmental dataset by creating a high-resolution, spatial and temporal isotope record for Olduvai Gorge upper Bed I and lower Bed II by exploring the correlation between shifting climates, ecological reorganization, and technological adaptations.

To explore the interactions between and among water accessibility and vegetation in various Olduvai paleo-habitats, terrestrial sediments were systematically sampled and processed for long-chain normal (*n*-) alkyl plant leaf wax compounds; specifically, *n*-alkanes and *n*-alkanoic acids lipid biomarkers. These compounds, consisting of covalently bonded carbon, hydrogen, and oxygen atoms are difficult to degrade without subjecting to high temperatures (>100°C) or catalytic enzyme and chemical activity, and thus the original isotopic content incorporated during

biosynthesis remains intact over geologic time as the molecules travel through the environment before settling in sediments (Eglinton and Eglinton, 2008). Normal alkanes and fatty acids (the biosynthetic precursors of the *n*-alkanes in plant cuticular wax (Kunst and Samuels, 2003; Samuels et al., 2008), are relatively long-lived compounds that are easily extracted and analyzed, and widely used as biomarkers in studies focusing on paleoenvironmental change (see Chapter 5: Plant Leaf Wax Lipid Marker Molecules). They pass into the environment as leaf debris, are often transported long distances by wind and water, and then the intact molecules are deposited in both terrestrial and aquatic sediments. These molecules eventually serve as proxy measures of the continental vegetation that synthesized them (Eglinton and Eglinton, 2008).

Assessing hydrogen and carbon isotope compositions of *n*-alkanes and *n*-acids act as a coupled proxy record for changes in water availability, vegetation communities, precipitation or aridity, evapotranspiration of leaf and soil moisture, and the relative abundance of C₃ and C₄ plants in response to climate changes (Liu and Yang, 2008; Liu et al., 2006; Lockheart et al., 1997; Magill et al., 2013b). Gas chromatography and mass spectrometry are used to quantitatively measure biomarkers and isotope ratios, as these techniques allow for the assessment of the environmental parameters in which these biomarkers formed (Castañeda and Schouten, 2011).

Following biomarker quantification, hydrocarbon identification differentiates *n*-alkane and fatty acid homologues and their sources of production (e.g. aquatic vs. terrestrial plants). The ubiquitous, well-preserved nature of *n*-alkyl compounds, particularly in lacustrine sediments (Wang et al., 2014), has led to their distributions being used to understand paleoenvironmental processes and the climatic context in which they originated (Castañeda and Schouten, 2011; Eglinton and Eglinton, 2008). Identifying specific carbon-hydrogen compounds allows for the differentiation of *n*-alkane and *n*-acid homologues between those produced by aquatic algae

(Cranwell et al., 1987), submerged and floating aquatic plants (Cranwell, 1984; Ficken et al., 2000), and terrestrial vegetation (Eglinton and Hamilton, 1967). This interpretation will serve as a paleoenvironmental proxy for habitat type in the greater Olduvai paleolandscape; i.e. lacustrine vs. fluvial vs. terrestrial settings.

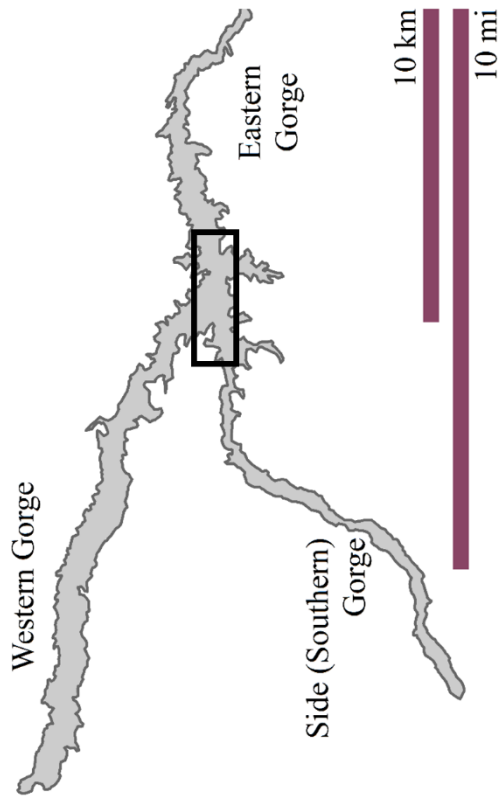
The hydrogen and carbon isotope compositions of *n*-alkyl lipids assess changes in plant type, atmospheric CO₂, plant water-use efficiency, temperature, aridity/humidity (including precipitation), and source water. Hydrogen isotopes of plant biomarkers are primarily influenced by the isotopic composition of precipitation water used during photosynthesis, and the isotopic fractionation associated with evapotranspiration (Sachse et al., 2012), but also temperature and successive evaporation-condensation events. Carbon on the other hand is primarily influenced by photosynthetic pathway (C₃ vs. C₄) and the discrimination against the heavy isotope (¹³C) during photosynthesis. Therefore, the hydrogen and carbon isotope compositions of *n*-alkanes and *n*-alkanoic acids function primarily as paleo-hydrological and paleo-vegetation proxies.

As a well-defined archaeological landscape (or ‘archaeo-sphere’) representing the fossil record of broader East Africa, Olduvai presents an opportunity to explore the validity of the proposed research objectives. The focus on Olduvai is befitting given that the region boasts archaeological remains with extraordinary evidence for human behaviour. This makes the study area the best place to track the impact shifting climates had on configuring local habitats, and the role ecological variability played in the development of Acheulean technology at Olduvai Gorge. Terrestrial sediments were sampled from the following Olduvai locations (Fig. 1-2) with the assistance of The Olduvai Paleoanthropology and Paleoecology Project (TOPPP):

- Frida Leakey Korongo North (FLK-N), a Bed I locality dated 1.831 ± 0.006 Ma to 1.803 ± 0.002 Ma (Deino, 2012), containing several hundred Oldowan stone tools and abundant faunal remains but no clear association between the two assemblages (n=8)
- Clays in contact below Tuff IF (1.803 ± 0.002 Ma), the marker tuff dividing Bed I from Bed II that is exposed for more than a kilometer throughout the main confluence of the gorge (n=30)
- Frida Leakey Korongo West (FLK-W), an excavation site dated between 1.698 ± 0.015 Ma and 1.664 ± 0.019 Ma, consisting of fluvial conglomerates and sands (Diez-Martín et al., 2015) that contains Olduvai's earliest known Acheulean assemblage (n=28)
- Along the Lower Augitic Sandstone (LAS), an unconsolidated sedimentary unit dated to between 1.698 ± 0.015 Ma and 1.664 ± 0.019 Ma, which is exposed for roughly one kilometer in the main confluence of the gorge and is stratigraphically related to the lower units of FLK-W (n=15)
- Clays in contact below the Bird Print Tuff (BPT), a roughly 200-meter long volcanic deposit exposed south of FLK-W in the main gorge, dated to Middle Bed II and found stratigraphically above FLK-W (n=11)
- Clays situated above Tuff IF (1.803 ± 0.03 Ma) and below Tuff IIA (1.74 ± 0.03 Ma) at Olduvai's geologic feature known as the *Castle*. These clays represent the paleoenvironment that followed the FLK-N sequence and preceded the FLK-W sequence in the lower portion of Bed II (n=14).

Sampling from these sites¹ presents an opportunity to combine temporal (column approach) with spatial (landscape approach) strategies to identify variations in lipid biomarkers and isotopes

¹ Archaeological *sites* are broadly defined as areas with stratified layers of varied sedimentology and different lithic (or fossil) material.



●	Bird Print Tuff (BPT)	
●	Lower Aurgitic Sandstone (LAS)	1.664 ± 0.019 Ma
⊠	FLK West	1.698 ± 0.015 Ma
■	Castle	1.740 ± 0.030 Ma

●	Clays below Tuff IF	1.803 ± 0.002 Ma
★	FLK North	1.831 ± 0.006 Ma

Bed II		

Bed I		

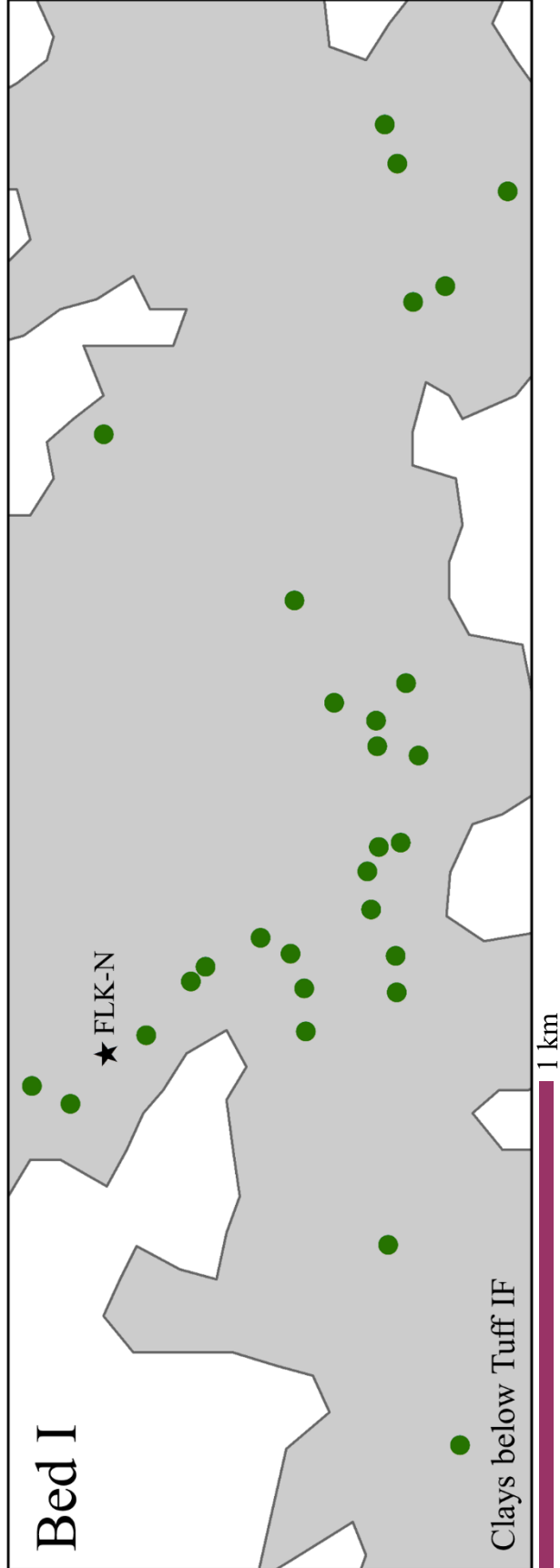


Figure 1-2A. Clays below Tuff IF sampling locations throughout the main confluence of the gorge. Sampling distance spans ~2.7 km east-to-west, and ~1.1 km north-to-south. ★ FLK North archaeological site.

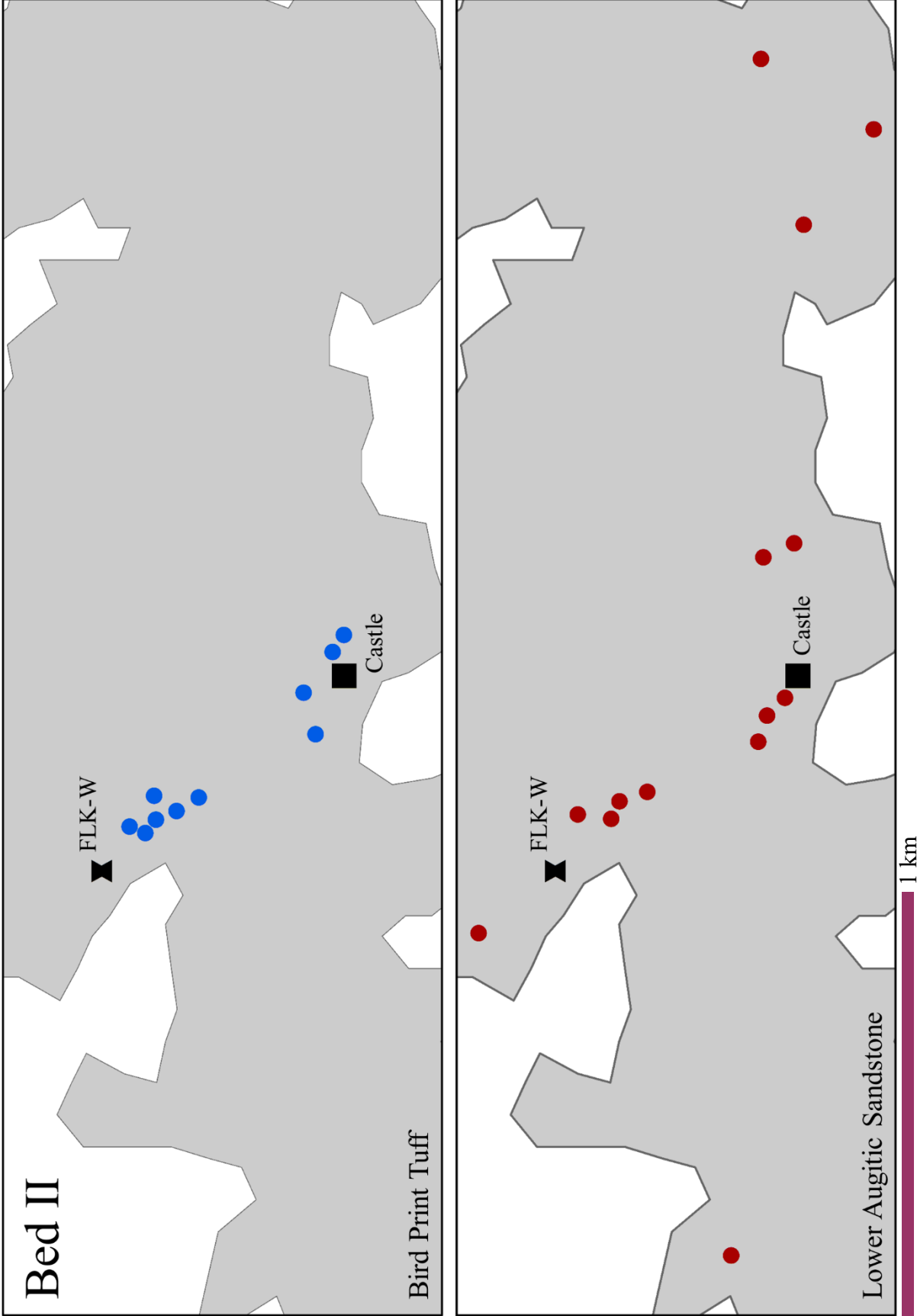


Figure 1-2B. Bird Print Tuff (BPT) sampling locations throughout the main confluence of the gorge. Sampling distance spans ~775 m NW-to-SE. **8-1C.** Lower Augitic Sandstone (LAS) sampling locations; distance spans ~1.2 km NW-to-SE and ~2.8 km east-to-west. **▲** FLK-W archaeological site, **■** Olduvai's Castle.

resulting from a mosaic ecosystem and changes in the environment over time. This will also allow for the classification of the patches of distinct landscape structure that existed at Olduvai Gorge ~1.7 Ma.

1.4 Importance to Human Evolution Scholarship

The scientific and technical originality of the project is the application of several proxies to assess the interaction between water accessibility, mosaic ecosystems, and dietary behavior in the various habitats that existed at Olduvai Gorge during upper Bed I and lower and middle Bed II. The focus on Olduvai is befitting given that the region boasts archaeological remains with extraordinary evidence for human behaviour, making the study area the best place to track the impact shifting climates had on configuring local habitats, and the role ecological variability played in the development of Acheulean technology at Olduvai Gorge. The research makes significant contributions to the science of human ecology and evolution studies by integrating environmental disciplines with archaeology to apply a wide array of data acquisition techniques and analyses to contribute to anthropological theory.

Changing hydrological conditions would have influenced plant community composition and imposed strong adaptive pressures on human evolution (Magill et al., 2013b). Even today, the role water availability plays in vegetation and resource distribution guides primate behaviors due to the impact water budget has on vegetation and resource distribution (Pruetz and Bertolani, 2009; Teaford and Ungar, 2000). However, much of our understanding on climatic controls and human evolution stem from reconstructions derived from indirect carbon or oxygen isotope proxies, specifically from tooth enamel, paleosols, or marine sediment sources (Feakins et al., 2013; Sponheimer and Lee-Thorp, 1999; Sponheimer et al., 2006; van der Merwe et al., 2008; Wynn,

2000). In addition, there are incomplete terrestrial records for environmental change that use stable hydrogen isotopes from lipid biomarkers preserved in terrestrial sediments. Therefore, the interpretation of the connection water accessibility and mosaic ecosystems had on human evolution is limited by both indirect proxies for hydrological and vegetation changes, and irregular terrestrial data for environmental fluctuations.

1.5 Chapters Summaries

The following chapters aim to establish a link between water availability and vegetation type during the emergence of the Acheulean stone tool industry at Olduvai Gorge, Tanzania through the isotopic characterization of *n*-alkyl lipid biomarkers from plant wax sources in ancient terrestrial sediments.

Chapter 2 introduces the ecological primers and theoretical foundations of studying extant African biomes and phytochoria. This chapter focuses on Sub-Saharan Africa by characterizing the geology, climate, and ecology of today, with an emphasis on East Africa and specifically, the Olduvai Gorge region. Flora on the Africa continent is addressed, as well as specific microhabitats and biomes; woodland, bushland, shrubland, grassland, desert, and Afroalpine vegetation. Sub-Saharan Regional Centers of Endemism according to White (1983) and major extant plant families are also introduced. Finally, an overview of present-day climate and vegetation of the greater Olduvai region is given, including modern referentials used for paleolandscape reconstructions.

Today, the regional centers of endemism and extant biomes are largely influenced by seasonal precipitation patterns which respond to regional topography and the convective activity of the Intertropical Convergence Zone; these features also play a critical role in the distribution of plant resources, which are largely determined by the availability of freshwater. These factors likely

had a similar role during the Pleistocene, and human activity would have been motivated by precipitation seasonality and vegetation distribution. As for the referential studies, caution must be taken when assigning any modern environment as a Pleistocene correlate, as interactions between CO₂ concentrations, rainfall amount, average temperature, or localized geology may have established Pleistocene vegetation communities and structures unlike those found today in the greater Olduvai region.

Chapter 3 reviews climate change and human evolution research. This chapter begins with an introduction to the controlling factors on climates and environments in Africa such as Milankovitch Cycles, tectonic uplift, and moisture-aridity cycles. It continues with a review on the discourse of intrinsic and extrinsic factors influencing human evolution, as well as habitat specific and variability hypotheses that explain the emergence of such human traits as bipedalism, brain enlargement, and tool use. Multiple hypotheses have been advanced linking climate change and human evolution and the environmental context of early human biological and technological adaptations in Africa. Both global and regional controls impact precipitation patterns and thus the available water to both plants and animals, including early humans. Therefore, these environmental parameters would have played a significant role in human evolution over both short and long timeframes, including the development of the Acheulean ~1.75 Ma.

Chapter 4 examines research at Olduvai Gorge, with an emphasis on the history of paleoanthropology at Olduvai, the geological interpretations for such things as the deposition on Beds I through IV, Masek, Ndutu, and Naisiusiu, volcanism and dating, and faulting and environmental (hydrological) reconfigurations. The primary focus of this chapter is the stratigraphy and geological characteristics of the seven Olduvai beds and the extent of which they can be found throughout the gorge. Although this chapter does not detail individual archaeological

sites, it provides the basis for understanding areas of the gorge discussed in other chapters and the stratigraphic correlations between Bed I and Bed II sites.

Chapter 5 is a comprehensive review of biological specific marker molecules diagnostic of terrestrial plants, specifically those from plant-derived normal (*n*-) alkyl lipids. This section introduces leaf wax lipid biomarkers, lipid biosynthesis, C₃ and C₄ photosynthetic pathway, and the controls influencing the carbon and hydrogen isotope content of leaves. Research on the environmental factors that effect isotope values in plants, such as temperature, aridity, evaporation, and source water is presented in addition to biomarker studies on modern plants and landscapes that inform our understanding of using this proxy as an environmental reconstruction tool. It also includes a brief summary of isotope fractionation and describes processes that affect the relative abundance of isotopes in lipids. It ends with an important discussion on the preservation and diagenesis of leaf wax lipid compounds, and why $\delta^{13}\text{C}$ and δD interpretations should be made with caution as isotope values may be altered due to (bio)degradation soon after deposition into soil horizons.

Chapter 6 examines East African paleo-reconstructions for Pleistocene habitats and biomes. It begins with a review of stable isotopes from pedogenic carbonates in both the Omo-Turkana Basin in Kenya and Ethiopia as well as Olduvai Gorge over the last ~2.5 Ma, with an emphasis on the major changes of the Early Pleistocene (1.806 Ma to 781,000 years ago). This chapter then reviews paleontological proxies for habitat reconstructions with a focus on avian, fish, and mammalian fossils. It continues with a discussion on biogenic silica in the form of plant phytoliths. Next, it reviews interpretations from a geological perspective on past environments, specifically in the Olduvai Gorge region. Finally, Chapter 6 looks at the recent advances in isotope analysis using lipid biomarkers to reconstruct hominin ecology in Kenya and Tanzania. These

different proxies are important for understanding Pleistocene East African archaeological sites because they exhibit how changing climate and environments altered the distribution of plant habitats and food resources which may have been the impetus for both biological and cultural adaptations in early humans.

The Acheulean stone tool industry and hypotheses on its emergence in East Africa are presented in Chapter 7. This section provides a general overview of the earliest known examples in Kenya, Ethiopia, and Tanzania, then follows with a review of proposed reasons for the Acheulean's emergence following nearly one million years of Oldowan tool use. A brief review of the Acheulean at Olduvai is then given before the chapter finishes with the environmental context of the earliest Acheulean in East Africa. The assemblage at Kokiselei (West Turkana, Kenya) is characterized by coarsely made proto-bifaces, unifacially and bifacially shaped crude handaxes, and pick-like tools, while those found at Konso-Gardula (Ethiopia) were large bifacially or unifacially modified flakes shaped into picks, handaxes, and cleavers. The Acheulean at FLK-W (Olduvai Gorge, Tanzania) on the other hand, displays evidence of relatively advanced knapping skills and provides evidence for the earliest stages of Acheulean development, and is the earliest site in which stone tools associate spatially and functionally with fauna exploitation.

Chapter 8 details methods and protocols, and the development of different analytical techniques for the analysis of leaf wax lipid biomarkers. This chapter begins with a discussion on sampling locations and collection strategy at Olduvai Gorge and reviews the geological and archaeological context of the investigated archaeological sites and geolocalities. Different methods used for the recovery of lipid extracts are then presented, and includes a review of the strengths and limitations of each extraction technique. This chapter follows with a comprehensive overview of technique development; this section highlights complications encountered during laboratory

analysis and the different protocols designed to mitigate such complications. It also presents the reasons why specific techniques and lipid biomarkers were used and summarizes the best approach to successfully analyzing terrestrial sediments from Pleistocene aged material. Chapter 8 continues with the gas chromatography mass spectrometry and the isotope ratio mass spectrometry protocols used for identifying and quantifying lipids compounds and their carbon and hydrogen isotopes. Finally, the most reliable and efficient method for extracting and analyzing *n*-alkanes and *n*-alkanoic acids is summarized at the end of the chapter. This section is given to provide an easy-to-follow method for future biomarker research in Pleistocene sediments.

Results are described in Chapter 9. Gas chromatography mass spectrometry compound quantitation is given for samples from each archeological site and geolocality investigated except for the Lower Augitic Sandstone which was mired by Unresolved Complex Mixtures. For both the *n*-alkanes and *n*-alkanoic acids (as Fatty Acid Methyl Esters), carbon preference index (CPI) and average chain length (ACL) were used to examine the odd-over-even or even-over-odd carbon number predominance and the weight-averaged number of carbon homologues, respectively. Quantitation results are also presented as histograms for each sample, but for some samples from FLK-W and BPT, *n*-alkane concentrations could not be calculated with confidence as they were either too low in concentration or had UCM interference; therefore, these were reported as relative abundance. The concentrations of all other samples are reported relative to a standard, but for the FLK-N sample set, only FAMES are given. The most dominant compounds detected were the C₃₁ *n*-alkane homologue and C₂₈ *n*-alkanoic acid, both of which derive from terrestrial plants, but the C₂₂ *n*-acid, which likely derive from mosses, was also very abundant especially at FLK-N.

The second half of Chapter 9 deals with the carbon and hydrogen isotope composition of the *n*-alkanes and *n*-acids. The $\delta^{13}\text{C}$ and δD isotopic composition of the C₂₂-C₃₂ even-numbered

FAMEs are reported for FLK North, the clays below Tuff IF, and the Castle Clays, while the $\delta^{13}\text{C}$ isotopic composition of the $\text{C}_{25}\text{-C}_{33}$ odd-numbered *n*-alkanes are given for FLK West. Only two Bird Print Tuff samples were successfully analyzed for $\delta^{13}\text{C}$, one for *n*-alkanes and one for *n*-alkanoic acids. This chapter ends with a summary table of the techniques used for each sample set and the overall findings.

Chapter 10 deals with the discussion of the results. A review of leaf wax lipid preservation is given, and how different sedimentological context result in differential preservation of the investigated biomarkers. This chapter begins with a discussion on the role sediment grain size has in preserving lipid biomarkers; for example, the different sediments comprising the six FLK-W archaeological levels lead to large disparities in lipid abundance between samples from the different levels. Although this may be attributed to the methods used to isolate the compounds, it could also be the result of microbial degradation as indicated by Unresolved Complex Mixtures. Following this, Chapter 10 deals with the abundances of plant waxes in the Castle Clays, FLK North, and clays below Tuff IF, as these were the best-preserved sample sets studied. This section ends with an examination of the taphonomy of lipid biomarkers from the Bird Print Tuff, Lower Aughtic Sandstone, and FLK-W and how (bio)degradation of the *n*-alkanes resulted in substantial UCMs. This is followed by a review of the different factors that result in UCM interferences such as elevated soil temperatures, soil pH, and seasonal differences in precipitation.

The proportions of plants using the C_3 or C_4 photosynthetic pathway is then addressed using $\delta^{13}\text{C}$ and end-member mixing models. Because there can be a significant estimation error associated with the end-member values used, three different end-member schemes and two separate mathematical models were employed to estimate the proportion of C_3 and C_4 plants at FLK-N, FLK-W, and the Castle. Chapter 10 continues with an overview of the possible

environmental factors dictating the $\delta^{13}\text{C}$ and δD isotope signatures of both *n*-alkanes and *n*-acids such as rainfall amount, changes in source precipitation, and plant type. This is followed by an analysis of the potential of using δD as a mechanism for tracking moisture source changes in East Africa and how distinct isotope signatures could result from a change in the direction of moisture delivery; e.g. northern or southern Indian Ocean. Additionally, the implications of this dissertation research are presented, and how leaf wax lipid biomarkers can be used to answer specific questions regarding environmental change and human evolution. Finally, the environmental context of the earliest Acheulean at Olduvai Gorge is proposed with both geochemical and archaeological evidence.

Lastly, Chapter 11 deals with the conclusions. A summary of the findings is discussed, specifically the data from leaf wax preservation, water availability and plant landscapes, plant ecosystems in Upper Bed I and Lower Bed II at Olduvai Gorge, and environments and stone tool technology. Recommendations for future biomarker research at Olduvai Gorge and East African paleoanthropological sites are offered at the end of this chapter, specifically regarding laboratory protocols and the need for proper baseline studies of extant African biomes.

CHAPTER 2: ECOLOGICAL PRIMERS AND THEORETICAL FOUNDATIONS

2.1 An Introduction to African Phytochoria and Biomes

Human-environment interactions and the relationship with evolutionary change is a prominent focus of anthropologists, biologists, ecologists, geoscientists or anyone interested in human evolution. As researchers continue investigating this relationship, they have concentrated their objectives on how evolutionary events correspond in time and space with particular environmental conditions, such as shifts in climate that result in shifts in habitat (Potts, 2013). Multiple hypotheses have been advanced in an effort to identify environmental triggers that influenced evolutionary change in humans and our ancestors throughout the Pleistocene (deMenocal, 2004; Feakins et al., 2005; Potts, 1998b, 2012a, b; Reed, 1997; Trauth et al., 2010; Trauth et al., 2006; Vrba, 1980). But, to truly recognize causal relationships between humans and their environment, we need an understanding of modern African ecology, as modern correlates are our only frame of reference to paleoenvironments. Therefore, a theoretical foundation regarding African climate, geomorphology, faunal communities, soil properties, and vegetation physiognomy or habitat structure can only be established by gathering as much information as possible on extant African habitats. Only then can we begin to reconstruct ancient vegetation physiognomy for Quaternary hominin environments.

The extant biomes of Africa are divided amongst sixteen major vegetation types, largely dependent on type of plant (tree, bush, grass, etc.), percentage of biomass each type of plant constitutes in each community, geography (e.g. coastal vs. mountain, tropical vs. temperate latitudes), and the structure of vegetation such as height, density, thorniness, and deciduousness. The sixteen types are further divided between five main groups; 1) formations of regional extent,

2) formations intermediate between those belonging to group 1 that have restricted distributions, 3) edaphic formations of distinct physiognomy, 4) formation of distinct physiognomy but with restricted distributions, and 5) unnatural (i.e. manmade) vegetation (White, 1983). In addition to the extensive anthropogenic modification of modern environments, we must also be aware that external mechanisms such as local tectonics, regional orbital forcing, and global climate changes are not operating precisely the same today as during the Pleistocene, and that the distribution of plants, percentage of biomass, or geographical extent may be quite different today than in the past. We also must be cautious when drawing parallels between extant and ancient vegetation communities, as many environments have been intentionally (Boivin et al., 2016), or non-intentionally (Marshall et al., 2018), modified by modern humans. Furthermore, the effects of external mechanisms like climate change on the distributions of animal and plant species, as well as the floristic composition of plant communities, is a complicated subject that can only begin to be understood through multidisciplinary research endeavors.

2.2 Flora and the African Continent

The continent of Africa measures approximately 8,000 kilometers north to south, with the Equator bisecting the landmass nearly at its center; the greater part of Africa's territory lies north of the Equator due to the westward extent of West Africa. Africa stretches to temperate regions in both the northern and southern hemispheres, but most of the land lies within the tropical region, bounded in the north by the Tropic of Cancer and in the south by the Tropic of Capricorn (Fig. 2-1A). Its vegetation includes several distinct types and floral zones (White, 1983). White identified twenty regional phytochoria (areas possessing a large number of endemic taxa) on the African continent, 18 on the African mainland and two on Madagascar (Fig. 2-1B). Phytochoria is the

science of the study of the distribution of taxa and floristic regions and their history, with phytochoria being defined by the richness of endemic floras found over a large geographic extent, and a relatively uniform composition of plant species. Phytochoria typically do not have a shared boundary, but rather, a transitional zone with many overlapping species.

Low altitude, gentle topography characterizes the majority of the African continent (Sept, 2013), but well-known highlands include Mt. Kilimanjaro, the Ethiopian and Kenyan Highlands, the Rwenzori Mountains on the border between Uganda and the Democratic Republic of the Congo, the Virunga and Albertine Rift Mountains, and the Drakensberg in South Africa. Other significant mountain regions are the Usambara Mountains in Tanzania, the Chimanimani Mountains of Zimbabwe, and the Cameroon Highlands. Considerable elevation in these ranges create temperature gradients that dictate strong vertical zonation in montane vegetation types, particularly in East Africa. In addition to changes in elevation, dramatic differences in rainfall across Africa create complex climate and vegetation zones. Convective activity in a narrow zone near the equator where northern and southern air masses converge, produces low atmospheric pressure and generates vigorous storms over large areas. Known as the Intertropical Convergence Zone (ITCZ) (Fig. 2-1C), this annual event creates seasonal rainfall patterns in the mid-latitudes north and south of the equator. Driven by solar insolation, the ITCZ produces singular rainy seasons in many parts of Africa; however in East Africa, Indian Ocean monsoons contribute to a biseasonal distribution of rainfall (Sept, 2013) (Fig. 2-1D). In conjunction with high rates of seasonal evapotranspiration, particularly in the tropics, seasonality limits plant growth, resulting in latitudinal belts of vegetation: humid equatorial forests are enclosed by regions of woodlands, which in turn are surrounded by grasslands, and subsequently deserts (Figs. 2-1B/D).

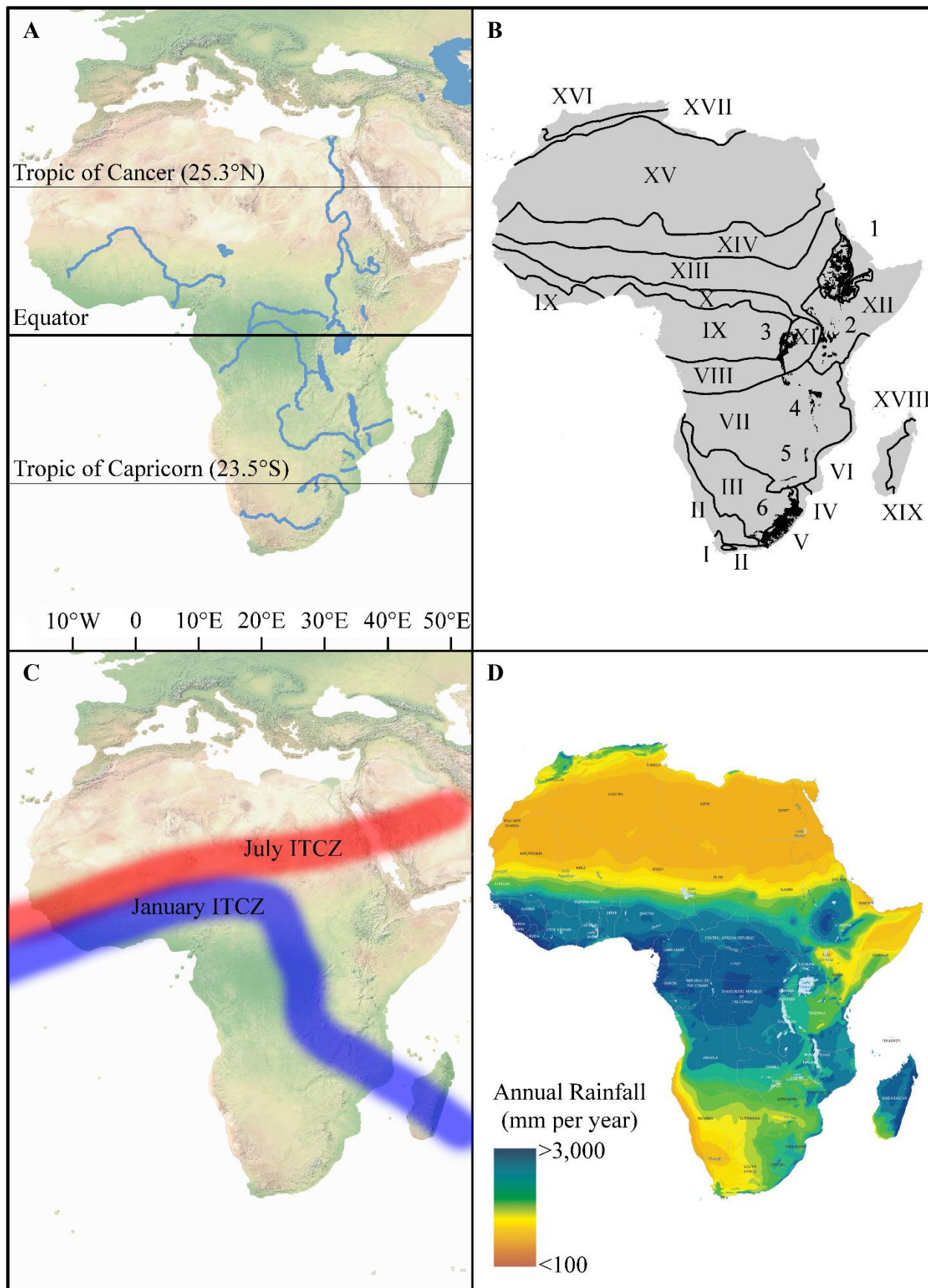


Figure 2-1A. Geographic extent of the African continent with major rivers and lakes.

Figure 2-1B. Regional Centers of Endemism according to White (1983): I. Cape. II. Karoo–Namib. III. Kalahari–Highveld. IV. Tongaland–Pondoland mosaic. V. Afromontane. VI. Zanzibar–Inhambane VII. Zambezian. VIII. Guineo–Congolian/Zambezian transitional zone. IX. Guineo–Congolian. X. Sudano/Guineo–Congolian/transition. XI. Lake Victoria. XII. Somalia–Masai. XIII. Sudanian. XIV. Sahel. XV. Sahara. XVI. Mediterranean. XVII. Mediterranean/Sahara regional transition zone. XVIII. West Malagasy. XIX. East Malagasy. Afroalpine archipelago-like region of extreme floristic impoverishment not shown separately. Major Afromontane regions: 1. Ethiopian Highlands. 2. Imatongs–Usambara. 3. Kivu–Ruwenzori. 4. Uluguru–Mlanje. 5. Chimanimani. 6. Drakensberg.

Figure 2-1C. Boreal and austral summer extent of the Intertropical Convergence Zone (ITCZ) and prevailing direction of monsoon winds.

Figure 2-1D. Annual average rainfall of the African continent (modified from UNEP’s *Africa Water Atlas*).

2.2.1 Microhabitats and Biomes

Within these broad vegetational units, the porosity and chemistry of soils help to create distinct microhabitat structures. Topography, and groundwater sources mediate local, microhabitat variation, while edaphic conditions influence vegetation structure and floristic patterns at a regional scale (Sept, 2013). The term *biome* is used here to describe areas covered by relatively uniform vegetation types (e.g. forest, wooded grassland, grassland, semidesert, and desert) that represent major biotic zones and correlate with various climatic indices such as rainfall seasonality, summer aridity, and minimum winter temperatures (Van Wyk and Smith, 2001)

The *woodland* biome is the most widespread vegetation type in tropical Africa. Woodlands are open stands of trees that are at least 8.0 meters high, but no more than 20 m, with woody coverage accounting for roughly 40% of the biomass over a field layer dominated by grasses. Unlike true forests, woodland canopies do not overlap extensively. The distinguishing characteristics of woodlands is that the dominance of trees combined with the open canopy and almost universal presence of sun-loving C₄ grasses, herbs, and small tree and shrub understories, separate woodlands from other types of vegetation. Most African woodlands are deciduous or semi-deciduous but nearly all types contain a few evergreen species (White, 1983).

True forests are continuous stands of 10 to 50 m high trees with a closed, multistory, overlapping canopies. Woody plants contribute most to the biomass and the sparse ground layer usually lacks trees though may contain shrubs. Nearly all the forests in Africa are evergreen or semi-evergreen, though deciduous forests occur as well. The forest biome is sub-divided into rainforests, dry, semi-evergreen, deciduous, and undifferentiated forests (White, 1983). In forests, the crown cover is usually more than 75%, with graminoids usually absent on the ground. Outside of Central Africa, forests often only occur as a series of scattered small (1.0 km²) to very small (<0.1 km²) patches (Mucina and Rutherford, 2006), and are typically found as *islands* within larger biomes such as grasslands or bushlands. For example, the tropical rainforests of Eastern Africa only encompass 10,000 km² and are highly fragmented (Wasser and Lovett, 1993). Forest types include gallery forests that develop along riparian zones adjacent to rivers, inundated freshwater swamp forests, true rainforests, groundwater fed forests, highland Afromontane forests, coastal forests with high atmospheric humidity, and mangrove forests (Mucina and Rutherford, 2006; Van Wyk and Smith, 2001; White, 1983). Water availability is the dominant factor dictating forest development, as forest vegetation is a function of amount of precipitation, evapotranspiration, availability of groundwater, soil structure, and seasonality of precipitation (Mucina and Rutherford, 2006). Riverine forests for example, develop in areas of low rainfall that would otherwise not support dense stands of woody plants. Interestingly, species richness varies more within a forest than between forests (suggesting that the high degree of similarity may have been established before forest fragmentation during the late Miocene (Geldenhuys, 1992)), and drier and warmer forests tend to be richer in species than wetter and cooler forests (Mucina and Rutherford, 2006).

Bushland and thicket usually accompany one another. *Bushland* is defined as an open stand of bushes, or woody plants intermediate between a tree and a shrub, usually 3-7 m tall, that cover 40% or more of the land. Bushes often flourish in rocky or stony substrates that are unfavourable to grasses. Rainfall is between 250 and 500 mm per year, and in some bushland and thicket biomes, droughts of several months are common and there is a 25% change of not receiving 80% of the mean annual precipitation in any given year (Mucina and Rutherford, 2006). *Thicket* is defined as a closed stand of bushes and climbers that are so densely interlocked that they form a nearly impenetrable obstacle that hinders movement. Bushland and thicket occur under a wide range of climatic and edaphic conditions that are inauspicious for taller woody plants (White, 1983). Bushland and thicket comprise a broad spectrum of physiognomic types reflecting gradients in climate, geology, soil, and herbivory with varying structure and species composition (Mucina and Rutherford, 2006). This biome also contains a high diversity of species and a wide span of ecological lifeforms including leaf and stem succulents, deciduous woody shrubs, geophytes, annuals, forbs, and grasses, and reflects the transitional, ecotonal nature of thicket vegetation.

Shrublands are landscapes dominated by shrubs that vary in height from 10 cm to 2 m or more. Usually, open or closed stands of shrubs occur where taller woody plants cannot gain a foothold because of low rainfall, extended drought periods, low temperatures, high rates of evapotranspiration, and oligotrophic or nutrient-poor soils. The most extensive and distinctive shrublands are found in western South Africa and Namibia (White, 1983). Important features of shrublands often include the presence of leaf spinescence, high sedge cover, and low grass cover, frequent summertime fires, and nutrient-poor sandy, clay, and gravelly soils (Monroe et al., 2007)

Grasslands develop anywhere woody plants cover 10% or less of a landscape. There are over a thousand species of grasses throughout the African continent, but plant communities

dominated by grasses are sporadic and have an infrequent distribution. Pure grasslands occur on deep sandy soils wherever rainfall is between 100 and 250 mm, but in areas where rainfall is between 250 and 500 mm 'wooded grassland', an intermediate between grassland and woodland with 10-40% woody plants, replaces grassland. African grasslands are subdivided into three distinct types; climatic, edaphic, and secondary. Secondary grasslands are now the most extensive community on African mountains due to human activity such as controlled fires and agriculture. Edaphic grasses, those caused by soil conditions, occur in shallow soils or in valleys where clays become waterlogged. They are widespread in most of Sub-Saharan Africa from ~20° S to ~15° N except in equatorial Central Africa. In any of the grassland types, dominant species may grow to 3 m or more. The well-known 'savanna' is a grass dominated ecosystem (White, 1983), however 'savanna' is not a useful term or classification system as it comprises vegetation composition with a grass dominated herbaceous layer and scattered low or tall trees, but also includes both closed and open woodlands with a tree cover ranging from less than 75% and greater than 1% (Mucina and Rutherford, 2006). Additionally, the general term 'grassland' is also problematic as it can be applied to any region dominated by grasses, making it neutral and basically all inclusive category (Mucina and Rutherford, 2006). Nevertheless, grasslands as referred to here, are structurally simple with less than 10% canopy cover, with woody species only occurring in specialized habitats that are dependent on the availability of moisture. Forbs also form an important component of grasslands, and may contribute more in terms of biome species richness than grass species do (Mucina and Rutherford, 2006). The major C₄ photosynthetic subfamily of the grassland biome is Panicoideae, while Pooideae, a C₃ subfamily, dominate only at high altitudes and in well-watered environs.

Arid landscapes with a sparse cover dominated by sandy, stony, or rocky substrate are termed deserts. The plant cover is scarce and shows various adaptations to unfavourable water conditions. Typical annual rainfall is less than 200 mm, but in some extreme deserts, precipitation can be as little as 10 mm. When rainfall is between 200 and 250 mm, semi-desert develops, however, the transition towards arid regions is gradual and it is difficult to differentiate desert vegetation from semi-desert (White, 1983). Although there are no true deserts in East Africa, the deserts of southwestern Africa include a number of species adapted to hyperarid conditions. Deserts are often characterized by ecological extremes (Mucina and Rutherford, 2006), as they have the greatest variability in rainfall, the highest temperatures, and in some regions, the highest occurrence of coastal fog. Like grasslands, the desert biome is often poorly defined, particularly when moisture emanating from fog results in perennial vegetation exceeding 10% of canopy coverage yet mean annual precipitation is less than 70 mm (Mucina and Rutherford, 2006). Additionally, different limits for the maximum amount of annual precipitation have been used to categorize deserts; 60 mm (Werger, 1978), 70 mm (Mucina and Rutherford, 2006), and 200 mm (White, 1983) have all been used to delimit the maximum amount of rainfall in desert biomes.

Finally, confined to the highest mountains of tropical Africa is *Afroalpine* vegetation. Transitional formations of local extent include scrub forest, transition woodland, and scrub woodland, which are intermediate between forest and bushland or thicket, forest and woodland, and woodland and bushland, respectively (White, 1983). Vegetation in these regions are often classified as alpine (2,800 - 3,500 m.a.s.l.) and subalpine (1,800 - 2,800 m.a.s.l.), and may be a separate phytogeographical region (Hedberg, 1965), although its total flora only includes about 280 species (in East Africa) but no endemic genera.

2.3 Extant Phytochoria and Biomes of Sub-Saharan Africa

The following section is an overview of White's (1983) descriptive memoir of extant African phytochoria termed *Regional Centers of Endemism*, defined as regions that consist of more than 1,000 endemic species, 50% of which are confined to the region (White, 1979). The Zambezian, Sudanian, Guineo-Congolian, Somalia-Masai, Karoo-Namib, and Cape regions are reviewed in the following sections by order of regional extent (Fig. 2-1B). The Afromontane, although not a Regional Center of Endemism in the strict sense, but unique in that it is an *Archipelago-like Center of Endemism* and important to the dissertation research objectives, is examined as well. As is the Zanzibar-Inhambane Regional Mosaic, a restricted biome that is nevertheless significant to the overall goals of the project. Endemism is a relative concept that refers to taxon limited in geographic range due to ecological and physiological parameters, but it should be noted that some plant taxa are present, even if marginally, in multiple centers as satellite populations (Van Wyk and Smith, 2001).

2.3.1 Zambezian Regional Center of Endemism

The 3,770,000 km² area that comprises the Zambezian Regional Center of Endemism (RCE) is situated between 3° and 26° south, and can be found in most of Angola, northern Namibia, all of Malawi, Zambia, and Zimbabwe, western Mozambique, southwestern Tanzania, southeastern Democratic Republic of the Congo, northern Botswana, and Limpopo Province, South Africa. Much of this RCE sits at an elevation greater than 900 meters above sea level (m.a.s.l.), but in some areas can be as high as 2,500 m.a.s.l. wherein the terrain supports Afromontane communities. Overall, the Zambezian is categorically identified as a dry, deciduous forest that rarely exceeds 25 m in height and is simple in structure compared to rainforests. After

the Sahara, the Zambebian RCE is the largest major phytochorion in Africa containing at least 8,500 species of which about 54% are endemic, though there are no endemic genera and only a few endemic families.

The Zambebian RCE has the richest and most diversified vegetation types of any of the African phytochoria. The biogeography of the Zambebian consists of dry forest, swamp and riparian forests, transition woodland, woodland, thicket, scrub woodland, and grassland; most of which include subdivisions based on soil types, rainfall, and elevation. Both dry evergreen and dry deciduous forests were once extensive in moisture rich areas of the Zambebian. However, cultivation and manmade fires have greatly diminished both types of forest. These two types are almost completely different in terms of their floristic compositions; dry evergreen forests rarely exceed 25 m in height, where deciduous trees are usually about 20 m high, but can vary between 12 and 25 m. Dry evergreen forests are confined to regions that receive more than 1,200 mm of rainfall a year while dry deciduous forests occur in parts where rainfall is between 600 and 900 mm. The dry deciduous forest also includes a large scrub forest component, particularly in the western range of the Zambebian RCE in Angola.

Permanent swamp forest occurs in the Zambebian where annual rainfall exceeds 1,000 mm. Swamp forests are associated with perennial, slow-moving or stagnant watercourses and tributaries of the Zambezi River, the fourth longest, and largest eastward-flowing river in Africa. Swamp forests often merge into riparian forests in areas where the water table remains below the land surface for part of the year because rainfall is less than 800 mm. Only beyond the floodplain of the Zambezi and its major tributaries, do trees reach a height of 18-24 m; on floodplains that are submerged for six months of the year, trees only grow between 9 and 12 m.

Three main types of woodland, miombo, mopane, and undifferentiated, are distinct enough to have their own classifications within the greater Zambezan woodland RCE. Miombo is the prevailing vegetation in well-drained, acidic, shallow, and stony soils throughout most of the Zambezan except for the Kalahari, western Zambia and eastern Angola, and along the low-lying Zambezi and Luangwa River valleys. Floristically, miombo is very different from other types of woodland and is dominated by the genus *Bracystegia* (of which the Swahili word is miombo), which rarely occurs in other vegetation types. Miombo is mostly 10-20 m tall, but some species can reach heights of 30 m when soil conditions are productive. Mopane forests are typically found in wetter soils along the valleys of the Zambezi, Luangwa, Limpopo, Shashi, and Savi rivers or in other regions where miombo is absent. Mopane species can survive elevations up to about 1,400 m, annual rainfall of 800 mm or less, and multiple edaphic conditions. Rarely, do miombo and mopane forests overlap. Undifferentiated woodland on the other hand, is defined by the absence of both the miombo and mopane dominants, rather than by its own floristic composition. Although it is relatively restricted in range, undifferentiated woodland is composed of many more tree species than either miombo or mopane and subdivided into those north of the Limpopo and those south of the Limpopo, with those in the north usually including large trees frequently exceeding 20 m, growing on well-drained soils at elevations intermediate to the river valleys and uplands. The southeastern part of the ecoregion is found in altitudes varying from 150 to 1,500 m.a.s.l. and is transitional between the Zambezan RCE and the Kalahari-Highveld regional transition zone to the south.

Thicket, transition and scrub woodland, and grassland make up the remainder of the Zambezan RCE. Several types of thicket occur scattered throughout the Zambezan region, particularly in drier parts along the periphery, such as in central Tanzania. The thicket is normally

6-7 m tall and nearly impenetrable. Scrub mopane and scrub woodland are often associated with the southern undifferentiated woodland, whereas miombo frequently occurs as scrub woodland at altitudes between 1,600 and 2,100 m. Scrub woodland also forms the ecotone between miombo woodland and Zambebian grassland, as well as between Kalahari woodland and grassland. Grasslands typically occur on seasonally waterlogged soils that contain heavy metals.

2.3.2 Sudanian Regional Center of Endemism

The Sudanian Regional Center of Endemism extends along a narrow belt for nearly 6,000 km from the coast of Senegal to the foothills of the Ethiopian Highlands. Mostly between 500 and 700 km wide and below 750 m altitude, it covers an area of 3,731,000 km² and lies within the tropical summer rainfall zone sharing similar rainfall patterns with the Zambebian region. With mean annual temperatures between 24° and 28°C, temperatures in the Sudanian region are considerably warmer, and the dry season is more severe than the Zambebian to the south. However, there is likely less than 2,750 species in the Sudanian RCE, a third of which are endemic and belong to three monotypic genera.

The predominant vegetation types of the Sudanian RCE are various woodlands, though there is no true forest apart from a few localized swamp and riparian forests because cultivation has had a major impact on the natural primary vegetation. In areas of secondary growth, the majority of tree species that are allowed to grow are those of economic importance. Edaphic and wooded grassland prevail along larger river valleys or on hydromorphic soils but are also found on rocky outcrops. Bushland and thicket are very poorly represented.

Because the Sudanian RCE is relatively low-lying, the climate over the entire region changes gradually, and this, combined with plant species wide tolerance for differing climate

regimes, prevents distinct vegetation zones from developing. However, two noticeable differences are observed, one in the drier north that lacks the genus *Isoberlinia* (family Fabaceae – legume), and another in the wetter south that is dominated by *Isoberlinia*. The southern woodland stretches without interruption from Mali in the west to northwest Uganda in the east. Trees are scarcely ever greater than 15 m in height. The northern woodland extends from Senegal to the Red Sea, acting as a ‘highway’ across the continent. However, the original vegetation is no longer recognizable due to extensive human modification.

As for the other, restricted vegetation types, dry forests are only found in western Mali, and in isolated regions from Guinea-Bissau to the Ivory Coast. Patches of riparian forest are localized in the northern half of the Sudanian range, but most have been degraded to riparian woodland. On the outer fringe of the riparian forests (particularly in Nigeria), well-developed transitional woodland exists. Pure grassland is rare, as there is usually a mixture of woody plants, but grassland and wooded grassland on soils formed from Pleistocene alluvium are very extensive.

2.3.3 Guineo-Congolian Regional Center of Endemism

Situated between five degrees north and south of the equator, the Guineo-Congolian Regional Center of Endemism stretches from Africa’s Atlantic coast in the west, to the Rwenzori Mountains in the east. It encompasses an area of 2,800,000 km², most of which is at an altitude of less than 1,000 m.a.s.l. except where it approaches the Rwenzori Mountains. Overall, the Guineo-Congolian is categorized as a rainforest with well-drained soils, whereby the upper canopy is 30 m tall or more. Both evergreen and semi-evergreen vegetation prevails, swamp and riparian forests are widespread, and typical shrublands are absent. Of the 8,000 species known to exist in the Guineo-Congolian region, 80% are endemic, including ten endemic families.

The Guineo-Congolian region receives between 1,600 and 2,000 mm of rainfall annually, which is slightly less than the global yearly minimum of rainforests of 2,000 mm (Turner, 2004). The biogeography of the Guineo-Congolian rainforest can be divided into four variants based on species of plants; 1) the hygrophilous species growing in moist places along coastal evergreen rainforest; 2) mixed, moist semi-evergreen rainforest that constitutes most of this RCE ; 3) single-dominant, moist evergreen and semi-evergreen rainforest 'islands' within variant 2; and 4) drier, semi-evergreen rainforest along the northern and southern periphery bordering the Sudania and Zambezia regional transition zones, respectively.

The hygrophilous coast evergreen rainforest occurs in two sections along the Atlantic coast from Sierra Leone to southern Ghana, and then from southern Nigeria to Gabon. The mean annual rainfall is often more than 3,000 mm and coastal proximity results in very high atmospheric humidity. However, there is a pronounced, yet short, dry season where many of the tree species shed their leaves.

Most Guineo-Congolian rainforest belongs to the mixed moist evergreen and semi-evergreen type. This variant comprises the vegetation in northeast Gabon, southeast Cameroon, southwest Central African Republic, northern Republic of the Congo, and most of the Congo Basin and its periphery in the Democratic Republic of the Congo. Rainfall is well distributed throughout the year, and warm moisture from the Atlantic persists over much of the western segments of this RCE. Found scattered throughout this variant are single-dominant, moist evergreen and semi-evergreen rainforest 'islands' (variant 3). These are often no more than a few hectares in extent and localized in the Congo Basin because of the extensive development of swamp forest; these 'islands' are virtually absent from the coastal regions of West Africa, however.

The fourth variant is drier, semi-evergreen rainforest found along the periphery of the Guineo-Congolian region, bordering the Sudania and Zambezia regional transition zones to the north and south, respectively. Rainfall is between 1,200 and 1,600 mm and there is relatively high humidity even during the dry season. Most trees are large deciduous species that lose their leaves during the dry season. This variant was once widespread in the adjoining transition zones, and even distributed in the Lake Victoria basin.

2.3.4 Somalia-Masai Regional Center of Endemism

The Somalia-Masai Regional Center of Endemism is quite an expansive region occupying a large part of East Africa between 16°N and 9°S and 34°E and 51°E. It encompasses an area of 1,873,000 km² and includes eastern and southern Ethiopia (except the mountains), most of Somalia and Kenya, Djibouti, eastern Eritrea, northcentral Tanzania, southeastern Southern Sudan, northeastern Uganda, and across the Red Sea into southern Arabia. This RCE, situated between 0 and 900 m.a.s.l, has an arid to semi-arid climate whereby rainfall is often less than 500 mm per year and can be as low as 20 mm, and mean monthly temperatures between 25° and 30°C. Overall, the Somalia-Masai has extensively developed deciduous bushland and thicket and various types of wooded grassland. Trees rarely exceed 8 m in height. There are about 2,500 species of flora, and possibly 50% of these are endemic. There is one endemic family, Dirachmaceae (*Dirachma socotrand*), which is found on the island of Socotra (Yemen) and in Somalia, and about 50 endemic genera occurring on both the African mainland and in Arabia and Socotra.

The biogeography of the Somalia-Masai region is dominated by deciduous bushland and thicket that grade into and are replaced by evergreen and semi-evergreen bushland and thicket on the lower slopes of mountains. Smaller areas of scrub forest, riparian forest, secondary grassland

and wooded grassland, seasonally waterlogged grassland, semi-desert grassland and shrubland, and desert are also found throughout this RCE.

Somalia-Masai *Acacia-Commiphora* deciduous bushland and thicket is a dense, 3-5 m tall impenetrable bushland that forms thickets of plants often armed with spines that hinder movement. Emergent, 9-10 m tall trees scatter throughout the bushland, particularly on rocky hills. Most species are deciduous, but evergreens contribute 2.5-10% of the biomass. Modern human activities, especially in areas where domestic animals are abundant, are responsible for the conversion of bushland into grassland over hundreds of square kilometers where grasses were once uncommon. *Acacia-Commiphora* deciduous bushland and thicket is widespread in the Ngorongoro Conservation Area, near Lake Eyasi, and in Olduvai Gorge. East African evergreen and semi-evergreen bushland and thicket occurs on the drier slopes of mountains and upland areas from central Tanzania to Eritrea and beyond, forming an ecotone between montane forest and the *Acacia-Commiphora* bushland and thicket.

Semi-desert grassland and shrubland dominate the Somalia-Masai RCE wherever rainfall is between 100 and 200 mm per year. Edaphic grassland covers large areas in Tanzania but is less well developed further north, and the near absence of trees on the Serengeti Plains is partly due to unfavourable edaphic conditions. In the ecotone between forest and grassland in Nairobi National Park, a combination of grazing, browsing, and fire has created grassland in areas capable of supporting evergreen bushland or forest.

As for forests, Somalia-Masai scrub forest develops at relatively low altitudes where rainfall is higher (>500 mm) than that of deciduous bushland and thicket but too low to support true forest. Scrub forest vegetation usually reaches between 7-10 m tall. Riparian forest occurs

only on the banks of the larger rivers, such as the Tana River (Kenya), and often includes many species that are widespread throughout Africa.

Special attention is paid to the Serengeti ecosystem that lies entirely within the Somalia-Masai Regional Centre of Endemism because within the Serengeti National Park, human activity has been minimal whereas outside the park, the intensity of human influence varies greatly from place to place. The Serengeti ecosystem comprises 35,000 km² of grassland and wooded grassland in northern Tanzania extending into southern Kenya. More than one hundred species of grass occur in the region but are mainly restricted to soils derived from volcanic ash that favor grasses rather than woody vegetation. *Acacia-Commiphora* bushland and thicket is very poorly represented inside the Serengeti National Park, but *Acacia-Commiphora* wooded grassland is the most extensive woody vegetation type in the Serengeti National Park and represents 88% of all woody vegetation.

2.3.5 Karoo-Namib Regional Center of Endemism

The Karoo-Namib Regional Center of Endemism occupies the central, northern, and northwestern parts of Northern Cape Province, South Africa, the western coast of Namibia, and the southwest coast of Angola. The biogeographic extent of the Karoo-Namib region ranges from sea level to 2,695 m.a.s.l. encompassing an 661,000 km² area that includes coastal plains, escarpments, and plateaus. Contained within this RCE is the Namib Desert, where precipitation varies from 2 mm in the most arid regions to 200 mm elsewhere. Almost the whole of the Karoo-Namib region, with the exception of the Namib Desert, is covered with various types of Karoo shrubland consisting almost entirely of shrubs less than 2 m tall. There are ~3,500 flora species,

of which more than half are endemic. There is only one endemic monotypic family, Welwitschiaceae (*Welwitschia mirabilis*), but about 260 endemic genera.

Four types of shrubland comprise the Karoo-Namib RCE: Bushy Karoo, Succulent Karoo, Dwarf Karoo, and Montane grassy Karoo. The remainder of the vegetation in the Namib and Karoo regions contains desert and semi-desert plants, respectively. The landscape represented by Bushy Karoo shrubland is dotted with small bushy trees and large shrubs, but succulents are usually abundant, and many species of grasses thrive. Succulent Karoo shrubland is confined to the sandy coastal plain of western South Africa and Namibia, and as the name suggests, succulents dominate throughout. These range in height from 0.3 to 1 m, but a few species can reach 2 m or more. Large shrubs and bushes are virtually absent from this shrubland type. Dwarf Karoo shrubland is by far the most extensive type of Karoo shrubland. Here, dwarf shrubs prevail while bushes and trees are absent, and succulents are only an insignificant component of the biomass. Grasses are also more abundant in the Dwarf Karoo region than any other and increase in proportion from west to east. Little is known about the Montane Grassy Karoo shrubland except that it is likely that grasses were more dominant in the past whereas today mountain wire grass is all that remains of what was once a grass-dominated environment.

The vegetation of the Namib Desert lives within a 100 km wide area, extending from the Atlantic coast to the foot of the escarpment that defines the interior highlands of southern Africa. In some parts of the desert, the mean annual rainfall is only 10 mm, and on average occurs only once every two years. However, there are between 100 and 215 fog days per year, providing some moisture to the vegetation, although the fog only penetrates as far as 50 km inland. Extremely sparse vegetation is found in the sand dunes of the Outer Namib Fog Desert, but the shifting sand dunes in this area prevent any plant growth whatsoever. North of Swakopmund, Namibia exists a

gravel desert cemented into a rock-hard layer by deposition of calcium (gypsum and lime). The only vegetation that typically survives here is lichen, as the gravel desert is devoid of plants. In the outer parts of the Central Namib, lichen covered rocks provide the only habitat where perennials can survive. Stem, leaf, and stem with deciduous leaves succulents are only able to survive by rooting in crevices between these rocks. Grasses and succulents represented by a single species grow in the transition zone between the Inner and Outer Namib Deserts. Also distributed in this region is the *Welwitschia mirabilis*, a plant that has leaves that can reach upwards to 3 m and are able to absorb half their water source from fog.

2.3.6 Cape Regional Center of Endemism

The Cape Regional Center of Endemism is located between 32° and 35° south, and 18° and 27° east in the southwestern part of Northern Cape, most of the Western Cape, and the southwestern portion of Eastern Cape, South Africa. It is one of the smallest RCEs covering only 71,000 km². Dispersed throughout this region are pockets of Namib-Karoo, Afromontane Archipelago-like Centre of Endemism and Tongaland-Pondoland Regional Transition Zone vegetation. The mountainous Cape landscape reaches altitudes between 1,000-1,500 m on average, with individual peaks exceeding 2,000 m. Rainfall mostly totals between 300 and 2,500 mm but can reach upward to 5,000 mm in parts of the mountains. Overall, this RCE is deprived of forest other than Afromontane and small patches of scrub forest. The prevalent vegetation is endemic fynbos shrubland, some of which reach heights equivalent to bushland and thicket. Although of limited extent, the Cape region has about 7,000 species, of which more than half are endemic, including 210 endemic genera, and 7 endemic families.

The prevailing vegetation of the Cape is fynbos shrubland, a 1-3 m tall hard-leaved plant. The term fynbos is applied to virtually all the vegetation in the Cape except for the Afromontane and riparian thicket and scrub forest species that are isolated throughout the region. Only about 50 fynbos species normally exceed 3 meters in height, and even fewer grow taller than 6 m. Fynbos communities often contain scattered bushes and, less often, widely spaced trees that vary greatly in height and density.

As for other vegetation in the Cape RCE, secondary cape shrubland occurs below 300 m on productive soils that were once intensively farmed. On the south coast, certain scrubs and trees form thicket or scrub forest up to 10 m tall, and arid adapted fynbos form the transition from typical Cape to typical Karoo vegetation.

2.3.7 Afromontane Archipelago-like Centre of Endemism

The Afromontane region is unique amongst the African phytochoria in that it is represented by interspersed mountain ranges throughout the continent, and not defined as a single area of large geographic extent. The combined extent of the Afromontane regions throughout the African Continent is 715,000 km². Climate in ACEs is extremely varied due to both altitudinal and longitudinal effects, and therefore on any particular mountain, there is usually a very wide range of vegetation type and distribution. There are at least 4,000 species of flora in the Afromontane regions, and nearly 3,000 of these species are endemic; though only two plant families are endemic. About one-fifth of the tree genera are endemic, but for smaller plants, the proportion is likely less.

Although some of the Afromontane ACEs are widely separated, they share an assortment of similar plant species that are often distinct from the surrounding lowland landscapes. For the most part, the lowermost vegetation in the Afromontane ACE is forest, with a transition zone

connecting the Afromontane forest to lowland phytochoria beneath. Above the forest belt, the vegetation diminishes in stature from the lower slopes to the summit, eventually transitioning into the Afroalpine.

Afromontane ACE vegetation consists of a combination of forests, bamboo, bushland and thicket, shrubland, grassland, and mixed communities depending on such factors as elevation, rainfall, latitude, soil characteristics, and geologic parent material (i.e. igneous vs. metamorphic rock). Forest types of the archipelagos vary between rainforest, undifferentiated forest, single-dominant forests, and dry transitional montane forest. Rainfall received by Afromontane forest ranges from 800 mm to upwards of 3,000 mm per year rainforests.

In terms of structure and composition, Afromontane rainforest is similar to certain types of Guineo-Congolian lowland rainforest, except at the species level it is almost completely different. Trees in the upper stratum can reach heights of up to 45 m tall, but are on average 30-38 m. In the middle stratum, trees range between 14 and 30 m, while the lower stratum is 6-15 m and forms a dense canopy. Below this level is a shrub layer 3-6 m high. Afromontane rainforest is typically found between 1,200 and 2,500 m.a.s.l. depending on latitude, distance from the coast, and rainfall.

Undifferentiated Afromontane forest usually replaces rainforest at higher altitudes on wetter slopes and at comparable altitudes on the drier slopes, but tree height is less. Although no single species can be found in every archipelago, the majority of tree species are widespread and each ACE's plant communities are represented by several species. However, some species that occur in South Africa do not cross the Limpopo River into eastern Africa, and some species that are found in the east are absent from West Africa.

When a single tree species characterizes much of a plant community, a single-dominant Afromontane forest develops. These typically occur at elevations greater than 1,500 m on East

African mountains chains. Dry transitional montane forest is also found in East Africa, but to a limited extent. These once more-widespread forests developed between the bushland Somalia-Masai plains and the drier, lower mountain slopes of East Africa.

In highland forests throughout Africa, Afromontane bamboo grows vigorously as thicket on deep volcanic soils where precipitation exceeds 1,250 mm per year at altitudes between 2,400-3,000 \pm 200 m. On most of the higher African mountains, Afromontane evergreen bushland and thicket grow on shallow soils inside the montane forest belt, and on the exposed summits of mountains. Bushland can grow between 3 and 13 m tall, but on exposed rocky ridges, they merge into Afromontane shrubland. These short shrublands are mixed communities of grasses, sedges, forbs, non-vascular plants, lichens, and often stunted individuals of bushland and thicket dominants. However, the most widespread vegetation type on the drier African mountains is grassland. Afromontane grassland benefit from human activity, particularly clearing of forests, but also from natural fires. Secondary grasslands, invading from the lowlands, developed more readily on drier mountains where forests were cleared.

2.3.8 Zanzibar-Inhambane Regional Mosaic

The Zanzibar-Inhambane Regional Mosaic is a complex transitional zone of different physiognomic types with different floristic relationships that covers a regional extent of 336,000 km². Afromontane forest and various Somali-Masai and Zambezian vegetation types merge and overlap with coastal mosaic endemics. This region occupies a coastal belt from southern Somalia to the Limpopo River in southern Mozambique, and while it only extends upwards to 200 km inland, lowland transitional rainforest thrives along broad river valleys as well as into the western, moisture-rich slopes of mountains below 1,500 m.a.s.l. About 3,000 species live in the regional

mosaic, and although the total number of endemic species is unknown, 48% of the forest trees are only found within the coastal forests. The greatest concentration of endemic trees is in the Shimba Hills of Kenya and the Usambara Mountains in Tanzania.

Rainfall is plentiful in the Zanzibar-Inhambane Mosaic, which receives between 800 and 1,200 mm of precipitation annually. Higher amounts of rainfall (~1,950 mm) occur in the eastern Usambara Mountains and on the islands of Pemba and Zanzibar; here, the amount and distribution of water supports true rainforests. In most other parts of the regional mosaic, precipitation is comparable to that of the Zambezian Region, but the dry season is less imposing due to greater relative humidity, and fewer (if any) dry days per month. Mean annual temperature is 26°C except in the southern extent where it is slightly lower.

Most of White's main vegetation types grow within the Zanzibar-Inhambane Regional Mosaic. Forest types include lowland and transitional rainforest, and undifferentiated, scrub, and swamp forests. Each of these are rich in species, but the floristic composition and physiognomy changes rapidly over short distances because of the distribution of rainfall, differences in atmospheric humidity during the dry season, and the regional availability of soil moisture. The Usambara Mountains transitional rainforest for example, has remarkably rich and diversified flora in relation to its limited extent, with more than 40% endemic large tree species. The majority of these species are closely related to those found in the lowland rainforest of the Guineo-Congolian RCE, suggesting that the Usambara Mountains serve as a refugium of flora that has become extinct in much of its former range.

Forest species also occur in a close assortment with Zambezian woodland species to form transitional woodland, but as the forest species become scarce, woodland, and scrub woodland communities develop. Transitional woodland tends to develop on soils that are unfavourable to the

growth of true forest species, whereas Zambebian linking woodland and scrub woodland species thrive in the dry, rain shadow areas on the western slopes and foothills of the Usambara Mountains. In addition, miombo woodland occurs in mosaics with floristically poor patches of forest and other vegetation south of the Ruvuma River, which separates Tanzania from Mozambique.

Bushland and thicket, and edaphic, secondary, and wooded grasslands develop on soil conditions unfavourable for the development of forests. Shallow soils overlying coral, waterlogged sites of former shallow lagoons or lake basins, seasonally flooded clay soils, or badly drained soils on the deltas of the larger rivers cannot support true forests or woodlands. In these locations, dense evergreen and semi-evergreen bushland and thicket develop on termite mounds in seasonally waterlogged edaphic grasslands that occupy parts of the offshore islands and coastal plains. For example, on the coastal plain of Mozambique between the Save and Buzi Rivers, flooded clay depressions overlying sandy deposits are covered with grasslands bordered by wooded grassland.

2.3.9 Other Criteria and Floristic Classifications

Unfortunately, the broad phytogeographic units classified by White (1983) tend to cover large geographical areas and are of little practical use when it comes to local-level ecological studies (Van Wyk and Smith, 2001). Because a plant community is not a random aggregate of species, but rather an organized complex with a relative composition and combination of floristic growth forms, structure, and physiognomy (Van Wyk and Smith, 2001), each plant community is an unique grouping of dictated by environmental conditions and the interaction of species populations through time.

2.4 Overview of Present-day Climate and Vegetation

2.4.1 The Olduvai Gorge Region

As a world-renowned paleoanthropological site, Olduvai Gorge is famous for both its archaeological and paleontological record.

Additionally, Olduvai is situated in one of the most fascinating geological settings on Earth, the East African Rift System (EARS). Rifting in East Africa was set in motion more than 30 million years ago when plumes of superheated rock rose beneath the crust, causing it to bulge and thin. The brittle crust fractured, creating valleys bound by mountains and

escarpments. Many of the valleys and rifts became inundated, forming Africa's Great Lakes, while the volcanic mountains, such as Kilimanjaro (Africa's largest peak) and the still-active Ol Doinyo Lengai in Tanzania (Fig. 2-2), released fertile volcanic ash, creating the wildlife-rich grasslands of the Serengeti Plain.

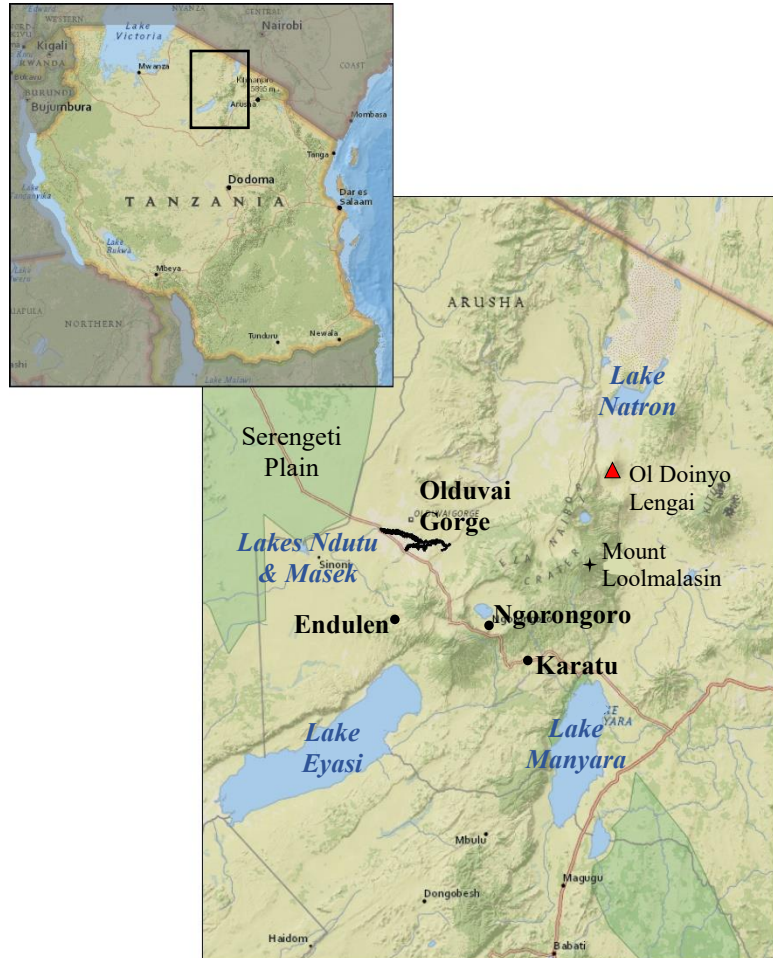


Figure 2-2. Olduvai's location in the Arusha Region of northern Tanzania. The Crater Highlands are to the south and east, and the Serengeti Plain is to the west. Basemap data from ESRI and National Geographic.

Olduvai is situated within the Eastern Rift, as is the Serengeti Plain to the northwest, the Ngorongoro Crater Highlands to the south and east, Lakes Ndutu and Masek to the west, and the rift lakes Eyasi, Manyara, and Natron, to the south, southeast, and northeast, respectively (Fig. 2-2). These rift lakes are mainly shallow and alkaline due to local volcanism. Lake Manyara (saline/alkaline), Lake Eyasi (saline/alkaline), and Lake Natron (saline) are found on the Rift Valley floor along the Nguruman Escarpment at about 1,000 m.a.s.l.

To the east of Olduvai are the Crater Highlands, famous for Ngorongoro Crater, a large, 260 km² volcanic caldera that is home to approximately 25,000 large animals. Though the elevation of the crater floor is only ~1,700 m.a.s.l., the crater rim rises 500 m above the floor creating a distinctive and prominent geological, biologic, and ecologic landform in the Olduvai region. Mount Loolmalasin is the highest peak in the Highlands at 3,682 m.a.s.l. Because the Crater Highlands rise far above the adjacent Serengeti Plain (which are about 1,500 m.a.s.l.), they capture moisture from passing air masses and host rainforests while creating a rain-shadow effect over Olduvai and the Serengeti to the west resulting in *Acacia-Commiphora* bushland and thicket.

Indian Ocean monsoons and the ITCZ contribute to a biseasonal distribution of rainfall in the Olduvai Region (Fig. 2-3). Extensive altitudinal changes result in temperature gradients that, along with precipitation, dictate strong vertical vegetation zonation throughout the Crater Highlands and Serengeti Plain. Rainy seasons occur when cold fronts arrive in April, and May, and again in November and December. Average annual precipitation in the Crater Highlands is about 1,037 mm with average temperatures of 21°C and 6°C on the crater floor and rim, respectively. Annual rainfall at Olduvai averages 550 mm with average temperature of 23°C (Deocampo, 2004). Higher amounts of rainfall (750-1250 mm) also fall in the western Serengeti (west of Lakes Masek and Ndutu), whereas the Lake Natron region receives the least

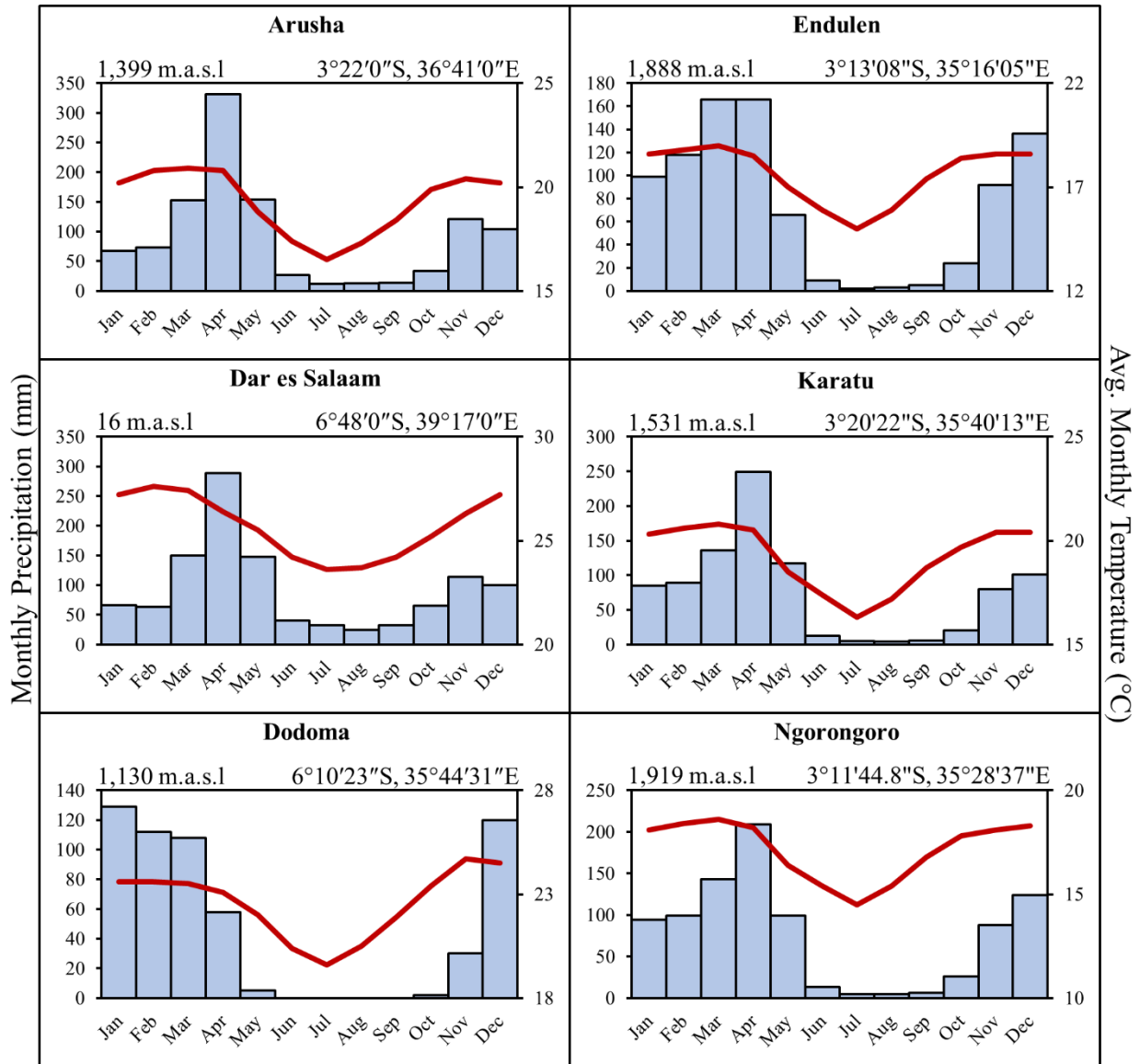


Figure 2-3. Monthly precipitation (histogram) and average temperature (line) data for six locations in Tanzania. Note the biseasonal distribution of rainfall peaking in April and December. Altitude (meters above sea level) and latitude and longitude (degrees, minutes, seconds) given for each location. See Figure 2-2 for geographic relation to Olduvai Gorge. Data from Climate-Data.org and the Global Network of Isotopes in Precipitation (GNIP).

(250-500 mm) and is accompanied by extensive evaporation (Barboni, 2014).

Olduvai Gorge and surrounding areas (minus the Crater Highlands) fall within the Somalia-Masai Regional Center of Endemism, with the vegetation communities consisting of various types of deciduous bushland and thicket where *Acacia* (e.g. *A. tortilis*, *A. kikii*, *A. seyal*, *A. mellifera*) and *Commiphora* trees (e.g. *C. africana*, *C. madagascariensis*) cover much of the region except west on the Serengeti Plain, where grasslands species (e.g. *Sporobolus marginatus*, *Digitaria macroblephara*) thrive on volcanic ash derived soils (Herlocker and Dirschl, 1972; White, 1983). Deciduous small shrubs and trees (<8 m) form discontinuous canopies in Olduvai Gorge and on the western and northern sides of the Crater Highlands below 1,500 m in elevation. Above 1,500 m.a.s.l., forests develop (such as the Lerai Forest of Ngorongoro). Afromontane vegetation dominates the eastern, moisture-rich slopes of the Crater Highlands (Fig. 2-4).

Lakes Manyara (Fig. 2-2) and Makat (Fig. 2-4) are often considered correlates for paleo-Lake Olduvai as they have vegetation types not in equilibrium with the regional climate (Barboni, 2014), and the stream/spring-fed wetlands are suggested as reminiscent of those found on Olduvai's paleo-lacustrine plain (Copeland, 2007). An evergreen forest with a dense canopy of interlocking crowns flourishes near freshwater springs that percolate out of rift escarpment on the northwestern shore of Lake Manyara, as these well-drained alluvial fans support a groundwater forest that would not otherwise be possible under the existing rainfall regime of 650 mm per year. Palms (*Phoenix reclinata*) are frequent in sections of the forest where the canopy is open, while C₄ sedges (Cyperaceae²) make up much of the vegetation on the ground (Barboni, 2014). Only a few hundred meters removed from the springs however, the forest is replaced by vegetation more

² The abundance of C₄ sedges may preclude the use of Lake Manyara as a modern referential for the FLK-N site (see Section 2.5).

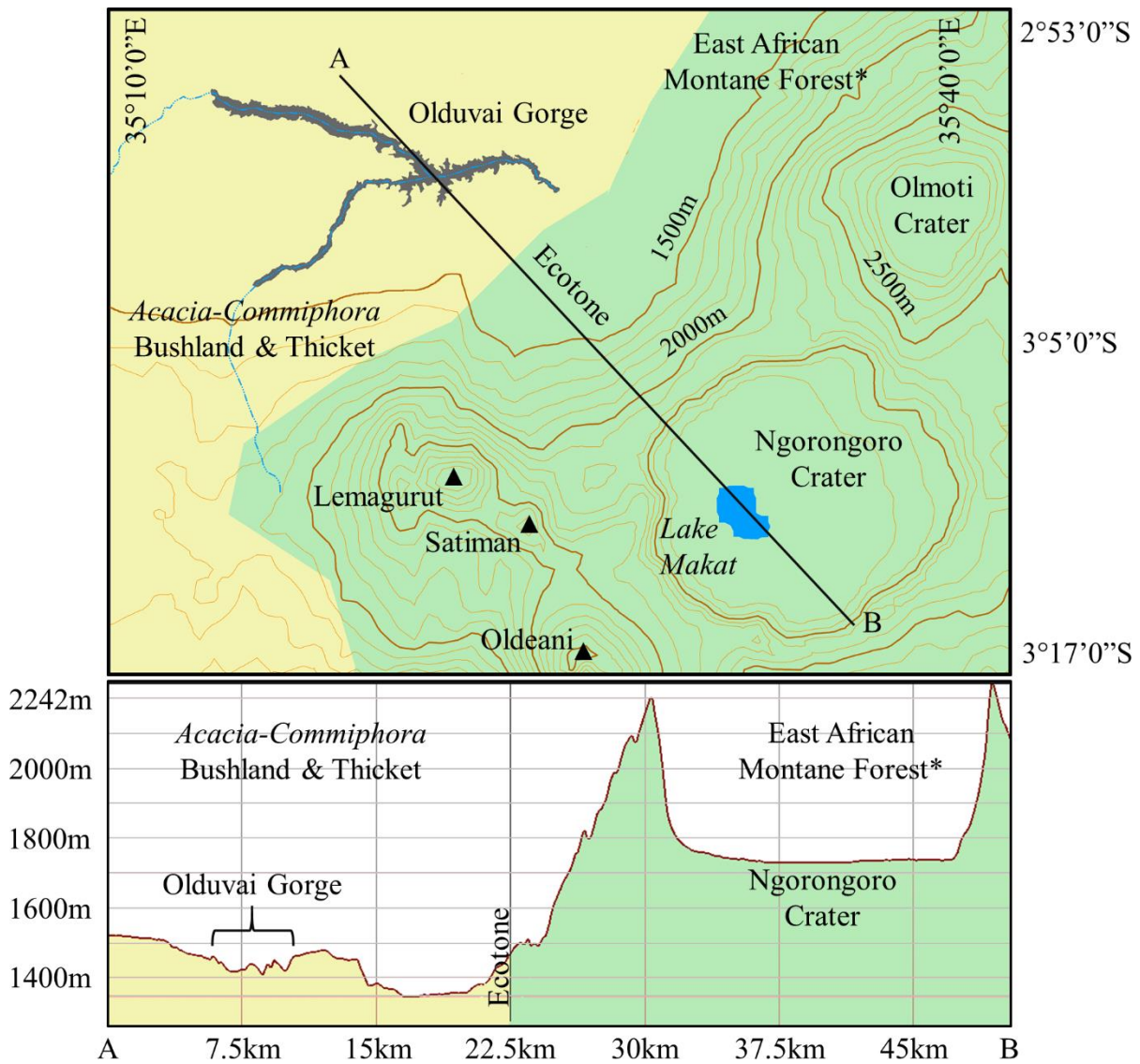


Figure 2-4. Elevation profile of a 50 km transect (A-B) extending from the *Acacia-Commiphora* bushland and thicket north of Olduvai to the montane forests of the Ngorongoro Crater rim. An ecotone exists beginning at ~1500 m.a.s.l. on the northwestern flank of the Crater Highlands separating the two ecoregions. *In Ngorongoro Crater, the montane forest transitions to open grassland that is interrupted by the Lerai Forest in the southwest, shallow Lake Makat, and numerous small spring-fed wetlands.

accustomed to drier conditions typically found in *Acacia* bushland and woodland. Lake Makat, the seasonally fluctuating, shallow soda lake near the center of Ngorongoro Crater is surrounded by short *Odyssea* grasses that colonize the saline/alkaline soils surrounding the lake, while medium grasses of *Sporobulus*, *Cynodon*, *Pennisetum*, and *Digitaria* grow around this perimeter and out onto the crater floor (Herlocker and Dirschl, 1972). Small spring-fed marshes of *Cyperus immensus* and *Cy. laevigatus* grow near the northern and western edges of the lake, while 3.0 km east of Lake Makat grows the ground water Ngoitokitok forest where *Acacia xanthophloea* forms a dense canopy.

2.4.2 Physiography of Olduvai Gorge

Olduvai Gorge is often divided into three distinct physiographic regions; the Eastern Gorge situated between the first and fourth faults, the Western Gorge set from the main confluence to Granite Falls, and the Southern Gorge produced by a Crater Highlands tributary stream originating on Mount Makarut (Fig. 2-5). The Main (Eastern and Western) Gorge is the result of downcutting by the low-energy, intermittent Ndutu Stream (sometimes referred to as the Oldupai River) which originates in Lakes Masek and Ndutu that travels nearly 50 km before emptying into the Olbalbal fault graben depression (Hay, 1976).

Olduvai is actually a misspelling of *Oldupaai*, Maa for the wild sisal plant (*Sansevieria ehrenbergii*), which occurs in proliferation throughout all sections of the gorge. In the east, the stream gradient is steep, and runoff is rapid, resulting in a deep gorge with vertically eroded walls and a narrower floor. The vegetation is variable and includes a mosaic of woodland, bushland, and grassland consisting of open tree cover and dense thicket along the stream bed margin. The woodland component is composed mainly of trees from the *Commiphora* and *Acacia* species (*Co.*

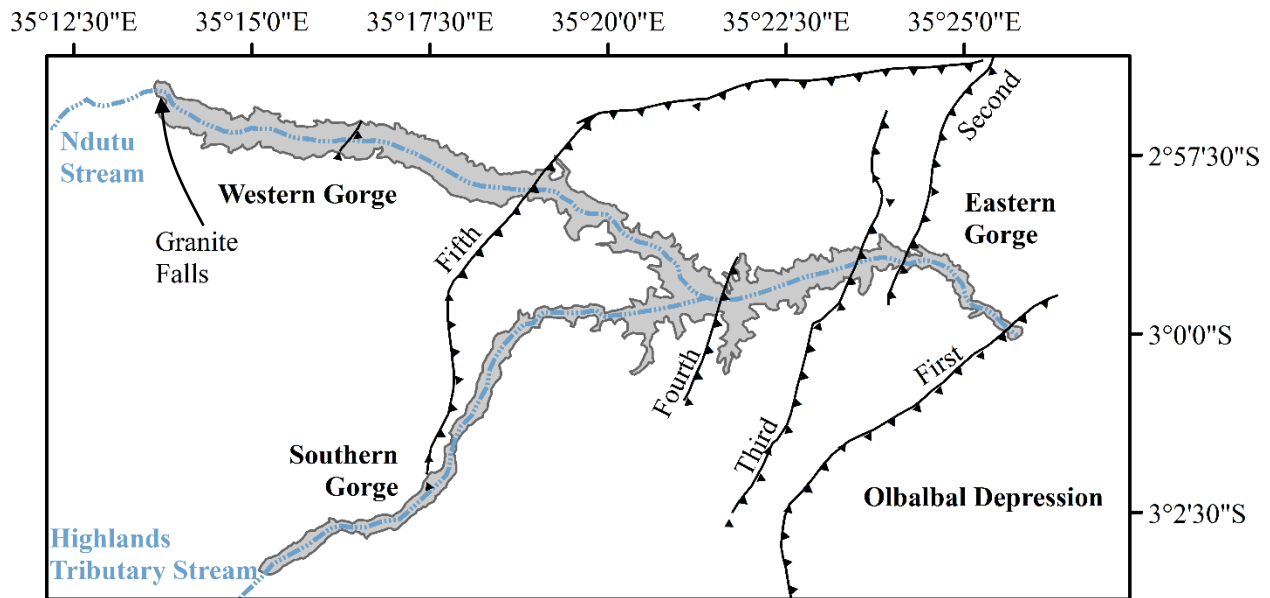


Figure 2-5. Physiographic distinctions of Olduvai Gorge. The Eastern Gorge extends from the First to the Fourth fault; the Western Gorge from Granite Falls to the main confluence; and the Southern Gorge follows the Highlands Tributary (or Norkuman) stream to the main confluence. Both streams are intermittent and only flow during the rainy seasons.

madagascariensis, *Co. merkeri*; *Ac. mellifera*, *Ac. tortilis*, *Ac. xanthophloea*), as well as *Salvadora persica*, *Balanites aegyptiaca*, and *Ximenia caffra*. Bushland species include *Achyranthes aspera*, *Cadaba farinose*, the herb *Justicia bentonica*, *Lycium europium*, and *Pluchea ovalis*. Associated short vegetation comprises grasses (*Pennisetum mezianum*, *Sporobolus panicoides*), fern (*Asparagus africanus*), succulents (*Aloe secundiflora*, *Euphorbia schimperi*, *Euphorbia tirucalli*), and woody vines (*Cissus quadrangularis*, *Cissus cactiformis*).

The southern reach of the gorge is characterized by bushes and thicket, especially near the stream channel, and narrow bands of shorter woodland. *Commiphora* and *Acacia* trees predominate in the south, while *Asparagus africanus*, *Salvadora persica*, and *Sporobolus panicoides* are also abundant. Additional grass species are *Aristida adoensis*, *Digitaria macroblephara*, and *Sporobolus marginatus*, while *Kyllinga* (a sedge) and *Barleria eranthemoides* (a bush) are also found.

Like the eastern and southern stretches of the gorge, the West is categorized by *Acacia-Commiphora* deciduous bushland and thicket, with *Ac. mellifera*, *Ac. nilotica*, *Ac. tortilis*, *Co. africana*, and *Co. habessinica* dominant. Other trees include *Ba. aegyptiaca*, *Cordia monoica*, *Sa. persica*, *Senna italica*, and *Ximenia caffra*. The layer of bush species range in density from low to medium and consists of *Barleria eranthemoides*, *Boscia angurtifolia*, and *Maerua triphylla*, while succulents found are *Aloe secundiflora* and *Sarcostemma viminale*, and the woody vine *Ci. cactiformis*. The grass layer is composed of *Ar. adoensis*, *Chloris gayana*, *Cynodon dactylon*, *Digitaria macroblephara*, *Odysea jaegeri*, *Pe. mezianum*, and *Sporobolus consimilis*, *Sp. homblei*, *Sp. panicoides*, and *Sp. spicatus*. Finally, *As. africanus* and the herbs *Heliotropium steudneri*, *Hypoestes torskaolii*, and *Ju. betonica* constitute the shorter vegetation in well-watered areas.

2.5 Referentials for Olduvai's Paleolandscape

Over the last few decades, different investigations have attempted to identify modern ecosystems as referential correlates to Olduvai's ancient vegetation structure for when hominins occupied the lakeside environment. Peters and Blumenschine (1995) developed a paleolandscape model for lowermost Bed II that attempted to predict possible hominin land use patterns based on reconnaissance surveys in eastern and southern Africa. Copeland (2007) modeled the vegetation of lowermost Bed II by examining modern habitats in northern Lake Manyara, Ngorongoro, and the Serengeti Plain as analogs to the paleolandscape in terms of climate, land forms, and soil types. Lake Manyara is an attractive referential as it is a Rift Valley lake with an associated lacustrine plain and terrace, and alluvial fans on the western margin provide abundant freshwater through seeps not otherwise delivered by local rainfall. The landscape facets of the southeastern side of

paleo-Lake Olduvai, including alluvial fans and freshwater seeps (Ashley et al., 2009), are thought to have been similar to the modern ecosystem surrounding Lake Manyara. Likewise, water flowing into Ngorongoro Crater from the northeast through the Lonyokie and Munge streams form a series of freshwater wetlands before terminating in Lake Makat. The level of Lake Makat varies widely from year-to-year in response to inflow amount, which is dictated by local rainfall that can be as low as 300 mm per year (Herlocker and Dirschl, 1972). It is the fluctuating lake level and the ensuing extent of the lacustrine plain and stream-fed wetlands that makes Makat a potential analog for the lacustrine plains of paleo-Lake Olduvai (Copeland, 2007).

Well-drained alluvial fans north of Lake Manyara support a lush groundwater forest that supports large trees such as the Cape Mahogany (*Trichilia emetica*) which grows to heights of up to 20 meters (Copeland, 2007). The ubiquitous groundwater and the small, spring-fed perennial rivers on the alluvial fans northwest of the lake have a dominant effect on the vegetation community and structure (Copeland, 2007) such that it changes rapidly within a few hundred meters of the freshwater sources. In addition to *Tr. emetica*, which has edible seed pods, other common trees include *Ficus sycomorus* which has both edible figs and leaves, *Croton macrostachyus* that produces fruits eaten by chimpanzees in western Tanzania, and the inedible species *Cordia goetzii* and *Tabernaemontana ventricosa* (Copeland, 2007 and references within). *Acalypha fruticosa* and *Acalypha ornate*, which also produce fruits and leaves eaten by chimpanzees, and *Hibiscus ovalifolius* and *Senna bicapsularis* are additional shrubs commonly found in the groundwater forest. The shade-adapted, inedible C₃ *Oplismenus hirtellus* is one of the rare grasses found on the forest floor.

The Lerai Forest of Ngorongoro Crater was a dense stand of deciduous *Acacia xanthophloea* (fever tree) and the evergreen *Rauvolfia caffra* (quinine tree), species that are

associated with abundant groundwater or found along rivers and streams and on floodplains and lake margins (Mills, 2006). Both species are regarded as indicators of water, and dense stands of closed woodlands often form in seasonally flooded areas on alluvial soils. The forest once acted as a refuge for nursing black rhinoceroses and their calves and was a critical habitat for hiding new-born rhinos from predators such as hyenas and lions. Recently however, the extent of the forest has contracted considerably, being replaced by woodland and grassland in many places (Mills, 2006). Multiple hypotheses have been advanced as to the cause of the contraction such as drought induced reductions in groundwater level and stream flow as well as increases in soil salinity due to flooding from nearby sodic Lake Makat and the intrusion of saline groundwater into the Lerai area.

Within a small rift valley to the east of Olduvai sits the Olbalbal Depression, a fault graben in which the Ndotu Stream empties. Olbalbal contains an assortment of fluvial, eolian, and semi-lacustrine sediments of Holocene age (Hay, 1976) and at about 1,300 m.a.s.l., the depression remains the lowest geologic feature in the greater Olduvai region and acts as the base level for streams draining the northwest slopes of the Crater Highlands and the eastern Serengeti Plain (Herlocker and Dirschl, 1972). Situated adjacent to Olduvai in the west and the Crater Highlands in the south and east, Olbalbal and the accompanying ecosystem were first recognized as a modern example of the type of lake basin in which Beds II and IV were deposited by Pickering (1960). Similarities include a narrow transition zone extending between the Olbalbal lake-margin and alluvial fans of the Crater Highlands, a zone corresponding to a lacustrine plain. Soils are somewhat alkaline and non-saline clays, sandy clays, and loams; whereas Olduvai had more of a saline-alkaline soil environment. Moisture regimes are similar, if not somewhat drier today, and depends mainly on local rainfall and drainage from local streams, with only marginal rainfall

coming during the dry season (June to October). *Pennisetum mezianum* and *Cynodon plectostachyus*, are the most common grasses, particularly in the poorly drained southern half of the depression, while *Cynodon dactylon* is dominant in the north (Herlocker and Dirschl, 1972). *Acacia tortilis* grow on the well-drained, gentle slopes on the alluvial fans to the east and the western graben fault, typically accompanied by *Cynodon* grasses. Groundwater forests of *Acacia xanthophloea* occur on sandy soils with moist, loamy troughs throughout the depression (Herlocker and Dirschl, 1972). In addition, many of the other plant species found in the eastern, southern, and western physiographic sections of Olduvai also grow throughout the Olbalbal Depression.

It should be noted that it is possible there are no modern correlates for paleo-Lake Olduvai and the surrounding ecosystems as Pleistocene climatic regimes dictating plant communities may not be properly represented today. For example, the interactions between CO₂ concentrations, rainfall amount, average temperature, or localized geology may have established Pleistocene vegetation communities and structures unlike those found today in the greater Olduvai and Manyara regions, and therefore, any modern referential might be missing key components of Pleistocene plant assemblages. Moreover, different proxy records (i.e. pollen, phytoliths, and leaf wax lipid biomarkers) used in paleo-reconstructions either do not correlate with one another or have not been systematically explored in modern environments. Ancient pollen data from Olduvai Gorge for instance, suggests a paleo-landscape dominated by grasses and sedges with tree species representative of those found today in the *Acacia-Commiphora* bushland and thicket (Bonnefille, 1984). Because the ancient pollen data is very similar to that of the main plant landscape surrounding Olduvai Gorge today, it is possible there was a sampling bias or modern contamination of the sediments studied by Bonnefille. However, Bonnefille also found pollen

representing species from the Afromontane phytogeographical zone (such as *Juniperus* and *Podocarpus*), an interesting discovery that is often disregarded (e.g. Barboni (2014)) when modern landscapes are being considered as referentials. Due to cooler temperatures and periods of increased rainfall in East Africa during the Pleistocene, Afromontane regions may be an attractive biome for comparison as highland species may have migrated to lower altitudes when climatic conditions favored their expansion. This has yet to be explored, however.

Both phytolith (Barboni et al., 2010) and isotope data (Cerling and Hay, 1986; Magill et al., 2013a) suggests a more mosaic environment surrounding paleo-Lake Olduvai and therefore studies (Barboni, 2014; Copeland, 2007) identifying modern biomes as Pleistocene correlates often target nearby habitats as their referential. However, no systematic study with properly designed sampling strategies using either phytoliths or leaf wax lipids have been conducted in the groundwater forest near Lake Manyara, in the Lerai Forest of Ngorongoro Crater, or other East African biome. And similar to how the pollen proxy data does not align with that of phytoliths or isotopes, the abundance of C₄ sedges in the forest near Lake Manyara does not seem to be represented by the isotope records; a further complication when using Lake Manyara as a modern correlate. Furthermore, Barboni et al., (2007) were unable to differentiate phytoliths of Afromontane vegetation from that of Somalia-Masai grasslands, attesting to the need for more comparative studies on modern habitats to better inform our interpretations of the ancient environments of early human paleoanthropological sites in East Africa.

One other issue, especially with leaf wax lipid biomarkers, is that most of our understanding of the isotopic concentrations of lipid compounds in sedimentary archives stem from studies on living plants. However, isotope diagenetic studies in soil forming horizons have not been characterized in East Africa and we do not have a full appreciation of the isotopic

differences between plant waxes (*n*-alkanes) and their depositional environments (see Section 5.7). Nevertheless, studies (Freier et al., 2010; Wang et al., 2009) have documented the isotope content of African soils and their relationship to living plants and can guide us in interpreting Pleistocene paleo-environments going forward, but much more work is needed on both living plants and soil horizons of the extant phytochoria and biomes of East Africa before we can confidently characterize Pleistocene environments in which early human activity occurred.

2.6 Chapter 2 Summary

The African phytochoria and extant biomes (as defined by White (1983)) include 16 major vegetation types, subdivided into five main groups as determined by regional extent and physiognomy. These are largely influenced by seasonal precipitation patterns which respond to regional topography and the convective activity of the Intertropical Convergence Zone; these features also play a critical role in the distribution of plant resources, which are largely determined by the availability of freshwater. These factors likely had a similar role during the Pleistocene, and human activity would have been motivated by precipitation seasonality and vegetation distribution.

The present-day climate and vegetation of the Olduvai Gorge region within the Ngorongoro Conservation Area falls under the Somalia-Masai Regional Center of Endemism, and more specifically, the *Acacia-Commiphora* bushland and ticket biome. Three distinct physiographic regions with a variety of trees, shrubs, and grasses define Olduvai Gorge today; the Eastern, Western, and Southern Gorges. Recently, different investigations have attempted to identify modern ecosystems as referential correlates for Olduvai's ancient vegetation structure around paleo-Lake Olduvai such as Lake Manyara or Lake Makat. However, caution must be taken

when assigning any modern environment as a Pleistocene correlate as interactions between CO₂ concentrations, rainfall amount, average temperature, or localized geology may have established Pleistocene vegetation communities and structures unlike those found today in the greater Olduvai region. Moreover, no systematic study with properly designed sampling strategies using either phytoliths or leaf wax lipids have been conducted in the groundwater forest near Lake Manyara, in the Lerai Forest near Lake Makat, or other East African biome.

CHAPTER 3: CLIMATE CHANGE AND HUMAN EVOLUTION

3.1 Introduction

Hypotheses linking climate change and human evolution focus on climatic variability that altered ecological processes in human environments (e.g. Potts, 1998a, b, 2012a, b). Dynamic climate and ecosystems necessitated that hominins, the members of the evolutionary group of bipedal species most closely related to *Homo sapiens*, effectively respond to adaptive and speciation pressures (Committee on the Earth System Context for Hominin Evolution, 2010), leading to genetic selection and technological innovation. Archaeological, paleontological, and paleoenvironmental records suggest that notable evolutionary events coincided with substantial changes in African (and Eurasian) climate, and that these changes and events influenced key junctures in human evolution. Although causal relationships are difficult to determine, noteworthy hominin extinction, speciation, and behavioral events appear to associate with changes in African climate over the past 6 million years (deMenocal, 2011). For example, the extinction of *Australopithecus afarensis* around 2.95 Ma, the emergence of *Paranthropus aethiopicus* about 2.7 Ma, and the appearance of *Homo habilis* and the earliest evidence for Oldowan stone tools at 2.6 Ma (and possibly as old as 2.8 Ma (Villmoare et al., 2015)) overlapped with Northern Hemisphere glacial intensification, faunal changes, aridification, and grassland expansion in Africa at about 2.7 Ma (Bobe and Eck, 2001; Committee on the Earth System Context for Hominin Evolution, 2010; deMenocal, 2011; Semaw, 2003). Additional developments, such as the evolution of *Homo erectus* and subsequent migration out of Africa occurred when subtropical temperatures cooled around 1.9 Ma (Ravelo et al., 2004), while the emergence of the Acheulean at ~1.75 Ma corresponds with increases in African wind-borne dust, indicative of long-term drying, which

peaked near 1.8 Ma (deMenocal, 2004), and *n*-alkanoic acid biomarkers from the Gulf of Aden that suggest C₄ expansion between 2.4 and 1.7 Ma (Feakins et al., 2005). However, a cause and effect relationship between specific climatic events and major evolutionary occurrences is difficult to establish as these records are geographically distant from archaeological and paleontological sites.

Although the impact aridity and remodeling of environments (i.e. grassland expansion (Soreng et al., 2017)) have on human evolution remains a topic of discussion (Bibi et al., 2018; Cerling et al., 2011; deMenocal, 2004; Magill et al., 2013a; Wood and Harrison, 2011), hominin-environment interactions between such things as water availability, mosaic ecosystems, and dietary behaviour certainly influenced natural selection, human evolution, and technological adaptations. Intrinsic (Klein, 2009; Wilson, 1979; Wolpoff, 1980) and extrinsic (Potts, 1998a, b, 2012b; Trauth et al., 2009; Trauth et al., 2007; Trauth et al., 2010; Vrba, 1995a) explanations have been advanced to explain how evolutionary change was initiated, particularly those that set the stage for major events like the development of bipedalism, hominin speciation, the appearance of *Homo* and manufactured stone tools, the dispersal out of Africa, and an increase in cranial capacity. Prior to the seminal work published in *Human Origins: Perspectives on Human Evolution* (Isaac and McCown, 1976), most proceedings dealing with human evolution used intrinsic explanations to relate hominin origins, specifically bipedalism, to a shift from forested/wooded habitat to an open grassland setting. (This is better known as the *Savanna Hypothesis*.) Intrinsic explanations stipulate that the environment was a relatively neutral agent, and the only requirement for the emergence of bipedality or tool use (for example) was the movement into the savanna, or an initial environmental shift to drier, less forested surroundings (Potts, 2012b). Beginning in the late 1970s however, an emphasis was placed on the importance of environmental complexity for

understanding hominin evolution, particularly in sedimentary, geomorphological, taphonomic, and ecological settings (Bishop, 1978), climatic, geologic, and paleoecological contexts (Butzer and Isaac, 1975; Jolly, 1978), and complex tectonic and climatic events (Bishop, 1976; Isaac, 1976).

3.2 Controlling Factors of Climate and Environment

3.2.1 Convention for Dating the Pleistocene

The Quaternary Period of the geologic time scale has traditionally encompassed the last 1.806 million years, defined by the Global Stratotype Section and Point (GSSP) at Vrica, Calabria, Italy. The base of the Quaternary however, has been redefined using the Gelasian Stage at Monte San Nicola in Sicily, Italy, and is currently dated at 2.58 Ma (Gibbard and Head, 2010). In 2009, the International Union for Geological Sciences (IUGS) ratified a proposal that the base of the Quaternary Period, and therefore the base of the Pleistocene Epoch, be lowered to that of the Gelasian Age, which was transferred accordingly from the Pliocene to the Pleistocene (Gibbard and Head, 2009). The GSSP at Monte San Nicola has an estimated age of 2.58 Ma and defines the lower boundary of the Gelasian Age, Pleistocene Epoch, and Quaternary Period. As this is a relatively recent demarcation, 1.806 Ma is regularly designated as the start of the Quaternary/Pleistocene, specifically in paleoanthropological literature. Nevertheless, this dissertation follows the updated 2.58 Ma date as the boundary between Pliocene-Pleistocene/Neogene-Quaternary because significant climatic episodes from this earlier period correspond with East African sites associated with human evolution.

The Pleistocene epoch is divided into four ages: the Gelasian, Calabrian, Ionian, and Tarantian, whereby the current IUGS-sanctioned (2009) timescale defines the Gelasian and Calabrian as the “Early” Pleistocene, and the Ionian and Tarantian as the “Middle” and “Late”

Pleistocene, respectively. However, in keeping with paleoanthropological tradition, “Gelasian” is used for the period that spans 2.58 to 1.806 Ma, but “Early” (1.806 Ma to 781,000 years ago), “Middle” (781,000 to 126,000 years ago), and “Late” (126,000 to 11,650 years ago) terminology is maintained in place of Calabrian, Ionian, and Tarantian.

The new base of the Pleistocene at 2.58 Ma corresponds to Marine Isotope Stage (MIS) 103, the first cold, glacial period of this epoch (Lisiecki and Raymo, 2005). Marine isotope stages are alternating warm/cool periods in the Earth's paleoclimate, deduced from the two isotopes of oxygen: oxygen-16 (^{16}O) which is the most-common, and the heavier, less-common oxygen-18 (^{18}O). Oxygen isotope data is recorded in the calcium carbonate (CaCO_3) shells of foraminifera collected from deep-sea cores and reflect changes in temperature and glaciation. The lighter isotope (^{16}O) evaporates more readily from the oceans, and therefore precipitation (and glacial ice) is enriched in ^{16}O . This results in a greater concentration of the heavier isotope (^{18}O) in ocean water during cold periods. Thus, during periods of extensive glaciation, more ^{16}O is frozen in glacial ice, so the concentration of ^{18}O in seawater, and foraminifera, increases. Conversely, during warmer interglacial periods when the amount of glacial ice decreases dramatically, more ^{16}O returns to the ocean, so the proportion of ^{18}O relative to ^{16}O in ocean decreases as well. The ratio between ^{18}O and ^{16}O ratio also varies with temperature; more ^{18}O evaporates with water vapor from the oceans when temperatures are high, and less when temperatures are low. Therefore, the heavy isotope is more abundant in the precipitation of warm eras and less abundant during colder periods.

Even-numbered marine isotope stages have seawater that is enriched in the heavier isotope (^{18}O) and represent cold glacial periods, while odd-numbered stages are depleted in ^{18}O and represent warm interglacial intervals (Fig. 3-1). The Early Pleistocene begins during the transition

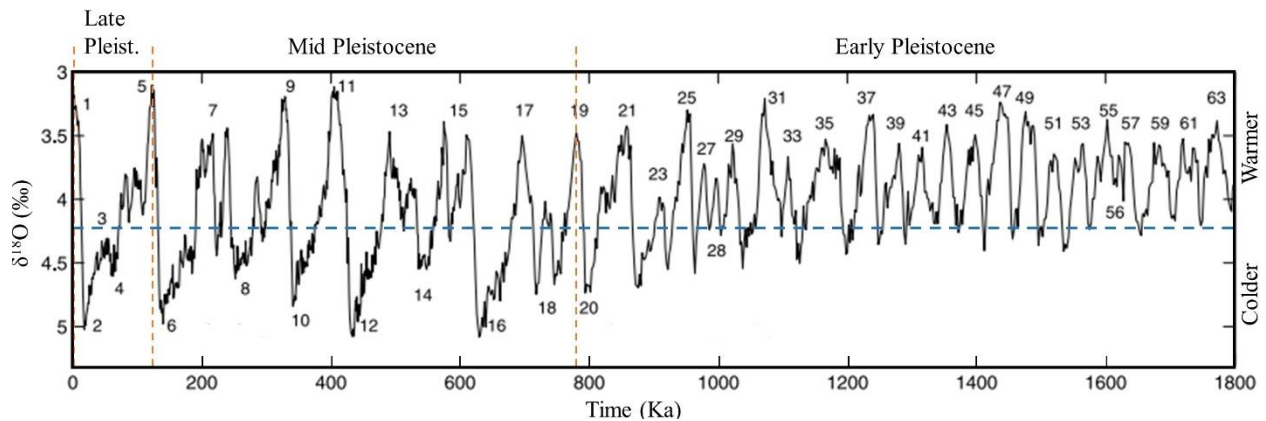


Figure 3-1. Average benthic foraminifera $\delta^{18}\text{O}$ record for the last 1.8 million years showing MIS 1-64. Warmer interglacials are marked with odd numbers, representing less ^{18}O in the ocean. Modified from Lisiecki and Raymo (2005).

from MIS 65 (warm) to MIS 64 (cold) and concludes during MIS 19 (warm). The Middle Pleistocene begins during MIS 19 (warm) and concludes with MIS 5 (warm), which is also the beginning of the last interglacial before the current period. The Late Pleistocene begins during MIS 5 (warm) and ends at MIS 1 11,650 years ago (warm). MIS 1 marks the start of the Holocene and continues to the present. (The Holocene, although technically an interglacial, is distinct from the Pleistocene due to the severe human impact on land and life.) One hundred and three marine isotope stages transpired since the start of the Pleistocene, signalling the fluctuating atmospheric conditions throughout this period (Lisiecki and Raymo, 2005).

The unique ability for *Homo sapiens* to adapt, thrive, and diversify in numerous and wide-ranging climatic and environmental settings has resulted in the nearly world-wide colonization of our species. An adaptation such as this may be the product of *Homo* speciation during the Pleistocene, a period of global climate variability (this may also be true for other species that evolved and subsequently survived the Pleistocene). The Pleistocene epoch was a very complex phase in Earth's history characterized by several advances and retreats of glacial ice that influenced worldwide climate change. Beginning 2.58 Ma, the *Ice Age* was a time of extensive glaciation, with glaciers being much more widespread than they are now, especially in the Northern

Hemisphere, and covering nearly three times as much of Earth's surface as they do today (Monroe et al., 2007). An uninterrupted record of climate cycles preserved in seafloor sediments suggests that there may have been as many as 20 significant warm-cold cycles that altered ocean circulation and the transport of heat and moisture around the planet, consequently impacting the ecological controls on terrestrial environments (Lutgens and Tarbuck, 2012).

Climatic instability during the Pleistocene was remarkable; as ice sheets advanced and retreated, they triggered global changes in sea level, at times as much as 100 meters lower than today (Dawson, 1996; Shackleton, 1987), and colder ocean temperatures and reduced evaporation caused by water being trapped in glacial ice caused widespread aridification that led to the expansion of grasslands and a reduction in forests. In East Africa, shifts toward cooler and drier climates resulted in the gradual replacement of woodlands by wooded-grasslands and open grasslands between 3.0 Ma and 1.0 Ma; although evidence for purely C₄ grasslands does not appear until about 1.0 Ma (Cerling, 1992).

During interglacial periods, rainfall patterns varied throughout Africa and precipitation increased, likely changing the availability of food resources (Peters and O'Brien, 1981). Because Pleistocene environmental variables dictated which foods were available for consumption, the ability to procure foods often depended on a species' ability to adapt to changing ecological conditions. Pleistocene hominins were opportunistic foragers and would have been able to cope with changing climates. Their highly variable diet and ability to exploit diverse environments for various food sources of fruits and leaves, large quantities of grasses and sedges, or animals (Sponheimer and Lee-Thorp, 1999; Sponheimer et al., 2006) was key to their adaptability. During the Pleistocene, hominin speciation was perhaps greater than any other time since the divergence of humans and chimpanzees between 6.0 and 10 Ma (Perelman et al., 2011), and it was during this

period that at least 14 different hominin species emerged. Therefore, the Pleistocene was a significant point in hominin evolution, as it was during this epoch that the genus *Homo* appeared, but also because the first, definitive stone tools occur in the archaeological record.

3.2.2 Orbital Forcing and Global Climate

Global and local environmental changes are a response to both external and internal forcing mechanisms that shape climatic patterns (Maslin et al., 2013). External forces include Earth's changing orbital parameters that alter the seasonal and latitudinal distribution of net solar radiation (Milankovitch, 1941), and orogenesis, or tectonic uplift, that alters the topography and altitude of a region (Sepulchre et al., 2006). Greenhouse gases, such as the amount of carbon dioxide (CO₂) in the atmosphere (Plass, 1956), and the patterns of deep circulation of ocean water that drive heat and moisture transport across hemispheres (Duplessy and Shackleton, 1985; Newell, 1974) are examples of internal forcing mechanisms. Because internal and external factors operate at different timescales, the environmental response time to climate systems is dependent on multiple factors in operation; e.g. long-term processes such as tectonic uplift gradually changing the precipitation patterns of a region over millions of years (Sepulchre et al., 2006), or short-term processes such as seasonal variations in localized lake levels (Trauth et al., 2010).

Glacial-interglacial oscillations, the most fundamental environmental characteristic of the Quaternary period, are primarily forced by changes in the Earth's orbital geometry (Hays et al., 1976), that is the combined effects of eccentricity, obliquity, and precession; better known as Milankovitch Cycles. Milankovitch Cycles regulate the amount of solar radiation received at different latitudes, and subsequently modify insolation and moisture systems.

3.2.3 Milankovitch Cycles

The three main orbital parameters that determine the variation in incoming solar radiation are the combined effects of eccentricity, obliquity, and precession. (Additional elements like tectonic uplift, sea surface temperatures, and atmospheric circulation modify insolation and moisture dynamics at a regional scale.) *Eccentricity*, or the deviation in the shape of the Earth's orbit around the Sun, varies from circular to elliptical over approximately 100,000 years (Hays et al., 1976), with an additional long cycle of about 400,000 (Maslin et al., 2013). Although changes in eccentricity cause only minor variations in the solar radiation that reaches the Earth's surface, it triggers substantial seasonal effects, particularly when the orbit deviates from a circular pattern. Milankovitch (1949) suggested that northern ice sheets are more likely to form in boreal summer when the Earth is in an orbit of greater eccentricity, or when the orbit takes it further from the sun, due to greater snowfall totals in mid to high latitudes. The greater snowfall totals, in conjunction with cooler summer temperatures, results in a net reduction of snowmelt. This produces a situation favorable for snow and glacial ice accumulation because as Earth's orbit becomes more-elliptically shaped, it creates greater seasonal exaggeration in the Northern Hemisphere.

Earth's axial tilt, called *obliquity*, varies between 21.8° and 24.4° over a 41,000 year period (Maslin and Christensen, 2007). Today the axis of rotation tilts at about 23.5° to the plane of Earth's orbit, and it is the tilt of the axis that causes the seasons. In boreal summer for example (June to September), the Northern Hemisphere angles towards the sun, and temperatures increase as the north receives over 12 hours of direct sunlight. At the same time in the Southern Hemisphere, the axis of rotation slopes away from the sun and the hemisphere cools as it receives under 12 hours of direct sunlight. Raymo and Nisancioglu (2003) show that obliquity drives differential heating between high and low latitudes and controls atmospheric meridional flux of heat, moisture,

and latent energy. Moreover, meridional temperature gradients controlling the poleward transport of moisture produced the strong obliquity signals now observed in Pleistocene geologic archives.

Increased seasonality and extreme differences between summer and winter temperatures are responses to larger obliquity, or greater axial tilt. As the Earth's axis of rotation decreases, high latitudes experience cooler summer temperatures while at the same time, enhanced delivery of moisture into polar regions promotes ice sheet growth. Therefore, obliquity, northward moisture transport, and glacial-interglacial cycles form a relationship in which the summer energy budget controlled Pleistocene glacial variability (Huybers, 2006).

The gravitational pull of the Sun and the Moon on the Earth causes axial *precession*, or the wobbling of Earth's axis. As the Earth rotates along its axis it slowly wobbles, or precesses, like that of a spinning top. There are two main components of precession; that of the Earth's axis of rotation, and the precession of the Earth's orbit around the sun which influences the equinoxes. Over time, the slow wobbling changes the direction in which Earth's north pole points, and because the wobble is constant, precession causes a change in the Earth–Sun distance for the seasonal equinoxes (Maslin et al., 2013). Consequently, it is the combination of the different orbital parameters that results in a 23,000-year precession period.

Precession dominates high-latitude summer insolation (Raymo and Nisancioglu, 2003), and the impact of precession on global climate systems is modulated by eccentricity; precessional forcing is enhanced during periods of pronounced eccentricity (Scholz et al., 2007). Precession has a significant impact on the tropics and regulates the duration and intensity of the precipitation-bearing monsoons along the equator. Although precession forcing is moderated at times by tropical sea-surface temperatures in the Indian Ocean and Atlantic Ocean (Scholz et al., 2007), long-term forcing of East African climate has been attributed to precessional processes (Trauth et al., 2003).

3.2.4 *Glacial-Interglacial Intensification*

Hays et al., (1976) added supporting evidence to the Milankovitch Cycle hypothesis by showing that major variations in climate over the past several hundred-thousand-years were closely associated with changes in the geometry of Earth's orbit. They showed that a 100,000-year climatic component is in phase with orbital eccentricity, a 23,000-year period of climate variance correlates with 23,000- and 19,000-year precessional changes, and a 42,000-year climatic component has the same period as variations in the obliquity of the Earth's axis. Hays et al. (1976) concluded that changes in the Earth's orbital geometry are the fundamental cause of Pleistocene glaciation.

Raymo and Nisancioglu (2003) showed that $\delta^{18}\text{O}$ ice volume proxies are dominated by the 41,000-year obliquity periodicity, while summer insolation is governed by the 23,000-year period of precession at nearly every latitude. Trauth et al., (2007) illustrated that water levels of lakes in the East African Rift System (EARS) were dictated by the precessional forcing of moisture availability in the tropics. Lake level changes coincided with major global events at: a) 2.7-2.5 Ma when Northern Hemisphere glaciation intensified due to incremental changes in the Earth's orbital obliquity (low tilt angle) and the gradual closing of the Isthmus of Panama (Haug and Tiedemann, 1998); b) 1.9-1.7 Ma with cooling subtropical temperatures and the onset of strong zonal, or Walker, circulation in the Pacific (Ravelo et al., 2004); and c) 1.1-0.9 Ma during the "Mid-Pleistocene Revolution" (Berger and Jansen, 1994), when a shift in global climate led from an obliquity-dominated periodicity to a precession-dominated regime (Maslin and Ridgwell, 2005). Kingston et al., (2007), also examining EARS lakes, showed extreme changes in water levels between 2.7 and 2.5 Ma using diatom assemblages and laminated diatomite in what is today the Baringo Basin of Kenya. They attribute variability in lake levels observed in diatomite

fragmentation, dispersal, and speciation to 23,000-year precessional forcing. East African lake records document the extreme climate variability relating to precession-forced wet and dry phases, and when coupled with variations in solar heating due to changes in the Earth's obliquity, create an important driving force of glacial cycles throughout the Pleistocene.

3.2.5 Differing Controls on Regional Climate

Glacial intensification at the start of the Pleistocene affected global climate by reducing Earth's water budget, increasing aridity, and cooling temperatures. However, orbital forcing alone was not the only driver of the intense glacial-interglacial oscillations over the last 2.58 Ma; instead, feedback mechanisms amplified solar insolation at the Earth's surface. For example, as ice accumulates, albedo increases and subsequently reflects more sunlight back into space while modifying the ambient environment. As ice sheets grew, they impacted both atmospheric circulation and ocean currents by reducing the amount of warm water flowing into the Nordic Seas, which led to increased cooling in the Northern Hemisphere and ultimately, the further expansion of northern ice sheets. Ice expansion and cooling also compresses both the northern and southern boundaries of the Intertropical Convergence Zone (ITCZ), which directly impacts East African moisture availability by increasing the sensitivity of East Africa to precessional forcing (Trauth et al., 2007). Furthermore, differing controls on regional climate result from local variations in orbital forcing, but also from unique geographic features like uplift in the East African Rift Valley, and circulation patterns of easterlies and westerlies in southern Africa.

Differential heating between marine and terrestrial areas generates landward convection of moisture-rich oceanic air. In East Africa moisture is obtained from the Indian Ocean, and this dynamic produces the East African monsoon. The timing of increased East African monsoonal

rainfall is a product of the migration of the ITCZ, which follows the seasonal and latitudinal movement of solar radiation from south to north during the rise of boreal summer (Lepre et al., 2007). When northern African landmasses warm, they build low-pressure systems that pull the ITCZ northward to where it settles in the northern low latitudes (Nicholson, 1993). The opposite occurs during austral summer, as the path of incoming sunlight pushes southward. The two migration periods of the ITCZ across the equator produces the characteristic biannual rains of the East Africa monsoon. Orbital precession and tropical sea-surface temperatures moderate the intensity of monsoonal rainfall and govern climate controls in the region (Scholz et al., 2007).

3.2.6 East African Tectonic Uplift

Tectonic activity, specifically the onset of volcanism and rifting in East Africa, has an important bearing on hydrological spatial patterns and amounts, which in turn induces strong shifts in vegetation. The progressive formation of the East African Rift System (EARS) increased aridity in the region, but also developed fault-graben basins as catchments for lakes (Maslin and Christensen, 2007). The EARS is a continental divergent plate boundary that extends through eastern Africa for approximately 3,000 kilometers and consists of several interconnected rift valleys that split into eastern and western sections around Lake Victoria (Chorowicz, 2005). The most recent period of rifting began about 20 million years ago when upwelling in the Earth's mantle intruded the base of the lithosphere and began stretching and deforming the Earth's surface. Uplifting reached a maximum around the Plio-Pleistocene boundary (Chorowicz, 2005; Wolfenden et al., 2004), with more recent phases of uplift between 5.0 and 2.0 Ma in the Tanganyika and Malawi rifting zone (Ebinger et al., 1993). Major Tanzanian escarpments, present

by 3.0 Ma, create a 6,000-kilometre-long, north-south oriented crest situated between 1,500 and 5,100 m.a.s.l. (Chorowicz, 2005; Foster et al., 1997).

Rainfall and general atmospheric circulation models by Sepulchre et al. (2006) demonstrate the influence of East African tectonic activity on precipitation patterns. In their model, elevated plateaus divided major air currents, and wind patterns became less zonal reducing the available moisture for precipitation. Additionally, increased elevation depleted the moisture content of the leeward sides of uplifted regions, producing strong aridification that would have had important effects on standing water, vegetation type, and resource distribution. This is due in part to increased elevation and upland depletion of air moisture and precipitation which causes a rain-shadow drying effect, a phenomenon partly responsible for the aridification of the eastern highlands and lowlands of the EARS (Hardt et al., 2015: 571). When areas of higher elevation block major air currents, areas of high- or low-pressure form over landmasses and oceans far from the plateaus (Ruddiman and Kutzbach, 1991), and when this is coupled with greater seasonal variations in heating and cooling in land regions adjacent to the plateaus, seasonal monsoons of varying strengths are generated. This is significant in that summer rainfall in East Africa varies according to the westerly airstream of the African monsoon (Nicholson, 1993), and summer monsoonal runoff drains into the Omo and the Nile rivers via the capture of moisture by the Ethiopian and Kenyan Highlands (Hardt et al., 2015).

Tectonic uplift exacerbated orbitally-forced periods of aridification. However, tectonics were essential for the formation of isolated lake basins in the rift system that would have supported mosaic environments within restricted geographic regions (Trauth et al., 2007), and possibly provided refugia for Pleistocene hominins (Shea, 2008). Moreover, evidence from soil carbonates (Levin et al., 2011; Levin et al., 2004; Quade and Levin, 2013; Wynn, 2001, 2004) and *n*-alkane

and *n*-alkanoic acid biomarker isotopes (Feakins et al., 2005; Feakins et al., 2007; Feakins et al., 2013) illustrate a progressive proliferation of C₄ plants throughout the Pleistocene in response to increased aridity attributed to rifting in East Africa (deMenocal, 2004).

3.2.7 East African Moisture-Aridity Cycles

Research throughout Africa supports strong precessional-driven moisture-aridity cycles. Larrasoña et al. (2003) present a high-resolution proxy record of northern Sahara dust supply to the eastern Mediterranean Sea for the past 3 million years. Their marine-dust record reflects moisture-aridity cycles that coincide with 400,000-year eccentricity minima and maxima and 41,000-year obliquity variations in dust flux in the eastern Algerian, Libyan, and western Egyptian lowlands. The dust record proxy shows that moisture-aridity cycles are in direct response to the northward penetration of the African summer monsoon beyond the central Saharan watershed. The northward dispersal of the monsoon front is subject to long-term modulation by orbital eccentricity, whereby precession dictates the northward extent of the monsoon front. Consequently, stronger monsoons lead to enhanced soil moisture and vegetation cover that inhibit dust production. Conversely, when the impact of precession weakens, the potential of the African summer monsoon front to extend beyond the watershed is lessened, and persistently dry, non-vegetated desert conditions prevail. There has been a tendency for the monsoon front to remain south of the central Saharan watershed since 0.95 Ma (Larrasoña et al., 2003).

The *Homo sapiens* fossils Omo I and Omo II from the Kibish Formation in southern Ethiopia dated to 195 ± 5.0 Ka coincide with sapropel formation in the Mediterranean Sea (McDougall et al., 2008). Rossignol-Strick et al. (1982) proposed that sapropels, or organic-rich dark colored sediments, develop in the Mediterranean following extensive Nile River freshwater

discharge; a response to precessional forcing and increased seasonal contrast between the Northern Hemisphere summer and winter (Rohling, 1994). Increased seasonal contrast intensifies monsoonal circulation in summer, leading to greater precipitation amounts in East Africa, especially in the Ethiopian highlands (McDougall et al., 2008). As a result, an upsurge in Nile discharge brings massive quantities of freshwater into the Mediterranean, promoting organic productivity and subsequently, the development of anoxic conditions in deeper waters that favor the preservation of sunken organic-rich sapropels.

McDougal et al., (2008) link sapropel formation in the Mediterranean with heightened Omo River discharge into Lake Turkana, reflecting greater precipitation in the highlands of Ethiopia during the deposition of the Kibish Formation. The correlation between the sapropels in the Mediterranean, greater water levels in Lake Turkana, and sedimentation of the Kibish Formation stems from a common cause; the intensification of the African monsoon. As the Omo River drainage network raised Lake Turkana water levels during periods of intensified rainfall in the eastern Ethiopian highlands, the Nile River system provided huge runoff into the Mediterranean at the same time from the northern Ethiopian highlands. McDougal et al., (2008) demonstrate that the link between the deposition of the Kibish Formation and the sapropels in the Mediterranean Sea was determined by the Milankovitch cycles.

Lepre et al., (2007) provide evidence for lake-level oscillations of Lake Turkana caused by variations in the intensity of monsoonal rainfall between 1.9 and 1.6 Ma. Lake-margin sediments of the Koobi Fora Formation in the northeast Turkana Basin of Kenya record climate changes caused by orbital cycles operating at 20,000- and 40,000-year frequencies. These time intervals are near the range of precession and obliquity timescales, respectively, and Lepre et al., (2007) show that stratigraphic shifts in facies environments correspond to transgressions and regressions

of lake levels, which implies alternating wetter and drier climatic conditions. They also note that major drops in lake levels repeat on a timescale consistent with obliquity, and that the ancient lake margin is responsive to changes in monsoonal rainfall resulting from orbital insolation and/or glacial forcing.

Scholtz et al., (2007) report continental evidence for several periods of pronounced tropical African aridity in the Late Pleistocene over the last ~145,000-years from cores taken in Lakes Bosumtwi, Malawi, and Tanganyika. They interpret an interval between 70 and 145,000 years as a period of enhanced precession-forced variability in the hydrologic cycle, marked by periods of extreme drought interceded by shorter intervals of greater precipitation. They attribute this variability to a peak in eccentricity-amplified precession as opposed to tectonic or glacial activity. In addition, the three lakes equivalently responded to regional changes in the evaporation-precipitation balance in tropical Africa. Sholtz and coauthors also observed overall wetter, more stable conditions after 70,000 years ago, which was likely widespread across tropical Africa. This transition to wetter, more stable conditions coincides with diminished orbital eccentricity and a reduction in precession-dominated climatic extremes.

3.2.8 Orbital Forcing and Paleo-Lake Olduvai

Hay and Kyser (2001) divided Paleo-Lake Olduvai's "Central Basin" into four differing lithologic units representing different lacustrine paleoenvironments. They inferred several episodes of higher and lower average lake levels in the central basin and eastern and western lake-margins based on the distribution of chert and calcite nodules, desiccation and cracking of claystones, extent of lacustrine claystones, and sedimentological chemistry determined using X-ray diffraction. Because Paleo-Lake Olduvai occupied a broad, shallow basin, it would likely have

increased to a much greater extent in surface area than in depth; in low-level episodes, the lake may have only increased to a maximum of 2.0 m deep, whereas in high-stands, the lake level may only have reached 4.0 m deep. Hay and Kyser determined that the lake of lower Bed II was larger than that of upper Bed I, and episodes of wetter climate alternated with drier episodes in which the lake extent changed accordingly.

Using lake-sediment stratigraphy between Tuff IF (1.803 ± 0.002 Ma) and Tuff IIA (1.74 ± 0.03 Ma) exposed in lower Bed II at Olduvai Gorge, Ashley (2007) following the interpretations of Hay and Kyser (2001), estimated the duration and cause of paleolake expansions and contractions. She was able to determine three discrete expansions represented by “waxy claystones” deposited by saline-alkaline lake water and two contractions identified through “earthy claystones” formed in a lakeshore freshwater wetland. The duration of these expansions and contractions averaged 21,000 years, consistent with orbital precession cycles. Precession likely influenced total rainfall amounts, which may have fluctuated between 400 and 800 mm at Olduvai Gorge for contraction and expansion periods, respectively.

Berry (2012) identified four lake cycles using X-ray fluorescence analyses for $\text{Al}_2\text{O}_3/\text{MgO}$ ratios, and TiO_2 and P_2O_5 between Tuffs IA (1.88 ± 0.05 Ma) and IF on sediments collected about 1.0 km west of the Fifth Fault (Location 80 of Hay (1976)). Lake cycles 1 and 4 encompass approximately 44,250 and 41,500 years, respectively (on par with the 41,000-year-cycle associated with obliquity), while lake cycles 2 and 3 covered 23,600 and 26,550 years, respectively (slightly longer than the 21,000-year precession cycle). Interestingly, the impact of obliquity on low latitude locations such as the Olduvai Gorge is not usually considered as significant as precession (Ashley, 2007; deMenocal, 1995). However, Berry’s lake transgression cycles correlate with Ashley’s

(2007) and show that orbital forcing likely produced variations in localized lake levels which would have had specific implications on human evolution.

3.3 Environmental Hypotheses for Human Evolution

Multiple hypotheses have been advanced in an effort to identify the environmental events that influenced evolutionary change in hominins throughout the Pleistocene (deMenocal, 2004; Feakins et al., 2005; Potts, 1998b, 2012a, b; Reed, 1997; Trauth et al., 2010; Trauth et al., 2006; Vrba, 1980). Furthermore, because climate in East Africa varied between humid and arid instances during this period (Potts, 2012a), the ability to deal with “ecological shocks” required that early humans be mobile and have a flexible diet; a fundamental characteristic to the development of the genus *Homo* (Hardy et al., 2015; Wells, 2012). In addition, wet to dry environmental shifts in the Pleistocene (Potts, 2012a) fragmented local ecosystems into ‘oasis-like’ concentrations of plants (Ashley et al., 2014; Ashley et al., 2010b; Ashley et al., 2009).

Early explanations of human evolution focused on intrinsic stimuli (Washburn, 1960; Wilson, 1979; Wolpoff, 1980), whereby a simple transition from one habitat type to another (forest to grasslands for example) set the stage for specific hominin characteristics like bipedalism and tool use. These *Habitat Specific Hypotheses* stipulate that the transition from closed woodlands to open grasslands underpinned the development of meat-eating, hunting, brain enlargement, fire use, food distribution, complex sociality, and even language (Potts, 2013). In this scenario, hominin environments were a passive agent and all that was required for human ancestors was to migrate into the open, drier environments. Once settled, adaptations such as bipedalism and tool use initiated the development of more-modern human behavior. Therefore, human traits evolved,

reinforced, and built upon previous adaptations creating a feedback mechanism for evolutionary change.

The discourse over the last decade surrounding the environmental impact on early human evolution however, asserts that grasslands were not the predominant habitat occupied by our ancestors, and that drier, open environments did not play a significant role in the emergence of certain evolutionary traits (Domínguez-Rodrigo, 2014). In fact, paleo-reconstructions show that the earliest, well-known bipedal hominins inhabited a mosaic environment with abundant tree coverage. For example, floral and faunal analyses and stable carbon isotope ratios in bone or soil carbonate (White et al., 2009a; White et al., 2009b; WoldeGabriel et al., 2009; WoldeGabriel et al., 2001; WoldeGabriel et al., 1994) demonstrate that *Ardipithecus* lived in a relatively wet and closed woodland/forest habitats. This is supported by bovid assemblages dominated by medium sized kudu fossils and abundant colobine monkey remains, both of which indicate the presence of a closed, wooded environment (WoldeGabriel et al., 1994). Furthermore, reconstructions indicate that both *Australopithecus anamensis* and *Au. afarensis* inhabited a mosaic environment and had access to a variety of habitats. Mammalian faunal analysis at Kanapoi (Kenya) suggest that *Au. anamensis* survived in a gallery forest along a river that supported a variety of primates, including galagos and colobines, which was surrounded by a fairly dry, open woodland or bushland landscape (Leakey et al., 1995).

The 1980s saw the focus on evolutionary change transfer to extrinsic factors as explanations for the environmental influence on key human features (Laporte and Zihlman, 1983), more than a decade before the above studies investigated the environments of early bipedal hominins. In opposition to the earlier intrinsic factors, the new paradigm generated the *Variability Selection Hypotheses* to examine changes initiated by the external environment. Studies proposed

that rapid increases in African aridity (deMenocal, 2004; Vrba, 1995a; Vrba, 1985, 2007), short-term climate variability (Potts, 1996, 1998b, 2013), and spatial unpredictability (Trauth et al., 2007; Trauth et al., 2010; Trauth et al., 2005) were responsible for human evolutionary change.

3.3.1 Habitat Specific Hypotheses

The most widely studied habitat specific hypothesis is the *Savanna Hypothesis*. Even Raymond Dart in as early as 1925 used the open savanna model to explain larger brains and bipedality in early *Homo*. The Savanna Hypothesis states that forest reduction and savanna expansion was a primary driver of hominin bipedalism because it was thought that these two trends occurred at about the same time (Lee-Thorp and Sponheimer 2007: 299). According to this hypothesis, adaptation to drier and increasingly open environments was the hallmark of hominin evolution from the late Miocene through the early Pleistocene. Savannas were believed to have driven natural selection in human evolution.

Coppens (1994) suggested that it was the formation of the EARS and separation of equatorial Africa into two distinct ecological regions (wet, forested west vs. dry, open east) that divided the common ancestor of *Homo* and *Pan* apart. Dubbed the *East Side Story* theory, Coppens posited that the western descendants of the last common ancestor continued evolving in a humid, arboreal setting eventually becoming *Pan*, while the eastern descendants of the same common ancestor had to “invent” new adaptations to life in open savanna ecosystems, thus becoming hominins. Coppens argued that the evolution of the australopithecines and *Homo* was driven by tectonic activity along the EARS that opened the landscape, and that bipedalism and an opportunistic diet developed as the most advantageous adaptations to this unfamiliar environment.

Over the last two decades the Savanna Hypothesis has become less popular due in large part to the older dating of the evolution of bipedalism in species like *Sahelanthropus tchadensis* dated to 7.0-6.0 Ma (Brunet et al., 2002; Vignaud et al., 2002), *Orrorin tugenensis* at 6.5-5.8 Ma (Pickford, 1975; Pickford and Senut, 2001b), and *Ardipithecus ramidus/kadabba* from 5.8-5.5 Ma (Haile-Selassie et al., 2004). In addition, even though paleoenvironmental reconstructions show that grasslands were a component at each of the *Sahelanthropus*, *Orrorin*, and *Ardipithecus* sites, they did not dominate over any other ecological zone. Studies (Boisserie et al., 2005; Le Fur et al., 2009, 2014; Vignaud et al., 2002) suggest that a mosaic of environments existed at the hominin bearing Toros-Menalla site 266 (TM 266) in Chad where *Sahelanthropus* was discovered. The paleolandscape was ecologically diversified, and composed of permanent aquatic habitats, as attested by the high abundance of semi-aquatic mammals (Boisserie et al. 2005; Le Fur et al., 2009) and abundant remains of freshwater fish, crocodiles, and turtles (Vignaud et al. 2002). Primate fossils (attributed to Colobinae) suggest that dense to moderately- dense woodlands or gallery forests with trees and bushes (Le Fur et al., 2009; Vignaud et al. 2002) were juxtaposed to wooded savanna, as demonstrated by the moderate abundance of browsers (such as proboscideans and giraffids) (Vignaud et al., 2002), and open grasslands, expressed in bovid remains (Vignaud et al., 2002). Interspersing these settings were both humid zones (floodplains and swamps) and dry areas.

Paleoenvironmental studies (White et al., 2009a; White et al., 2009b; WoldeGabriel et al., 2009; WoldeGabriel et al., 2001; WoldeGabriel et al., 1994) of *Ardipithecus kadabba* and *Ar. ramidus* sites present relatively humid and closed woodland/forest habitats with 20-45% grass biomass. Furthermore, the multiproxy approach taken by WoldeGabriel et al. (2009) suggests that the Middle Awash *Ardipithecus*-bearing locality was a former floodplain that supported a wooded

“biotope” rather than a grassland savanna. Using paleosols isotope data from Aramis, another *Ardipithecus* bearing site, Cerling et al., (2010) revealed a high abundance of grasses with only 5-25% tree cover, a landscape which they refer to as a tree- or bush-savanna, with less woody canopy cover.

As detailed environmental data reveal more information on the ecological conditions in which human evolutionary traits emerged, revisions to the Savanna Hypothesis have also materialized (Domínguez-Rodrigo, 2014). First and foremost is the definition of “savanna”: at times it is associated with mosaic environments with a strong wooded component (Cerling et al., 2010; Cerling et al., 2011; White et al., 2009a), whereas others simply use it synonymously with grassland (White et al., 2009b; White et al., 1994).

The discovery of ≥ 3.7 Ma hominins (*S. tchadensis*, *O. tugenensis*, *Ardipithecus*, and *Au. anamnesis*) living in woodland mosaics questions the open-landscape version of the Savanna Hypothesis. The *Forest Hypothesis* on the other hand, alleges that selective pressures associated with densely vegetated environments played a key role in the evolution of bipedalism (Potts, 1998a), as Late Miocene-Pliocene hominin species appear to have lived in varied settings. The available paleoenvironmental data from 7.0-3.7 Ma suggests that early hominins were attracted to closed habitats and exploited resources from their mosaic surroundings. Heterogeneity of vegetation is difficult to identify in the archaeological or paleontological record, but it is likely that differing hydrological conditions, topographic barriers, and volcanism resulted in a patchy network of wooded habitat that was essential to the development of complex hominin foraging strategies.

Multiyear studies document foraging-based tool making and use by wild chimpanzee populations throughout Central and West African forests (Boesch and Boesch, 1990, 2000; Hernandez-Aguilar, 2009). Observations on a population living in a 27 km² home range in western

Tai National Park, Côte d'Ivoire documented tools used for ant-dipping, killing of wood-boring bees and nest probing with sticks, honey-fishing, eating of bone marrow, brain, and cleaning of eye orbits, and nut-cracking. The Tai chimpanzees show the highest known incidence of hunting and tool use among any wild chimpanzee populations (Boesch and Boesch, 2000), and Boesch-Achermann and Boesch (1994) argue that key hominin traits – tool use, hunting, social cooperation, and food sharing – manifest more often in forested-adapted chimpanzees than those in open environments. These discoveries prompted Boesch and Boesch to suggest that woodlands or forests provided the initial setting in which hominins evolved.

As previously mentioned, paleoenvironmental reconstructions indicate that both *Au. anamensis* and *Au. afarensis* inhabited a mosaic environment and had access to a variety of habitats. Mammalian faunal analysis at Kanapoi (Kenya) suggest that *Au. anamensis* lived in a gallery forest along a river surrounded by a fairly dry, open woodland or bushland landscape (Leakey et al., 1995), while evidence from Hadar suggests that *Au. afarensis* accessed a mixture of dry bushland and riparian woodland on a seasonal floodplain along riverine forest habitats (Johanson et al., 1982). Additionally, data from Laetoli propose that *Au. afarensis* lived in an open grassland near a densely wooded environment (Andrews, 1989), and in South Africa, fossil pollen from Makapansgat suggests that *Au. africanus* inhabited settings resembling that of a tropical forest (Rayner et al., 1993).

Finally, Cavallo and Blumenschine (1989), using evidence from modern seasonal scavenging opportunities in riparian woodlands in the Serengeti, propose that toolmakers exploiting meat and marrow preferentially took advantage of wooded zones within the savanna mosaic of East Africa. Sikes (1994) then reconstructed hominin environments in lower Olduvai Bed II at ~1.74 Ma, showing that artifacts were abandoned in a riparian forest adjacent to grassy

woodland. However, Cerling et al., (2011) attempted to redevelop the Savanna Hypothesis by widening its foundation to incorporate the “savanna mosaic” as an ecological component that influenced human evolution. This is interesting in that it changes the fundamental principle of the hypothesis by saying that human traits evolved with a diverse, variable landscape as opposed to a relatively open grassland.

Habitat Specific Hypotheses see adaptations as responses to the constant challenges imposed by a change from one specific habitat to another. Alternate explanations postulate that important adaptive changes arise in response to climate and environmental variation.

3.3.2 *Variability Hypotheses*

Laporte and Zihlman (1983) initially argued for the impact environmental change had on driving early human evolution. They proposed that adaptive changes appearing in the Plio-Pleistocene represented responses to both changing environments caused by global cooling or orogeny, or new habitats in which hominins migrated. Vrba (1985) expanded upon these ideas by introducing the *Turnover Pulse Hypothesis*, which posits that rapid speciation and extinction events (turnover) are the result of environmental change.

The Turnover Pulse Hypothesis (TPH) stresses that species turnover and the emergence of new adaptations were concentrated during periods of heightened aridity and the expansion of open habitats (Vrba, 1985). It focuses on species’ surroundings and on the dynamic relationships between physical change, habitats, and species, and that speciation follows rare, large *pulses* in response to major environmental changes. Synchronous change in African bovids, micromammals, and hominins (Vrba, 1995a; Wesselman, 1995) are attributed to a shift from warm, moist conditions to cooler, drier, and more open habitat due to intense global cooling that

led to pulses of aridification in Africa. Therefore, this hypothesis strongly links hominin evolution with global climatic events; the origins of *Homo* and of the robust australopithecines around 2.5 Ma were considered part of a turnover pulse, as this pulse coincides with the 2.7-2.5 Ma Northern Hemisphere glacial intensification and closing of the Isthmus of Panama. Vrba et al. (1989) advocated that another turnover pulse coincided with the “Mid-Pleistocene Revolution” at 0.9 Ma, and that this event was responsible for the dispersal of *H. erectus* into Eurasia. (They also suggested that this pulse was responsible for the extinction of *Paranthropus boisei*, but subsequent fossil discoveries proved this to not be the case.)

The TPH has been modified over the years, first by broadening the range of pulse events to encompass timeframes as large as 400,000 years (Vrba, 1995b), and second by suggesting that specialized organisms should experience turnover first, followed later by more-generalized organisms (Vrba, 1995c). Recent treatises (Vrba, 2007) on the TPH also broaden the hypothesis by stating that environmental changes that trigger turnover are diverse and vary in nature, intensity, timing (how long they endure), amount of fluctuation, degree of changes, and geographic extent (localized to global). In this regard, it is difficult to pinpoint what can be considered a “pulse”.

Behrensmeyer et al. (1997) tested the Turnover Pulse Hypothesis at the Turkana-Omo basin, a locale containing a fossil mammal assemblage spanning the Plio-Pleistocene transition as well as the Gelasian and Early Pleistocene periods (i.e. 3.0 to 1.8 Ma). This study found no statistically significant pulse in either first or last appearances between 2.8 and 2.5 Ma and instead showed that mammalian lineages displayed a prolonged period of turnover up until 1.8 Ma. The authors argued that (what is now predominately the case in all recent paleoanthropological literature) a complex mosaic landscape coupled with global climate fluctuations over hundreds of

thousands of years explain both the persistence of more-generalized organisms as well as prolonged periods of turnover.

Bibi and Kiessling (2015) analyzed eastern African Bovidae (antelopes) and Turkana Basin large mammal fossil databases assembled from the Turkana Public Database and the International Omo Research Expedition and Omo Group Research Expedition databases to test the TPH for a period between 3.75 Ma and 1.25 Ma. Their results indicate that speciation and extinction proceeded continuously throughout the Plio-Pleistocene, as did increases in the relative abundance of arid-adapted bovids, thereby contesting the Turnover Pulse Hypothesis. The authors did note however that there was a single pulse present at 2.0 - 1.75 Ma, but other than this, found no evidence for rapid evolutionary or ecological changes in the East African record. Bibi and Kiessling's analyses suggest that African large mammal evolution tracked global climatic trends over millions of years, with local, Turkana Basin-scale changes (e.g., tectonic or hydrographic) influencing at shorter timescales.

Important adaptive changes may arise in response to environmental variation in both the short-term or long-term (Potts, 1998a). Short-term variations are those experienced by an organism over its lifetime, whether it is seasonal fluctuations or enduring climate trends. Long-term variations play a critical role in the adaptive processes of a population over generational timeframes. The long-term, or *Variability Selection Hypothesis* (VSH) predicts that new adaptations originate during periods of heightened environmental variability, whether due to climate or other factors (Potts 1996). In this model, adaptability refers to an organism's ability to adjust to changes in its surroundings and the ability to inhabit a wide diversity of environments. In a general sense, the VSH argues that environmental instability is a main factor of selection among hominin responses to variable habitats, and that climate-driven habitat fluctuations caused habitat-

specific adaptations to be replaced by morphological and behavioral adaptations to complex environmental changes.

The VSH seeks to explain how the ability of an organism to adjust to change in its surroundings, to inhabit a wide diversity of environments, and to interact with its surroundings in novel ways may evolve (Potts, 2012b). Interestingly, at its essence, the VSH attempts to explain the basic principles of evolutionary theory within an environmental framework by stating that adaptable phenotypes are favored over habitat-specific adaptations. Similar to the TPH, Variability Selection has been modified over time to include factors such as gene pools and thus the genetic basis for adaptable phenotypes (Potts, 2013). Furthermore, VSH emphasizes the role of landscape remodeling, changes in vegetation and animal communities, and regional hydrological fluctuations as drivers of selective adaptations; ideas which are applicable to the evolutionary history of all species.

The Variability Selection Hypothesis fits well within the complex intersection of orbitally forced changes in insolation and feedback mechanisms described above. As orbital forcing and differing controls on regional climate produce extreme environmental variability, behavioral and morphological mechanisms that enhance adaptive fitness are therefore selected. Moreover, there is compelling evidence for the preferential evolution of hominins during periods of highly variable East African climate between very dry to very wet conditions from 5.0 and 0.5 Ma (Maslin et al., 2013; Trauth et al., 2005).

Maslin and Trauth (2009) present an update on the Variability Hypothesis through their *Pulsed Climate Variability Hypothesis*. From updated paleoclimate records (Garcin et al., 2009; Garcin et al., 2006; Kingston et al., 2007), they propose that precession-forced lake-level changes in the East African Rift Valley and ocean-derived wind-borne dust records signify that the long-

term drying trend in East Africa was punctuated by short episodes of both extreme humidity and aridity. They attribute these short punctuations (which coincide with Northern Hemisphere Glaciation (2.7-2.5 Ma), the development of the Walker circulation (1.9-1.7 Ma), and the Mid-Pleistocene Revolution (1.1-0.9 Ma)), to the compression of the Intertropical Convergence Zone; consequently, East Africa becomes more susceptible to precessional forcing, resulting in rapid shifts from wet to dry conditions. Building on The Variability Selection Hypothesis, Trauth and Maslin suggest that pulsed climate periods provided a catalyst for evolutionary change and drove key speciation and dispersal events amongst mammals and hominins in Africa.

3.4 Chapter 3 Summary

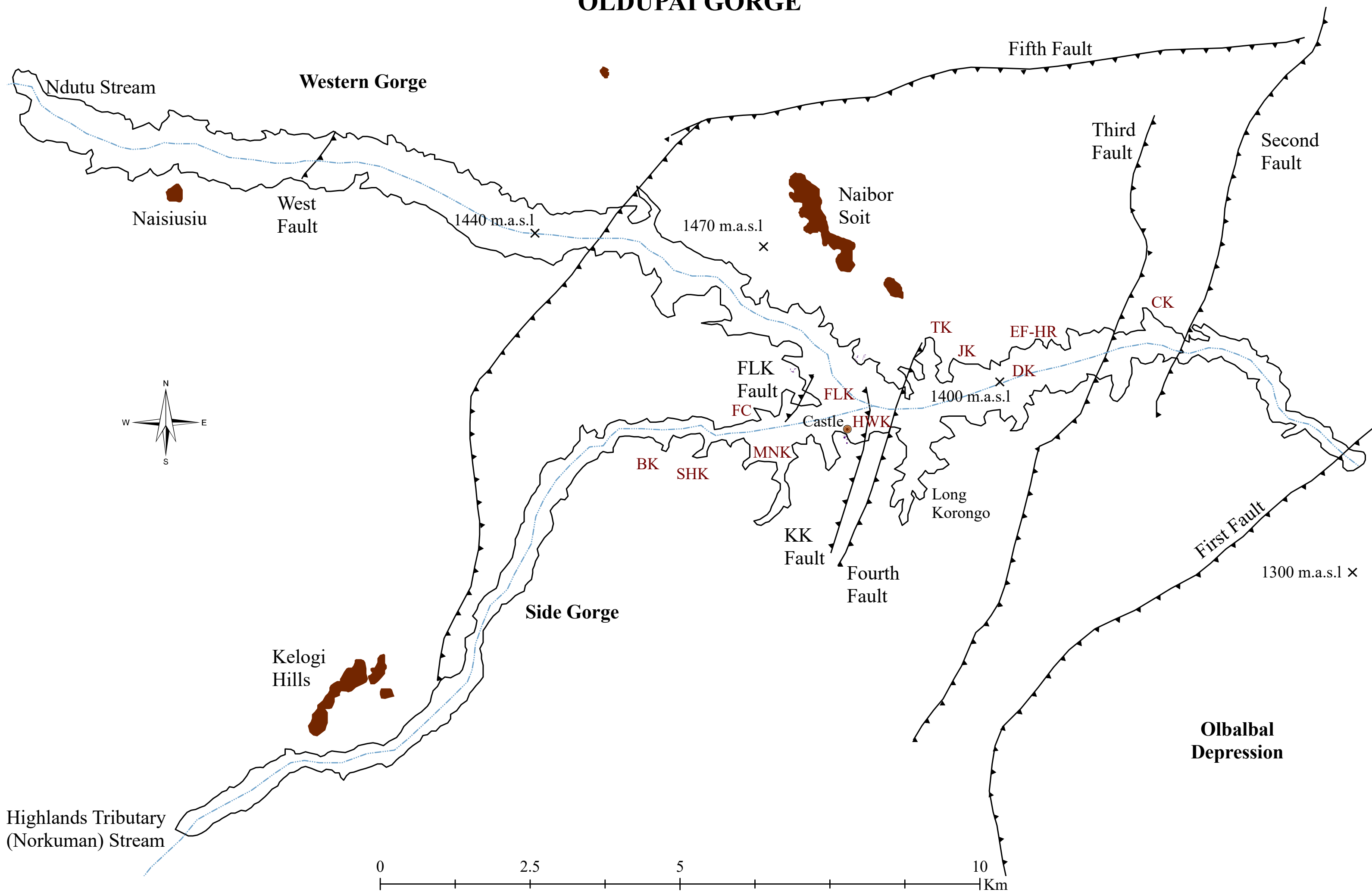
Multiple hypotheses have been advanced linking climate change and human evolution and the environmental context of early human biological and technological adaptations in Africa. Our understanding of these hypotheses results from studies on the controlling factors of climate and environment in East Africa such as global mechanisms like orbital forcing (Milankovitch Cycles) and northern hemisphere glaciation, and regional processes like tectonic uplift and moisture-aridity cycles related to monsoon weather patterns. Both global and regional controls impact precipitation patterns and thus the available water to both plants and animals, including early humans. For example, global and regional climatic systems influenced the extent of paleo-Lake Olduvai and the amount of freshwater flowing from the highlands into the Olduvai basin. In addition, early explanations of human evolution focused on intrinsic stimuli, but in recent decades, the discourse has changed in favor of extrinsic impetuses setting the stage for the development of specific hominin characteristics. This led to the development of both habitat specific and variability hypotheses such as the Turnover Pulse and Variability Selection hypotheses.

CHAPTER 4: OLDUVAI GORGE

4.1 Introduction

Olduvai Gorge, the UNESCO World Heritage site in northern Tanzania ($2^{\circ}59'46.87''\text{S}$, $35^{\circ}21'7.50''\text{E}$), has one of the most continuous paleoanthropological records in the world, exceptional archaeological site preservation due to a low-energy sedimentary environment, and a timeframe of human evolution that spans the transition from the Oldowan to the Later Stone Age. Located on the western flank of the Gregory Rift in Tanzania's Ngorongoro Conservation Area, Olduvai is situated between the volcanic Crater Highlands to the south and east, metamorphic topographic complexes to the north, and the celebrated Serengeti Plain in the west. Although Olduvai is best known for its paleontological and archaeological record, it also contains well-defined sedimentological strata (Beds I-IV ($2.038 \pm 0.005 - 0.6$ Ma), Masek (600,000 - 400,000), Ndutu (400,000 - 32,000), and Naisiusiu ($17,550 \pm 1,000 - 10,400 \pm 600$ BP) (Deino, 2012; Diez-Martín et al., 2015; Domínguez-Rodrigo et al., 2013; Hay, 1976; Leakey, 1971), that help situate two million years of evolutionary and technological history. Today, the primary branch of the gorge, the Main Gorge, has its origin in Lakes Masek and Ndutu, while the southern branch, named the Side Gorge, originates on the western slopes of Lemagrut volcano (Fig. 4-1). Both the intermittent Ndutu and Highlands Tributary (or Norkuman) Streams, originating in Lakes Masek and Ndutu, and the slopes of Lemagrut, respectively, have exposed the Pleistocene-to-Holocene aged beds through erosional downcutting over the last $\sim 400,000$ years. The Ndutu Stream flows roughly 40 km eastward from its source lakes in the west before connecting with the ~ 30 km long Highlands Tributary Stream at Olduvai's main confluence, whereby the two combined intermittent waterways continue for another 10 km before emptying into the Olbalbal Depression. This fault

OLDUPAIGORGE



graben depression acts as the base level for surface waters draining the northwest slopes of the Crater Highlands and the eastern Serengeti Plain (Herlocker and Dirschl, 1972). Furthermore, Pickering, who first geologically mapped Olduvai, used Olbalbal as a modern example of the type of lake basin in which Beds II and IV were deposited (Pickering, 1960).

In 1931, Louis and Frida Leakey led the Third East African Archaeological Expedition to Olduvai Gorge, accompanied by German geologist Hans Reck, who previously worked in the gorge prior to World War I and discovered a human skeleton (Olduvai Hominid 1) (Tobias, 2003). Soon after their arrival at Olduvai³ an Acheulean handaxe was recovered by one of their African workers, thus proving that Olduvai was a “unique showcase not only of animal fossils, but also of tool forms and associated human occupation sites over a period of a million and a half years or more” (Leakey, 1974: 13). This handaxe was the forerunner to the thousands of stone tools that would be excavated in the Gorge over the next 85 years and would help Leakey establish a preliminary cultural sequence he named the *Chellean* (which would later be subsumed into the Acheulean). Leakey would go on to designate one of the richest fossil and stone tool assemblages in the gorge “Frida Leakey Korongo” (FLK); *korongo* being the Swahili word for “gully.” Coincidentally, in 1959, Leakey’s second wife Mary would find the remains of *Zinjanthropus* (*Paranthropus boisei*) at the FLK site, a discovery that would significantly alter the research history of the gorge; following the find, Louis and Mary entered into a long-standing arrangement with the National Geographic Society, in which their research was supported through salaries and the supplying of field equipment. After nearly thirty years of field work in Kenya and Tanzania, the importance of *Zinj* “...convinced the National Geographic Society in the United States that

³ Exaggerated reports claim that within a half hour of arrival at Olduvai, the Acheulean hand axe was found. However, Philip Tobias, a long-time friend of Louis Leakey, said that in reality, “Leakey won a small wager with Reck when, within 24 hours of arriving at Olduvai, one of the Kikuyu team-members found a fine hand-axe. Soon after, one was found in situ” (Tobias, 2003).

Louis and [Mary] and Olduvai were worth financial support on a scale that exceeded [their] wildest dreams, starting with \$20,200 in 1960.” (Leakey, 1984: 122). In fact, the discoveries at Olduvai Gorge had perhaps the most important impact in the 20th century on the theories of human evolution; for example, the discovery of *Zinjanthropus* in 1959 (Leakey, 1959) was a defining moment in the history of paleontology as it vindicated Louis Leakey’s decision to work in East Africa, and was the specimen that convinced people that East Africa was a sensible place to look for the earliest evidence of human ancestry (Gibbons, 2006: 25).

4.2 Stratigraphic Summary of the Olduvai Beds

The monograph *Geology of the Olduvai Gorge* by Richard Hay (1976) lay the groundwork for the current understanding of the geology of Olduvai Gorge. Hay defined seven geological bed formations within the gorge adopting Reck’s nomenclature for Beds I-IV while replacing Beds V and VA with the Ndutu and Naisiusiu Beds, respectively (Table 4-1). The sequence of the seven beds exposed in Olduvai Gorge is as much as 100 m thick, with Bed I being the thickest of the major subdivisions. In the eastern part of the Main Gorge, Bed I can be up to 60 m thick and consists of basaltic lavas overlain by lacustrine and alluvial sedimentary deposits. In the Western Gorge, it is less-exposed at a maximum of 43 m, and to the southwest near the Kelogi inselbergs (Fig. 4-1), it thins towards the Laetoli Beds. Bed I lavas, tuffs, and claystones are also exposed in the Fifth Fault about 5.0 km north of the Main Gorge and south of Engelosin. Bed I is dated to between 2.005 ± 0.007 Ma and 1.803 ± 0.002 Ma (Deino, 2012), and six tuffs provide the principal basis for correlations; Tuffs IA-IF. However, below Bed I lies the pyroclastic Naabi Ignimbrite, the oldest known stratigraphic unit at Olduvai, which is dated to 2.038 ± 0.005 Ma. Additionally, the lowermost dated unit in Bed I is a ~30 cm thick tuff exposed west of the Fifth Fault in the Main

Table 4-1. Olduvai Gorge geochronology with selected archaeological sites.

Epoch	Stratigraphy	Subdivisions	Markers	Marker Dates	Sites	
Holocene			Namorod Ash	1,250 BP		
Pleistocene	Naisiusiu Beds		Tuff XXX			
	Ndutu Beds	Upper Unit	Tuff XXX			
		Lower Unit	Tuff XXX			
	Masek Beds	Norkilili Member				
		Lower Unit	Tuff XXX Tuff XXX			
	Bed IV		Tuff IVB Tuff IVA			
	Bed III		Tuff 4 Tuff 3 Tuff 2 Tuff 1	1.33 ± 0.06 Ma	JK, WK	
	Bed II	Upper Bed II	Tuff IID Tuff IIC	1.48 ± 0.05 Ma and 1.338 ± 0.024 Ma	BK, JK, PLK, TK	
		Middle Bed II	Upper Augitic Sandstone Bird Print Tuff Middle Augitic Sandstone Tuff IIB		CK, EFHR, SHK	
			Upper Lemuta Tuff FLK W B	1.664 ± 0.019 Ma	MNK	
Lower Bed II		Lower Augitic Sandstone Tuff FLK W A Tuff IIA Lower Lemuta Twiglet Tuff	1.698 ± 0.015 Ma 1.74 ± 0.03 Ma	FLK West, HWK-EE		
Bed I	Upper Bed I	Tuff IF	1.803 ± 0.002 Ma	HWK		
		Tuffs between tuffs IE and IF	1.828 ± 0.005 Ma			
		Tuffs between tuffs IE and IF	1.836 ± 0.015 Ma			
		Tuffs between tuffs IE and IF	1.833 ± 0.005 Ma	FLK North		
		Tuffs between tuffs IE and IF	1.831 ± 0.006 Ma			
		Kidogo Tuff				
		Ng'eju Tuff	1.818 ± 0.006 Ma			
	Tuff IE	1.831 ± 0.004 Ma				
	Tuff IE Vitric	1.837 ± 0.006 Ma				
	Tuff ID (Plagioclase)	1.854 ± 0.011* Ma				
	Tuff IC	1.832 ± 0.003 Ma and 1.848 ± 0.008* Ma	FLK Level 22, PTK, DS			
	Chapati Tuff					
	Tuff IB	1.848 ± 0.003 Ma				
	Bed I Lavas	1.911 ± 0.016 Ma and 1.891 ± 0.010 Ma	DK Levels 1-3, FLK NN			
Lower Bed I	Tuff above IA	2.060 ± 0.018* Ma				
	Mafic Tuff					
	Tuff IA	1.88 ± 0.05 Ma				
	Coarse Feldspar Crystal Tuff	2.015 ± 0.006 Ma				
	Tuff between NI and CFCT	2.005 ± 0.007 Ma				
		Naabi Ignimbrite	2.038 ± 0.005 Ma			

Dates from Deino, 2012; Diez-Martín et al., 2015; Domínguez-Rodrigo et al., 2013; Hay, 1976; Leakey et al., 1972; Manega (1993)

*Provisional according to Deino, 2012

Red indicates uncertainty as to stratigraphic position, nomenclature, and age

Gorge and is dated to 2.005 ± 0.007 Ma (Deino, 2012). As for the six marker tuffs, IA (1.88 ± 0.05 Ma) is only located west of the Fifth Fault, IB (1.848 ± 0.003 Ma) is found near the Second Fault and west of the Fifth Fault, IC (1.832 ± 0.003 Ma) is fluvially reworked in the east, but represented in the west, at the FLK complex, and near the confluence of the Main and Side Gorges, ID (1.854 ± 0.011 Ma) is exposed at the FLK complex and to the west of the Fifth Fault, IE (1.831 ± 0.004 Ma) in the eastern part of the Main Gorge, and IF (1.803 ± 0.002 Ma), which is widespread and the most recognizable stratigraphic marker found throughout much of the Olduvai Basin from FLK to Kelogi, and near to and west of the Fifth Fault (Deino, 2012; Hay, 1976).

Bed II is 20-30 m thick and divided into two deposits below and above a regional disconformity (named the Lower Disconformity by Hay (1976); below the disconformity, deposits have many similarities with Bed I, while those overlying are unique within the Olduvai sequence (Hay, 1976). Moreover, above the Lower Disconformity faunal remains suggest open, wooded grassland and fluvial-lacustrine and fluvial deposits, counter to the lake, lake-margin, alluvial-fan, and eolian deposits below. Bed II is widespread and can be observed on the southwestern margin of Olbalbal, much of the eastern gorge, 5.0 km north of the Main Gorge in the Fifth Fault, and 6.0 km into the Side Gorge. Located just below the disconformity is the Lemuta Member, a widespread, distinctive sequence of eolian tuffs comprised of reworked tephra mixed with minor limestone and claystone components that reflect a relatively dry episode that lasted at least 20,000 years (Hay, 1976). Tuff IIA (1.74 ± 0.03 Ma) is found within the lower section of the Lemuta Member, while Tuff IIB (no firm date but <1.66 Ma) caps it and marks the start of Middle Bed II (Stanistreet, 2012). Tuffs IIC and IID, the two other principal Bed II marker tuffs, are typically reworked and discontinuous, and not easily recognizable. Dating for Tuff IIC has been problematic but it is younger than 1.66 ± 0.01 Ma (McHenry and Stanistreet, 2018), while Tuff IID has been

recently dated to 1.338 ± 0.024 (Domínguez-Rodrigo et al., 2013). Overall, the stratigraphy of Bed II is complex, and correlation is difficult but, it is in Bed II that the transition from the Oldowan to the Acheulean is documented.

Other marker deposits located within Bed II are the Lower, Middle, and Upper Augitic Sandstones and the Bird Print Tuff (BPT). After the deposition of Tuff IIA and the Lemuta Member, a depressed graben formed between the FLK and Fifth Faults, forming the Lower Disconformity (Uribelarrea et al., 2017). The Lower Augitic Sandstone (LAS) unit is deposited on top of this disconformity in eastern fluvial lacustrine deposits flowing towards the lake in the northwest. The MAS can be found near Vivian Evelyn Korongo (VEK) on the south side of the Main Gorge, and from Juma's Korongo (JK) west to between the Fourth and KK Faults, while the UAS forms a continuous deposit in the Side Gorge as far west as Sam Howard Korongo (SHK) (Hay, 1976). The augitic grains of the sandstones indicate a fundamental change in the pyroclastic origin of volcanic rock fragments arriving in the Olduvai Basin (Stanistreet, 2012).

The Bird Print Tuff is a 2.5 to 12 cm thick yellow laminated, fine- to medium-grained tuff exposed in outcrops between FLK North North and Henrietta Wilfrida Korongo (HWK) that is also found west of the Fifth Fault in the Western Gorge at Richard Hay Cliff and Mary Nicol Korongo (MNK) in the Side Gorge (Hay, 1976; McHenry et al., 2016). This pyroclastic tuff is characterized by fragmented bits of glass and is always situated above the LAS. The BPT is named for the presumably abundant trace fossils of shore bird footprints preserved in the tuff (Hay, 1976); this feature, along with its mineral composition, makes it one of the most easily identifiable marker tuffs in the gorge.

A widespread episode of faulting affected the Olduvai basin around 1.33 Ma., causing erosion of Bed II and a change in the topography; Beds III and IV were deposited on this new

terrain (Hay, 1976). Beds III and IV are only distinguishable in the eastern part of the basin, specifically at JK, and west of the Fifth Fault where the contact with Bed II is generally sharp. Bed III is 4.5 to 11 m thick and Bed IV is 2.4 to 10 m thick (Hay, 1976), but dating for these beds have been problematic; Tuff IID is dated to 1.338 ± 0.024 (Domínguez-Rodrigo et al., 2013), while Tuff IIIA, also designated Tuff 1 of Bed III, was given an age of 1.33 ± 0.06 Ma (Manega, 1993). Bed III is a reddish-brown deposit that is easily identifiable when it is exposed (Fig. 4-2), and consists of four marker tuffs of which only Tuff 1 is dated. Tuff 2 is 15 to 30 cm thick and lies 1.5 to 2.4 m above the base of Bed III, Tuff 3 is 30 to 45 cm thick and about 2.6 m below the top of Bed III, and Tuff 4 is 30 to 60 cm thick and only 1.2 to 1.5 m below the top of Bed III (Hay, 1976). Bed IV varies in thickness from 2.4 to 7.3 m in the Main Gorge but up to 10 m in the Side Gorge; this variation is due to fault movements during the deposition of the bed. Only two tuffs are identified in Bed IV, IVA and IVB, but these have not been dated radiometrically. However, based on sedimentation rates and using the Matuyama-Brunhes polarity chron boundary, the contact between Beds III and IV is estimated at 800,000 years before the present while the top of Bed IV is about 600,000 years old (Hay, 1976).

The Masek Beds were the last deposited prior to the initial erosion of the gorge ~400,000 years ago. They have a maximum thickness of about 25 m and are found along the rim of the modern gorge. The Masek Beds are divided into two units that were laid down between 600,000 (contact with Bed IV) and 400,000 years ago; potassium-argon dating of volcanic rocks near the Kerimasi Volcano east of Olduvai, which provided the Masek tephra, was minimum age dated to 400,000 years ago. The Olduvai basin was an alluvial plain during the deposition of the Masek Beds, with drainage flowing into the depression between the First and Second Faults. The Ndutu Beds were deposited over stretches of faulting, erosion, and partial filling of the gorge (Hay, 1976:

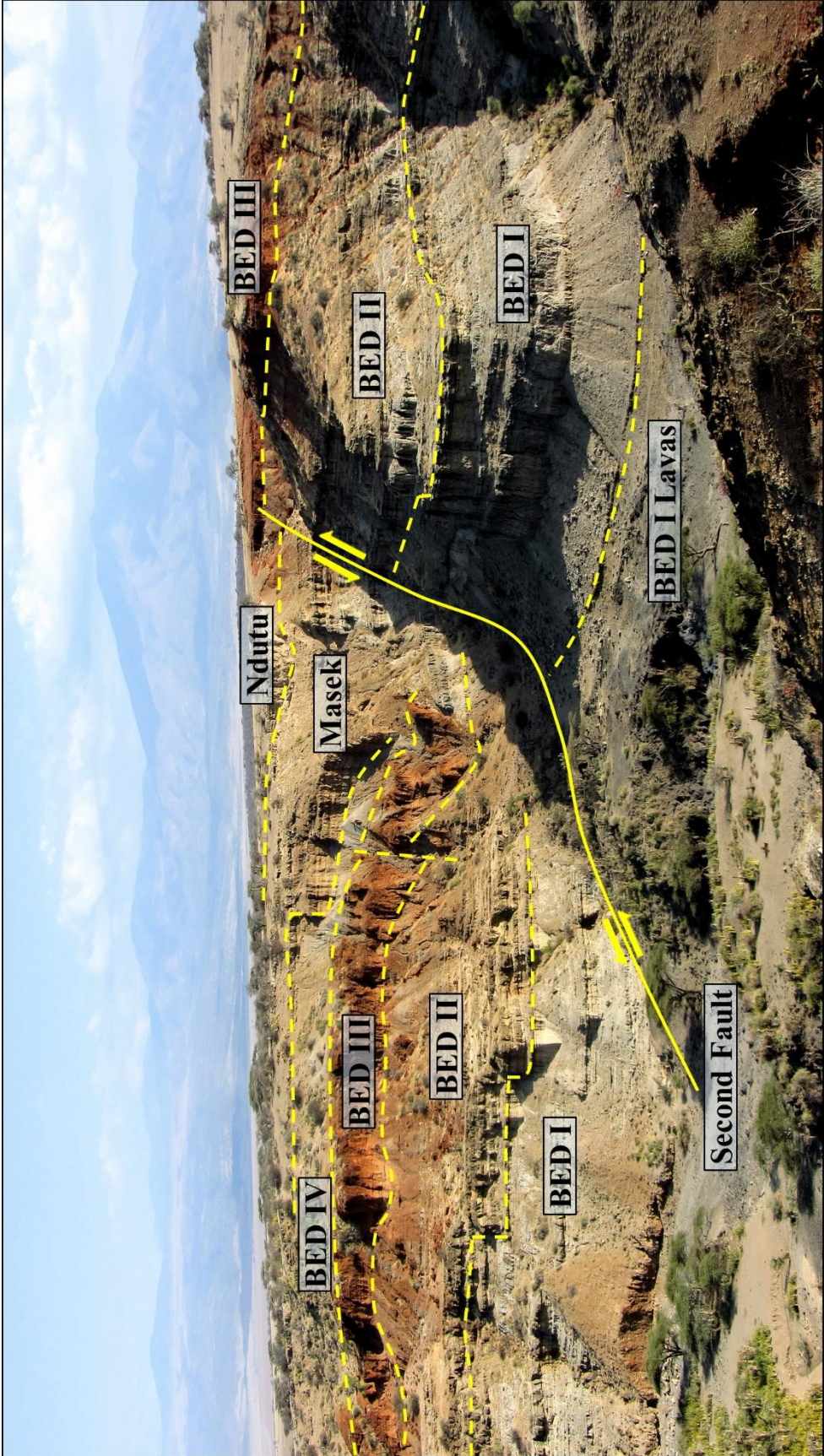


Figure 4-2. View of the Second Fault in the eastern part of the Main Gorge and the displacement of the Olduvai Beds due to normal faulting. On the left (hanging wall), all beds except for Naisiusiu are exposed, while on the right (foot wall), only the Bed I lavas and Beds I-III are still visible. Photo was taken on the northern rim of the gorge facing south. Mount Lemagrut is in the background.

146), during which the Olbalbal Depression became the drainage basin, as it remains today. The maximum thickness of Ndotu sediments in the Side Gorge is 12 m south of Kelogi, but there are thicker exposures east of the Second Fault of up to 14 m. The Ndotu Beds is separated into two units, the Lower and Upper dated to 400,000 to 60,000 and 60,000 to 32,000 years ago, respectively (Leakey et al., 1972). Deposition of the Ndotu Beds ended with a significant period of faulting that resulted in further subsidence of the Olbalbal Depression and increased fluvial erosion. Finally, the Naisiusiu Beds were deposited after the upper unit of the Ndotu Beds but have been largely eroded to its current maximum thickness of 1.0 to 3.0 m. These beds are primarily composed of eolian tuffs and dated between $17,550 \pm 1,000$ and $10,400 \pm 600$ BP (Leakey et al., 1972). Isolated artifacts of *Homo sapiens* are found 110 m west of the Second Fault on the northern rim of the gorge, in which the assemblage contains abundant microliths.

4.3 Chapter 4 Summary

Olduvai Gorge is world-renowned for its archaeological and paleoanthropological record, but also contains a ~100 m thick sedimentary beds exposed through erosional downcutting over the last 400,000 years. The Olduvai marker tuffs allow for well-defined dating of Beds I-IV (2.038 ± 0.005 - 0.6 Ma), Masek (600,000 - 400,000), Ndotu (400,000 - 32,000), and Naisiusiu ($17,550 \pm 1,000$ - $10,400 \pm 600$ BP). This helps situate specific archaeological sites and their relative positioning with one another in each bed. Due to erosion and faulting, the beds are disproportionally exposed throughout the gorge; Bed I can be up to 60 m thick and is best represented in the eastern part of the Main Gorge, while in the Western and Southern parts of the gorge, it is less-exposed at a maximum of 43 m; Bed II is 20-30 m thick and can be observed on the southwestern margin of Olbalbal, much of the eastern gorge, and in the Fifth Fault north of the

Main Gorge; Beds III and IV are only distinguishable in the eastern part of the basin, specifically at Juma's Korongo, and west of the Fifth Fault where the contact with Bed II is generally sharp, with Bed III being 4.5 to 11 m thick while Bed IV varies in thickness from 2.4 to 7.3 m in the Main Gorge but up to 10 m in the Side Gorge; the Masek Beds have a maximum thickness of about 25 m and are found along the rim of the modern gorge; in the Side Gorge, the Ndotu sediments are about 12 m thick, but exposures east of the Second Fault are up to 14 m; Finally, the Naisiusiu Beds have been largely eroded to its current maximum thickness of 1.0 to 3.0 m.

CHAPTER 5: PLANT LEAF WAX LIPID MARKER MOLECULES

5.1 Leaf Wax Lipid Biomarkers

Biologically specific marker molecules, or *biomarkers*, diagnostic of a terrestrial plants are powerful tools for understanding paleoenvironmental processes and the climatic context in which they originated (Castañeda and Schouten, 2011; Eglinton and Eglinton, 2008; Sachse et al., 2012). The external surface of vascular plant leaves and other aerial parts are coated with protective waxes that contain a wide range of organic compounds (Eglinton and Hamilton, 1967). The cuticle, or the hydrophobic coating on the outer surface of leaves, is a layer of cutin and cutan composed of polymerized hydroxy (-OH) fatty acids and hydrocarbons (Fig. 5-1 & Table 5-1) that preserve the water balance of the plant and minimizes damage to leaf cells from fungal and insect attack, wind abrasion, and excessive ultraviolet radiation (Eglinton and Hamilton, 1967). The lipid components of the protective waxes are environmentally persistent and typically comprise of mixtures of long, straight-chain (i.e., normal, *n*-) alkanes, alkanols, alkanolic acid (Tables 5-2 and 5-3), as well as ketones, aldehydes, acetals, and esters (Eglinton and Hamilton, 1967). Strong covalent bonds fuse straight-chain hydrocarbons, making them, for the most part, chemically inert and resistant to biodegradation in sediments over geologic time and an excellent biomarker proxy measure of the continental vegetation that synthesized them (Eglinton and Eglinton, 2008). They pass into the environment as leaf debris and are often transported long distances by wind and water before the intact molecules are deposited.

Primarily, the leaf lipid components of terrestrial plants are described in terms of carbon-number range (e.g. C₂₅-C₃₅), or as the most abundant compound (C_{max}) in a series containing the same molecular formula but different carbon-carbon (C-C) chain lengths. For example, *n*-alkanes

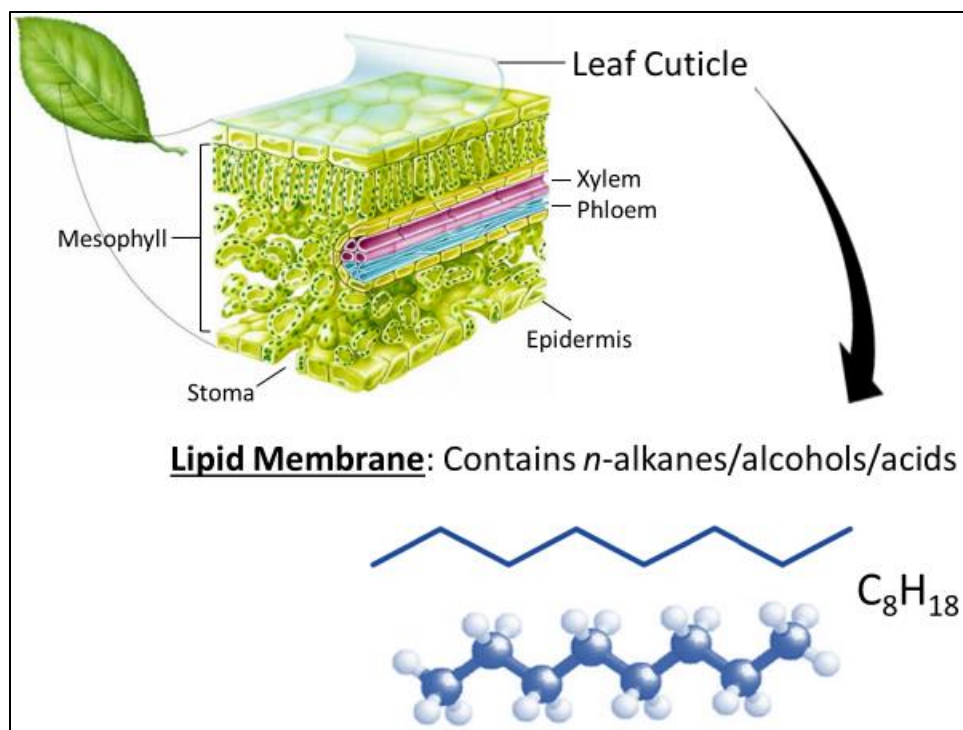
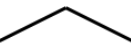


Figure 5-1. Schematic of leaf anatomy highlighting the location and makeup of the lipid membrane in leaf cuticles. The C_8H_{18} hydrocarbon chain is represented in two formats, with (bottom) and without (top) the hydrogen atoms represented. Leaf cross-section adapted from Graham et al., 2006 and Mauseth, 2009.

Table 5-1. Straight-chain leaf wax lipid biomarkers and their molecular and structural formulas.

Component	Molecular Formula	Structural Formula	Structure
<i>n</i> -alkane	C_nH_{2n+2}	$CH_3(CH_2)_nCH_3$	H_3C  CH_3
<i>n</i> -alkanol	$C_nH_{2n+1}OH$	$CH_3(CH_2)_nCH_2OH$	H_3C  OH
<i>n</i> -alkanoic acid	$C_nH_{2n+1}COOH$	$CH_3(CH_2)_nCO_2H$	H_3C  $COOH$

have the molecular formula C_nH_{2n+2} (Table 5-1), whereby $C_{27}H_{56}$ (C_{27}) and $C_{29}H_{60}$ (C_{29}) are homologues with the same formula that differ in the number of repeating carbon units they contain; often, molecular studies use the most abundant homologue for analysis (e.g. Schefuß et al., 2003; Tierney et al., 2008). Average chain length (ACL), carbon-number preference index (CPI), and the stable isotope values of individual homologues or their averages are ancillary techniques for describing the distribution of long-chain biomarker compounds (Eglinton and Eglinton, 2008). Additionally, the dominant chain lengths, carbon number distributions, and isotopic compositions of *n*-alkanes, *n*-alkanols, and *n*-alkanoic acids vary depending on the source of biosynthesis (Castañeda and Schouten, 2011).

The ubiquitous, well-preserved nature of lipid biomarkers, particularly in lacustrine sediments (Wang et al., 2014), allows for their distribution to differentiate between homologue series and sources of production (Castañeda and Schouten, 2011; Eglinton and Eglinton, 2008). Generally, short-chain homologues (C_{17} - C_{21} *n*-alkanes) characterize aquatic algae (Cranwell et al., 1987), mid-chain homologues (C_{21} - C_{25} *n*-alkanes) characterize submerged and floating aquatic macrophytes (Barnes and Barnes, 1978; Cranwell, 1984; Ficken et al., 2000), and long-chain homologues (C_{27} - C_{35} *n*-alkanes) characterize terrestrial vegetation (Eglinton and Hamilton, 1967). Furthermore, terrestrial plants generally contain a higher abundance of C_{26} - C_{32} *n*-alkanoic acids (Chikaraishi and Naraoka, 2007; Ficken et al., 2000; Gao et al., 2011), submerged and floating aquatic plants display a higher abundance of C_{20} - C_{24} *n*-acids (Ficken et al., 2000; Wang and Liu, 2012), while C_{14} - C_{18} *n*-acids derive from algae (Liu and Liu, 2017; Liu et al., 2018); however, submerged and terrestrial plants may also exhibit abundant C_{16} and C_{18} acid components (Huang et al., 2004; Huang et al., 2002), as they comprise the two major monomer families of cutin.

Some other notable exceptions have been observed amongst chain length and biosynthesis source. Sachse et al., (2006) found that the C₂₃ *n*-alkane, often attributed to submerged aquatic plants, is a significant component of leaf lipids in birch trees (genus *Betula*), while Aichner and colleagues (Aichner et al., 2010a; Aichner et al., 2010b) report that emergent macrophyte samples from Lake Koucha on the Tibetan Plateau contain abundant long-chain C₂₇ and C₂₉ *n*-alkanes. Regardless of chain length, many organisms exhibit strong odd-over-even carbon number predominance in *n*-alkanes, whereas the *n*-alkanols and *n*-alkanoic acids exhibit strong even-over-odd carbon number predominance (Fig. 5-2) (Castañeda and Schouten, 2011; Patalano et al., 2015; Yang and Leng, 2009).

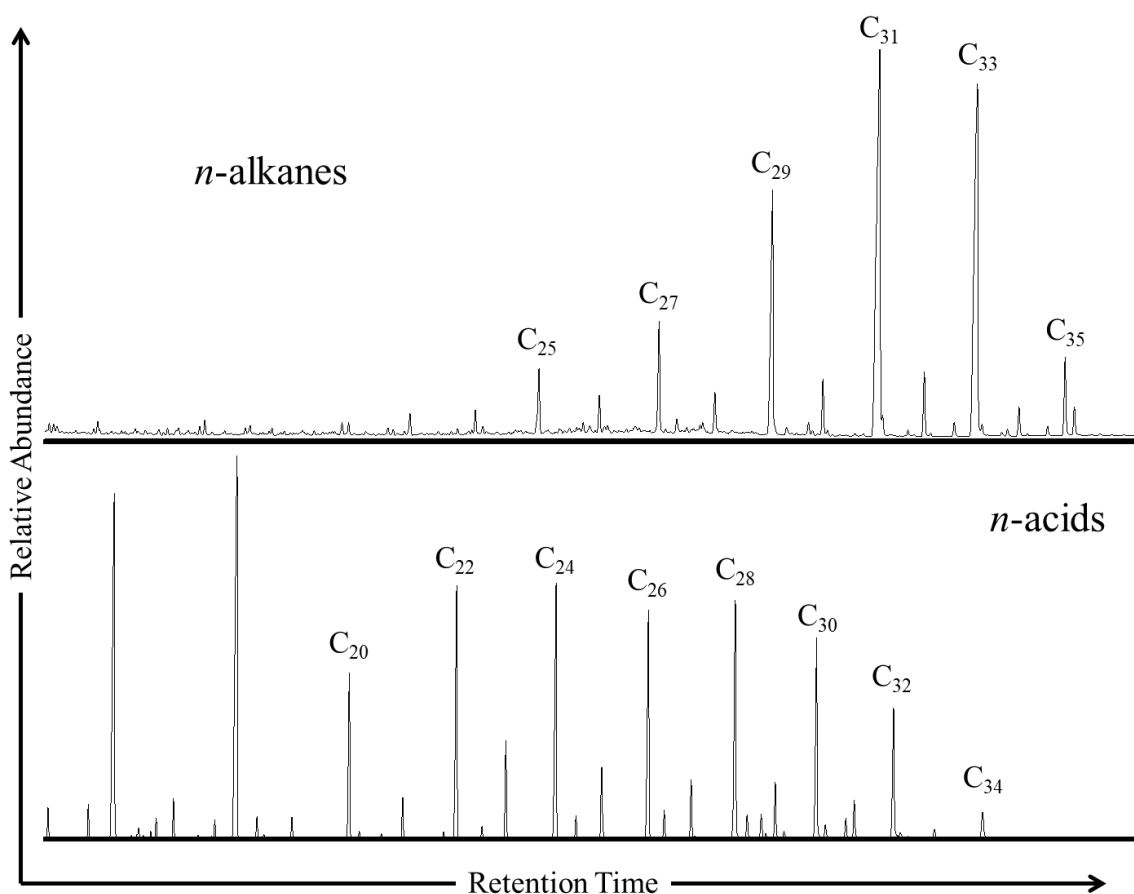


Figure 5-2. Typical GC-MS trace of *n*-alkane odd-over-even carbon chains (top) and *n*-alkanoic acid even-over-odd carbon chains (bottom) from a Castle Clay sample at Olduvai Gorge. Note the standard homologues for terrestrial vegetation (e.g. grasses) in the *n*-alkane signature, but the extensive range of the *n*-acids signal, indicative of both aquatic and terrestrial vegetation.

In some instances, the distribution patterns of *n*-alkanes are used to distinguish between different vegetation types (Schwark et al., 2002), as the C₃₁ alkane is often the most-dominant homologue in grasses, while C₂₇ or C₂₉ abound in deciduous trees (Cranwell, 1973; Schwark et al., 2002). Vogts et al., (2009) examined 45 savanna⁴ species and 24 rainforest plants from across Africa and found that the C₂₉ alkane is the most abundant homologue in five rainforest lianas, seven shrubs, and five trees (17/24 species; 70.8%), while C₃₁ dominated the distribution patterns in one liana, four shrubs, and two tree species (7/24 species; 29.2%). In 45 savanna species, they observed that the C₂₇ alkane was most abundant in six trees (6/45 species; 13.3%), the C₂₉ alkane proliferated in two herbs, two shrubs, and 10 trees (14/45 species; 31.1%), the C₃₁ was most dominant in three herbs, seven shrubs, and 12 trees (22/45 species; 48.9%), while three herbs (3/45 species; 6.7%) had C₃₃ as the most plentiful homologue. Vogts et al., (2009) presented the C₂₇ homologue to be the most abundant in 8.7% of the total assemblage, whereas C₂₉ accounted for 44.9%, C₃₁ for 42.1%, and C₃₃ for 4.3% of the 69-plant species dataset. As the C₂₉ alkane is the most abundant homologue in rainforest species and the C₃₁ was most dominant in savanna plants, plant growing environment, physiographic variables (i.e. latitude, longitude, elevation, precipitation), and plant type factor into alkane-homologue biosynthesis.

Rommerskirchen et al., (2006) assessed long-chain *n*-alkanes (C₂₇ to C₃₅) of 33 C₄ grasses of the subfamilies Aristidoideae, Chloridoideae, and Panicoideae from southern African grasslands and savannas⁵ and three C₃ grasses of the subfamily Pooideae from Peru and Australia. They found that wax signatures of C₄ grasses are distinguishable from C₃ species by the higher C₃₁ and C₃₃ alkane content, as well as heavier isotopic values (Sections 5.4 & 5.5). Rommerskirchen and

⁴ “Savanna” is not defined by the authors, but plant species were collected in the Karoo-Namib, Somalia-Masaai, and Sudanian Regional Centers of Endemism.

⁵ The authors define “savanna” as ecozones where woody species are significant but do not form a closed canopy or a continuous cover.

coauthors' (2006) data show that the C₃₁ compound is most abundant in all nine Aristidoideae species studied (9/9 species; 100%), whereas for Chloridoideae the C₂₇ alkane was most abundant in one plant (1/14 species; 7.1%), C₂₉ alkane was also foremost in one plant (1/14 species; 7.1%), the C₃₁ was most dominant in six grasses (6/14 species; 42.9%), while six other grasses (6/14 species; 42.9%) had C₃₃ as the most plentiful homologue. The 10 Panicoideae species were evenly distributed, with five having maximum distributions at C₃₁ (5/10 species; 50%), and five others at C₃₃ (5/10 species; 50%). Therefore, for the C₄ grasses, the C₂₇ and C₂₉ homologues only accounted for 3.0% of the total assemblage each (1/33 species, respectively), whereas C₃₁ accounted for 61% of the total assemblage (20/33 species) and C₃₃ for 33.3% (11/33 species) of the 33-C₄-plant species dataset. In their limited dataset from C₃ Pooideae grasses, Rommerskirchen et al., (2006) identified two species to have C₂₉ as their dominant homologue (2/3 species; 66.7%), while the third plant had C₃₁ as the most abundant compound (1/3 species; 33.3%). Although limited, the *n*-alkane distribution patterns separate the Pooideae from the subfamilies comprising the C₄ grasses whereby the C₃ grasses have slightly shorter-chain homologues than those that characterize the C₄ species.

BOX V-I: HYDROCARBON NOMENCLATURE

- **Aliphatic** hydrocarbons consist of linear chains of carbon atoms
- **Aromatic** hydrocarbons contain benzene (C₆H₆) as a part of their structure
- **Branched** hydrocarbons are isomers with the same number of C atoms but different physical and chemical properties
- **Cyclic** hydrocarbons have carbon chains that join to itself in a ring
- **Saturated (normal)** hydrocarbons have only single bonds that contains the maximum number of hydrogen atoms for each carbon atom
- **Unsaturated** hydrocarbons contain multiple bonds and contain less than the maximum number of hydrogens per carbon.

5.2 Lipid Biosynthesis

5.2.1 Fatty Acid Biosynthesis

Synthesis of wax compounds occurs in the epidermal cells of the photosynthetic tissue of plants (Samuels et al., 2008). In vascular plants, all lipid compounds including *n*-alkanes, *n*-alkanols, and *n*-alkanoic acids form via the fatty acid biosynthetic pathway whereby acetate ($C_2H_3O_2^-$), produced by

Table 5-2. Saturated (normal) Alkanoic Acids

Carbon Atoms	Hydrogen Atoms	Oxygen Atoms	Systematic Name
1	2	2	Methanoic acid
2	4	2	Ethanoic acid
3	6	2	Propanoic acid
4	8	2	Butanoic acid
5	10	2	Pentanoic acid
6	12	2	Hexanoic acid
7	14	2	Heptanoic acid
8	16	2	Octanoic acid
9	18	2	Nonanoic acid
10	20	2	Decanoic acid
11	22	2	Undecanoic acid
12	24	2	Dodecanoic acid
13	26	2	Tridecanoic acid
14	28	2	Tetradecanoic acid
15	30	2	Pentadecanoic acid
16	32	2	Hexadecanoic acid
17	34	2	Heptadecanoic acid
18	36	2	Octadecanoic acid
19	38	2	Nonadecanoic acid

the decarboxylation of pyruvate ($C_3H_4O_3^-$), is subsequently synthesized into straight-chain hydrocarbons with $>C_{20}$ carbon atoms (Hitchcock and Nichols, 1971). The first stage of wax biosynthesis involves the joining of the C_2 building blocks of acetyl-coenzyme A (acetyl-CoA)⁶ together to form C_{16} and C_{18} fatty acids (FAs) (Table 5-2) within the leucoplasts, the small non-photosynthetic plastids found in the epidermis (Samuels et al., 2008). The second stage involves the elongation of C_{16} and C_{18} FAs in the endoplasmic reticulum into *very-long-chain fatty acids* (VLCFAs) with C_{20} - C_{34} carbon atoms. The second stage is responsible for generating cuticular waxes that are subsequently modified into other major wax products such as alkanes.

⁶ Coenzyme A is the ubiquitous acyl-transfer cofactor in biological systems: its derivatives are known to be necessary for the activity of a large number of enzymes which catalyze a variety of reactions involving *acyl groups* ($R-C=O$ group, where *R* represents an alkyl group (an alkane missing one hydrogen) that is linked to the carbon atom (C) of the group by a single bond (Hitchcock and Nichols, 1971).

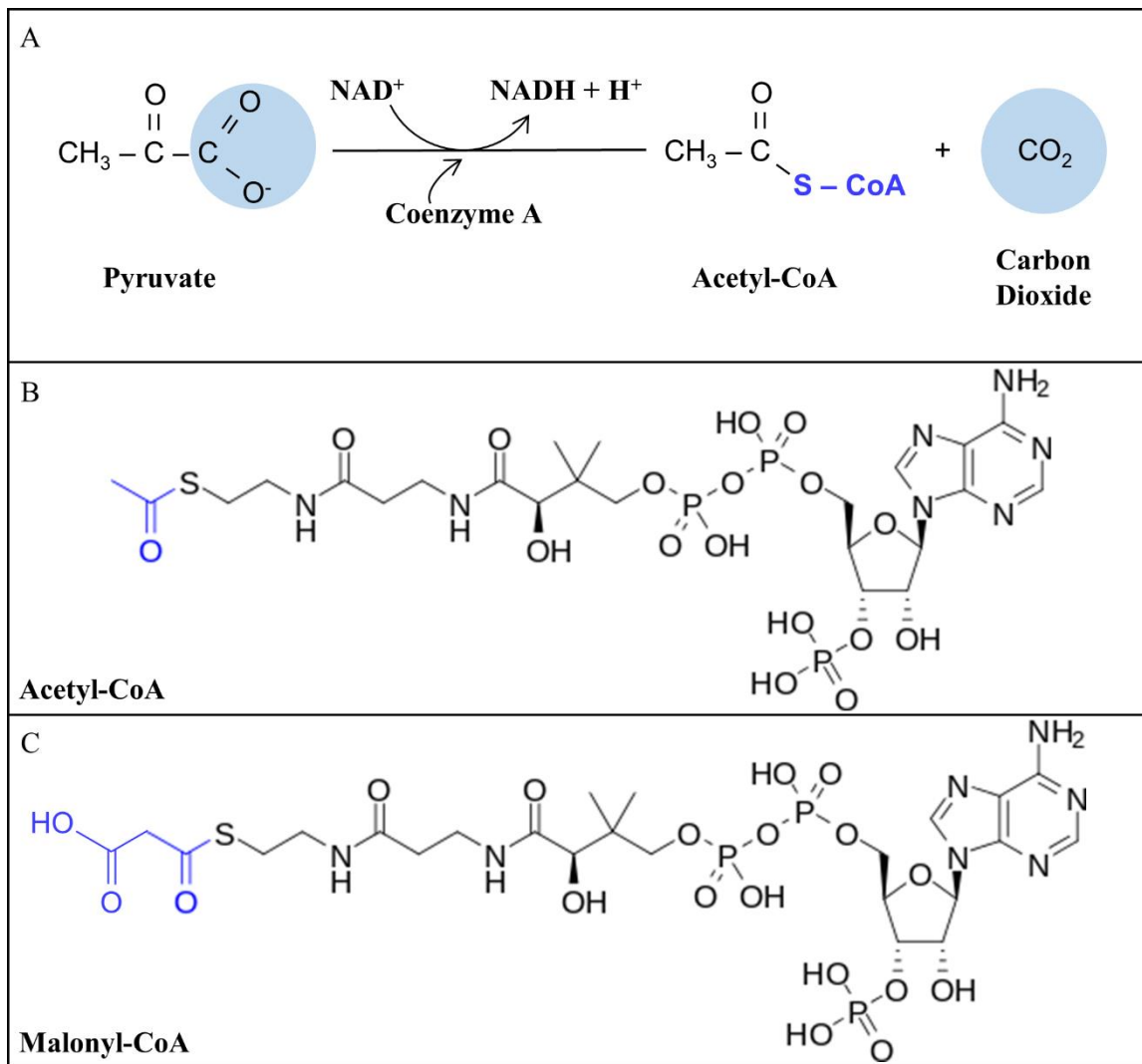


Figure 5-3. **A.** The process by which pyruvate is attached to Acetyl Coenzyme A releases a carbon dioxide molecule and forms NADPH. **B.** Acetyl-CoA is the result of acetyl being attached to the carrier molecule coenzyme A during photosynthesis. **C.** Malonyl-CoA is produced by acetyl-CoA carboxylase, becoming the central donor for fatty acid synthesis. Adapted from Mauseth, 2009.

The enzyme Fatty Acid Synthase (FAS) catalyzes the synthesis of de novo C₁₆ and C₁₈ acyl chains (Jetter and Kunst, 2008). This begins with the oxidation and decarboxylation of pyruvate (C₂H₃OCOO⁻), the anion of pyruvic acid, in which the coenzyme nicotinamide adenine dinucleotide (NAD⁺) reacts with the pyruvate molecule to liberate CO₂ and produce a 2-carbon fragment called *acetyl* (C₂H₃O) (Fig. 5-3). The acetyl attaches to the carrier molecule *coenzyme A* (CoA), resulting in acetyl-CoA (C₂₃H₃₈N₇O₁₇P₃S), which is subsequently transferred to an acceptor molecule (the 4-carbon oxaloacetate; C₄H₂O₅⁻²) and converted to a six-carbon compound

(citrate; $C_6H_5O_7^{3-}$) (Mauseth, 2009). During synthesis, the growing acyl chain is attached to an acyl carrier protein (ACP), an essential protein component of FAS (Kunst and Samuels, 2003). In this process, the central donor for fatty acid synthesis is a C_2 moiety functional group originating from a malonyl-CoA produced by acetyl-CoA carboxylase (Ohlrogge and Browse, 1995). The malonyl

Table 5-2 cont. Saturated (normal) Alkanoic Acids

Carbon Atoms	Hydrogen Atoms	Oxygen Atoms	Systematic Name
20	40	2	Eicosanoic acid
21	42	2	Heneicosanoic acid
22	44	2	Docosanoic acid
23	46	2	Tricosanoic acid
24	48	2	Tetracosanoic acid
25	50	2	Pentacosanoic acid
26	52	2	Hexacosanoic acid
27	54	2	Heptacosanoic acid
28	56	2	Octacosanoic acid
29	58	2	Nonacosanoic acid
30	60	2	Triacontanoic acid
31	62	2	Henatriacontanoic acid
32	64	2	Dotriacontanoic acid
33	66	2	Tritriacontanoic acid
34	68	2	Tetatriacontanoic acid
35	70	2	Pentatriacontanoic acid
36	72	2	Hexatriacontanoic acid
37	74	2	Heptatriacontanoic acid
38	76	2	Octatriacontanoic acid

group is transferred from CoA to malonyl-ACP, where it enters a series of condensation reactions with acyl-ACP and acetyl-CoA acceptors (Fig. 5-4). After each condensation, the ACP product is reduced, dehydrated, and reduced again by ACP reductase enzymes, which use NADH or NADPH to form saturated fatty acids (Ohlrogge and Browse, 1995). The combined action of these reactions leads to the lengthening of the precursor fatty acid by 2-carbon units and commits them to fatty acid chain synthesis (Jetter and Kunst, 2008; Samuels et al., 2008). At least three different fatty acid synthases complexes, which differ in their protein synthase condensing enzyme, participate in the production of C_{16} and C_{18} fatty acids (Jetter and Kunst, 2008; Kunst and Samuels, 2003; Ohlrogge and Browse, 1995; Samuels et al., 2008). These enzymes synthesize saturated hexadecanoic ($C_{16}H_{32}O_2$) and octadecanoic ($C_{18}H_{36}O_2$) acids, but also oleic acid ($C_{18}H_{34}O_2$), the

most widely distributed and abundant unsaturated fatty acid in nature (Hitchcock and Nichols, 1971).

The second stage of fatty acid synthesis, the extension of the C₁₆ and C₁₈ fatty acids to VLCFAs, is carried out by Fatty Acid Elongases (FAE), multienzyme complexes bound to the endoplasmic reticulum membrane (Kunst and Samuels, 2003). Analogous to primary stage synthesis, VLCFA formation involves four consecutive enzymatic reactions that results in a 2-carbon extension of the acyl chain in each elongation cycle (Samuels et al., 2008). However, unlike the FAS which uses malonyl-ACP as a C₂ donor, FAE utilizes C₂ units from malonyl-CoA (Fig. 5-3). Multiple elongation cycles are needed to generate C₂₄ to C₃₄ acyl chains for the production of straight-chain, saturated wax compounds (Jetter and Kunst, 2008).

5.2.2 *Alkane Biosynthesis*

Although fatty acids are the biosynthetic precursors of the *n*-alkanes in plant cuticular wax, knowledge of the enzymes involved in alkane biosynthesis remains limited (Kunst and Samuels, 2003). However, after elongation, fatty acids are processed according to two different biosynthetic pathways: the alcohol-forming pathway, yielding fatty alcohols and alkyl esters, and the alkane-forming pathway, generating fatty aldehydes, alkanes, and their derivatives (Fig. 5-4) (Samuels et al., 2008). The alkane-forming pathway is responsible for the formation of compounds with predominantly odd-number carbon atoms and among these, the alkanes are the most ubiquitous in plant waxes where they accumulate in high concentrations. The primary reaction that makes the transition from even- to odd-numbered carbon chains is thought to involve the loss of one carbon

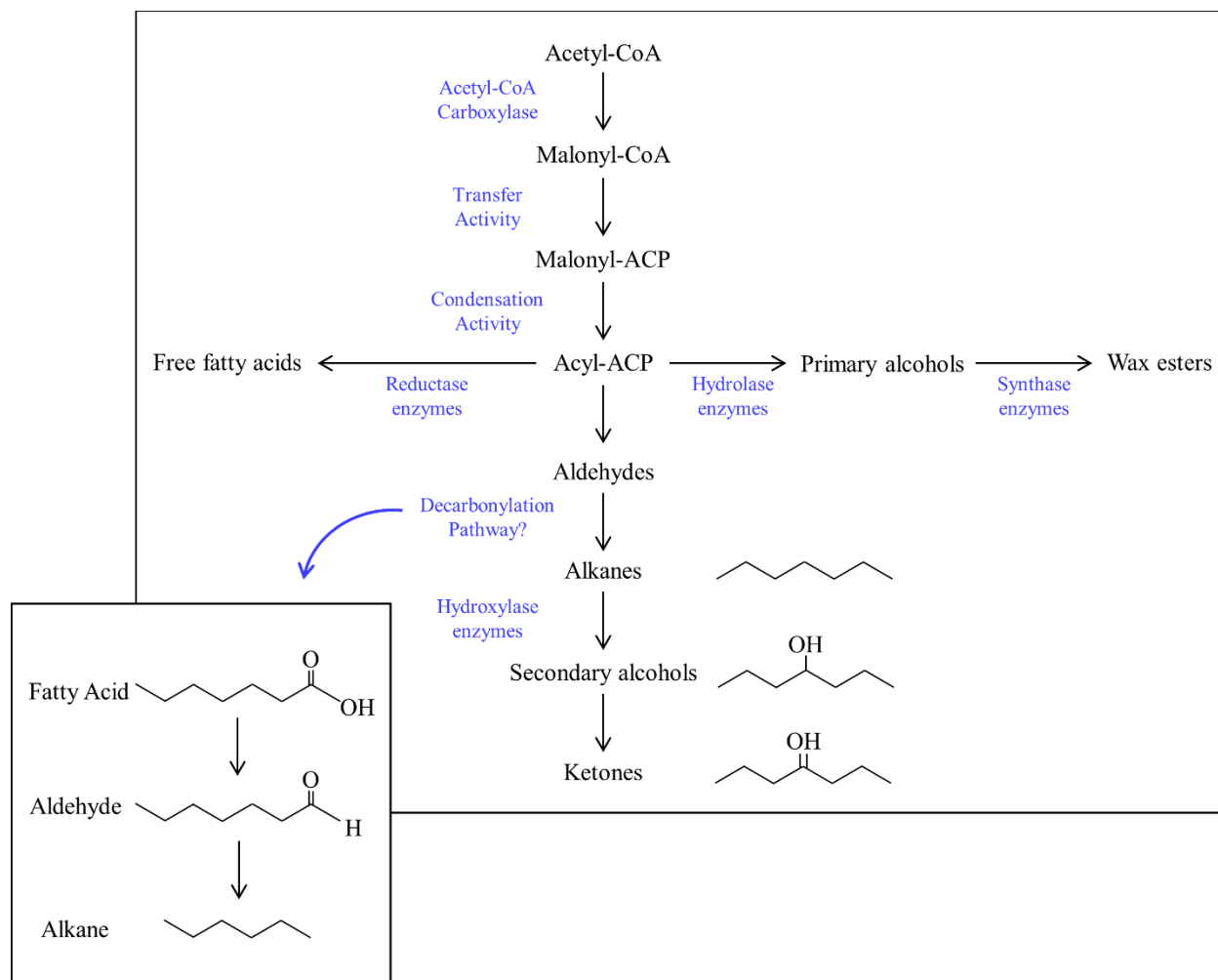


Figure 5-4. Proposed metabolic pathway for leaf wax biosynthesis. VLCFAs are modified into major wax products, through either the acyl reduction pathway, which gives rise to primary alcohols and wax esters, or through the decarboxylation pathway that leads to the formation of aldehydes, alkanes, secondary alcohols and ketones. After Kunst and Samuels, 2003 and Samuels et al., 2008.

atom from acyl precursors rather than an addition of a carbon atom (Samuels et al., 2008).

Biochemical experiments showed that carbon atoms were lost in reactions when C₃₀ and C₃₂ acids were converted into C₂₉ and C₃₁ alkanes, respectively (Khan and Kolattukudy, 1994; Kolattukudy et al., 1972). Though the overall carbon loss is well established, the reaction details are not fully understood. One hypothesis suggests that the central C–C cleavage step is through decarboxylation (the loss of a CO molecule) by an aldehyde intermediate (Bognar et al., 1984). In order to refine the plant alkane-forming pathway and test the decarboxylation hypothesis, Bernard et al., (2012) utilized the small flowering plant *Arabidopsis thaliana* ECERIFERUM1 (CER1) protein as it is

Table 5-3. Saturated (normal) Alkanes

Carbon Atoms	Hydrogen Atoms	Systematic Name	Carbon Atoms	Hydrogen Atoms	Systematic Name
1	4	Methane	28	58	Octacosane
2	6	Ethane	29	60	Nonacosane
3	8	Propane	30	62	Triacosane
4	10	Butane	31	64	Hentriacontane
5	12	Pentane	32	66	Dotriacontane
6	14	Hexane	33	68	Tritriacontane
7	16	Heptane	34	70	Tettratriacontane
8	18	Octane	35	72	Pentatriacontane
9	20	Nonane	36	74	Hexatriacontane
10	22	Decane	37	76	Heptatriacontane
11	24	Undecane	38	78	Octatriacontane
12	26	Dodecane	39	80	Nonatriacontane
13	28	Tridecane	40	82	Tetracontane
14	30	Tetradecane	41	84	Hentetracontane
15	32	Pentadecane	42	86	Dotetracontane
16	34	Hexadecane	43	88	Tritetracontane
17	36	Heptadecane	44	90	Tetratetracontane
18	38	Octadecane	45	92	Pentatetracontane
19	40	Nonadecane	50	102	Pentacontane
20	42	Eicosane	52	106	Dopentacontane
21	44	Heneicosane	54	110	Tetrapentacontane
22	46	Docosane	60	122	Hexacontane
23	48	Tricosane	62	126	Dohexacontane
24	50	Tetracosane	64	130	Tetrahexacontane
25	52	Pentacosane	66	134	Hexahexacontane
26	54	Hexacosane	67	136	Heptahexacontane

an essential element of wax alkane synthesis. The authors identified a physical interaction between CER1 and CER3 (ECERIFERUM3) in both yeast and *Arabidopsis*, suggesting that they associate to form an enzymatic complex necessary for catalyzing the conversion of VLCFAs to *n*-alkanes. In this reaction, CER1 (as an aldehyde decarbonylase) and CER3 (as a fatty acyl reductase) catalyze a two-step reaction starting with the reduction of acyl-CoA to an intermediate aldehyde that is subsequently decarbonylated to an alkane with the loss of one carbon, potentially as carbon monoxide. Therefore, by successfully demonstrating the catalytic functions of CER1 and CER3

for long-chain alkane production, Bernard et al., (2012) identified the enzymatic components of plant alkane synthesis in *Arabidopsis thaliana*.

5.3 Photosynthetic Pathways

In most plants, the series of reactions by which carbon dioxide is reduced is called the *Calvin cycle*, the only known pathway for making carbohydrates from carbon dioxide. Because the first detectable product of the Calvin cycle is the 3-carbon molecule phosphoglycerate (3-PGA) ($C_3H_7O_7P$) (Fig. 5-5), this metabolic pathway is known as C_3 photosynthesis. The C_3 pathway is the most widespread carbon-fixation pathway, and of the estimated 250,000 species of land plants, about 85–89% use the C_3 photosynthetic pathway (Sage, 2004). Almost all trees, shrubs, and herbs,

and temperate or shade-adapted grasses follow the C_3 pathway, while C_4 photosynthesis is common among grasses and sedge families in warm, often dry environments with strong solar radiation in the growing season. As several C_3 grasses are most abundant in cooler, humid growing seasons, they are known as *cool-season grasses*. *Warm-season grasses* on the other hand, typically use C_4 photosynthesis, an

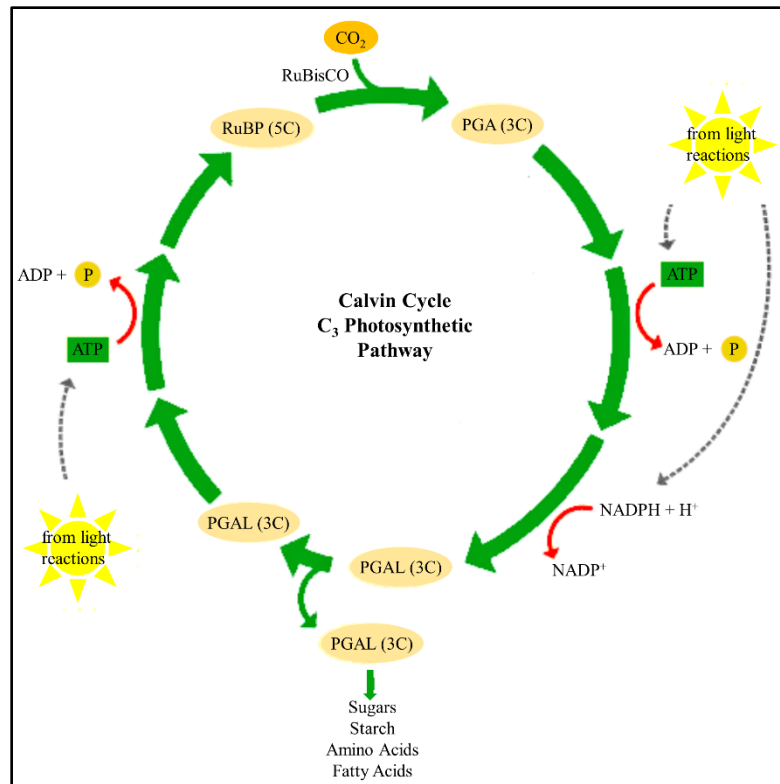


Figure 5-5. In the **Calvin-Benson Cycle**, RuBisCO combines CO_2 with RuBP to yield 3-PGA. ATP and NADPH convert 3-PGA to PGAL, some of which is used to make sugars and other carbon-containing compounds. Three turns of the cycle are required to produce one molecule of PGAL. After Graham et al., 2006.

adaptation that improves productivity during hot, dry conditions (Fig. 5-6). Most C₄ plants are grasses (4,500 species), followed by sedges (1,500 species) and dicots (1,200 species) (Sage, 2004). Of the 213 major families of Angiosperms, a mere twenty contain C₄ plants (Judd et al., 2007); within the primary C₄ biome of grasslands, the average C₄ contribution is only 36% of the total species (Raven et al., 2004).

During C₃ photosynthesis, carbon dioxide (CO₂) and water (H₂O) are converted into simple sugars (C₆H₁₂O₆) and oxygen gas (O₂). This is the result of chlorophyll absorbing visible-light energy that excites electrons within leaf tissue and splits water molecules through *photolysis* into molecular oxygen (O₂), most of which enters the atmosphere, and into electrons and protons. The organic compound adenosine triphosphate (ATP) (C₁₀H₁₆N₅O₁₃P₃) captures any remaining energy that does not dissipate as heat, while electrons (e⁻) and protons (H⁺) from photodissociated water combine with the electron acceptor nicotinamide adenine dinucleotide phosphate (NADP⁺) (C₂₁H₂₉N₇O₁₇P₃), to form the energy carrier NADPH; the added electron reduces NADP⁺ to NADPH (Graham et al., 2006).

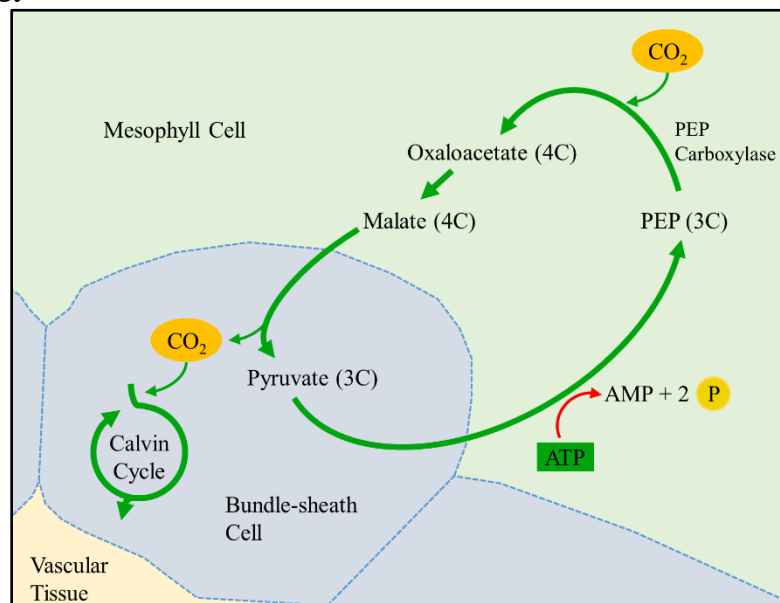


Figure 5-6. The initial fixation of carbon in the **Hatch-Slack** pathway is mediated by the enzyme PEP Carboxylase, which combines CO₂ with 3-carbon PEP to form 4-carbon oxaloacetate. The oxaloacetate is converted to malate, which is transported to specialized bundle-sheath cells and split into pyruvate and CO₂ that is used in the Calvin cycle and fixed by RuBisCO. After Graham et al., 2006.

The Calvin-Benson cycle (Calvin and Benson, 1948) (Fig. 5-5) begins and ends with a 5-carbon sugar called ribulose 1,5-bisphosphate (RuBP) ($C_5H_{12}O_{11}P_2$). The enzyme ribulose 1,5-bisphosphate carboxylase/oxygenase, better known as *RuBisCO*, fixes CO_2 or O_2 to RuBP through carboxylase or oxygenase reactions, respectively. When RuBisCO enzymes combine CO_2 with RuBP, it creates a 6-carbon sugar that is subsequently fragmented into two molecules of 3-PGA; the first detectable product of the Calvin cycle (Fig. 5-5). An endergonic reaction that absorbs energy from ATP and NADPH reduces 3-PGA into the 3-carbon molecule phosphoglyceraldehyde (PGAL) ($C_3H_5O_6P^{-2}$), which is either converted to starch, the main storage product in plants and green algae, or exported from chloroplasts and becomes sucrose, the principal transport sugar in plants.

Warm-season grasses typically use the *Hatch-Slack* photosynthetic pathway (Slack and Hatch, 1967) to fix carbon (Fig. 5-6), whereby the first product of carbon fixation is the 4-carbon compound oxaloacetate ($C_4H_4O_5$). In the mesophyll cells of C_4 plant leaves, CO_2 combines with the 3-carbon molecule phosphoenolpyruvate (PEP) ($C_3H_5O_6P$) to form oxaloacetate in a reaction

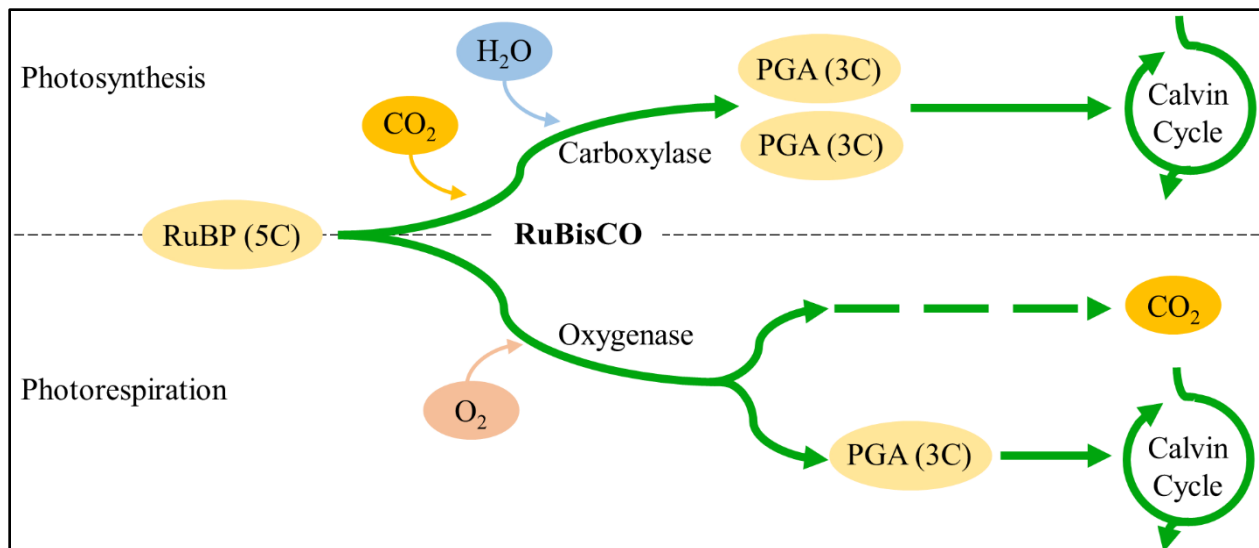


Figure 5-7. Photosynthesis (top) and photorespiration (bottom) pathways. When RuBisCO combines RuBP with CO_2 , it produces two 3-PGA molecules, which continue through the Calvin cycle. When CO_2 levels are low, RuBisCO acts as an oxygenase and combines RuBP with oxygen, yielding only one 3-PGA molecule (and CO_2). Therefore, photorespiration reduces the efficiency of photosynthesis by causing the loss of a carbon. After Graham et al., 2006.

catalyzed by the PEP carboxylase enzyme. (Because PEP carboxylase is not an oxygenase, it has a higher rate of carbon assimilation than the Calvin-Benson cycle (Hatch, 1987).) Oxaloacetate is reduced to malate ($C_4H_4O_5^{2-}$) by a molecule of NADPH, and malate is transported from the mesophyll into bundle-sheath cells that surround leaf vascular tissue. Malate is broken down into CO_2 and the 3-carbon pyruvate ($C_3H_3O_3^-$), whereby CO_2 enters the Calvin cycle and is fixed to PGA by RuBisCO, while pyruvate returns to the mesophyll cells and is converted back into PEP by ATP; water breakdown and oxygen production also occur. Because all the malate from a large volume of mesophyll decarboxylates in the small volume of bundle-sheath cells, CO_2 concentration in the bundle-sheath is very high (Mauseth, 2009). Therefore, C_4 plants spatially separate the Hatch-Slack and Calvin-Benson cycles by operating C_4 metabolism in the mesophyll cells and the Calvin cycle in the bundle-sheath cells.

Plants acquire CO_2 from the atmosphere through their stomata, but also lose water when the stomata are open. When C_3 plants are stressed during hot or arid periods, they close their stomata to prevent water loss. As a result, the concentration of leaf CO_2 decreases, the enzyme RuBisCO combines oxygen with RuBP rather than carbon dioxide, and only one molecule of 3-PGA is created instead of two (Fig. 5-7). This process is termed *photorespiration* because it consumes oxygen and releases carbon dioxide. In C_3 plants, photorespiration increases with light intensity and temperature making them less-metabolically efficient in hot, dry climates. Under present atmospheric conditions, high rates of photorespiration in C_3 plants reduce the overall photosynthetic rate by 30-40% (Ehleringer et al., 1986). C_4 plants on the other hand, virtually eliminate photorespiration by concentrating carbon dioxide in the bundle-sheath cells to levels ten times greater than that in the atmosphere (Graham et al., 2006). With these elevated levels of CO_2 available to RuBisCO, C_4 vegetation have higher net rates of photosynthesis than C_3 plants,

particularly under increased light and temperature conditions. Concentrating CO₂ within bundle-sheath cells improves water-use efficiency (Llorens et al., 2009) and prevents photorespiration in high- temperature, light, or salinity environments and in places with limited water supplies or low CO₂ concentrations (Ehleringer et al., 1986; Farquhar et al., 1989; Sage, 2004).

Although large areas of Earth's surface are spatial and temporal mosaics of both photosynthetic types, C₄ grasses dominate the grasslands that encircle the globe at sub-tropical latitudes in Africa, South America, and parts of Australia, India, and Pakistan (Still et al., 2003). These zones reflect the distribution of arid, open environments that respond to the impact of prevailing weather patterns on the continents. Still et al., (2003) estimate that the global coverage of C₄ vegetation is 18.8 million km², while C₃ vegetation covers 87.4 million km².

5.4 Isotope Signatures from Lipid Biomarkers

The biochemical approach for paleoclimate reconstructions is much more widespread now that techniques for extracting and analyzing leaf wax lipid biomarkers are becoming more precise (Hilkert et al., 1999). Traditionally, the most common isotope used as both an environmental and dietary indicator is $\delta^{13}\text{C}$ (ratio between carbon-13 and carbon-12 (written ¹³C and ¹²C, respectively)). This is due in part to its effectiveness as an environmental proxy, which enables us to trace plant type, plant water-use efficiency, and relative paleo-temperature based on the distinct ratio between the ¹³C and ¹²C isotopes found within leaf lipid compounds (Castañeda and Schouten, 2011; Cerling et al., 2011; Cerling et al., 1997c; Collister et al., 1994; Farquhar et al., 1989; Lockheart et al., 1997; Sponheimer and Lee-Thorp, 1999; Sponheimer et al., 2006). Our understanding of environmental change in East Africa throughout the Pleistocene results from research that utilizes stable carbon isotopes from both terrestrial and marine sediment sources, as

well as palynological and terrestrial dust archives (Feakins et al., 2013; Wynn, 2000). The stable carbon isotopic composition of all higher plants is a function of the carbon isotopic composition of atmospheric CO₂ ($\delta^{13}\text{C}_{\text{CO}_2}$), and the ratio of atmospheric CO₂ partial pressure ($p\text{CO}_2$) inside leaves relative to atmospheric $p\text{CO}_2$ (Farquhar et al., 1989; O'Leary, 1981).

Analysis using stable hydrogen isotopes on the other hand, is a relatively new approach for reconstructing paleoecology (Leng et al., 2010; Liu et al., 2006; Magill et al., 2013a, b; Raynard and Hedges, 2007; Yang and Huang, 2003). Gas Chromatography – Isotope Ratio Mass Spectrometry (GC-IRMS) has only recently made the molecular examination of hydrogen isotopes in modern and fossil plants possible (Burgoyne and Hayes, 1998; Hilkert et al., 1999; Scrimgeour et al., 1999). Using hydrogen to trace paleoenvironmental conditions is now being seriously considered because stable hydrogen isotope values, expressed as δD (ratio between deuterium and hydrogen (written D/H or $^2\text{H}/^1\text{H}$)), are well preserved in terrestrial sediments (Epstein et al., 1977; Estep and Hoering, 1980; Feng and Epstein, 1994; Sessions et al., 1999; Sternberg, 1988; White et al., 1985; Xie et al., 2000; Yang and Leng, 2009; Yapp and Epstein, 1982). Compound-specific biomarkers preserve the hydrogen isotopic signature of precipitation as well as relative humidity, and when combined with the carbon isotopic signature, can help determine paleoenvironmental conditions of specific geographic regions (Andersen et al., 2001; Huang et al., 2004; Sachse et al., 2004; Sauer et al., 2001). Furthermore, most lipid hydrogen atoms are covalently bound to carbon atoms and are not readily exchanged at temperatures below 100°C (Sessions et al., 2004).

When coupled, $\delta^{13}\text{C}$ and δD present a unique opportunity to analyze both paleo-atmospheric and hydrological conditions as well as C₃ vs. C₄ dominated ecosystems. As methodologies for paleoenvironmental reconstructions become more advance, particularly those for analyzing δD (Burgoyne and Hayes, 1998; Hilkert et al., 1999; Scrimgeour et al., 1999; Yang

and Leng, 2009), further-detailed information on human Pleistocene environments will supplement the existing carbon isotope data from East Africa. In both cases, the proxies are entirely based on compound-specific isotope measurements and are therefore completely independent of the more conventional proxies based on inorganic isotopic variations (e.g. carbonates).

5.5 Controls on $\delta^{13}\text{C}$ and δD of Lipid Compounds

5.5.1 Plant Type

Differences in C_3 and C_4 plant physiologies result in distinct stable carbon isotope signatures (Tippie and Pagani, 2007). The carbon isotopic composition ($\delta^{13}\text{C}$) of leaf lipid biomarkers is distinguishable between vegetation utilizing the different photosynthetic pathways as the distinct mechanisms for CO_2 fixation causes characteristic differences in the stable carbon isotope composition of plant material. Leaf wax lipid $\delta^{13}\text{C}$ values of *n*-alkanes have been shown to vary between -29‰ and -39‰ in C_3 plants and between -14‰ and -26‰ in C_4 vegetation (Bi et al.,

2005; Collister et al., 1994; O'Leary, 1981; Rommerskirchen et al., 2006; Vogts et al., 2009). Bulk isotope values of C_3 leaves range between -20 and -35‰ while bulk C_4 values span from -7 to -15‰ (Ehleringer, (1989): p. 41). Moreover, Ballentine et al., (1998), Chikaraishi et al., (2004),

Box V-II: Isotope Nomenclature

Enrichment – A process by which the relative abundance of the heavier isotope increases, thus making isotope values more positive.

Depletion – A process by which the relative abundance of the heavier isotope decreases, thus making isotope values more negative.

Delta (δ) – Notation used to represent the differences between heavier and lighter isotopes relative to a standard.

Per mil (‰) – Isotopes values are reported in parts per thousand relative to a standard.

Isotope Abundances:

- ^{12}C : 98.89%
- ^{13}C : 1.11%
- ^1H : 99.984%
- ^2H or D: 0.016%

and Gao et al., (2015) demonstrated that the bulk carbon isotopic signature of fatty acids is also diagnostic of photosynthetic pathway, with C₃ fatty acids ranging from -31‰ to -42‰ and C₄ from -19‰ to -25‰. The source for this discrimination, specifically in C₃ photosynthesis, is the RuBisCo enzyme, which discriminates strongly against heavier ¹³C; PEP in C₄ plants on the other hand, does not appear to differentiate against ¹³C (Ehleringer, 1989). Additionally, C₃ plants generally contain proportionally less ¹³C than the atmosphere having a 91:1, ¹²C:¹³C ratio, with greater discrimination following increases in the ratio between leaf and atmospheric partial pressure of CO₂ (Farquhar et al., 1989).

The hydrogen isotopic composition (δ D) of leaf lipid biomarkers is not as well-defined, however. Bi et al., (2005) found no significant differences in δ D from *n*-alkanes isolated from C₃ and C₄ plants collected in South China and concluded that δ D_{*n*-alkanes} are not diagnostic discriminators of photosynthetic pathway. Other studies have found inverse relationships between metabolic pathway and δ D: Chikaraishi and Naraoka (2003) for example, presented depleted average δ D values ($-171 \pm 12\text{‰}$) of *n*-alkanes from C₄ plants compared to both C₃ angiosperms ($-152 \pm 26\text{‰}$) and gymnosperms ($-149 \pm 16\text{‰}$). (Inversely, average $\delta^{13}\text{C}$ value of C₄ plants was more enriched ($-20.5 \pm 2.1\text{‰}$) than both angiosperm ($-36.1 \pm 2.7\text{‰}$) and gymnosperm ($-31.6 \pm 1.7\text{‰}$) values.) Contrariwise, Smith and Freeman (2006) observed a $\sim 25\text{‰}$ D-enrichment in *n*-alkanes from greenhouse-grown C₄ plants ($-140 \pm 15\text{‰}$) compared to C₃ grasses ($-165 \pm 12\text{‰}$), and found that on average, the C₂₉ *n*-alkane for C₄ grasses was $+21 \pm 6\text{‰}$ more enriched than that of C₃ grasses studied on the US Great Plains. Liu et al., (2006) suggest that the stable hydrogen isotope ratio of plant leaf waxes is more closely related to ecological lifeform of terrestrial plants (tree, shrub, and grass), whereby grasses have more negative δ D values than the cooccurring trees and shrubs, regardless of photosynthetic pathway. They found no significant differences between

average (C_{27} , C_{29} , and C_{31} *n*-alkanes) δD values in C_3 and C_4 plants among trees, shrubs, or grasses growing on the Chinese Loess Plateau. The authors did however show that the δD values of C_4 grasses from northwestern China have slightly more positive values (-196‰ to -127‰) than C_3 grasses (-210‰ to -148‰) from the same region. Moreover, Liu and Yang (2008) compiled a global database using previously published results from the preceding studies (Bi et al., 2005; Chikaraishi and Naraoka, 2003; Liu et al., 2006; Smith and Freeman, 2006), as well as others from Asia (Chikaraishi and Naraoka, 2001), North America (Hou et al., 2007b), and Europe (Sachse et al., 2006), and presented statistically (one-way ANOVA) that there was no apparent differences in plant leaf wax δD between C_3 and C_4 grasses at the global scale. Liu and Yang (2008) did find that when comparing C_4 and C_3 Gramineae plants from the same sites in China and the United States, that *n*-alkanes from C_4 Gramineae are D-enriched relative to C_3 Gramineae.

Smith and Freeman (2006) attribute the δD enrichment of *n*-alkanes from C_4 plants to the degree of transpiration related to different plant physiologies. Chikaraishi and Naraoka (2003) interpret the hydrogen isotopic differences between C_3 and C_4 plants as a reflection of the isotope effects associated with evapotranspiration and *n*-alkane biosynthesis. Liu et al., (2006) and Liu and Yang (2008) suggest that plant ecological lifeform (trees vs. shrubs vs. grasses) exert a greater influence on δD than differences in photosynthetic pathway, and that in any geographic region that utilizes the same precipitation as source water, differences in water absorption systems between plant-form plays a significant role in influencing *n*-alkane δD values amongst grasses and woody plants. As the δD of precipitation varies with moisture source, latitude, and degree of continentality, and the δD values of leaf water are directly enriched by transpiration and indirectly by evaporation of soil waters, the δD of *n*-alkanes register integrated signals from the collective effects of evapotranspiration, precipitation, and other environmental components. Therefore, the

effect of the photosynthetic pathway on the δD of modern plant *n*-alkanes must be further explored for better paleoenvironmental interpretations.

Of note to the tropics or in areas where meteorological conditions lead to similar deuterium enrichment in leaf water, Sachse et al., (2006) found that plants with leaves having very thick wax layers are better protected from evaporative water loss and avoid strong deuterium enrichment in leaf water. For example, samples of Myrtle (*Myrtus*) collected in Finland were 50‰ depleted in deuterium relative to Birch (*Betula pendula*) gathered at the same site, and Sachse et al., suggest that a thick wax layer might restrict evaporative enrichment of leaf water. Because a more complex wax-layer with higher concentrations of hydrocarbons may minimize plant water loss (e.g. Maffei et al., (1993)), plants with thick waxy leaves found in arid regions of East Africa should be considered when using modern correlates to reconstruct paleoenvironments.

A limitation of biomarker studies for reconstructing ancient vegetation structure is that sedimentary accumulations of plant leaf waxes cannot be attributed to individual species (Sachse et al., 2012). This is because such accumulations integrate plant inputs over time and across landscapes; for example, lacustrine or marine sedimentary samples obtain wax inputs from small catchment areas to large river basins while terrestrial archives are susceptible to the deposition of aerosols containing waxes that are transported long distances by wind (Eglinton and Eglinton, 2008). Therefore, sedimentary archives' isotope values may either represent only a subset of the full range of values that are documented in modern ecosystems or mixtures of plants at different stages of their lifecycles which could have a significant impact on δD (Sachse et al., 2012; Sessions, 2006).

5.5.2 Atmospheric CO₂

The C₄ photosynthetic pathway concentrates CO₂ within leaves when atmospheric partial pressure is low, enriching them in ¹³C. Changes in the carbon isotope ratios of fossil tooth enamel in Asia, Africa, and North and South America between 8.0 and 6.0 million years ago suggests a global increase in the biomass of plants using C₄ photosynthesis (Cerling et al., 1997b). This discovery prompted Cerling et al., to attribute the global expansion of C₄ plants to a decrease in the atmospheric partial pressure of CO₂ (*p*CO₂) and argue that crossing a critically low CO₂/O₂ threshold triggered an ecological response (i.e. C₄ expansion) as physiological mechanisms provide an advantage to C₄ plants under low *p*CO₂. Using long-chain unsaturated ketones⁷ and surface-dwelling planktonic foraminifera δ¹³C records from deep sea cores encompassing the early, middle, and late Miocene ~30 to 5.0 Ma, Pagani and colleagues evaluated the role of *p*CO₂ as a mechanism forcing C₄ expansion (Pagani et al., 1999a; Pagani et al., 1999b). They show that *p*CO₂ first decreased 130 parts per million by volume (ppmv) near the Oligocene/Miocene boundary 23 Ma from 350 to 220 ppmv before decreasing again to a low of ~180 ppmv 14 Ma. During most of the early and middle Miocene, *p*CO₂ concentrations ranged between 190 and 260 ppmv, but increased to concentrations between 250 and 320 ppmv 9.0 Ma. Therefore, nearly 15 million years elapsed between the onset of low *p*CO₂ at the start of the Miocene to the major expansion of C₄ grasses between 8.0 and 6.0 Ma. Due to this time-gap, the authors posit that *p*CO₂ level alone was not a sufficient trigger of the late Miocene event as suggested by Cerling and coauthors (1997b), and that it was regional controls, the development of low-latitude seasonal aridity, and changes in growing conditions on a global scale rather than a decrease in *p*CO₂ that led to the sudden expansion of C₄ vegetation at ~7.0 Ma.

⁷ An organic compound with the structure RC(=O)R', where R and R' can be a variety of carbon-containing substituents.

In a complimentary study, Huang et al., (2001) analyzed the carbon isotopic composition of leaf wax *n*-alkanes in sediment cores from two Mesoamerican lakes to test the relative impacts of aridity, seasonal precipitation, and $p\text{CO}_2$ on the abundance of C_3 and C_4 plants, and whether such climatic factors can counteract an increase in C_4 distributions due to lower $p\text{CO}_2$. The cored lakes are situated in two distinct ecozones with different mean annual precipitation (map), temperature, and vegetation structure, with sedimentary deposits spanning the last 20,000 years. One lake, situated in northern Mexico (500 mm map; 20°C avg.), is surrounded by shrub grassland with a significant C_4 component on lower elevations, and mixed forest of pine, oak, and juniper at higher altitudes. The other, in the central Yucatan of northern Guatemala (1,600 mm map; 25°C), has modern lowland vegetation of semi-evergreen forest. Huang et al., (2001) results from C_{27} - C_{31} *n*-alkanes indicate that complex interactions between several environmental factors such as rainfall, precipitation seasonality, temperature, and $p\text{CO}_2$ control the relative abundance of C_4 and C_3 plants in each lake region, and that greater concentrations of C_4 plants only occurred over the last 20,000 years when low $p\text{CO}_2$ coincided with increased aridity. Although the two sites show generally opposing temporal trends in the relative abundance of C_3 and C_4 plants, enrichment in $\delta^{13}\text{C}$ from both cores indicate periods where strong evaporative conditions combined with frequent fires, and in Guatemala, anthropogenic forest clearing during the Holocene, favored C_4 grasses. However, during the Last Glacial Maximum when $p\text{CO}_2$ was at a minimum, the combined effect of high winter precipitation and low temperatures led to an expansion of C_3 plants, specifically in the northern Mexico lake. Therefore, C_4 plant abundance only increased when low $p\text{CO}_2$ coincided with increased aridity. Huang et al., (2001) conclude that during times of adverse climatic conditions, low $p\text{CO}_2$ is insufficient on its own to trigger the expansion of C_4 plants.

Both Pagani et al., (1999a; 1999b) and Huang et al., (2001) suggest that although $p\text{CO}_2$ levels during the past 15 million years were sufficiently low to create conditions favorable to C_4 plant expansion, major changes in precipitation and temperature in low-latitude regions (initiated by late Miocene Asian tectonic uplift) triggered the large-scale radiation of C_4 vegetation. With sufficiently high precipitation, C_3 plants can increase in abundance relative to C_4 plants even at low $p\text{CO}_2$ levels (Scheffuß et al., 2003), but low $p\text{CO}_2$ does prohibit C_3 growth under average or below-average precipitation levels due to changes in plant water-use efficiencies (Huang et al., 2006).

On the other hand, in a study utilizing compound-specific $\delta^{13}\text{C}$ measurements on n -alkyl lipids (alkanes, acids, and alkanols) extracted from a ~35,000-year sediment core sampled in high-altitude (2,350 m a.s.l.) Sacred Lake, Mt. Kenya, Huang et al., (1999) found that low $p\text{CO}_2$ and temperatures prior to the onset of the Holocene allowed C_4 grasses to have a significant competitive advantage over C_3 vegetation during the Last Glacial Maximum (LGM). As $p\text{CO}_2$ plays a major role in controlling plant photosynthetic pathways (Cerling et al., 1997b), and because C_4 plants possess a CO_2 -concentrating mechanism which is more efficient than C_3 plants under low CO_2 concentrations, C_4 plants have a selective advantage over C_3 vegetation, specifically during climatic cool intervals such as the LGM when $p\text{CO}_2$ was only about 190 ppm (Huang et al., 1999). Terrestrial plant biomarkers show large glacial-interglacial variations in $\delta^{13}\text{C}$ of up to 15‰, with the highest values (-18.5‰ $\text{C}_{27/29}$ n -alkanes; -17‰ C_{26} n -acid) coinciding with the lowest CO_2 concentration and temperature as recorded in the Vostok Station ice core (Antarctica) at roughly 20,000 years ago. Following this $\delta^{13}\text{C}$ maximum, the isotope values deplete rapidly at the onset of the Holocene, reaching a $\delta^{13}\text{C}$ minimum of -35 to -30‰ while both temperature and $p\text{CO}_2$ increased. Furthermore, Huang et al., noted a significant time lag between the $\delta^{13}\text{C}$

maximum and evidence for the partial desiccation of Lake Kenya, suggesting that CO₂ may have played a more important role than aridity in controlling the abundance of C₄ plants around Sacred Lake during Late Pleistocene stadial. Therefore, the low atmospheric partial pressure of CO₂ favored terrestrial C₄ grasses and had a significant impact on both terrestrial ecosystems on Mt. Kenya prior to the onset of the Holocene.

Schubert and Jahren (2012) conducted laboratory experiments in which C₃ plants were grown in chambers across a wide range of atmospheric CO₂ partial pressures (370-4,200 ppm) to quantitate the effect of *p*CO₂ level on land-plant δ¹³C values (specifically, the net isotopic difference between atmospheric and plant tissue CO₂, written Δ¹³C_P (Farquhar et al., 1989)). The environmental characteristics within the growth chambers were controlled so that photon flux/light levels, maximum daylight hours, temperature, excess nitrogen, phosphorous, and trace nutrients, soil water, and daytime relative humidity were maintained across 15 different chambers having variable *p*CO₂ range. Accordingly, Schubert and Jahren did not find any significant relationship between *p*CO₂ and temperature, nor was there a significant correlation between *p*CO₂ level and relative humidity. They did however find that all plant tissues (C₃₁ *n*-alkanes from 191 plants) in this study showed an increase in carbon isotope discrimination with increasing *p*CO₂ and that the amount of carbon isotope fractionation varied between 0.01 and 0.35‰ Δ¹³C_P per unit increase in 100 ppm *p*CO₂.

Schubert and Jahren note that a change in *p*CO₂ will cause a change in Δ¹³C_P under any moisture regime, even though relative humidity exerts a strong control over stomatal openness and subsequently evapotranspiration and leaf/atmosphere water balance, thus influencing the δ¹³C of lipid biomarkers. They advocate that for paleoenvironmental reconstructions, the impact of *p*CO₂ level on leaf lipid δ¹³C must be considered, specifically during wet periods (e.g. interglacials of

the Pleistocene) where depleted $\delta^{13}\text{C}$ data could be misinterpreted as stomatal opening during relatively wet/humid intervals. This interpretation only applies to ever-wet, non-grassland ecosystems comprised on C_3 vegetation, which can be difficult to identify in ancient sediments, especially in East Africa. Nevertheless, Schubert and Jahren show that atmospheric CO_2 does factor into leaf lipid $\delta^{13}\text{C}$ values, specifically in wetland ecosystems where water accessibility is unrestricted to C_3 vegetation.

5.5.3 Plant Water-Use Efficiency

Carbon (Farquhar et al., 1989) and hydrogen (Hou et al., (2007a) (but cf. Bi et al., (2005) and Chikaraishi and Naraoka (2007)) isotope ratios are indicators of plant water-use efficiency (WUE), the ratio of the rate of carbon assimilation (photosynthesis) to the rate of water loss (transpiration) in plants (Farquhar et al., 1989; Hou et al., 2007a). WUE is influenced by temperature, precipitation, sunlight exposure, and other environmental factors, but also by plant-type physiological mechanisms. For example, the ability of C_4 plants to increase their internal leaf CO_2 concentrations and decrease their stomatal conductance increases their WUE while providing an advantageous adaptation to hot, high-light, water-stressed conditions (Hatch, 1987; Mauseth, 2009). During photosynthesis, plants fix carbon as CO_2 enters leaves through stomata. Amplified stomatal conductance generates an increase in the partial pressure of CO_2 within leaves, thereby expanding the rate of CO_2 assimilation. However, the rate of transpirational water loss also intensifies when plants augment stomatal conductance. The sensitivity of CO_2 assimilation rate to changes in stomatal conductance differs between plants using the Calvin-Benson or Hatch-Slack cycles, but also in C_3 species that have different rates of lipid biosynthesis; e.g. in evergreen vs. deciduous trees (Chikaraishi and Naraoka, 2003; Farquhar et al., 1989; Huang et al., 2006). In

addition, as C₄ plants are able to augment stomatal conductance and reduce transpiration, they fix CO₂ at rates equal or greater than C₃ plants while under similar conditions, resulting in water-use efficiency that is twice that of C₃ plants (Hatch, 1987). Therefore, higher rates of carbon assimilation are maintained when growing under elevated water-stressed conditions.

In terms of carbon-13 isotope values, plants in arid environments have greater WUE and are proportionally enriched in ¹³C than well-watered analogs (Farquhar et al., 1989). This typically registers in more-positive $\delta^{13}\text{C}$ values in leaf wax lipid biomarkers. More-positive $\delta^{13}\text{C}$ of leaf wax *n*-acids also corresponds with greater WUE in various types of C₃ trees (Hou et al., 2007a). Studies (Chikaraishi and Naraoka, 2003; Huang et al., 2006) have shown that evergreen trees have both higher $\delta^{13}\text{C}$ values and WUE than cooccurring deciduous species, likely due to different plant classes having distinguishable isotope effects on carbon (and hydrogen) during *n*-alkane synthesis. Zhang and Marshall (1994) suggest that WUE can be estimated from carbon isotopes for plants from a given region where environmental variables such as soil type, temperature, precipitation, and evaporation are relatively constant.

Hou et al., (2007a) found that trees with greater WUE (as inferred by more-positive $\delta^{13}\text{C}$ values) were negatively correlated with δD values for C₂₆, C₂₈, and C₃₀ *n*-acids, meaning that $\delta^{13}\text{C}$ enrichment correlated with δD depletion. As all their samples were collected within 50 m of the same pond, precipitation, temperature, humidity, soil, and source water should be comparable across sampled trees. Water-use efficiency is likely an important factor in the hydrogen isotope ratios of leaf lipids, so observed differences in hydrogen isotopic variation can, at times, be attributed to tree-type physiological mechanisms; plants with better WUE transpire less water to produce the same amount of leaf biomass compared to species with lower WUE. Smaller transpiration rates result in lessened hydrogen isotopic enrichment of leaf water; when water

transpires from the stomatal cavities, remaining leaf water becomes enriched in deuterium (Farquhar et al., 1989). Therefore, plants with greater WUE should subsequently synthesize leaf waxes with depleted δD . However, Bi et al., (2005) and Chikaraishi and Naraoka (2007) did not observe the same relationship as Hou and coauthors, but instead found variations in the relationships between $\delta^{13}C$ and δD . Because their data was collected from multiple sites and botanical gardens across China, Japan, and Thailand, other factors such as temperature, relative humidity, and precipitation likely impacted the carbon and hydrogen isotope ratios in complex ways. Consequently, water-use efficiency may only be diagnostic in areas where environmental variables influencing hydrogen isotope abundance are consistent and known.

5.5.4 Temperature

At high latitudes, the δD (and $\delta^{18}O$) of precipitation is a function of temperature wherein light isotopes evaporate faster than their heavier counterparts as temperatures decrease. Moreover, the heavy isotope content in precipitation reduces with successive condensation events, as condensation is caused by cooling and heavier isotopes *rainout* first (Dansgaard, 1964). Therefore, initial water condensed from vapor is usually in equilibrium with source water (standard mean ocean water (SMOW)) and will have the same isotopic composition as the source. The variations in deuterium content of natural waters caused by condensation and evaporation lie between +100‰ and -400‰ in regard to the deuterium content of the ocean (Ziegler, 1989). Through further condensation/precipitations episodes, water vapor loses the heavier isotope component and becomes depleted in deuterium. Progressive cooling of air masses leads to precipitation of water depleted in δD (though enriched compared to the vapor remaining in the air), specifically when air masses are transported to high latitudes with lower temperatures (Alley and Cuffey, 2001;

Dansgaard, 1964). Consequently, colder climates have depleted δD precipitation values, with nearly a 5‰ change of δD per degree Celsius (Alley and Cuffey, 2001).

As a paleoclimate indicator for warm vs. cool conditions, more-positive δD may reflect increases in temperature (Feng and Epstein, 1994), particularly at high latitudes (Niedermeyer et al., 2010; Thomas et al., 2012). However, on a seasonal time-scale, Sessions (2006) observed summertime D-depletion in *Spartina alterniflora* from a single location in a coastal Massachusetts marsh; opposite of what would be expected during hotter, drier summer months where leaf-water evaporation should intensify, thus producing more-positive δD values. Investigating fatty acids, *n*-alkanes, and phytol, Sessions (2006) recorded D-depletion by up to 40‰ during the summer in each biomarker class, even though δD of environmental water remained constant. Sessions attributes summertime depletion of deuterium to changes in biosynthetic fractionation, as lipids synthesized during this period utilize acetate and NADPH derived from the decarboxylation of pyruvate. Lipids produced during the fall and spring on the other hand, are more D-enriched as biomass is synthesized from energy reserves stored as carbohydrates. Therefore, biosynthetic fractionation may offset the effect of temperature on δD in some, well-watered plant species.

Sachse et al., (2004) measured the hydrogen isotopes on C_{12} - C_{31} *n*-alkanes of sediments from 13 European groundwater-fed lakes along a north-south transect between 40° and 70° N latitude. Although sample size was limited due to low *n*-alkane concentrations in some samples, Sachse et al., identified correlations between lipid compound, source water, and temperature. Algal derived C_{17} and terrestrial plant derived C_{29} show strong correlations with latitude in that samples from more northern latitudes with lower mean annual temperatures had more-negative δD values compared to lower latitude counterparts. (Meteoric water displayed the same trend.) The δD of C_{17} also recorded lake and meteoric water δD , suggesting that meteoric water is the source of hydrogen

for the C₁₇ biomarker, and that in terms of paleohydrological implications, demonstrates that this alkane can be used to reconstruct the δD of lake water (Cf. Garcin et al., (2012)). The C₂₅-C₃₁ *n*-alkanes are also isotopically lighter in the north than in the south (though temperature does not seem to be a factor) and are generally 30‰ heavier than C₁₇ due to evaporation processes in the leaves of the plants. The more-negative δD of plant wax lipids correlates positively with more negative meteoric source water δD , suggesting that the difference between C₁₇ and C₂₅-C₃₁ (when both share the same source water) can serve as a proxy for evapotranspiration of lake ecosystems.

Wirth and Sessions (2016), studying the hydrogen isotopic composition of C₂₈ *n*-alkanoic acid from Younger Dryas and Holocene aged lake sediments from the southern European Alps, noted δD variability coincident with temperature fluxes. Between 12.9 and 12.8 thousand years ago (Ka), a 14‰ δD decrease corresponded to an early cooling event marking the onset of the cold Younger Dryas period. However, during the subsequent Younger Dryas interval, δD does not correlate with further climate cooling as evident in other climate proxies from the Alps and western Mediterranean. Wirth and Sessions posit that a moisture-source change and a significant reorganization of the vegetation composition (from primarily trees to shrubs) overrode the effect of lower temperatures on δD . ($\delta^{13}C$ was not measured, and therefore the authors could not comment on the impact vegetation changes had on the δD signal.) Again, at the end of the Younger Dryas (11.6 Ka), there was no statistically significant change in δD even though other proxies from the region document that air temperatures rose by ~2-3°C.

During the Holocene, Wirth and Sessions identified punctuated periods of more-positive δD values at 8.9, 8.0, and from 7.4-6.8 Ka, phases that associate with various lines of evidence for warm conditions; however, a northern shift of the ITCZ and changes in precipitation patterns may also have influenced δD values. Depleted δD mark a thousand-year period from 6.2-5.2 Ka that

experienced cold temperatures, and Wirth and Sessions' lowest δD (-180‰) correlates to late Holocene cooling around 700 years BP. Interestingly, during the Little Ice Age (~1450-1850 AD), δD values increase, signaling that changes in source moisture outweighed the temperature effect in their record.

In the tropics however, the temperature effect is not generally detectable because initial cloud formation and precipitation are spatially and temporally narrow (Niedermeyer et al., 2010), resulting in a negligible impact of tropical temperature change on rainwater δD . The dominant mechanism influencing precipitation δD within the tropics is the "amount effect" (Dansgaard, 1964; Ziegler, 1989), whereby rainfall intensity controls the (re)evaporation and isotopic enrichment of rain. This leads to lower (more-depleted) δD values in areas of high precipitation and higher values (more-enriched) δD when precipitation is low, and evaporation enhanced. Niedermeyer suggests that the potential influence of temperature on the isotopic composition of precipitation in the tropics is small compared to the amount effect. Therefore, provided that the local controls on the δD of precipitation are stable over time, changes in the isotopic composition of plant wax *n*-alkanes reflect changes in the amount of precipitation with stronger depletion in δD at higher rainfall rates (Niedermeyer et al., 2010).

Plants utilizing the C_3 , C_4 , or crassulacean acid metabolism (CAM) photosynthetic pathways show characteristically different discrimination against ^{13}C during photosynthesis, but for each photosynthetic type, CAM plants are the only that show large variations in isotope fractionation with temperature, while C_3 and C_4 plants do not (O'Leary, 1981). O'Leary (and references therein) report that $\delta^{13}C$ becomes slightly depleted (~2‰) over a six-degree temperature increase from 7° to 13° in C_3 *Phleum pretense* (Timothy-grass), but this effect decreased to less than 1‰ over a temperature range increase from 26° to 32°. Although the temperature effect on

$\delta^{13}\text{C}$ is negligible, Maffei et al., (1993) noticed an accumulation of epicuticular hydrocarbons (*n*-alkanes) in Rosemary (*Rosmarinus officinalis*) in low-temperature growth experiments, but also found an overall decrease in epicuticular fatty acids under the same conditions. Garcin et al., (2012) also detected higher *n*-alkane concentrations in lake surface sediments from Cameroon coinciding with higher elevation and cooler temperatures. An increase in *n*-alkane concentrations may be an adaptive metabolic response for protecting leaf surfaces in lower temperatures, but the impact of the accumulation of hydrocarbons on $\delta^{13}\text{C}$ is not well understood. Indirectly however, the $\delta^{13}\text{C}$ of lipid biomarkers may be used as a proxy for relative temperatures; C_4 plants improve productivity under hot, dry conditions and thus, a positive isotope shift may indicate an increase in C_4 biomass due to elevated temperatures.

δD , and to an extent $\delta^{13}\text{C}$, display a systematic trend towards more-negative values with increasing altitude, presumably the result of decreasing temperature with higher elevation (Jaeschke et al., 2018; Wirth and Sessions, 2016). Wirth and Sessions identified an altitude effect of $-3.7\text{‰}/100\text{ m}$ for δD in the southern European Alps over an altitudinal range from 440 to 1,130 m a.s.l. This gradient is due to the δD of precipitation, which is dependent on altitude and becomes sequentially more-depleted with increasing elevation because of the *rainout* of heavy hydrogen (Dansgaard, 1964). Jaeschke et al., (2018) noted an altitude effect on δD of $-17\text{‰}/1,000\text{ m}$ and on $\delta^{13}\text{C}$ of $-5\text{‰}/1,000\text{ m}$ in forest soil *n*-alkanes from the southwest Ethiopian highlands over an altitudinal range from 1,600 to 2,700 m a.s.l. This is contrariwise to a global dataset of C_3 plants from mountain ranges around the world that displays increases in $\delta^{13}\text{C}$ values coinciding with rising altitude due to higher water-use efficiency in response to both lower temperature and atmospheric partial pressure of CO_2 at greater elevation (Körner et al., 1988). The average species-level $\delta^{13}\text{C}$ response to altitude change is between $+1.1$ and $+1.2\text{‰}/1,000\text{ m}$, and is attributed to the

physiological effect of lower temperature and $p\text{CO}_2$ above ~2,000 m.a.s.l. (Körner et al., 1988; Wei and Jia, 2009). Below ~2,000 m however, precipitation plays an important role in C_3 and C_4 plant distributions, with vegetation shifts from arid shrub and grass ecosystems to moist evergreen broad-leaved forests explaining the depleted $\delta^{13}\text{C}$ values coincident with elevation increases up to ~2,000 m (Jaeschke et al., 2018; Wei and Jia, 2009).

5.5.5 Aridity/Humidity

Because precipitation plays an important role in C_3 and C_4 plant distributions, the $\delta^{13}\text{C}$ of leaf wax lipids preserved in sediments provides an indirect method of examining moisture content and the pronounced effect on vegetation type. Tropical vegetation is a sensitive indicator of moisture and aridity because its distribution is mainly controlled by precipitation, which in tropical East Africa, is influenced by the seasonal migrations of the Intertropical Convergence Zone (ITCZ) (Castañeda et al., 2007) and altitude (Jaeschke et al., 2018). Furthermore, as elevated temperatures, high-light intensity, and aridity intensify rates of photorespiration and therefore enrich leaf lipids in ^{13}C , it is possible to use $\delta^{13}\text{C}$ as an inference for changes in aridity and humidity. However, aridity is best interpreted using a combination of carbon and hydrogen isotopes as competing factors must also be considered when interpreting sedimentary $\delta^{13}\text{C}$ values (Diefendorf and Freimuth, 2017).

Applying compound-specific $\delta^{13}\text{C}$ measurements on long-chain *n*-alkyl lipids from Sacred Lake, Mt. Kenya, Huang et al., (1999) observed 10 to 15‰ glacial-interglacial changes in $\delta^{13}\text{C}$ values, a reflection of changes in the proportion of C_3 and C_4 plants. During the Last Glacial Maximum lower $p\text{CO}_2$ (see above) coupled with a drier and colder climate allowed C_4 vegetation to prevail in the Sacred Lake catchment area. But, as indicated by $\delta^{13}\text{C}$, the onset of the Holocene

signalled the colonization by montane C₃ forest, albeit punctuated by periods of enhanced aridity and $\delta^{13}\text{C}$ enrichment resulting from an increased abundance of dry adapted C₄ plants.

Liu et al., (2011) evaluated hydrological changes over the last ~800 years in the Tarim Basin of northwestern China using bulk carbon isotopes of plant remains from a 10.5 m long eolian sand sediment core. Large negative isotopic excursions of up to 6‰ during the ‘Little Ice Age,’ a relatively cold period dated to approximately 1450 to 1850 AD, are much lower than values from before and after this period, suggesting wetter climatic in the Tarim Basin at that time. Additionally, more-positive carbon values before the Little Ice Age and a sharp increase in $\delta^{13}\text{C}$ around 1890 AD correlate with part of the ‘Medieval Warm Period’ and the current warm/dry period of northwestern China, respectively. This suggests that the Tarim Basin was relatively humid between 1500 and 1850 and that the bulk $\delta^{13}\text{C}$ recorded changes in aridity/humidity over this 800-year period. Moreover, the isotope data was corroborated with geologic indicators for wet depositional environments; silty clay layers deposited under an alluvial fan/flood delta plain environment.

By combining plant wax $\delta^{13}\text{C}$ values with pollen, indicators for fire, and sea surface temperature, Sikes et al., (2013) identified changes in aridity during the most recent deglaciation of New Zealand and a shift from cold and dry conditions during the Last Glacial Maximum to a seasonally warm and wet climate. Since New Zealand has no native C₄ plants, any isotopic variations in $\delta^{13}\text{C}$ is ascribed to changes in moisture availability during the growth season rather than plant-ecosystem changes. Positive shifts in *n*-alkanoic acid values indicated cold and dry conditions in the Last Glacial Maximum, while at the deglacial boundary, depletions of $\delta^{13}\text{C}$ suggested significant moisture/precipitation events and seasonally wetter conditions.

Analyzing $\delta^{13}\text{C}$ of dust-borne C_{31} *n*-alkanes from a deep sea core in the eastern tropical Atlantic Angola Basin, Schefuß et al., (2003) correlated C_4 plant distributions with sea surface temperatures (SST) attained from C_{37} alkenones between 1.2 Ma and 450,000 years ago and showed that aridity is a dominant control on the large-scale distribution of C_3 versus C_4 vegetation in tropical Africa. Their vegetation distributions correlate with SST during the middle Pleistocene (after 650,000 years), in that lower SST reduced tropical evaporation and the total atmospheric moisture content, the main source of southwest African rainfall, resulting in an increase of C_4 vegetation. The authors interpret C_3/C_4 plant variations as an ecological response to changes in continental aridity driven by monsoonal precipitation; these results indicate that aridity is the dominant climatic control of continental-scale C_4 plant distributions and that changes in the strength of monsoons and atmospheric moisture balance, controlled by tropical SST, determined Pleistocene African vegetation structure.

These interpretations however, only hold for the middle Pleistocene period and do not correlate with their >650,000-year record where increases in temperature co-vary with increases in C_4 vegetation. It is feasible that prior to the middle Pleistocene, temperature was the dominant control of C_3 or C_4 distribution, and that increases in temperature regardless of available moisture, influenced the overall percentage of C_3 or C_4 vegetation perhaps through changes in plant water-use-efficiency.

Castañeda et al., (2007), using $\delta^{13}\text{C}$ values of $\text{C}_{29}\text{-C}_{33}$ *n*-alkanes extracted from late Pleistocene and early Holocene aged sediment cores in Lake Malawi, the southernmost lake in the western branch of the East African Rift Valley, also highlighted the sensitivity of C_3 and C_4 vegetation as aridity indicators. Noting increases in abundances of C_4 vegetation during times of low, intermediate, and high $p\text{CO}_2$, they suggest that $p\text{CO}_2$ fluctuation alone are not sufficient for

driving vegetation changes. Therefore, Castañeda et al., (2007) correlated their $\delta^{13}\text{C}$ evidence with that of Lake Malawi temperature data (of Powers et al., (2005)) and noted strong links between temperature and aridity in southeastern Africa for late Pleistocene sediments; atypically, their C_4 abundances increased with cooler temperatures, implying an association between warm and wet, and cool and dry growing conditions. Because C_4 expansion coincided with cooler, drier conditions around Lake Malawi, vegetation changes in East Africa during this time were mainly driven by changes in aridity likely brought on by greater solar insolation, consistent with previous studies of tropical Atlantic Africa by Schefuß et al., (2003). Castañeda et al., (2007) propose that latitudinal shifts in the position of the ITCZ is the mechanism by which warmer/wetter or cooler/drier conditions prevailed in southern East Africa during the late Pleistocene.

The relationship between aridity and C_4 expansion is asynchronous in the early Holocene, however. Although C_4 vegetation coincides with cooler temperatures, $\delta^{13}\text{C}$ values and moisture index inferred from ice-core methane (CH_4) records from Antarctica and Greenland antiphase, with C_4 abundance increasing around Lake Malawi during global-scale wetter intervals. It is possible that decreases in solar insolation in the southern hemisphere at the start of the Holocene decreased surface evaporation and the moisture availability for precipitation in southern East Africa.

Because both studies only identified synchronous relationships between aridity and C_4 expansion in certain sections of their cores, $\delta^{13}\text{C}$ alone is not in and of itself a powerful indicator of aridity and humidity. δD on the other hand, may be better suited for identifying aridity or humidity in paleo-records, as regional meteoric water is the primary control on the leaf wax δD signatures, and δD of terrestrial plants is a function of atmospheric relative humidity (Barbour and

Farquhar, 2000; Bi et al., 2005; Garcin et al., 2012; Polissar and Freeman, 2010; Sachse et al., 2004, 2006; Yang and Leng, 2009; Yapp and Epstein, 1982).

Additionally, under conditions of low atmospheric relative humidity, evapotranspiration increases, leading to deuterium enrichment of plant leaf water and the organic compounds synthesized within (Yapp and Epstein, 1982). Drier conditions exacerbate soil water evaporation, enriching soil water δD values while at the same time, concentrating deuterium in plant leaf water due to enhanced evapotranspiration (Yapp and Epstein, 1982). Both occurrences lead to higher δD values of plant leaf wax lipid biomarkers. Therefore, changes in D/H ratios of leaf waxes may be used to reconstruct past changes in relative humidity when such effects as temperature and plant type can be independently constrained by using $\delta^{13}C$ (Liu and Huang, 2005).

Andersen et al., (2001) interpreted D-enriched C_{22} *n*-alkanes (and isoprenoids) in upper Miocene (7-5 Ma) sediments from the Mediterranean Sea as a response to large fluctuations in δD values (up to 160‰) resulting from intensive evaporation and changes in relative humidity. Hydrogen has the largest relative mass difference between its stable isotopes 1H (1.007947 amu) and 2H or D (2.014102 amu), and when seawater ($\delta D = 0‰$) evaporates, the resultant water vapor is depleted in heavy hydrogen because $^1H_2^{16}O$ is lighter, has a higher vapor pressure, and evaporates faster than $^1H^2H^{16}O$ or $^2H_2^{16}O$ (Sachse et al., 2012). Conversely, when water vapor condenses into precipitation, the resulting rain is enriched in heavy hydrogen relative to the D-depleted vapor. Because deuterium enrichment increases with decreasing humidity, the D-enriched composition of the two biomarkers indicate intense evaporation and low relative humidity in and around the Mediterranean Sea during the late Miocene (Andersen et al., 2001).

Similarly, Liu and Huang (2005) attributed considerable variations in C_{27} - C_{31} *n*-alkane δD values over a 14 meter, 130,000-year sequence from the Chinese Loess Plateau to increased aridity

and the ensuing impact on local precipitation. Alternating sequences of paleosol and loess depositional phases of the Chinese Loess Plateau correspond to relatively wet and dryer phases, respectively, whereby more-positive δD correlated to dryer loess deposition while more-negative δD values linked to the wetter paleosol horizons. The loess depositional phases are characterized by dryer conditions which resulted in more-positive δD values of soil water and the concentration of deuterium in plant-leaf-water due to enhanced evapotranspiration; both of which results in D-enriched *n*-alkanes.

Huang et al., (2007) likewise linked C_{27} - C_{33} *n*-alkane δD values to hydrological changes in precipitation and evaporation in an 11-million-year record from Miocene sediments in the Arabian Sea. Dramatic changes in hydrogen (and carbon) isotopic ratios of leaf waxes suggest major transformations in integrated continental vegetation communities driven by increases in aridity and fluctuations in rainfall patterns and timing. Their data suggest significant variability in C_4 plant abundances, particularly between 7.9 and 5.5 Ma when the proportion of C_4 plants increased from 15% to 65%, and after 5.5 Ma when the amount reached 75%. Huang and coauthors ascribe δD enrichments of $\sim 50\text{‰}$ between 8.3 to 6 Ma, and an additional $+30\text{‰}$ between 6.0 to 1.0 Ma to increases in aridity that subsequently drove the late Miocene expansion of C_4 plants. Moreover, the major phases of increasing δD values slightly precede the $\delta^{13}C$, thus implying that aridity was the dominant driver for the late Miocene expansion of C_4 plants in the Arabian Peninsula and southern Asia.

Diatom-based oxygen isotope data and palmitic acid derived δD isotope values from Lake Malawi depict century-to-millennial scale humid/arid episodes over the last 25,000 years in southeast Africa (Barker et al., 2007). *n*-Acid δD records obtained from lipids of aquatic-algae origin show major shifts in precipitation and evaporation in the Late Pleistocene/Holocene Lake

Malawi region, overlapping with seasonal variation in algal groups and total biomass. Furthermore, the authors compared their $\delta^{18}\text{O}$ and δD evidence with that of Lake Malawi temperature data (of Powers et al., (2005)), and found that warmer lake temperatures correlate with depleted δD values, likely due to heightened rainfall in the lake catchment area during these intervals. These warm, wet periods also match with warm periods depicted in Greenland ice cores and fall within cycles for postglacial expansion of more-northerly EARS lakes. Alternatively, Barker et al., found that dry events in Lake Malawi coincide with cool periods represented in Greenland ice core temperature reconstructions. Therefore, it appears that stages of cooling in the tropics over the last 25,000 years reduced overall humidity levels and rainfall in the Lake Malawi region, resulting in the more-positive δD isotope values in dry periods, and more-negative values in wet periods, correlating with Castañeda et al., (2007) $\delta^{13}\text{C}$ interpretations for the same period.

Finally, Sachse et al., (2012) assembled a global data set of site-averaged $\delta\text{D}_{\text{C}_{29}}$ from living plants and mean annual precipitation δD ($\delta\text{D}_{\text{MAP}}$), and emphasized a trend toward more-positive, D-enriched isotope records in drier regions. Moreover, they identified more-positive $\delta\text{D}_{\text{C}_{29}}$ values in long-lived shrubs and shrub-like trees, which are common and widespread in seasonally dry, arid, and hyperarid environments. Sachse et al., advocate that D-enriched shrub waxes may be due in part to climatic factors favoring evaporative D-enrichment signals.

5.5.6 Source Water

Ultimately, source water hydrogen is the primary signal recorded in the δD values of *n*-alkanes, *n*-alcohols, and *n*-alkanoic acids derived from terrestrial plants (Bi et al., 2005; Garcin et al., 2012; Hou et al., 2007b; Sachse et al., 2004; Sauer et al., 2001). Although variability exists in the δD of plant waxes in regard to plant source water (Chikaraishi and Naraoka, 2003; Huang et

al., 2004; Sachse et al., 2004, 2006; Sessions et al., 1999), regional meteoric water δD is the primary control on leaf wax signatures (Bi et al., 2005; Garcin et al., 2012; Sachse et al., 2012). Different organisms use different environmental water as their source of hydrogen, and several environmental factors influence the isotopic signature of precipitation δD . As discussed above, the *rainout* process is interrelated with the ‘temperature effect’, specifically in high latitudes. This has a pronounced effect on the fractionation of hydrogen with precipitation being enriched by approximately 74‰ relative to water vapor at 25°C, whereas at colder temperatures, the fractionation is about 100‰ at 0°C (Sachse et al., 2012). In tropical regions characterized by strong seasonality in rainfall rather than seasonal temperature variations, the ‘amount effect’ (Dansgaard, 1964; Ziegler, 1989) dictates the isotopic composition of precipitation in which greater depletion of δD corresponds to higher precipitation rates. Finally, when water vapor travels further inland, deuterium is preferentially lost during subsequent rainfall events, resulting in isotopically lighter precipitation with increasing distance from the source. Known as the ‘continental effect’ (Dansgaard, 1964), this pattern has been observed in the hydrogen isotopic composition of higher plant leaf waxes, and may prove particularly useful in tracing precipitation with high fidelity, especially in dry regions with less than 400 mm mean annual precipitation (Hou et al., 2008a).

During the biosynthesis of lipids, aquatic organisms such as cyanobacteria, algae, and submerged and floating plants utilize environmental water from lakes, wetlands, or rivers (water sourced from precipitation), as their hydrogen pool. The δD of *n*-alkane C₁₇ records meteoric water δD , and in terms of paleohydrology, can be used to reconstruct the δD of environmental source water (Sachse et al., 2004). (However, Garcin et al., (2012) found that the δD values of aquatic *n*-C₁₇ alkane from 11 lake surface sediments in Cameroon were not correlated with the δD values of lake water.) In arid regions where evaporation exceeds precipitation, source water becomes

enriched in deuterium, and therefore, the degree of evaporation experienced by lake, wetland, or river systems may be estimated using aquatic organisms' wax biomarkers.

Soil moisture and groundwater are the main water source for terrestrial plants, but fog, dew, and cloud water also provide additional moisture for photosynthesis and leaf wax biosynthesis (Tipple et al., 2013). Because precipitation is the original source of both soil moisture and groundwater, the variability of the leaf-water isotopic composition recorded in leaf wax lipids reflects an amount-weighted average of precipitation inputs (Sachse et al., 2012). Ecological lifeform however, plays an important role in controlling the hydrogen isotopic composition of leaf wax *n*-alkanes and *n*-acids as different plants tap into different water pools (Garcin et al., 2012; Yang and Leng, 2009). For example, grasses, often having short roots, tend to use near-surface soil water deriving from recent precipitation events, whereas trees and shrubs usually have longer and deeper roots, which allow them to absorb water from deep soil horizons or groundwater aquifers (Liu et al., 2006). In areas with adjacently growing grasses and woody plants, grasses have been found to possess more-negative δD values than their woody counterparts because they absorb surface soil water, which in many places is seasonally controlled (Liu et al., 2006). In contrast, trees and shrubs have more-positive δD values because they absorb water from deep soil horizons. In fact, Dawson and Ehleringer (1991) documented through xylem water hydrogen isotopes that trees growing next to a stream used little to no surface water because their roots penetrate deep underground. Therefore, the difference in plant water absorption system may be one of the primary reasons why grasses have more-negative δD values than woody plants from the same ecosystem.

Konecky et al., (2011) examined a 140,000-year record of leaf wax δD from two lacustrine sediment cores taken in Lake Malawi's northern and central basins for the relative influence of

source region, transport history, and convective, evaporative, and distillation processes on C_{28} *n*-acid δD in the lake catchment area. Contrary to what one would expect for the tropics, Konecky and coauthors identified long-term D-enrichment beginning 56,000 years ago coinciding with the onset of wetter conditions in the Lake Malawi region as evident by a nearly 300 meter lake level rise; opposite to what is expected due to the amount effect (Dansgaard, 1964). This led the authors to suggest that changes in transport history between Indian and Atlantic Ocean source moisture, not the amount effect, act as the dominant control on δD in the Lake Malawi region.

Comparing the δD of precipitation deriving from the Indian and Atlantic Oceans and estimating the fractionation (see Section 5.6) between water vapor and leaf wax lipids, Konecky et al., noted changes in precipitation sources for Pleistocene-to-Holocene Lake Malawi. Specifically, the majority of their Lake Malawi record reflects predominant moisture originating from the northern Indian Ocean driven by the winter Indian monsoon. Depletions in leaf wax δD of up to -35‰ however, were determined to be the result of a source change to southeasterly winds transporting vapor from the southern Indian ocean, which loses much of its moisture in the Madagascar highlands before reaching the African continent. The *rainout* process (Dansgaard, 1964) helps explain the δD depletion corresponding to a moisture source change, as the heavier isotopes would fall in Madagascar first, with the more-depleted rain falling on the Lake Malawi region.

In tropical western Africa, Garcin et al., (2012) studied the δD of C_{17} , C_{29} , and C_{31} *n*-alkanes from across a highly ecologically diverse transect in Cameroon, which included both lacustrine and terrestrial sediment samples encompassing steep climate and vegetation gradients as well as the δD of lake water, precipitation, river water, groundwater, and plant-xylem water. Although the aquatic algae-derived C_{17} did not correlate with lake water δD (such as that of Sachse

et al., (2004)), the isotopic composition of surface waters (i.e., river water and groundwater) were found to exert the primary control on C₂₉ δD values, whereas plants with a dominant C₃₁ alkane chain derived their source water either from lakes or other, non-surface waters. Garcin and coauthors suggest that plants growing in the Cameroon transect have different dominant long-chain *n*-alkane homologues and utilize source waters with dissimilar isotopic compositions. Furthermore, they demonstrated that C₂₉ δD correlated with river and groundwater, while C₃₁ and lake water δD were synchronized, and thus plants with a dominant C₃₁ alkane sourced their water from different pools than that of the C₂₉ alkane-dominant plants.

Garcin et al., (2012) hypothesized that while terrestrial plants with a dominant C₂₉ homologue occupied catchment areas and sourced their water from river or groundwater, plants with a dominant C₃₁ homologue inhabited lakeshore environments. Extrapolating this finding to paleoenvironmental reconstructions, the C₃₁ *n*-alkane could be used as a proxy for plants growing along or near paleo-Lake Olduvai, while the C₂₉ alkane could be an indicator of plants growing along rivers or streams that emptied into the paleo-lake. However, vegetation type (i.e., C₃ vs. C₄ plants; grasses vs. trees and shrubs) should be considered using δ¹³C to determine whether the dominant *n*-alkane homologue is a product of ecological lifeform rather than source water.

Source water identification using leaf wax biomarker analysis also pinpointed the hydrogen isotopic composition at the Paleocene/Eocene Thermal Maximum 55 million years ago. Pagani et al., (2006) identified different water sources using the δD of C₁₇, C₂₇, and C₂₉ *n*-alkanes, whereby C₁₇ recorded the δD of Arctic surface waters, while C₂₇ and C₂₉ reflected the hydrogen isotopic composition of precipitation in the Arctic region. Their results suggest that Arctic precipitation 55 Ma was substantially D-enriched relative to today, and that the hydrogen isotopic compositions of source water was comparable with modern, mid-latitude precipitation. Pagani et al., interpret their

isotope record as documenting decreased rainout and increased moisture delivery during poleward moisture transport to the Arctic, likely due to a global decrease in latitudinal temperature gradients that would have reduced rainout, and therefore more water vapor would have been transported to high latitudes.

5.6 Isotope Fractionation

The complex relationship between and among the controls on $\delta^{13}\text{C}$ and δD of lipid biomarkers (Section 5.5) results in the *fractionation* of carbon and hydrogen isotopes between the source (i.e. atmosphere or water) and synthesized leaf waxes such as *n*-alkanes and acids. Isotope fractionation is the partitioning of isotopes between two substances (e.g. the atmosphere and plant leaf material) leading to different isotope ratios (Hoefs, (2009): 6), that transpires during the exchange between different physiochemical mechanisms such as photosynthesis or through kinetic effects like evaporation. The main fractionation process in plants is carbon fixation during photosynthesis, specifically during the intracellular diffusion of CO_2 and the biosynthesis of organic compounds such as carbohydrates, lignin, proteins, and lipids (Collister et al., 1994; Hoefs, 2009). Photosynthetic pathway plays a substantial role in the fractionation of carbon because ultimately, the observed differences in *n*-alkyl $\delta^{13}\text{C}$ values between C_3 and C_4 plants is a function of ^{13}C discrimination during the Calvin-Benson and Hatch-Slack cycles. Hydrogen isotope fractionation on the other hand is not as well understood; complex factors including taxonomy (Hou et al., 2007b), lifeform (Liu et al., 2006), climate gradient (Sachse et al., 2006), and light irradiation (Yang et al., 2009) influence the isotopic offset between source water and biosynthesized compounds and makes for difficulties in determining the fractionation pathway of hydrogen from source water absorption to synthesized organic compounds.

5.6.1 $\delta^{13}\text{C}$ Fractionation

It is the exchange of CO_2 between the atmosphere and leaf tissue through stomata, and subsequent photosynthesis within leaves, that causes the larger carbon-13 depletion in C_3 vegetation, depleted in $\delta^{13}\text{C}$ by about 15‰ on average compared to C_4 plants; C_4 flora eliminate this free exchange by concentrating carbon dioxide in bundle-sheath cells (Farquhar et al., 1989). Transfer of CO_2 across the leaf cuticle into the mesophyll and to the chloroplasts causes an initial fractionation of about -4.4‰ (Tcherkez et al., 2011), but because the carboxylation enzyme RuBisCo discriminates strongly against heavier ^{13}C (whereas PEP in C_4 plants does not appear to differentiate against ^{13}C (Ehleringer, 1989)), C_3 plants generally contain proportionally less ^{13}C than the atmosphere (Farquhar et al., 1989). Photorespiration (Fig. 5-7) is another mechanism that produces differences in ^{13}C patterns between C_3 and C_4 plants, as photorespiration is an important reaction in C_3 metabolism but not in C_4 (Hobbie and Werner, 2004). The isotope fractionation associated with RuBisCO and photorespiration results in an average C_3 bulk-biomass $\delta^{13}\text{C}$ value of -29‰, depleted by about -18 to -20‰ in comparison to the current atmospheric CO_2 value of -8‰ (Hoefs, 2009; Tcherkez et al., 2011). The isotope effect of C_4 plants on the other hand, is much smaller, only about -4 to -6‰ (Hoefs, 2009; O'Leary, 1981).

^{13}C is irregularly distributed between carbohydrates, proteins, and lipids, with lipid compounds being considerably depleted in ^{13}C relative to other biosynthetic products (Hoefs, 2009). Total lipids are depleted in ^{13}C by 5-8‰ relative to the bulk biomass, while *n*-alkanes are further depleted in ^{13}C relative to bulk tissue by 6.5-14‰ and 2-9‰ in C_4 and C_3 plants, respectively (Collister et al., 1994). Therefore, *n*-alkane $\delta^{13}\text{C}$ values from modern plants can range between -29‰ and -39‰ in C_3 flora and between -14‰ and -26‰ for C_4 (Bi et al., 2005; Chikaraishi and Naraoka, 2001; Collister et al., 1994; Vogts et al., 2009).

Straight-chain *n*-alcohols and *n*-acids are closely related to *n*-alkanes biosynthetically, and thus these three compounds are expected to have isotopic compositions similar to one another (Collister et al., 1994). For example, Conte et al., (2003) showed that the $\delta^{13}\text{C}$ of these compounds fell within 1‰ of each other in nine northern mixed mesic prairie species growing in southern Alberta. Chikaraishi and Naraoka (2007) also demonstrated a similar pattern by showing that in 14 C_3 angiosperms, four C_3 gymnosperms, five C_4 grasses, and two CAM plants from Japan and Thailand, *n*-alkanes and *n*-alkanols were enriched in ^{13}C by 1.4‰ and 1.3‰, respectively relative to the corresponding carbon-numbered *n*-alkanoic acids. In addition, because these *n*-alkyl compounds are synthesized from acetate, which is produced from the decarboxylation of pyruvate, the depletion of lipids relative to biomass is associated with the isotopic fractionation during the oxidation of pyruvate to Acetyl-Coenzyme A (Fig. 5-3) (O'Leary, 1981). The similar isotopic distribution among the *n*-alkyl compounds recognized by Conte et al., and Chikaraishi and Naraoka, indicates that for individual plant species, *n*-alcohols, *n*-acids, and *n*-alkanes originate from the same straight-chain compound produced by a common acyl-acyl carrier protein (Section 5.2). For instance, the C_{30} alkanolic acid, C_{29} alkane, and C_{30} alkanol are synthesized from a shared C_{30} acyl-ACP predecessor (e.g. Fig. 5.2) and will share similar $\delta^{13}\text{C}$ values.

5.6.2 δD Fractionation

The hydrogen isotopic composition of plant leaf tissue is affected by two major fractionation processes; evapotranspiration in both soil- and leaf-water which contributes to the overall net fractionation within plants by enriching leaf water δD , and enzymatic reactions during biosynthesis which depletes organic products through hydrogen exchange (Sachse et al., 2012; Yang and Leng, 2009). Relative humidity, plant lifeform (e.g. tree, shrub, grass), physiological

differences in photosynthetic pathways, light irradiation, water-use efficiency, and the original δD content of source water are additional factors that influence leaf-water δD and subsequent synthesized organic products (Castañeda and Schouten, 2011; Hoefs, 2009; Yang et al., 2009; Ziegler, 1989). The sum of these chemical and physical fractionation processes can result in large D-depletions of up to -150‰ or more, especially during lipid biosynthesis.

For the most part, water is not altered isotopically during uptake by roots (but Cf. Ellsworth and Williams (2007) regarding xerophytes), rather transpiration from leaves due to evaporation and strong discrimination against H_2O but in favor of HDO during evapotranspiration is associated with δD fractionation enrichment of up to 40-50‰ in terrestrial plants (White, 1989; Ziegler, 1989). Evaporation of source water determines the hydrogen isotope content of vapor relative to liquid water, whereby water in the oceans is more enriched than vapor due to vapor losing the heavier isotope component, becoming depleted in δD in the process (Alley and Cuffey, 2001; Dansgaard, 1964). However, the extrinsic effect of external factors on plant- δD isotope fractionation and composition of intercellular water is still poorly understood, even after numerous studies (see references throughout Section 5.5) investigated relationships between hydrological variables and leaf wax lipid biomarkers and identified climatic and physiological drivers impacting lipid δD values. These studies, and others on cellulose and bulk organic matter (Yapp and Epstein, 1982), indicate that D/H ratios of terrestrial plants are primarily influenced by source water (rather than metabolic or physiological mechanisms) before D-depletion from enzymatic reactions during biosynthesis.

Like carbon, there is an irregular distribution in δD between carbohydrates, proteins, and lipids, with lipid compounds being considerably depleted in deuterium relative to proteins and carbohydrates. Straight chain lipids for example, are depleted in D by 150-200‰ relative to source

water (Hoefs, 2009). Alkyl lipids synthesized along the Acetyl-CoA pathway have the smallest D-depletion relative to source water, and because these products are synthesized from an acetate progenitor, they inherit hydrogen from Acetyl-CoA, NADPH (the most D-depleted), and directly from water (the most D-enriched) resulting in large δD ranges between -400 and +200‰ in lipids biomarkers (Chikaraishi and Naraoka, 2003, 2007; Sessions et al., 1999). Another important reaction during lipid synthesis is the formation of *n*-alkanes through the decarboxylation of *n*-alkanoic acids; Generally, *n*-alkane and *n*-alkanol are depleted in D by -25‰ and -15‰, respectively relative to the corresponding carbon-numbered *n*-alkanoic acid (Chikaraishi and Naraoka, 2007; Sessions et al., 1999) which could be due to differences in the hydrogen isotopic composition of acetate and/or NADPH used in biosynthesis.

5.7 Leaf Wax Diagenesis

5.7.1 Preservation

As mentioned in the chapter opening, straight, long-chain hydrocarbons are for the most part, chemically inert and resistant to biodegradation in sediments over geologic time (Eglinton and Eglinton, 2008), and due to their small size, readily dispersed into the environment. Water insoluble leaf waxes exhibit great resistance to hydrolytic enzyme microbial degradation, and are therefore some of the best-preserved biomolecules (Killops and Killops, 2005). Additionally, some compounds, such as carboxylic acids, contain polar and reactive functional groups and adsorb into mineral matrices like clay or silt that then travel throughout the environment (Eglinton and Eglinton, 2008), which also limits them as bioavailable compounds. Multiple factors contribute to the preservation of biomarkers during sedimentation and burial (Peters et al., 1993), including sedimentation rate and grain size, oxic or anoxic deposition, and depositional setting.

Sedimentation rate and grain size play a key role in leaf wax lipid preservation as organic matter is preferentially deposited with fine-grained sediments, specifically in marine or lacustrine settings (Peters et al., 1993). Because fine-grained sediments often limit the infiltration of oxygen-rich waters, they enhance anoxic conditions which subsequently inhibits aerobic microbial biodegradation and detritivore bioturbation. Under oxic conditions, aerobic bacteria readily degrade organic matter but with anoxic conditions, aerobic degradation is limited (Peters et al., 1993). Thus, in anoxic environments, anaerobic degradation is less efficient and there is enhanced preservation of lipid-rich organic matter in sediments. One way this can be tested is through hopanes, bacterial lipid precursors that can form in reducing environments (Peters et al., 1993), as their presence in Total Lipid Extracts can be used as a tracer for bacterial activity in anoxic conditions (Wang et al., 2014). The rate of sedimentation and burial improves biomarker preservation by reducing the residence time of organic matter in zones of bioturbation and aerobic activity (Peters et al., 1993), and fine-grained sediments are often organic rich and generally finely-laminated and not bioturbated (Killops and Killops, 2005). Moreover, the sedimentation rate in lakes exceeds that of the deep ocean, and therefore organic matter is buried more rapidly, and preservation is enhanced in lacustrine settings. Regarding *n*-alkanes, an even-over-odd predominance in short-chain (C₁₅-C₂₂) homologues has been attributed to the microbial breakdown of fatty acids or waxy alcohols in sedimentary organic matter, among other activity (Grimalt et al., 1985; Wang et al., 2010), resulting in short-chain *n*-alkanes with dominant even-numbered carbon compounds (opposite of leaf wax *n*-alkanes). Additionally, some species utilize *n*-alkanes as their sole carbon source in sediments (Lattuati et al., 2002) resulting in rapid and extensive degradation. Global climatic events have also been shown to play a role in *n*-alkane preservation or degradation; Wang et al., (2014) found that the production and preservation of *n*-alkanes were common during

interglacial periods in Paleo-Lake Tianyang, South China, while lower production and poor preservation (and possibly greater bacterial activity) was evident in glacial times.

Studies investigating the contributing factors to the preservation of organic matter in sedimentary environments have largely focused on marine and lacustrine conditions under which petroleum source-rocks form. In terrestrial sediments, wind and dust act to ablate leaf waxes, a portion of which accumulate in the air as micrometer-sized particles before being removed by precipitation (Conte and Weber, 2002; Conte et al., 2003; Hadley and Smith, 1989; Rogge et al., 1993; Zafiriou et al., 1985). Because air masses moving across land surfaces accumulate and integrate wax signatures from continental-scale vegetation sources (Conte and Weber, 2002) they must also be considered in terms of area of erosion and rate of wax transfer (Eglinton and Eglinton, 2008), especially during deposition. Although the isotope composition of plant waxes in aerosols have been shown to accurately record a large integrated signal of regional vegetation sources (Conte et al., 2003), and lipid molecules are relatively unaltered during passage through the environment (Eglinton and Eglinton, 2008), most soils are oxygenated and organic matter within can be efficiently degraded by microbial enzymatic activity (Killops and Killops, 2005), even generally well-preserved leaf wax lipids.

5.7.2 Diagenesis and Fractionation

Diagenesis is the biological, physical, or chemical alteration of organic matter in sediments prior to significant changes caused by heat or pressure (Peters et al., 1993). When utilizing the isotope composition of individual leaf wax lipid biomarkers for paleo-reconstructions, it is often assumed that diagenesis does not generate significant fractionation at the molecular level, and studies (Naraoka and Ishiwarati, 2000; Nguyen Tu et al., 2004; Wu et al., 2019) that have

isotopically characterized diagenetic processes have had mixed results in identifying carbon (^{13}C) alteration through chemical and microbial activity. For example, Naraoka and Ishiwarati (2000) suggested that early diagenesis and bacterial reworking does not affect the isotope composition of long-chain ($\text{C}_{20}\text{-C}_{30}$) fatty acids from near-surface marine sediments, while on the other hand, Harvey and Macko (1997) detected a ^{13}C enrichment in short-chain ($\text{C}_{12}\text{-C}_{18}$) fatty acids from mixed sources after 40 days of experimental biodegradation. Moreover, straight chain alkanes, the most commonly used biomarker for compound specific isotope analysis, were found to exhibit a ^{13}C enrichment when transported from river to open ocean (Naraoka and Ishiwarati, 1999). However, no evidence was found for carbon isotope fractionation of individual *n*-alkanes during decomposition in a peat soil (Huang et al., 1997), which may be due to the acidic nature of peat environments (Killops and Killops, 2005). In petroleum samples, microbial degradation of alkanes is often reported and characterized by Unresolved Complex Mixtures (UCM) identified on gas chromatograms of hydrocarbons (Broman et al., 1987; Peters et al., 1993; Venkatesan and Kaplan, 1982), but UCMs and their formation are usually overlooked in studies focusing on the isotopic composition of leaf wax biomarkers in terrestrial sediments. Grimalt et al., (1988) however, showed that *n*-alkanes can suffer from biodegradation soon after deposition due to bacterial alteration of hydrocarbons and the reworking of sedimentary lipids which results in UCMs.

The isotope fractionation of lipid biomarkers resulting from diagenesis is now being investigated, especially for the implications to paleoenvironmental reconstruction studies. In an analysis of fresh (living) and degrading (litter) *Gingko biloba* leaves, Nguyen Tu et al., (2004) observed ^{13}C enrichment in *n*-alkanes during the early stages of diagenesis as lipids extracted from litter leaves were enriched by +3.0‰ compared to fresh leaves. The authors suggest that according to the residence time of plant debris in surface soils before burial, diagenesis may strongly affect

the isotope composition of *n*-alkanes. Additionally, they documented decreasing $\delta^{13}\text{C}$ values coincided with increasing chain length ($\text{C}_{21}\text{-C}_{27}$) in living leaves, but the isotope composition of *n*-alkanes became homogeneous in litter leaves; that is, there was no relationship between chain length and $\delta^{13}\text{C}$ values in degraded leaves. Nguyen Tu et al., (2004) propose that isotope homogeneity of *n*-alkanes could therefore be used as a marker of diagenetic alteration of the original leaf wax isotope signal. Wu et al., (2019), who analyzed both carbon and hydrogen isotope fractionation in tropical leaf litter-to-soil profiles for both the C_{29} *n*-alkane and C_{30} *n*-alkanoic acid, did not find any evidence for systematic changes in δD values due to diagenesis but did document a +4.0‰ to +6.0‰ enrichment in $\delta^{13}\text{C}$ soil lipids. This finding corroborates other leaf-litter-soil studies from different environmental settings (Chikaraishi and Naraoka, 2006; Huang et al., 1996) which documented $\delta^{13}\text{C}$ enrichment between leaf and surface soils for $\text{C}_{27}\text{-C}_{31}$ *n*-alkanes of 2.0-4.0‰.

Even though there seems to be an apparent 2.0-4.0‰ $\delta^{13}\text{C}$ enrichment in both *n*-alkanes and *n*-alkanoic acids as a result of diagenesis, Brittingham et al., (2017) found a $\delta^{13}\text{C}$ depletion of -4.2‰ in sedimentary samples stored at room temperature for three years and the accompanying bacteria containing gene coding for *n*-alkane degrading enzymes. Because sampling and storage may promote bacteria proliferation by exposing them to different oxygen and moisture conditions, the unique setting created during storage may be responsible for the $\delta^{13}\text{C}$ depletion rather than an enrichment that is seen in litter studies. This is corroborated by Nguyen Tu et al., (2011) who provide evidence for microbial contributions to decaying litter for specific alkanes ($\text{C}_{25}\text{-C}_{29}$) through litterbag studies but also note that there is disparity in reported $\delta^{13}\text{C}$ values depending on the environment investigated; e.g. oxic vs. anoxic, well-drained vs. stagnant water. Nevertheless, both bacteria and filamentous fungi efficiently degrade long-chain hydrocarbons (Leahy and

Colwell, 1990; Verstraete et al., 1976), and because they may be the driving force of leaf wax lipid biodegradation in soils, additional studies on their metabolic process and the impact on lipid biomarkers are needed, especially in East African soils.

5.7.3 Taphonomy

The archaeological applications of leaf wax lipid biomarkers for environmental reconstruction is promising, but the future of this research depends on the taphonomic understanding of the preservation of lipid molecules, specifically in East African sediments. The complex interactions between lipid marker molecules, microbial (fungal and bacterial) communities, and soil pH, alkalinity, temperature, and moisture content, is currently not well understood, and future studies must investigate the transport, preservation, and diagenesis of plant waxes in modern habitats to better interpret the isotope signal from archaeological sediments. First, a systematic investigation of leaf wax lipid biomarkers and the controls on $\delta^{13}\text{C}$ and δD from the *Acacia-Commiphora* biome must be undertaken in living plant material, soil-surface litter, and buried soils. This will inform researchers on the diagenetic and fractionation effects of isotopes from plant-to-soil and the potential mechanism(s) responsible for isotopic differences. Additionally, studies on microbial communities through genomics, proteomics, and lipidomics will aid in how these microbiomes respond to different soil pH or alkalinity, plant biomass abundance, and seasonal differences in moisture content and temperature, and what this means for the preservation and diageneses of leaf wax lipids. With these properly investigated, a better understanding of the long-term preservation of leaf wax lipids from Pleistocene sediments is achievable.

5.8 Chapter 5 Summary

Leaf waxes preserve the water balance of plants and minimize damage to leaf cells from fungal and insect attack, wind abrasion, and excessive ultraviolet radiation. Their synthesis and isotopic characteristics are governed by leaf physiognomy, ecological lifeform, plant-growing environments, and photosynthetic pathways. Furthermore, the major factors determining the $\delta^{13}\text{C}$ and δD of *n*-alkane and *n*-alkanoic acid compounds of East African plants are photosynthesis type, that is C_3 or C_4 pathways, and rainfall amount, or the “amount effect.” Temperature and CO_2 also play a role and were likely important factors that helped C_4 plants spread during the Pliocene-Pleistocene, but today, moisture and aridity are the dominant controls shaping plant landscapes as C_3 plants thrive with readily available freshwater. Plant water-use efficiency (WUE), or the ratio of the rate of carbon assimilation to the rate of water loss, is another important mechanism acting on carbon and hydrogen isotope values during leaf wax biosynthesis.

Isotope fractionation occurs with carbon fixation during photosynthesis, specifically during the intracellular diffusion of CO_2 and the biosynthesis of organic compounds such as carbohydrates, lignin, proteins, and lipids. Furthermore, hydrogen fractionation associated with evapotranspiration in both soil- and leaf-water contributes to the overall net fractionation within plants by enriching leaf water δD . Leaf wax preservation and diagenesis must also be considered when using lipid biomarkers for paleo-reconstructions; although leaf wax lipids are geologically persistent molecules, recent research has shown that isotope fractionation can occur during diagenesis, especially between leaf, litter, and soil organic matter. This is an important component of paleo-reconstructions that must be considered when using *n*-alkanes or *n*-alkanoic acid because if significant changes in the isotopic signature of these compounds result from (bio)degradation, then our interpretations of Pleistocene environments may need to be reevaluated.

CHAPTER 6: PALEO-RECONSTRUCTIONS IN EAST AFRICA

6.1 Stable Isotopes of Pedogenic Carbonates

The research connection between climate, ecology, evolution, and in the case of hominins, technological development, has led to the utilization of various proxies for paleoclimate and paleoenvironmental reconstructions for African Plio-Pleistocene archaeological sites. Fossil vertebrates, primarily mammals, birds, and fish (Bibi and Kiessling, 2015; Bibi et al., 2018; Prassack et al., 2018), micro- and macrobotanical remains like pollen, phytoliths, and wood (Barboni et al., 1999; Bonnefille, 1995; Bonnefille, 1984), and stable isotopes of hydrogen, carbon, nitrogen, oxygen, and strontium (Cerling et al., 1997a; Sealy, 1986; Sillen and Balter, 2018; Styring et al., 2010) are paleoecological methods applied in the reconstructions of past habitats, climates, and behaviors of early human ancestors. These proxies, when combined, provide a robust picture of hominin-occupied environments in East Africa throughout the Pleistocene.

Paleosols are one such important proxy for interpreting changing environmental conditions, as stable isotopes of carbon (^{13}C and ^{12}C) and oxygen (^{18}O and ^{16}O) reveal the proportion of C_3 to C_4 plants growing on a soil surface and local water-balance and climate, respectively. Both paleosols and carbonate (CO_3^{2-}) horizons found within fossilized soils have been used to reconstruct early human environments, often complimenting each other, but at times, providing completely different interpretations of the past (Cerling et al., 2010; White et al., 2010). The primary basis for using stable carbon isotopes from pedogenic (soil forming) carbonates as a paleoecological proxy is that, the differences in the way C_3 and C_4 plants use distinct photosynthetic pathways to *fractionate* isotopes from atmospheric carbon are well-established (Garrett et al., 2015). Plants utilizing C_3 carbon fixation (trees, shrubs, sedges such as *Typha*, and

"cool-season" grasses) discriminate against ^{13}C during photosynthesis and uptake of atmospheric CO_2 (O'Leary, 1981). C_4 plants on the other hand ("warm-season" grasses and most other sedges), discriminate less against ^{13}C from atmospheric carbon (O'Leary, 1981). The result is that C_3 plants tend to have more-negative isotopic values (reported in per mille notation ‰, or parts per thousand) relative to a standard⁸ (modern C_3 mean $\delta^{13}\text{C}$: $-27.4 \pm 1.6\text{‰}$), whereas C_4 plants tend to have a more-positive isotopic value relative to a standard (modern C_4 mean $\delta^{13}\text{C}$: $-12.7 \pm 1.1\text{‰}$) (Collister et al., 1994; Farquhar et al., 1989; Kohn, 2010). The $\delta^{13}\text{C}$ of soil carbonate indicates the proportion of C_3 and C_4 plant biomass contributing to soil CO_2 that diffuses downward to form carbonates. Consequently, the carbon isotope composition of pedogenic carbonate in paleosols is used to infer the relative proportions of C_3 vs. C_4 plants during pedogenesis (Cerling and Quade, 1993).

Soil carbonate oxygen isotope compositions are moderated by the isotopic configuration of soil water which derives from localized meteoric water (Cerling and Quade, 1993). Pedogenic carbonate $\delta^{18}\text{O}$ values are therefore largely controlled by climate, which ultimately determines local water-balance through precipitation and evaporation, and soil temperature which is related to ambient temperatures and solar radiation (Quade and Levin, 2013). The $\delta^{18}\text{O}$ of modern, deeply formed soil carbonate is correlated with the $\delta^{18}\text{O}$ of meteoric water, though typically offset by 2‰ - 10‰ due to the effects of evaporation (Koch et al., 2003) particularly in arid environments, but also by the distanced traveled from the source of moisture, elevation, and extent of rainout from local cloud masses (Quade and Levin, 2013; Rozanski et al., 1993). The oxygen isotope composition of pedogenic carbonate in paleosols is subsequently used as a proxy to infer relative paleo- precipitation and temperatures.

⁸ The standard established for $\delta^{13}\text{C}$ is the Pee Dee Belemnite (PDB). This standard is often used for $\delta^{18}\text{O}$ when studying carbonates, but the Vienna Standard Mean Ocean Water (VSMOW) standard is used as well.

Pedogenic carbonate (CaCO_3) forms in soils that become supersaturated with calcite when CO_2 -soil-levels decrease, when carbonate precipitates in soils due to weathering processes at the land surface, or when there is a net water loss due to evaporation (Cerling and Quade, 1993). Supersaturation due to evaporation is regarded as the primary mechanism for CaCO_3 precipitation, particularly in well-drained soils in the unsaturated zone above the influence of the groundwater table (Sikes and Ashley, 2007). Because pedogenic carbonates form in soils with a net water deficit, they occur globally in soils today where annual rainfall is less than 1,000 mm per year (Retallack, 1990). Current climate regimes with rainfall less than 1,000 mm per year include most of East Africa at elevations below $\sim 1,000$ meters, explaining pedogenic carbonates under much of the modern East African landscape (Quade and Levin, 2013).

Pedogenic carbonates preserved in paleosols are important for paleoenvironmental reconstructions but have relatively restricted distributions as they only form in arid to semiarid environments (Lee-Thorp and Sponheimer, 2007). Cerling and Quade document (1993) that *true* pedogenic carbonates form well below the active soil horizon, and carbonates that precipitate at depths greater than 50 cm in soils with moderate to high evaporation rates reflect the isotopic composition of plant-derived CO_2 with no direct contribution from the atmosphere (Cerling, 1991).

6.1.1 Olduvai Gorge

Extensive reconstructions of Quaternary hominin paleoenvironments using stable isotopes from paleosols exist for Olduvai Gorge. The pioneering study by Cerling and Hay (1986) compiled a comprehensive dataset of the carbon and oxygen isotopic composition of carbonates from each of Olduvai's seven beds (I-IV, Masek, Nduku, and Naisiusiu). The $\delta^{13}\text{C}$ and $\delta^{18}\text{O}$ Olduvai data vary considerably with time, but overall, there is a trend toward warmer and drier conditions

beginning around 1.67 Ma. The isotopic composition of calcretes, other pedogenic carbonates, and carbonates from fluvial facies from Olduvai Gorge range between -7.0 and +1.0‰ for both $\delta^{13}\text{C}$ and $\delta^{18}\text{O}$. The isotopic composition of carbonates from the lake-margin, fluvial-lacustrine, alluvial fan, and perennial saline lake facies are similar, ranging from -8.0 and -1.0‰ for $\delta^{13}\text{C}$, and -7.0 to -2.0‰ for $\delta^{18}\text{O}$. (Pedogenic carbonates formed under 100% C_3 vegetation, which has a $\delta^{13}\text{C}$ average value of -27‰, will have $\delta^{13}\text{C}$ values of about -12.5‰, whereas pedogenic carbonates formed under 100% C_4 vegetation, which has a $\delta^{13}\text{C}$ average value of -12‰, will have $\delta^{13}\text{C}$ values of about +2.5‰ (Cerling and Quade, 1993; Wynn, 2001).

Cerling (1984) developed a model to describe the isotopic composition of soil carbonate $\delta^{13}\text{C}$ values in terms of the proportion of biomass using the C_4 photosynthetic pathway: the model predicts $\delta^{13}\text{C}$ values for carbonates produced under pure C_4 flora to be about +2.0‰ and for pure C_3 flora to be about -12.0‰. In Olduvai Bed I and lower Bed II (~1.9-1.6 Ma), the percentage of C_4 plants varied between less than 40% at 1.74 Ma ($\delta^{13}\text{C}$, -5.8‰) to as high as 80% at 1.695 Ma ($\delta^{13}\text{C}$, -0.9‰). However, the best-fit estimate of the percentage of C_4 biomass at Olduvai Gorge based on the carbon isotopic composition of paleosol carbonate for Bed I and lower Bed II is 40-60%.

Cerling suggests a “major” climatic event coinciding with the Lemuta Member of Bed II. Carbon isotopes from Lemuta Member samples show a 3-4‰ enrichment at 1.66 Ma ($\delta^{13}\text{C}$, -0.6‰) and at 1.65 Ma ($\delta^{13}\text{C}$, -1.1‰) compared to other samples from this stratigraphic subsection and from Bed I. (Specifics on sampling methods are not provided in the manuscript and therefore, it is difficult to ascertain the relationship between location and stratigraphy of individual samples.) Cerling puts forward that the two $\delta^{13}\text{C}$ “spikes” are drastic increases in C_4 biomass to percentages between 50-80%, correlating with bovid faunal remains indicative of savannah grassland with

scrub and bush (Hay, 1976). Yet, when considering each of the Lemuta Member samples (n=15), the data demonstrates that there could be less than 30% C₄ grass at times, and more than 80% C₄ biomass at others. It is possible that there could be anywhere from 20-90% C₄ biomass between 1.67 and 1.62 Ma.

Oxygen isotopes from the Lemuta Member offer additional information, and show a 4-5‰ enrichment at 1.655 Ma ($\delta^{18}\text{O}$, -1.8‰) and at 1.635 Ma ($\delta^{18}\text{O}$, -2.5‰) compared to other samples from this stratigraphic subsection and from Bed I. The 1.655 Ma sample has a $\delta^{13}\text{C}$ value of -1.9‰ making it the only sample that shows significant enrichment in both carbon and oxygen isotopes. It is likely that the period from 1.66 to 1.65 Ma experienced significant warming, decreased rainfall, and an expansion of C₄ biomass. This data also suggests a climatic event when the Lemuta Member was deposited, albeit one that was relatively short lived (~50,000 years), as conditions during most of middle and upper Bed II were similar to the prevailing conditions of Bed I and lower Bed II.

Cerling (1984) groups the period from middle Bed II (1.62 Ma) through the end of Bed IV (0.62) together and states that during this time, the $\delta^{18}\text{O}$ isotopic composition of meteoric water of -2.0 to -5.0‰ represents a major change from middle Bed II. Although there is no explanation on how this change differed from middle Bed II or what caused the change, there is a general trend toward a higher percentage of C₄ biomass beginning at 1.62 Ma; from Bed II to Bed IV there was anywhere from 20-70% C₄ biomass. From 0.62 Ma, this trend continued and C₄ plants began to dominate in the landscape from anywhere between 70 and 80%.

Following Cerling's (1984) work, further studies began narrowing the focus of pedogenic carbonate research to specific Olduvai sites. Research conducted by Sikes (1994) at the HWK-E 'occupation floor' site located above Tuff IF (1.803 ± 0.002 Ma) in Olduvai basal Bed II, found

that four co-existing pedogenic carbonates had a mean $\delta^{13}\text{C}$ value of -4.8‰ and $\delta^{18}\text{O}$ average values of -5.6‰ . The carbon isotopic ratios indicate that the eastern paleo-Lake Olduvai margin supported a local floral biomass of 20-45% C_4 plants during the period of soil formation ~ 1.74 Ma. This percentage range suggests that for basal Olduvai Bed II, paleosols formed under riparian forest to grassy woodland conditions, not under wooded or open C_4 dominant grasslands such as those that characterize the nearby Serengeti Plain today.

This interpretation corresponds with Cerling's (1984) analysis of the same time period, but Sikes' reconstruction contrasts with previous explanations using different proxies that depicted the basal Bed II paleo-lake margin as a mudflat, *Typha* swamp, or open grassland (Blumenschine and Masao, 1991; Bonnefille, 1984; Hay, 1976). It is likely that hominins from this period concentrated their activities around river channels surrounded by riparian forest or grassy woodlands, as was documented for the SHK and BK sites in middle and upper Bed II, respectively (Diez-Martín et al., 2014; Domínguez-Rodrigo et al., 2009). Furthermore, it is possible that this type of environment was resource-abundant, and would have offered plant foods, scavenging opportunities, predator refuge, access to water, aquatic resources, and stone sources compared to C_4 dominated settings.

Sikes and Ashley (2007) employed stable isotopes of pedogenic carbonates as indicators for paleoecology for a $\sim 60,000$ -year interval (~ 1.845 to ~ 1.785 Ma) above Tuff IB in Bed I of Olduvai Gorge. This research differentiates from most other Olduvai studies by reconstructing paleoecology of the westernmost extent of the main gorge; investigations have primarily been situated at the confluence of the gorge which represents the southern extent of paleo-Lake Olduvai. Sikes and Ashley present stable carbon and oxygen isotope values of paleosol carbonate and organic matter from fluvial and lake deposits, volcanic ash, eolian sediments, and paleosols.

Building upon Cerling (1984) and Sikes (1994), Sikes and Ashley used stable isotope values preserved within pedogenic carbonates to reconstruct local climatic conditions and variation in tropical vegetation communities with different proportions of C₄ (grasses) to C₃ (woody) vegetation from eight distinctive lithostratigraphic units beginning at Tuff IB.

Contrary to Cerling (1984), Sikes and Ashley (2007) only included discrete forms of pedogenic CaCO₃ (nodules, rhizoliths, and calcrete) in their paleosol study. Paleosol CaCO₃ δ¹³C values had a fairly narrow range of variation, from -6.6 to -3.3‰ with a mean of -4.8‰. These data indicate a local biomass of about 40-60% C₄ plants during pedogenic carbonate formation 1.845 to 1.785 Ma. δ¹⁸O values from Bed I range from -5.6 to -3.8‰, with a mean of -4.7‰. Over the eight stratigraphic units, there is a general increase in δ¹⁸O values indicating a change in local climate from cooler or moister to warmer or drier conditions. However, two significant episodes are identified by decreases in δ¹⁸O values whereby rainfall increased, and the lake expanded.

Based on the paleosol δ¹⁸O values, rainfall may have been as high as 800 mm during these two episodes. Today, annual rainfall at Olduvai averages 566 mm (Hay, 1976), a substantial decrease than that of Bed I times which was probably slightly less than 850 mm since pedogenic carbonate is relatively uncommon where rainfall is >750-850 mm (Cerling, 1984; Cerling and Hay, 1986). This increased moisture content contrasts today's savanna grassland mosaic on the semiarid Serengeti Plain, but was adequate to support higher proportions of woody C₃ vegetation presented in Sikes and Ashley's study in Bed I. A local biomass of about 40-60% C₄ plants in Bed I suggests variable proportions of grassy woodland to wooded grassland, reiterating Sikes (1994) earlier study.

Another study focusing on Bed I was performed by Ashley et al. (2010a) at the FLK-NN site. This investigation analyzed carbon and oxygen isotopes from carbonates deposited in a tufa

mound, not pedogenic carbonates. Tufa is a highly porous, sedimentary rock composed of calcium carbonate that forms by biological and chemical precipitation of calcite or aragonite. The term is used to describe cool water deposits of highly porous freshwater carbonate associated with persistently high water tables, extensive ground cover by macrophytes, and moderate levels of CaCO_3 in the groundwater (Pedley, 1990). Warm, humid, temperate climates appear most favorable to freshwater tufa development. The narrow range of optimum tufa developmental conditions is used as a proxy in the paleoenvironmental interpretation of ancient tufa-bearing sequences, such as those from Olduvai Gorge. Interpretations of isotopic investigations in lacustrine carbonates however, are sophisticated and difficult because of the complex nature of sedimentation, influenced by a number of physicochemical and biological factors (Pzadur et al., 2002). Nevertheless, the tufa at FLK-NN is blanketed by Tuff IC and dated to 1.832 ± 0.003 Ma.

Tufa $\delta^{18}\text{O}$ values range from about -5‰ to -1.0‰, and according to Ashley et al., (2010a) suggest a “robust ‘freshwater’ isotopic signature...which indicates a groundwater-fed water source (Cerling and Quade, 1993).” Although $\delta^{18}\text{O}$ values form in equilibrium with soil water whose isotopic composition is related to meteoric water, Cerling and Quade (1993) focused their study on pedogenic carbonates, not tufa, so the interpretation that a groundwater-fed water source was responsible for the FLK NN tufa based on this reference may be misleading. Regardless, the $\delta^{18}\text{O}$ values of the tufa could indicate a meteoric source for the water when groundwater seeps onto the surface (Cerling et al., 1993). Compared to the carbonate record of a freshwater wetland in lowermost Bed II (Liutkus et al., 2005), the tufa $\delta^{18}\text{O}$ is more positive in Bed I, likely because of warmer or drier conditions and increased evaporation, similar to what is suggested for the westernmost segment of the gorge by Sikes and Ashley for this timeframe.

The $\delta^{13}\text{C}$ signature is less straightforward as these values may have incorporated carbon from weathered rock and soil that the groundwater passed through, in addition to diffusion of carbon from the atmosphere. Even though this data is not very informative, other paleoenvironmental proxies used in this study (phytoliths) suggest a closed habitat consisting of woody trees, shrubs or bushes, and palms at the FLK complex.

6.1.2 Omo-Turkana Basin

The paleosol isotope record from the Koobi Fora Formation, Kenya by Cerling et al., (1988) was the first of its kind for the Omo-Turkana Basin. Following the deposition of the KBS Tuff at East Turkana 1.869 ± 0.021 Ma (Lepre et al., 2007), C_4 grasses became well established as a result of increased aridity and temperature. Unlike Olduvai Gorge, there are few calcrete deposits in the Koobi Fora Formation, likely due to the less reactive parent material and higher sedimentation rates in the Turkana Basin, but pedogenic carbonates (nodules) do exist. The $\delta^{13}\text{C}$ values for modern soil carbonate from the Koobi Fora region are about -4.0 to -2.0‰, and according to Cerling's (1984) model, this would correspond to a biomass made up of about 60-80% C_4 flora. Differences in the isotopic composition of paleosol carbonates from the Koobi Fora Formation are attributed to changes in the isotopic composition of meteoric and soil waters over the past 3.5 Ma.

Prior to 2.1 Ma, which corresponds to the Lonyumun and Lower Burgi Members (Cerling et al., 1988), $\delta^{13}\text{C}$ values in the Koobi Fora Formation ranged from -10 to -6.0‰, corresponding to a percentage of C_4 plants of only 20-40%. A change is first recognized in the upper Burgi Member (1.945 ± 0.004 to 1.869 ± 0.021 Ma (Joordens et al., 2013) in which $\delta^{13}\text{C}$ pedogenic carbonate values range from -10 to -3.0‰ and $\delta^{18}\text{O}$ values from -3.0 to -6.0‰ (lower stratigraphic

units) and -3.0 to +1.5‰ (upper stratigraphic units). These values likely coincide with changes in the isotopic composition of lake water resulting from changes in the lake's water budget or changes in the isotopic composition of inflowing water. Major changes are evident beginning in the KBS member (1.869 ± 0.021 Ma) and continue through the Chari Member (~ 0.7 Ma). Average $\delta^{13}\text{C}$ values in sediments below the KBS Tuff are from -9.0 to -6.0‰, whereas those above the tuff are -4.0 to -3.0‰. This likely represents a change in the proportion of C_4 flora from about 25% below the KBS Tuff to about 65% above. This would also indicate significant drying in the basin, or increased temperatures, or both.

This trend is more apparent in the $\delta^{18}\text{O}$ record. The average $\delta^{18}\text{O}$ value for paleosol carbonates at the KBS Tuff was 0.7‰, increasing to 0.9‰ in the Okote unit dated between 1.53 ± 0.01 and 1.38 ± 0.03 Ma, and finally to 1.2‰ in the Chari Member between 1.38 ± 0.03 and ~ 0.74 Ma (Lepre and Kent, 2015). This trend toward more positive carbon and oxygen isotope values suggests that prior to 1.9, paleosols were developed on the Omo River floodplain, but the later soils formed in more arid climatic conditions. Drying conditions are also represented at Olduvai Gorge for this period.

In his synthesis of $\delta^{13}\text{C}$ values from Kanapoi, the Nachukui, and the Koobi Fora Formations, Wynn (2004) also identified a change in C_4 biomass through time in both the eastern and western parts of the Turkana Basin. Wynn marked three episodes of aridification in the basin by spatial and temporal changes in open and closed habitats from 3.58-3.35 Ma (Kanapoi Formation), another between 2.52-2.0 Ma (Lokalalei Member at West Turkana), and lastly from 1.81-1.58 Ma (KBS Member at East Turkana).

Prior to 2.52 Ma, $\delta^{13}\text{C}$ values from east and west Turkana were depleted and less variable with a mean of -8.0‰. Between 2.52 and 1.82 Ma, $\delta^{13}\text{C}$ became enriched and ranged between -

7.5 and -4.9‰ with a mean value of -6.2‰. At 1.81 Ma, isotope values became further enriched whereby the mean $\delta^{13}\text{C}$ value of paleosol carbonate approached modern soil carbonate value of -3.8‰ but ranged from -5.8 to -1.8‰. Following 1.58 Ma, $\delta^{13}\text{C}$ values would return to around -4.38‰, but would never become as depleted as they were prior to 1.81 Ma. The basin-wide ^{13}C enrichment represents an increase of C_4 biomass through time, with major punctuations at 2.52 and 1.81 Ma, but at no point in the record is there evidence for pure C_4 habitats. The stable carbon isotopic values are more characteristic of mixed grassy woodlands and low tree-shrub savannas, which would have been slightly more open than the contemporary Olduvai environment.

Quinn et al., (2007) presented a follow-up study in which they detail a $\delta^{13}\text{C}$ record for the Koobi Fora Formation between 2.0 and 1.5 Ma by showing a pronounced increase in $\delta^{13}\text{C}$ values after 1.8 Ma. This change however is not uniform throughout the Turkana Basin as it is only represented in some regions (Koobi Fora Ridge) but not in others (Karari Ridge). $\delta^{13}\text{C}$ values of pedogenic carbonates from the Koobi Fora Formation have a mean value of -5.5‰ but range from as low as -10.4‰ to as high as +0.4‰. This would indicate that over time, the environmental setting fluctuated from a nearly closed C_3 forest (-10.43‰) to an open C_4 grassland (+0.43‰), but likely resembled a mosaic composition of grassy woodland or wooded grassland (-5.5‰) for the majority of this period, according to Cerling's (1984) model. What is interesting is that the $\delta^{13}\text{C}$ values from the Koobi Fora Ridge subregion corroborates the previous interpretation of C_4 expansion after 1.8 (Wynn, 2004), but this trend is not shown in the data from the Karari Ridge which is about 20-30 km northeast of the Koobi Fora Ridge today. This is likely due to the paleogeographic history of the Karari Ridge and that it may have had a different water-availability regime that was supplying a consistent supply of water to C_3 floral communities.

Isotopic data from Omo Group (Ethiopia) paleosol carbonates are presented by Levin et al. (2011), and document systematic environmental variability within the Omo-Turkana Basin from three formations, the Shungura, Nachukui, and Koobi Fora, for the past 4 million years. The Shungura Formation (~3.9-1.0 Ma) is located north of Lake Turkana along the modern Omo River. Pooled together over the nearly three-million-year period, the carbon isotopic composition of nodules from the paleosol ranged from -10.2 to -4.2‰ with an average value of -8.1‰. $\delta^{18}\text{O}$ values from all paleosols sampled from the Shungura Formation range from -8.3 to -0.3‰ and average -4.0‰. The Shungura Formation can be divided in two distinct strata based on $\delta^{13}\text{C}$ values; those older than ~1.9 Ma that yield an average $\delta^{13}\text{C}$ value of -8.9‰, and those younger than ~1.9 Ma that yield an average $\delta^{13}\text{C}$ value of -6.3‰. The positive shift after 1.9 Ma signifies a major restructuring of vegetation along the ancestral Omo River from a C_3 dominated ecosystem (~20% C_4 biomass) to a more mixed grassy woodland (~40% C_4 biomass).

The Nachukui Formation is located west of modern Lake Turkana and dated to between ~4.2-0.5 Ma. Though this is a nearly four-million-year exposure, few paleosols were sampled between 2.03 and 1.5 Ma or in the Nariokotome Member younger than 1.2 Ma due to an absence of calcareous paleosols in the region. When data from the entire formation are compiled together however, the carbon isotopic composition of nodules from the paleosol ranged between -9.1 and -0.4‰ with an average value of -6.1‰. $\delta^{18}\text{O}$ values from all paleosols sampled from the Nachukui Formation range from -6.9 to 4.5‰ and average -2.6‰. Both $\delta^{13}\text{C}$ and $\delta^{18}\text{O}$ values increase from the early Pliocene to the top of the section at 0.7 Ma, again indicating an increase in C_4 biomass and a shift toward warmer temperatures.

The Koobi Fora Formation is located east of modern Lake Turkana and dated to between ~4.4-0.6 Ma. Pedogenic carbonates sampled within the Koobi Fora Formation yielded $\delta^{13}\text{C}$ values

that range from -10.6 to -2.0‰ and average -6.7‰. $\delta^{18}\text{O}$ values range from -7.6 to +1.6‰ and average -3.1‰. Like both the Shungura and Nachukui formation, the $\delta^{13}\text{C}$ values from Koobi Fora increase throughout the stratigraphic section suggesting a change toward more arid conditions. Additionally, more positive $\delta^{13}\text{C}$ values at Koobi Fora at 1.88 Ma (-2.0‰), coincides with the transition to C_4 environments at 1.8 Ma that was recognized by Cerling et al. (1988) and Quinn et al. (2007).

The isotopic results from the basin-wide sampling demonstrate that the soils in the Omo-Turkana Basin supported a mosaic vegetation community and diverse hydrologic regimes, contrasting in water availability, slope, and drainage across short distances. The $\delta^{13}\text{C}$ values from the Shungura Formation are lower than $\delta^{13}\text{C}$ values from contemporary paleosols in the Nachukui and Koobi Fora formations, whereas the $\delta^{18}\text{O}$ values in the Nachukui Formation are higher than $\delta^{18}\text{O}$ values from concurrent paleosols upstream in the Shungura Formation.

Beginning around 2.5 Ma, the abundance of C_4 grasses in East Africa increased as identified in the $\delta^{13}\text{C}$ carbonate records first at West Turkana, and later by ~2.0-1.8 Ma, at Koobi Fora, the Shungura Formation, and in the KBS Tuff Member. At Olduvai, a wetter or cooler phase persisted from about 1.845 to 1.74 Ma at the top of Bed I and lower Bed II, but more arid conditions become evident again at ~1.7 Ma in the Lemuta Member of Bed II. This drying trend continued in East Africa and is recognizable starting around 1.62 in Olduvai Bed II and in the Okote Unit in the Turkana Basin, and continues through 0.7 Ma in the Omo-Turkana Basin and 0.62 Ma at Olduvai Gorge. Furthermore, an extensive C_4 grassland has been identified on Rusinga and Mfangano Islands of Lake Victoria for Late Pleistocene Middle Stone Age sites, 100-45 thousand years ago (Garrett et al., 2015), showing that the trend toward more arid and warm conditions of East Africa today has gradually developed over at least the last two million years.

Prior to 2.0 Ma, $\delta^{18}\text{O}$ values from Shungura are lower than those from the Nachukui and Koobi Fora Formations suggesting that pedogenic carbonates from the ancestral Omo River floodplain formed from meteoric water with more-negative $\delta^{18}\text{O}$ values, possibly sourced in the Ethiopian highlands. Pedogenic carbonates from Nachukui and Koobi Fora on the other hand, formed from meteoric water with more-positive $\delta^{18}\text{O}$ values sourced near modern day Lake Turkana. An alternate explanation is that the more-positive $\delta^{18}\text{O}$ values at Koobi Fora and Nachukui reflect increased soil evaporation and generally more arid conditions than that of the Shungura Formation, a hypothesis that is also supported by the more-negative $\delta^{13}\text{C}$ values from Shungura. Gallery and riparian forest, and grassy woodland conditions persisted along ancient waterways nevertheless, and the data from Olduvai and Shungura suggests that these habitats were likely resource-abundant, and would have offered plant foods, scavenging opportunities, predator refuge, access to water, aquatic resources, and stone sources compared to C_4 dominated settings. Although there is a general trend toward more open conditions, mosaic environments in East Africa played a major role in human evolution.

6.2 Paleontological Proxies

The most common data recovered at early human sites in East Africa are typically other mammalian fossils (Reed et al., 2013), and are thus targeted as proxies to answer questions relating to evolutionary paleoecology as most African faunal analyses are used in reconstructing ancient habitats. Typically, two approaches are taken in early human paleoecology using fossil material; the first being the analysis of individual fossil bird, mammal, or fish species at particular localities to reconstruct specific habitats, while the second focuses on communities as a whole.

6.2.1 The 'Earliest' Hominins

As discussed in *Section 3.3.1 Habitat Specific Hypotheses*, the discourse over the last decade surrounding early hominin studies asserts that savannas may not have played as significant a role in the emergence of human evolutionary processes (Domínguez-Rodrigo, 2014), instead densely wooded environments and sometimes forests may have had a larger impact. This is true for some of the earliest hominin sites, such as the Toros-Menalla site 266 (TM 266) in Chad where *Sahelanthropus tchadensis* was discovered. Paleoenvironmental data were established through carbon and oxygen isotope composition of tooth-enamel samples (Boisserie et al., 2005; Zazzo et al., 2000), and extensively through vertebrate faunal analyses (Boisserie et al., 2003; Le Fur et al., 2009, 2014; Louchart et al., 2005; Vignaud et al., 2002). The faunal assemblage is comprised of more than 9,000 mammal remains from 55 species (Le Fur et al., 2014), abundant turtles, lizards, snakes, and crocodiles skeletal material (Vignaud et al., 2002), and an aquatic bird fossil (Louchart et al., 2005). The extensive collection has generated detailed information on the paleoenvironmental context in which *S. tchadensis* lived.

Studies (Boisserie et al. 2005; Le Fur et al. 2009; Le Fur et al. 2014; but also originally proposed by Vignaud et al., 2002) suggest that a mosaic of environments existed at TM 266; the paleolandscape was ecologically diversified, composed of 1) permanent aquatic habitats, as attested by the high abundance of semi-aquatic mammals (Boisserie et al. 2005; Le Fur et al., 2009) and abundant remains of freshwater fish, crocodiles, and turtles (Vignaud et al. 2002); 2) dense to moderately dense woodlands or gallery forests with trees and bushes, as suggested by primate fossils (likely attributed to Colobinae) (Le Fur et al., 2009; Vignaud et al. 2002); 3) wooded savanna, demonstrated by the moderate abundance of browsers (such as proboscideans and giraffids) (Vignaud et al., 2002) and scarcity of frugivorous taxa, suggesting the reduced extent

of wooded habitats (Le Fur et al., 2009); and 4) open landscape of grasslands, expressed in bovid remains (Vignaud et al., 2002) interspersed by humid zones (floodplains and swamps) and dry areas. Therefore, the vertebrate fauna contemporary with *S. tchadensis* suggests a mosaic of environments from gallery forest at the edge of a lake area, to a large savanna and grassland.

The discovery of *Orrorin tugenensis* in association with fauna and flora indicative of woodland to forest habitats also suggests that this species lived in relatively closed habitat (Pickford and Senut, 2001b). Analyzing the faunal assemblage from the Lukeino Formation, Tugen Hills, Kenya, Pickford and Senut (2001a) identified medium to small bovids and small colobines, and recorded that impalas dominated the assemblage. The predominance of impalas suggests that the surrounding landscape of the *Orrorin* site was probably open woodland, while the presence of several specimens of colobus monkey indicate that there were denser stands of trees in the vicinity, and lacustrine shales and sedimentary facies imply a lake margin, floodplain, and fluvial environment (Pickford and Senut, 2001a).

For *Ardipithecus* fossil bearing sites, fossil bovid assemblages are dominated by medium sized kudu fossils and abundant colobine monkey remains, both of which indicate the presence of a closed, wooded environment (WoldeGabriel et al., 1994). Furthermore, the multiproxy approach taken by WoldeGabriel et al. (2009) utilizing geologic, floral, invertebrate, and vertebrate paleontological and taphonomic data associated with the localities that contain *Ardipithecus*, suggest that the site was a former floodplain that supported a wooded “biotope” rather than a grassland savanna as no evidence for lowland humid Guineo-Congolian rainforest, subdesertic arid vegetation, or highland C₃ grasses exist. Finally, according to White et al. (2009b), *Ardipithecus* preferred a woodland-to-forest habitat, not savanna grasslands, and was adapted mainly to tree-dwelling.

In spite of this faunal data and the evidence from *Ardipithecus* anatomy, independent isotope measurements from paleosols and fossil teeth paint a distinctly different picture of the paleolandscape in Aramis and Gona, Ethiopia (Cerling et al., 2010; Levin et al., 2008). Using paleosols isotope data from Aramis, Cerling et al. (2010) revealed a high abundance of grasses and only 5-25% tree cover, a landscape which they refer to as a tree- or bush-savanna, with less woody canopy cover. They further assert that the faunal assemblage does not necessarily represent a closed woodland environment, but instead riparian forest to grassland ecosystems. For Gona hominin environments (~100 km from Aramis), Levin et al. (2008) used stable carbon isotope measurements on fossil teeth to show that *Ardipithecus* lived in an ecosystem in which C₄ grasses dominated the landscape and supported a large number of grazing mammals as opposed to browsers. White et al. (2010) dispute these results and claim that the body of evidence they collected for paleoenvironmental information is inconsistent with an open environment. Nevertheless, the combined evidence from the two sites appears to indicate a degree of spatial and temporal variability in the proportion of grass and trees coverage.

6.2.2 Olduvai Fauna

Frida Leakey Korongo (FLK) is perhaps the most famous locality at Olduvai Gorge, as it was here at “Level 22” that Mary Leakey discovered *Paranthropus boisei* in 1959 (Leakey, 1959). This level, situated between Tuffs IB (1.84 ± 0.003 Ma) and IC (1.832 ± 0.003 Ma), was interpreted as an occupation or living floor (Leakey, 1959; Leakey, 1971), whereby hominins (*Homo habilis* and even perhaps *P. boisei*) made stone tools to butcher mammals from diverse habitats (Blumenschine, 1995; Bunn and Kroll, 1986). Blumenschine et al., (2012) conducted 13 excavations across the *Zinj* paleolandscape to compare environments and Oldowan hominin land

use patterns through bird, rodent, and larger mammal taxonomy and taphonomy, in addition to macroplant fossils and phytoliths, tephrostratigraphy, and sedimentary facies analyses. The avifaunal assemblage (n=226) was dominated by sandpipers, rails, and ducks, which are extant in nearshore, wetland, and open water environments, but barn and eagle owl remains attest to nearby woodland and short/mixed grassland settings. Rodent remains, many of which were found as owl pellets, included species indicative of wooded habitats, such as those from the genus *Thallomys* which are associated with Acacia trees. Additionally, large mammal accumulations, including bones with tooth and stone tool marks, included arboreal frugivores that indicate a diverse closed woodland, but species of *Kobus*, a C₄ grazer associated with marshes, floodplains, or other grassy areas near water, was the most common ungulate documented at Level 22. The high mammalian variety suggests the juxtaposition of distinct landscape ecologies with woodland, bushland, grassland, and marshland biomes situated nearby FLK, with a diversity of species greater than that of modern gallery forests along the Serengeti's Mara River.

Over the last decade, the Olduvai Geochronology and Archaeology Project (OGAP) has excavated fossil and stone tool sites in Olduvai's Middle and Upper Bed II, uncovering multiple paleontological and archaeological assemblages to answer questions on the emergence of the Acheulean. Bibi et al., (2018) reevaluated mammalian and fish collections from Mary Leakey's 1972 Henrietta Wilfrida Korongo East East (HWK-EE) excavations (Pante and de la Torre, 2018) as well as those collected by OGAP over the last 10 years from Lower Bed II (HWK-EE), Middle Bed II (Fuch's Cliff East and West (FC-E, FC-W) and Mary Nicol Korongo (MNK)), and above Tuff IIC in Upper Bed II (Evelyn Fuchs Hans Reck (EF-HR) and FLK-W⁹). This timeframe,

⁹ OGAP FLK-W is different from FLK-W described by Diez-Martín (2015) in that it is located in Upper Bed II above Tuff IIC, whereas the Diez-Martín excavation is in Lower Bed II between Tuffs IIA and IIB.

roughly 1.7 to 1.5 Ma, covers the local emergence of the Acheulean at Olduvai Gorge (Diez-Martín et al., 2015).

The fish and mammal assemblages studied by Bibi et al., (2018) suggests open and seasonal grassland habitats at the margins of an alkaline lake. Mammalian fossils from Middle Bed II are dominated by grazing ungulates, indicating open grassland, with higher proportions of bovids (Alcelaphini and Antilopini) in lower Middle Bed II, but a greater abundance of equids hippopotamus (*H. gorgops*) in upper Middle Bed II. However, hominin butchery played a role in the formation of these assemblages and likely account for the abundances and differences across Middle Bed II (Pante et al., 2018), particularly at HWK-EE. Furthermore, these faunae differ from Lower and Middle Bed I which had larger proportions of forest adapted spiral-horned antelopes (Tragelaphini) and antelopes that inhabit well-watered areas (Reduncini). Bibi and coauthors propose that tree cover throughout Middle Bed II must have been low and true woodlands practically absent (cf. Kovarovic et al., (2013)).

Overall, fish diversity was found to be low, with only two taxa identified, Clarias (*C. gariepinus*) and Cichlidae which accounted for 94.3% of the assemblage. These fish likely entered paleo-Lake Olduvai through streams or rivers flowing into the eastern side of the lake, and at MNK and HWK-EE, were stranded in evaporating water pools either at the end of the dry season or during sudden fluctuations in waters before subsequently being covered by floodwater sediments during the rainy season (Bibi et al., 2018). Because cichlids, and to a lesser extent *C. gariepinus*, are generally highly tolerant of saline and alkaline lake water, Bibi et al., compare paleo-Lake Olduvai to Lakes Singida and Magadi, which are saline but contain a diverse number of endemic fish species (Kavembe et al., 2016). At Olduvai, cichlids are well represented at all sites suggesting

predominantly saline conditions, while *C. gariëpinus* is rare except in MNK and FC-W, sites located in the Side Gorge where fresher water stream channels were present (Hay, 1976).

Both the mammalian and fish collections suggest open grassland habitats adjacent to an alkaline and saline lake with inflowing freshwater in Bed II. Throughout Middle and Upper Bed II, habitats remained consistently dry, with no observable species turnover or ecological change. Therefore, Bibi and coauthors suggest that the transition toward drier, more open conditions occurred earlier in Upper Bed I, prior to the appearance of the Acheulean in Bed II around 1.7 Ma (Diez-Martín et al., 2015). However this contradicts pedogenic carbonate isotope data that shows major C₄ expansion beginning around 1.6 Ma (Cerling, 1984; Sikes, 1994) in the upper Middle Bed II.

Olduvai's Pleistocene bird fossils remain the largest and richest avifaunal assemblage known in Africa (Prassack et al., 2018), and have been used to study the ecology of Bed I across the 1.84 Ma FLK *Zinj* landscape (Prassack, 2010), as well as to infer the environmental context of the Oldowan-Acheulean transition in Middle Bed II (Prassack et al., 2018). Prassack (2010) recognized shorebirds like plovers and sandpipers as the most common avifauna across the *Zinj* landscape (FLK Level¹⁰ 22, FLK-N, level 1 of FLK-NN, and FLK-S), but also recovered a variety of lake and wetland species such as grebes, rails, and ducks as well as birds typical of bushland, grassland, and open woodland like doves, mousebirds, and lovebirds. The abundance of small shorebirds at FLK-NN suggests near shore environments and close proximity to mudflats, diving birds (cormorants, teals, and grebes) at FLK Level 22 attest to lake depth, while the presence of raptors indicates roosting trees or rocky outcrops nearby. Marsh birds (moorhen, crane, swamphen, and flufftail) imply suitable emergent vegetation at FLK-N, but trees and bushes likely grew in

¹⁰ An archaeological *level* is a conglomeration of lithics and/or fauna within a vertically defined unit within a site (Leakey, 1971).

this location due to the occurrence of doves and mousebirds attesting to the ecotonal nature of FLK-N. These arboreal refugia likely served as relatively safe centers for hominins processing carcasses brought in from the more-open environments nearby.

The Bed II avifaunal community suggests a shift from the dominant wetland and lacustrine habitats to a mosaic of more-open dry and wet grasslands and open woodlands through Middle and Upper Bed II (Prassack et al., 2018). Studying multiple assemblages from Lower (below Tuff IIB), Middle (between IIB and IIC), and Upper (between IIC and IID) Bed II, Prassack et al., (2018) revealed a wetland signal in Lower and lowermost Middle Bed II, with cormorant, anhinga, pelican, duck, and flamingo fossils indicating the presence of well-watered environments, contrasting the mammal and fish data and paleoreconstruction presented by Bibi et al., (2018). The site HWK-EE, the richest in avian taxa, is interpreted by Prassack and coauthors as tree and flooded grassland ecosystem with a body of water deep and fresh enough to sustain a variety of fish.

Rails are common and diverse in lowermost Bed II but are restricted in Middle Bed II to open water taxa (gallinules and moorhens), with those preferring thick, emergent vegetation noticeably absent. Low duck and other algae-feeder diversity in Middle Bed II suggests clearer permanent waters that would have supported fish and piscivorous birds, likely an open permanent water source with an exposed shoreline. Additionally, the presence of wattled crane (*Grus carunculata*) and northern bald ibis (*Geronticus eremita*) in Middle Bed II, support the presence of open, drier grassland signal that was missing in lowermost Bed II. Although avian remains are limited overall in Middle Bed II, the documented high incidence of rodent modified bird bones, and a number of perching and roosting taxa (i.e., owls, raptors), suggest a wooded grassland. Upper Bed II is only represented by two fossil bird bones; a cormorant at the Acheulean EF-HR and a

duck at OGAP's FLK West. This suggests a more-open landscape, such as an intermittent riverbank that would preserve lower avian diversity overall.

Like the mammalian faunal data (Bibi et al., 2018), there does not appear to be any major avifaunal turnover; rather, changes from wetland habitats to more-open environments may have played a role in the preservation of the Bed II avian community. Although the fossils themselves may not suggest changes in the landscape through time, the better preservation and abundance of avian fauna in Lower Bed II compared to Upper Bed II attests to changes in local environmental conditions from those that better preserve fossils (wetlands) to those that do not (open grasslands).

Another study that used Olduvai mammalian fossils to investigate the paleoecological conditions which characterized the transition between Lower and Upper Bed II was conducted by Kovarovic et al., (2013). (In this study Bed II was only divided into two subsets; sediments below (Lower) and above (Upper) Tuff IIA, or those older than 1.74 ± 0.03 Ma and those which are younger.) The authors utilized revised mammalian faunal lists for Bed II and applied ecological diversity/correspondence analysis which considers the niche exploitation of the entire mammalian community as an indicator for available habitats and compared these paleontological profiles to known modern habitats. Data for modern mammal communities were collected in 26 tropical and subtropical African localities grouped into nine broad ecological categories: seasonal tropical forest, tropical forest, montane forest, summer rainfall woodland, miombo woodland, mixed woodland-bushland, woodland-grassland ecotone, tropical grassland, and tropical arid bushland.

Kovarovic et al., (2013) recognized that very large mammals (≥ 180 kg) both proportionately and absolutely dominate both Bed II fauna collections, and that there is a near lack of small mammals (< 1000 g) in Upper Bed II (Fig. 6-1). Furthermore, the total number of large mammal species (≥ 90 kg) in Bed II exceeds the numbers found in any modern locality, implying

that the Olduvai communities had a greater affinity to open habitats, which have proportionally greater numbers of large grazers and carnivores today. Semi-arboreal taxa and those in the smallest body mass category (1-100 g) disproportionately represent extant montane and tropical forests, while seasonal tropical forests have more species in 100-1000 g and 1-10 kg body mass and a greater number of browsers (Kovarovic et al., 2013). Olduvai fossil communities therefore do not represent forested environments as they seem to be influenced by mammals in 90-180 kg body mass range.

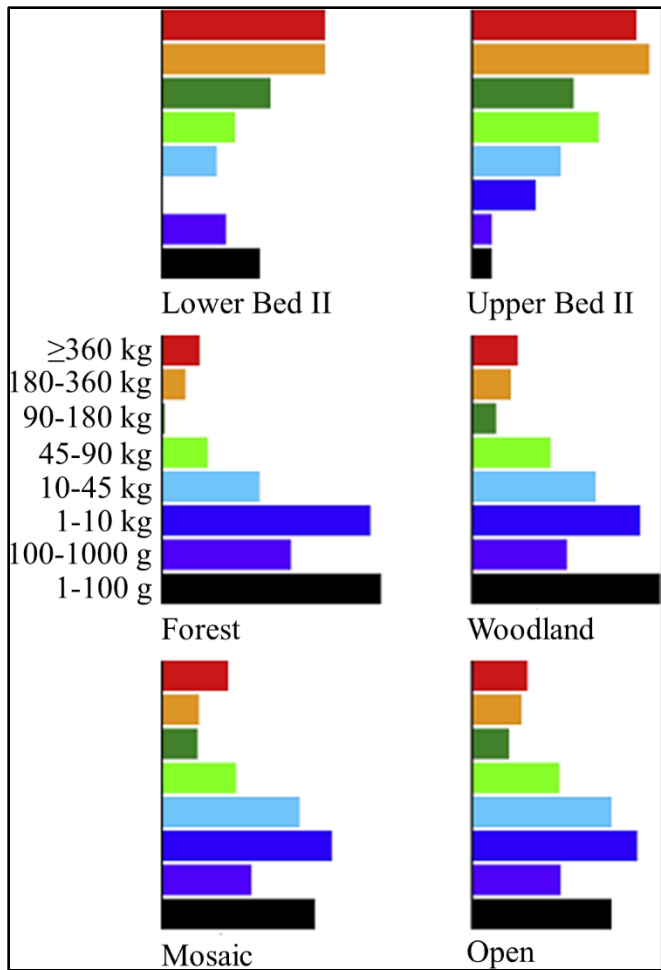


Figure 6-1. Proportions of species allocated to each body mass category for Lower and Upper Bed II, as well as mean proportions for the major habitat categories. Modified from Kovarovic et al., 2013.

When forest localities are dropped from the ecological diversity/correspondence analysis, Kovarovic et al., found that there is much better differentiation among the remaining broad ecological categories, with woodland localities distributed opposite to mosaic and open habitats. In this situation, Lower Bed II falls within an open environment. However, when large mammals are removed from the analyses instead, Lower Bed II is more closely associated with woodlands. This prompted the authors to situate Lower Bed II within a mosaic environment and suggest the tropical grassland of Kafue National Park in Zambia as a modern correlate for the environmental setting of pre-1.74 Ma Olduvai Gorge. The

modern area of Kafue is *Brachystegia* and *Isoberlinia* dominated Miombo woodlands interspersed with seasonal floodplains adjoining major rivers and tributaries. This compares well with other paleontological evidence (e.g. Prassack et al., (2018)) that suggests the lowermost portion of Bed II was predominantly comprised of wetland, lacustrine, and riverine habitats.

Upper Bed II (which in this case includes Middle Bed II of Bibi et al., (2018)) is represented mostly by fauna in the ≥ 180 kg body size (Fig. 6-1), with abundant terrestrial, grazing, and carnivorous species and fewer arboreal, frugivorous types. In fact, large bodied mammals disproportionately represent Upper Bed II. Species with a body mass of 45-90 kg are also well represented in Upper Bed II, helping situate this unit well within the woodland category even though there are fewer taxa in the ≤ 10 kg range that categorize modern woodland biomes. Kovarovic and coauthors compare Upper Bed II with the woodland habitats at Zinave National Park (Mozambique) or Kruger National Park (South Africa), but also to Kafue because of Upper Bed II's propensity of larger bodied mammals. Overall however, the greater proportion of ≥ 180 kg taxa imply less vegetative cover than the ecological diversity/correspondence analysis suggests.

Although the total number of species in Upper Bed II is very close to the average for all modern localities investigated, the distribution of species highlights a taphonomic impartiality toward smaller mammals. Furthermore, the absolute abundance of large mammals in Bed II suggests differences between Pleistocene Olduvai communities and any potential modern correlate, but these differences are likely related to taphonomy and the proportional preservation of large mammals over small (Kovarovic et al., 2013).

One cause of the differences in mammalian profiles between Lower and Upper Bed II is likely due to changes in depositional environment; that is, a reduction in waterlogged environments in Upper Bed II reduced preservation potential of small to medium sized animals. Therefore,

Kovarovic et al., suggest that the environmental differences between Lower and Upper Bed II may be overstated (e.g. Bibi et al., 2018) and that although the disappearance of paleo-Lake Olduvai near the top of Bed II was likely driven by changing climatic conditions, changes in local hydrology and geomorphology had a significant impact on fossilization and preservation on the mammal communities.

Altogether, Kovarovic et al., (2013) analyses imply that Lower Bed II was a Miombo-like woodland interspersed with seasonal floodplains adjoining Lake Olduvai and its major rivers and tributaries, while in Upper Bed II, there was an overall reduction in wetland environments, but wooded coverage retained its importance. The authors acknowledge that there are difficulties when assessing mammalian communities and their ecological significance, but also do not rule out that Olduvai may have been more open than any of the modern environments used in comparison and that this interpretation (Bibi et al., 2018) based on the large mammal assemblage must remain a viable alternative hypothesis.

6.2.3 Omo-Turkana Basin

In the Omo-Turkana Basin, faunal turnover, estimated using first and last appearance dates, began amongst bovids, equids, suids, and primates between 2.5 Ma and 1.8 Ma (Bobe and Behrensmeyer, 2004; Bobe and Eck, 2001). For example, Bobe and Behrensmeyer (2004) used the abundances of different mammalian species documented in faunal catalog databases from multiple formations in the northern Turkana Basin (e.g. Koobi Fora and Nachukui) to show changes in environments from the Late Pliocene to Early Pleistocene. Although the authors focused on taxa that indicate grassland habitats, such as Alcelaphini, Antilopini, and *Equus*, other species included in the study also demonstrate ecological change in the basin. Suids, an overall

minor component of the Omo faunal assemblages, declined in the Pliocene but recovered in the Early Pleistocene after 1.8 Ma, while bovids increased in abundance throughout the Gelasian. Cercopithecids on the other hand, peaked in richness in the Late Pliocene but numbers dropped after 2.0 Ma. At the start of the Pleistocene 2.58 Ma, *Oryx*, *Tragelaphus* (spiral-horned antelopes), and *Antilope* (now only found in India, Pakistan, and Nepal) appear for the first time, while species associated with closed and wet ecosystems such as the suid *Nyanzachoerus kanamensis* and the bovid *Menelikia leakeyi* have their last appearance. (however, *Antilope* is also not found after this period highlighting an issue with using first and last appearance dates). Also at this time, *Australopithecus sp.* is found in association with the closed adapted suid *Kolpochoerus limnetes*, and colobine primates *Rhinocolobus turkanaensis*, demonstrating that *Australopithecus* inhabited wooded environments.

During the Early Pleistocene, *Homo erectus* appears alongside hypsodont suids and Alcelaphinae bovids which are characterized as open-habitat species, while arboreal colobine monkeys become extinct (or not represented in the fossil record). However, *H. erectus* shows associations with woodland adapted species such as baboons (*Papio*) and the Kudu-like *Tragelaphus gaudryi*. Interestingly, *Paranthropus aethiopicus* also appears alongside *H. erectus* in the same showing that they may have shared the same habitats but exploited different food resources.

Equids never reach high concentrations, suggesting that although grasslands were beginning to expand in East Africa beginning about 2.5 Ma, they may not have dominated the northern portion of the Omo-Turkana basin. Furthermore, because the appearance of *Homo erectus* is associated with a transition to a complex mosaic of habitats that included grasslands, woodlands,

and bushlands (Bobe and Eck, 2001), the heterogeneity of the Omo-Turkana Basin may have been well suited to the dispersal of *Homo* into the region ~1.8 Ma.

6.3 Macro- and Microbotanical Remains at Olduvai Gorge

Fossil plants, root casts, leaf impressions, and biogenic silica (phytoliths) are often used to identify paleoenvironments and to track vegetational changes (Albert and Bamford, 2012; Albert et al., 2009; Bamford et al., 2006; Bamford et al., 2008; Barboni et al., 2010; Mercader et al., 2010; Mercader et al., 2009). At Olduvai Gorge, these proxies have been employed with varying results in Beds I and II, with some studies showing well-preserved plant material (e.g. Barboni et al., 2010), while others were unable to make reliable morphological interpretations of plant remains (e.g. Blumenschine et al., 2012). Nevertheless, phytolith research from Olduvai for example, provides evidence for a mosaic paleolandscape with a diversity of plant ecological lifeforms present in and around some of the early hominin sites. Albert et al., (2018) reconstructed the habitat of the HWK-W site located between Tuffs ID (1.854 ± 0.011 Ma) and IE (1.831 ± 0.004 Ma) (Deino, 2012) using phytoliths, macroplants, and diatoms. Both phytoliths and plant fossils were dominated by palms while grasses and sedges were also present, prompting the authors to suggest that the site was a river-fed, freshwater wetland or a riparian river channel. Barboni et al., (2010) used phytoliths from samples collected in the 5.0 cm immediately below Tuff IF to reconstruct the vegetation at FLK-N and surrounding landscape at the top of Bed I (1.803 ± 0.002 Ma). They show that at FLK-N, there was heterogenous woody coverage associated with a groundwater forest or dense woodland and that silica cells diagnostic of grasses were rare. Comparing this with samples collected in the HWK area east of the Castle, Barboni et al., (2010) demonstrated that in the upper part of Bed I, grass phytoliths were in greater abundance and perhaps more expansive than in the

younger sedimentary horizons between Tuffs ID and IE. Additionally, Bamford (2012) used plant fossils from trees, shrubs, grasses, and sedges to describe the paleo-vegetation at Olduvai from Tuff IIB (1.848 ± 0.003 Ma) in Bed I to immediately above Tuff IF in Bed II. Bamford identified rare leaf impressions from *Typha* in upper Bed I as well as in situ, silicified root horizons in the area of HWK-E which was interpreted as a growing surface with woody vegetation and flowering plants, while to the north and east, dry grasslands were common.

6.4 Geology and Stratigraphy

In *Geology of the Olduvai Gorge* (Hay, 1976), Hay documented physical sedimentation processes and used the chemical environment of sedimentation and post-depositional activities for paleogeographic reconstructions to indicate that during Bed I, the Olduvai region was governed by a fluctuating saline and alkaline paleolake. An alluvial fan, positioned on the eastern margin of the fault basin, drained the volcanic highlands through freshwater intermittent streams into the paleolake. Deposits of stream-laid trachyte igneous-rock attest to this, as coarser materials are found in the east, with particle size decreasing in a down-current westward direction. Cross-bedding, ripple marks, and cut-and-fill channeling, diagnostic features for determining sedimentation processes, helped establish stream patterns, and Hay determined that the paleolake did not have an outlet and consequently fluctuated between flooding and receding episodes controlled by the balance of inflow and evaporation.

Water of the perennial part of the lake was saline, alkaline, and rich in dissolved sodium carbonate-bicarbonate. Modern lakes rich in dissolved sodium carbonate-bicarbonate include Lakes Natron, Ndutu, and Singida, which yield diagnostic minerals (e.g. Gaylussite, searlesite) and distinct rock types (e.g. dolomite). Sand-sized calcite crystals are widespread in lake deposits

of Bed I, as well as beds of fine-grained dolomite, inorganic sodium-silicate chert nodules, and zeolite, potassium feldspar, and fluorite minerals, all of which demonstrate that the lake of Bed I was chemically similar to sodium carbonate-bicarbonate lakes in the rift valley today (Hay, 1976). The high salinity of the paleolake also suggests that Pleistocene Olduvai was closed basin in an arid or semiarid climate somewhat wetter than that of today. Furthermore, the paleolake appears to have been smallest between the deposition of Tuffs ID and IF, as indicated by a period of relative desiccation at FLK North (Hay and Kyser, 2001), but expanded abruptly just before Tuff IF was deposited, suggesting an increase in regional precipitation.

In Bed II, the perennial section of the lake was highly saline, more so than that of Bed I, as it did not have an outlet; this was determined by the abundance of trona, a non-marine evaporative mineral (Hay, 1976). Moreover, lithofacies, different but contemporaneous stratigraphic units deposited in a closely related series of environments, exhibit a common occurrence of zeolitic mineral alteration on the paleosurface, demonstrating that saline, alkaline soils were widespread. In the eastern fluvial and fluvial-lacustrine facies (east of the Second Fault), mudflows and coarse conglomerates deposited on a relatively flat surface suggest flash flooding caused by torrential downpours in an arid or semiarid climate.

Caliche limestones and calcareous nodules occur throughout the Olduvai sequence and provide another line of evidence for a semiarid climate at Olduvai through the Pleistocene (Hay, 1976). These are specifically widespread in the uppermost part of Bed II and are found in abundance in the eastern fluvial-lacustrine facies as well as in the western part of the basin. Caliche, a sedimentary rock consisting of calcium carbonate and other materials (e.g. sand, clay, silt) allude to a climate where evapotranspiration exceeds rainfall, indicating that standing water was rare in Upper Bed II. These deposits are also associated with eolian tuffs, which implies that

sparse, or shallow-rooted vegetation was unable to prevent the wind-blown movement of sediments.

Eolian tuffs of the Lemuta Member reflect a relatively dry episode that lasted at least 20,000 years. The Lemuta Member is a widespread sequence of tuffs comprised of reworked tephra mixed with minor limestone and claystone components; Tuff IIA (1.74 ± 0.03 Ma) is found within the lower section of the Lemuta Member, while Tuff IIB caps it and marks the start of Middle Bed II. It is this boundary that signals an increase in the relative extent of grassland, a decrease in the size of the lake, and abrupt faunal changes in Bed II. Caliche limestones and calcareous nodules are much more widespread above this unit, and fauna suggests wetland and closed-woodland species predominated below the Lemuta Member while open-savannah adapted species flourished above.

6.5 Isotopes of Lipid Biomarkers

Molecular proxies for paleoclimatology include environmentally persistent compounds sampled in lake sediments, loess deposits, ice cores, and terrigenous materials. These proxies are typically comprised of mixtures of long, straight-chain (i.e., normal, *n*-) alkanes, alkanols and alkanolic acids with 22-36 carbon atoms that record the composition and characteristics of continental vegetation. Molecular-proxy studies focus on these lipid components found in the protective waxes that coat leaf surfaces because they record information on atmospheric CO₂, the pathway employed during photosynthesis (C₃ or the C₄ biosynthetic pathway), and on factors such as aridity/humidity that affect the conductance of the plant's stomata (Eglinton and Eglinton, 2008). For a comprehensive review, see *Chapter 5: Plant Leaf Wax Lipid Marker Molecules*.

Abell and Margolis (1982) conducted the first study identifying terrestrial plant waxes in East Africa. They found *n*-alkanes in Plio-Pleistocene sediments of paleo-Lake Turkana in northern Kenya. Following this, Ficken et al., (1998) comprehensively analyzed a lake core encompassing the transition from MIS 5 to 4 in high-altitude Lake Nkunga (1,820 m.a.s.l.) on Mt. Kenya for *n*-alkanes, *n*-alkanols, and *n*-alkanoic acids. Mount Kenya is a large, extinct stratovolcano that receives most of its rainfall in northern spring and autumn, coinciding with the movement of the ITCZ and African monsoon, and displays the characteristic effects of orogenic rain-shadow; the southeastern flank receives more than 2,500 mm of rain annually, while the northern flank is dry and receives less than 1,500 mm per year (Ficken et al., 1998). Due in part to rainfall variations, vegetation on both flanks exhibits significant altitudinal zonation, ranging from wooded grassland to montane rainforest on the southeastern flank, and wooded grassland transitioning directly into high-altitude vegetation types (ericaceous moorland, afroalpine grassland) on the north.

Ficken and coauthors found that input from both terrestrial and emergent aquatic plants formed a relatively high proportion of the organic matter in the modern lake sediments. Focusing on compounds typical of higher terrestrial plants (C_{29} , C_{31}), they found that low ambient CO_2 and widespread aridity promoted the expansion of C_4 grasses in Pleistocene sediments. (Dating the core was problematic, a basal age was ^{14}C dated to $41,395 \pm 750$ years, but a nearly 30,000-year time gap separates Pleistocene from Holocene sediments). The $\delta^{13}C$ data for terrestrial-plant biomarkers in the late Holocene sediments exhibit values within the C_3 range, showing that C_3 vegetation returned on Mt. Kenya after being displaced by C_4 grasses during the last glacial period. They attribute the expansion of C_4 grasses and sedges in the glacial phase to lower atmospheric CO_2 and

reduced rainfall and reconstructed the Pleistocene environment as a dry *Juniperus-Olea* forest with an understory of mixed C₃ and C₄ grasses.

Using marine sediment cores from the Gulf of Aden, Feakins et al., (2005) recorded northeast African vegetation change spanning the late Neogene to Holocene (9.4 – 0.05 Ma), by systematically sampling in two- to three-thousand-year timeframes, with a goal of resolving orbital-scale variability. At the time of publication, the Gulf of Aden core was the closest marine site, and subsequently lipid biomarker record, to the East African hominin fossil sites. In accordance with East African carbonate isotope studies (Cerling, 1992), Feakins et al., show that C₃ woody and herbaceous vegetation was ubiquitous in Miocene sediments older than 4.0 Ma, but at around 3.8 Ma, large-scale isotopic variations coinciding with the 100,000-year precession cycle revealed variability in East African vegetation structure. This suggests that plant-landscape variability in this region began one million years before the onset of Northern Hemisphere glacial intensification and the closing of the Isthmus of Panama at 2.8 Ma. $\delta^{13}\text{C}$ values also demonstrate C₄ expansion between 2.4 and 1.7 Ma and that progressively more open environments spread when subtropical temperatures cooled around 1.9 Ma (Ravelo et al., 2004) and African wind-borne dust peaked near 1.8 Ma (deMenocal, 2004). Feakins et al., (2005) attribute the large-amplitude, northeast African vegetational changes to orbital precession variability.

Feakins et al., (2007) compared the Gulf of Aden marine isotope record to biomarkers from a terrestrial site ~2,000 km away in the Turkana Basin, Kenya. Although they were unable to directly compare the terrestrial and marine sediments for vegetation patterns due to possible microbial and diatom interference, they suggest that precessionally-forced environmental changes in the Turkana Basin were more pronounced than the northeast African vegetation changes recorded in marine sediments. They also showed that C₃ vegetation increased in East Africa during

periods of heightened monsoons, whereas C₄ vegetation spread when monsoons were weakened; precipitation is one of the most influential mechanisms for lipid biomarker biosynthesis. Furthermore, Feakins et al., (2007) showed that Rift Valley lakes (i.e. Paleo-Lake Turkana) responded to monsoon intensity and that they likely experienced cyclical changes in water levels and water chemistry. Therefore, hominins in the area were potentially susceptible to environmental oscillations that impacted local water supplies and vegetation structure.

Building upon their 2005 work, Feakins et al., (2013) extended the Gulf of Aden record back to 11.3 Ma and compared lipid biomarkers with diagnostic grass pollen. Interestingly, they found decreases in total grass pollen to coincide with more-positive $\delta^{13}\text{C}$ isotope values, what they claimed to be an indication of C₄ biomass expansion. Feakins et al., (2013) surmise that reductions in C₃ coverage outpaced the spread of C₄ grasses, even though overall grass pollen abundance did not increase significantly until after 1.6 Ma.

In the first major biomarker study at a specific East African archaeological locale, Magill (Magill et al., 2013a, b) studied lipid isotope signatures from a 100,000-year sequence of paleo-Lake Olduvai sediments recovered at outcrops exposed near the hypothesized center of the lake (Ashley, 2007; Hay, 1976). Using the C₃₁ *n*-alkane, Magill and coauthors (2013a) observed repeated shifts in $\delta^{13}\text{C}$ values between -36‰ and -20‰ starting about 1.8 Ma, changes that suggest ecosystem oscillations between closed C₃ woodlands and open C₄ grasslands. In addition, these values imply that vegetation composition varied along with orbital precession which regulates the duration and intensity of the precipitation-bearing monsoons in eastern Africa. To track these changes in precipitation, Magill et al., (2013b) used the δD of the C₃₁ *n*-alkane and algal-derived C₁₇, and detected values ranging from -148‰ to -132‰ and -150‰ to -30‰ for C₃₁ and C₁₇, respectively. Interestingly the C₃₁ δD and $\delta^{13}\text{C}$ only had a slight correlation, while the C₁₇ δD , with

hydrogen derived directly from lake water, correlated strongly with $C_{31} \delta^{13}C$. The lake water δD values revealed that significant fluctuations in water availability accompanied ecosystem changes identified through $\delta^{13}C$, and that drier conditions for this period, specified by more-positive δD values, complemented the more-positive stable carbon-isotopic evidence for C_4 ecosystems. Conversely, wetter conditions, indicated by more-negative $C_{17} \delta D$, associated with increased woody cover across the paleolandscape.

In a follow up study that evaluated plant distributions at a spatial scale, Magill et al., (2015) examined the C_{23} and C_{31} *n*-alkanes, as well as sedge-synthesized phenolic compounds and fern-produced mid-chain diols, across the FLK *Zinj* paleolandscape. Through these compounds, the authors were able to document spatial vegetation changes across the landscape; $C_{23} \delta^{13}C$ of sediments collected nearer to the presumed paleo-lake at the FLK North-North site had values of around -24‰, likely indicative of a more-aquatic ecosystem, while more-negative $C_{31} \delta^{13}C$ from archaeological trenches at the FLK *Zinj* Level 22 suggest dense, woody cover. Samples collected at FLK South, from the southeastern section of the transect, show more-positive $\delta^{13}C$ values thus demonstrating open C_4 grassland. These data show the potential for lipid biomarkers as a proxy for vegetation structure over spatial distances of 10 to 100+ meter scales.

Recent investigations on lipid biomarkers have also been achieved in the Turkana Basin of Kenya. Uno et al., (2016) studied the $\delta^{13}C$ from the C_{31} *n*-alkane and the C_{30} *n*-alkanoic acid of sediments from the Nachukui Formation to reconstruct the vegetation history of a roughly 600,000-year period; about 2.3 to 1.7 Ma. The Nachukui Formation, along the northwestern margin of Lake Turkana, belongs to the Omo Group which also includes the more famous Koobi Fora Formation on the eastern side of Lake Turkana and the Shungura Formation located to the north of Lake Turkana along the western side of the Omo River. Sediments within the Nachukui

Formation are associated with the Kokiselei archaeological complex that contains the earliest evidence of the Acheulean stone tool industry estimated at an age of 1.76 Ma (Lepre et al., 2011), and also includes co-occurring Oldowan and Acheulian lithic artifacts. The carbon isotope record shows that throughout the Nachukui, mixed C₃ and C₄, and C₄-dominated landscapes are most common, specifically after 2.0 Ma. The only instance of a C₃-dominated environment occurs at around 2.25 Ma and may be associated with riparian forests of the ancestral Omo River (Uno et al., 2016). Following this, gradually more-positive $\delta^{13}\text{C}$ values for *n*-acids show an increase in C₄ flora up until about 1.9 Ma suggesting an opening of the landscape, but at 1.9 Ma both *n*-alkanes and *n*-acids show large $\delta^{13}\text{C}$ variability for the next ~200,000 years, implying a plant composition structure between 40 and 80% C₄ vegetation, with inputs of up to 95% C₄ around 1.75 Ma.

Uno et al., interpret these changes in $\delta^{13}\text{C}$ as representing a decrease in mean annual precipitation for the Turkana Basin after 2.0 Ma, likely caused by changes in seasonality toward longer and more intense dry seasons. Because C₄ plants have an adaptive advantage in such conditions, they therefore would have outcompeted C₃ flora in times of extreme seasonality. Moreover, changes to the ancestral Omo River drainage network may have led to a reorganization of the plant landscape, especially in the positioning of riparian forests. Both scenarios would result in more positive $\delta^{13}\text{C}$ values in the C₃₀ *n*-acid and C₃₁ *n*-alkane records from the Nachukui Formation.

In an analogous study, Lupien et al., (2018) presented carbon and hydrogen isotope ratios from terrestrial plant waxes recovered in a 216 m borehole sample (Hominin Sites and Paleolakes Drilling Project Core WTK13) cored in the Nachukui Formation of West Turkana. The core spans about 500,000 years and was $^{40}\text{Ar}/^{39}\text{Ar}$ dated to between 1.870 and 1.388 Ma. The authors reported on the $\delta^{13}\text{C}$ and δD of the C₂₈ *n*-alkanoic acid due to its high abundance in samples throughout the

core, with δD values ranging from -58‰ to -181‰ with an average of -110‰, and $\delta^{13}C$ between -31‰ to -15‰ and an average of -22‰. The δD data correlate with both the 41,000-year obliquity cycle and closely to the 21,000-year precession cycle; periodicity in hydrogen isotopes were documented at 18,000 years, slightly shorter than orbital precession. Lupien and coauthors' evidence suggests that changes in precession-controlled summer insolation is the dominant factor driving Early Pleistocene hydrologic change in the Turkana region. In addition, the authors observed average δD values to be depleted by about -25‰ than late Holocene aged sediments from modern Lake Turkana samples, which suggests that the Turkana Basin was wetter throughout the Early Pleistocene than today. Over the 500,000-year period investigated, Lupien et al., (2018) found no statistically significant trend toward drier conditions such as that of Uno et al., (2016), but do find high-amplitude variations in $\delta^{13}C$ and δD for the overlapping 1.8 to 1.7 Ma records; possibly due to oscillations between much-wetter and much-drier conditions than average for the rest of the core.

6.6 Chapter 6 Summary

Various proxies for paleoclimate and paleoenvironmental reconstructions for African Pliocene Pleistocene archaeological sites have been published, including reconstructions using carbonate isotopes, faunal and botanical remains, geomorphology, and leaf wax lipid biomarkers. Carbonate isotope data at Olduvai suggest a trend toward warmer and dryer conditions starting around 1.65 Ma and that there was likely a major change in the amount of precipitation in the region. A shift toward dryer conditions began in Middle to Upper Bed II and persisted through Bed IV. In the Omo-Turkana region, there is also a trend toward dryer conditions and greater C4 biomass, especially after 1.9 Ma, but due to its larger geographic extent, the Omo-Turkana basin supported

a mosaic vegetation community with diverse hydrologic regimes, contrasting in water availability, slope, and drainage across short distances. As for paleontological proxies, there is high mammalian diversity at Olduvai Gorge, suggesting the juxtaposition of distinct landscape ecologies with woodland, bushland, grassland, and marshland biomes, especially in Bed I. In Bed II however, there is a shift to a mosaic of more-open dry and wet grasslands according to the avifaunal assemblages, while mammalian remains imply an overall reduction in wetland environments, but wooded coverage retained its importance. In the Omo-Turkana region, equids never reach high concentrations suggesting that grasslands may not have dominated, at least in the northern portion of the basin. Furthermore, the appearance of *Homo erectus* is associated with a complex mosaic of grasslands, woodlands, and bushlands. Finally, lipid biomarkers from both Olduvai and Turkana show that vegetation composition varied along with orbital precession which controlled summer insolation and the intensity of the precipitation-bearing monsoon in eastern Africa. Therefore, C₃ and C₄ dominated environments correlated with changes in precipitation as governed by both the 41,000-year obliquity cycle and the 21,000-year precession cycle.

CHAPTER 7: THE ACHEULEAN STONE TOOL INDUSTRY

7.1 Introduction

The appearance of the Acheulean in East Africa at ~ 1.75 Ma (Beyene et al., 2013; Diez-Martín et al., 2015; Lepre et al., 2011) (Fig. 7-1), marks the first major transition in stone tool technology whereby the more-complex and systematically-shaped tools of the Acheulean overlap and then supplant the earlier Oldowan cobble-core tradition. As the Acheulean signifies early complex behavior through the repeated manufacture of large-sized, standardized tools (Diez-Martín et al., 2015), it is indicative of advance foresight requiring developments in spatial perception beyond those known for apes or earlier (>2.0 Ma) hominins. Acheulean archaeological assemblages, typified by handaxes, cleavers, and other Large Cutting Tools (LCTs) such as picks, are found up until about 125,000 years ago (Bruggemann et al., 2004; Walter et al., 2000), making it the longest-lasting technology. Artifact assemblages containing handaxes and cleavers are also the first indicators of a Stone Age technology appearing outside of Africa, reaching the Middle East (Bar-Yosef, 1994; Bar-Yosef and Goren-Inbar, 1993; Clark, 1975) and South Asia by 1.4 Ma (Paddayya et al., 2002; Pappu et al., 2011; Petraglia et al., 1999), Western Europe by

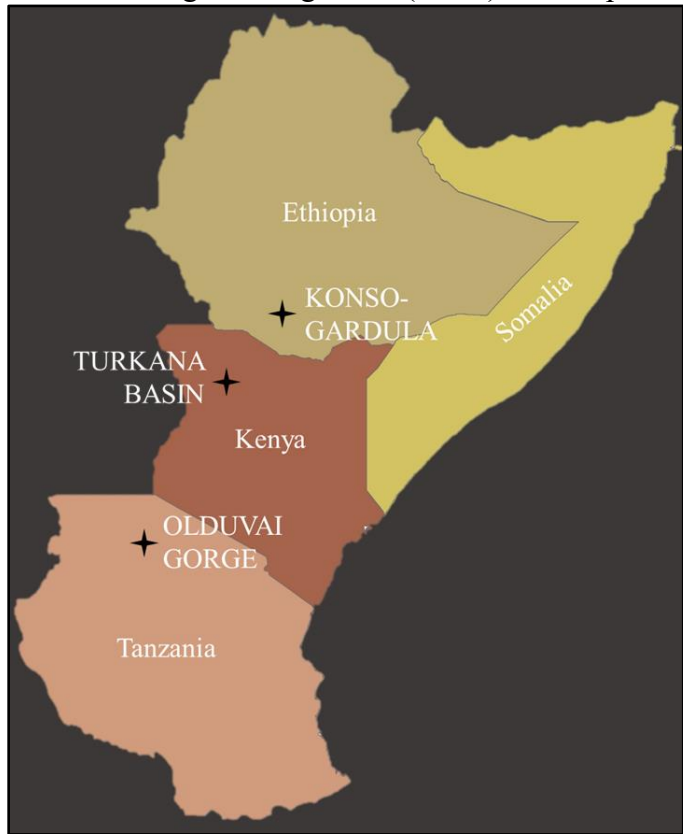


Figure 7-1. The earliest known examples of the Acheulean in East Africa, 1.76 to 1.70 Ma.

500,000 years ago (Falguères et al., 1997; Lebreton et al., 2016; Roebroeks, 2011; Santonja and Villa, 2006), and possibly East Asia by 0.8 Ma (Hou et al., 2000; Kuman et al., 2014; Yamei et al., 2000); however debate continues over whether the term *Acheulean* is applicable to assemblages in eastern Asia.

The distinctive Acheulean tool forms are often divided into two major types (handaxes and cleavers), with a third (picks) that is sometimes subsumed into the handaxe category (Schick and Toth, 1993). Handaxes are symmetrically designed, bifacially flaked tools with pointed tips that are lanceolate-, triangular-, ovate-, or pear-shaped (Fig. 7-2). They are characteristically flaked around all or most of their circumference, producing sharp convex, concave, or straight cutting edges (Roe, 1996). Cleavers, although more “axe like” in appearance, are tools with broad transverse cutting edges oriented perpendicular to the long axis of the tool, but with less emphasis on side cutting edges than those on handaxes. Additionally, cleavers are most abundant in regions where raw material does not need extensive shaping prior to the removal of large flakes (Santonja and Villa, 2006). Picks are very similar in appearance to handaxes except with less emphasis placed on creating sharp cutting edges; instead, they tend to be thicker and have a trihedral tip.

Handaxes and cleavers dominate the perception of Acheulean stone tool kits because they are easily recognizable, but Acheulean assemblage also contain other implements made from retouching simple flakes into points, knives, and scrapers (Roe, 1996). Furthermore, although the terms *biface* or *Large Cutting Tool (LCT)* are used to refer to Acheulean assemblages, not all handaxe-bearing sites (e.g. China; see Kuman et al., 2014) are considered *Acheulean*. Demarcating Acheulean archaeological sites has been problematic for some time now; for example, Mary Leakey (1971) excavated and described the Acheulean at Olduvai Gorge but felt that Kleindienst earlier criterion (1961) for classifying Acheulean sites (i.e. they must contain 40-60% bifaces)



Figure 7-2. The two *typical* Acheulean tools, the cleaver and handaxe, found exposed on the surface in the Side Gorge in 2014 (Sharpie is approximately 14 cm).

should be revised to include sites which have a lower percentage of bifaces. Nevertheless, Acheulean LCTs persisted for 1.5 million years, serving as a multitool for bone breaking, butchering, chopping, digging, hide-working, nut-cracking, scraping, and wood-working (Clark, 2001; Domínguez-Rodrigo et al., 2001; Goren-Inbar et al., 2002; Leakey, 1971; Schick and Toth, 1993). In addition, although Acheulean tools found in different regions with distinct geomorphology, raw material sources, and ecology are broadly similar in terms of typology, there is variability in the shape and size of bifaces, manufacturing techniques, raw material source, and artifact assemblage composition (Jones, 1995; McPherron, 2000; Wynn and Tierson, 1990).

7.2 Earliest Examples of the Acheulean

The earliest known examples of the Acheulean in East Africa are found at Kokiselei 4, West Turkana, Kenya at an estimated age of 1.76 Ma (Lepre et al., 2011), and at Konso-Gardula, Ethiopia, $^{40}\text{Ar}/^{39}\text{Ar}$ dated to 1.74 ± 0.03 Ma (Beyene et al., 2013). Slightly younger, but chronologically well-bracketed material that is more technologically and morphologically

complex is found at Olduvai's Frida Leakey Korongo West (FLK-W) site, $^{40}\text{Ar}/^{39}\text{Ar}$ dated to 1.698 ± 0.015 Ma (Diez-Martín et al., 2015). There is about a 200,000-year gap before the Acheulean becomes widespread, but shortly after 1.5 Ma, the technology disperses across Africa (Chazan et al., 2008; Gibbon et al., 2009; Kuman and Clarke, 2000), the Near East (Bar-Yosef and Goren-Inbar, 1993), India (Pappu et al., 2011), and then later in China (Hou et al., 2000; Zhu et al., 2004), and Indonesia (Simanjuntak et al., 2010).

7.2.1 Kenya

The Kokiselei 4 Acheulean assemblage is stratigraphically positioned ~30 m above the 1.869 ± 0.021 Ma KBS (Kay Behrensmeyer) Tuff at the base of the Kaitio Member of the Nachukui Formation in West Turkana, Kenya, and 4.5 m above the boundary between the Olduvai *subchron* and Matuyama *polarity chron* boundary. (A subchron is a short time interval (≤ 0.1 Ma) of an alternate polarity occurring within a polarity chron; e.g. the normal-polarity Olduvai subchron within the Matuyama reversed-polarity chron. The top of the Olduvai subchron dates to 1.778 ± 0.003 Ma (Hilgen et al., 2012).)

The age of Kokiselei 4 is estimated through a sediment accumulation rate model using the KBS Tuff and the Olduvai subchron, as well as other $^{40}\text{Ar}/^{39}\text{Ar}$ dated

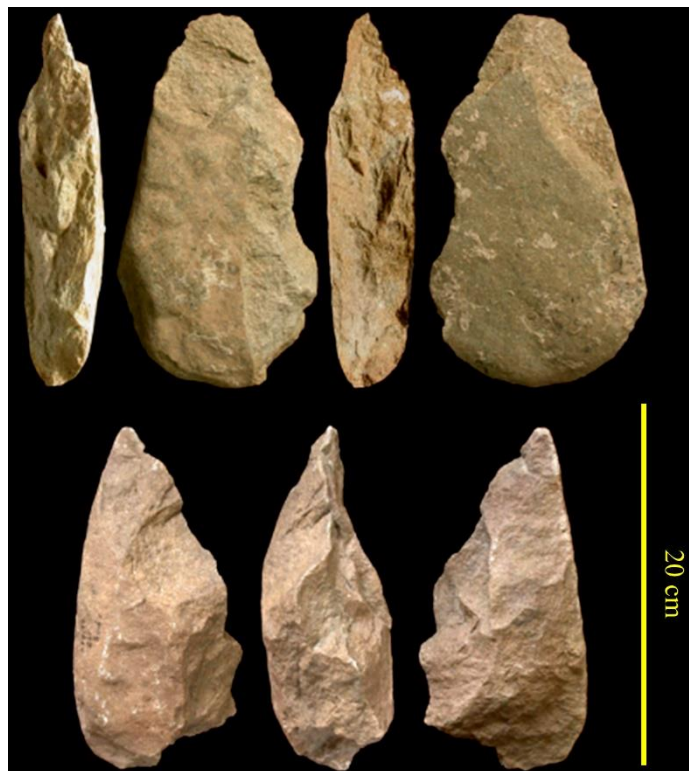


Figure 7-3. Partial crude handaxes made on a flat large phonolite cobble (top) and a thick split phonolite pebble (bottom). Modified from Lepre et al., 2007.

tuffs in the Nachukui Formation (Kalocho, Lower Koobi Fora) to place the Acheulean assemblage at 1.76 Ma. The collection is characterized by coarsely made proto-bifaces, unifacially and bifacially shaped crude handaxes, pick-like tools with a trihedral section manufactured on thick phonolite pebbles, and scrapers and notches crafted on cobble cores and flakes (Lepre et al., 2011; Roche et al., 2003) (Fig. 7-3).

7.2.2 Ethiopia

At Konso-Gardula (KGA), Ethiopia, the youngest recognizable Acheulean assemblage occurs at KGA6, a site stratigraphically situated within 2.0 m above the Konso Kayle Tuff-2 (KYT2). This tuff is 6.0 m above the top of the Olduvai subchron, and is $^{40}\text{Ar}/^{39}\text{Ar}$ dated to 1.74 ± 0.03 Ma (Beyene et al., 2013). At KGA6, 47 large bifacially or unifacially modified flakes were recovered, 18 of which were shaped into picks, handaxes, and cleavers. The raw material was almost exclusively locally available basalt, while the largest tools exceed 20 cm in maximum length.

Picks are dominant and mostly asymmetrically made on flake blanks with thick pointed tips. Handaxes are crudely shaped and exhibit curved to linear bilateral cutting edges that converge into a somewhat rounded to rectilinear tip. At the KGA6 site, 28 total tools were documented, with cleavers accounting for 11%, handaxes 14%, picks 39%, and other types 36%. One hundred percent of the cleavers and picks were made on flakes, while 88% of the handaxes were manufactured on flakes but 12% were fashioned from cobbles. Furthermore, 100% of the cleavers were unifacial, whereas 75% and 91% of the handaxes and cleavers were unifacial, respectively. The mean pick length was 179.5 mm and the mean for the handaxes was 161 mm.

One of the most interesting aspects of the Konso-Gardula Acheulean assemblage is that it spans nearly one million years, from ~1.75 to ~0.85 Ma (Fig. 7-4). The earliest “typical” Acheulean tools are found around 1.57 Ma (KGA4), and are broadly comparable to the early Acheulean of Olduvai Bed II sites EF-HR (1.6-1.5 Ma) and BK (1.4-1.3 Ma) (Leakey, 1971). The younger KGA4 handaxes exhibit *near-symmetrical* designs in some portion of the tools compared to the older KGA6 assemblage, with a clear increase in workmanship in edge modification and tip thinning (Beyene et al., 2013). More sophisticated Acheulean tools were gathered between 1.5 and 1.2 Ma; these are extensively bifacial, have greater symmetry, a higher frequency of tool types, sizes, and shapes, and seemingly standardization of edge and tip shape and form.

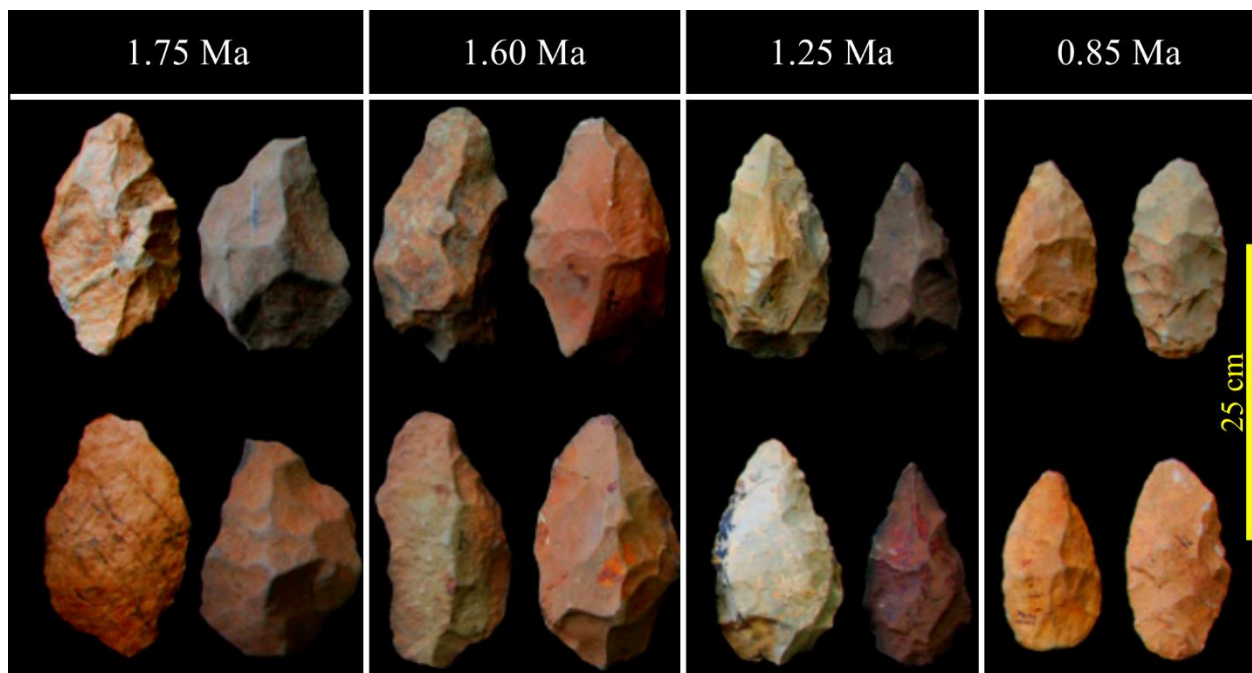


Figure 7-4. Handaxe refinement through time at Konso-Gardula, Ethiopia. Near-unifacial (left) and more extensively bifacial (right) examples shown. Approximate age at top. Modified from Beyene et al., 2013.

7.2.3 Tanzania

The slightly younger Frida Leakey Korongo West (FLK-W) site, is a chronologically well-bracketed Acheulean assemblage at Olduvai Gorge that is more technologically and morphologically complex than either Kokiselei 4 or Konso-Gardula (Diez-Martín et al., 2015). Situated between Tuffs FLK-Wa (1.698 ± 0.015 Ma) and FLK-Wb (1.664 ± 0.019 Ma), the lithic collection totals 2,120 artifacts distributed across six “archaeo-stratigraphic” units consisting of fluvial conglomerates and sands. In all six stratigraphic levels, a variable representation of Oldowan percussive elements (hammerstones, battered cobbles, anvils, and percussion flakes) were found alongside the Acheulean assemblage. Truly bifacial handaxes were amongst the 28 large cutting tools discovered, most of which were shaped through bifacial and preferential non-invasive reduction. The LCT artifacts had mean length, width, and thickness sizes of 143, 85, and 53 mm, respectively.

The most significant accumulations of stone tools occur in levels 6 (39.38% of the total sample), 5 (37.12%), and 4 (13.49%), with the majority of the collection knapped on large flake blanks or tabular Naibor Soit quartz clasts (73.67%), followed by volcanic basalts and phonolite (18.19%), and chert (7.07%), especially in archaeological level 6 (Diez-Martín et al., 2015). Interestingly, most artifacts can scarcely be attributed to the *classic* Acheulean, as most lack any form of symmetry. However, these simpler tools co-exist with another extremely sophisticated, highly symmetrical and bifacially flaked handaxe (Fig. 7-5). This



Figure 7-5. Bifacially-flaked basalt handaxe from FLK-W Level 6, measuring 310 mm from tip to end. Modified from Diez-Martín et al., 2015.

handaxe exhibits traits similar to the earlier examples found at Kokiselei 4 and Konso-Gardula; however, the FLK-W handaxe (and other LCTs) displays evidence of relatively advanced knapping skills as it was bifacially flaked with extreme symmetry obtained. Moreover, the FLK-W site provides evidence of the earliest stages in developing the Acheulean technology as it is found along cobble and percussion tools and is the oldest Acheulean site in which stone tools associate spatially and functionally with fauna exploitation.

The co-occurrence of the Oldowan and Acheulean at Kokiselei 4 and FLK-W shows that the two technologies are not mutually exclusive, time-successive components of an evolving stone tool tradition, as the behavioral repertoire of early hominins in both regions incorporated both technologies for food processing, wood working, digging, or bone breaking (Beyene et al., 2013). Although the overlap of the two industries may indicate different species of hominins with different tool-production behaviors, an alternative is that the Acheulean represent new activities within the same species and population (Semaw et al., 2008). Additionally, the emergence of the Acheulean in East Africa appears to have been rapid (as exemplified by the three studies above), and the slightly younger (~1.6 Ma) appearance of abundant bifaces and picks at Gona, Ethiopia (Semaw et al., 2008) and abundant handaxes and crudely made bifaces at 1.3 Ma Peninj, Tanzania (de la Torre et al., 2008). Other important Early Acheulean sites in East Africa include Koobi Fora (Harris and Isaac, 1997), Gadeb (Clark, 1987), and Melka Kenture (Piperno, 2001), while in South Africa early Acheulean artifacts are found in the Sterkfontein Valley (Kuman, 2007), Wonderwerk Cave (Chazan et al., 2008), and the Reitputs Formation (Gibbon et al., 2009) (Fig. 7-6).



Figure 7-6. Acheulean sites of Eastern and Southern Africa.

7.3 Emergence of the Acheulean

The emergence of the Acheulean has been linked to the appearance of *Homo erectus* about 1.9 Ma; a partial occipital bone (KNM-ER 2598) was found 4 m below the KBS Tuff in the Koobi Fora Formation (Feibel et al., 1989; Gathogo and Brown, 2006). In fact, Mary Leakey (1967) considered the possible connection between different hominins and stone tool technologies, and hypothesized that the Oldowan was made by *H. habilis*, and the Acheulean by *H. erectus*. However, *H. erectus* remains have yet to be found in association with the earliest Acheulean in West Turkana (Kokiselei 4), Konso-Gardula (KGA6), or Olduvai Gorge (FLK-W, EF-HR)¹¹, nor have Acheulean tools been documented at Koobi Fora with the earliest *H. erectus* material (de la Torre, 2016). When hominin remains and early Acheulean tools do associate with a given archaeological horizon, the species is always *Homo erectus*, rather than the contemporaneous *Homo habilis* or *Paranthropus boisei* (Larick and Ciochon, 1996).

If the early age of KNM-ER 2598 is acknowledged, then *H. erectus* emerged about 150,000 years before the Acheulean, therefore implicating a biological framework for this technology. For example, Oldowan hominins (i.e. *H. habilis*) primarily utilized fine-grained cobbles for the production of sharp-edged cutting flakes, whereas in the Early Pleistocene, *H. erectus* toolmakers (i.e. at Gona, Ethiopia) sought large size raw materials irrespective of their fine-grained nature (Semaw et al., 2008). At Olduvai on the other hand, de la Torre and Mora (2014) show that (presumably) *H. erectus* at the upper Bed II TK site (~1.5 Ma) selected for large quartzite cores without significant irregularities for the production of LCTs, contrasting with Bed I Oldowan sites where small lava cobbles and quartzite regardless of irregularities were used.

¹¹ All *H. erectus* fossils at Olduvai appear in handaxe-bearing deposits (de la Torre and Mora, 2014), but no hominin remains have been recovered at FLK-W or EF-HR yet.

Because Acheulean toolmakers appear cognizant of the textural quality of raw materials used in the production of bifaces, the two-dimensional (and later three-dimensional) symmetry of early handaxes required developments in spatial perception beyond those known for Oldowan hominins, while the congruent symmetries of later handaxes required mental rotation. The calculated, technical workings of the third dimension first began to materialize at Kokiselei 5, a short-term occupation site on the margin of paleo-Lake Turkana which is slightly older than Kokiselei 4 and demonstrates technological aspects akin to the earliest Acheulean in West Turkana (Gallotti and Mussi, 2018a; Texier et al., 2006). The Kokiselei 5 hominins (*H. habilis*, *H. rudolfensis*, *P. boisei*, or *H. erectus*) did not impose stringent selection criteria on raw materials, utilizing a wide range of rock types and cores of no specific shape to create a series of flakes; this contrasts with the earlier Oldowan manufacturers that were constrained by the initial morphology of raw material sources (Texier et al., 2006). Furthermore, this *technological leap* enabled the Kokiselei 5 individuals to bypass the restraints imposed by specific raw material, such as the size, quality, and shape, and granted them the ability to create new striking platforms to further flake production after initial flake removal (Gallotti and Mussi, 2018a).

Although the archaeological level is relatively thin at only about 20 cm, The Kokiselei 5 assemblage consists of 1,766 lithics. Flakes make up roughly 90% of the collection, while natural clasts or manuports make up about 8.0%, and cores slightly more than 2.0% (Texier et al., 2006). Flakes are evenly distributed at the site and refitting on 140 lithics show that cores and débitage were within a 2.5 m radius of each other; this also suggest that flaking activity occurred in a low post-depositional environment away from fast moving streams. Most of the assemblage was constructed of phonolite and trachyte (similar to the Acheulean assemblage of Kokiselei 4), rocks that were abundantly and locally available. Both unifacial and bifacial flaking is evident on

chopper-core technology, and bifacial flaking of thick nodules and cores reveal concrete evidence of the technical capabilities of the local individuals, and their ability to modify platform angles. Perhaps the most important aspect of the archaeological assemblage is a proto-biface that was crafted on medium-grained phonolite. This tool evokes a slow transition towards the Acheulean as it was made on an elongated nodule fractured along its long-axis, with a trihedral pointed tip subsequently obtained through unifacial flaking on one half (Texier et al., 2006). Therefore, Kokiselei 5 provides an opportunity to study the transition from the Oldowan and emergence of the Acheulean, as the manufacturers reached a level of technological expertise that allowed them to work a variety of raw material types in order to create specific bifacial morphology through the successive removal of flakes (Gallotti and Mussi, 2018a).

7.4 The Acheulean at Olduvai Gorge

The Acheulean, which persisted for about 1.5 million years, was the first technology that became widely distributed, with sites ranging from the southern edge of Africa, across the continent and into the Middle East, and all the way from western Europe to south and east Asia. However, it would be the rich archaeological record from Olduvai Gorge, first presented by Louis Leakey (1951) and then redefined by Mary Leakey (1971), that established the Acheulean as one of the best known and well-studied cultural industries. Olduvai is the location where the transition from the Oldowan to the Acheulean was first documented, and where the original earliest archaeological evidence of this technology was discovered before being supplanted by Kokiselei 4 and Konso-Gardula.

One of the best known and perhaps most representative sites of an early Acheulean assemblage at Olduvai Gorge is EF-HR, named for Evelyn Fuchs and Hans Reck who first

identified its potential in 1931. EF-HR, which is approximately 1.3 km west of the Third Fault on the northern rim of the gorge, was originally excavated by Mary Leakey in 1963 (Leakey, 1971) whereby she recovered a large number of bifaces (53.8% of all tools) made on large flakes struck from boulders or large cobbles, as well as heavy-duty picks, and well-made cleavers. The assemblage also included a small number of Oldowan choppers (3.3% of all tools). Leakey (1971) proposed that the assemblage represented a living floor of a camp situated along a shallow stream channel. Recent excavations (de la Torre et al., 2017; de la Torre and Wehr, 2018) found that the site is positioned between Tuffs IIC and IID and falls between an age of 1.66 ± 0.01 Ma (McHenry and Stanistreet, 2018) and 1.338 ± 0.024 (Dominguez-Rodrigo et al., 2013), placing it within Upper Bed II, and thus younger than the Acheulean at FLK-W. Additionally, de la Torre et al., (2017) interpreted hominin activity and artifact accumulation to be concentrated within an incised valley created by a river system sourced in the Crater Highlands, and that hominins occupied a lacustrine floodplain along an ancient river valley. The largest concentration of Acheulean handaxes so far documented in Bed II at Olduvai have also been reported from the EF-HR site (de la Torre and Mora, 2018). With over 2,300 artifacts recovered, two distinct reduction sequences were documented in the EF-HR assemblage (de la Torre and Mora, 2018), one utilized for producing large cutting tools and a second employed for flaking small debitage. This standardization emphasizes advance mental foresight and the management of raw materials for specific tool manufacturing signifies both technological and cognitive advancements from the Oldowan to the Acheulean.

Another location first identified by Louis Leakey (1951), then further explored by Mary Leakey (1971), and more recently excavated by Santonja et al., (2014), is the Upper Bed II site of Thiongo Korongo (TK). Divided into two subsections, the TK Upper Floor is positioned between 2.80 and 3.16 m below the contact of Beds II and III, while the TK Lower Floor is between 3.95 and 4.30 m below the contact (Santonja et al., 2014). Currently, TK has only been dated through stratigraphic correlations using the top of Bed II and Tuff IID exposed at the Juma Korongo site 800 m to the southeast of TK; Tuff IID at the Bell's Korongo (BK) site of the Side Gorge has been $^{40}\text{Ar}/^{39}\text{Ar}$ dated to 1.338 ± 0.024 (Domínguez-Rodrigo et al., 2013). Originally, Mary Leakey (1971) defined the lithic assemblage at TK as the Developed Oldowan B (see Box VII-I) but showed that the TK Lower Floor contained bifaces similar in morphology to those excavated at EF-HR yet in low frequencies. Subsequently, she attributed the Lower Floor to the Acheulean based on the typological aspects of the bifacial tools even though they were found in low abundance and did not meet Kleindienst's criterion (1961) for classifying Acheulean sites (i.e. they did not contain 40-60% bifaces) but kept the Upper Floor as part of the Developed Oldowan B. de la Torre and Mora (2005) however, suggested that the entire site is consistent with the Acheulean technology and that separate classifications for the two floors was unwarranted as both the Lower

BOX VII-I: IS THERE A DEVELOPED OLDOWAN?

Mary Leakey (1971) categorized several Olduvai artifact assemblages into a transitional industry called the *Developed Oldowan*. The Developed Oldowan-A contains cores, choppers, and flakes but differentiated from the *typical* Oldowan in that it consists of many spheroids and proto-bifaces. The Developed Oldowan-B contains crudely-worked small bifaces on cobbles, as well as awls, burins, and well-made large bifaces formed on large flakes that are similar to the Early Acheulean but found in small numbers. However, there is uncertainty in the status of the Developed Oldowan as a valid tradition, as variations in the tools are mainly the result of differences in the flaking potential of raw materials (de la Torre and Mora, 2014; Semaw et al., 2008).

and Upper floors contained handaxes that were indistinguishable from one another in terms of raw materials used, large flakes utilized as blanks, or final tool form and shape. After analyzing 2,174 and 5,319 lithics from the Lower and Upper floors, respectively, Santonja et al., (2014) attributed the entirety of TK to the Acheulean technological complex. One of the most interesting aspect of the TK assemblage is that the majority of the tools originated on quartzite sourced at the nearby (~2.0 km) Naibor Soit outcrop, the proximity of which may have been the impetus for hominin activity at the site.

Two other archaeological sites that were originally designated Developed Oldowan (Leakey, 1971) but later reclassified as Acheulean (de la Torre and Mora, 2005) are the Side Gorge assemblages Sam Howard Korongo (SHK), set below Tuff IIC, and the younger Bell's Korongo (BK), the highest known occupation site in Bed II. At BK, a high proportion of quartzite bifaces similar to those at TK were recovered (Leakey, 1971), while SHK was one of the early sites investigated by Louis Leakey (Leakey, 1965) that helped him establish a preliminary cultural sequence he named the *Chellean* which would later be subsumed into the Acheulean. Although the number of recovered bifaces at SHK is relatively small (68 (Leakey, 1971)) the original assemblage included ten flakes larger ranging in length from 11 to 17 cm that were likely generated during the manufacture of LCTs as they were used without further modification. Overall, Leakey found that choppers were the second most common tool form at SHK after spheroids, while crude and poorly made bifaces only accounted for 7.4% of the total assemblage. Of the 68 bifaces recovered, most were made on quartzite and there was one well-made example that was larger and more symmetrical than the other specimens. Additionally, Mary Leakey identified one biface that allegedly resembled a Middle Stone Age bifacial point. A single bifacial cleaver, two oblong picks, and a heavy-duty pick were also excavated at SHK (Leakey, 1971). At the stratigraphically higher

BK, heavy flakes weighing more than 2.0 kg were recovered alongside massive cores that suggest the use of large flakes as blanks (de la Torre and Mora, 2014). In the initial excavation, Leakey recovered over 6,800 lithics while in subsequent excavation (Diez-Martín et al., 2009), more than 1,500 flaked tools were found. Similar to SHK and TK, quartz is the predominant raw material type at BK, accounting for 95% of all tools (Diez-Martín et al., 2009). Furthermore, at both sites, handaxes are intensively reduced and show symmetrical manufacturing through both bipolar, bifacial, and centripetal flake removal (de la Torre and Mora, 2005; Diez-Martín et al., 2009).

7.5 Environmental Context of the Earliest Acheulean

Isaac (1971) and then Hay (1976) were the first to recognize that the early Acheulean sites at Olduvai Gorge were seemingly located in paleo-riverine environments at least 1.0 km beyond the paleo-lake margin, as opposed to the Oldowan/Developed Oldowan sites positioned closer to the lake shore. At Gona and West Turkana however, Oldowan localities were deposited within fluvial sediments associated with the meandering or braided paleo- Awash and Omo rivers and were located within perennial river systems that included a mosaic, riparian environment (Rogers and Semaw, 2008). Nevertheless, faunal reconstructions at SHK, TK, and BK (Domínguez-Rodrigo et al., 2014a; Domínguez-Rodrigo et al., 2014b; Yravedra et al., 2016) indicate that the sites were dominated by open habitat taxa, but whether or not these taxa were brought into the site by hominins or other carnivores similar to that of FLK West (Diez-Martín et al., 2015), is currently unknown. Similarly, at Kokiselei the presence of bovid, wetland adapted antelope, impala, gazelle, and spiral-horned antelope remains indicate a wooded grassland ecosystem (Lepre et al., 2011). Sedimentological facies on the other hand, provide evidence for beach, lagoon, and riverine habitats and hippopotamus fossils indicate a perennial water source and the presence of grassy

environments along riverbanks and the lake margin (Lepre et al., 2011). Additionally, pedogenic carbonates suggest that wooded grassland was dominant in and around Kokiselei, but woodland, bushland, and shrubland were also present (Quinn et al., 2013). At Konso-Gardula, fossils and lithic artifacts occur in fluvial sediments in river systems equivalent to modern tributaries of the Omo River, such as lake-margin floodplains and alluvial fan settings (Suwa et al., 2003). At KGA6 for example, lacustrine and floodplain depositional settings dominate the sedimentary sequences, suggesting a consistent water source for Acheulean manufacturers. Interestingly, bovids (*Antelopinae* and *Alcelaphinae*) are poorly represented in the faunal assemblage of KGA6 (Suwa et al., 2003), suggesting a relatively closed setting at Konso-Gardula.

At Olduvai, Mary Leakey (1971) ruled out the paleoecological hypotheses of Isaac and Hay, in which the Acheulean was utilized in riverine settings whereas the Oldowan was confined to lakeshore habitats, on the grounds that there was no clear ecological distinction between Middle and Upper Bed II. Moreover, Bibi et al., (2018) show that uppermost Bed I and all Bed II faunal assemblages advocates the dominance open grassland habitats and that tree coverage would have been minimal and true woodlands practically absent. Because they argue that habitats remained consistently dry and open throughout the entire Bed II sequence, there was no major turnover or paleoecological changes that took place across the Oldowan to Acheulean transition. Although this supports Mary Leakey's claim of there being no clear ecological distinction between Middle and Upper Bed II, Bibi et al., (2018) dismissal of woodland habitats is likely misguided as riparian woodlands would have established along water courses flowing into paleo-Lake Olduvai similar to those at Kokiselei and Konso-Gardula.

Taken as a whole, the environmental context of the earliest Acheulean is still poorly represented, and more direct, site specific analyses are needed to clearly define the ecological

context of hominin tool use and assemblage accumulation for this period. Generalizations, such as Acheulean artifact utilization occurring in river channels along lake-margin floodplains and alluvial fans, do not provide specific evidence for an environmental causality for the emergence of this industry and thus cannot help us define its origins in East Africa. Therefore, new methods designed to assess the environmental context of both the Oldowan and the Acheulean are necessary for determining whether hominin paleo-habitats acted as a driving force in the implementation and widespread use of Acheulean stone tools.

7.6 Chapter 7 Summary

Kokiselei 4, West Turkana, Kenya, Konso-Gardula, Ethiopia, and Frida Leakey Korongo West, Olduvai Gorge, Tanzania; these three sites represent the earliest evidence for the Acheulean stone tool industry. The collection at Kokiselei is characterized by coarsely made proto-bifaces, unifacially and bifacially shaped crude handaxes, and pick-like tools, while those found at Konso-Gardula were large bifacially or unifacially modified flakes shaped into picks, handaxes, and cleavers. The Acheulean at FLK-W on the other hand, displays evidence of relatively advanced knapping skills and provides evidence for the earliest stages of Acheulean development, and is the earliest site in which stone tools associate spatially and functionally with fauna exploitation. Moreover, the co-occurrence of the Oldowan and Acheulean at Kokiselei 4 and FLK-W shows that the two technologies are not mutually exclusive, time-successive components of an evolving stone tool tradition, as the behavioral repertoire of early hominins in both regions incorporated both technologies for food processing, wood working, digging, or bone breaking.

CHAPTER 8: METHODS

8.1 Sample Collection

Olduvai Gorge is an exceptional locality for examining evolutionary events that associate with environmental stability and change as the region boasts archaeological remains with extraordinary evidence for human paleobiology. This makes the study area the best place to track the impact shifting climates had on configuring local habitats, and the role ecological variability played in the emergence of Acheulean technology at Olduvai ~1.7 Ma. The emphasis is on the environmental and archaeological transition between Olduvai Beds I and II, a nearly 200,000-year period (1.83 to 1.66 Ma), which includes a key shift in stone tool technology from the Oldowan to the Acheulean, and a general opening of the landscape. Terrestrial sediments were sampled from the following Olduvai locations (Fig. 8-1; 8-2A, B, C.):

- Frida Leakey Korongo North (FLK-N), a Bed I locality dated 1.831 ± 0.006 Ma to 1.803 ± 0.002 Ma (Deino, 2012), containing several hundred Oldowan stone tools and abundant faunal remains but no clear association between the two assemblages (n=8)
- Clays in contact below Tuff IF (1.803 ± 0.002 Ma), the marker tuff dividing Bed I from Bed II that is exposed for more than two kilometers throughout the main confluence of the gorge (n=30)
- Frida Leakey Korongo West (FLK-W), an excavation site dated between 1.698 ± 0.015 Ma and 1.664 ± 0.019 Ma, consisting of fluvial conglomerates and sands (Diez-Martín et al., 2015) that contains Olduvai's earliest known Acheulean assemblage (n=28)

Along the Lower Augitic Sandstone (LAS), an unconsolidated sedimentary unit dated to between 1.698 ± 0.015 Ma and 1.664 ± 0.019 Ma, which is exposed for roughly three

kilometers in the main confluence of the gorge and is stratigraphically related to the lower units of FLK-W (n=15)

- Clays in contact below the Bird Print Tuff (BPT), a nearly 800-meter long volcanic deposit exposed south of FLK-W in the main gorge, dated to Middle Bed II and found stratigraphically above FLK-W (n=11)
- Clays situated above Tuff IIA (1.74 ± 0.03 Ma) and below the LAS at Olduvai's geologic feature known as the *Castle*. These clays represent the paleoenvironment that followed the FLK-N sequence and preceded the FLK-W sequence in the lower portion of Bed II (n=14).

Sampling from these sites presents an opportunity to combine temporal (column approach) with spatial (landscape approach) strategies to identify variations in lipid biomarkers and isotopes resulting from a mosaic ecosystem and changes in the environment over time. For all samples, between 5.0 and 10 mm of the outer surface of excavation trench walls or geologic exposures were cleaned with a trowel to limit modern airborne hydrocarbon contamination prior to sediment collection.

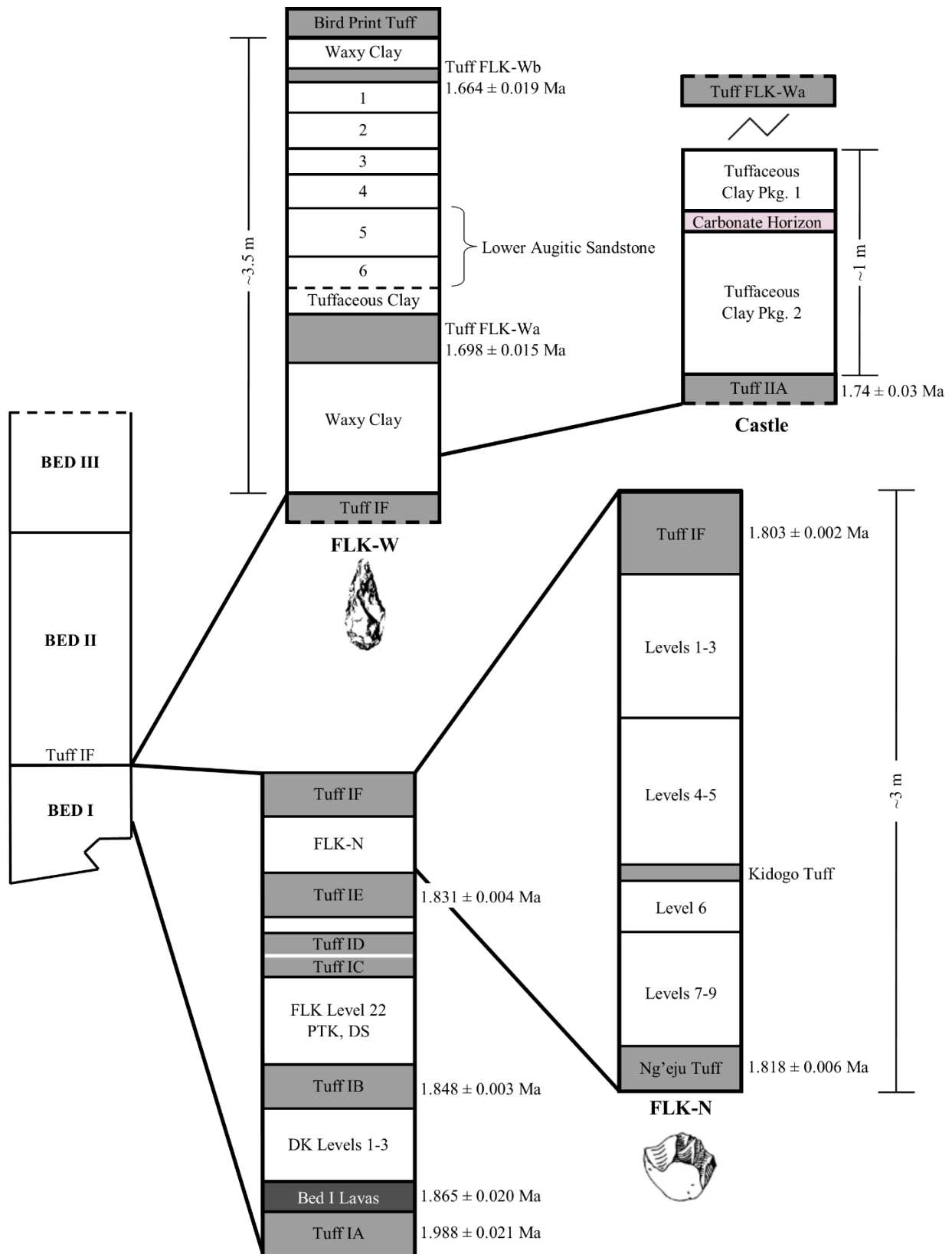
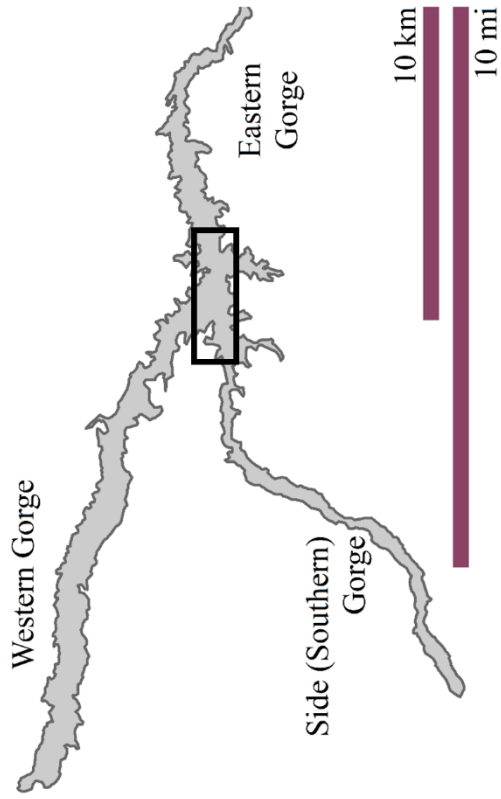


Figure 8-1. Stratigraphic subsections of Bed I, with expanded view of the FLK-N Oldowan site, and the Bed II FLK-W Acheulean site. The Castle, about 700 m southeast of FLK-W, is stratigraphically related to the clays below Tuff FLK-Wa. Stratigraphic and archeological units are not necessarily to scale (Dates and stratigraphy adapted from Ashley et al., 2010; Deino, 2012; Diez-Martín et al., 2015; Domínguez-Rodrigo et al., 2007; Hay, 1976; McHenry and Stanistreet, 2018; Stanistreet, 2012).



●	Bird Print Tuff (BPT)	
●	Lower Augitic Sandstone (LAS)	1.664 ± 0.019 Ma
✕	FLK West	1.698 ± 0.015 Ma
■	Castle	1.740 ± 0.030 Ma

●	Clays below Tuff IF	1.803 ± 0.002 Ma
★	FLK North	1.831 ± 0.006 Ma
Bed II		
Bed I		

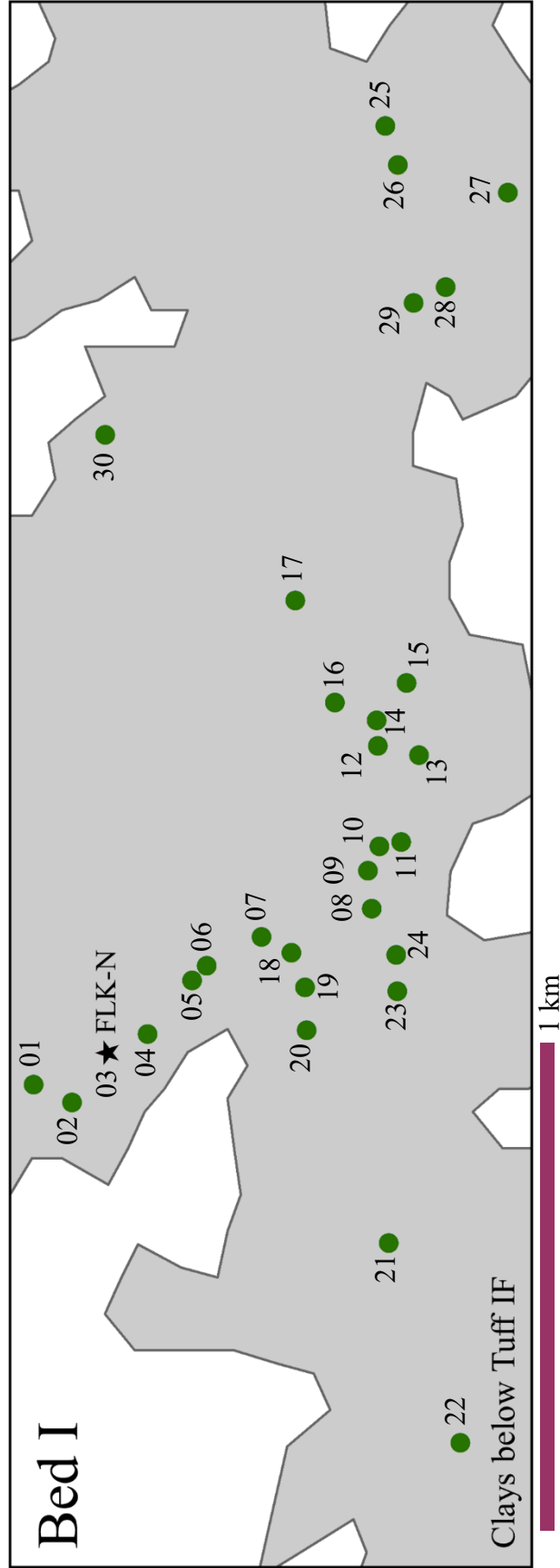


Figure 8-2A. Clays below Tuff IF sampling locations throughout the main confluence of the gorge. Sampling distance spans ~2.7 km east-to-west, and ~1.1 km north-to-south. ★ FLK-N archaeological site.

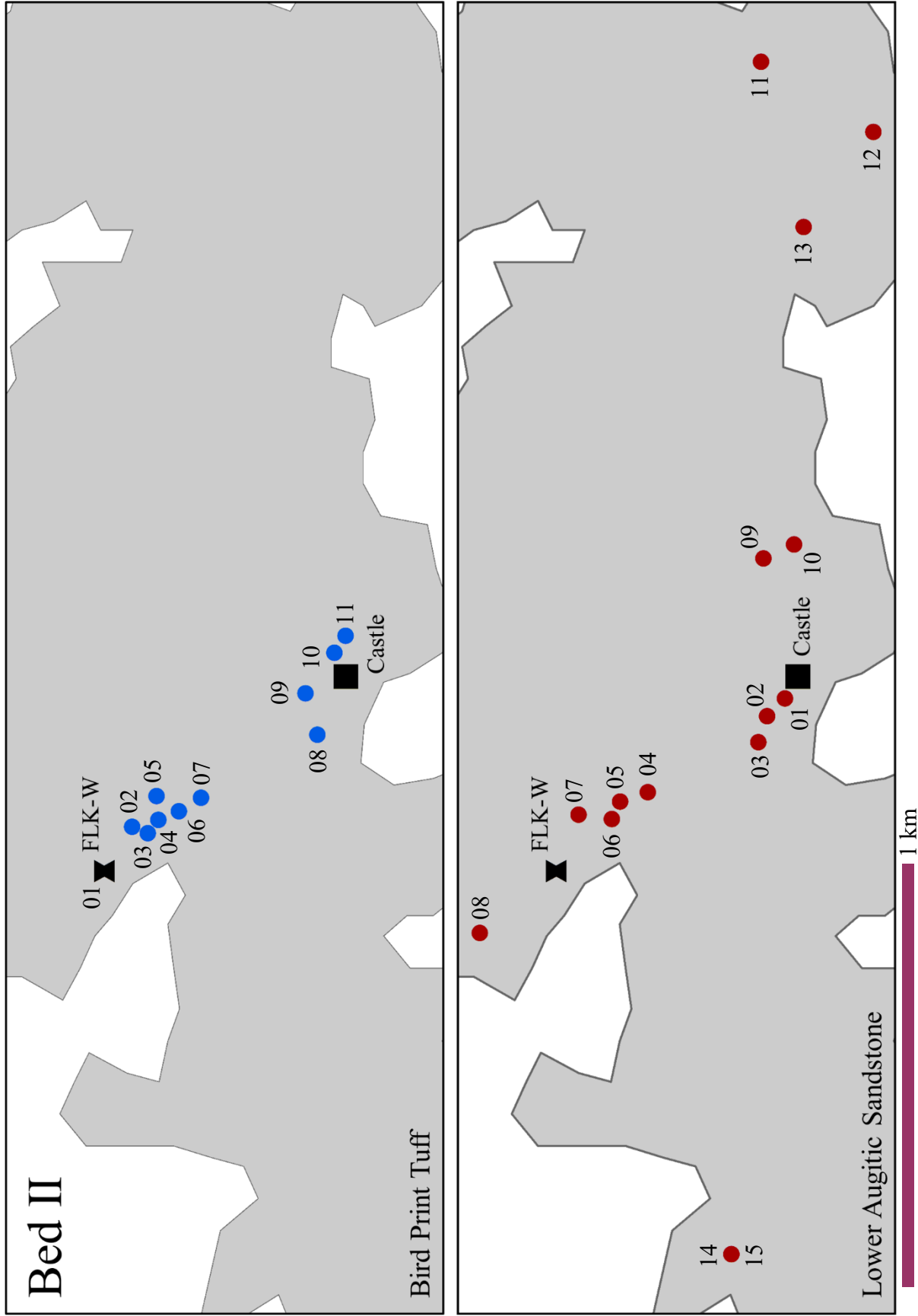


Figure 8-2B. Bird Print Tuff (BPT) sampling locations throughout the main confluence of the gorge. Sampling distance spans ~775 m NW-to-SE. **8-2C.** Lower Augitic Sandstone (LAS) sampling locations; distance spans ~1.2 km NW-to-SE and ~2.8 km east-to-west. **▲** FLK-W archaeological site, **■** Olduvai's Castle.

8.1.1 FLK-N

Underlying Tuff IF, Frida Leakey Korongo North (2° 59' 21.08"S, 35° 20' 53.4"E) is a 3.0 m, 15,000-year sequence in Upper Bed I subdivided into nine archaeological units dated between 1.803 ± 0.002 Ma (Tuff IF) and 1.818 ± 0.006 Ma (Ng'eju Tuff) (Deino, 2012), that is rich in cultural and faunal material (Leakey, 1971). (Interestingly, FLK-N contains three archaeological horizons above Tuff IF that extend into Lower Bed II, one of which corresponds to Levels 1, 2, and 3 of HWK-E.) Of the nine units below Tuff IF, Levels 1-5 sit above the Kidogo Tuff, while 6-9 are between the Kidogo and Ng'eju Tuffs (Fig. 8-3). Mary Leakey (1971) arbitrarily subdivided Levels 1-3, as this unit was uniform in composition, and consists of about 80 cm of a grey-brown silty/waxy clay. Archaeologically, she combined Levels 1 and 2 but excluded Level 3 on the grounds that it was poor in artifact and faunal remains; overall however, there is no tangible basis for distinguishing between Levels 1 and 2, and 3 (Domínguez-Rodrigo and Barba, 2007). Level 4 is a dark chocolate-brown silty/waxy clay varying in thickness from 8 to 45 cm. The lack in association among faunal remains and hominin butchering activities in FLK-N Levels 1-4 suggest carnivore accumulated bone assemblages by felids, most likely leopard (Domínguez-Rodrigo et al., 2007b). Level 5 is a greenish-yellow clay that includes a hominin toe bone (OH 10) and is situated atop the 10 cm fine-grained pyroclastic Kidogo Tuff (Ashley et al., 2014), which separates Levels 1-5 from 6-9; Leakey (1971) interpreted Levels 1-5 as hominin "living floors." Level 6 is a dark greyish-brown silty/waxy clay 20-50 cm thick, which Leakey described as an elephant (*Elephas recki*) butchery site (c.f. Domínguez-Rodrigo et al., 2007a; Potts, 1988), that also contained a 75 mm proto-biface made on basalt (Leakey, (1971): p. 66). Levels 7-9 have not yet been extensively excavated, but were described by Domínguez-Rodrigo et al., (2010) as a 15-

20 cm light-grey clay (Level 7), a 13-18 cm light-grey to yellowish clay (Level 8), and a 16-31 cm dark waxy clay (Level 9).

Samples (n=8) were collected in 5 cm intervals from directly below Tuff IF to a depth of 40 cm in Levels 1 and 2 of FLK-N Geological Trench 7 (Fig 8-3). It is within these levels that a high-density concentration of faunal remains were recovered in association with Oldowan stone tools (Bunn et al., 2010; Diez-Martín et al., 2010; Domínguez-Rodrigo et al., 2010; Leakey, 1971). Levels 1 and 2 have been described as a living floor (Leakey, 1971), a central foraging place (Bunn, 1986), a spot for intensive percussion behavior, particularly on long bone shafts (de la Torre and Mora, 2005; Diez-Martín et al., 2010), a palimpsest of non-related animal and hominin activity (Bunn et al., 2010), a felid-responsible bone accumulation site (Diez-Martín et al., 2010), and a hammer-and-anvil location for plant resource processing (Domínguez-Rodrigo and Barba, 2007).

Table 8-1. FLK-N Trench 7 samples, stratigraphic position, and amount (g) used in Soxhlet extraction.

Sample	Depth below Tuff IF (cm)	Amount (g)
8	0-5	40.1
7	5-10	40.5
6	10-15	40.1
5	15-20	41.1
4	20-25	41.1
3	25-30	42.0
2	30-35	41.7
1	35-40	39.4

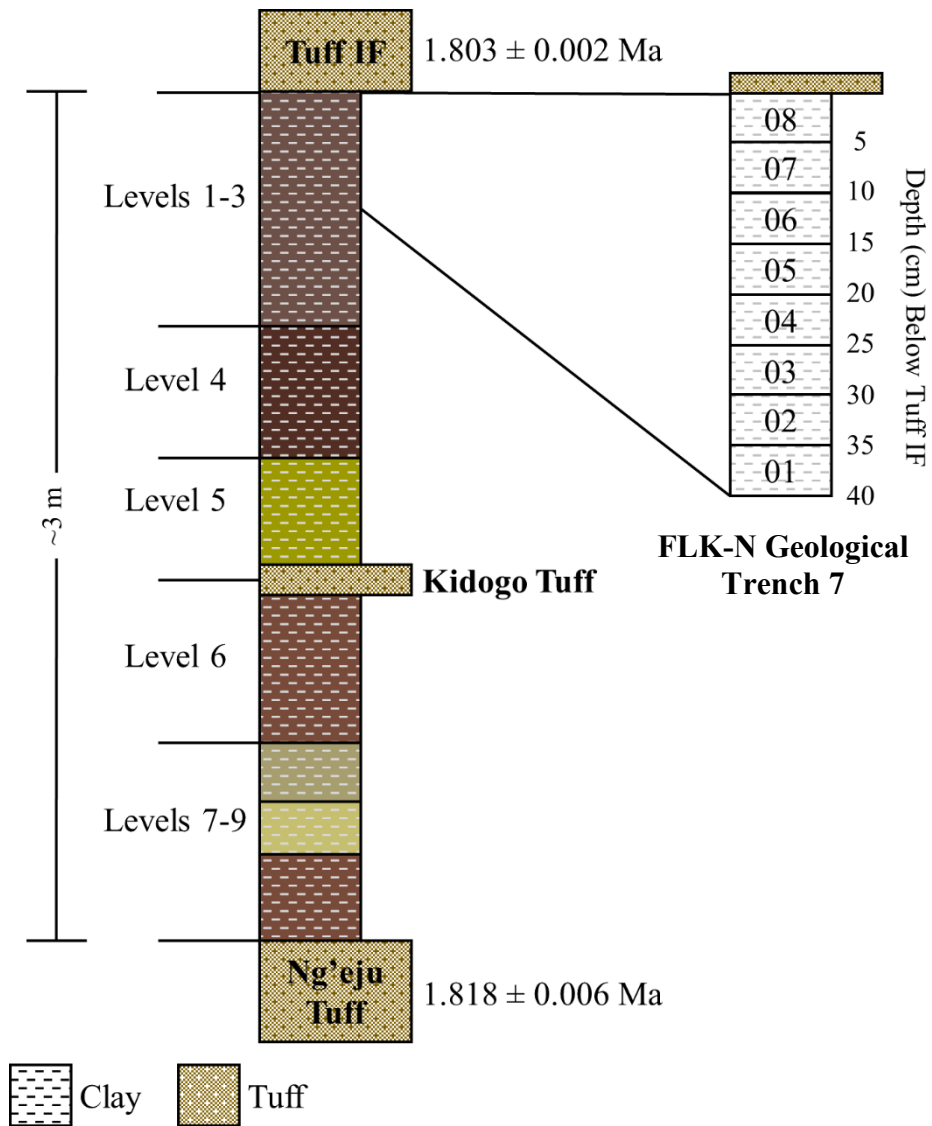


Figure 8-3. Stratigraphy of the FLK-N archeological levels and FLK-N Trench 7 column sampling. Through Levels 1-3, materials appear vertically dispersed without showing any sedimentary intervals (Adapted from Ashley et al., 2010; Hay, 1976; Leakey, 1971).

8.1.2 *Clays Below Tuff IF*

Tuff IF divides Bed I from Bed II and is the most widespread of the Bed I tuffs (Hay, 1976). Samples (n=30) were collected in the clays directly in contact below the tuff for more than two kilometers throughout the main confluence of the gorge (Fig. 8-2A; Table 8.2) to track spatial changes in vegetation before the transition to Bed II. The clays are generally waxy, and greenish brown to dark brown in color, and were likely deposited through fluvial and lacustrine processes on the alluvial fans and floodplains surrounding paleo-Lake Olduvai. However, no systematic geologic survey has been conducted on the depositional history of the clays themselves outside of those at specific archaeological sites (e.g. FLK-N). Climatologically, the region was in a drying phase toward the top of Bed I (Ashley, 2007; Hay, 1976; Sikes and Ashley, 2007), whereby changes in precipitation had a long-term effect on the water level of paleo-Lake Olduvai. Landscape sampling was designed to track changes in vegetation, mainly difference between C₃ vs. C₄ dominated localities, in relation to Bed I archaeological sites to answer questions on whether hominin activity was concentrated in areas with a greater abundance of woody (C₃) cover.

8.1.3 *FLK-W*

Frida Leakey Korongo West (2° 59' 23.78"S, 35° 20' 54.27"E) is a Bed II excavation site within a ~40 m wide and 130 cm deep fluvial river channel infilled with a sequence of six archaeo-stratigraphic levels (Diez-Martín et al., 2015). This channel represents a high-energy depositional environment, isolated in a wide and flat area that includes concentrations of hominin activities situated near paleo-Lake Olduvai. The lowermost levels (L6 and L5) are the most dense and important in terms of their archeological contents. Based on a recent geological model, the FLK-W sequence is dated 1.698 ± 0.015 Ma (Tuff FLK-Wa) to 1.664 ± 0.019 Ma (Tuff FLK-Wb)

Table 8-2. Clays below Tuff IF samples, amount (g) used in ultrasonic extraction, and coordinates in decimal degrees.

Sample	Amount (g)	Latitude	Longitude
01	10.4	-2.9878	35.34755
02	10.4	-2.9885	35.34722
03	10.8	-2.9891	35.34814
04	10.5	-2.9899	35.34848
05	11.0	-2.9907	35.34947
06	11.0	-2.9910	35.34974
07	10.4	-2.9920	35.35027
08	10.3	-2.9940	35.35079
09	11.2	-2.9939	35.35149
10	11.0	-2.9941	35.35194
11	10.2	-2.9945	35.35202
12	10.9	-2.9941	35.35379
13	10.5	-2.9949	35.35362
14	10.0	-2.9941	35.35426
15	10.1	-2.9946	35.35495
16	10.2	-2.9933	35.35459
17	10.3	-2.9926	35.35647
18	10.3	-2.9925	35.34998
19	10.9	-2.9928	35.34934
20	10.2	-2.9928	35.34855
21	11.6	-2.9943	35.34463
22	10.2	-2.9956	35.34095
23	11.3	-2.9945	35.34927
24	10.2	-2.9944	35.34994
25	10.1	-2.9942	35.36521
26	10.2	-2.9945	35.36449
27	10.7	-2.9965	35.36398
28	10.3	-2.9954	35.36224
29	10.3	-2.9948	35.36195
30	10.1	-2.9891	35.35952

and consists of fluviatile conglomerates and sands fixed within a clay unit at the base of Bed II (Figs. 8-2B, C; 8-4). Diez-Martín et al., (2015) describe the six archaeo-stratigraphic levels as Level 1 (L1), a homogeneous fine-grained sand and silt, overlaid by Tuff FLK-Wb; Level 2 (L2), an erosive unit of cut-and-fill up to 50 cm wide and 20 cm deep, which corresponds to small braided channels that reworked the previous fluvial deposit; Level 3 (L3), a 30 cm layer of massive clayish silt without flow structures; Level 4 (L4), a medium-grained mafic (upper) and felsic (lower) sand and tuffaceous sand unit, increasing in thickness from 15 to 30 cm; Level 5 (L5), three layers of coarse sand 20–30 cm thick, with cross bedding and horizontal lamination in the lower and western parts of sequence; and Level 6 (L6) a 20 cm thick conglomerate composed of blocks, cobbles, and gravels within a matrix of coarse sand. The most significant Acheulean artifacts are featured in L5 and L6, where 26 large cutting tools (LCT), including truly bifacial handaxes, were found (Table 8-3). Both simple LCTs and a highly symmetrical and bifacially flaked handaxes co-exist in the lower level assemblage.

Samples (n=28) were collected throughout the 155 cm sedimentary sequence in a 2 cm high, by 9.5 cm wide (on average), and 4.5 cm deep (on average) arrangement, with 4 cm intervals between each sample (Fig. 8-4; Table 8-4). Of the total samples, 23 were collected in the six archaeo-stratigraphic levels (samples 1 to 23), four in the tuffaceous clays below L6 (samples 24 to 27), and one from the waxy clays above Tuff FLK-Wb and below the Bird Print Tuff (sample 28).

Table 8-3. Summary of total lithics recovered and the number of LCTs from the six archaeo-stratigraphic levels at FLK-W (data from Diez-Martín et al., 2015).

Level	Total Lithics	% of Total	LCTs
L1	26	1.22	0
L2	89	4.19	0
L3	97	4.57	0
L4	286	13.49	0
L5	787	37.12	2
L6	835	39.38	24

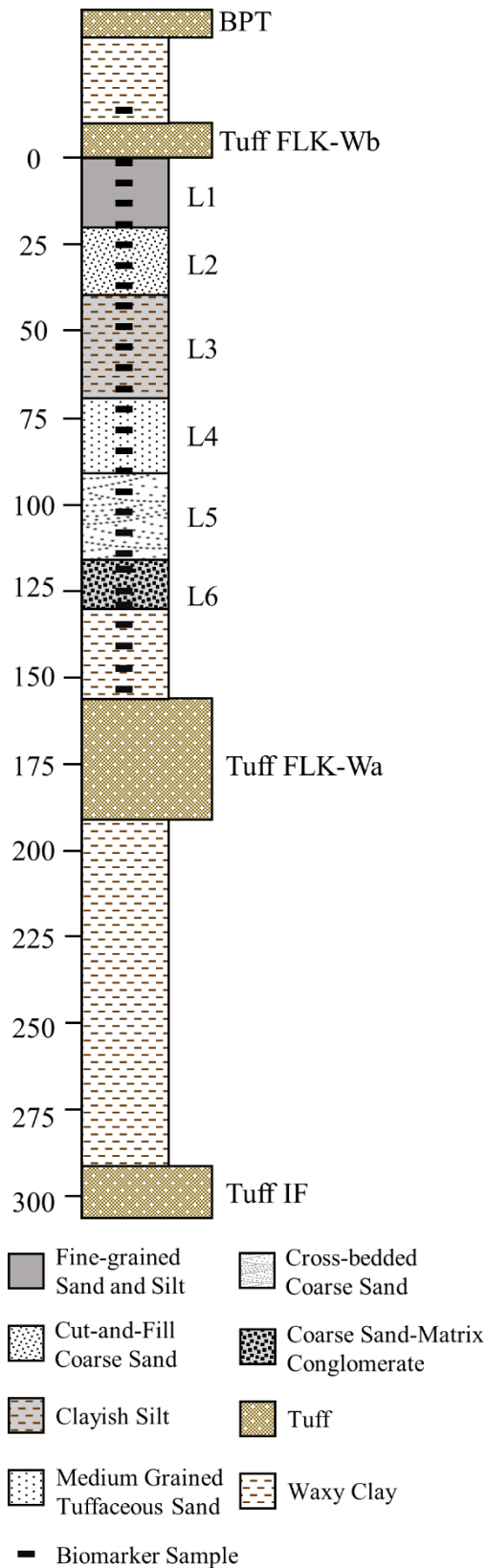


Figure 8-4. Column sampling at the FLK-W site through the 6 archaeo-stratigraphic levels and in the above and below clay units. Sampling strategy is 4 cm intervals between 2 cm high samples (Adapted from Diez-Martín et al., 2015; Uribealrrea et al., 2017).

Table 8-4. FLK-W samples, depth below Tuff FLK-Wb, amount used in Soxhlet extraction, and the archaeo-stratigraphic level.

Sample	Depth (cm) below FLK-Wb	Amount (g)	Level
28	-	51.5	Clays above FLK-Wb
23	0-2	49.4	L1 - Fine-grained Sand and Silt
22	6-8	56.7	
21	12-14	43.8	
20	18-20	44.2	
19	24-26	40.8	L2 - Cut-and-Fill Coarse Sand
18	30-32	54.1	
17	36-38	40.7	
16	42-44	33.2	L3 - Massive Clayish Silt
15	48-50	43.5	
14	54-56	48.2	
13	60-62	50.4	
12	66-68	48.1	
11	72-74	56.1	L4 - Medium Grained and Tuffaceous Sands
10	78-80	47.5	
9	84-86	42.3	
8	90-92	35.5	
7	96-98	50.0	L5 - Cross-bedded Coarse Sand
6	102-104	44.2	
5	108-110	25.4	
4	114-116	41.3	
3	118-120	47.6	L6 - Coarse Sand- Matrix Conglomerate
2	124-126	30.8	
1	128-130	44.4	
27	134-136	51.3	Clays below L6
26	140-142	16.8	
25	146-148	17.0	
24	152-154	18.6	

8.1.4 LAS

The Lower Augitic Sandstone (LAS) is an unconsolidated sedimentary unit belonging to the same fluvial system as FLK-W archaeological Levels 5 and 6. This unit is exposed for ~2.0 km NW-SE and ~3.0 km E-W in the main confluence of the gorge (Fig. 8-2C). It was deposited over the Lemuta Member that erodes Tuff IIA at several places on the south side of the Main Gorge (Hay, 1976). LAS sediments are mafic, and mainly augitic with 50-75% augite and 10-30% volcanic rock fragments of pyroclastic origin. The LAS unit was deposited along the eastern paleo-lake-margin as a braided stream channel flowing northwest towards the central lake, likely converging into a single channel at FLK-W (UribeArrea et al., 2017). This deposit is also positioned 5.0 m above Tuff IF in Long Korongo just east of the Fourth Fault. Both Acheulean FLK-W and the Oldowan HWK sites belong to the same fluvial system (Fig. 8-5), but HWK was within the braided stream system while FLK-W was located along a sinuous stream channel (UribeArrea et al., 2017). UribeArrea and coauthors suggest that although the two sites share the same fluvial system, the difference in stone tool technology could be explained by ecological or landscape related limitations.

Samples (n=15) were collected in the unconsolidated sandstones that comprise the LAS for ~2.8 km E-W and ~1.2 km NW-SE in the main confluence of the gorge (Fig. 8-2C; Table 8.5) to track spatial changes across the fluvial system and to compare with FLK-W L6 and L5. The sandstone is either loosely consolidated or unconsolidated; most samples were collected as loose sands (1-4, 9-12), while the others were consolidated into singular units (5-8, 13-15). On average, unconsolidated samples were collected in a 6 cm high, by 6 cm wide, and 4 cm deep arrangement (Max: 12x9x8; Min: 2x4x3 (HxWxD)), while consolidated samples were collected as sandstone blocks.

Figure 8-5. Geologically inferred braided stream channel reconstruction that deposited the Lower Augitic Sandstone in Lower Bed II. Flow direction is northwest. LAS Samples 01-10 were sampled within this section, while 11-15 were collected in Long Korongo and the Side Gorge in separate sandstone units (Fig. 8-2C). HWK sites and the FLK-W site belong to the same fluvial system but archaeologically, HWK is Oldowan while FLK-W is Acheulean. Stream interpretation from Uribe Larrea et al., 2017.

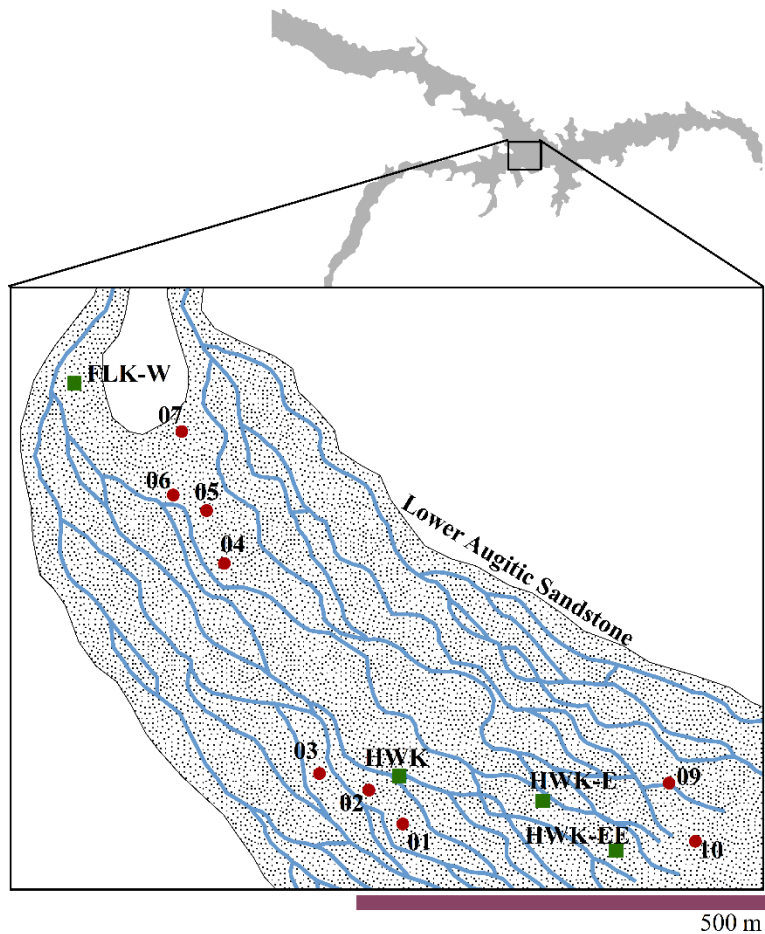


Table 8-5. Lower Augitic Sandstone samples, name of Olduvai geolocality, amount (g) used in Soxhlet extraction, and coordinates in decimal degrees.

Sample	Geolocality	Amount (g)	Latitude	Longitude
01	Lava Tongue Korongo	44.0	-2.9948	35.3520
02	Lava Tongue Korongo	31.7	-2.9944	35.3516
03	Playground	43.9	-2.9942	35.3511
04	Leakey's Road	31.4	-2.9919	35.3501
05	Maiko Gully	46.8	-2.9913	35.3499
06	Maiko Gully	40.0	-2.9912	35.3495
07	Maiko Gully	49.6	-2.9905	35.3496
08	FLK-NW	41.4	-2.9884	35.3471
09	HWK-E	36.5	-2.9943	35.3550
10	HWK-EE	40.6	-2.9950	35.3552
11a	Long Korongo	41.8	-2.9943	35.3653
11b	Long Korongo	43.7	-2.9943	35.3653
12	Long Korongo	44.0	-2.9966	35.3639
13	Long Korongo	39.4	-2.9952	35.3619
14	Side Gorge	50.4	-2.9937	35.3404
15	Side Gorge	44.5	-2.9937	35.3404

8.1.5 BPT

The Bird Print Tuff is a 2.5 to 12 cm thick yellow laminated, fine- to medium-grained tuff exposed in outcrops between FLK-NN and HWK that is also found west of the Fifth Fault in the Western Gorge at Richard Hay Cliff and at MNK in the Side Gorge (Hay, 1976; McHenry et al., 2016). This pyroclastic tuff is characterized by fragmented bits of glass and is always situated above the LAS; it appears 25 cm above Tuff FLK-Wb, 40 cm above the LAS unit in “Maiko Gully” southeast of FLK-W, and 3.0 m above the LAS throughout the HWK area (Uribelarrea et al., 2017). The BPT is named for the presumably abundant trace fossils of shore bird footprints preserved in the tuff (Hay, 1976); this feature, along with its mineral composition, makes it one of the most easily identifiable marker tuffs in the gorge.

Samples (n=11) were collected in the waxy, silty clays that underlie the BPT; 10 of the samples came from a 780-meter, NW-SE transect in the main confluence of the gorge (Fig. 8-2B; Table 8.6), with the eleventh taken from the clays above Tuff FLK-Wb at FLK-W. On average, samples were collected in a 3.5 cm high, by 12 cm wide, and 6.45 cm deep arrangement (max: 5x21x11; min: 2x7x3 (HxWxD)) and came from clays directly in contact with the BPT, or slightly below. The clays below the Bird Print Tuff were likely deposited within the lake-margin zone that connected the alluvial fans and streams draining the Crater Highlands from the southeast with paleo-Lake Olduvai.

Table 8-6. Bird Print Tuff samples, sampling code, name of Olduvai geolocality, amount (g) used in Sohlet extraction, and coordinates in decimal degrees.

Sample	Code	Geolocality	Amount (g)	Latitude	Longitude
FLK-W 28	BPT1	FLK-W	51.5	-2.9900	35.3484
01	BPT2	Maiko Gully	46.7	-2.9906	35.3493
02	BPT3	Maiko Gully	45.3	-2.9903	35.3492
03	BPT4	Maiko Gully	47.6	-2.9911	35.3495
04	BPT5	Maiko Gully	53.4	-2.9911	35.3500
05	BPT6	Maiko Gully	43.4	-2.9916	35.3497
06	BPT7	Leakey's Road	40.0	-2.9920	35.3499
07	BPT8	OGAP Mine	46.0	-2.9920	35.3513
08	BPT9	Lava Tongue Korongo	56.1	-2.9942	35.3521
09	BPT10	Castle	51.8	-2.9948	35.3530
10	BPT11	HWK	47.8	-2.9951	35.3533

8.1.6 Castle Clays

Perhaps the most prominent and recognizable feature in the gorge, Olduvai's Castle is also one of its most understudied geolocality, likely due to its lack of archaeological contents. Only separated from HWK by a ~50 m gully, the Castle is a striking promontory on the southern edge of the gorge (Fig. 8-2B, C) that resisted erosive forces and exposes Beds I through III (Fig. 8-6). All of Bed II is visible as well as the characteristic red sediments belonging to Bed III, and Tuffs IF, IIA, IIB, BPT, and IID, in addition to the Lower and Middle Augitic Sandstones have all been identified (McHenry and Stanistreet, 2018; Uribe-larrea et al., 2017). Tuff IIA is positioned about 1-2 meters above Tuff IF, while the LAS and the BPT are ~3.5-4.0 m and ~8.0 m above IIA, respectively (Tuff IIB is between the LAS and BPT). Tuffaceous silt, silty clay/claystones, and sands are sandwiched between the marker tuffs (Fig. 8-6). The clays situated above Tuff IIA (1.74 ± 0.03 Ma) and below the LAS represent the paleoenvironment that followed the FLK-N sequence and preceded the FLK-W sequence in the lower portion of Bed II, while the LAS is contemporary with levels 5 and 6 of FLK-W.

Samples (n=14) were collected from two *packages* separated by a ~10 cm carbonate horizon in the tuffaceous clays above Tuff IIA; four samples came from above the carbonate horizon, nine from below the horizon, and one sample from underneath Tuff IIA (Fig. 8-6; Table 8.7). (Tuff IIA is about 30 cm thick at the Castle, and sample 14 was collected 2.0 cm below Tuff IIA, or roughly 32 cm below the top of Tuff IIA.) Sample dimensions were irregular with an average width of 7.9 cm (max: 12; min: 4) and height of 4.8 cm (max: 9; min: 2).

Table 8-7. Castle Clays, height above Tuff IIA, amount used in Soxhlet extraction, and tuffaceous clay package sampled.

Sample	Depth (cm) below LAS	Amount (g)	Package	
14	0-5	38.3	Upper	Carbonate Horizon
13	10-13	40.7		
12	17-21	40.1		
11	25-28	39.6		
10	40-46	42.5	Lower	Tuff IIA
09	55-61	44.4		
08	75-79	30.4		
07	93-96	37.4		
06	104-110	40.0		
05	124-133	40.0		
04	147-149	41.1		
03	163-167	22.1		
02	181-186	32.4		
01	226-235	34.0	Below IIA	

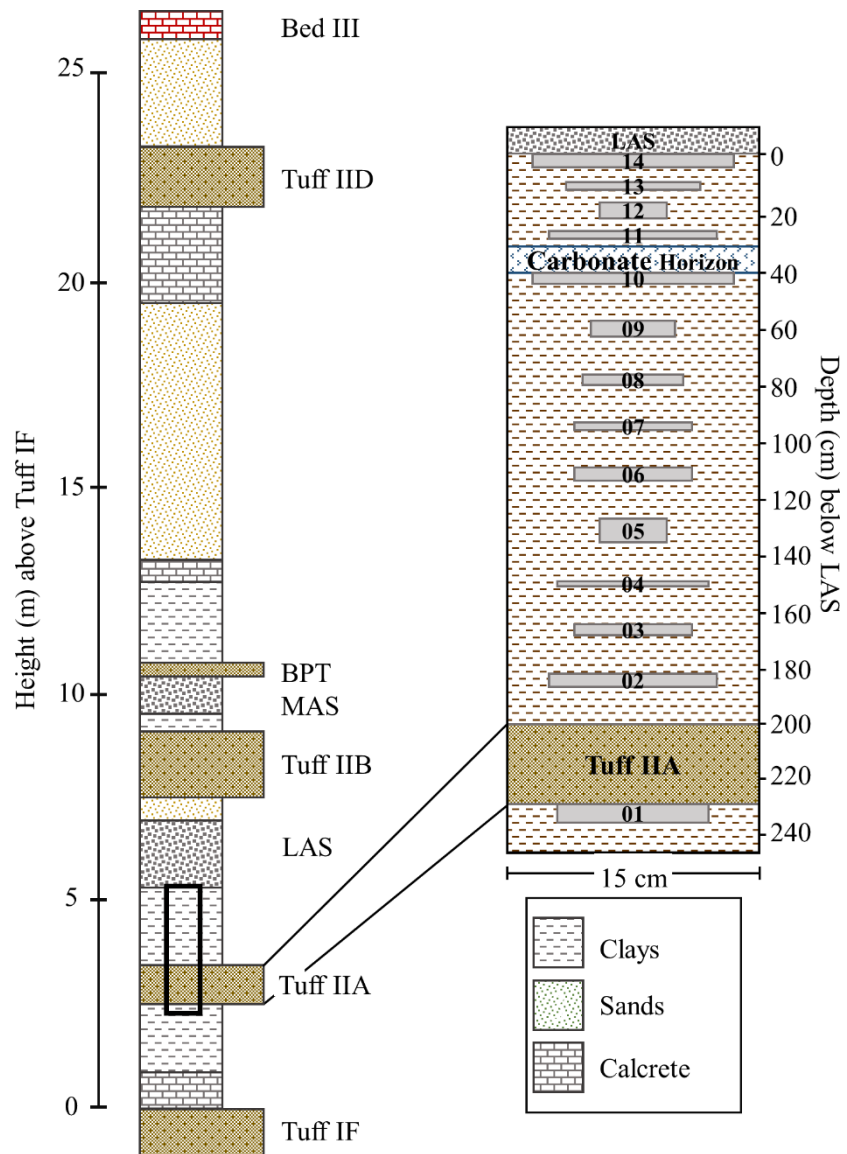


Figure 8-6. General stratigraphic section of Olduvai's Castle (left) showing the exposed geologic features of Bed II sandwiched between Beds I and III. Sampling strategy of the Castle Clays (right) from below Tuff IIA to the LAS (Adapted from McHenry and Stanistreet, 2018; Uribealarea et al., 2017).

8.2 Sample Preparation and Total Lipid Extraction

8.2.1 Sample Preparation

To prepare for isotope analysis, all samples were lyophilized using benchtop Freeze Dry apparatus in either the Geomicrobiology Group (Energy Environment Experiential Learning building) or Bone Chemistry Preparation (Earth Sciences (759) building) laboratories for 24 to 48 hours at -50°C and 0.016 mbar. Clay or consolidated sandstone samples were crushed with oven-cleaned mortar and pestles, while unconsolidated sediments were homogenized with either mortar and pestles or a vortex. Prior to lipid extraction, the mass of each sample was recorded directly in individual Soxhlet extraction thimbles before being placed into the Soxhlet apparatus. The clays in contact below Tuff IF samples however were weighed in 40 mL glass vials, as these were ultrasonically (as opposed to Soxhlet) extracted. Sample amounts ranged from 16.8 to 56.7 grams for Soxhlet samples, and 10.0 to 11.6 grams for ultrasonic samples (Table 8-8).

8.2.2 Soxhlet Extraction

Soxhlet (Fig. 8-7) is an extraction technique based on the *like-dissolves-like* principle of solvent separation, whereby solvents readily dissolve analytes of approximately the

Table 8-8. Summary of sample amounts used in lipid extraction. Minimum, maximum, and average weight in grams given for each project. See previous tables for individual sample amounts.

Project	Maximum (g)	Minimum (g)	Average (g)
FLK-N T7	42.0	39.4	40.8
FLK-N Landscape	11.6	10.0	10.5
FLK-W	56.7	16.8	41.9
LAS	50.4	31.4	41.8
BPT	56.1	40.0	48.1
Castle Clays	44.4	22.1	37.4

same polarity. Typically, an azeotrope mixture of solvent is refluxed through a crushed rock or unconsolidated sediment sample to isolate biologically-derived compounds. Soxhlet however,

suffers from several drawbacks including a time-consuming extraction period (up to 72 hours), expends a large volume of solvent (200-300 mL per sample), and requires a constant flow of water to act as a condensing medium (if interrupted, the solvent typically evaporates). On the other hand, this technique is one of the most efficient and reliable for isolating lipid marker molecules. During the extraction, organic solvent is evaporated and travels up the side arm into an Allihn condenser (Fig. 8-7). Here, cool temperatures condense the vapor back into liquid solvent, which then drips into the extraction chamber. The condensed solvent fills the extraction chamber, bonds to lipids, and siphons the extracted organics into the boiling-flask. The evaporation-condensation process is repeated, while the Total Lipid Extract (TLE) accumulates in the flask.

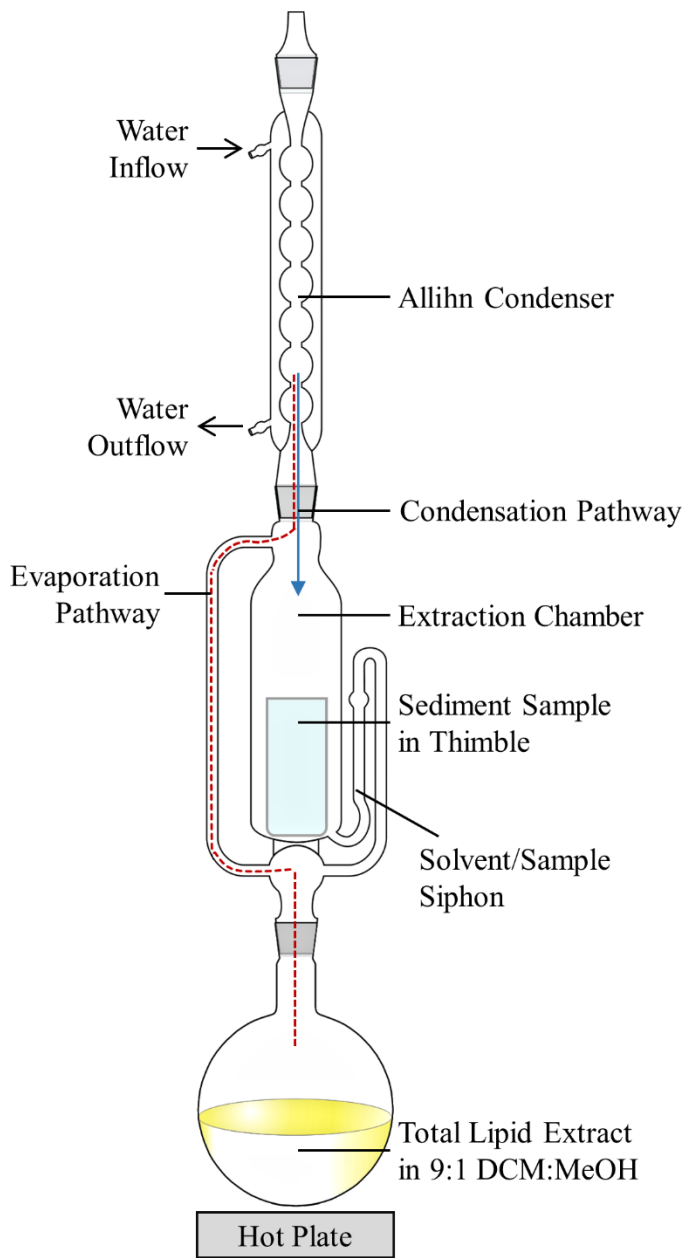


Figure 8-7. Schematic of the complete Soxhlet apparatus: boiling flask, extraction chamber, and Allihn condenser. Solvent vapor moves along the Evaporation Pathway until it reaches the Allihn Condenser, where it condenses back into liquid and drips into the extraction chamber. When the solvent reaches the top of the siphon, it empties into the flask bringing with it the Total Lipid Extract removed from the sediment sample.

Soxhlet extraction chambers (Kimble™ KIMAX™) and flat-bottom boiling flasks (VWR® Short-neck 250 mL Flasks) were oven-cleaned for 8-12 hours at 400°C in the Tropical

Archaeology Lab. Extraction thimbles (GE Whatman High Performance Cellulose Extraction Thimble, double thickness (2 mm wall), 33×94 mm) were solvent-cleaned using a 2:1 mixture of Dichloromethane (DCM; 39.7°C boiling point) and Methanol (MeOH; 64.7°C boiling point) (EMD Millipore OmniSolv® grade solvents) for 24 hours with the Soxhlet. (Flasks used to collect cleaning solvent were then hand washed with Alconox® powdered detergent and oven-cleaned again.) Pre-cleaned extraction thimbles were then filled with ~40 g of sediment (Tables 8-1–8-2, 8-4–8-8) and placed in the extraction chamber. 200 mL of 9:1 DCM:MeOH, boiling chips (EMD Millipore ~1-2 mm), and copper granules (Millipore Sigma ACS reagent 10-40 mesh, ≥99.90%) were added to the 250 mL flat-bottom flasks. About 50-100 mL of the DCM:MeOH solution was poured from the flask into the extraction chamber containing the thimbles with sample; flasks were then connected to extraction chambers, which were subsequently connected to Allihn Condensers (Kimble™ KIMAX™). Extractors were placed on a hot plate set to 40°C and the condensers were connected to a water chiller to promote condensation. The solvent (with aid of the boiling chips) was brought to vaporization but not a rolling boil and left for 72 hours. After the 72-hour period, lipid-containing-solvent was evaporated to ~4.0 mL by disconnecting the water flow, and then pipette-transferred to oven-cleaned and labeled 4.0 mL vials (Thermo Scientific™ National™ 15x45mm screw thread glass vials fitted with National™ PTFE-lined storage caps). These vials contained the Total Lipid Extracts (TLEs).

8.2.3 Ultrasonic Extraction

Due to the total number of samples (n=30), the clays in contact below Tuff IF were ultrasonically extracted in DCM and MeOH at 40°C for four, 15-minute cycles. Ultrasonic extraction has the benefit of being able to process many samples in a short amount of time (~2

hours) and uses lower solvent volumes (40-80 mL per sample). However, ultrasonic extraction is most efficient with small sample amounts (10 g or less) and therefore does not yield as high a concentration of lipids as Soxhlet. The two extraction techniques were compared and will be discussed in Section 8.4 Technique Development.

For each sample, roughly 10 g of sediment was measured directly in 40 mL glass vials (Fisherbrand® 28 x 108 mm, 11 Dram screw thread vial) fitted with a polypropylene cap (Supelco® screw cap with 24 mm hole for septa). Solvent was added to the vials and then vortexed for 20 seconds. Samples were extracted in groups of 12 at 40°C in four, 15-minute ultrasonic cycles of different solvent concentrations: Cycle 1) 20 mL MeOH; Cycle 2) 20 mL 2:1 MeOH:DCM; Cycle 3) 20 mL 2:1 DCM:MeOH; Cycle 4) 20 mL DCM. Between each cycle, vials were centrifuged for five minutes at 4,000 RPM and then the lipid extracts were filtered through five-inch, oven-cleaned glass pipettes (VWR® Pasteur Pipet, Disposable Borosilicate Glass, 5 ¾”) plugged with glass wool. Two new, oven-cleaned and labeled 40 mL vials were used for each sample as the total volume of solvent used during extraction exceeded 40 mL. Samples were rotary evaporated, each sample set was then consolidated into a single vial, and rotary evaporated again to dryness. These vials contained the TLEs.

BOX VIII-I: COLUMN CHROMATOGRAPHY NOMENCLATURE

- **Mobile Phase:** The liquid solvent that moves through the column
- **Stationary Phase:** Adsorbent solid substance (e.g. Silica Gel) that stays fixed inside the column
- **Eluent:** The solvent used to pass compounds through the column (e.g. Hexane)
- **Eluate:** The organic compounds extracted through the column and accumulates in collection vials
- **Elution:** The process of extracting a compound through the column
- **Analyte:** The mixture of individual components to be separated and analyzed by GC-MS.

8.3 Leaf Wax Lipid Compound Separation

Column chromatography is an analytical technique used to separate organic compounds into individual components, so that these components can be analyzed with gas chromatography and mass spectrometry. Like Soxhlet and ultrasonic extraction, column separations are based on the principle of *like-dissolves-like*, whereby solvents readily elute analytes of approximately the same polarity. Generally, the targeted analyte is dissolved in various organic solvents and loaded onto the column, and due to solvent polarity, the different compounds of the analyte either adhere to, or elute through the column. Three different stationary phase separation techniques were employed; 1) Silica Gel Column Chromatography (SGCC); 2) Silver nitrate infused silica gel (SiAgNO_3); and 3) Aminopropyl columns (ApCC). Justification for these techniques and why they were used is given in Section

8.4 Technique Development.

8.3.1 Silica Gel Column Chromatography

Silica Gel Column Chromatography (SGCC) separates organic compounds according to polarity; silica is a polar adsorbent so non-polar compounds (e.g. *n*-alkanes) elute before more polar ones (e.g. *n*-alkanoic acids). Columns (Fig. 8-8) are constructed by first creating a glass wool filter near the base of a 5-inch pipette (the “column”), slowly adding 1.0 g activated¹² silica gel

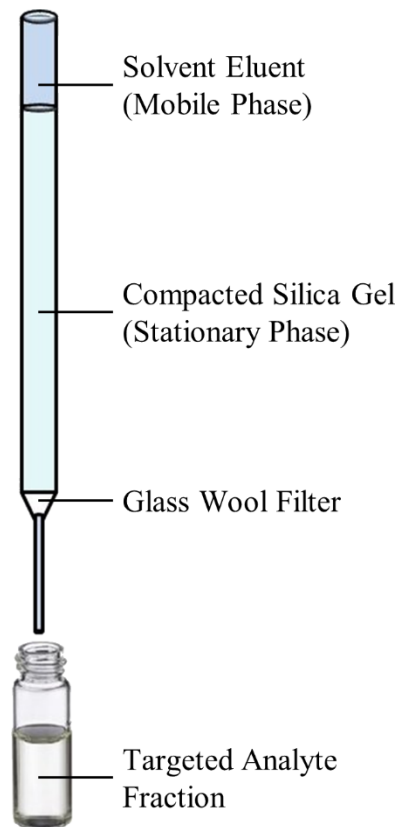


Figure 8-8. Schematic of a silica gel column for chromatography. Lipids are eluted through the stationary silica gel with mobile solvents of increasing polarity.

¹² Overnight at 110°C then stored at 65°C until use.

(pre-weighed, high-purity grade (Davisil Grade 923), pore size 30 Å, 100-200 mesh (Sigma-Aldrich)), and then compacting the silica using a Dremel® tool to remove spaces in the matrix, thus preventing the formation of air pockets when adding solvent. Before analyte separation, columns are rinsed with ~3.0 mL Hexane (EMD Millipore OmniSolv® grade solvent), which is collected in a “waste” vial.

The TLEs are separated into individual compound classes using solvents of increasing polarity; the non-polar aliphatic hydrocarbon fraction containing the *n*-alkanes is eluted with Hexane (Polarity Index 0.1), the ester, ketone, and alcohol fraction is eluted with DCM (Polarity Index 3.1), and the polar fraction is eluted with MeOH (Polarity Index 5.1). Silica acts as the stationary phase, while the solvents, acting as the mobile phase, elute through the column under gravity. In the Hexane fraction, the compounds adhering to the silica (esters, ketones, alcohols, polar compounds) travel more slowly compared to the non-polar aliphatic hydrocarbons but are subsequently removed with DCM and MeOH. As the *n*-alkanes are non-polar in nature, they readily elute with the non-polar mobile phase (Hexane) without adhering to silica. Once removed, the mobile phase is changed to the more-polar DCM, forcing the esters, ketones, and alcohols to detach from the silica. Finally, the mobile phase is changed again, this time to MeOH, to elute any remaining polar components.

For each sample, three 4.0 mL vials were labeled with the sample name (e.g. FLK-W 01), date, and solvent fraction (Hex, DCM, or MeOH). One milliliter of Hexane was added to the TLE vial with an oven-cleaned 5-inch pipette, and then using a separate pipette (separate for each sample), the Hexane was used to “wash” the inside of the TLE vial three times; the 1.0 mL Hexane, now containing the non-polar compounds, was then added to the top of the column. As this first milliliter eluted through the column under gravity, an additional 1.0 mL of Hexane was added to

the TLE vial, washed six times, and then added to the top of the column again. A third 1.0 mL was added to the TLE vial, thoroughly washed 10 times, and again added to the top of the column. Finally, 1.0 mL of straight Hexane was added to the top of the column and allowed to elute through to remove any remaining non-polar compounds. The four total milliliters of Hexane were collected in the “Hex”-labeled 4.0 mL vial. While the straight Hexane was eluting through the column, 1.0 mL of DCM was used to wash the TLE vial, and after the Hexane reached the top of the silica, the new DCM fraction containing the esters, ketones, and alcohols was added to the column. The “DCM”-labeled 4.0 mL vial was switched in once the DCM fraction traveled through the silica gel. The same procedure ensued using DCM (1.0 mL x 3 washes, 1.0 mL x 6 washes, 1.0 mL x 10 washes, and straight DCM). While the straight DCM was eluting through the column, 1.0 mL of MeOH was added to the TLE vial, and after the DCM reached the top of the silica, the final “MeOH”-labeled 4.0 mL vial was switched in, and the new MeOH fraction containing the polar compounds was added to the column with the (1 x 3 x 10) wash process repeating. All fractions were evaporated with a steady stream of N₂.

8.3.2 Silver Nitrate Column Chromatography

Silver Nitrate Column Chromatography follows the same principles as SGCC, except that its use is based on the ability of silver ions (Ag⁺) to interact with unsaturated compounds (e.g. alkenes) (McWilliams and Angelici, 2016; Nikolova-Damyanova, 2009). Silver ions form weak reversible electron-donor-acceptor complexes with multiple-bonded compounds to separate lipids based on their degree of unsaturation and resolve complex lipid mixtures into simpler molecular species (Nikolova-Damyanova, 2009). Therefore, Silver Nitrate Column Chromatography is better suited for isolating saturated *n*-alkanes and *n*-alkanoic acids from unsaturated compounds than

standard SGCC because it helps to resolve chromatographic issues arising from compound (bio)degradation.

Silver Nitrate (AgNO_3) columns were prepared by infusing activated silica gel with silver nitrate solution (0.1N (N/10)/Certified, Fisher Chemical). Five or 10 grams of silica gel were added to an aluminum foil wrapped beaker, then submerged under 29.5 or 59 mL of 0.1N AgNO_3 solution, respectively. The beaker was loosely covered with aluminum foil and left to dry in an oven set to 75°C for at least two days. Because of AgNO_3 's sensitivity to light (the Ag^+ ion decomposes into elemental silver), the dried silver nitrate-infused silica gel (SiAgNO_3 ; 10%) remained covered in aluminum foil in a drying oven (65°C) until use. Columns (Fig. 8-9) were constructed by placing a glass wool filter near the base of a 5-inch pipette, followed by adding 0.5 g SiAgNO_3 , 0.5 g activated silica gel, and then by compacting the two stationary phases with a Dremel® tool to remove spaces in the matrix. Before analyte separation, columns were rinsed with ~ 3.0 mL Hexane, which were collected in a “waste” vial.

Like SGCC, TLEs are separated into individual compound classes over the SiAgNO_3 using solvents of increasing polarity; Hexane, DCM, and MeOH. The same method was used of 4.0 mL total solvent in 1.0 mL increments of 3 x 6 x 10 washes followed by straight solvent. The 0.5 g SiAgNO_3 with 0.5 g silica gel technique was adopted after experimenting with different amounts of SiAgNO_3 (see 8.4 Technique Development) and learning that this set up was best suited for

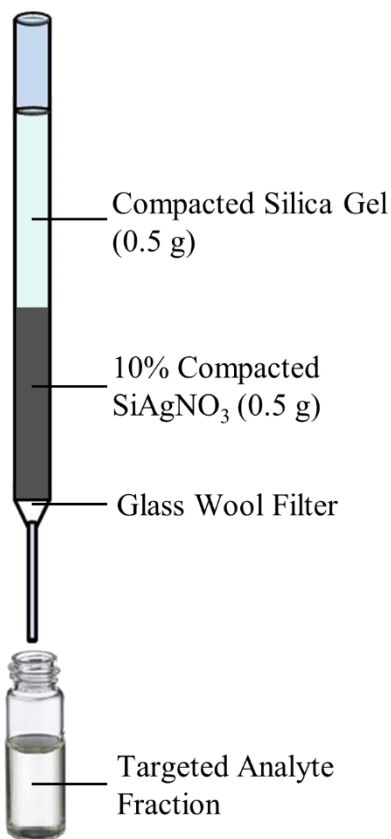


Figure 8-9. Schematic of a silver nitrate-infused silica gel column for chromatography. The 10% SiAgNO_3 binds to unsaturated hydrocarbons, trapping them in the matrix. (Colors are for visualization only, SiAgNO_3 is white, just like silica gel.)

separating saturated and unsaturated compounds while also preventing analyte loss through repeated column extractions; that is, a silica gel column first, followed by a SiAgNO₃ column.

8.3.3 Aminopropyl Column Chromatography

Aminopropyl (NH₂(CH₂)₃) column chromatography is another silica-based stationary phase extraction technique where the silica gel is functionalized with amino groups. This is a normal-phase ion exchange chromatographic type that uses stationary phase columns (Agilent Bond Elut NH₂ cartridge, 500 mg, 6 mL, 40 μm) (Fig. 8-10) to retain polar analytes, and non-polar mobile-phase solvents to separate neutral lipids from fatty acids and phospholipids. Like SGCC and SiAgNO₃, the retention ability of Aminopropyl columns decreases as the eluting solvent becomes more polar. Neutral lipids, or those soluble only in solvents of very low polarity such as hydrocarbons, are eluted through with 2:1 DCM:Isopropanol (VWR® ≥99.5% ACS grade), fatty acids, such as those found in waxes, with 4% Glacial Acetic Acid (Thermo Scientific, HPLC Grade) in Diethyl Ether (ACROS Organics™, HPLC Grade, Stabilized), and phospholipids with MeOH. The ability of Aminopropyl columns to retain acids when total extracts are eluted with DCM:Isopropanol and then release the acids when eluted with acetic acid in ether make it the ideal technique for quickly separating carboxylic acids from the neutral lipid fractions (Huang et al., 1999; Yang and Huang, 2003) before further separation into individual *n*-alkanes and *n*-alkanoic acids.

The elution protocol followed the same format as SGCC and SiAgNO₃, except that it uses different solvents. Moreover, though this technique is presented as the third separation technique, it ended up being the first employed on TLEs, followed by SiAgNO₃ (See Section 8.4.5). For each sample, three 4.0 mL vials were labeled with the sample name (e.g. FLK-W 01), date, and solvent

fraction (Neutral, Acids, or Polar). One milliliter of 2:1 DCM:Isopropanol was added to the TLE vial with an oven-cleaned 5-inch pipette, and then using a separate pipette, the DCM:Isopropanol was used to “wash” the inside of the TLE vial three times; the 1.0 mL DCM:Isopropanol now containing the neutral compounds was added to the top of the Aminopropyl column. An additional 1.0 mL of DCM:Isopropanol was added to the TLE vial, this time washed six times, and then added to the column again. A third 1.0 mL was then added, the TLE vial was thoroughly washed 10 times, and again pipetted to the column. Because of the 6.0 mL volume of the Bond Elut column, each wash cycle could be added once prepared; this differs from the

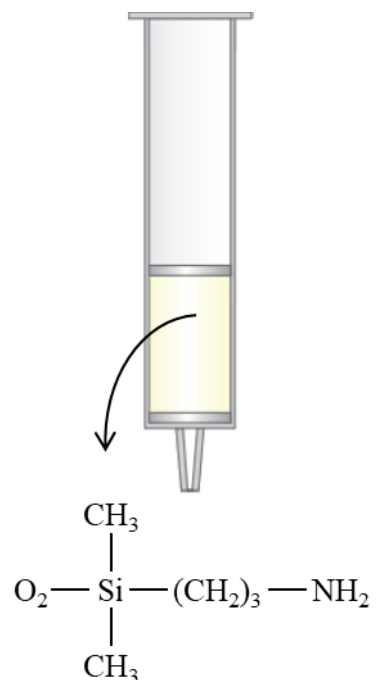


Figure 8-10. Schematic of a 6.0 mL Agilent Bond Elut NH2 column showcasing the structural formula of the Aminopropyl-silica.

pipette columns in that they only had about 1.5 mL of excess space above the silica gel. After the lipid-containing-solvent eluted through the silica, 1.0 mL of straight DCM:Isopropanol was allowed to elute any remaining neutral compounds. The four total milliliters of DCM:Isopropanol were collected in the “Neutral”-labeled 4.0 mL vial. While the straight DCM:Isopropanol was eluting through the column, 1.0 mL of 4% Acetic Acid in Diethyl Ether (96:4 v:v) (AADE) was used to wash the TLE vial three times. After the DCM:Isopropanol reached the top of the NH2-silica, the new AADE fraction containing the fatty acids was added, and the “Acids”-labeled 4.0 mL vial was switched in. The 1.0 mL x 3 washes, 1.0 mL x 6 washes, 1.0 mL x 10 washes, and straight solvent procedure was followed again, only this time with the Acetic Acid in Diethyl Ether, and then finally with MeOH (and “Polar”-labeled vial). All fractions were then evaporated with a

steady stream of N₂ before being separated further into *n*-alkanes and alkanols (Neutral fraction) or methylated (Acids fraction) with 2.0% HCl in Methanol (94.5:5.5mL v:v, MeOH:37% HCl).

8.4 Technique Development

8.4.1 Lipid Extractions

An Accelerated Solvent Extractor (ASE) is an automated system for extracting organic compounds from a variety of solid and semisolid samples. ASE uses a combination of elevated temperature and pressure with common solvents to increase the efficiency of the extraction process. During a run, an extraction vessel containing the sample is filled with solvent and heated and pressurized to maintain the solvent in a liquid state at temperatures >100°C. The TLE is then collected in a vial, and the process is repeated 3-5 times. This technique has the advantage of being able to extract a sample in less than 30 minutes, holds up to 24 extraction vessels for automatic processing, and significantly reduces total solvent volume (for example, a 10 g sample can be extracted in less than 15 minutes, using less than 15 mL of solvent). Unfortunately, an ASE system is expensive, both in the initial purchase and in its maintenance, and suffers from an inability to thoroughly clean contamination as it is made up of many moving parts and inner tubing for the flow of gasses and liquids. There is one ASE (Thermo Scientific™ Dionex™ ASE® 200) at the University of Calgary managed by the Petroleum Reservoir Group; however, this machine had not been used in about ten years and remained dormant until January 2016.

The FLK-W set of samples was the first project to be processed in 2016. Because of background training in ASE operation, this extraction technique was initially employed on a subset of the FLK-W sediments after the machine was made functional again. Although at first the ASE performed and “extracted” lipids from the sediments in collection vessels, after about three or four

automated extractions, issues arose with the AutoSeal Arm that pumps solvent into the extraction vessel; the vessel would fill with solvent (9:1 DCM:MeOH) but began to leak from the AutoSeal arm onto the collection vessel, activating a hydrocarbon alarm. This was likely an issue with the AutoSeal arm not properly fitting into the O-rings in the vessel cap as it occurred on multiple caps fitted with entirely new O-rings. Furthermore, this problem was inconsistent in that the seals would not always leak, but because of the sporadic interruptions, the ASE had to be monitored and therefore was not truly “automated”. Nevertheless, a few samples were run on the ASE, silica gel extracted, and tested on GC-MS.

The second issue encountered involved the contamination of the samples with low-molecular weight (<C₂₀) compounds, at first assumed to be contaminants from the last time the machine was operational. Contamination is not typically an issue with ASE as there are thorough solvent rinses before and after sample extraction that are designed to clean the system of any lingering organic residue. However, due to the dormancy of the machine and previously processed samples being of unknown origin (but likely petroleum-rich sediments), contamination issues persisted. These residues may have adhered to the inner tubing of the ASE, and after sitting for a decade, were not easily removed during rinse cycles; these contaminants may also have slowly released during actual sample runs. Contamination was first recognized in blanks that were processed alongside the FLK-W samples, and although the target compounds for study were >C₂₃, the presence of contaminants precluded any reliable GC-MS and GC-IRMS analyses. To pinpoint the cause of the contamination, different blanks were analyzed to test whether contamination stemmed from certain stages of the extraction process:

- 1) Hexane blank eluted through an oven-cleaned silica gel column with an ASE extracted glass wool filter to test whether the ASE contaminated the glass wool. Evaporated with N₂ gas and transferred to a GC-MS 2.0 mL vial.
- 2) Hexane blank eluted through a silica gel column with a 500°C oven-cleaned glass wool filter to test whether the silica gel was contaminated (regardless of ASE). Evaporated with N₂ gas and transferred to a GC-MS 2.0 mL vial.
- 3) A modern plant sample ASE extracted and eluted through a silica gel column with oven-cleaned glass wool and silica gel. Evaporated with N₂ gas and transferred to a GC-MS 2.0 mL vial.
- 4) A modern plant sample manually extracted and eluted through a silica gel column with oven-cleaned glass wool and silica gel. Evaporated with N₂ gas and transferred to a GC-MS 2.0 mL vial.
- 5) Pure Hexane in a 4.0 mL vial that was evaporated with N₂ and transferred to a GC-MS 2.0 mL vial.

All samples came back positive for contamination (Fig. 8-11), showing that the ASE was not the only instrument contaminated, as the manually extracted plant and pure Hexane blank tested positive, and that something other than the ASE, glass wool, or silica gel was responsible. The only other apparatus used with every sample was the nitrogen evaporator, which was originally ruled out due to nitrogen being an inert gas. Each blank was completely evaporated with a steady stream of N₂ then reconstituted in 200 µL of Hexane and transferred to 2.0 mL GC-MS vials (Agilent screw top, clear, write-on spot, certified vial, 12 x 32 mm) fitted with 200 µL glass inserts (Agilent glass, flat bottom insert, 4.8 x 31 mm) and analyzed with GC-MS. To confirm the nitrogen

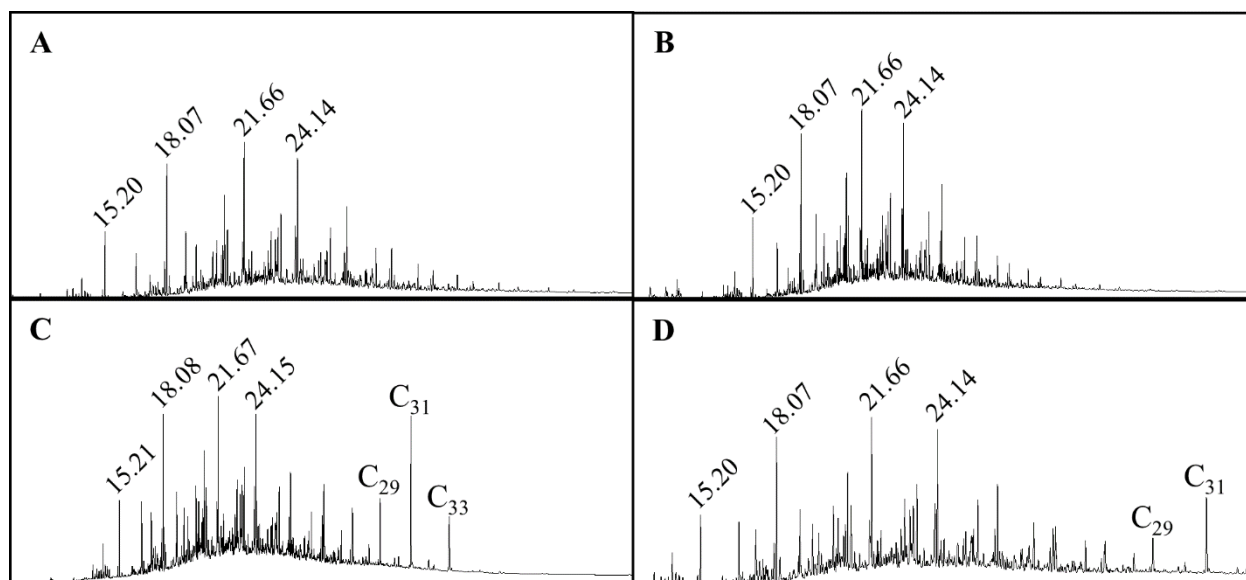


Figure 8-11. GC-MS chromatograms for the contamination isolation tests. A) Hexane blank SGCC with ASE-cleaned glass wool; B) Hexane blank SGCC with oven-cleaned glass wool; C) Modern plant ASE extracted and SGCC with oven-cleaned glass wool; D) Modern plant manually extracted and SGCC with oven-cleaned glass wool. Both modern plant samples (C, D) have *n*-alkanes (C₂₉-C₃₃) that do not appear in the *blanks* (A, B). Major contaminants on all samples labeled with their GC retention times.

evaporator was contaminated, additional blank Hexane samples were evaporated with a second evaporator and tested on the GC-MS again. No contaminants were detected in this subset.

As some of the FLK-W samples were ASE extracted and evaporated with the contaminated N₂ apparatus, they were abandoned for further analyses; fortunately, extra sample had been collected in the field in 2015, allowing for the reanalysis of this project. Although the ASE itself may not have been contaminated, the inconsistency with the AutoSeal arm determined that the instrument would not be suitable for thorough lipid extractions, and Soxhlet was implemented as the glassware can be oven cleaned and was the technique consistently utilized by the Petroleum Reservoir Group. In addition, a new nitrogen evaporator (Supelco Mini-Vap L × W 7 1/2 in. (19 cm) × 1 1/2 in. (4 cm)) was purchased and has since been contaminant free. Soxhlet was used for all other projects except for the clays below Tuff IF.

8.4.2 Soxhlet vs. Ultrasonic Extraction

To determine that there were no substantial differences between samples extracted with Soxhlet and those with ultrasonics, three samples from the Castle Clays (1-3) and all the BPT samples were both Soxhlet and ultrasonic extracted. The Castle Clays and ultrasonic BPT samples were subsequently separated by Aminopropyl and SiAgNO₃ column chromatography, while the Soxhlet BPT was first eluted over a silica gel column, then the MeOH fraction was separated on an Aminopropyl column, and finally on SiAgNO₃ column chromatography. The reasoning for this sequence is explained in the following sections.

Other than the total concentration of analytes, each sample, regardless of extraction technique, displayed the same lipid compounds (Fig. 8-12). This is significant in that it showed both extraction methods could be used for isolating target *n*-alkyl lipids, especially for the spectrographic identification and quantification of these biomarkers to differentiate *n*-alkane and fatty acid homologues and their sources of production (e.g. aquatic vs. terrestrial plants). However, because manual extraction recovers a lower total concentration of lipids compared to Soxhlet, sediment samples with initial low total organic carbon may be problematic for carbon ($\delta^{13}\text{C}$) and hydrogen (δD) isotope analysis as the isotope ratio mass spectrometer (IRMS) is not as sensitive as a gas chromatograph mass spectrometer (GC-MS). That is, analytes identified on the GC-MS may not have the same quantifiable abundance on the IRMS. Nevertheless, the two extraction techniques are comparable, and the clays below Tuff IF samples, which were manually extracted, were successful in both carbon and hydrogen isotope analysis.

Manual extraction has the benefit of being conducted in one day, so this method is ideal for the preliminary analysis of samples to check the overall preservation of *n*-alkyl lipids before running the more time consuming Soxhlet. Additionally, because this technique only uses ~10 g

of sample, there is typically surplus material for further analyses or to rerun samples if any issue occurs during the extraction and purification processes. Soxhlet's benefit lies in its ability to thoroughly extract total lipids from sediment samples ranging from 10-50 g, therefore resulting in more abundant lipid concentrations. Furthermore, when samples are Soxhlet extracted and made GC amenable with column chromatography, they have the added advantage of multiple GC-MS or IRMS injections; that is, the total concentration on analytes allows for multiple MS analyses without worrying about using the entire sample for examining only carbon or hydrogen.

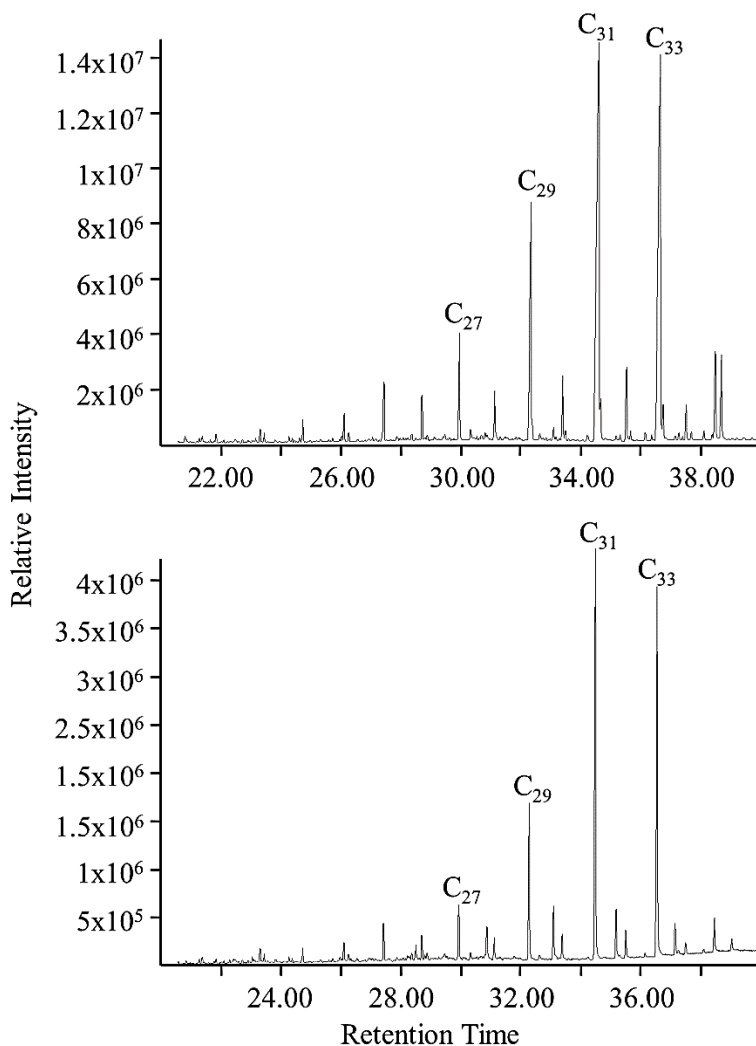


Figure 8-12. Chromatograms of the same sample (Castle Clays 01) extracted using ultrasonics (top) and Soxhlet (bottom) showing the same compound distribution only with differences in relative intensity. Other than the total amount of lipids recovered, both extraction techniques were satisfactory in isolating lipids from sediment samples.

8.4.3 Silica Gel

Silica Gel Column Chromatography is the traditional method for separating total lipid extracts into GC amenable products. It is the standard, proven technique for extracting *n*-alkanes from living plants as well as archaeological and geological sediments ranging in age from the Holocene to the late Palaeocene (Magill et al., 2013b; Marlow et al., 2000; Pagani et al., 2006; Patalano et al., 2015; Uno et al., 2016; Yang and Huang, 2003; Yang and Leng, 2009). Furthermore, because most lipid hydrogen atoms are covalently bound to carbon atoms and not readily exchanged at temperatures below 100°C (Sessions et al., 2004), isotope fractionation does not occur when eluting *n*-alkanes or *n*-acids of silica gel columns. Due to familiarity and former training with this technique, it was initially employed to isolate the *n*-alkanes from the total lipid extracts. The FLK-W samples were the first to be processed with SGCC and analyzed with GC-MS. TLEs were eluted through the silica gel column with 4.0 mL of Hexane to separate the *n*-alkanes, followed by 4.0 mL each of DCM and MeOH. Each fraction was N₂ evaporated and stored at 4°C. The *n*-alkane fraction was then reconstituted in ~200 µL Hexane, transferred to a 2.0 mL GC vial with 200 µL insert, evaporated to dryness again, and then immersed in exactly 200 µL of Hexane. Finally, 2.0 µL of the *n*-alkane-containing Hexane was injected into the GC-MS (Agilent 7890B GC coupled with 5977A MSD; PRG lab) for quantification and identification.

Rather than easily identifiable and clearly defined *n*-alkanes, nearly all the 28 samples examined on the GC-MS displayed broad, unimodal Unresolved Complex Mixtures (UCMs), a phenomenon that occurs when structurally complex organic compounds cannot be resolved (i.e. separated) by gas chromatography due to an overabundance of degraded isomers and homologues of cyclic and branched hydrocarbons (Bouloubassi and Saliot, 1993; Gough and Rowland, 1990) (Fig. 8-13). This term is usually applied to low-maturity crude oils or petroleum hydrocarbons

isolated from marine sedimentary samples (Farrington and Quinn, 2015), as the UCM becomes more pronounced the more degraded oils become. However, at Olduvai Gorge we do not expect to find petroleum hydrocarbon contamination. Instead, chemical, physical, and microbial action are likely responsible for the (bio)degradation of

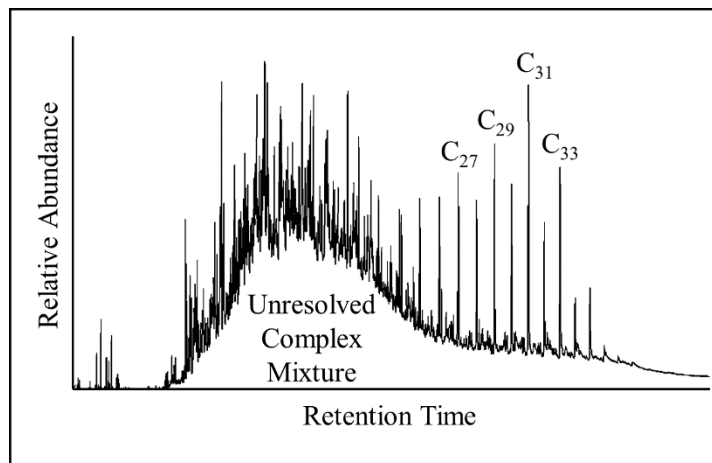


Figure 8-13. Unresolved Complex Mixture (UCM) visible in the chromatogram of a FLK-W sample. Alkanes were identifiable to the right of the UCM and carbon isotope analysis was possible. However, due to the messy baseline, hydrogen analysis was not as successful or reliable.

sedimentary organic matter and the formation of the UCMs in depositional environments.

UCM distributions in the lower molecular weight range have been attributed to bacterial degradation of organic inputs (Broman et al., 1987; Venkatesan and Kaplan, 1982), and typically have a chromatographic output between C_{16} and C_{22} (Grimalt et al., 1988). For the FLK-W samples, the UCM appeared in nearly all samples in the C_{15} to C_{25} range, with the maximum height of the UCM usually occurring between C_{17} and C_{20} . Additional evidence for microbial degradation of organic matter and production of UCMs comes from topsoil samples collected at Olduvai; even these “modern” soils, ultrasonically extracted and eluted using SGCC, suffered from UCM interference (Fig. 8-14). Because biologically produced mixtures have a GC-MS retention window of C_{16} to C_{22} , and control experiments on the reworking of sedimentary lipids show bacterial alteration of hydrocarbons within one month’s time (Grimalt et al., 1988), *n*-alkanes can suffer from biodegradation soon after deposition. Moreover, the multifaceted interactions between microbial activity, alkaline soil chemistry, soil temperature, and the extreme variance in seasonal

precipitation, factors not well understood in East African soils, subject the Olduvai *n*-alkanes to (likely¹³) higher degrees of alteration.

The LAS and BPT samples were also subjected to SGCC after Soxhlet extraction but contained far greater UCM

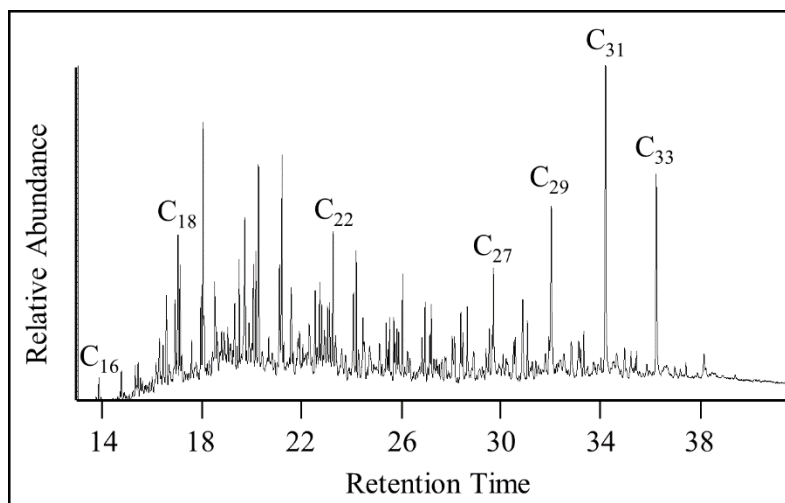


Figure 8- 14. A less-pronounced UCM of a "modern" topsoil sample collected at Olduvai Gorge in 2014. It is possible that a combination of soil temperature and chemistry, microbial activity, and variable seasonal precipitation have an impact on leaf wax soon after deposition.

interference than many of the FLK-W samples. In fact, nearly all these samples had no discernible *n*-alkanes, showing that they were heavily degraded upon deposition. These initial results guided protocol development and method implementation for the remaining laboratory analyses. SiAgNO₃ was applied to reduce the UCM and obtain IRMS amenable products. *n*-Alkanoic acids were isolated as they are the biogenic precursors to *n*-alkanes and were found to preserve much better in modern and ancient terrestrial sediments.

8.4.4 Implementation of SiAgNO₃

The ability of silver ions (Ag⁺) to interact with unsaturated compounds and form weak bonds with branched and cyclic hydrocarbons helps to resolve complex lipid mixtures into amenable GC products. Silver-infused silica is therefore better suited for isolating saturated *n*-alkanes and *n*-alkanoic acids from UCMs as it corrects chromatographic complications deriving

¹³ Samples from the Ngorongoro Crater Highlands also studied for *n*-alkanes do not have UCM chromatographic outputs. This could be due to differing environmental characteristics between Olduvai and the Crater Highlands; e.g. overall vegetation structure, more-shaded ground cover and greater total precipitation in the Highlands, or elevated soil temperatures and soil alkalinity in the Olduvai region.

from compound (bio)degradation. After unsuccessfully trying other *n*-alkane purification techniques (i.e. Urea Adduction and Molecular Sieves), a literature review of the application of SiAgNO₃ to UCM resolution was conducted (Frysiner et al., 2003; Li et al., 1995; McWilliams and Angelici, 2016; Nikolova-Damyanova, 2009; Polissar and Freeman, 2010), and it was found that most studies trying to resolve UCMs, or separating saturated from unsaturated hydrocarbons use between 5 and 10% (w/w) silver nitrate to silica gel. Therefore, different SiAgNO₃ preparation methods were attempted based on the following publications:

- *Li et al., 1995 Method* – 5.0 g of silver nitrate (Crystalline/Certified ACS, Fisher Chemical) dissolved in 30 mL of reverse osmosis deionized (RODI) water was mixed with 50 g silica gel and ground with mortar and pestle for five minutes. The mortar was covered with aluminum foil and the mixture was oven dried at 110°C overnight.
- *Frysiner et al., 2003 Method* – 20 g of silica gel and 4.0 g of silver nitrate crystals were mixed within a beaker in 50 mL of MeOH:H₂O (4:1 v/v) until the silver nitrate dissolved. The slurry was covered with aluminum foil and dried overnight at 110°C. A second iteration of this method was attempted whereby the slurry was dried using rotary evaporation.
- *Alex Sessions' Lab Method* – 5.0 g activated silica gel was inundated with 29.5 mL 0.1N silver nitrate solution (0.1N (N/10)/Certified, Fisher Chemical) in an aluminum foil covered beaker and dried in an oven at 75°C. A second iteration of this method was attempted whereby 0.5 g of silver nitrate crystals were dissolved in 29.5 mL of RODI water and then added to 5.0 g silica gel. Test on both iterations showed that they worked equally well, but due to the simplicity of using the solution, it was the preferred method utilized.

The Fryinger et al., (2003) method was the least successful of the attempted protocols. After the drying period, the Ag^+ ion decomposed into elemental silver turning the silver-infused silica black, even though it was covered with aluminum foil and stored in a dark oven. A second attempt at this method was performed whereby the mixture was evaporated under reduced pressure using rotary evaporation to limit the drying period. This time, the SiAgNO_3 slurry was mixed in a 250 mL flat bottom flask, covered with aluminum foil, and rotary evaporated until completely dry. It was then transferred to an aluminum foil covered beaker and stored in a dark drying oven at 65°C overnight. Again, the Ag^+ ion decomposed into elemental silver. The catalyst for Ag^+ decomposition may have been the amount of AgNO_3 used as this was the only method employed that resulted in 20% SiAgNO_3 (4.0 g AgNO_3 in 20 g Silica), or possibly the inclusion of methanol in the mixing solution in addition to water. Because this method for preparing SiAgNO_3 could not be replicated, it was abandoned and not used for compound purification.

The initial attempt at the Li et al., (1995) protocol worked sufficiently in that the 10% SiAgNO_3 combination retained the characteristic white coloring of the silica gel. A stationary phase experiment was then conducted in which 1.0 g of the SiAgNO_3 was added to a 5-inch pipette and eluted with a previously GC-MS analyzed *n*-alkane fraction from FLK-W¹⁴ with Hexane. The initial results were promising in that the silver nitrate successfully reduced the UCM, but at the same time, reduced the relative concentration of the target *n*-alkanes. Additional FLK-W column samples were purified the same way, but with inconstant results; for many samples, the UCM was reduced allowing for *n*-alkane identification and quantification as well as carbon isotope analysis. Conversely, the UCM was not affected in some samples, and therefore these were not used for

¹⁴ This sample, FLK-W 00041, was collected in bulk in L6 at the FLK-W site, though not from the same column as the samples described above. Collected 2.0 m east of the column, this sample was initially studied for particle size analysis, phytolith preservation, and biomarker concentrations and helped guide protocol development.

isotope analysis. One hypothesis for the inconsistencies is that the mortar and pestle mixing method was inadequate for thoroughly infusing the dissolved silver nitrate onto the silica gel, as 30 mL H₂O did not inundate the entirety of 50 g silica. It is possible the samples that did not have reduced UCMs were eluted over silica insufficiently infused with silver nitrate (i.e. <10%) due to the uneven distribution of AgNO₃ across the silica using mortar and pestle mixing, while those that reduced the *n*-alkanes in addition to the UCMs may have had >10% infused silica.

A revised version of the Li et al., method was designed to A) test the effectiveness by first dissolving silver nitrate crystals in water using a magnetic stirrer (as opposed to mortar and pestle), and B) compare the effectiveness of 5% vs. 10% SiAgNO₃ on UCM and *n*-alkane reduction. Two subsets of SiAgNO₃ were obtained by dissolving 1.0 g (subset 1) and 0.5 g (subset 2) silver nitrate crystals in 30 mL RODI H₂O within an aluminum foil covered beaker using a magnetic stirrer, and then adding 10 g silica gel to each beaker. Both the 5% and 10% (w/w) SiAgNO₃ were then oven dried overnight at 110°C and stored at 65°C to make sure they remained deactivated from water.

A third protocol, adopted from the Alex Sessions Stable Isotope Biogeochemistry laboratory (obtained through personal communication, Dr. Zheng Wang, State Key Laboratory for Loess and Quaternary Geology), was used in a comparison study with the two modified Li et al.,

BOX VIII-II: WHY 29.5 mL SILVER NITRATE SOLUTION FOR 5.0 g SILICA?

In order to get SiAgNO₃ of 10% (w/w) using 5.0 g activated silica gel, 29.5 mL of 0.1N solution was determined to equate to 0.5 g AgNO₃ using the following equation:

$$(\text{Grams Equivalent to 10\%}) \div (\text{Normality of Solution}) \div (\text{Molar Mass of AgNO}_3) = \text{Volume in Liters}$$

$$0.5 \text{ g} \div 0.1\text{N} \div 169.87 \text{ g/mol} = 0.0295 \text{ L or } 29.5 \text{ mL}$$

The volume of solution needed is easily adjusted when using different amounts of silica gel; e.g. SiAgNO₃ of 10% using 10 g silica requires 59 mL of solution. Both 5 and 10 grams of silica were used in column chromatography preparation depending on the number of samples being processed on a given day.

methods. For this protocol, 29.5 mL of 0.1N silver nitrate solution ((N/10)/Certified, Fisher Chemical) was added to 5.0 g silica gel in an aluminum foil covered beaker and oven dried for at least two days at 75°C. This approach was the simplest in terms of preparation, as silver nitrate crystals did not have to be dissolved initially. After drying, the resulting SiAgNO₃ retained its characteristic white coloring and was therefore the preferred method for preparing SiAgNO₃; it was subsequently used in column chromatography for reducing UCMs and isolating saturated *n*-alkanes and fatty acids.

An experiment designed to test the efficiency of the different SiAgNO₃ preparation methods was conducted using a fatty acid methyl ester (FAME) standard (Supelco 37 Component FAME Mix, 1.0 mL in DCM) consisting of known saturated and unsaturated compounds. (FAMES are *n*-alkanoic acids that have been derivatized with methanol making them GC amenable; see Section 8.4.5 for further details.) Three columns were constructed using SiAgNO₃ prepared by the two modified Li et al., methods (5% and 10%) and the Sessions 0.1N protocol. Each column consisted of a Soxhlet extracted glass wool filter and 1.0 g of the respective SiAgNO₃. They were then eluted with 100 µL of the FAME 37 standard and 4.0 mL DCM to test how effective each method was at trapping unsaturated fatty acids; that is, those with carbon-to-carbon double bonds. The FAME 37 standard contains 15 saturated compounds, eight compounds containing 1 double bond, and one compound each for 3, 4, 5, and 6 double bonds. Figure 8-15A is the GC chromatographic output (or chromatogram) for a 1.0 µL injection of the FAME 37 standard showing each of the compounds and their respective number of carbon-to-carbon double bonds.

Before chromatography, each column was rinsed with ~3.0 mL of DCM which was collected in a waste vial and discarded. 100 µL of FAME 37 standard was then added to the top of each column and subsequently eluted with 4.0 mL of DCM; this was collected in an oven-cleaned

4.0 mL vial. The experimental samples were evaporated with N₂, reconstituted in ~200 μL Hexane, transferred to 2.0 mL GC vials with 200 μL inserts, evaporated again, and then immersed in exactly 100 μL of Hexane. Figure 8-14A–D show the chromatograms for 1.0 μL injections of the FAME 37 standard (in 100 μL DCM) and the three SiAgNO₃ columns (in 100 μL Hexane); in 8-15A, all saturated and unsaturated compounds are identified and each carbon-to-carbon double bond is symbolized; 8-15B is the modified Li et al., 10% SiAgNO₃; 8-15C is the modified Li et al., 5.0% SiAgNO₃; and 8-15D is the Sessions 0.1N SiAgNO₃. The Li et al., methods were successful in removing all carbon-to-carbon compounds containing 3 or more double bonds, but was not as effective for those containing only 1 double bond; this may be due in part to silver ions' ability to resolve fatty acids on the basis of the number of their double bonds, meaning that they become more effective as the number of double bonds increase. Although the 5.0 and 10% SiAgNO₃ columns reduced the overall concentration of the carbons containing 1 double bond, they did not eliminate them entirely. The Sessions method on the other hand, completely removed all double bonded compounds, but also reduced the total concentration of saturated FAMEs considerably (Table 8-9), especially in the lower carbon number range (<C₁₅). In fact, three of the saturated FAMEs were completely lost.

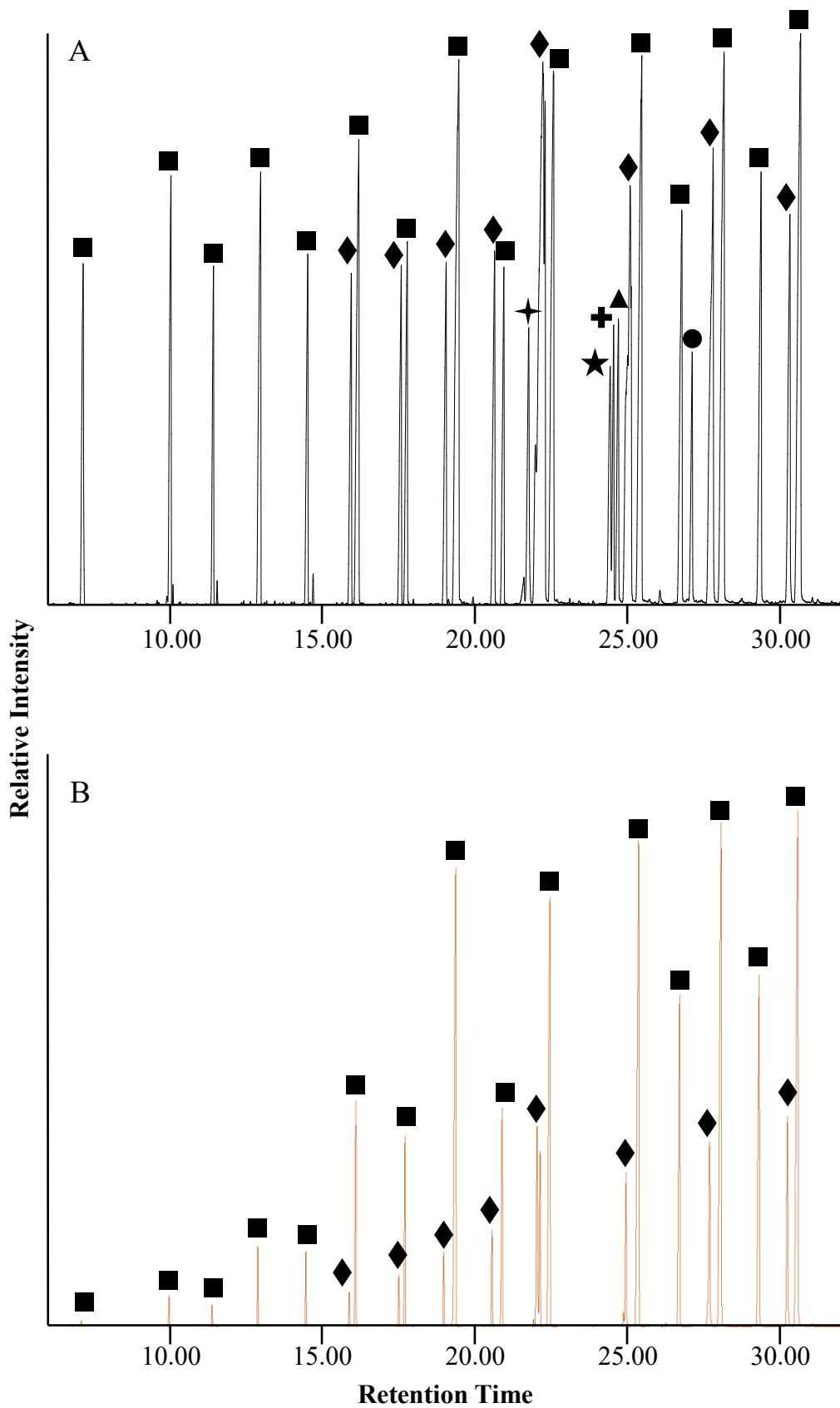
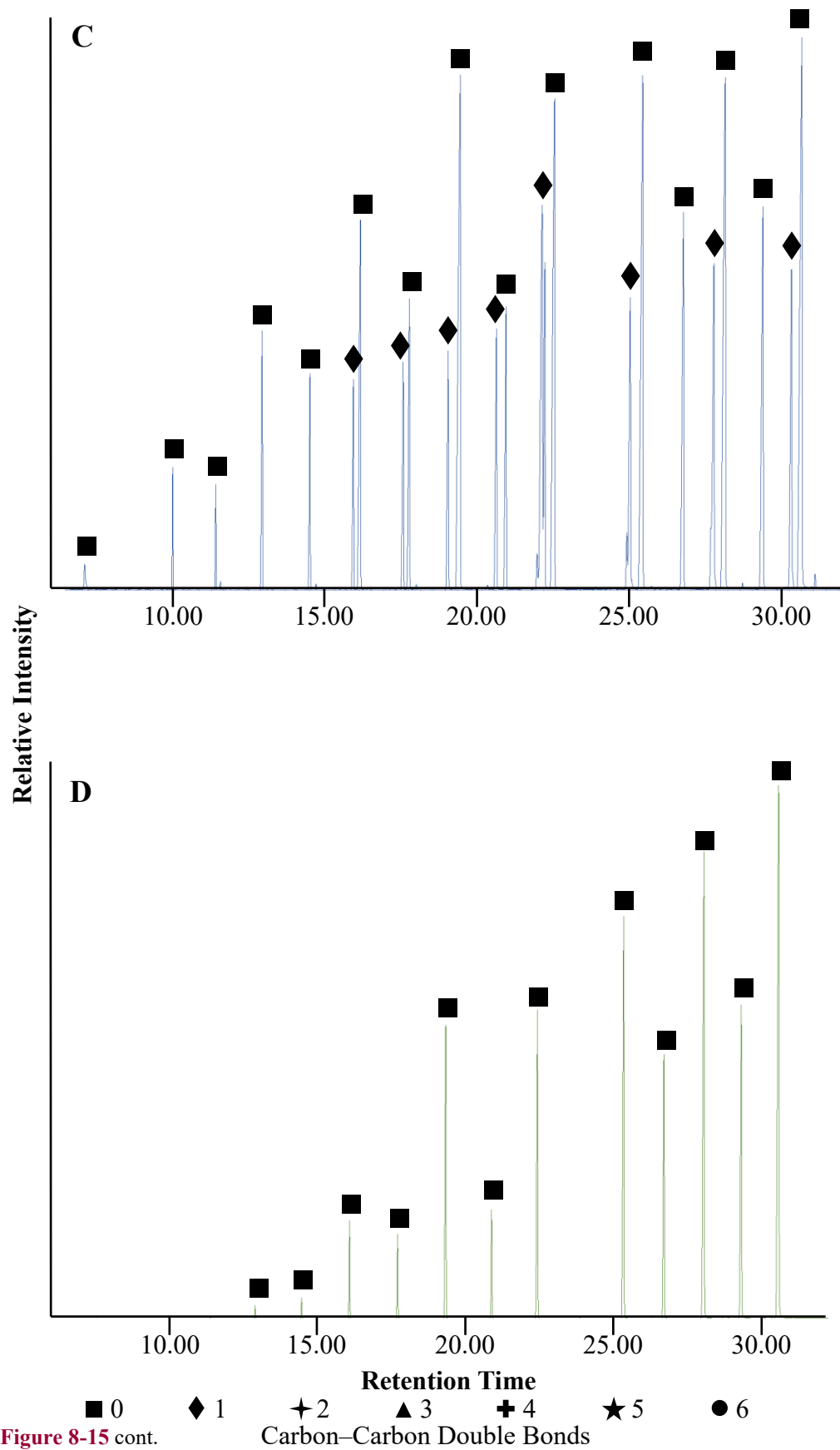


Figure 8-15. GC-MS chromatogram for FAME 37 Standard (A) and experimental using different SiAgNO_3 preparation methods of 10% (B), 5% (C), and 0.1N (D). The C_{24} saturated FAME is the last peak represented on each chromatogram.



Overall, the 0.1N silver nitrate solution was the most effective in terms of isolating saturated FAMES during column chromatography. However, because this method also significantly reduced the total concentration of these analytes, it was slightly modified for all subsequent analyses; instead of using 1.0 g SiAgNO₃, only 0.5 g were used for column chromatography. Additionally, silica gel and silver nitrate column chromatography were no longer divided into two separate procedures. Rather, they were combined in one column, with 0.5 g SiAgNO₃ situated below 0.5 g silica gel (Fig. 8-9). This setup limits analyte loss by both reducing the number of columns needed to separate lipids from two to one, and by lessening the total amount of SiAgNO₃ from 1.0 to 0.5 g. Consequently, this approach was used for isolating both the *n*-alkanes and *n*-alkanoic acids from the total lipid extracts.

Table 8-9. Total concentration of the C₂₄ saturated FAME (top) and C₂₄ unsaturated FAME with the double bond between carbons 15 and 16 (bottom) for the standard and three SiAgNO₃ chromatography methods. Peak area and height determined by GC-MS. Percentages are of the total concentration of the FAME 37 standard.

	Peak Height	Peak Area	% Height	% Area
FAME 37	26,618,608	1,751,661,621	-	-
5%	21,524,431	1,113,478,371	80.9%	63.6%
10%	15,734,620	645,799,973	59.1%	36.9%
0.1N	12,018,363	418,249,776	45.2%	23.9%

	Peak Height	Peak Area	% Height	% Area
FAME 37	17,914,093	834,701,753	-	-
5%	12,485,846	445,067,286	69.7%	53.3%
10%	6,420,568	176,912,434	35.8%	21.2%
0.1N	0	0	0.0%	0.0%

8.4.5 Fatty Acid Methyl Esters

Fatty acids are the biosynthetic precursors of the *n*-alkanes in plant cuticular wax and have similar $\delta^{13}\text{C}$ values with the *n*-alkanoic acids being depleted by 1.3‰ to 1.4‰ relative to the corresponding carbon-numbered *n*-alkanes. The alkanes are the most ubiquitous component of plant waxes as they accumulate in high concentrations and due to their non-polar nature, can easily be extracted from leaf material or total lipid extracts using only Hexane and silica gel column chromatography. This makes them the more traditional method for environmental reconstructions

using carbon and hydrogen isotopes. The *n*-alkanoic acids on the other hand, are more-polar compounds that tend to form hydrogen bonds due to carboxyl (-COOH) functional groups. They require neutralization through esterification in order to reduce their polarity so that they are more amenable for GC analysis. Not only are multiple chromatographic columns required to isolate them from TLEs, *n*-alkanoic acids must be methylated before carbon and hydrogen isotope analysis, and then isotope values must be

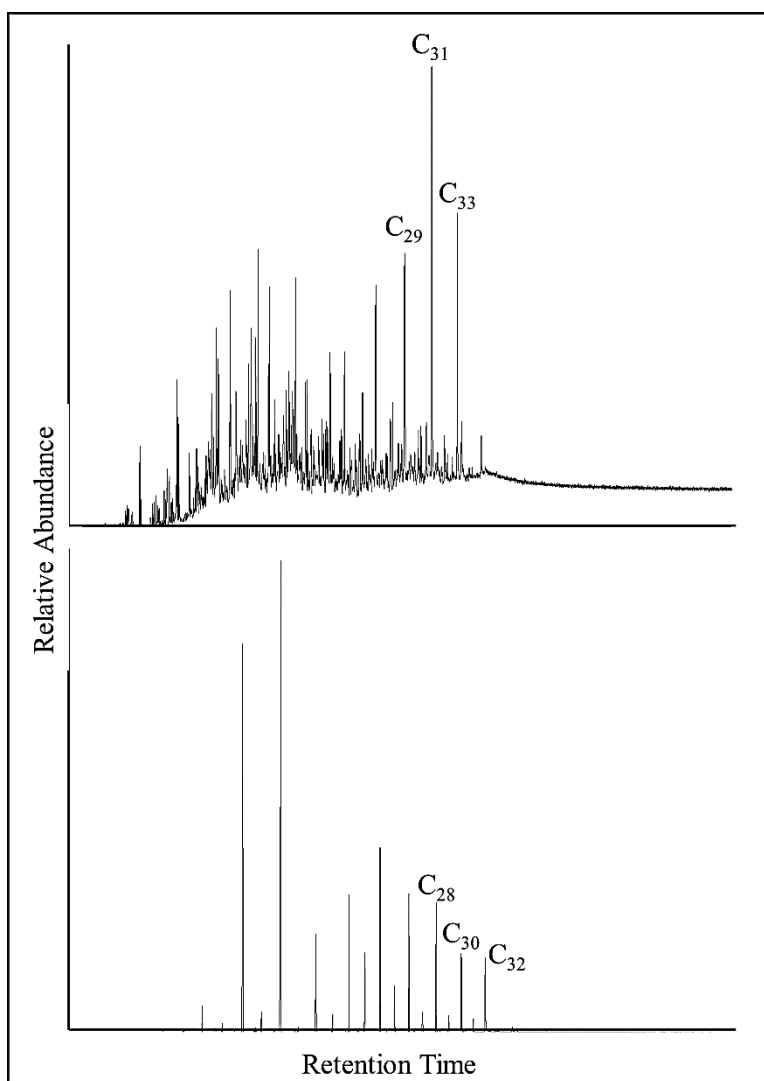


Figure 8-16. *n*-Alkane GC trace with UCM interference (top) vs. *n*-alkanoic acids (as FAMES) (bottom) from the same sample. It is the UCM interference that justified using FAMES for the majority of $\delta^{13}\text{C}$ and δD analyses.

mathematically corrected to account for the added methanol (see Section 8.7.6). The fatty acids, however, tend to preserve much better in East African terrestrial sediments and do not seem to suffer the same effects of (bio)degradation as the *n*-alkanes, such as the inclusion of UCMs (Fig. 8-16).

Aminopropyl columns retain acids when total lipid extracts are eluted with DCM:Isopropanol, which allows for the removal of neutral compounds such as *n*-alkanes. These acids are subsequently released when the column is eluted with 4% Acetic Acid in Diethyl Ether, making it the paradigm for quickly separating carboxylic acids (i.e. *n*-alkanoic acids) from neutral fractions. However, free, underivatized fatty acids are difficult to analyze with GC-MS due to their polarity that leads to GC column adsorption issues. In order to make them GC amenable, following Aminopropyl column chromatography and N₂ evaporation (Section 8.3.3), the *n*-alkanoic acid fraction was converted to Fatty Acid Methyl Esters (FAMES) through methylation by adding 1.0 mL of 2% HCl in Methanol (94.5:5.5 mL v/v, MeOH:37% HCl) to the 4.0 mL vials, capping under nitrogen to force out oxygen, vortex mixing for 10 seconds, and storing in an oven set to 50°C for 20-24 hours. FAMES are stable compounds that can be quantitatively analyzed using GC-MS. During the esterification reaction, the 2% HCl catalyst protonates an oxygen atom of the carboxyl group on the *n*-alkanoic acid (Fig. 8-17), making it more reactive. The Methanol then combines with the protonated acid to yield a methyl ester and water as a by-product; the Cl is removed with water. To isolate the FAMES from the solution, 1.0 mL of 5.0% aqueous NaCl and 1.0 mL Hexane were each added to the 4.0 mL vials, shaken for 5.0 seconds and vortexed for 20 seconds. The mixture was then left to settle for ~30 seconds until the two phases (water and Hexane) separated due to differences in density. The Hexane portion (containing the FAMES) was then carefully

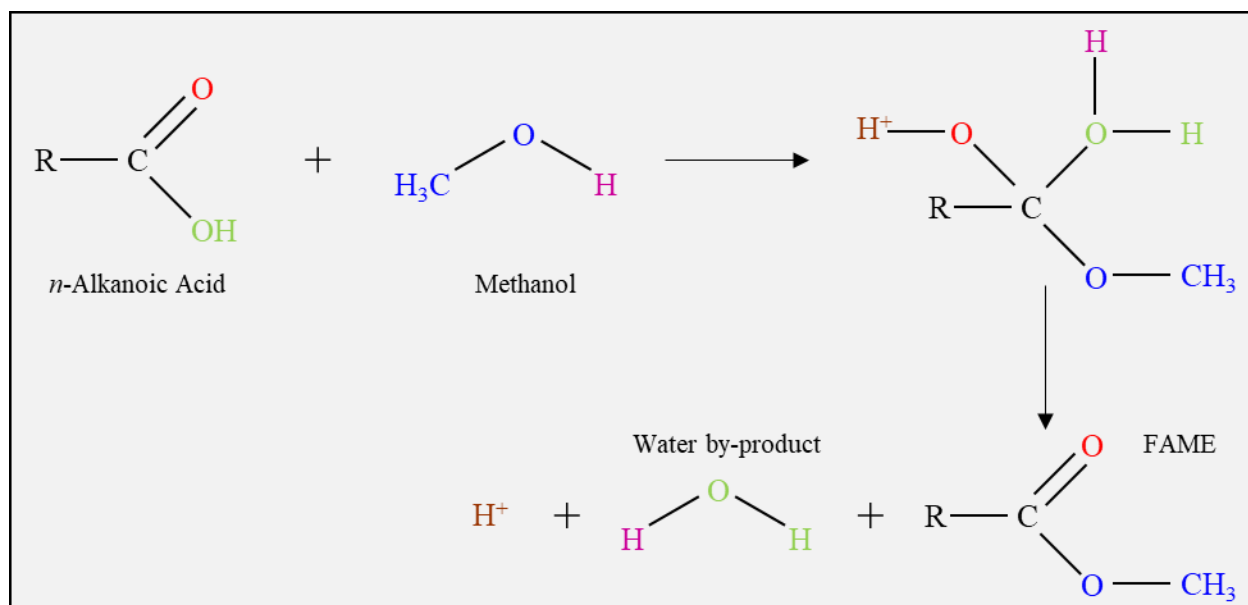


Figure 8-17. Methylation reaction in which 2% HCl in Methanol protonates an oxygen atom of the carboxyl group on the *n*-alkanoic acid converting it to a GC amenable FAME.

pipetted into a new, oven-cleaned 4.0 mL vial; 1.0 mL of Hexane was added three additional times, and shaken, mixed, and pipetted to the new vial to ensure extraction of all the FAMES. Samples were evaporated with N₂, and then the FAMES were isolated from other acids using 0.5:0.5 g (w/w) SiAgNO₃:Silica column chromatography (Fig. 8-9) with Hexane and DCM eluents; where the DCM fraction contained the FAMES.

Fatty acid methyl esters were not originally targeted for analysis. That is, at the onset of this project, they were not considered in terms of their environmental reconstruction potential due to the anticipated use of the *n*-alkanes. Only after the issues with the UCMs became prevalent (they interfered in the FLK-W, LAS, and BPT samples, and then later in “modern” topsoil), were *n*-alkanoic acids targeted for carbon ($\delta^{13}\text{C}$) and hydrogen (δD) isotope data. Aminopropyl column chromatography was therefore applied at two different stages during compound separation. The first involved using the polar (MeOH) fraction from SGCC of the FLK-W, LAS, and BPT samples to isolate FAMES using Aminopropyl columns. The second stage used the TLEs from the FLK-N,

clays below Tuff IF, and Castle Clays sample so that the neutral and acid fractions could be divided initially, before being partitioned into *n*-alkanes and *n*-alkanoic acids respectively with SiAgNO₃.

In terms of technique development, the protocol for Aminopropyl column chromatography and FAME isolation was modified from Yang and Huang (2003) (obtained through personal communication, Dr. Hong Yang, Bryant University), specifically for the methylation of the *n*-alkanoic acids. The polar fraction of the FLK-W samples was the first to be eluted over Aminopropyl. The N₂ evaporated polar fraction, which was eluted with MeOH over silica gel, was first reconstituted in 4.0 mL 2:1 DCM:Isopropanol to extract the neutral components, then with 4.0 mL 4% Glacial Acetic Acid in Diethyl Ether to release the carboxylic acids, and then finally with 4.0 mL MeOH to recover any phospholipids. The neutral and MeOH fractions were stored at -40°C because; A) the neutral extracts were originally separated with SGCC and had therefore already been isolated (this was confirmed with GC-MS), and B) phospholipids were not a focus of this study but may be a potential research avenue in the future. The acids fraction was methylated and Hexane-extracted as described above, and then eluted over ~1.5 g silica gel with 4.0 mL each of Hexane and DCM, with the DCM fraction containing the FAMEs. Next, the FAMEs were quantitated with GC-MS (Agilent 7890B GC coupled with 5977A MSD; PRG lab). To note, this was conducted before the implementation of SiAgNO₃, and through GC analysis it was found that some of the samples had unsaturated acids containing single carbon-carbon double bonds. However, quantitatively the *n*-alkanoic acids preserved exceptionally well and did not seem to suffer the same issues of (bio)degradation as the *n*-alkanes. Therefore, the MeOH fractions from the BPT and LAS samples (also eluted with SGCC beforehand) were separated using Aminopropyl columns, but then the methylated acids were eluted over SiAgNO₃ with Hexane and DCM to isolate only the saturated FAMEs.

For the second set of samples (FLK-N, clays below Tuff IF, and the Castle Clays), total lipid extracts were first separated using the Aminopropyl columns instead of being SGCC-divided first. The resulting neutral fraction and methylated acids were then individually eluted over a combined SiAgNO₃-Silica column (Fig. 8-9) to yield *n*-alkanes (with Hexane) and FAMEs (with DCM), respectively. This procedural setup was the preferred method as it allowed for the separation of the TLEs into neutral and acids fractions without having to perform SGCC first, and the combination of the SiAgNO₃-Silica in a single column was successful in eliminating UCMs and limiting analyte loss, specifically for the *n*-alkanes.

8.5 Summary of Extraction Techniques

The most reliant protocol for the separation of individual plant leaf wax lipid biological markers from Olduvai terrestrial sediments was Soxhlet extraction of TLEs, followed by Aminopropyl column chromatography, and then SiAgNO₃-Silica separation. Figure 8-18A and B are *methodological dendrograms* for the two main protocols used in the isolation of biomarkers:

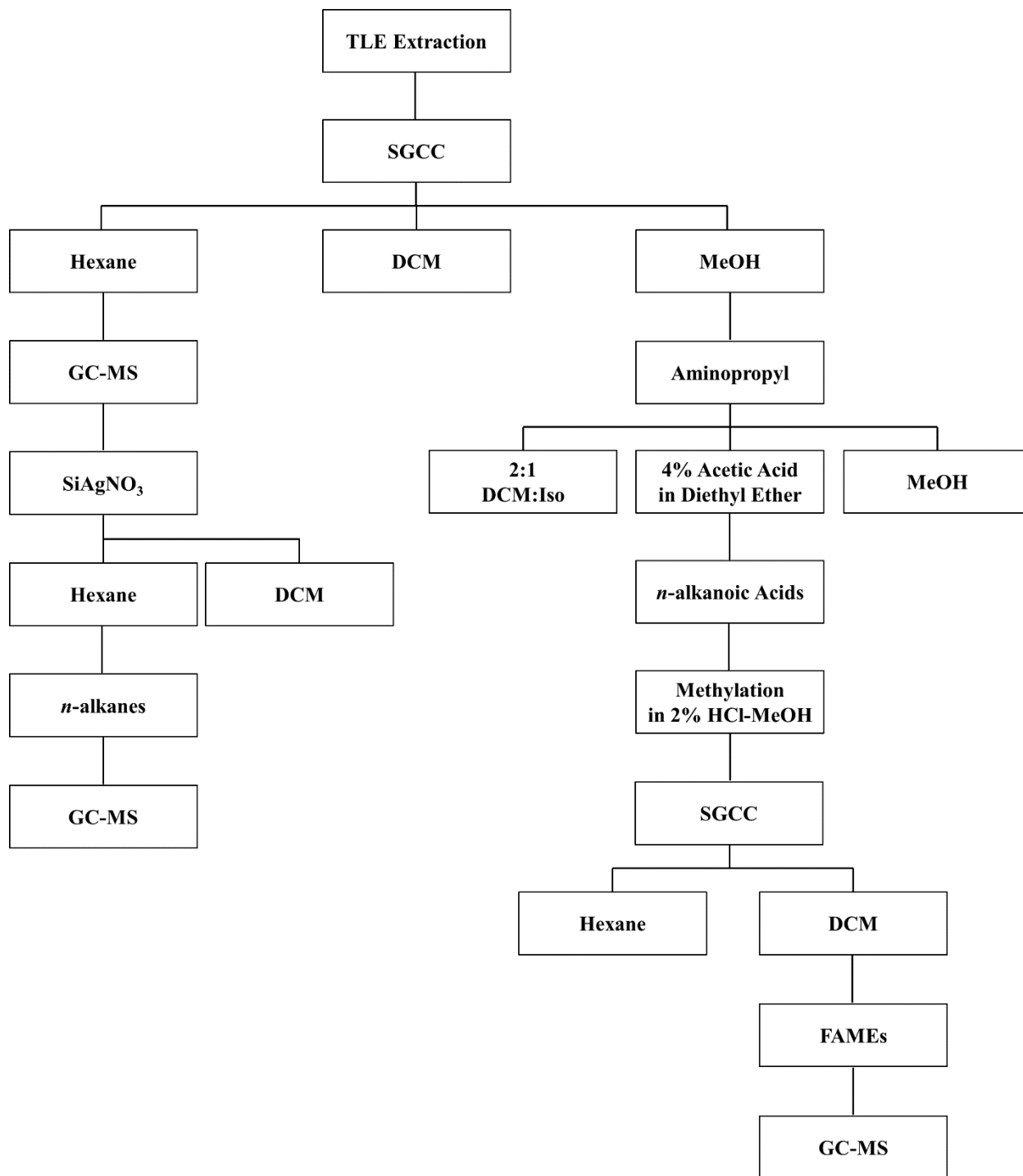


Figure 8-18A. The original protocol outline for *n*-alkane and FAME isolation. Soxhlet was used to extract total lipids from sediments, and then the TLEs were separated over silica gel using solvents of increasing polarity. After UCMS were found to dominate in the *n*-alkane fraction, they were subjected to SiAgNO₃ which improved the chromatographic baseline. Fatty acids were then targeted by using Aminopropyl columns for the MeOH polar fraction. The *n*-alkanoic acids were recovered using Acetic Acid in Diethyl Ether and then methylated. The FAMES were then eluted over silica gel with DCM and analyzed with GC-MS. This protocol was then modified (Fig. 8-18B) due to the presence of UCMS in the original non-polar Hexane fraction and double bonded fatty acids in the FAMES.

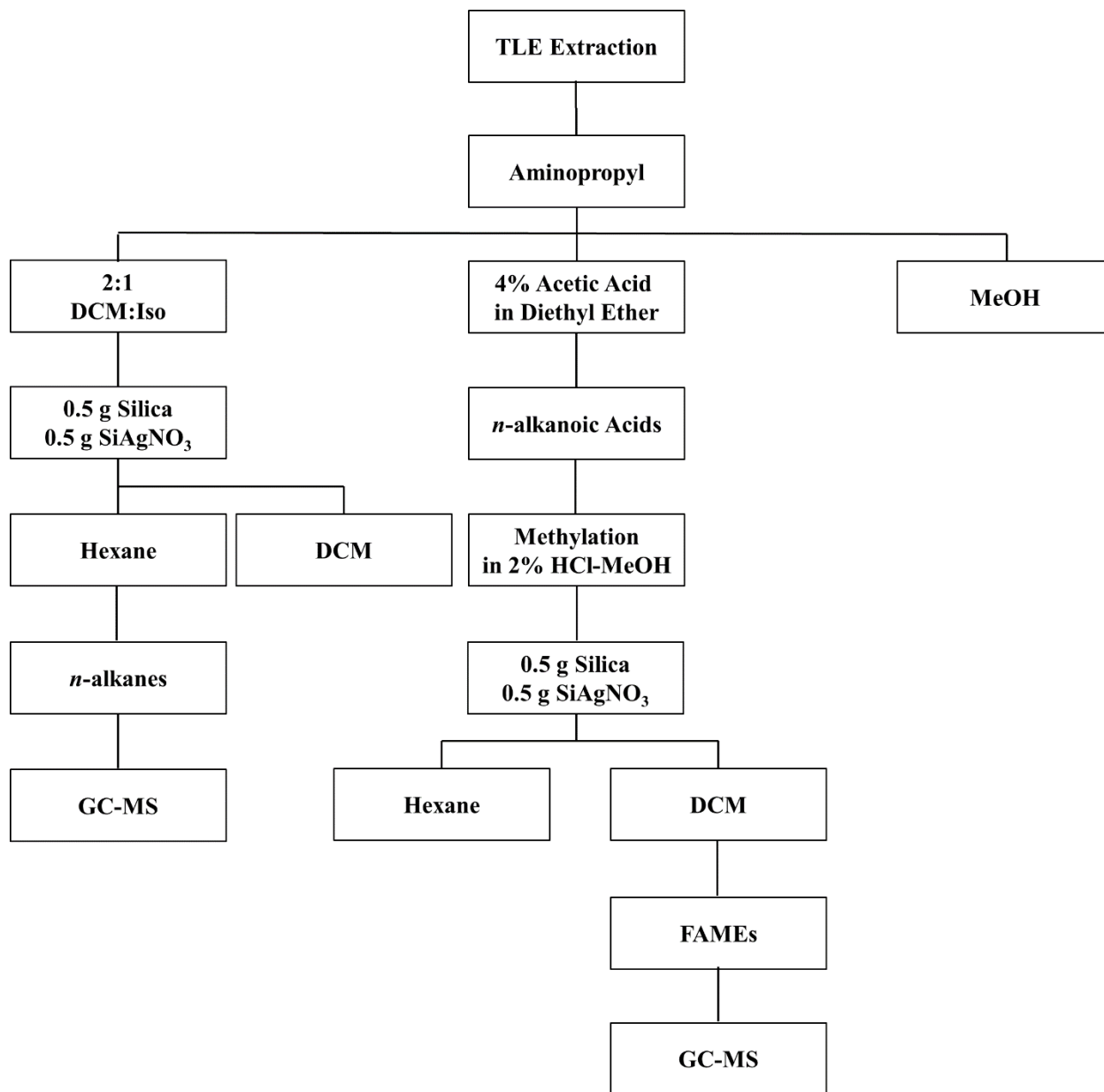


Figure 8-18B. The updated protocol outline for *n*-alkane and FAME isolation. Soxhlet was still used to extract total lipids, but the TLEs were first separated on Aminopropyl columns with the neutral and acid fractions eluted with DCM:isopropanol and Acetic Acid in Diethyl Ether, respectively. A combination column of SiAgNO₃ and silica gel was used to recover the *n*-alkanes and eliminate UCMs from the neutral fraction, whereby Hexane contained the *n*-alkanes. After methylation of the *n*-alkanoic acids, they too were eluted over a combination column of SiAgNO₃ and silica gel to eliminate double bonded compounds, with the FAMEs being recovered with DCM. Finally, samples were quantified with GC-MS. This was the preferred protocol as it eliminated unwanted chromatographic interference while also allowing for the most efficient recovery of target leaf wax lipid compounds.

8.6 Gas Chromatography and Isotope Ratio Mass Spectrometry

8.6.1 Gas Chromatography Mass Spectrometry (GC-MS)

Gas Chromatography Mass Spectrometry is an analytical technique for identifying and quantitating organic compounds in complex matrices. The gas chromatograph (GC) separates compounds by first volatilizing a sample in a heated inlet, uses an inert carrier gas (e.g. Helium) to then transfer the sample from the inlet through a fused silica capillary column containing a stationary phase coating, and then finally passes the sample from the column into the mass spectrometer (MS) which provides structural information on the injected compounds. Individual ovens heat the injector inlet, the column, and the MS detector. The column oven allows for the temperature to be programmed to increase at regular rates during the separation of samples; it is this temperature ramp that dictates analyte movement through the capillary column, and the ensuing elution as sharp peaks on the chromatographic output. The retention time of a compound therefore varies with the length of the column, the thickness of the stationary phase, temperature ramp conditions, and carrier gas flow. Thus, these parameters determine the relative tendency of when compounds move from the stationary phase into mobile carrier gas phase and subsequent discharge into the mass spectrometer.

The mass spectrometer ionizes the analytes eluting through the GC column as they enter the detector, the ions are then deflected by a magnetic field, and finally distinguished electrically according to their mass-to-charge ratio (m/z) (Fig. 8-19 – 8-21). The fragmentation of the ions, which represents the original molecule injected into the GC, is then used to determine the structure of targeted compounds. The data resulting from GC-MS are known as “mass spectra” and represent the m/z value and abundance of a molecular ion (M^+).

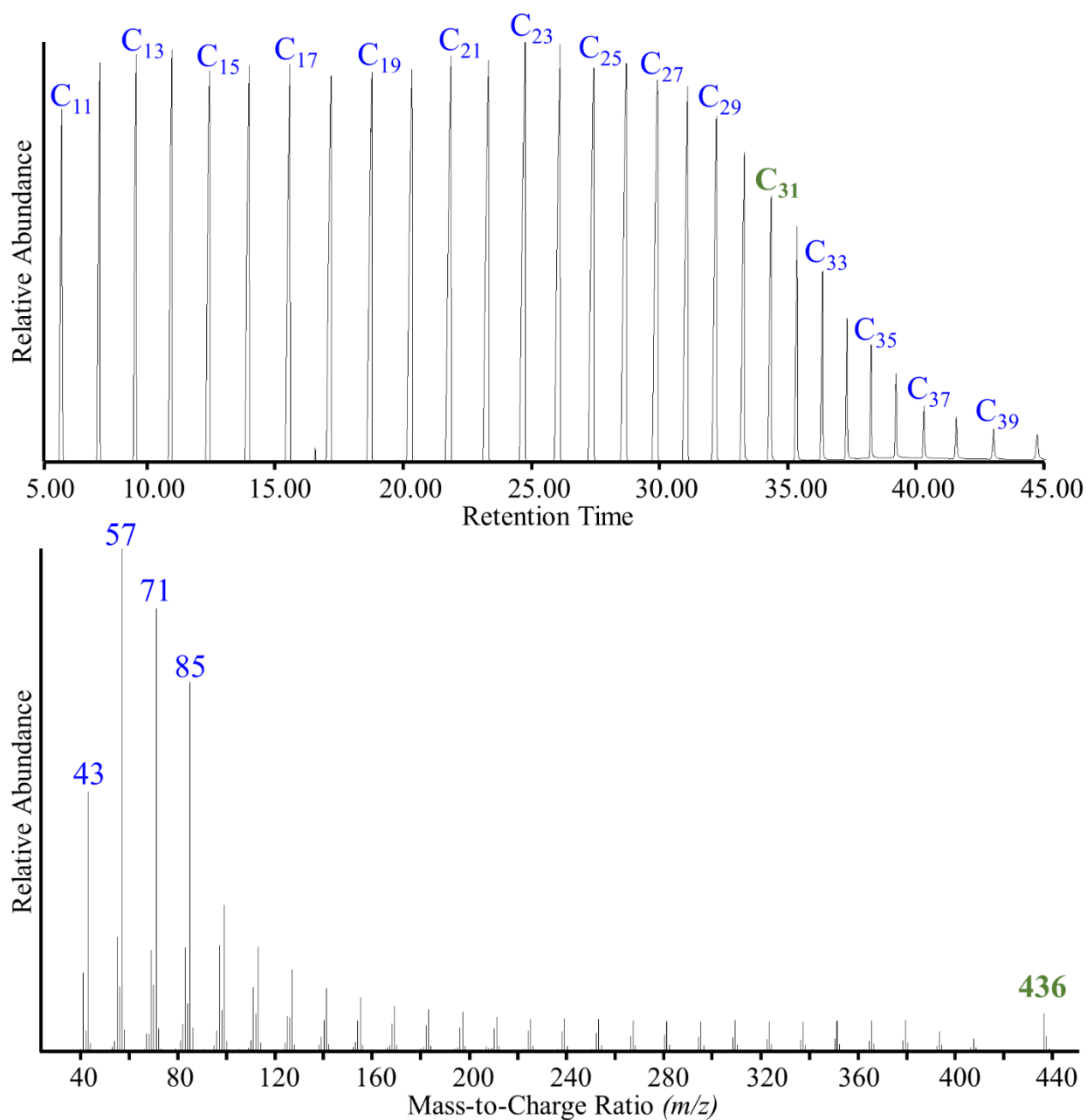


Figure 8-19. Top: A typical chromatogram of a C₁₀-C₄₀ *n*-alkane standard used in identifying compounds based on their retention time (C₁₀ not shown as it falls below 5.00 min). **Bottom:** The mass spectra of the C₃₁ *n*-alkane (in green) with the identifying molecular ion (M⁺) unit of 436 (also in green). The *m/z* value of ions formed using GC-MS is also representative of the molecular weight of the analytes, so in this case, the molecular weight and M⁺ value of C₃₁ is 436. The 43 to 85 *m/z* units are base peaks common in all *n*-alkane mass spectra, and ions with greater *m/z* values produce lower responses than those of lower *m/z* values.

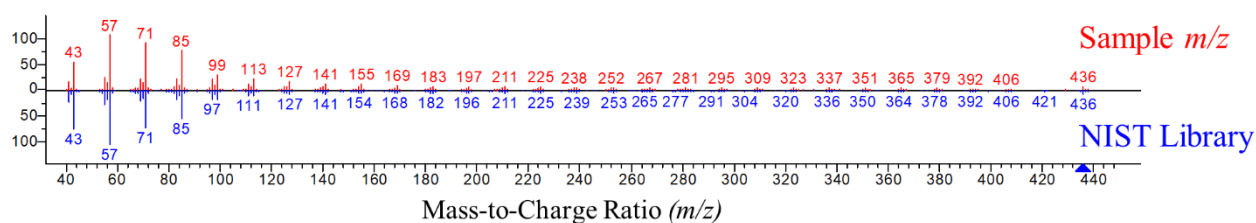
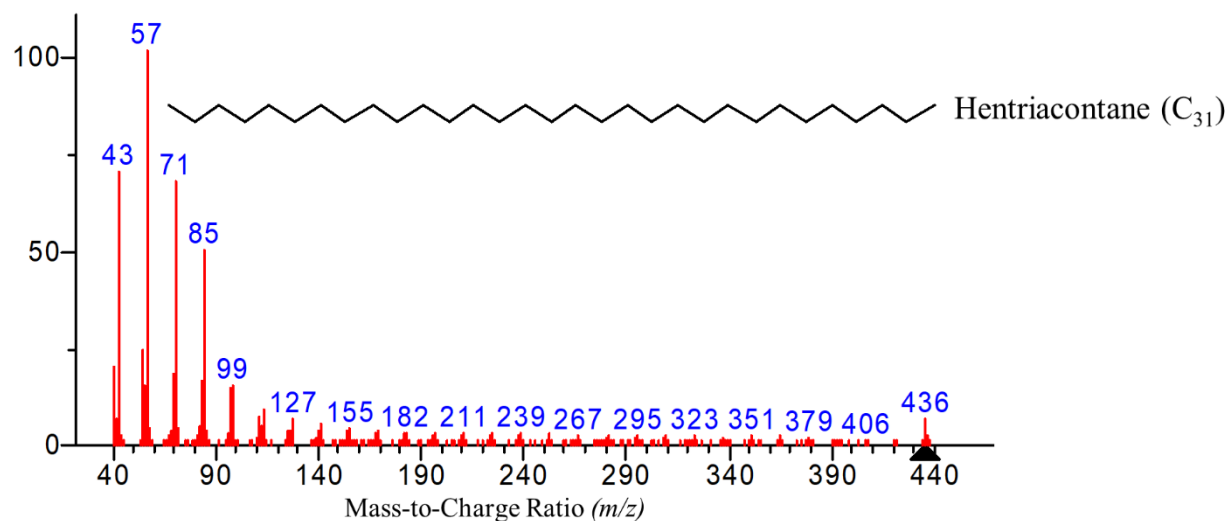
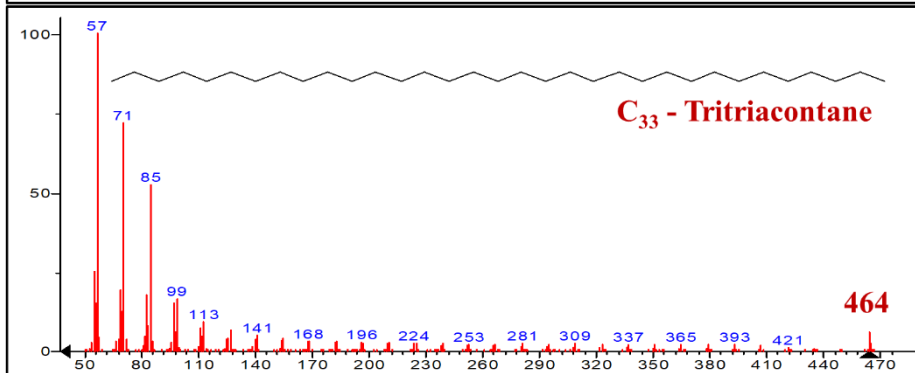
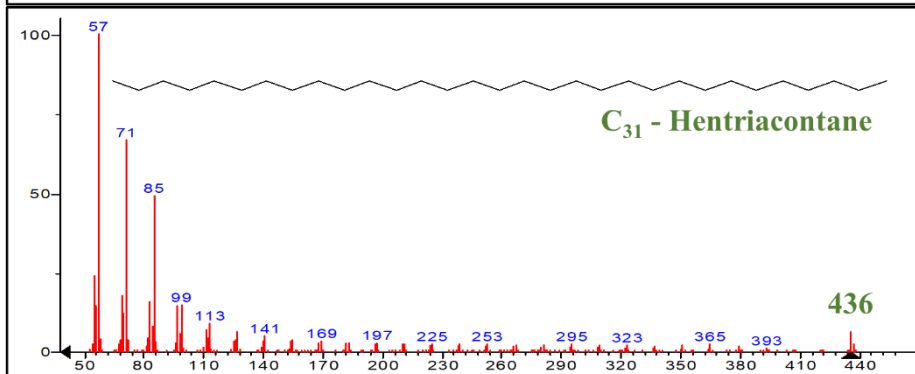
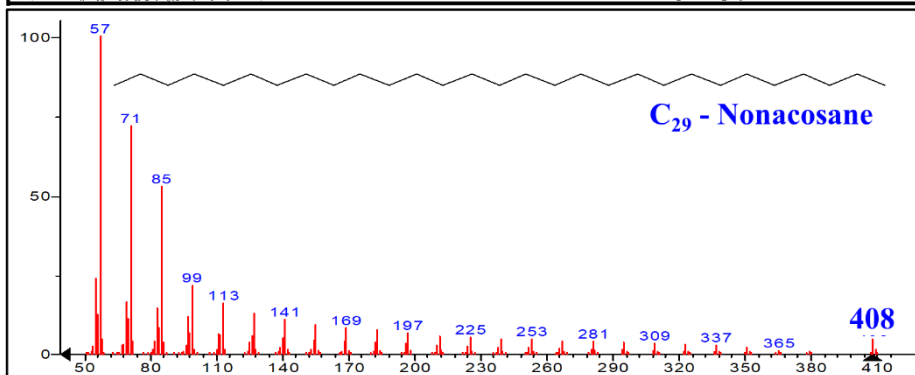
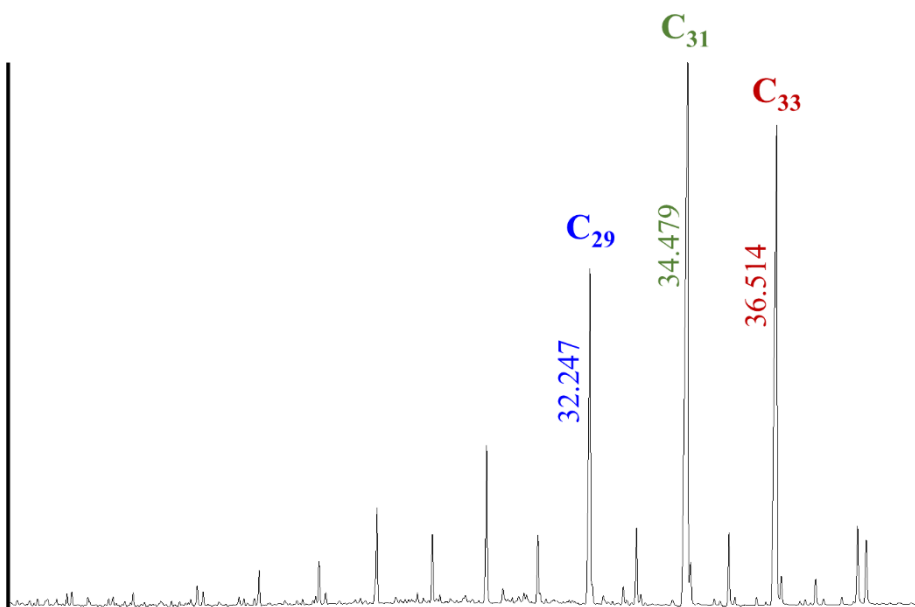


Figure 8-20. National Institute of Standards and Technology (NIST) provides a library search report for comparing m/z spectra of samples to their reference library. For example, the top figure shows the NIST spectra for the n -alkane Hentriacontane (C_{31}), while the bottom figure is a m/z comparison of a target sample (in red) to the NIST C_{31} spectra (in blue). The mass spectra of an unknown sample, the NIST library, and the GC retention time can therefore help in the identification of an analyte.

Following page:

Figure 8-21. Three mass spectra for the molecular ions representing the mass of the C_{29} - C_{33} n -alkanes. Each additional carbon homologue adds 14 mass units (one Carbon (12 amu) and two Hydrogen (2 amu)), so when comparing the odd numbered n -alkane compounds, 28 mass units are added between each compound. Therefore, C_{33} has a molecular ion identifier (464) that is 28 mass units greater than C_{31} (436), which is also 28 mass units greater than C_{29} (408). (This same pattern applies to the n -alkanoic acids as well.) It is this fragmentation patterns that help to identify leaf wax compounds using GC-MS.



The M^+ peak, always located on the right side of the mass spectra, provides information on the elemental composition of the sample analyzed with GC-MS. Intense molecular ion peaks indicate that the analyte is an aromatic compound or an unsaturated ring, usually accompanied by a lot of fragment ions (Sparkman et al., 2011). Low intensity, as in the figures above, indicate straight-chained or branched aliphatic hydrocarbons, which can prove challenging when interpreting an electron ionization mass spectrum.

Gas chromatography mass spectrometry was performed using two different instruments; an Agilent 7890B GC Series with an Agilent HP-5 capillary column (30 m length, 0.25 mm i.d. and 0.25 μm film) coupled with an Agilent 5977A mass selective detector (MSD), and an Agilent 6890N Network GC System joined with an Agilent HP-5 capillary column (30 m length, 0.25 mm i.d. and 0.25 μm film) to an Agilent 5973 MSD. One major difference in the instruments is that the 5977A MSD, a newer model, is more sensitive when measuring ions; however, the 6890N GC and 5973 MSD were used for most analyses.

Before GC analysis, *n*-alkane and FAME samples were reconstituted in ~ 200 μL Hexane, transferred to 2.0 mL GC vials with 200 μL inserts, evaporated, then immersed in exactly 100 μL of Hexane (Section 8.3). One microliter (μL) of the 100 μL Hexane containing sample was injected into a pulsed splitless inlet set at 250°C. In GC splitless mode, the sample is injected into an inlet with its solvent purge vent temporarily closed. After an experimentally optimized period (usually $\frac{1}{2}$ to 1 minute), the vent is opened to purge volatile solvent from the injector while the analytes in the sample are deposited onto the head of the column. Splitless injection is used for trace analysis, with pulsed splitless allowing for sharper peaks than in traditional splitless injection. The injector temperature of 250°C was high enough to volatilize all analytes of interest so that they condensed in a narrow band on the stationary phase of the column. The column oven was programmed from

an initial temperature of 60°C (9°C below the boiling point of Hexane) and held for 1.00 min, at which point the splitter was opened and the oven was ramped to 150°C at 10°C/min then to 320°C at 6°C/min, and held for 20.00 min. As the components of the sample are carried onto the column by the carrier gas, compounds are slowly released from the stationary phase into the mobile phase as temperature successively increases. Although *n*-alkanes and FAMES elute before maximum temperature was reached, the final temperature and hold time were designed to elute extraneous higher molecular weight compounds from the sample; however, no extraneous compounds were detected. Helium was used as the carrier gas and set at a constant flow rate of 1.1 mL/min. The MS electron ionization (EI) source, the most widely used type of ionizer, was

Table 8-10. GC-MS parameters used in the analysis of *n*-alkanes and FAMES.

Oven Temperature	
Initial Temp.	60°C
Hold Time	1.00 min
#1 Rate	10 °C/min
#1 Value	150°C
#1 Hold Time	0.00 min
#2 Rate	6 °C/min
#2 Value	320°C
#2 Hold Time	10 min
Front Inlet	
Mode	Pulsed Splitless
Initial Temp.	250°C
Pressure	13.5 psi
Pulse Pressure	21.8 ps1
Pulse Time	1.00 min
Purge Flow	30.0 mL/min
Purge Time	1.00 min
Total Flow	34.0 mL/min
Column	
Description	HP-5MS (5%-Phenyl)-methylpolysiloxane
Max Temp.	325°C
Length	30 m
Internal Diameter	250 µm
Film Thickness	0.25 µm
Mode	Constant Flow
Initial Flow	1.1 mL/min
Nominal Pressure	13.5 psi
Average Velocity	28 cm/sec

operated at 230°C with conventional 70 electron volt (eV) ionization energy. 70 eV assures that the EI spectrum of a compound will be the same when obtained on different instruments. Furthermore, electron ionization occurred under vacuum so that the ion source was subjected to everything eluting off the GC column in order to produce ions of the target compounds. The MS Quadrupole mass analyzer, which separates ions travelling from the ion source according to their

m/z , was set to 150°C and a full scan rate of m/z 50-550 units so that all target *n*-alkanes and FAMES could be detected. Table 8-10 summarizes the GC-MS parameters used for sample analysis.

8.6.2 Isotope Ratio Mass Spectrometry (IRMS) and the δ Notation

Gas Chromatography Isotope Ratio Mass Spectrometry (GC-IRMS or IRMS) follows the same principles as GC-MS, except instead of yielding structural information by scanning fragmented ions, IRMS instruments measure with high precision, small variations in the relative abundance of carbon ($^{13}\text{C}/^{12}\text{C}$), hydrogen ($^2\text{H}/^1\text{H}$ or D/H), nitrogen ($^{15}\text{N}/^{14}\text{N}$), oxygen ($^{18}\text{O}/^{16}\text{O}$) or sulphur ($^{34}\text{S}/^{32}\text{S}$) isotopes. During isotope measurement, samples are converted to gas (e.g. H_2 , CO_2) before the MS calculates the corresponding ratio of ions within the gas and monitors the mass to charge ratios of the target compounds. For example, in the analysis of carbon-13 to carbon-12, the mass spectrometer monitors the ions with m/z values of 44, 45, and 46 which correspond to the ions produced from CO_2 molecules containing ^{12}C and ^{13}C , as well as ^{16}O , ^{17}O , and ^{18}O in various combinations (Carter and Barwick, 2011). Therefore, minute variations of the heavier isotope can be detected in the presence of large amounts of the lighter isotope. During isotope analysis, a standard reference gas is compared to the gas produced from combusting samples, and it is the difference in the signals between the standard and the sample gases that is used to calculate the isotope ratio of the sample. Moreover, even though the absolute ratios are measured for a given gas (e.g. $^{45}/_{44}$ and $^{46}/_{44}$ for CO_2), it is the difference between the sample and the standard ratios that is of interest in the isotope ratio calculation (Ehleringer and Rundel, 1989).

The isotope composition of a sample is expressed using the “ δ ” notation in units of per mil (‰), which reports changes in isotopic abundance as deviations compared to a designated isotope standard (Table 8-11). Isotope composition of a sample is expressed with the differential notation:

$$\delta^H X = (R_{\text{Sample}} \div R_{\text{Standard}} - 1) \times 1000 \quad (1)$$

Where:

- $\delta^H X$ is the heavy isotope mass of element X (e.g. ^2H , ^{13}C) relative to a standard
- R_{Sample} is the ratio of the heavy isotope to the lighter isotope of element X in the sample (e.g. $^2\text{H}/^1\text{H}$, $^{13}\text{C}/^{12}\text{C}$)
- R_{Standard} is the ratio of the heavy isotope to the lighter isotope of element X in the standard.

Table 8-11. Hydrogen and Carbon Isotope Composition of International Reference Standards.

Standard	Ratio H/L	Value H/L	% Heavy	% Light
Vienna Standard Mean Ocean Water (VSMOW)	$^2\text{H}/^1\text{H}$	0.00015576	0.0155740	99.9844260
Vienna PeeDee Belemnite (VPDB)	$^{13}\text{C}/^{12}\text{C}$	0.01117960	1.1056	98.8944

H and *L* denote *Heavy* and *Light* isotopes, respectively.

The carbon isotope composition ($\delta^{13}\text{C}$) for each sample is expressed relative to the Vienna PeeDee Belemnite (VPDB) international standard and is defined as:

$$\delta^{13}\text{C} = [((^{13}\text{C}/^{12}\text{C})_{\text{Sample}} \div 0.01117960) - 1] \times 1000 \quad (2)$$

And the hydrogen isotope composition (δD) for each sample is expressed relative to the Vienna Standard Mean Ocean Water (VSMOW) international standard and is defined as:

$$\delta\text{D} = [((^2\text{H}/^1\text{H})_{\text{Sample}} \div 0.00015576) - 1] \times 1000 \quad (3)$$

Multiplying by 1,000 allows the values to be expressed in parts per thousand (‰), commonly referred to as “per mil”, and to amplify small differences between samples and the standard. For

instance, a small difference of 1.0‰ between a sample and the standard becomes 10‰, whereas an apparently large value of 100‰ is only a 10% sample-to-standard difference. However, because percentage values have only slight differences in their absolute values, δ notation allows for the focusing in on meaningful differences between samples; as an example, if one sample has a $^{13}\text{C}/^{12}\text{C}$ composition of 1.0788‰ and another has a value of 1.0934‰, the significance of these values may not appear obvious. But, when these values are expressed on a $\delta / \text{‰}$ basis, the values become -35‰ and -22‰, respectively, relative to VPDB, and the significance of the differences between the two values becomes apparent (in fact, these are the average $\delta^{13}\text{C}$ values for C_3 and C_4 plants, respectively). Negative δ values indicate relatively less of the heavy isotope in a sample compared to a standard, which always have δ values of 0‰, while samples with more-positive δ values are relatively enriched in the heavy isotope. So, for our example above, we know that C_4 plants do not discriminate against ^{13}C as do C_3 plants, and therefore have enriched or more-positive $\delta^{13}\text{C}$ values. Therefore, values closer to 0‰ means that the ratio between heavy and light isotopes is more equivalent to the standard, rather than there being no light isotope present. Finally, the δ notation allows for mixing and fractionation calculations, as it can be converted to Heavy Atom % ($^{\text{H}}\text{AP}$) or Ratio notation (R) (Fry, 2006).

Isotope $\delta^{13}\text{C}$ and δD values were obtained at the Isotope Science Laboratory, Department of Geoscience, University of Calgary; this was the first time compound specific isotope analysis on leaf wax lipid biomarkers from terrestrial vegetation was conducted at the University. GC-IRMS was performed with a Thermo Scientific™ Trace GC IsoLink™. Both *n*-alkane and FAME $\delta^{13}\text{C}$ values were determined by converting samples to CO_2 using a combustion reactor set to 1,000°C, while δD values were calculated by converting organic H to H_2 using high temperature pyrolysis at 1,420°C. Each gas was then introduced to a Restek Rxi-1ms GC column (60 m length,

0.32 mm i.d. and 0.25 μm film) coupled to FinniganTM MAT 253 isotope ratio mass spectrometer which determines $^{13}\text{C}/^{12}\text{C}$ and D/H ratios of individual compounds by integrating beams of different mass signals (Hilkert et al., 1999). Samples, in Hexane, were injected in splitless mode with an inlet temperature set to 270°C. The column oven was programmed from an initial temperature of 40°C, directly ramped to 160°C at 24°C/min, then to 295°C at 5°C/min and held for 20.00 minutes, and finally to 330°C at 20°C/min and held for 5.00 minutes. Helium was used as the carrier gas and set at a constant flow of 1.9 mL/min.

The accuracy of the δ values were evaluated by routine measurement using external isotope standards of known $\delta^{13}\text{C}$ and δD values for both *n*-alkanes and fatty acid esters (*n*-Alkane Mixture B4 and Fatty Acid Ester Mixture F8-2, supplied by Arndt Schimmelmann, Biogeochemical Laboratories, University of Indiana), which were injected at the beginning and end of each sample set, or after every five injections for larger sets. These standard mixtures were also used for correction of carbon and hydrogen isotope values. For FAMEs, isotope values were also recorded daily for a C₄-C₂₄ even carbon saturated FAMEs standard (Supelco®) to monitor the overall state of the GC-IRMS. The standard deviation for the $\delta^{13}\text{C}$ of the CO₂ reference gas was $\leq 0.5\text{‰}$, while δD was evaluated relative to pulses of a CH₄ reference gas and the H₃⁺ factor (the contribution of H₃ species formed by ion/molecule reactions in the ion source (Carter and Barwick, 2011)) was calculated daily, having an average value of 6.01 ppm/nA, thus confirming the stability of the analytical system. (The isotope software automatically corrected for H₃ contributions using the H₃⁺ factor.)

During isotope analysis, complications with unresolved complex mixtures in the FLK-W samples made it difficult to measure hydrogen isotopes, while issues stemming from the IRMS sample injection syringe initially made the clays below Tuff IF samples appear as blanks. Although

many of the FLK-W *n*-alkane samples had UCMs that eluted in the early part of the chromatogram, they did not interfere with carbon isotope analysis. However, due to messy GC “baselines” associated with the UCM, only a few samples were successfully measured for δD and therefore proper paleo-hydrological conditions could not be ascertained. Fortunately, UCMs were not an issue with FAME sample sets, so this problem did not impede δD measurements beyond the FLK-W samples. When analysing the clays below Tuff IF samples, a second setback associated with the injector syringe caused initial concerns during $\delta^{13}C$ measurements. The syringe, which picks up solvent containing the organic samples and injects it into the IRMS, was set for 2.0 μL injections; this is then combusted in the inlet and gas chromatography ensues. However, with the clays below Tuff IF samples, the syringe was misaligned and not properly collecting the solvent from some of the GC vial inserts, thus resulting in blank analyses. Because this issue was sporadic and did not occur with every sample, samples were rerun on the GC-MS to confirm that the vials contained FAMES before being tested on the IRMS again. Once it was verified that FAMES remained in the sample vials and were not diminished due to repeated IRMS injections, they were retested on the IRMS. Unfortunately, the issue persisted until the GC vial inserts were slightly angled so that the syringe was not directly over the center of the vial inserts and picked up solvent from the edge of the inserts. Once realigned, all samples injected came back positive for FAMES and $\delta^{13}C$ and δD were successfully measured.

8.6.3 Standards

Several standards of known analytes and concentrations were used for the identification and quantification of *n*-alkanes and fatty acid methyl esters using GC-MS. Both the alkane (C_{21} - C_{40} , 40 $\mu g/mL$; C_{10} , C_{20} - C_{40} , 50 $\mu g/mL$; C_7 - C_{40} , 1,000 $\mu g/mL$ (Supelco®)) and FAME (C_4 - C_{24}

1,000 µg/mL; 37 Component FAME Mix, varied concentrations (Supelco®)) solutions were compared to extracted samples to quantify the concentration of lipids in Olduvai sediments (see Section 8.7.4). Hydrogen and carbon isotope ratio reference material (*n*-Alkane Mixture B4; Fatty Acid Ester Mixture F8-2 (Arndt Schimmelmann, Biogeochemical Laboratories, University of Indiana)) were used to measure δD and δ¹³C relative to VSMOW and VPDB, respectively.

8.7 Data Analysis

8.7.1 CPI

The carbon preference index (CPI) of *n*-alkanes is used to examine the odd-over-even carbon number predominance, which can be used to distinguish sedimentary organic matter deriving from terrestrial plants and that from bacterial or petroleum sources (Bray and Evans, 1961; Castañeda and Schouten, 2011; Diefendorf et al., 2011; Jaeschke et al., 2018), and as an indicator for hydrocarbon maturity (Duan and Xu, 2012). Alkanes deriving from land plants display carbon chains typically with CPI >5.0¹⁵, while petrogenic and marine inputs or mature samples are characterized by considerably lower CPI values of ≤1.0. The same principles apply to the *n*-alkanoic acids, except that they have an even-over-odd carbon number predominance. CPI values were calculated using the following formulas for *n*-alkanes and *n*-alkanoic acids:

$$\text{CPI}_{25-33} = \frac{1}{2} \times \left[\frac{C_{25} + C_{27} + C_{29} + C_{31} + C_{33}}{C_{24} + C_{26} + C_{28} + C_{30} + C_{32}} + \frac{C_{25} + C_{27} + C_{29} + C_{31} + C_{33}}{C_{26} + C_{28} + C_{30} + C_{32} + C_{34}} \right] \quad (4)$$

$$\text{CPI}_{24-32} = \frac{1}{2} \times \left[\frac{C_{24} + C_{26} + C_{28} + C_{30} + C_{32}}{C_{23} + C_{25} + C_{27} + C_{29} + C_{31}} + \frac{C_{24} + C_{26} + C_{28} + C_{30} + C_{32}}{C_{25} + C_{27} + C_{29} + C_{31} + C_{33}} \right] \quad (5)$$

¹⁵ Lower values have been reported in plants (e.g. Bush and McInerney, 2013), while the CPI for *n*-alkanoic acids and *n*-alkanes in sedimentary samples from West Turkana were 1.5–4.9 and 1.1–4.5, respectively (Uno et al., 2016).

8.7.2 ACL

Although CPI reflects the degree of plant wax preservation, the wide range observed in living plants precludes its use as a single metric on which to base sample integrity (Bush and McInerney, 2013). Therefore, it is often characterized alongside other hydrocarbon measures. The composition of *n*-alkanes and fatty acids are often compared using average chain length (ACL), or the weight-averaged number of carbon homologues in higher plant and sedimentary samples. ACL can be used (cautiously) as both a vegetation and climate proxy, as ACL values have been shown to be higher in C₄ grasses (Rommerskirchen et al., 2006) coinciding with more-positive δ¹³C values, while the mean δD values of *n*-alkanes decrease with increasing ACL value (Duan and Xu, 2012). Moreover, Wang and Liu (2012) found that for the C₁₆-C₃₂ fatty acids, terrigenous and aquatic plants have significantly different average chain lengths from algal sources, and Hughen et al. (2004), using C₂₄-C₂₈ fatty acids, identified higher ACL and more-positive δ¹³C values in sedimentary samples deposited during drier, cooler glacial periods. However, Bush and McInerney (2013) found that chain length could not distinguish graminoids from woody plants and that climate influences ACL values, but in indistinct or inconsistent ways. Additionally, Liu and Liu (2017) suggest that ACL for C₁₄-C₃₂ cannot be used to distinguish fatty acids originating from terrigenous and submerged plants but can be used to differentiate algal sources from plants. Furthermore, Liu and Liu showed that ACL cannot distinguish fatty acid sources deposited in lake sediments as algae and submerged and terrigenous plants have large chain length overlap. Nevertheless, average *n*-alkane chain lengths were calculated using the following equation:

$$\text{ACL}_{25-33} = \frac{25 \times C_{25} + 27 \times C_{27} + 29 \times C_{29} + 31 \times C_{31} + 33 \times C_{33}}{C_{25} + C_{27} + C_{29} + C_{31} + C_{33}} \quad (6)$$

Average FAME chain lengths were calculated using the following equations:

$$ACL_{20-34} = \frac{20 \times C_{20} + 22 \times C_{22} + 24 \times C_{24} + 26 \times C_{26} + 28 \times C_{28} + 30 \times C_{30} + 32 \times C_{32} + 34 \times C_{34}}{C_{20} + C_{22} + C_{24} + C_{26} + C_{28} + C_{30} + C_{32} + C_{34}} \quad (7)$$

$$ACL_{26-34} = \frac{26 \times C_{26} + 28 \times C_{28} + 30 \times C_{30} + 32 \times C_{32} + 34 \times C_{34}}{C_{26} + C_{28} + C_{30} + C_{32} + C_{34}} \quad (8)$$

Because of the difficulty in distinguishing fatty acid sources deposited in lake sediments, both ACL_{20-34} (for the entire fatty acid range) and ACL_{26-34} (for those from terrestrial vegetation) to see if there is an identifiable difference in using the two formulas.

8.7.3 Mixing

To estimate the contribution of C_3 and C_4 vegetation to sedimentary n -alkane $\delta^{13}C$, a leaf tissue n -alkane $\delta^{13}C$ database was compiled from published studies on living plants (Bi et al., 2005; Chikaraishi and Naraoka, 2003; Collister et al., 1994; Garcin et al., 2014; Kristen et al., 2010; Rommerskirchen et al., 2006; Vogts et al., 2009). Due to the distinct $\delta^{13}C$ signature of both C_3 and C_4 plants (Figure 8-22), mixing models that use plant $\delta^{13}C$ values allow for the estimation of the relative contribution of C_3 and C_4 vegetation sources to sedimentary carbon archives, whereby the C_{29} and C_{31} n -alkanes are used most often due to their abundance and ubiquity in both plant and sedimentary material.

A simple linear mixing model with two end-members representing C_3 and C_4 $\delta^{13}C$ values was used to reconstruct percent C_3 vs. C_4 paleo-landscape composition. However, this model assumes that the relative proportions of C_3 and C_4 leaf waxes are identical to the relative proportions of C_3 and C_4 plants; this is likely not the case, but biome-specific end-member values, which would produce a better estimate of the vegetation composition than global or pan-African

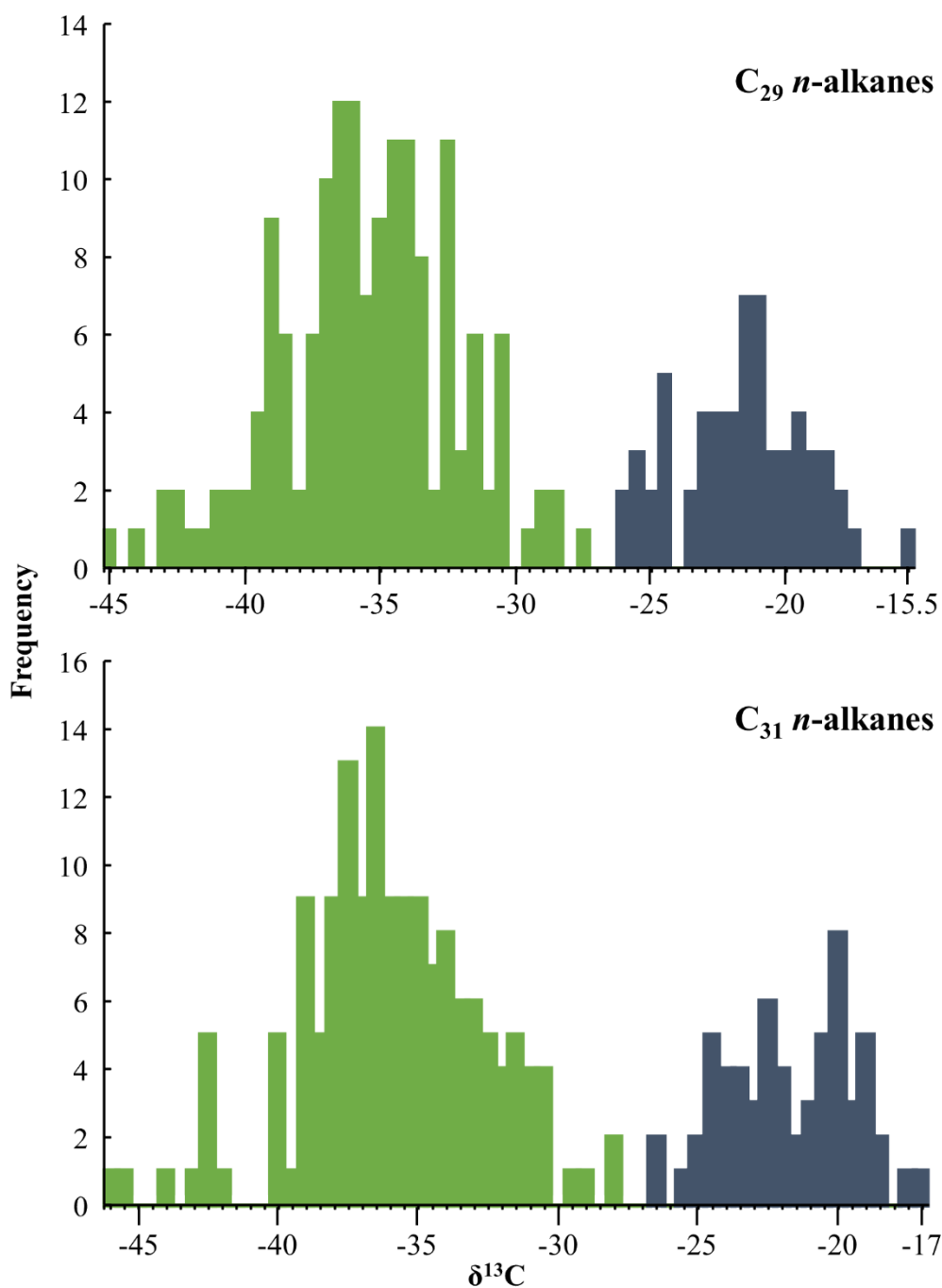
end-members, are relatively scarce for East Africa (Freier et al., 2010; Rommerskirchen et al., 2006; Vogts et al., 2009). Additionally, these values are based on individual plant species, some of which may be over/under represented in sedimentary $\delta^{13}\text{C}$ records due to differences in the total production of leaf wax lipids between species. Nevertheless, end-member values were calculated as the arithmetic mean of all plant species utilized in the published studies for each photosynthetic pathway (Figure 8-22).

The mean (end-member) values of C_{29} *n*-alkanes are -35.1‰ ($n=158$) and -21.2‰ ($n=59$) for C_3 and C_4 plants, respectively, and the mean of C_{31} *n*-alkanes are -35.4‰ ($n=156$) and -21.4‰ ($n=60$) for C_3 and C_4 plants, respectively. These mean end-member values were used in the following linear mixing model to estimate the contribution of C_3 and C_4 plants to Olduvai sedimentary records:

$$\% \text{C}_3 = (\delta_{\text{Sample}} - \delta_{\text{Source2}}) \div (\delta_{\text{Source1}} - \delta_{\text{Source2}}) \quad (9)$$

Where:

- δ_{Sample} represents the measured $\delta^{13}\text{C}$ of the C_{29} or C_{31} *n*-alkane (or C_{28} or C_{30} FAME)
- δ_{Source1} is the average $\delta^{13}\text{C}$ end member value of published C_3 plants
- δ_{Source2} is the average $\delta^{13}\text{C}$ end member value of published C_4 plants
- and $1 - \% \text{C}_3 = \% \text{C}_4$.



	Count		Average		Max.		Min.	
	C ₂₉	C ₃₁						
C ₃	158	156	-35.1	-35.4	-20.1*	-20.1*	-44.9	-45.9
C ₄	59	60	-21.2	-21.4	-15.3	-16.7	-25.8	-25.9

Figure 8-22. Histogram showing the distribution of *n*-alkane C₂₉ and C₃₁ δ¹³C values for C₃ (green) and C₄ (blue) plants. Most of the dataset (71%) comes from African plants, so the average (end-member) values do not change significantly when excluding non-African species; there is a 1.0‰ C₃ difference for *n*-alkane C₂₉ and no change for C₃₁ when excluding non-African species in the linear model. *Note that *Typha*, a C₃ plant, has δ¹³C values that fall within the C₄ range (-20.1‰); thus, *Typha* growing in paleo-wetlands could be falsely interpreted as a C₄ grassland.

A sine-squared model was also applied, as the relationship between C₃ and C₄ abundance is nonlinear (Cerling et al., 2011), and this model can be used to characterize small variations in % C₃, specifically when nearing minimum or maximum δ¹³C end-member values (Garcin et al., 2014). This equation has been used to determine the relative proportions of such factors as woody cover in particular regions (Cerling et al., 2011; Magill et al., 2013a), and is obtained by applying a sine-squared function to the linear model above:

$$\% C_3 = \sin \left[\frac{(\delta_{\text{Sample}} - \delta_{\text{Source2}})}{(\delta_{\text{Source1}} - \delta_{\text{Source2}})} \times \frac{\pi}{2} \right]^2 \quad (10)$$

Published δ¹³C data for C₂₈ and C₃₀ *n*-alkanoic acids from living plant material are inadequate in comparison to the abundant data for *n*-alkanes as detailed isotopic information of *n*-alkanoic acids in higher plants have not been explicitly examined. Thus, if we consider that *n*-alkanoic acids are depleted by -1.3‰ to -1.4‰ relative to the corresponding carbon-numbered *n*-alkanes, then the C₃₀ *n*-acid (corresponding to the C₂₉ *n*-alkane) would have average δ¹³C values of ~-36.5‰ and ~-22.6‰ for C₃ and C₄ plants, respectively. However, based on a small database (29 plants; 24 C₃, 5 C₄) compiled from Chikaraishi et al., (2004), Gao et al., (2015), and from this study, the δ¹³C average values for the C₃₀ *n*-acid are -37.43‰ and -21.43‰ for C₃ and C₄, respectively; a depletion of -0.93‰ for C₃ and enrichment of +1.17‰ for C₄ plants (the C₂₈ *n*-acid values are -36.45‰ and -22.04‰ for C₃ and C₄, respectively). These values are likely too depleted however, as Uno et al., (2016) determined a C₃ end-member value for the C₃₀ *n*-acid of -32.9‰ using modern δ¹³C values in soils collected from C₃ riparian forests along the Omo River in the Lower Omo Valley, Ethiopia. They also determined a C₄ value for the C₃₀ *n*-acid of -22.7‰ from

modern soils collected from C₄-dominated ecosystems in the Lower Omo Valley, but used an end-member value of -19‰ after Tipple and Pagani (2010). These values, determined from soils and not plants directly, speak to the uncertainty in using plant end-member values when reconstructing C₃ vs. C₄ paleo-landscapes.

Finally, as modern δ¹³C values of *n*-alkanes and *n*-acids were used to derive ancient end-member values for C₃ and C₄ plants for paleo-landscape composition, end-member values were also adjusted by +1.5‰ to correct for variations between modern (-8.0‰) and Pleistocene (-6.5‰) atmospheric δ¹³C associated with the ¹³C Suess effect (Garcin et al., 2014; Tipple et al., 2010).

8.7.4 Quantification

Leaf wax lipid biomarkers were quantified by comparing chromatogram peak areas of individual *n*-alkanes and FAMES with an external standard (Section 8.6.3) containing individual compounds of known concentrations to estimate the concentration for each biomarker sample. A single point external calibration was determined by analyzing standards using GC-MS to first calculate a Response Factor based on GC peak area (Equation 11), and then using the Response Factor to calculate concentration of sample analytes (Equation 12):

$$\text{Response Factor} = \frac{\text{Standard Peak Area}}{\text{Concentration Amount}} \quad (11)$$

$$\text{Analyte Concentration} = \frac{\text{Analyte Peak Area}}{\text{Response Factor}} \quad (12)$$

The single point external calibration assumes analyte response to be linear over a range of concentrations, and any error in the determination of Response Factor extends into the concentration calculation of target analytes. This is not an issue with the *n*-alkane standard as it extends to C₄₀ while target analytes max at C₃₃ (and occasionally C₃₅) so each compound can be

compared individually but is problematic when using the FAME standard which only has a range up to C₂₄ while target analytes extend to C₃₂ (and occasionally C₃₄). Therefore, a multipoint external calibration method was also applied whereby different concentrations of individual standard compounds (e.g. C₂₉ at 50, 100, and 500 µg/µL) were averaged to create a mean response factor which was then used in Equation 12. This was then compared to a linear least squares calibration curve as GC response was variable.

8.7.5 Modern H-isotopes from Precipitation

The δD values of the *n*-alkanes and FAMES were compared to modern δD values of meteoric water obtained from the International Atomic Energy Agency Global Network of Isotopes in Precipitation database (IAEA-GNIP) (IAEA/WMO, 2015) using measurement stations nearby Olduvai Gorge; Dar es Salaam, Tanzania, and Kericho and Nairobi, Kenya (Fig. 8-23). Additionally, the Online Isotope Precipitation Calculator (Bowen et al., 2005), which uses the GNIP database and interpolation algorithms, was used for Olduvai Gorge where no monthly δD values exist (Table 8-12). This information, when used in comparison with the *n*-alkane and FAME data from Olduvai paleo-sediments,

can be used to estimate paleo-precipitation δD values or amounts by using the biosynthetic apparent fractionation (Konecky et al., 2011) between precipitation and the C_{28} *n*-acid or C_{29} *n*-alkane and leaf wax δD values from modern plants and topsoil from the greater Ngorongoro Conservation Area. However, this assumes consistent precipitation patterns and source δD through time, which is likely inaccurate.

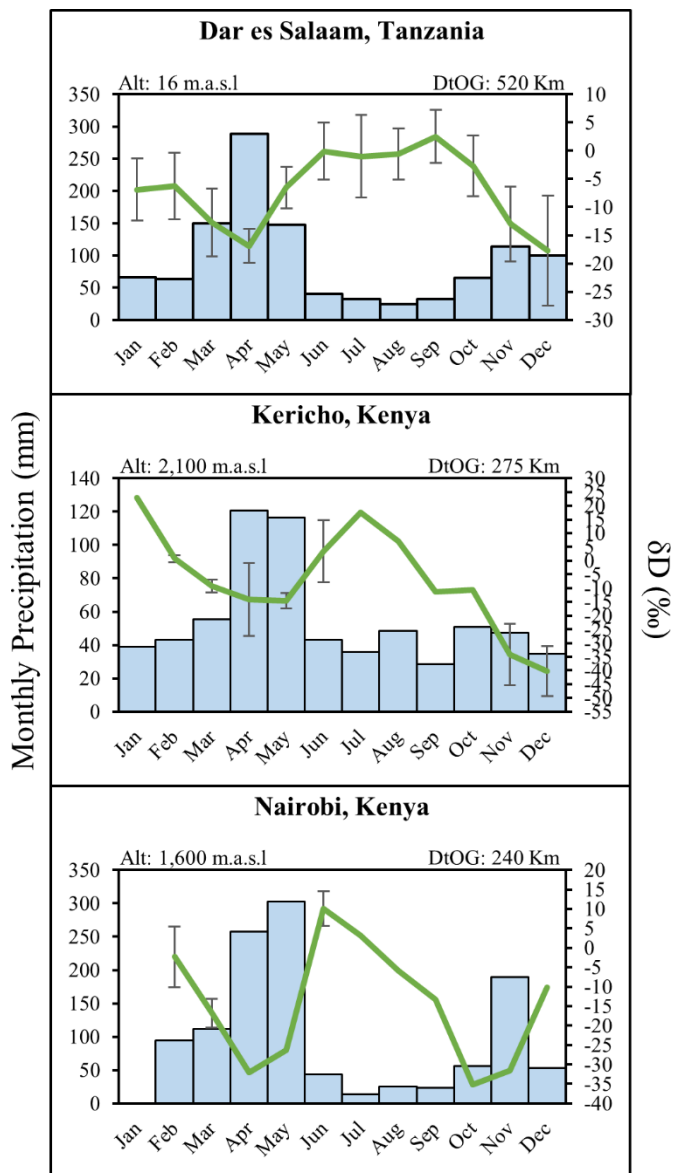


Figure 8-23. Monthly precipitation data in relation to precipitation δD (‰, VSMOW) for three East African measurement stations near Olduvai Gorge. Data retrieved from GNIP. “DtOG”: Distance to Olduvai Gorge.

Table 8-12. Monthly δD estimates for Olduvai Gorge using the Online Isotopes in Precipitation Calculator. More-positive values occur during the dry seasons.

δD (‰, VSMOW)	Jan	Feb	Mar	Apr	May	Jun
	5.0	13	-7.0	-7.0	-13	5
	Jul	Aug	Sept	Oct	Nov	Dec
	5.0	12	-2.0	-8.0	-9	0.0

8.7.6 FAME Corrections

Corrections were made on the fatty acid methyl esters to remove the isotopic contribution from the methyl group added during methylation using the following formulas for carbon and hydrogen:

$$\delta^{13}C_{FA} = \frac{(n + 1) \times \delta^{13}C_{FAME} - -25.48}{n} \quad (13)$$

Where:

- $\delta^{13}C_{FA}$ represents the $\delta^{13}C$ of the given FA prior to methylation
- $\delta^{13}C_{FAME}$ is the $\delta^{13}C$ value of the measured FAME
- -25.48 (± 0.08) is the $\delta^{13}C$ of the methanol used for preparation of the FAME
- n is the number of carbon atoms in the (non-methylated) fatty acid.

$$\delta D_{FA} = \frac{(2n + 2) \times \delta D_{FAME} - -102.5 \times 3}{2n - 1} \quad (14)$$

Where:

- δD_{FA} represents the δD of the given FA prior to methylation
- δD_{FAME} is the δD value of the measured FAME
- -102.5 (± 1.84) is the δD of the methanol used for preparation of the FAME
- n is the number of carbon molecules in the (non-methylated) fatty acid.

8.8 Methods Summary

The following outlines the most reliable protocol for obtaining $\delta^{13}\text{C}$ and δD from *n*-alkanes and *n*-alkanoic acids. Total Lipid Extracts (TLEs) were recovered using the Soxhlet extraction technique. Pre-cleaned extraction thimbles were filled with ~40 g of sediment and extracted with 200 mL of 9:1 DCM:MeOH into 250 mL flat-bottom flasks. Extractors were placed on a hot plate set to 40° to bring solvent to vaporization and samples were extracted continuously over a period of 72 hours. TLEs were evaporated to dryness using a steady stream of N₂ gas.

The TLEs were first separated on Aminopropyl columns with neutral, acid, and polar fractions eluted with 4.0 mL each of DCM:Isopropanol, Acetic Acid in Diethyl Ether, and Methanol, respectively. All fractions were evaporated to dryness using a steady flow of N₂ gas. The neutral fraction was then eluted over a column consisting of 0.5 g silver nitrate impregnated silica gel and 0.5 silica gel with Hexane and DCM; the *n*-alkanes were recovered in the Hexane fraction. The acid fraction was converted to Fatty Acid Methyl Esters (FAMES) through methylation by adding 1.0 mL of 2% HCl in Methanol, vortex mixing for 10 seconds, and storing in an oven set to 50°C for 20-24 hours. To isolate the FAMES from the solution, 1.0 mL of 5.0% aqueous NaCl and 1.0 mL Hexane were added, shaken for 5.0 seconds and vortexed for 20 seconds. The mixture was then left to settle for ~30 seconds until the two phases (water and Hexane) separated due to differences in density. The Hexane portion was pipetted into a separate vial and the process (adding and pipetting Hexane) was repeated three times. The Hexane containing FAMES was then evaporated with a steady stream of N₂ gas. The FAMES were eluted over a column consisting of 0.5 g silver nitrate impregnated silica gel and 0.5 silica gel with Hexane and DCM; the FAMES were recovered in the DCM fraction. Both *n*-alkanes and FAMES were reconstituted in Hexane and analyzed with GC-MS and IRMS.

CHAPTER 9: RESULTS

9.1 GC-MS Compound Quantitation

In order to quantify compounds with GC-MS, peak areas from individual sedimentary derived *n*-alkyl compounds were compared with external standards (containing C₂₅, C₂₇, C₂₉ or C₂₀, C₂₂, C₂₄) of known concentrations to calculate the *n*-alkane and *n*-alkanoic acid concentration for each sample. For the *n*-alkanes, the C₂₁-C₃₅ homologues were analyzed, while the C₂₀-C₃₄ homologues were studied for the *n*-alkanoic acids (as FAMES). Because each series covers large carbon chain ranges, they likely contain compounds deriving from aquatic or emergent plants in addition to terrestrial vegetation. Therefore, more-limited ranges are also presented to see whether it is possible to distinguish specific lipid producing sources in the Olduvai depositional environments. Because the C₂₇ to C₃₅ *n*-alkanes are major constituents of plant leaf waxes (Eglinton and Hamilton, 1967), homologue ranges were subdivided into C₂₅-C₃₃, C₂₅-C₃₅, C₂₇-C₃₃, and C₂₇-C₃₅. The *n*-acids were subdivided into C₂₄-C₃₂, C₂₄-C₃₄, C₂₆-C₃₂, and C₂₆-C₃₄. These ranges were used to determine if the different groupings had a significant impact on the interpretation of the distribution of *n*-alkyl lipids found in paleo-sediments.

The carbon preference index (CPI) of *n*-alkanes or *n*-alkanoic acids is used to examine the odd-over-even or even-over-odd carbon number predominance, respectively, which may distinguish sedimentary organic matter deriving from terrestrial plants from that of bacterial or petroleum sources (Bray and Evans, 1961; Castañeda and Schouten, 2011; Diefendorf et al., 2011; Jaeschke et al., 2018), or as an indicator for hydrocarbon maturity (Duan and Xu, 2012). Although CPI has a wide range in plants (0.4 to 99), values greater than or equal to 1.0 indicate an odd-over-even or even-over-odd predominance (Bush and McInerney, 2013). For soils, *n*-alkane CPI values

collected from a 2,700 km transect through the central USA from Minnesota to Texas ranged between 2.4 and 10.0 (Bush and McInerney, 2015); a much narrower range. CPI was therefore used to determine level of maturity or (bio)degradation of sedimentary lipids with values ≤ 1.0 indicating greater overall hydrocarbon degradation.

Though it has been shown that submerged and terrigenous plants have large chain length overlap (Liu and Liu, 2017), average chain length (ACL) is also reported for the weight-averaged number of carbon homologues in sedimentary samples. ACL was subdivided into two separate categories for each *n*-alkyl lipid, with the C₂₁-C₃₅ and C₂₀-C₃₄ homologues used for the *n*-alkanes and *n*-acids, respectively, but also C₂₅-C₃₅ (*n*-alkanes) and C₂₆-C₃₂ (*n*-acids) as terrestrial vegetation generally contain greater abundances of the higher carbon compounds.

9.1.1 FLK-N

The distribution of *n*-alkanoic acids in the Frida Leakey Korongo North (FLK-N) samples range from C₂₀ to C₃₄ and display an obvious even-over-odd predominance, specifically in compounds $>C_{26}$. Concentrations for individual *n*-acids range from 0.0 to 22.83 $\mu\text{g/g}$ of dry sediment, with an average value of 4.27 $\mu\text{g/g}$ (Appendix A). CPI values in this sample subset were 3.03-3.67 with an average of 3.37 ± 0.08 (CPI₂₀₋₃₄); 2.60-3.27 with an average of 2.93 ± 0.09 (CPI₂₄₋₃₂); 2.63-3.32 with an average of 2.96 ± 0.10 (CPI₂₄₋₃₄); 3.06-4.31 with an average of 3.64 ± 0.17 (CPI₂₆₋₃₂); and 3.11-4.40 with an average of 3.70 ± 0.17 (CPI₂₆₋₃₄) (Table 9-1). These values, regardless of chain length subcategory, indicate that these compounds derived from terrestrial plant leaf waxes and do not exhibit (bio)degradation. ACL spans from 24.64-24.97 with an average of 24.77 ± 0.05 (ACL₂₀₋₃₄), and 28.48-28.63 with an average of 28.55 ± 0.02 (ACL₂₆₋₃₂). The lower ACL from the 20-34 category results from abundant C₂₂ in all samples. The distributions and

abundances of *n*-acids in FLK-N Trench 7 are shown as histograms in Fig. 9-1. The carbon number with the maximum abundance in all samples is C₂₂, followed by C₂₈, C₂₄, and the C₃₀.

Table 9-1. Carbon Preference Index and Average Chain Length for FLK-N Trench 7 *n*-alkanoic acids.

		<i>n</i> -Alkanoic Acids						
Sample	Depth (cm)	CPI ₂₀₋₃₄	CPI ₂₄₋₃₂	CPI ₂₄₋₃₄	CPI ₂₆₋₃₂	CPI ₂₆₋₃₄	ACL ₂₀₋₃₄	ACL ₂₆₋₃₂
8	0-5	3.17	2.67	2.70	3.21	3.25	24.64	28.54
7	5-10	3.63	3.24	3.29	4.13	4.21	24.88	28.59
6	10-15	3.13	2.65	2.67	3.16	3.19	24.65	28.59
5	15-20	3.49	3.03	3.06	3.85	3.91	24.67	28.56
4	20-25	3.03	2.60	2.63	3.06	3.11	24.97	28.50
3	25-30	3.42	2.92	2.96	3.50	3.56	24.90	28.48
2	30-35	3.67	3.27	3.32	4.31	4.40	24.67	28.63
1	35-40	3.41	3.04	3.08	3.88	3.94	24.77	28.48

n-Alkanoic Acids

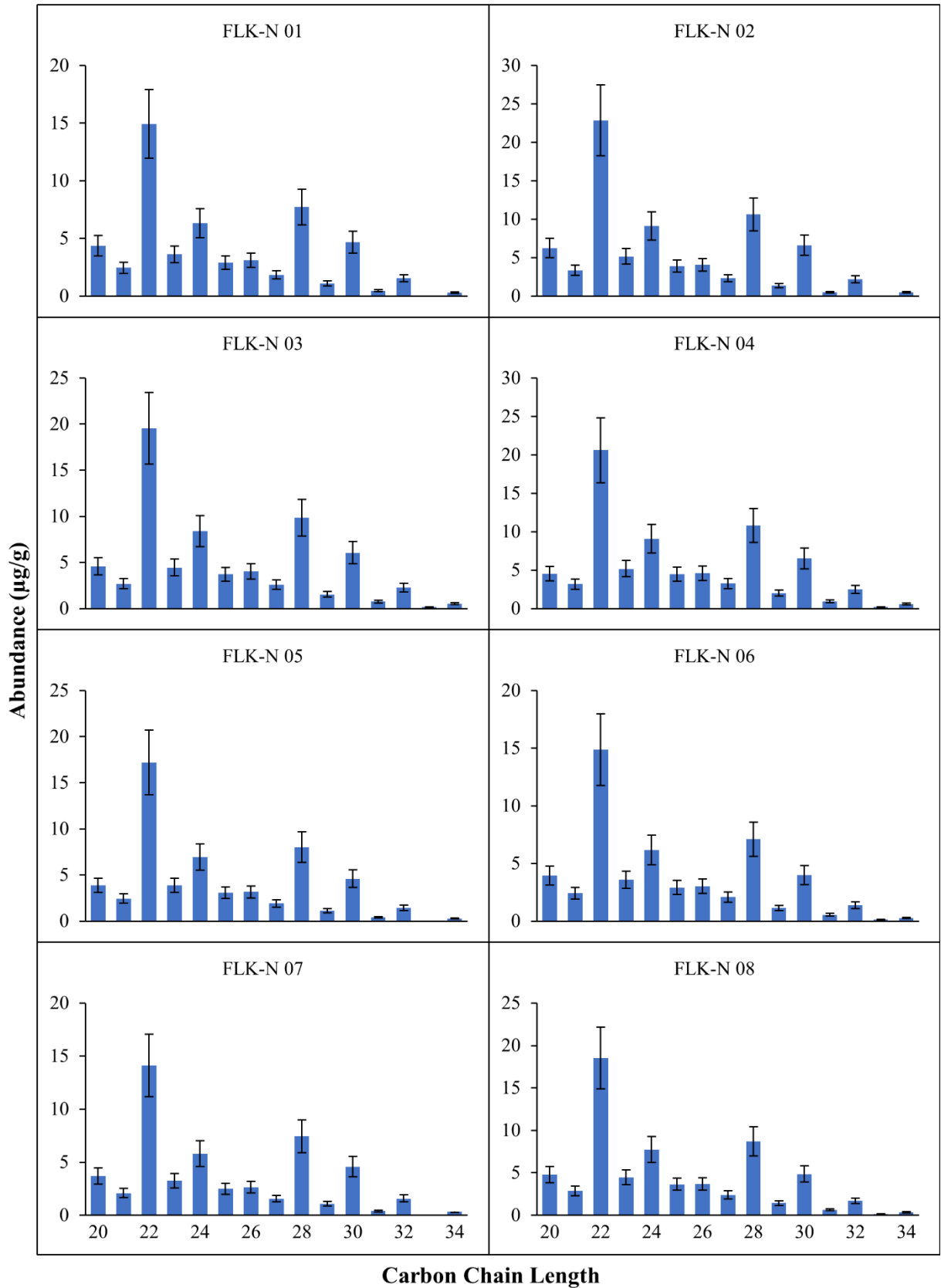


Figure 9-1. Homologue distribution and abundances (µg/gdw) of *n*-alkanoic acids from FLK-N Trench 7.

9.1.2 Clays Below Tuff IF

The distribution of *n*-alkanoic acids in the clays below Tuff IF samples range from C₂₀ to C₃₄ and for the most part, display an even-over-odd predominance; however, Tuff IF 02 does not have a characteristic even-over-odd pattern such as in Tuff IF 01 for example (Fig. 9-2A). Concentrations for individual *n*-acids range from 0.0 to 55.79 µg/g of dry sediment, with an average value of 3.11 µg/g (Appendix A). CPI values in this sample subset were 1.46-4.83 with an average of 3.02 ± 0.19 (CPI₂₀₋₃₄); 1.36-4.59 with an average of 2.73 ± 0.19 (CPI₂₄₋₃₂); 1.38-4.59 with an average of 2.75 ± 0.19 (CPI₂₄₋₃₄); 1.37-4.89 with an average of 2.87 ± 0.21 (CPI₂₆₋₃₂); and 1.40-4.89 with an average of 2.89 ± 0.21 (CPI₂₆₋₃₄) (Table 9-2). Of the 30 Tuff IF samples, only six had CPI values <2.0, and of these, only one sample (Tuff IF 02) had a CPI <1.5 (though still >1.0). Therefore, although some of these values were low, most of the samples have CPI scores indicative of terrestrial plant leaf waxes that have not been significantly (bio)degraded. Furthermore, the extent of deviation among CPI between carbon chain length subcategory is small, with the largest deviation being 0.61 (variance of 0.37) for samples 25 and 26. Tuff IF 25 was one of the poorest samples in terms of preservation, as carbon compounds C₂₁, C₂₃-C₂₇, and C₃₁-C₃₄ were not detected through GC-MS. Sample 26 on the other hand, was one of the best preserved and had a total C₂₀-C₃₄ concentration of 127.67 µg/g of dry sediment; the deviation may be due to a maximum abundance at C₂₂ but a greater even-over-odd predominance from C₂₆-C₃₄ (CPI 4.47). ACL spans from 24.14-29.44 with an average of 27.44 ± 0.27 (ACL₂₀₋₃₄), and 28.13-30.15 with an average of 29.11 ± 0.08 (ACL₂₆₋₃₂).

The distribution of *n*-alkanes in the clays below Tuff IF samples range from C₂₁ to C₃₅ but most samples only have detectable compounds in the C₂₅-C₃₃ range. All samples, apart from those with concentrations too low to detect on the GC-MS, display an odd-over-even carbon number

preference (Figs. 9-2A-E). Concentrations for individual *n*-alkanes range from 0.0 to 24.61 $\mu\text{g/g}$ of dry sediment, with an average value of 1.15 $\mu\text{g/g}$; lower than the *n*-alkanoic acids. CPI values in this sample subset were 3.69-28.58 with an average of 12.68 ± 1.73 (CPI₂₁₋₃₅); 3.96-26.63 with an average of 12.45 ± 1.64 (CPI₂₅₋₃₃); 4.26-28.58 with an average of 12.82 ± 1.70 (CPI₂₅₋₃₅); 4.09-26.63 with an average of 12.85 ± 1.62 (CPI₂₇₋₃₃); and 4.43-28.58 with an average of 13.27 ± 1.69 (CPI₂₇₋₃₅) (Table 9-2). All samples had CPI >3.0, indicating that they derive from terrestrial plant leaf waxes that have not been (bio)degraded. Five samples (09, 13, 14, 19, and 23) had Unresolved Complex Mixtures, but these were small and did not interfere with compound identification or quantification. The extent of deviation amongst the CPI for the *n*-alkanes between carbon chain length subcategory is small, apart from samples Tuff IF 01, which has the largest variation of 2.40 (variance of 5.74), Tuff IF 10, which has a deviation of 1.12 (variance of 1.26), and Tuff IF 27, which has a deviation of 1.13 (variance of 1.27). This may be due in part to the odd numbered carbon compounds >28 not being detected by the GC-MS. ACL spans from 29.45-32.01 with an average of 30.85 ± 0.12 (ACL₂₁₋₃₅), and 30.02-32.01 with an average of 31.00 ± 0.08 (ACL₂₇₋₃₃).

The distributions and abundances of *n*-acids and *n*-alkanes in the clays below Tuff IF are shown as histograms in Figs. 9-2A-G. Most samples have the C₂₈ *n*-acid as the most abundant compound (52%), but C₃₂ is the most abundant in 22% of the samples. When C₂₈ is the most prolific, the C₃₀ acid is the second most dominant homologue (50%), followed by C₃₂ (71%) as the third most dominant, and then C₂₆ (100%) as the fourth. For the *n*-alkanes, 91% of the samples had C₃₁ as the most abundant component, while two samples had C₃₃. C₃₃ was always the second most abundant compound after C₃₁, except for one sample (Tuff IF 20) that had C₂₉ as the second richest homologue.

Table 9-2. Carbon Preference Index and Average Chain Length for Clays Below Tuff IF *n*-alkanes and *n*-alkanoic acids.

Sample	<i>n</i> -Alkanes										<i>n</i> -Alkanoic Acids									
	CPI ₂₁₋₃₅	CPI ₂₅₋₃₃	CPI ₂₅₋₃₅	CPI ₂₇₋₃₃	CPI ₂₇₋₃₅	ACL ₂₁₋₃₅	ACL ₂₇₋₃₃	CPI ₂₀₋₃₄	CPI ₂₄₋₃₂	CPI ₂₄₋₃₄	CPI ₂₆₋₃₂	CPI ₂₆₋₃₄	ACL ₂₀₋₃₄	ACL ₂₆₋₃₂						
01	12.77	12.77	12.77	17.15	17.15	30.55	31.05	3.70	3.72	3.77	3.86	3.91	27.83	28.96						
02	7.73	7.38	7.73	8.47	8.88	31.08	31.08	1.46	1.36	1.38	1.37	1.40	28.02	29.00						
03	4.86	5.26	5.26	6.16	6.16	30.47	30.69	1.80	1.68	1.70	1.67	1.70	29.16	29.64						
04								3.77	2.94	2.94	3.73	3.73	24.14	28.50						
05	18.23	18.23	18.23			29.45	30.55	3.88	3.67	3.79	3.94	4.09	27.72	28.79						
06						30.47	30.79	4.83	4.59	4.59	4.89	4.89	27.24	28.74						
07	13.39	13.39	13.39	13.39	13.39	30.89	30.89	2.11	1.79	1.79	1.84	1.84	26.98	29.35						
08	24.22	24.22	24.22	24.22	24.22	30.95	30.95	2.63	2.27	2.27	2.29	2.29	26.62	29.19						
09						31.69	31.29	2.12	1.95	1.77	1.87	1.69	26.74	28.99						
10	21.09	19.04	21.09	19.04	21.09	31.93	31.60	1.54	1.42	1.45	1.41	1.45	29.08	29.60						
11						30.39	30.65	2.83	2.73	2.76	2.88	2.93	27.84	28.90						
12	23.81	23.81	23.81	22.91	22.91	30.71	30.94	2.94	2.72	2.74	2.79	2.82	27.38	28.97						
13	3.69	4.18	4.46	4.84	5.18	30.21	31.02	1.75	1.64	1.70	1.64	1.70	29.43	29.80						
14	4.26	3.96	4.26	4.09	4.43	30.76	30.95	1.68	1.55	1.61	1.54	1.61	28.81	29.42						
15						32.01	32.01	3.77	3.32	3.36	4.07	4.14	24.81	28.63						

Table 9-2 cont. Carbon Preference Index and Average Chain Length for Clays Below Tuff IF *n*-alkanes and *n*-alkanoic acids.

Sample	<i>n</i> -Alkanes										<i>n</i> -Alkanoic Acids											
	CPI ₂₁₋₃₅	CPI ₂₅₋₃₃	CPI ₂₅₋₃₅	CPI ₂₇₋₃₃	CPI ₂₇₋₃₅	ACL ₂₁₋₃₅	ACL ₂₇₋₃₃	CPI ₂₀₋₃₄	CPI ₂₄₋₃₂	CPI ₂₄₋₃₄	CPI ₂₆₋₃₂	CPI ₂₆₋₃₄	ACL ₂₆₋₃₂	ACL ₂₆₋₃₄	CPI ₂₀₋₃₄	CPI ₂₄₋₃₂	CPI ₂₄₋₃₄	CPI ₂₆₋₃₂	CPI ₂₆₋₃₄	ACL ₂₆₋₃₂	ACL ₂₆₋₃₄	
16	6.09	6.01	6.28	6.73	7.05	30.68	31.06	3.99	3.80	3.84	3.78	3.84	28.11	29.31	3.99	3.80	3.84	3.78	3.84	28.11	29.31	
17	4.57	4.57	4.57	5.65	5.65	31.01	31.01	2.04	1.83	1.87	1.77	1.83	29.37	30.15	2.04	1.83	1.87	1.77	1.83	29.37	30.15	
18	15.24	14.58	15.24	14.06	14.71	31.19	31.25	3.83	3.47	3.52	3.52	3.58	28.44	29.52	3.83	3.47	3.52	3.52	3.58	28.44	29.52	
19	28.58	26.63	28.58	26.63	28.58	31.70	31.46	4.45	4.44	4.43	4.54	4.54	27.70	29.12	4.45	4.44	4.43	4.54	4.54	27.70	29.12	
20	13.52	13.25	13.52	13.97	14.26	30.41	30.43	3.11	3.03	3.06	3.10	3.14	29.44	29.68	3.11	3.03	3.06	3.10	3.14	29.44	29.68	
21						31.09	31.09	1.89	1.81	1.83	1.81	1.85	27.39	28.88	1.89	1.81	1.83	1.81	1.85	27.39	28.88	
22	7.36	7.63	7.63	8.49	8.49	31.17	31.39	1.63	1.61	1.65	1.65	1.71	28.07	29.03	1.63	1.61	1.65	1.65	1.71	28.07	29.03	
23						29.59	30.22	4.36	3.36	3.36	3.27	3.27	26.43	28.90	4.36	3.36	3.36	3.27	3.27	26.43	28.90	
24						31.96	31.96	2.56	1.58	1.58	1.48	1.48	25.10	28.95	2.56	1.58	1.58	1.48	1.48	25.10	28.95	
25						31.00	31.00	3.82	2.46	2.46	2.46	2.46	26.13	28.99	3.82	2.46	2.46	2.46	2.46	26.13	28.99	
26						30.02	30.02	3.66	3.26	3.26	4.47	4.47	24.45	28.53	3.66	3.26	3.26	4.47	4.47	24.45	28.53	
27	9.05	9.62	9.85	11.34	11.63	30.71	30.78	3.47	3.19	3.22	3.23	3.27	28.23	29.37	3.47	3.19	3.22	3.23	3.27	28.23	29.37	
28	8.89	8.98	9.26	9.86	10.18	30.63	30.98	4.10	4.24	4.22	4.28	4.27	28.62	29.18	4.10	4.24	4.22	4.28	4.27	28.62	29.18	
29																						
30	13.51	13.02	13.51	14.29	14.82	31.01	30.86	3.86	3.80	3.83	3.99	4.03	25.58	28.13	3.86	3.80	3.83	3.99	4.03	25.58	28.13	

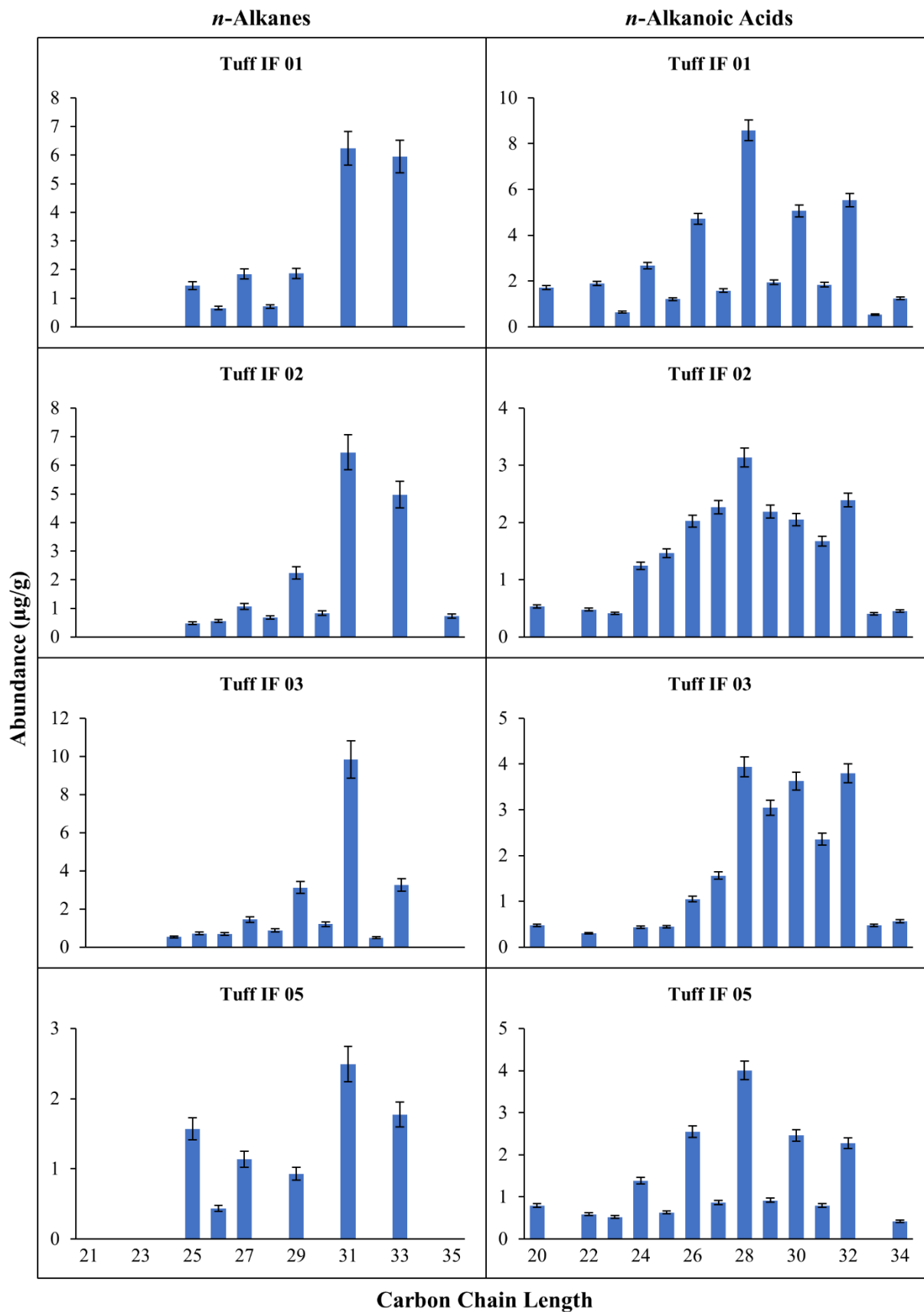


Figure 9-2A. Homologue distribution and abundances ($\mu\text{g/gdw}$) of *n*-alkanes and *n*-alkanoic acids from the clays below Tuff IF.

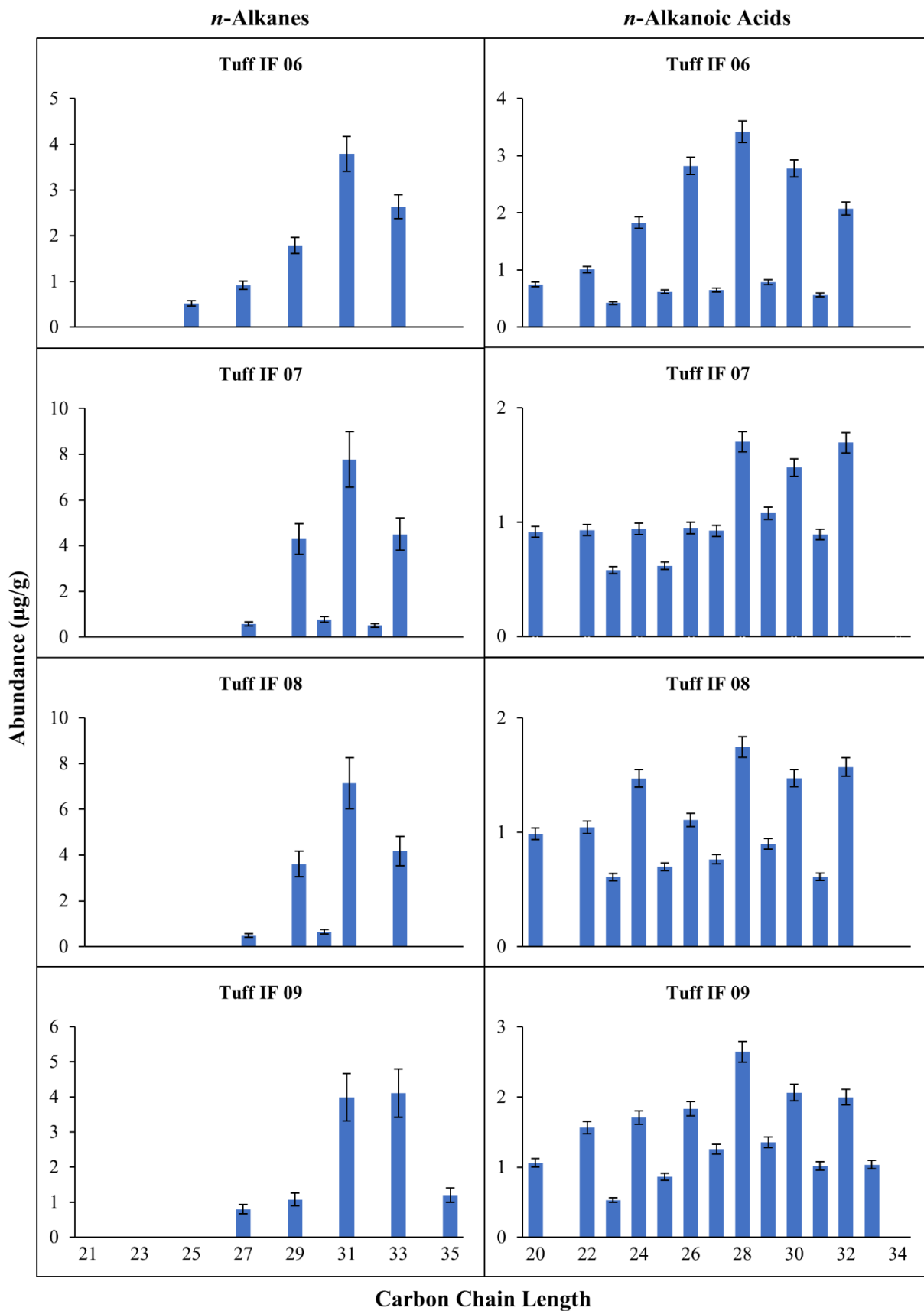


Figure 9-2B. Homologue distribution and abundances ($\mu\text{g/gdw}$) of *n*-alkanes and *n*-alkanoic acids from the clays below Tuff IF.

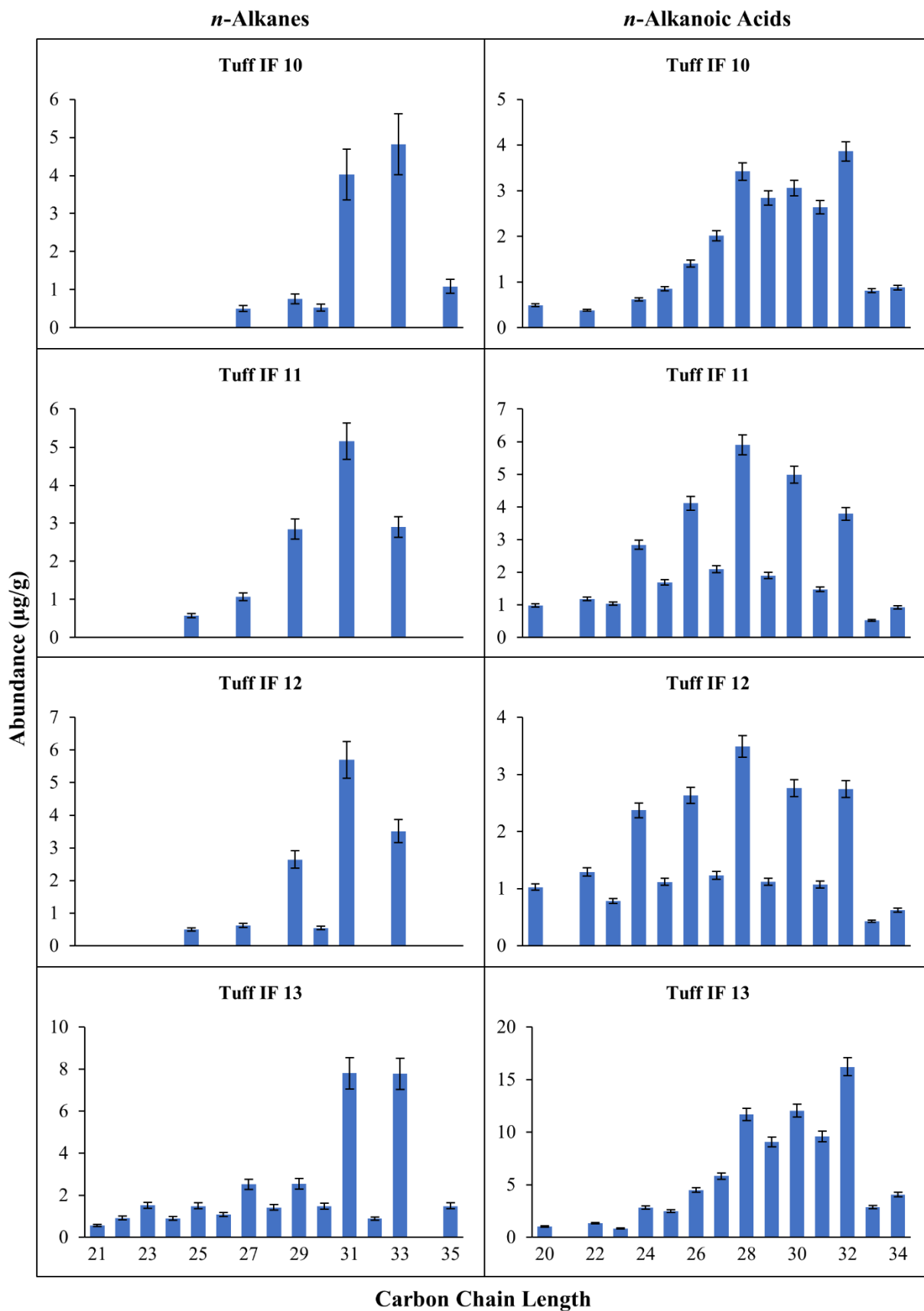


Figure 9-2C. Homologue distribution and abundances ($\mu\text{g/gdw}$) of *n*-alkanes and *n*-alkanoic acids from the clays below Tuff IF.

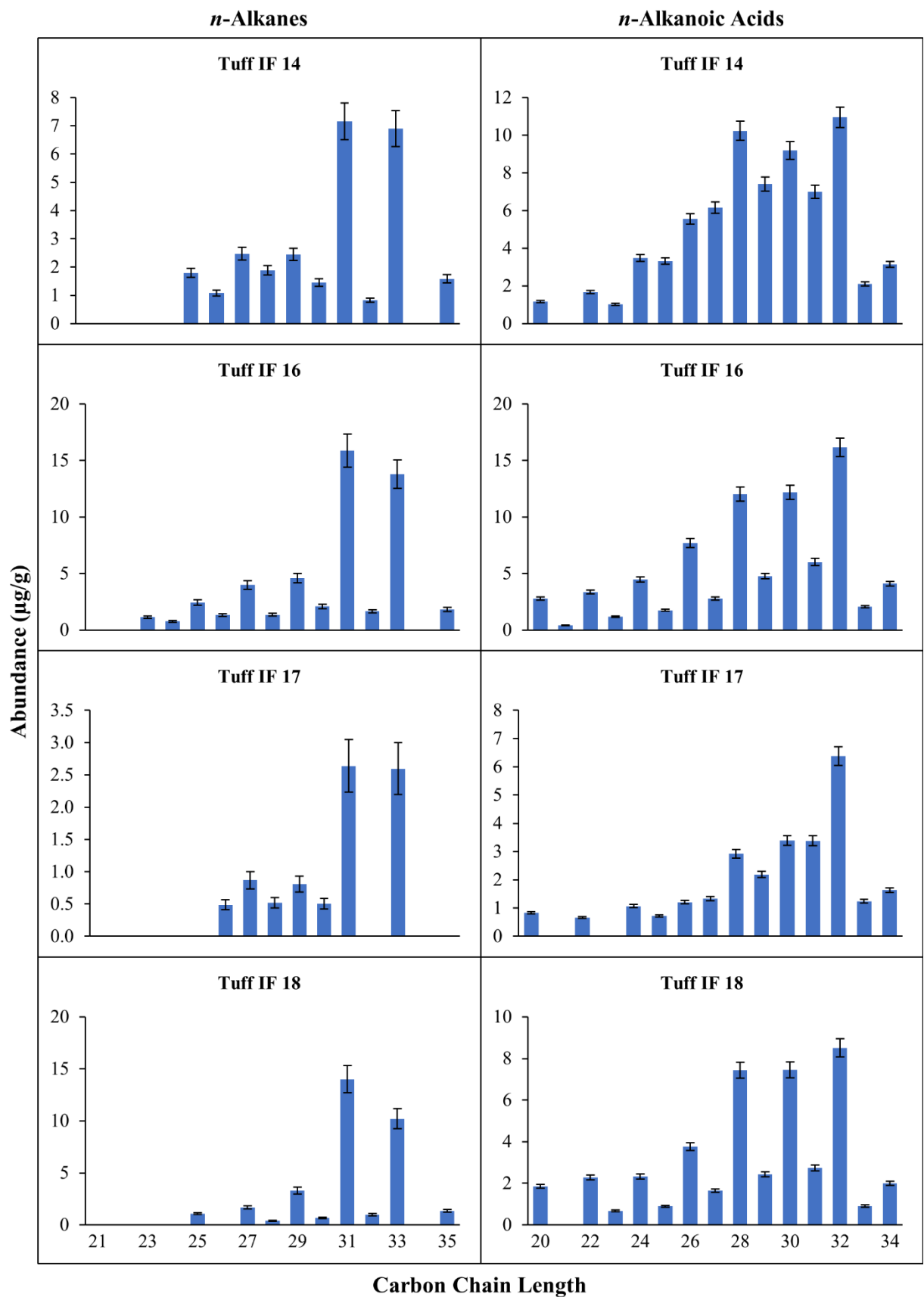


Figure 9-2D. Homologue distribution and abundances ($\mu\text{g/gdw}$) of *n*-alkanes and *n*-alkanoic acids from the clays below Tuff IF.

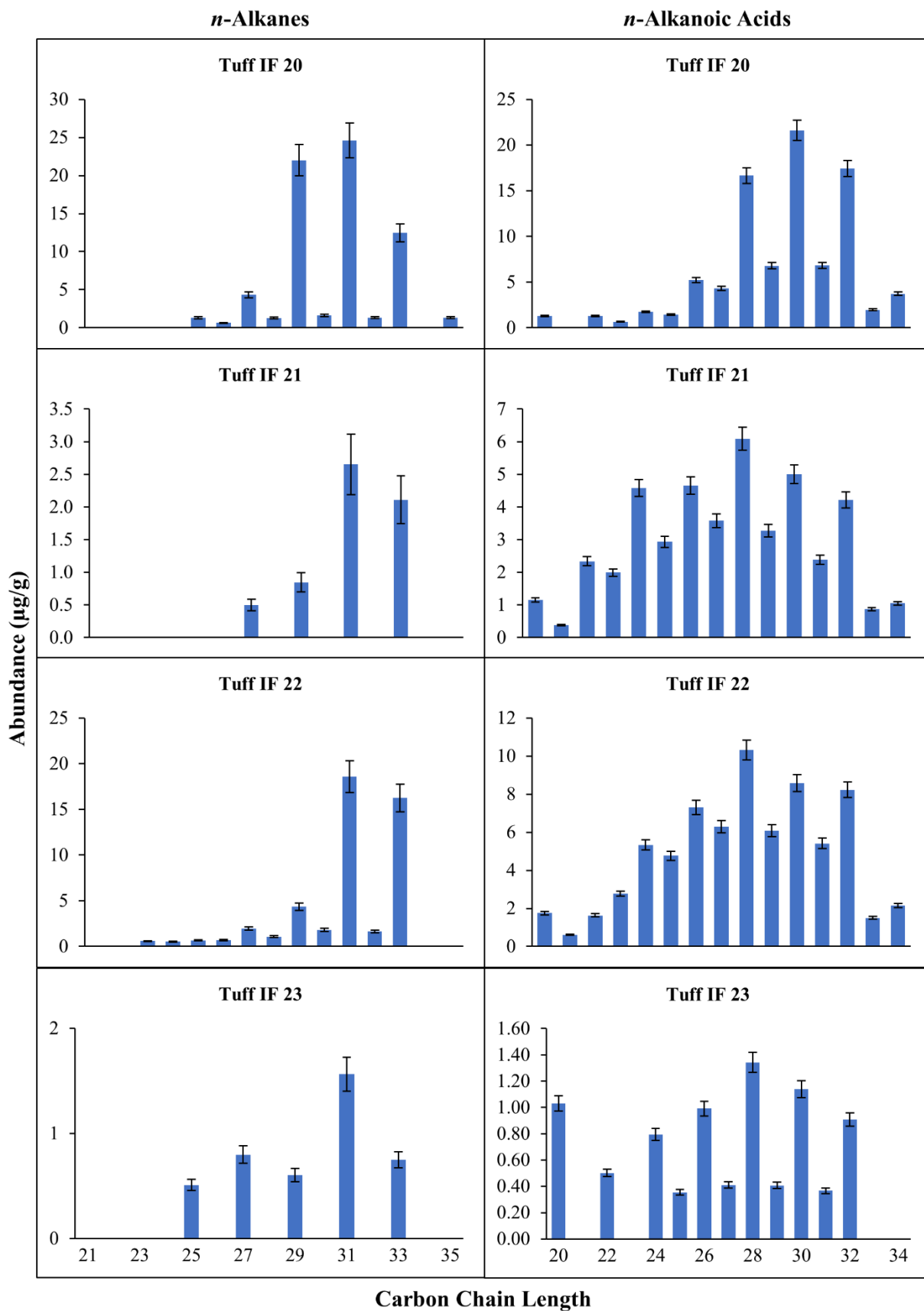


Figure 9-2E. Homologue distribution and abundances ($\mu\text{g/gdw}$) of *n*-alkanes and *n*-alkanoic acids from the clays below Tuff IF.

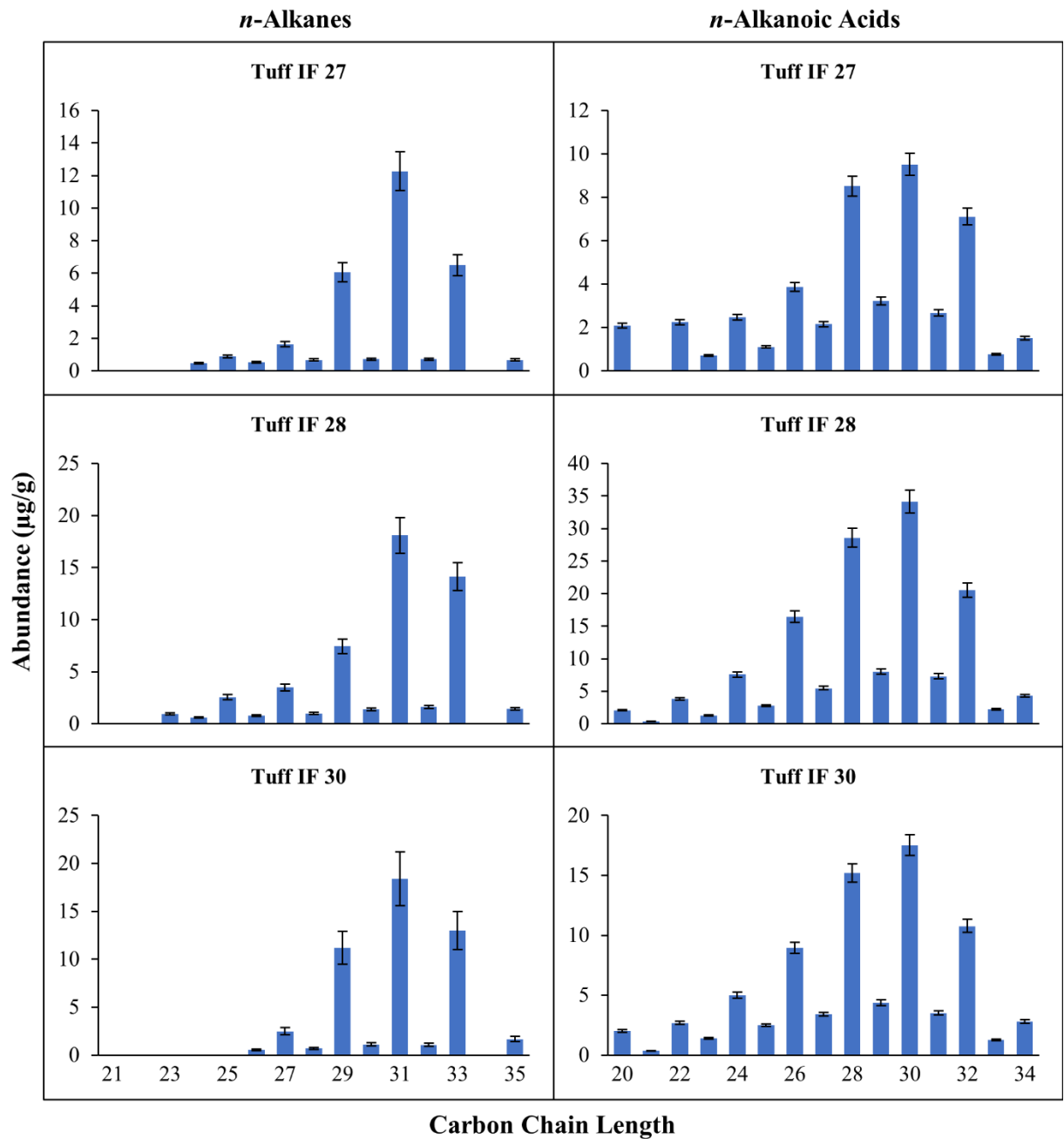


Figure 9-2F. Homologue distribution and abundances ($\mu\text{g/gdw}$) of *n*-alkanes and *n*-alkanoic acids from the clays below Tuff IF.

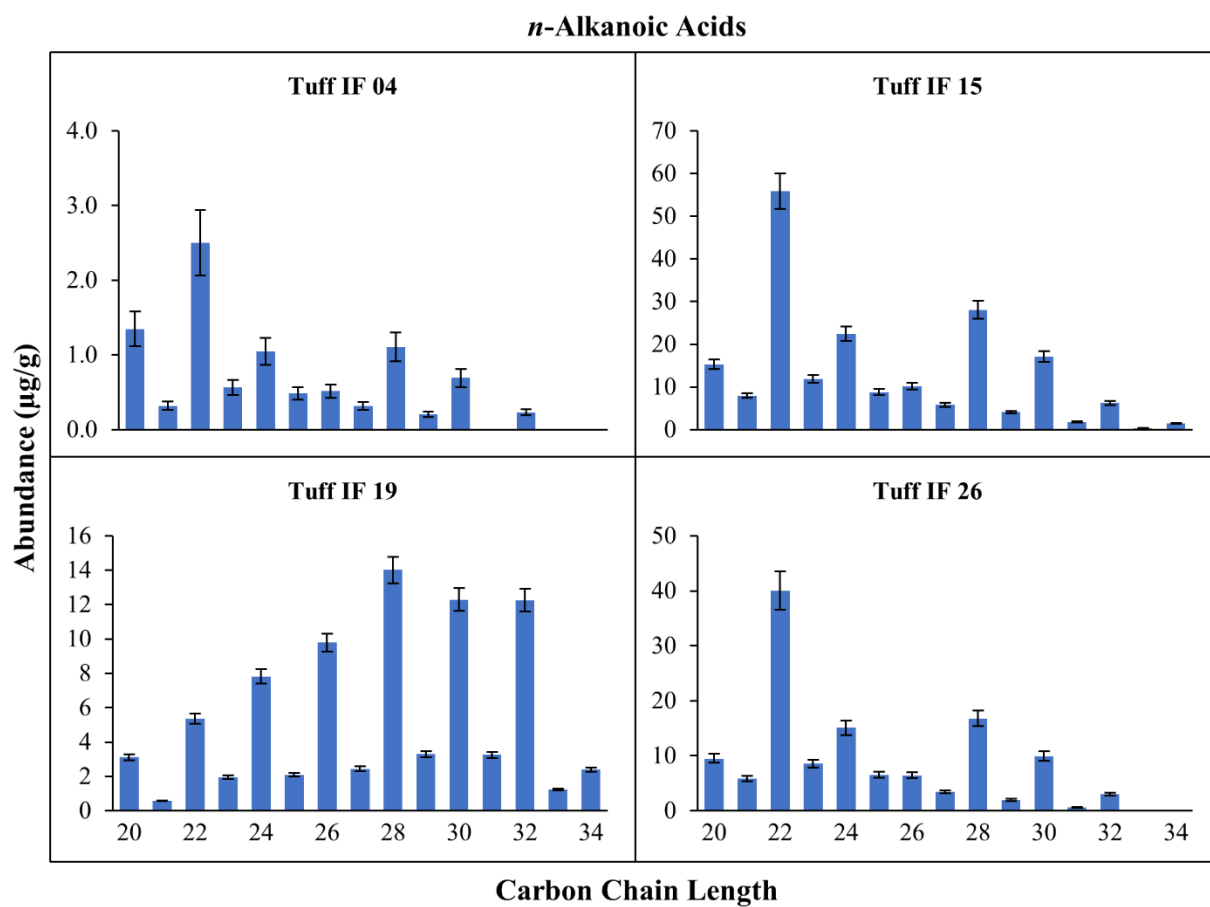


Figure 9-2G. Homologue distribution and abundances ($\mu\text{g/gdw}$) of *n*-alkanoic acids from the clays below Tuff IF.

9.1.3 FLK-W

The distribution of *n*-alkanoic acids in the Frida Leakey Korongo West samples range from C₂₀ to C₃₄ excluding C₃₃, whereby the abundance was too low to detect with GC-MS for every sample. Many of the samples display an even-over-odd predominance, however samples FLK-W 11, FLK-W 18, and FLK-W 27 had extremely abundant C₂₅, though this is likely an artefact of a double-bonded fatty acid interfering with the quantification of this compound due to the FLK-W samples not being eluted over silver nitrate infused silica gel. Concentrations for individual *n*-acids could not be calculated with confidence, so they are reported in relative abundance (Fig. 9-3A-G). CPI values in this sample subset were 1.10-3.43 with an average of 2.46 ± 0.13 (CPI₂₀₋₃₄); 0.75-5.35 with an average of 2.39 ± 0.20 (CPI₂₄₋₃₂); 0.76-5.41 with an average of 2.40 ± 0.20 (CPI₂₄₋₃₄); 1.22-5.82 with an average of 3.05 ± 0.21 (CPI₂₆₋₃₂); and 1.23-5.91 with an average of 3.08 ± 0.22 (CPI₂₆₋₃₄) (Table 9-3). Of the 28 FLK-W samples, two have CPI values <1.0 (FLK-W 11, 27) but only for the 24-32 and 24-34 ranges; when the entire spectrum (20-34) or 26-32 and 26-34 ranges were analyzed, CPI was >1.0. Nevertheless, most samples have CPI scores >1.0, indicating that the *n*-acids derive from terrestrial plant leaf waxes that have not been substantially (bio)degraded. The extent of deviation among CPI between carbon chain length subcategory is also small, with the largest deviation being 1.05 (variance 1.10) for samples FLK-W 01 and FLK-W 10. Sample FLK-W 07 was the only one in which acids were not detected; interestingly, the *n*-alkanes preserved better for this sample, which is not typical. ACL spans from 24.22-27.35 with an average of 25.05 ± 0.14 (ACL₂₀₋₃₄), and 28.05-28.92 with an average of 28.41 ± 0.04 (ACL₂₆₋₃₂). Over the 20-34 range, the average ACL of 25.05 may suggest a heavier input of lipids from non-terrestrial vegetation sources.

The distribution of *n*-alkanes in the FLK-W samples are significantly impacted by Unresolved Complex Mixtures (UCMs), specifically in archaeological levels 2 and 3 (Table 9-3, and orange bars in Fig. 9-3A-G). The odd-over-even carbon preference is consistent only for compounds ≥ 27 , mainly because compounds shorter than C₂₇ are impacted by the UCM. Moreover, six samples (13-16, 19-20) had such intense UCMs that *n*-alkanes could not be identified or quantified. Concentrations for individual *n*-alkanes could not be calculated with confidence, so they are reported in relative abundance. CPI values in this sample subset were 1.03-2.97 with an average of 1.66 ± 0.14 (CPI₂₁₋₃₅); 1.12-2.97 with an average of 1.71 ± 0.13 (CPI₂₅₋₃₃); 1.12-2.97 with an average of 1.74 ± 0.13 (CPI₂₅₋₃₅); 1.18-3.28 with an average of 1.90 ± 0.15 (CPI₂₇₋₃₃); and 1.19-3.28 with an average of 1.94 ± 0.16 (CPI₂₇₋₃₅) (Table 9-3). CPI values are generally low, but none of the 22 samples in which carbon chains could be identified and quantified had a CPI <1.0; the lowest value of 1.03 was from FLK-W 17 and calculated in the 21-35 range. ACL spans from 25.39-31.06 with an average of 28.63 ± 0.34 (ACL₂₁₋₃₅), and 28.83-30.78 with an average of 29.88 ± 0.11 (ACL₂₇₋₃₃).

The distribution and abundances of *n*-acids and *n*-alkanes in FLK-W are shown as histograms in Figs. 9-3A-G. Most samples have the C₂₂ *n*-acid as the most abundant compound (66%), with C₂₈ the second most prolific component (and most prolific when focusing on the C₂₆₋₃₂ range). The C₂₄ acid is the third most dominant homologue, followed by C₃₀. For the *n*-alkanes, 77% of the samples had C₃₁ as the most abundant component, while two samples had C₂₉ as the most dominant peak, and one had C₂₇. Two samples (FLK-W 17 and 18) have C₂₆ as the most prominent compound, but this may be an artefact of the UCM. C₂₉ was the second most abundant compound in 10 samples that had a dominant C₃₁ component.

Table 9-3. Carbon Preference Index and Average Chain Length for FLK-W *n*-alkanes and *n*-alkanoic acids.

Sample	Depth (cm)	<i>n</i> -Alkanes										<i>n</i> -Alkanoic Acids									
		CPI ₂₁₋₃₅	CPI ₂₅₋₃₃	CPI ₂₅₋₃₅	CPI ₂₇₋₃₃	CPI ₂₇₋₃₅	ACL ₂₁₋₃₅	ACL ₂₇₋₃₃	CPI ₂₀₋₃₄	CPI ₂₄₋₃₂	CPI ₂₄₋₃₄	CPI ₂₆₋₃₂	CPI ₂₆₋₃₄	ACL ₂₀₋₃₄	ACL ₂₆₋₃₂						
28	-	2.01	2.33	2.33	2.77	2.77	2.77	27.81	29.49	1.90	1.70	1.70	1.81	1.81	25.27	28.38					
23	0-2	1.91	2.14	2.15	2.50	2.51	29.10	29.80	2.90	2.76	2.79	3.17	3.21	25.66	28.66						
22	6-8	2.33	2.67	2.67	3.28	3.28	29.37	30.01	3.00	2.97	3.00	3.01	3.05	27.35	28.44						
21	12-14	2.78	2.43	2.78	2.83	3.27	31.06	30.22	2.36	1.95	1.96	3.41	3.44	24.35	28.26						
20	18-20								2.64	2.49	2.55	3.07	3.16	25.93	28.79						
19	24-26								2.58	2.52	2.56	3.26	3.32	25.33	28.53						
18	30-32	1.17	1.16	1.18	1.21	1.24	28.51	29.64	1.42	1.08	1.09	2.13	2.14	25.07	28.22						
17	36-38	1.03	1.12	1.12	1.18	1.19	27.29	28.83	1.83	2.02	2.03	1.90	1.92	25.29	28.47						
16	42-44								2.05	1.66	1.68	2.28	2.33	24.88	28.55						
15	48-50								2.43	2.37	2.40	2.90	2.95	25.30	28.45						
14	54-56								2.51	2.32	2.32	2.97	2.97	24.62	28.35						
13	60-62								2.21	3.06	3.06	3.37	3.37	25.79	28.29						
12	66-68	1.43	1.48	1.54	1.64	1.71	29.52	30.17	1.81	1.66	1.66	1.48	1.48	24.78	28.39						
11	72-74	1.77	1.90	1.99	2.15	2.27	28.02	30.38	1.10	0.75	0.76	1.22	1.23	24.68	28.35						
10	78-80	1.76	1.76	1.76	1.76	1.76	29.97	29.97	3.35	5.35	5.41	5.82	5.91	25.03	28.49						
09	84-86	2.97	2.97	2.97	2.97	2.97	30.78	30.78	3.23	3.03	3.06	3.90	3.95	25.31	28.92						
08	90-92	1.52	1.66	1.70	1.88	1.94	29.13	30.18	3.15	3.02	3.04	4.23	4.27	24.67	28.59						
07	96-98	2.44	1.26	1.27	1.39	1.40	25.39	29.68													
06	102-104	1.38	1.63	1.63	1.88	1.88	29.08	30.01	2.97	2.78	2.78	3.89	3.89	24.38	28.05						
05	108-110	1.39	1.55	1.55	1.67	1.67	29.17	29.99	2.79	2.71	2.71	3.47	3.47	25.44	28.48						
04	114-116	1.54	1.63	1.69	1.83	1.91	29.84	30.06	2.90	2.74	2.76	3.54	3.57	24.94	28.48						
03	118-120	1.54	1.62	1.62	1.79	1.79	27.83	29.95	2.53	2.37	2.37	3.02	3.02	24.67	28.17						
02	124-126	1.18	1.25	1.25	1.36	1.36	28.21	29.47	2.56	2.44	2.48	3.06	3.13	25.08	28.64						
01	128-130	1.27	1.38	1.38	1.51	1.51	27.76	29.84	3.43	2.95	2.95	4.99	4.99	24.22	28.13						
27	134-136	1.21	1.26	1.25	1.34	1.32	28.54	29.65	1.38	0.96	0.96	2.53	2.53	24.36	28.14						
26	140-142	1.45	1.65	1.65	1.88	1.88	28.30	29.75	2.49	2.22	2.22	2.71	2.71	24.42	28.35						
25	146-148	1.19	1.38	1.37	1.52	1.50	27.24	29.74	2.24	2.01	2.05	2.29	2.36	24.99	28.29						
24	152-154	1.24	1.37	1.36	1.50	1.47	27.92	29.66	2.78	2.51	2.51	2.96	2.96	24.55	28.13						

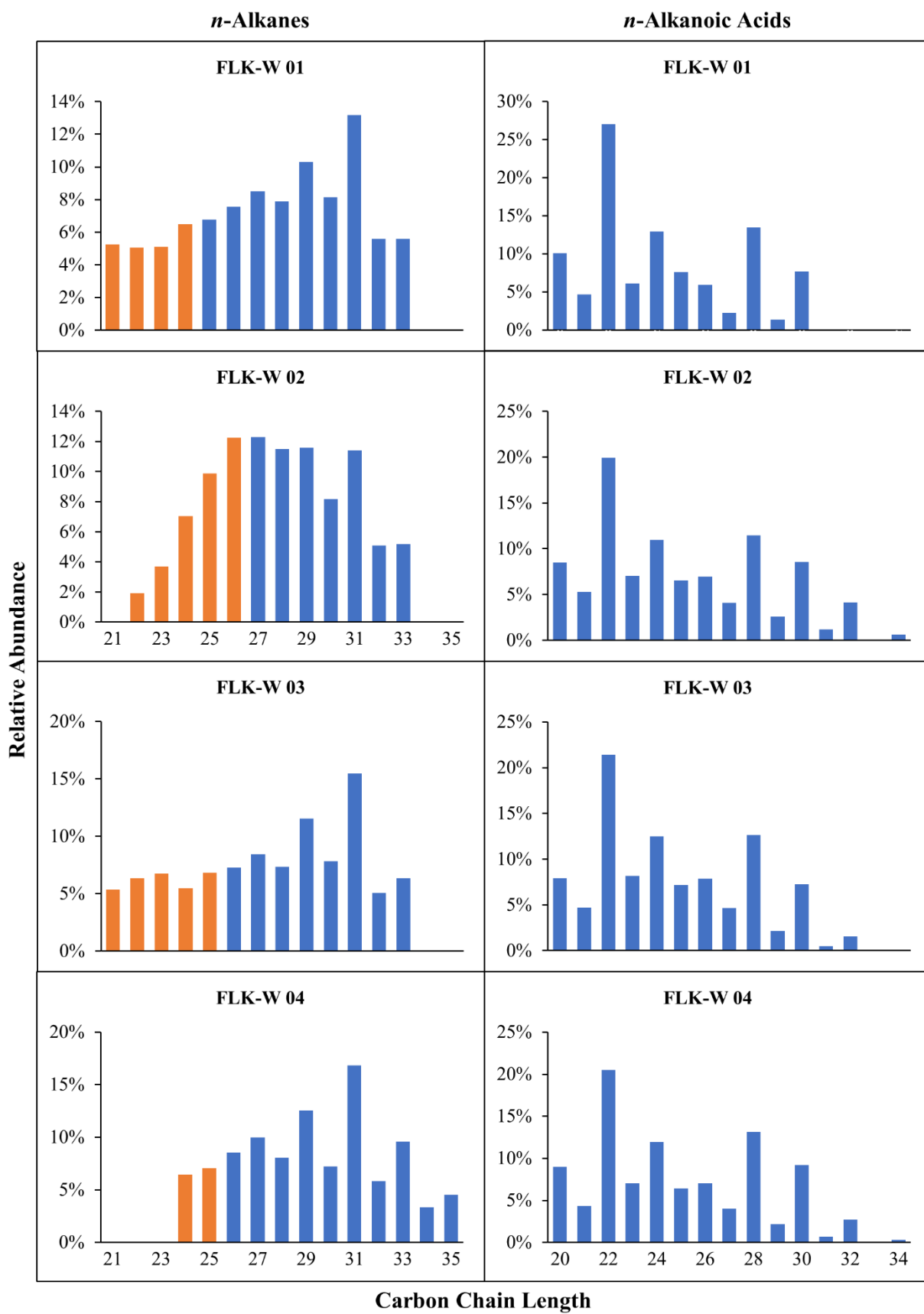


Figure 9-3A. Homologue distribution and relative abundances of *n*-alkanes and *n*-alkanoic acids from FLK-W. Orange bars represent extent of the UCM and the compounds impacted by its presence.

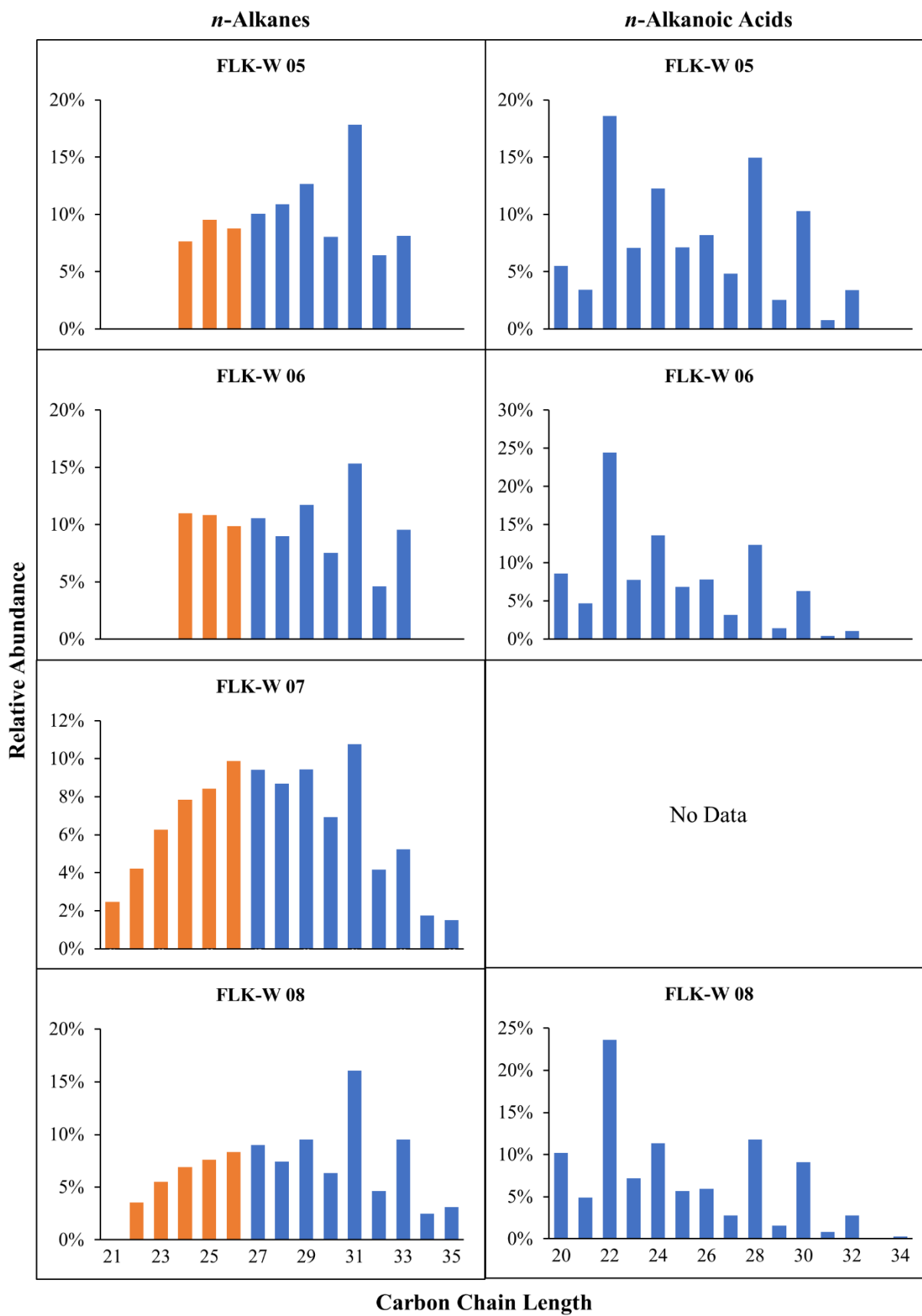


Figure 9-3B. Homologue distribution and relative abundances of *n*-alkanes and *n*-alkanoic acids from FLK-W. Orange bars represent extent of the UCM and the compounds impacted by its presence.

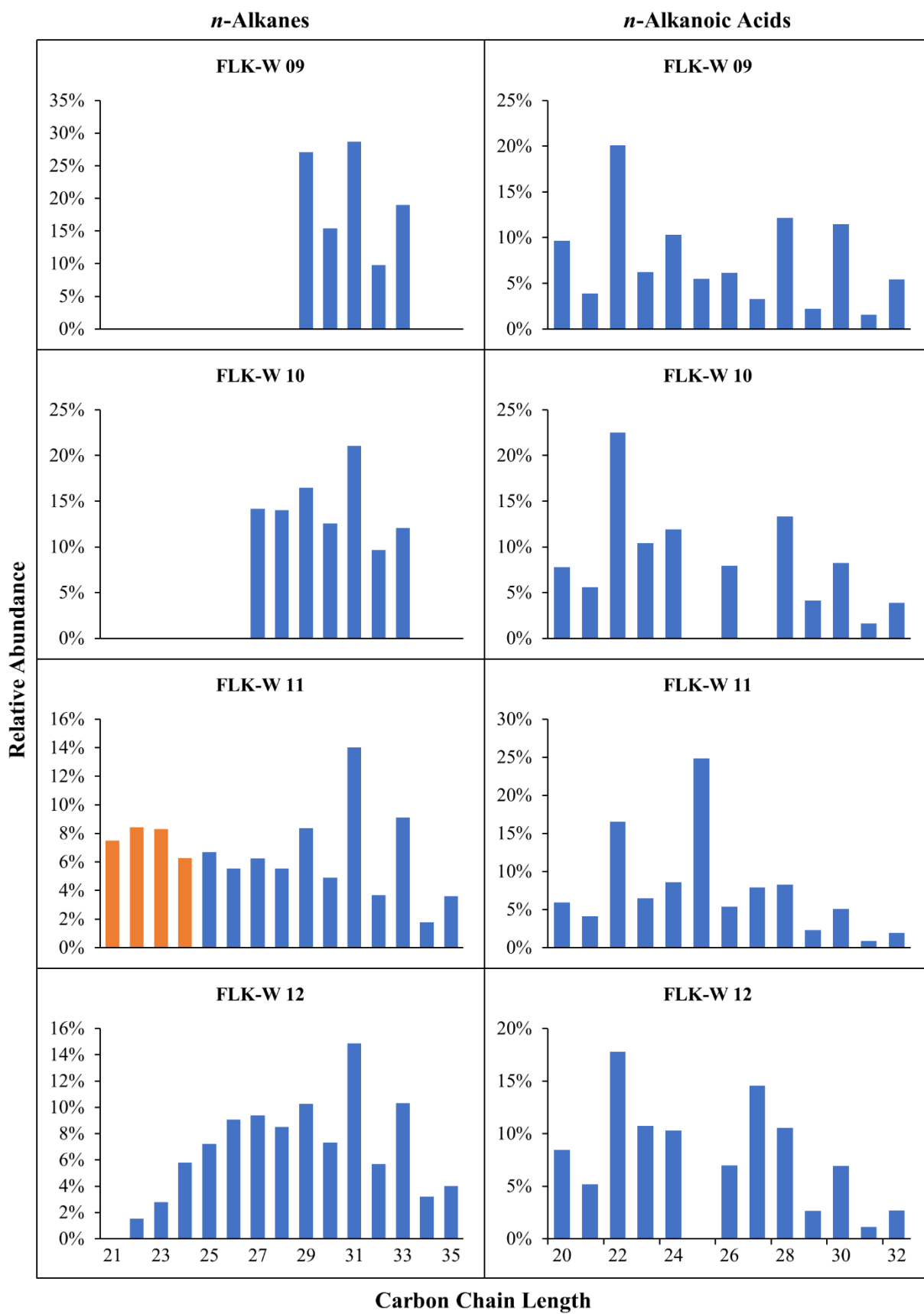


Figure 9-3C. Homologue distribution and relative abundances of *n*-alkanes and *n*-alkanoic acids from FLK-W. Orange bars represent extent of the UCM and the compounds impacted by its presence.

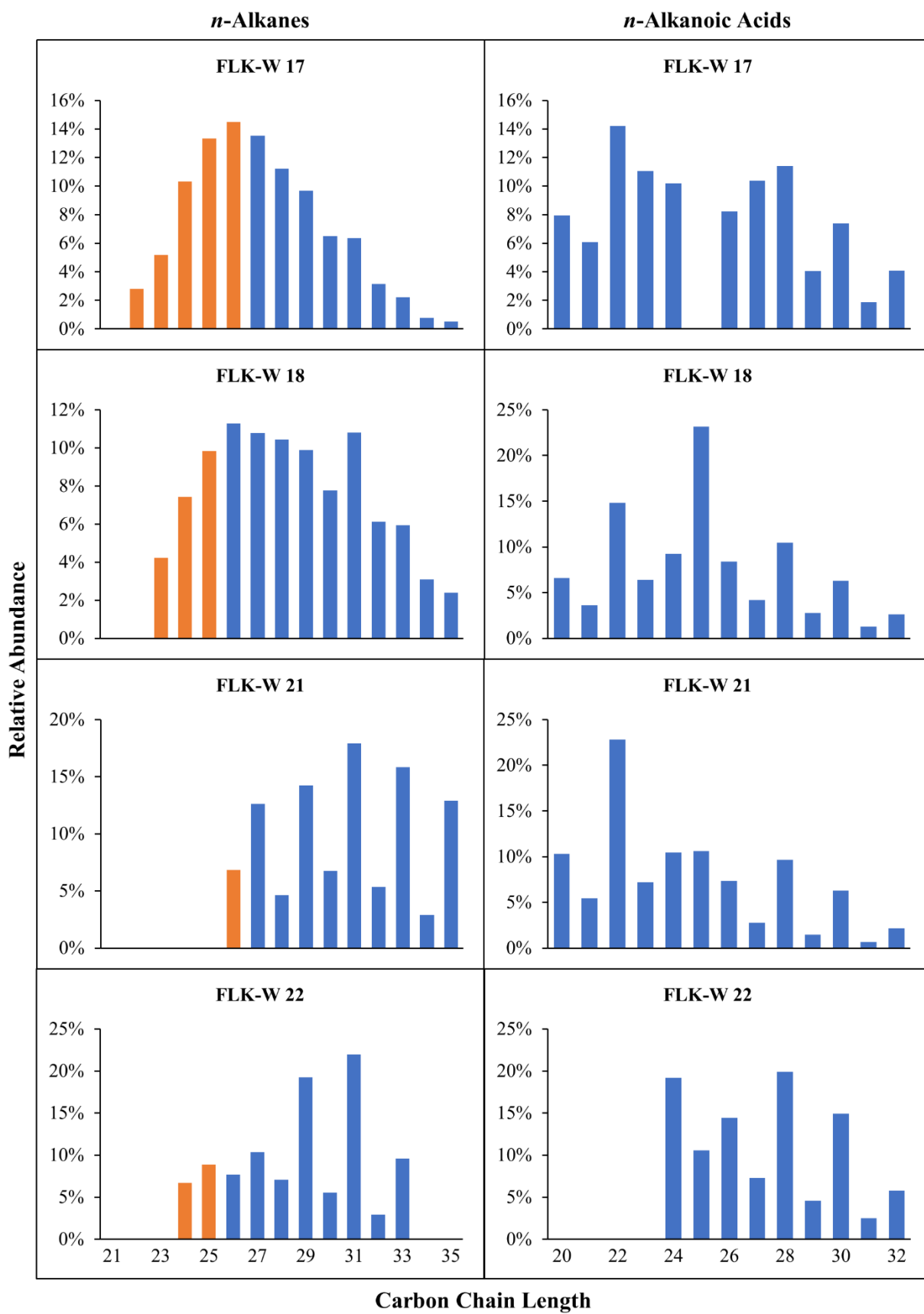


Figure 9-3D. Homologue distribution and relative abundances of *n*-alkanes and *n*-alkanoic acids from FLK-W. Orange bars represent extent of the UCM and the compounds impacted by its presence.

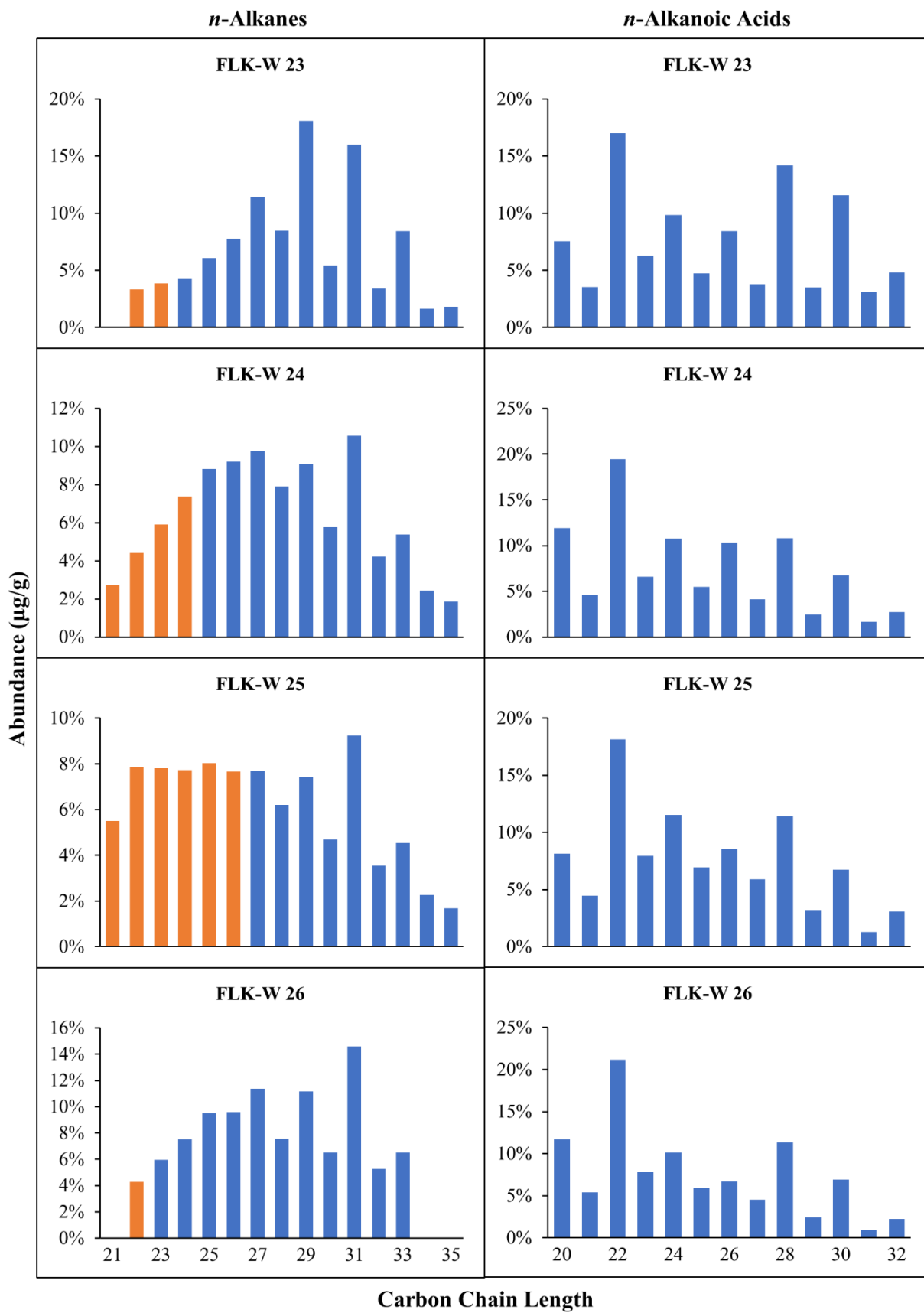


Figure 9-3E. Homologue distribution and relative abundances of *n*-alkanes and *n*-alkanoic acids from FLK-W. Orange bars represent extent of the UCM and the compounds impacted by its presence.

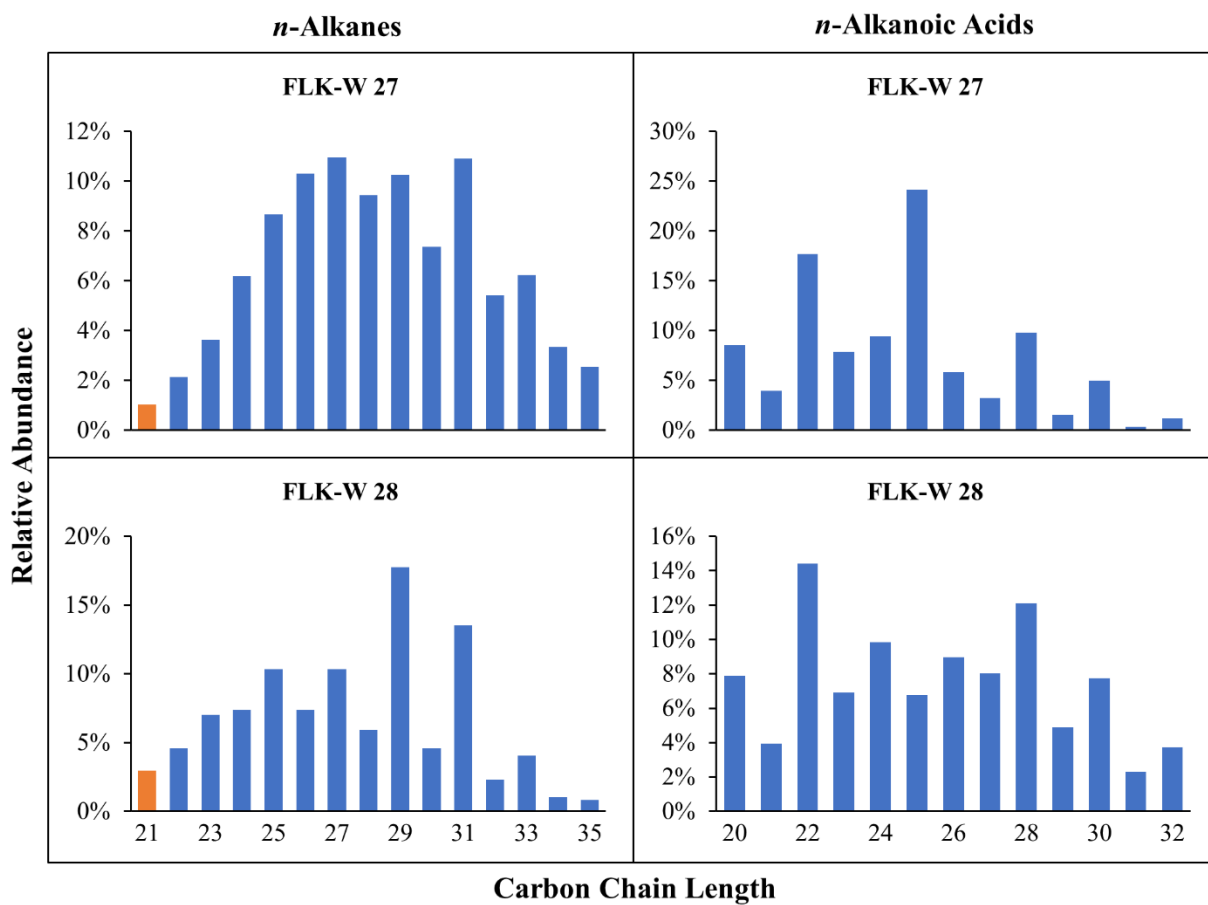


Figure 9-3F. Homologue distribution and relative abundances of *n*-alkanes and *n*-alkanoic acids from FLK-W. Orange bars represent extent of the UCM and the compounds impacted by its presence.

n-Alkanoic Acids

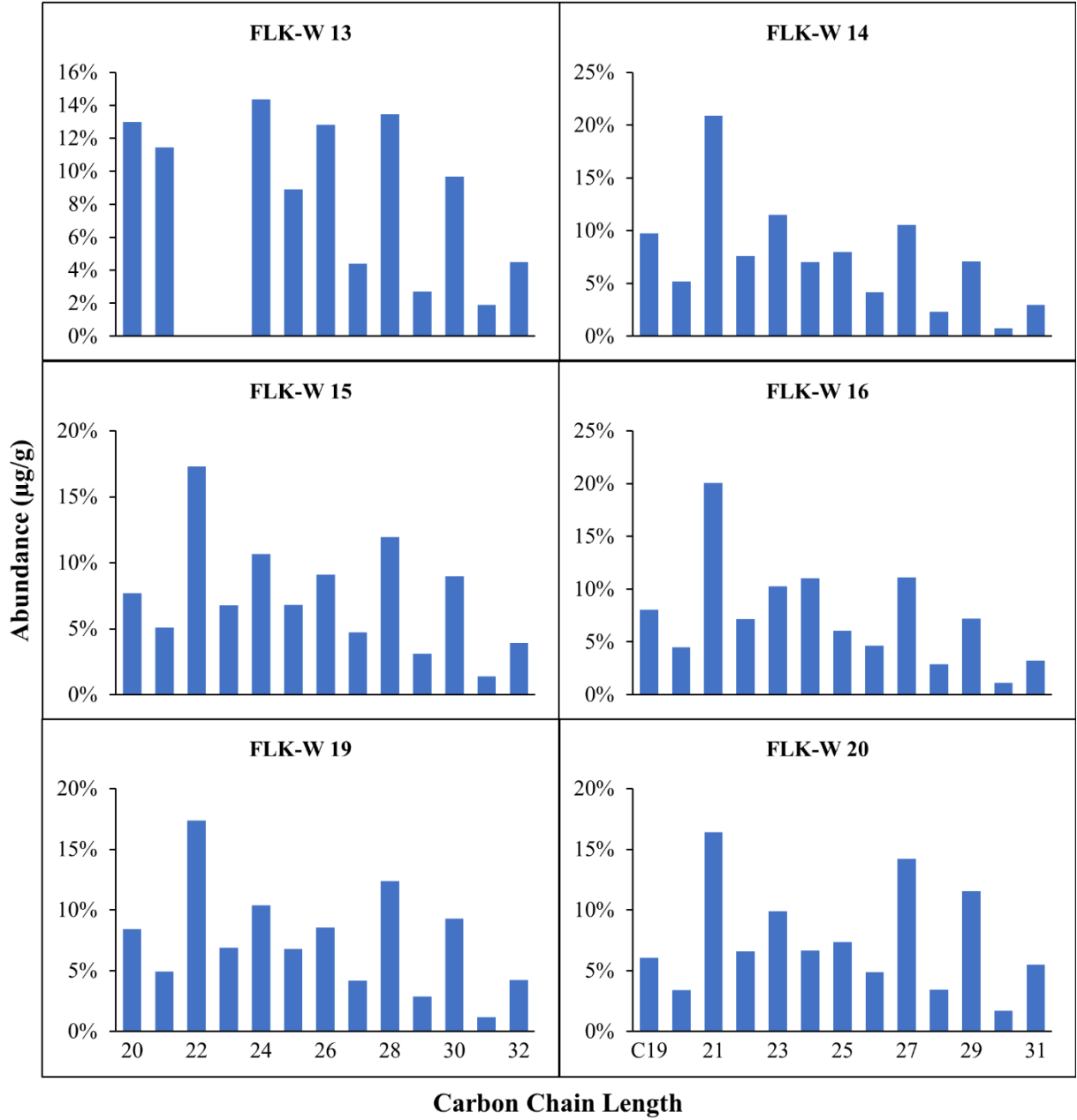


Figure 9-3G. Homologue distribution and relative abundances of *n*-alkanoic acids from FLK-W.

9.1.4 BPT

The distribution of *n*-alkanoic acids in the Bird Print Tuff samples range from C₂₀ to C₃₄ and display an even-over-odd preference (Fig. 9-4A-B). Concentrations for individual *n*-acids range from 0.0 to 24.46 µg/g of dry sediment, with an average value of 1.72 µg/g. CPI values in this sample subset were 1.90-5.71 with an average of 4.07 ± 0.66 (CPI₂₀₋₃₄); 1.70-5.73 with an average of 3.87 ± 0.72 (CPI₂₄₋₃₂); 1.70-5.73 with an average of 3.88 ± 0.72 (CPI₂₄₋₃₄); 1.81-7.13 with an average of 4.38 ± 0.88 (CPI₂₆₋₃₂); and 1.81-7.13 with an average of 4.39 ± 0.88 (CPI₂₆₋₃₄) (Table 9-4). None of the 11 BPT samples had a CPI <1.0, but BPT1 (FLK-W 28) had values falling between 1.70 and 1.90. Although this sample set had CPI scores indicative of terrestrial plant leaf waxes that have not been (bio)degraded, the overall concentrations were low and some samples' (BPT5-7, 9-10) *n*-acids could not be quantified with GC-MS. The extent of CPI deviation between carbon chain length subcategory amongst those samples that could be quantified is relatively small, with the largest deviation being 0.79 (variance 0.63) from BPT8. ACL spans from 23.83-27.22 with an average of 25.39 ± 0.38 (ACL₂₀₋₃₄), and 26.88-28.81 with an average of 27.93 ± 0.28 (ACL₂₆₋₃₂).

The distribution of *n*-alkanes in the BPT range from C₂₁ to C₃₅ but only in two samples, BPT1 and BPT11; all other samples had UCMs that interfered with compound quantitation. These two samples, however, display odd-over-even carbon number predominance (Fig. 9-2A). Concentrations for BPT1 and BPT11 could not be calculated with certainty and are reported in relative abundance. CPI values in BPT1 were 2.01 (CPI₂₁₋₃₅); 2.33 (CPI₂₅₋₃₃); 2.33 (CPI₂₅₋₃₅); 2.77 (CPI₂₇₋₃₃); and 2.77 (CPI₂₇₋₃₅) (Table 9-4). CPI values in BPT11 were 3.38 (CPI₂₁₋₃₅); 3.39 (CPI₂₅₋₃₃); 3.47 (CPI₂₅₋₃₅); 3.69 (CPI₂₇₋₃₃); and 3.79 (CPI₂₇₋₃₅). These values indicate that the *n*-alkanes derive from terrestrial plant leaf waxes that have not been substantially (bio)degraded. ACL for

BPT1 was 27.81 (ACL₂₁₋₃₅) and 29.49 (ACL₂₇₋₃₃), and 29.93 (ACL₂₁₋₃₅) and 30.51 (ACL₂₇₋₃₃) for BPT11.

The distributions and abundances of *n*-acids and *n*-alkanes for the BPT are shown as histograms in Figs. 9-4A-B. All samples have the C₂₈ *n*-acid as the most abundant compound except for BPT1 and BPT5 which have C₂₂ and C₂₀ as the richest component, respectively. C₂₆ was the second most abundant compound, except for BPT4 where C₃₀ is the second most abundant. For the *n*-alkanes, C₂₉ is the most dominant compound in BPT1, while C₃₁ is richest in BPT11. C₃₁ is the second most abundant component of BPT1, while C₃₃ succeeds C₃₁ in BPT11.

Table 9-4. Carbon Preference Index and Average Chain Length for BPT *n*-alkanes and *n*-alkanoic acids.

Sample	<i>n</i> -Alkanes						<i>n</i> -Alkanoic Acids							
	CPI ₂₁₋₃₅	CPI ₂₅₋₃₃	CPI ₂₅₋₃₅	CPI ₂₇₋₃₃	CPI ₂₇₋₃₅	ACL ₂₇₋₃₃	CPI ₂₀₋₃₄	CPI ₂₄₋₃₂	CPI ₂₄₋₃₄	CPI ₂₆₋₃₂	CPI ₂₆₋₃₄	ACL ₂₆₋₃₂	ACL ₂₀₋₃₄	ACL ₂₆₋₃₂
BPT1	2.01	2.33	2.33	2.77	2.77	27.81	1.90	1.70	1.70	1.81	1.81	1.81	25.27	28.38
BPT2							2.34	1.82	1.82	1.91	1.91	1.91	24.91	27.03
BPT3							4.54	4.19	4.19	4.68	4.68	4.68	25.79	28.49
BPT4							5.71	5.61	5.65	5.97	6.03	6.03	27.22	28.81
BPT5													23.83	27.77
BPT6														
BPT7														
BPT8							5.61	5.73	5.73	7.13	7.13	7.13	25.42	28.11
BPT9														
BPT10														
BPT11	3.38	3.39	3.47	3.69	3.79	29.93	4.31	4.16	4.16	4.77	4.77	4.77	25.28	26.88

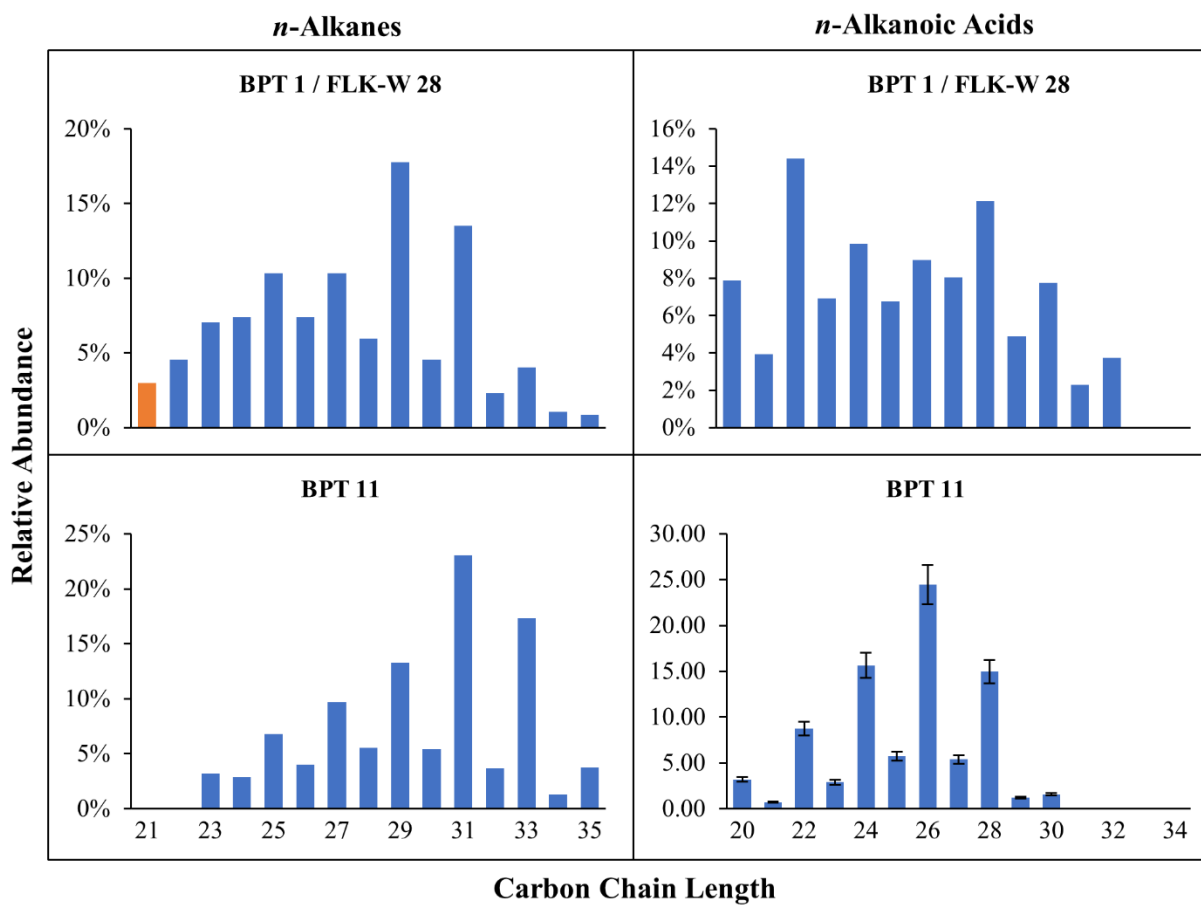


Figure 9-4A. Homologue distribution and relative abundances of *n*-alkanes and *n*-alkanoic acids from BPT. The *n*-acids for BPT11 are presented as $\mu\text{g/g}$ of dry sediment. Orange bar in BPT1 represents the extent of UCM.

n-Alkanoic Acids

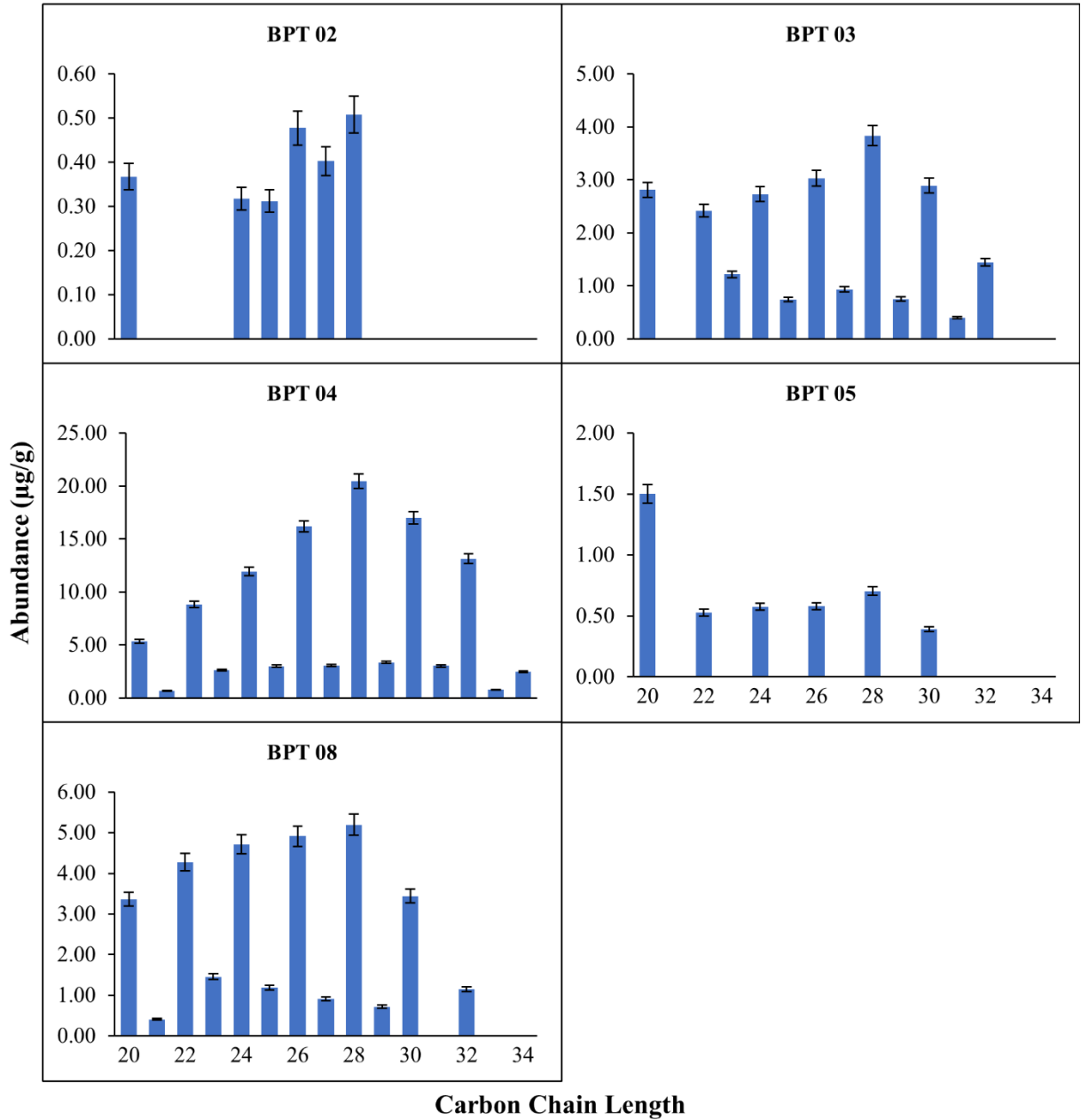


Figure 9-4B. Homologue distribution and abundances (µg/gdw) of *n*-alkanoic acids from BPT.

9.1.5 Castle Clays

The distribution of *n*-alkanoic acids in the Castle Clays range from C₂₀ to C₃₄ and display an even-over-odd predominance in all samples except Castle Clays 01, in which there is a relatively pronounced C₂₃ peak that is roughly as abundant as C₂₂. Concentrations for individual *n*-acids range from 0.0 to 56.64 µg/g of dry sediment, with an average value of 3.25 µg/g (Appendix A). CPI values in this sample subset were 2.00-4.89 with an average of 3.48 ± 0.32 (CPI₂₀₋₃₄); 1.84-4.75 with an average of 3.33 ± 0.31 (CPI₂₄₋₃₂); 1.84-4.83 with an average of 3.36 ± 0.31 (CPI₂₄₋₃₄); 1.91-5.37 with an average of 3.64 ± 0.34 (CPI₂₆₋₃₂); and 1.91-5.45 with an average of 3.69 ± 0.35 (CPI₂₆₋₃₄) (Table 9-5). All samples had CPI values >1.0, with the lowest value of 1.84 (CPI₂₄₋₃₂ & CPI₂₄₋₃₄) calculated in Castle Clays 08. Therefore, all samples have CPI scores indicative of terrestrial plant leaf waxes that have not been (bio)degraded. Furthermore, the extent of deviation among CPI between carbon chain length subcategory is relatively small, with the largest deviation being 0.70 (variance of 0.49) from Castle Clays 01. Castle Clays 09 was one of the best-preserved samples of all samples analyzed, having a total C₂₀-C₃₄ concentration of 311.37 µg/g of dry sediment. ACL spans from 23.80-27.10 with an average of 25.98 ± 0.24 (ACL₂₀₋₃₄), and 27.81-28.86 with an average of 28.52 ± 0.07 (ACL₂₆₋₃₂).

The distribution of *n*-alkanes in the Castle Clays range from C₂₁ to C₃₅ with most of the samples having the full range of homologues present (however, no data was obtained from samples 04 (compounds could not be identified with confidence) and 07 (concentrations were too low for quantification)). All remaining samples display obvious odd-over-even carbon number preference (Figs. 9-5A-D). Concentrations for individual *n*-alkanes range from 0.0 to 81.33 µg/g of dry sediment, with an average value of 3.50 µg/g (Appendix A). CPI values in this sample subset were 2.52-9.87 with an average of 6.45 ± 0.82 (CPI₂₁₋₃₅); 3.34-10.89 with an average of 7.59 ± 0.76

(CPI₂₅₋₃₃); 3.34-10.60 with an average of 7.49 ± 0.73 (CPI₂₅₋₃₅); 4.48-11.22 with an average of 8.80 ± 0.72 (CPI₂₇₋₃₃); and 4.48-11.22 with an average of 8.69 ± 0.69 (CPI₂₇₋₃₅) (Table 9-5). All samples have CPI >2.5 indicating that they derive from terrestrial plant leaf waxes and have not been (bio)degraded. Furthermore, the extent of deviation among CPI between carbon chain length subcategory is relatively small, apart from Castle Clays 10, which has the largest variation of 1.73 (variance of 2.99), Castle Clays 03, which has a deviation of 1.68 (variance of 2.84), and Castle Clays 09, which has a deviation of 1.11 (variance of 1.24). Like the *n*-acids, Castle Clays 09 was also the richest sample analyzed, with a total C₂₁-C₃₅ concentration of 259.90 µg/g. ACL spans 28.36-31.12 with an average of 30.04 ± 0.29 (ACL₂₁₋₃₅), and 29.75-31.17 with an average of 30.67 ± 0.14 (ACL₂₇₋₃₃).

The distributions and abundances of *n*-acids and *n*-alkanes in the Castle Clays are shown as histograms in Figs. 9-5A-D. Most samples have the C₂₈ *n*-acid as the most abundant compound (64%), but C₂₂ is the most abundant in three samples (21%), while C₂₀ was the most prolific in Castle Clays 01. When C₂₈ is the most dominant component, the second most plentiful homologue is either C₃₀, C₂₆, or C₂₂. For the *n*-alkanes, all samples have C₃₁ as the most abundant component, followed by C₃₃ (75%), then C₂₉.

Table 9-5. Carbon Preference Index and Average Chain Length for the Castle Clays *n*-alkanes and *n*-alkanoic acids.

Sample	Depth (cm)	<i>n</i> -Alkanes										<i>n</i> -Alkanoic Acids									
		CPI ₂₁₋₃₅	CPI ₂₅₋₃₃	CPI ₂₅₋₃₅	CPI ₂₇₋₃₃	CPI ₂₇₋₃₅	ACL ₂₁₋₃₅	ACL ₂₇₋₃₃	CPI ₂₀₋₃₄	CPI ₂₄₋₃₄	CPI ₂₆₋₃₂	CPI ₂₄₋₃₄	CPI ₂₆₋₃₂	CPI ₂₆₋₃₄	ACL ₂₀₋₃₄	ACL ₂₆₋₃₂					
14	0-5	9.87	10.89	10.60	11.55	11.22	30.94	31.07	4.84	4.74	5.10	4.83	5.20	26.43	28.86						
13	10-13	8.04	9.10	8.96	10.26	10.08	30.62	30.91	4.89	4.75	5.37	4.80	5.45	25.65	28.50						
12	17-21	8.37	9.35	9.15	10.38	10.14	30.97	31.15	4.68	4.59	5.02	4.66	5.12	25.92	28.56						
11	25-28	7.03	7.87	7.80	9.09	8.99	30.79	31.05	4.47	4.08	4.36	4.08	4.36	25.22	28.26						
10	40-46	5.41	7.52	7.54	9.57	9.54	29.82	30.65	2.90	3.13	3.35	3.19	3.44	27.10	28.58						
09	55-61	7.52	8.97	8.90	10.25	10.13	30.70	31.05	3.30	3.03	3.24	3.10	3.34	26.51	28.52						
08	75-79	2.52	3.34	3.34	4.48	4.48	28.36	29.75	2.00	1.84	1.91	1.84	1.91	26.10	28.72						
07	93-96								2.39	2.22	2.20	2.24	2.23	26.76	28.60						
06	104-110	9.27	10.03	9.89	10.85	10.70	30.13	30.38	4.51	4.19	4.63	4.25	4.72	24.81	28.26						
05	124-133	3.02	4.17	4.17	5.54	5.54	28.36	29.99	2.30	2.17	2.22	2.17	2.22	26.46	28.74						
04	147-149								3.31	2.99	3.04	3.03	3.08	25.67	28.44						
03	163-167	2.85	5.33	5.33	6.96	6.96	29.24	30.46	2.03	1.93	2.01	1.93	2.01	26.98	28.68						
02	181-186	9.86	10.14	9.86	11.10	10.87	31.12	31.17	4.89	4.69	5.01	4.77	5.11	26.31	28.78						
01	226-235	3.67	4.39	4.39	5.57	5.57	29.47	30.37	2.18	2.23	3.49	2.23	3.49	23.80	27.81						

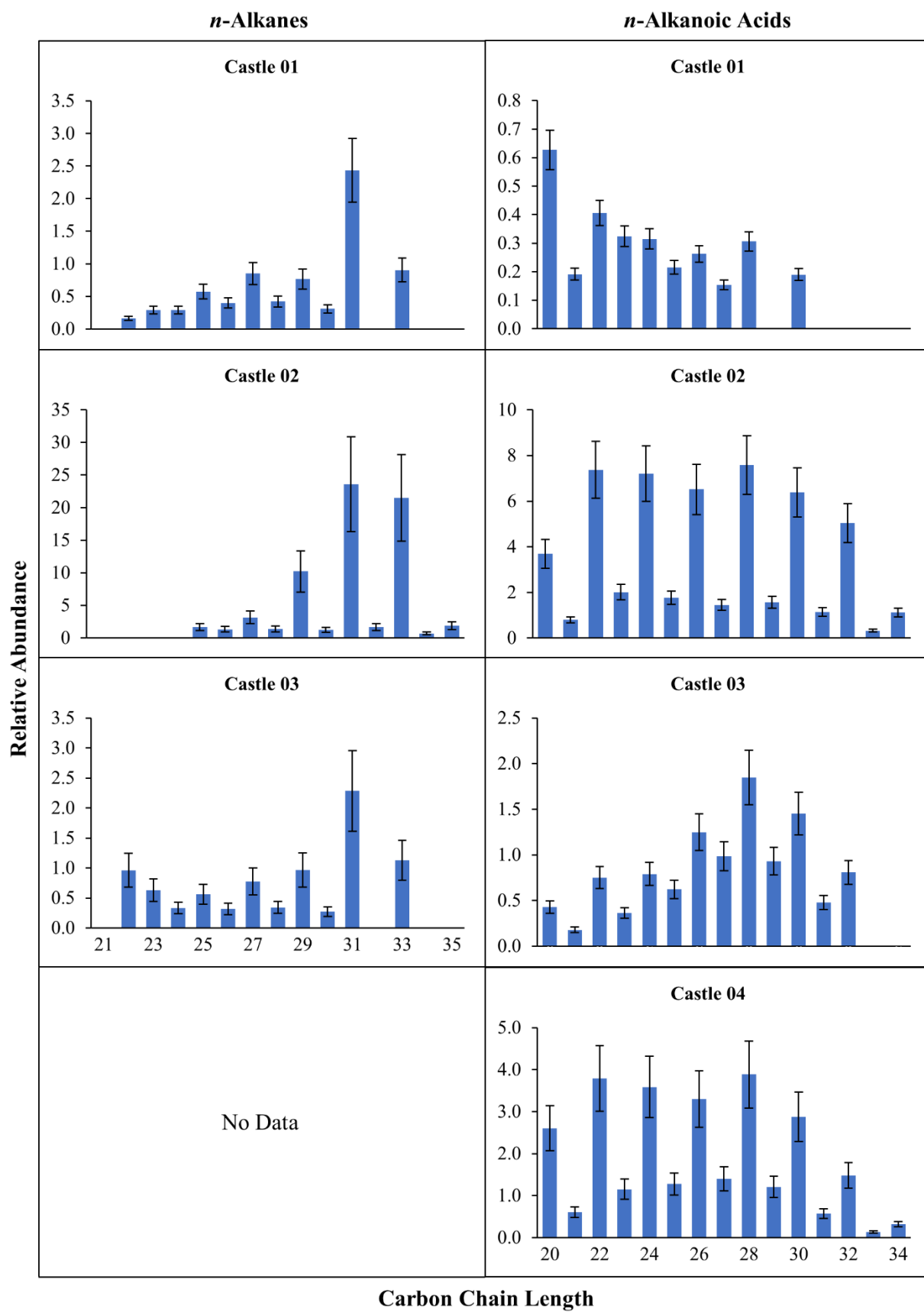


Figure 9-5A. Homologue distribution and abundances ($\mu\text{g/gdw}$) of *n*-alkanes and *n*-alkanoic acids from the Castle.

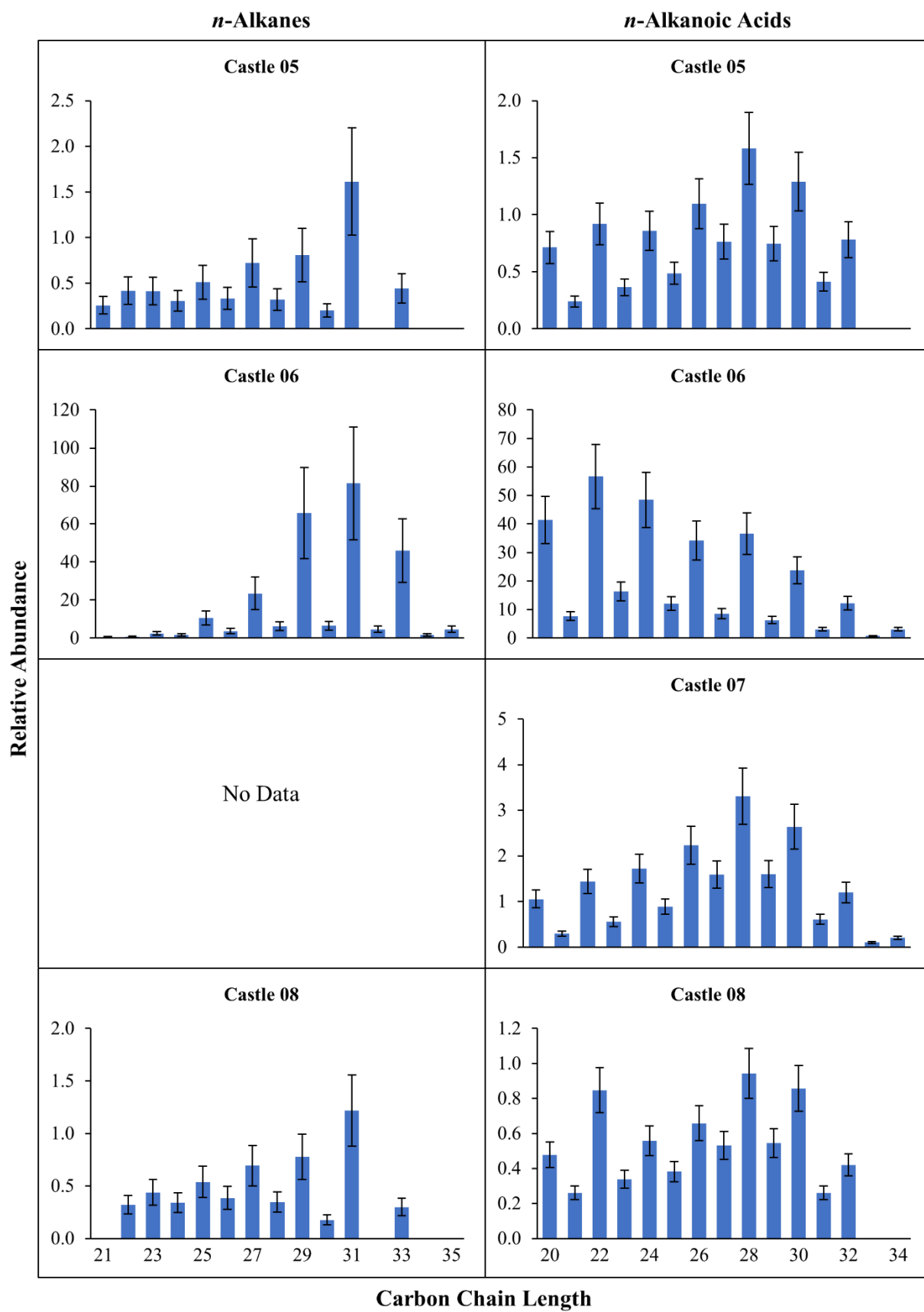


Figure 9-5B. Homologue distribution and abundances ($\mu\text{g/gdw}$) of *n*-alkanes and *n*-alkanoic acids from the Castle.

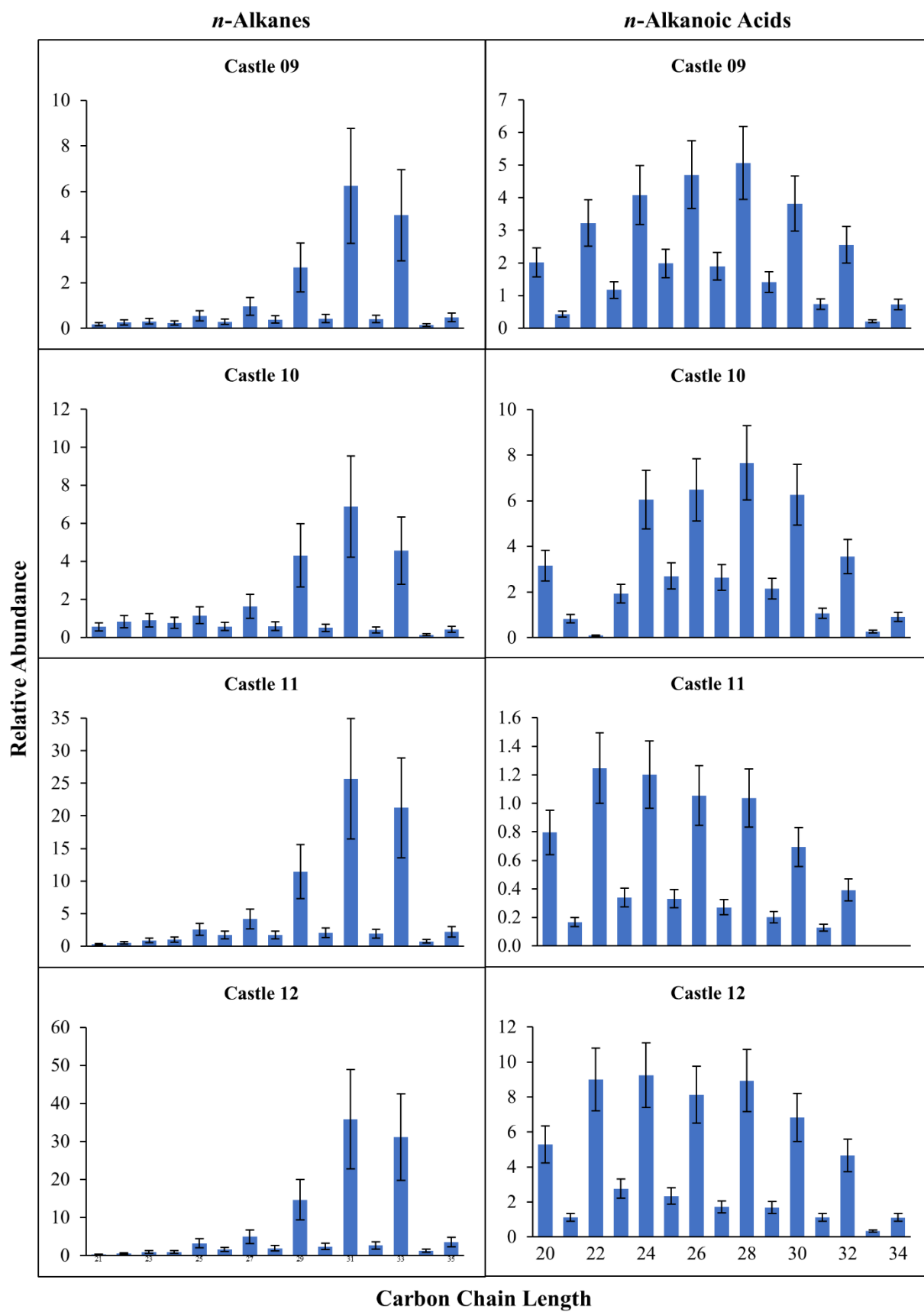


Figure 9-5C. Homologue distribution and abundances ($\mu\text{g/gdw}$) of *n*-alkanes and *n*-alkanoic acids from the Castle.

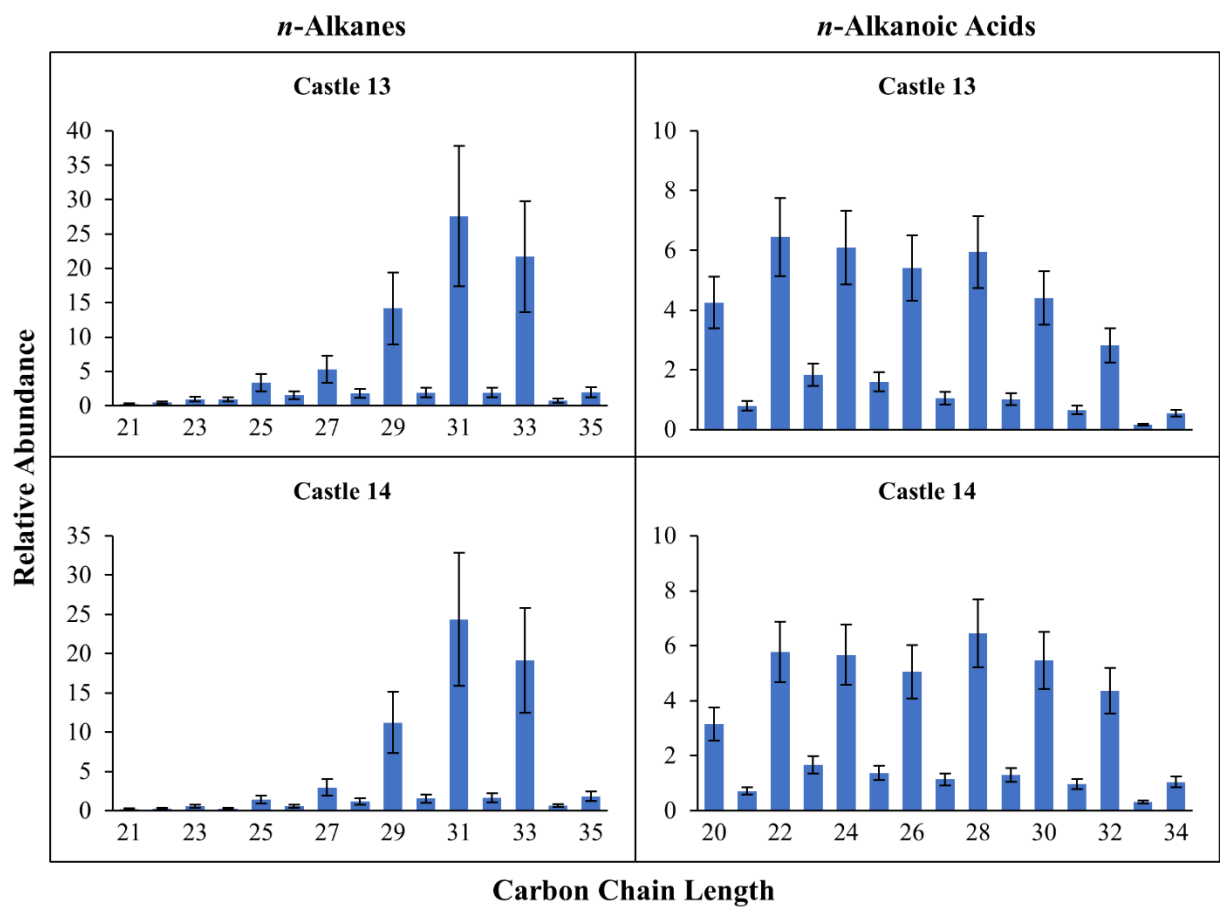


Figure 9-5D. Homologue distribution and abundances ($\mu\text{g/gdw}$) of *n*-alkanes and *n*-alkanoic acids from the Castle.

9.1.6 LAS

Data for higher molecular weight compounds were not obtained from the Lower Augitic Sandstone. The LAS *n*-alkanoic acids had a maximum homologue of C₂₄ in all but one sample, with C₂₀ and C₂₂ also being identifiable and quantified. Only LAS 11 had homologues above C₂₄, which has a maximum *n*-acid of C₃₀, but the overall concentration of all compounds was small and difficult to quantify with GC-MS; for example, C₃₀ had a concentration of $0.41 \pm 0.27 \mu\text{g/g}$ of dry sediment. Unresolved Complex Mixtures dominated samples analyzed for *n*-alkanes. Only two samples had identifiable *n*-alkanes, but of these, there was no odd-over-even preference (Fig. 9-6), and CPI was low (though only compounds C₂₃-C₃₀ could be quantified). Therefore, LAS samples were not analyzed for $\delta^{13}\text{C}$ and δD .

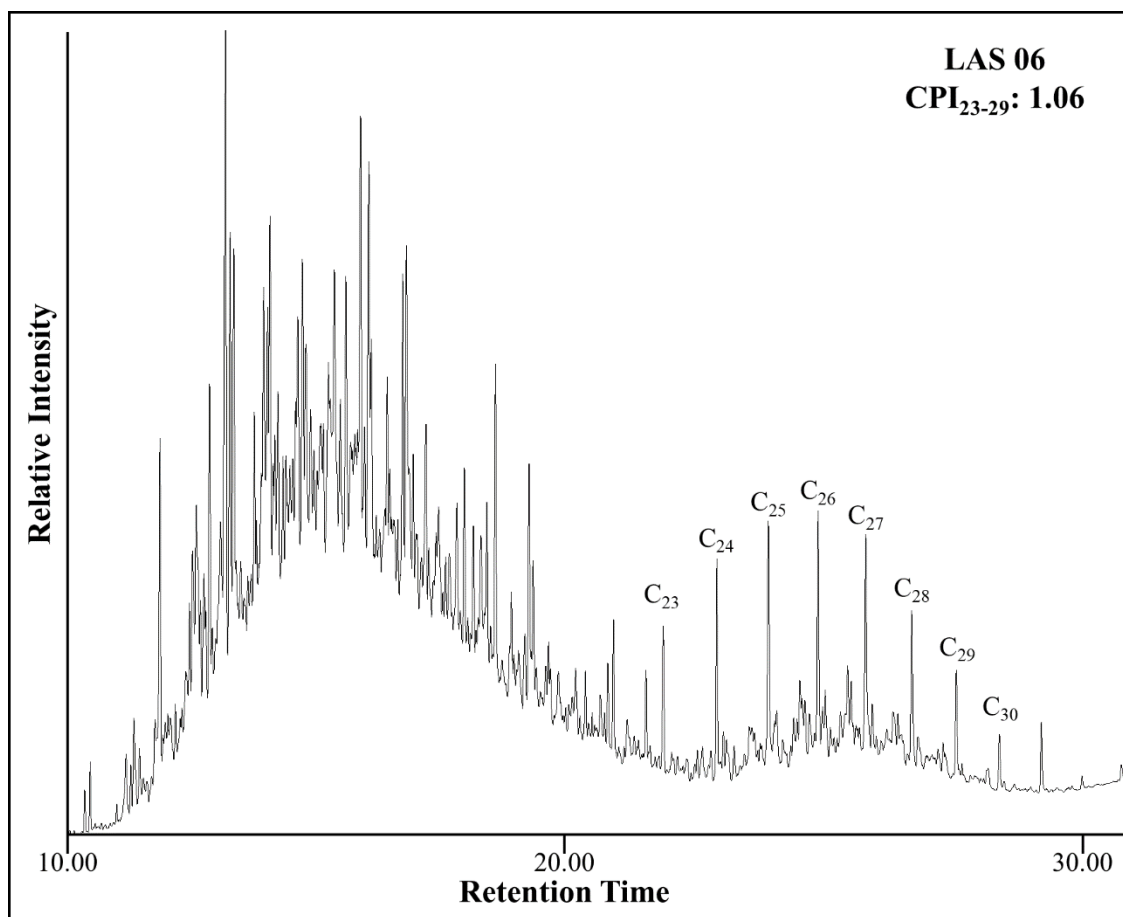


Figure 9-6. LAS chromatogram of *n*-alkanes dominated by an Unresolved Complex Mixture. There is no odd-over-even carbon number preference, CPI is low, and only compounds up to C₃₀ could be accurately identified.

9.2 $\delta^{13}\text{C}$ and δD

9.2.1 FLK-N

The $\delta^{13}\text{C}$ and δD isotopic composition of the C_{22} - C_{32} even-numbered FAMES are reported in Tables 9-6 and 9-8, and Figures 9-7 and 9-8 (raw data are presented in Appendix B). All FLK-N samples were measured for both carbon and hydrogen isotopes, but not all samples yielded data for both; sample 05 has no $\delta^{13}\text{C}$ value for C_{24} and samples 01 and 02 have no $\delta^{13}\text{C}$ data for C_{26} . The variation in carbon isotopes across the samples throughout Trench 7 involves oscillating changes in distribution, with the C_{24} , C_{26} , and C_{32} FAMES having larger variations between samples than the more-subtle changes of C_{28} and C_{30} . Nevertheless, C_{24} - C_{32} covary (Fig. 9.7) suggesting terrestrial vegetation as the biosynthesis source. C_{22} on the other hand, is anti-phased compared to the other compounds (e.g. it has negative isotope shifts when the others have positive), implying its origin is in aquatic or emergent plants or algae.

The highest $\delta^{13}\text{C}$ correlation between compounds is for C_{26} and C_{32} (r^2 0.94), followed by C_{24} and C_{32} (r^2 0.91), C_{28} and C_{30} (r^2 0.79), and then C_{24} and C_{26} (r^2 0.77) (Table 9-7). C_{22} does not correlate with the other compounds, except slightly with C_{32} (r^2 0.44); this is difficult to explain in that the two compounds anti-phase throughout the column, but perhaps only the slight changes in $\delta^{13}\text{C}$ between samples 04, 05, and 06 around 15-20 cm for C_{22} explicates the weak correlation.

The greatest δD correlation between compounds is for C_{28} and C_{30} (r^2 0.94), followed by C_{24} and C_{28} (r^2 0.89), C_{24} and C_{30} (r^2 0.84), and then C_{30} and C_{32} (r^2 0.65) (Table 9-9). Interestingly, C_{26} does not correlate well with any of the other compounds, but this may be due to the two extreme deviations in δD between samples below 15 cm compared to the other *n*-acids (Fig. 9-8). When samples 01 and 03 are omitted from the analysis, C_{26} and C_{32} correlate much better (r^2 0.71). C_{22}

also does not correlate with the other compounds even though it covaries with them below 25 cm (it is however anti-phased above 25 cm).

Terrestrial plants generally contain a higher abundance of C₂₆-C₃₂ *n*-alkanoic acids (Chikaraishi and Naraoka, 2007; Ficken et al., 2000; Gao et al., 2011), while submerged and floating aquatic plants display a higher abundance of C₂₀-C₂₄ *n*-acids (Ficken et al., 2000; Wang and Liu, 2012). For FLK-N Trench 7, the C₂₂ *n*-acid was the most abundant compound in all samples (Section 9.1.1). It also displayed the most-negative (depleted) δ¹³C values in five of the eight samples. The C₂₆ *n*-acid was the most-positive (enriched) compound in five of the six samples in which data was collected for it. The largest isotopic variation between any two samples was also found in C₂₆, whereby sample 05 is depleted by -2.9‰ compared to sample 04. The greatest isotopic difference between compounds from the same sample is in FLK-N 08, where C₃₀ is depleted by -3.3‰ compared to C₂₆. FLK-N 08 also has the largest variation between C₂₂ and C₂₄, in which C₂₂ is depleted by -2.9‰. However, due to the higher correlation between C₂₄ and C₂₆-C₃₂, C₂₂ is likely the only compound deriving from an alternative biosynthetic source. Therefore, C₂₄-C₃₂ δ¹³C values range from -34.7‰ to -30.2‰ with an average of -32.9 ± 0.2‰. C₂₂ values range from -34.9‰ to -32.8‰ with an average of -34.1 ± 0.2‰.

Regarding δD, C₂₆ displayed the most-negative (depleted) values in six of the eight samples while the C₂₄ *n*-acid was the most-positive (enriched) compound in seven of the eight samples. (Interestingly, C₂₆ was most-positive component in the one sample that did not have C₂₄ as most-enriched (FLK-N 03).) The largest isotopic variation between any two samples was also found in C₂₆, whereby sample 03 is enriched by +35.0‰ compared to sample 02. If C₂₆ samples 01 and 03 are excluded due to their extreme variability (Fig. 9-8), the largest isotopic variation between any two samples is in C₃₂, whereby sample 02 is depleted by -11.1‰ compared to FLK-N 01. The

greatest isotopic difference between compounds from the same sample is in FLK-N 01, where C₂₆ is depleted by -52.9‰ compared to C₂₄. When C₂₆ is omitted, the largest isotopic difference between compounds from the same sample is in FLK-N 03, where C₃₀ is depleted by only -12.5‰ compared to C₂₄. The δD of the C₂₆ *n*-alkanoic acid suggests that a different water/hydrogen source was utilized for biosynthesis compared to C₂₄, C₂₈-C₃₂ compounds; however, this might be an artefact of the extreme variability seen in samples 01 and 03, and when these are removed from analysis, the data suggests that the C₂₆ was in fact synthesized using the same source water. When compared, C₂₄-C₃₂ δD values (excluding C₂₆ FLK-N 01 and 03) range from -178.4‰ to -155.5‰ with an average of $-165.8 \pm 1.0\text{‰}$. C₂₂, which is likely the only compound deriving from an alternative biosynthetic source, has δD values range from -169.2‰ to -163.3‰ with an average of $-166.5 \pm 0.7\text{‰}$.

Table 9-6. $\delta^{13}\text{C}$ (VPDB) values for FLK-N Trench 7 samples. Isotope values are corrected to account for the isotopic contribution from the methyl group added during methylation.

$\delta^{13}\text{C}$ *n*-Alkanoic Acids

Sample	Depth (cm)	C ₂₂	C ₂₄	C ₂₆	C ₂₈	C ₃₀	C ₃₂
8	0-5	-34.97	-32.11	-30.66	-33.75	-33.96	-30.90
7	5-10	-34.07	-33.28	-32.66	-34.66	-34.61	-33.26
6	10-15	-34.87	-32.28	-31.34	-34.18	-34.38	-31.35
5	15-20	-34.80		-33.21	-34.16	-34.14	-33.12
4	20-25	-34.75	-32.22	-30.22	-33.27	-32.78	-30.65
3	25-30	-33.74	-32.17	-31.26	-33.39	-33.59	-31.76
2	30-35	-32.98	-33.54		-34.35	-34.69	-33.90
1	35-40	-32.80	-32.51		-33.31	-33.72	

Table 9-7. $\delta^{13}\text{C}$ Correlation (r^2) table for the C₂₂-C₃₂ *n*-acids from FLK-N Trench 7.

	C ₂₂	C ₂₄	C ₂₆	C ₂₈	C ₃₀	C ₃₂
C ₂₂	1.00					
C ₂₄	0.30	1.00				
C ₂₆	0.04	0.77	1.00			
C ₂₈	0.01	0.54	0.58	1.00		
C ₃₀	0.04	0.48	0.47	0.79	1.00	
C ₃₂	0.44	0.91	0.94	0.58	0.54	1.00

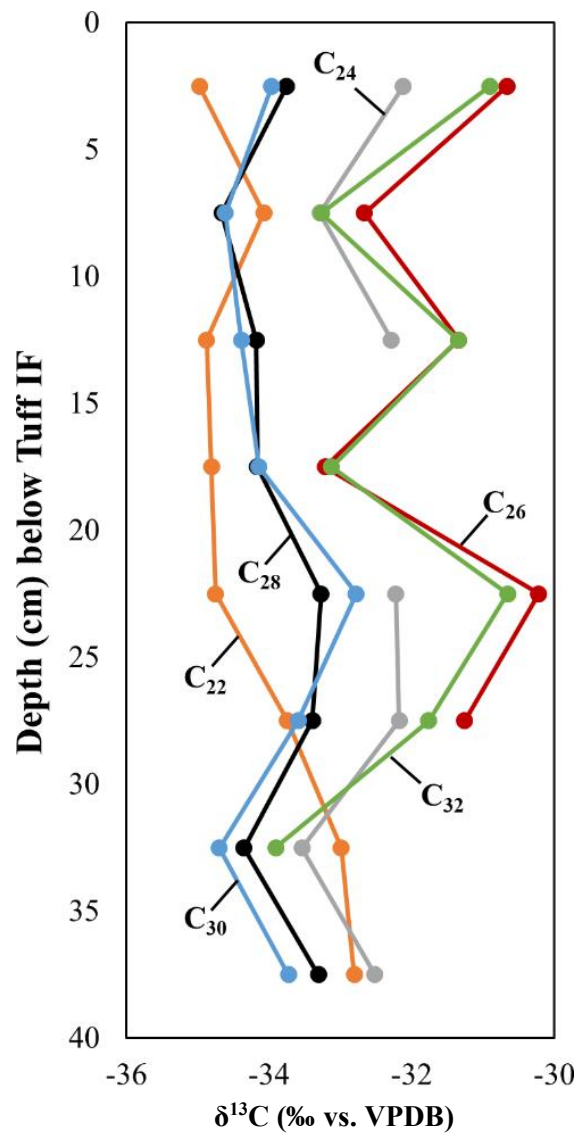


Figure 9-7. Carbon isotope values ($\delta^{13}\text{C}$ VPDB) from FLK-N Geological Trench 7 Level 1 for *n*-alkanoic acids C₂₂-C₃₂. Compound C₂₂ is anti-phased with the other *n*-acids, suggesting it was biosynthesized by non-terrestrial vegetation; i.e. an emergent plant or macrophyte. All other compounds have the same general positive-to-negative oscillation trend, suggesting they derive from the same biosynthetic source.

Table 9-8. δD (VSMOW) values for FLK-N Trench 7 samples. Isotope values are corrected to account for the isotopic contribution from the methyl group added during methylation.

δD <i>n</i>-Alkanoic Acids							
Sample	Depth (cm)	C₂₂	C₂₄	C₂₆	C₂₈	C₃₀	C₃₂
8	0-5	-165.22	-155.45	-161.48	-161.15	-164.30	-157.40
7	5-10	-165.47	-161.57	-172.56	-167.34	-170.29	-165.50
6	10-15	-166.02	-156.81	-167.56	-161.16	-166.38	-166.95
5	15-20	-167.83	-159.52	-178.37	-167.20	-171.18	-167.32
4	20-25	-169.15	-157.50	-175.96	-161.31	-166.25	-167.34
3	25-30	-163.29	-157.98	-142.91	-164.94	-170.51	-170.04
2	30-35	-169.00	-164.03	-177.95	-171.50	-175.69	-172.88
1	35-40	-165.77	-157.46	-210.41	-161.15	-166.13	-161.78

Table 9-9. δD Correlation (r^2) table for the C₂₂-C₃₂ *n*-acids from FLK-N Trench 7.

	C₂₂	C₂₄	C₂₆	C₂₈	C₃₀	C₃₂
C₂₂	1.00					
C₂₄	0.17	1.00				
C₂₆	0.18	0.02	1.00			
C₂₈	0.09	0.89	0.01	1.00		
C₃₀	0.08	0.84	0.01	0.94	1.00	
C₃₂	0.12	0.45	0.05	0.44	0.65	1.00

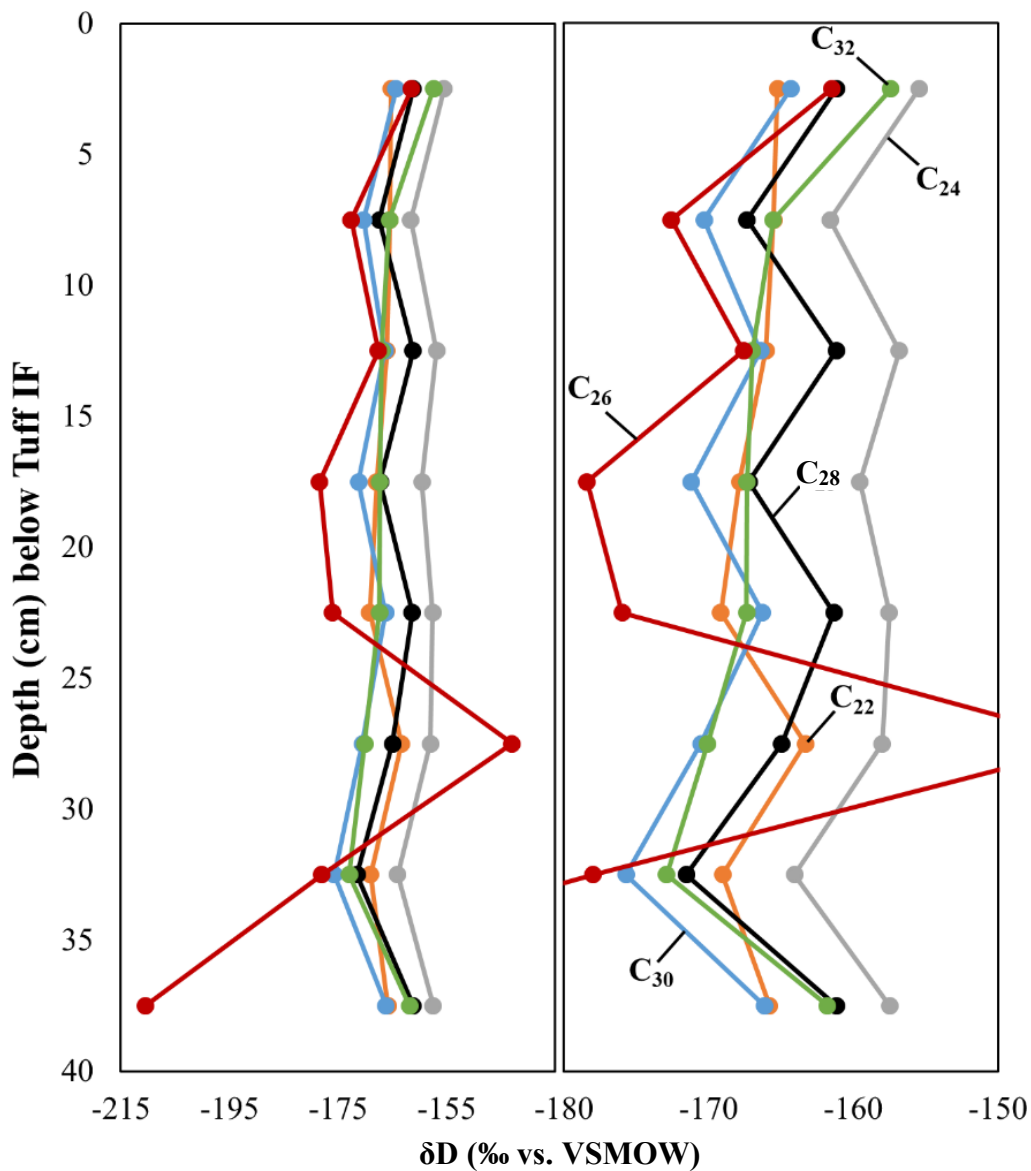


Figure 9-8. Hydrogen isotope values (δD VSMOW) from FLK-N Geological Trench 7 Level 1 for *n*-alkanoic acids C₂₂-C₃₂. The left panel shows all compounds and the large variation in δD below 25 cm for C₂₆. The right panel shows a zoomed view of the *n*-acids excluding δD C₂₆ from samples 01 and 03. Beginning around 25 cm, C₂₂ becomes anti-phased with the other *n*-acids, suggesting it was biosynthesized by non-terrestrial vegetation. All other compounds have the same general positive-to-negative oscillation trend, suggesting they derive from the same biosynthetic source, except for C₂₆, which has much larger fluctuations than the other *n*-acids.

9.2.2 Clays Below Tuff IF

The $\delta^{13}\text{C}$ isotopic composition of the C_{22} - C_{32} even-numbered FAMES from the clays below Tuff IF are reported in Table 9-10. Unfortunately, technical issues with Isotope Ratio Mass Spectrometer prevented many samples from being successfully analyzed for $\delta^{13}\text{C}$ (see Section 8.6.2). Of the 30 total samples processed for *n*-alkanoic acids, 22 had concentrations suitable for IRMS analysis, but of these, only 12 were successfully evaluated for $\delta^{13}\text{C}$ (Table 9-10)¹⁶. An issue with the IRMS sample injection syringe prevented the acquisition of *n*-acids from the 10 additional samples and therefore, only limited data is available for the clays below Tuff IF. (*n*-Alkanes were not analyzed as their concentrations were generally lower than that of the *n*-acids.) Nevertheless, some general inferences can be made with the data, specifically in terms of lipid production. When all 12 samples are compared, even though they were collected in spatially distinct locations throughout Olduvai Gorge, the C_{22} - C_{32} *n*-alkanoic acids are highly correlated, as r^2 values are all ≥ 0.90 (Table 9-11). This might suggest that all *n*-acids derive from the same biological source. However, some samples (03, 21, 28) have fairly large ($>4.0\%$) discrepancies between the C_{22} and C_{24} - C_{32} *n*-acids implying that the C_{22} compound derives from a non-terrestrial plant source. For example, in sample 03, C_{22} is depleted by -4.3% and -4.1% against the C_{26} and C_{32} *n*-acids, respectively. In clays below Tuff IF 21, C_{22} is depleted by -5.3% and -4.9% compared to C_{26} and C_{32} , respectively. Additionally, in sample 28, C_{22} is depleted by -4.8% from C_{32} .

For the clays below Tuff IF, C_{22} displayed the most-negative (depleted) $\delta^{13}\text{C}$ values in five of the 12 samples, and both the C_{26} and C_{32} *n*-acids were the most-positive (enriched) compound in five of the 12 samples each. The greatest isotopic difference between compounds originating in terrestrial plants from the same sample is in 15, where C_{30} is depleted by -3.4% in comparison to

¹⁶ Sample 14 also had $\delta^{13}\text{C}$ data, but only for C_{32} yet none of the other *n*-alkanoic acids.

C₃₂. Across all compounds, $\delta^{13}\text{C}$ values range from -35.2‰ to -18.2‰ with an average of $-24.9 \pm 0.7\%$. In C₂₈-C₃₂, values range from -35.2‰ to -19.0‰ with an average of $-24.3 \pm 1.0\%$. Overall, $\delta^{13}\text{C}$ displays large variety in the clays below Tuff IF, indicating that the *n*-alkanoic acids with more-positive values originated in C₄ grasses likely growing in an open landscape, while the more-depleted values developed in C₃ vegetation from closed or woody surroundings. Although limited, this data suggests a mosaic environment at the top of Bed I before Tuff IF was deposited.

Table 9-10. $\delta^{13}\text{C}$ (VPDB) values for the clays below Tuff IF. Isotope values are corrected to account for the isotopic contribution from the methyl group added during methylation.

Sample	$\delta^{13}\text{C}$ <i>n</i> -Alkanoic Acids					
	C ₂₂	C ₂₄	C ₂₆	C ₂₈	C ₃₀	C ₃₂
1			-20.37	-21.87	-20.13	
2			-19.11	-20.19	-20.99	-20.05
3	-34.97	-32.11	-30.66	-33.75	-33.96	-30.90
4						
5						
6						
7						
8						
9						
10						
11						
12						
13		-22.07	-18.16	-19.35	-20.17	-19.01
14						-19.42
15	-34.44	-33.26	-33.50	-34.71	-34.86	-31.50
16	-23.01	-22.94	-21.10	-22.54	-22.45	-20.76
17						
18						
19						
20				-19.52	-20.07	-19.26
21	-26.15	-22.34	-20.89	-22.30	-23.29	-21.17
22		-19.63	-20.36	-19.91	-20.27	-19.80
23						
24						
25						
26	-34.50	-34.22		-35.21	-35.15	-34.34
27						
28	-27.02	-26.39	-25.19	-25.29	-23.43	-22.26
29						
30	-23.50	-22.13	-21.54	-21.64	-21.99	-21.60

Table 9-11. $\delta^{13}\text{C}$ Correlation (r^2) table for the C₂₂-C₃₂ *n*-acids from the clays below Tuff IF.

	C ₂₂	C ₂₄	C ₂₆	C ₂₈	C ₃₀	C ₃₂
C ₂₂	1.00					
C ₂₄	0.93	1.00				
C ₂₆	0.90	0.93	1.00			
C ₂₈	0.96	0.98	0.97	1.00		
C ₃₀	0.96	0.95	0.93	0.98	1.00	
C ₃₂	0.92	0.94	0.95	0.97	0.98	1.00

9.2.3 FLK-W

The FLK-W $\delta^{13}\text{C}$ isotopic composition of the C_{25} - C_{33} odd-numbered *n*-alkanes are reported in Tables 9-12 and in Figure 9-9. Only samples that were not influenced by an Unresolved Complex Mixture, specifically for compounds $\geq\text{C}_{25}$, were measured for carbon isotopes. Of the 28 samples originally processed, only 18 were successfully analyzed for $\delta^{13}\text{C}$. Moreover, only seven samples yielded δD data and therefore, it is difficult to discuss trends in hydrogen isotopes across the FLK-W sedimentary column. There is also an uneven distribution in terms of preservation of the samples, with more data available from the clays and Levels L6 and L1 than from L5 through L2 (Table 9-12). Nevertheless, trends between compounds are obvious throughout the FLK-W sequence, with the overall tendency in $\delta^{13}\text{C}$ being towards more positive values. C_{29} and C_{31} covary throughout, as does C_{25} and C_{27} . But, C_{29} - C_{31} diverge from C_{25} - C_{27} in L5 through L3 (Fig. 9.9). C_{33} , which had fewer successfully analyzed samples than the other compounds (12/28 samples), appears to follow similar movements as C_{31} but with generally more-positive $\delta^{13}\text{C}$ values.

The highest $\delta^{13}\text{C}$ correlation between compounds was for C_{31} and C_{33} (r^2 0.86), followed by C_{29} and C_{31} (r^2 0.79), C_{27} and C_{29} (r^2 0.61), and then C_{27} and C_{31} (r^2 0.60) (Table 9-13). This suggests that compound C_{27} - C_{33} derive from similar biogenic sources, such as terrestrial plants. C_{25} does not correlate with the other compounds, except slightly with C_{27} (r^2 0.41); this is difficult to explain in that the two compounds covary throughout the column, but perhaps C_{25} is recording a mixed isotopic signature from multiple organic sources.

Mid-chain homologues (C_{21} - C_{25} *n*-alkanes) typically characterize submerged and floating aquatic macrophytes (Barnes and Barnes, 1978; Cranwell, 1984; Ficken et al., 2000), while long-chain homologues (C_{27} - C_{35} *n*-alkanes) characterize terrestrial vegetation (Eglinton and Hamilton, 1967). For FLK-W, C_{29} displays the most-negative (depleted) $\delta^{13}\text{C}$ values in 10 of the 18 samples,

and the C₂₅ *n*-alkane was the most-positive (enriched) compound in seven of the 18. The largest isotopic variation between any two samples was found in C₂₇, whereby sample 23 is depleted by -3.93‰ compared to sample 22. The greatest isotopic difference between compounds from the same sample is in FLK-W 22, where C₂₅ is depleted by -4.9‰ relative to C₂₉. The *n*-alkanes deriving from terrestrial plants, C₂₇-C₃₂, have δ¹³C values ranging from -31.5‰ to -23.0‰ with an average of -28.3 ± 0.25‰. For C₂₅, values extend from -29.7‰ to -26.2‰ with an average of -28.2 ± 0.2‰.

Table 9-12. $\delta^{13}\text{C}$ (VPDB) values for FLK-W *n*-alkanes.

			$\delta^{13}\text{C}$ <i>n</i> -Alkanes				
Level	Sample	Depth (cm)	C ₂₅	C ₂₇	C ₂₉	C ₃₁	C ₃₃
Above FLK-Wb	28	-	-27.73	-27.17	-27.14	-25.86	-24.60
L1	23	0-2	-28.53	-28.19	-25.98	-24.16	-24.69
	22	6-8	-27.87	-24.27	-23.00	-24.38	-24.64
	21	12-14	-26.72	-25.63		-24.43	
	20	18-20					
L2	19	24-26					
	18	30-32	-28.69	-28.84	-29.40	-29.61	-28.85
	17	36-38	-27.81	-27.81	-27.97	-27.96	-27.04
L3	16	42-44					
	15	48-50					
	14	54-56					
	13	60-62					
	12	66-68	-28.40	-27.78	-29.58	-27.95	-26.21
L4	11	72-74	-27.34	-27.73	-31.49	-29.03	
	10	78-80					
	09	84-86					
	08	90-92	-29.65	-28.96	-30.10	-28.72	-26.24
L5	07	96-98	-29.50	-29.44	-29.98	-29.73	-27.40
	06	102-104					
	05	108-110					
	04	114-116	-27.59	-28.52	-31.43	-31.02	
L6	03	118-120	-28.08	-28.39	-30.42	-30.33	
	02	124-126	-27.46	-28.07	-29.26	-29.09	
	01	128-130	-28.47	-28.45	-29.77	-29.70	
Clays below L6	27	134-136	-28.16	-28.50	-28.90	-29.47	-28.69
	26	140-142	-29.27	-29.58	-30.77	-31.03	-29.11
	25	146-148	-28.33	-28.79	-30.15	-30.18	-28.92
	24	152-154	-28.59	-28.23	-29.62	-29.58	-28.28

Table 9-13. $\delta^{13}\text{C}$ Correlation (r^2) table for the C₂₅-C₃₃ *n*-alkanes from FLK-W.

	C ₂₅	C ₂₇	C ₂₉	C ₃₁	C ₃₃
C ₂₅	1.00				
C ₂₇	0.41	1.00			
C ₂₉	0.03	0.61	1.00		
C ₃₁	0.14	0.60	0.79	1.00	
C ₃₃	0.10	0.43	0.56	0.86	1.00

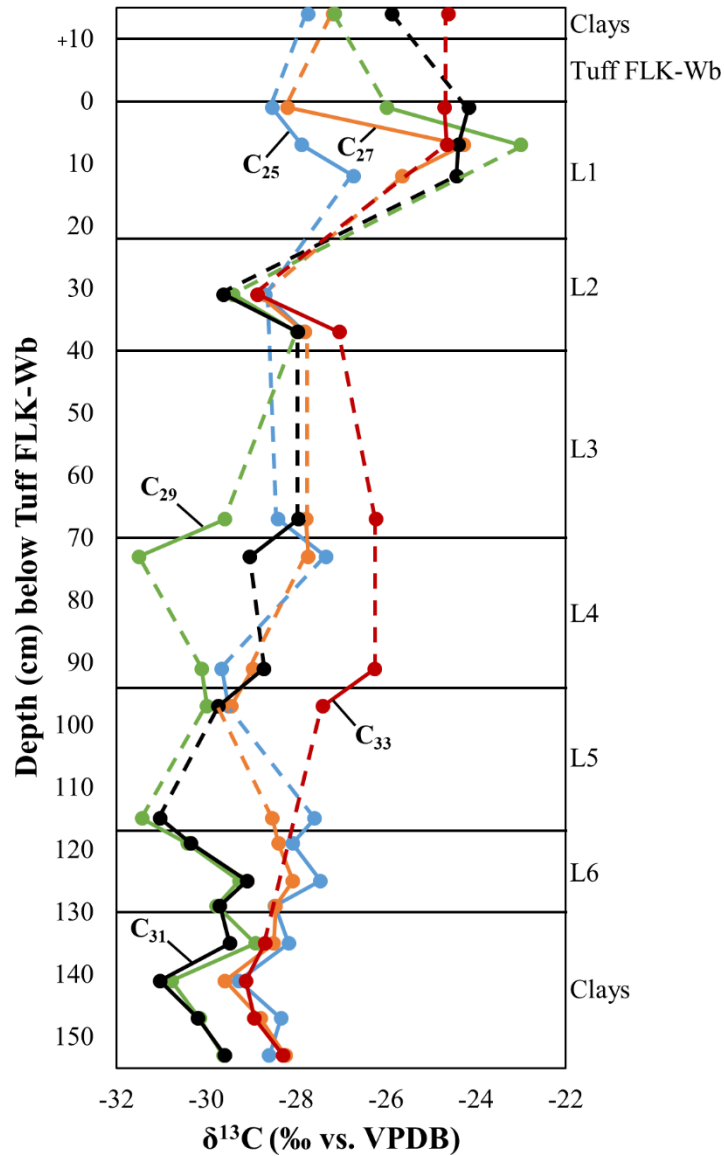


Figure 9-9. Carbon isotope values ($\delta^{13}\text{C}$ VPDB) from FLK-W for *n*-alkanes C₂₅-C₃₃. In Level 6 and the clays below L6, all samples covary and have similar positive-to-negative tendencies. Beginning in L5, C₂₉ and C₃₁ anti-phase with C₂₅ and C₂₇ until L2, where all compounds oscillate together once again. Overall, there is a general trend toward more-positive isotope values until Tuff FLK-Wb. Dotted lines represent discontinuous samples and inferred trend direction.

9.2.4 BPT

Only two Bird Print Tuff samples were successfully analyzed for $\delta^{13}\text{C}$, BPT1 (*n*-alkanes) and BPT11 (*n*-alkanoic acids). This is due in part to the poor preservation and presence of UCMs in the *n*-alkane samples, and low concentrations and issues with the IRMS injector syringe in the *n*-acids. Nonetheless, the $\delta^{13}\text{C}$ data is presented in Table 9-14. Carbon isotope values range from -27.7‰ to -24.6‰ with an average of $-26.5 \pm 0.6\text{‰}$ for C₂₅-C₃₃ in BPT1. The C₂₅-C₂₉ *n*-alkanes are similar in $\delta^{13}\text{C}$ concentration (having an average value of $-27.4 \pm 0.2\text{‰}$), while C₃₁ is intermediary in that it is enriched by +1.3‰ compared to C₂₉ but depleted by -1.3‰ relative to C₃₃. C₃₃ is the most-enriched compound (-24.6‰), and was likely produced by C₄ grasses only, whereas C₂₅-C₃₁ record a mixed C₃/C₄ signal with C₃₁ having a greater input from C₄ plants than C₂₅-C₂₉. For the *n*-alkanoic acids, carbon isotope values range from -23.4‰ to -21.5‰ with an average of $-22.4 \pm 0.3\text{‰}$ for C₂₂-C₃₀ in BPT11. The largest variation between compounds is in C₂₂ and C₂₈, in which C₂₈ is depleted by -1.9‰ compared to C₂₂. Both C₂₂ and C₂₄ (average $-21.7 \pm 0.2\text{‰}$) are enriched relative to C₂₈ and C₃₀ (average $-23.1 \pm 0.3\text{‰}$), possibly suggesting mixed organic sourcing with C₂₆ incorporating an overlap between the two sources; C₂₆ is enriched by +0.7‰ from the C₂₈-C₃₀ average and depleted by -0.7‰ from C₂₂-C₂₄.

Table 9-14. $\delta^{13}\text{C}$ (VPDB) values for the Bird Print Tuff *n*-alkanoic acids and *n*-alkanes. Isotope values for the *n*-acids are corrected to account for the isotopic contribution from the methyl group added during methylation.

$\delta^{13}\text{C}$ <i>n</i> -Alkanoic Acids					
Sample	C ₂₂	C ₂₄	C ₂₆	C ₂₈	C ₃₀
BPT11	-21.46	-21.92	-22.42	-23.42	-22.85

$\delta^{13}\text{C}$ <i>n</i> -Alkanes					
Sample	C ₂₅	C ₂₇	C ₂₉	C ₃₁	C ₃₃
BPT1	-27.73	-27.17	-27.14	-25.86	-24.60

9.2.5 Castle Clays

The $\delta^{13}\text{C}$ and δD isotopic composition of the C_{22} - C_{32} even-numbered FAMES from the Castle Clays are reported in Tables 9-15 and 9-17, and Figures 9-10 and 9-11. All Castle Clay samples were measured for both carbon and hydrogen isotopes, but not all samples yielded data for both; sample 10 returned no $\delta^{13}\text{C}$ data, while sample 09 did not yield δD , and sample 14 had concentrations too low to collect either $\delta^{13}\text{C}$ or δD . The variation in carbon isotopes throughout the Castle below the carbonate horizon includes subtle changes in distribution, with the largest $\delta^{13}\text{C}$ fluctuations occurring between ~90-130 cm depth, specifically in compounds C_{24} , C_{26} and C_{32} , and to a lesser extent C_{28} and C_{30} . For the most part C_{24} - C_{32} covary and become more-positive or more-negative collectively. However, C_{26} , which has the largest variability between individual samples, has an anti-phased $\delta^{13}\text{C}$ value at 167-163 cm (Sample 03). Additionally, C_{30} has very little change in $\delta^{13}\text{C}$ above 130 cm, while the other compounds have large negative shifts at this depth. C_{22} is completely anti-phased compared to C_{26} (Fig. 9-10), and for the most part, anti-phased with C_{24} , C_{28} - C_{32} ; below 150 cm, they slightly covary. Above the carbonate horizon, C_{24} - C_{32} vary together and contrast with C_{22} . For hydrogen, C_{28} - C_{32} have remarkable consistency throughout the entire column both above and below the carbonate horizon. C_{24} on the other hand, anti-phases with the larger chains at two major depths below the carbonate horizon; at 167-163 cm and 96-93 cm (Fig. 9-11). C_{26} also diverges from C_{28} - C_{32} at 96-93 cm but displays similar positive-to-negative-trends for the remainder of the column. Again, C_{22} is anti-phased, except at 96-93 cm where it covaries with both C_{24} and C_{26} . Above the carbonate horizon, C_{22} and C_{24} fluctuate together, opposite to compounds C_{26} - C_{32} . Therefore, C_{22} likely derives from a non-plant source, while C_{24} and C_{26} have overlapping input from multiple biogenic sources, and C_{28} - C_{32} derive exclusively from terrestrial vegetation.

The highest $\delta^{13}\text{C}$ correlation between compounds was for C_{30} and C_{32} (r^2 0.59), followed by C_{28} and C_{30} (r^2 0.45 entire column, but 0.91 below the carbonate horizon), and then C_{26} and C_{28} (r^2 0.44) (Table 9-16). C_{22} correlates slightly with C_{26} (r^2 0.35) but does not with any other compound. C_{24} also has poor correlation with the other *n*-acids, with its greatest association being with C_{32} (r^2 0.23). The greatest δD correlation between compounds was for C_{28} and C_{30} (r^2 0.78), followed by C_{30} and C_{32} (r^2 0.69), C_{28} and C_{32} (r^2 0.56), and then C_{24} and C_{26} (r^2 0.54) (Table 9-18). C_{24} also shows a relationship with C_{22} (r^2 0.47) but is poorly associated with any other compound besides C_{26} . These correlations suggest that for C_{22} - C_{26} , there is overlapping biosynthesis sources, while C_{28} - C_{32} derive from terrestrial plants that utilize the same source water.

For the Castle Clays, C_{24} displayed the most-negative (depleted) $\delta^{13}\text{C}$ values in six of the 12 samples, and the C_{32} *n*-acid was the most-positive (enriched) compound in five of the 12 samples. The largest isotopic variation between any two samples was in C_{22} , whereby sample 03 is depleted by -9.1‰ compared to sample 02. In the terrestrial plant-derived compounds (C_{28} - C_{32}), the largest difference between any two samples is in C_{28} , where sample 12 is depleted by -1.9‰ compared to sample 11. The greatest isotopic difference between compounds from the same sample is in Castle Clays 03, where C_{22} is depleted by -6.9‰ compared to C_{26} . For terrestrial plants, the largest variation comes from sample 11, where C_{30} is depleted by -2.3‰ in comparison to C_{28} . C_{28} - C_{32} $\delta^{13}\text{C}$ values range from -25.1‰ to -21.9‰ with an average of $-23.4 \pm 0.2\%$. The C_{22} values range from -29.8‰ to -20.8‰ with an average of $-24.4 \pm 0.7\%$. Finally, C_{24} and C_{26} (compounds likely deriving from multiple sources) range from -25.9‰ to -22.1‰ with an average of $-24.1 \pm 0.2\%$.

Regarding δD , C_{26} displayed the most-positive (enriched) values in seven of the 12 samples while the C_{22} *n*-acid was the most-negative (depleted) compound in nine of the 12 samples. The

largest isotopic variation between any two samples was found in C₂₆, whereby sample 08 is enriched by +59.9‰ compared to sample 07. The largest isotopic variation between any two samples in the C₂₈-C₃₂ compounds is in sample 11, which is enriched by +24.0‰ relative to sample 10; however, this enrichment happens across the carbonate horizon. When the samples are divided between *above* and *below* the carbonate horizon, the largest δD variation between samples is in Castle Clays 12, which is depleted by -23.19‰ from Castle Clays 11 (above the carbonate horizon) (Fig. 9-11). The greatest isotopic difference between compounds from the same sample is in sample 07, where C₂₆ is depleted by -55.9‰ compared to C₃₂. When focusing on C₂₈-C₃₂, the highest disparity is in sample 12, where C₃₀ is enriched by +11.7‰ against C₃₂. The δD of the C₂₂ and C₂₄ *n*-alkanoic acids suggests that a different water/hydrogen source was utilized for biosynthesis or that the isotope fractionation is different from that of the C₂₈-C₃₂ compounds. Therefore, when compared, C₂₂-C₂₄ δD values range from -177.3‰ to -128.7‰ with an average of $-147.4 \pm 3.5\%$. C₂₈-C₃₂ have δD values going from -150.9‰ to -115.6‰ with an average of $-137.1 \pm 1.4\%$. Finally, C₂₆, the compound that likely derives from multiple biogenic sources, has δD from -188.6‰ to -121.3‰ with an average of $-138.7 \pm 5.1\%$.

Table 9-15. $\delta^{13}\text{C}$ (VPDB) values for the Castle Clays. Isotope values are corrected to account for the isotopic contribution from the methyl group added during methylation.

		$\delta^{13}\text{C}$ <i>n</i> -Alkanoic Acids					
Sample	Depth (cm)	C ₂₂	C ₂₄	C ₂₆	C ₂₈	C ₃₀	C ₃₂
14	0-5	-22.96	-24.19	-23.13	-23.09	-22.60	-21.93
13	10-13	-23.15	-24.99	-24.33	-24.28	-24.26	-23.27
12	17-21	-23.40	-25.09	-23.95	-23.94		
11	25-28	-23.24	-25.20	-22.27	-22.07	-24.34	-23.66
10	40-46						
09	55-61	-24.47	-23.85	-22.92	-23.29	-23.19	-23.20
08	75-79	-26.87	-24.45	-22.12	-22.96	-23.16	-22.07
07	93-96	-25.97	-24.56	-22.83	-22.52	-22.96	-21.88
06	104-110	-23.32	-25.91	-25.03	-23.51	-23.07	-23.34
05	124-133	-25.06	-24.11	-22.63	-22.84	-23.04	-22.12
04	147-149	-24.12	-24.54	-23.78	-23.68	-23.56	-22.86
03	163-167	-29.84	-24.81	-22.92	-24.87	-25.13	-23.65
02	181-186	-20.79	-24.41	-25.15	-25.08	-25.01	-23.43
01	226-235						

Table 9-16. $\delta^{13}\text{C}$ Correlation (r^2) table for the C₂₂-C₃₂ *n*-alkanoic acids from the Castle Clays.

	C ₂₂	C ₂₄	C ₂₆	C ₂₈	C ₃₀	C ₃₂
C ₂₂	1.00					
C ₂₄	0.01	1.00				
C ₂₆	0.35	0.18	1.00			
C ₂₈	0.00	0.01	0.44	1.00		
C ₃₀	0.00	0.05	0.07	0.45	1.00	
C ₃₂	0.02	0.23	0.17	0.25	0.59	1.00

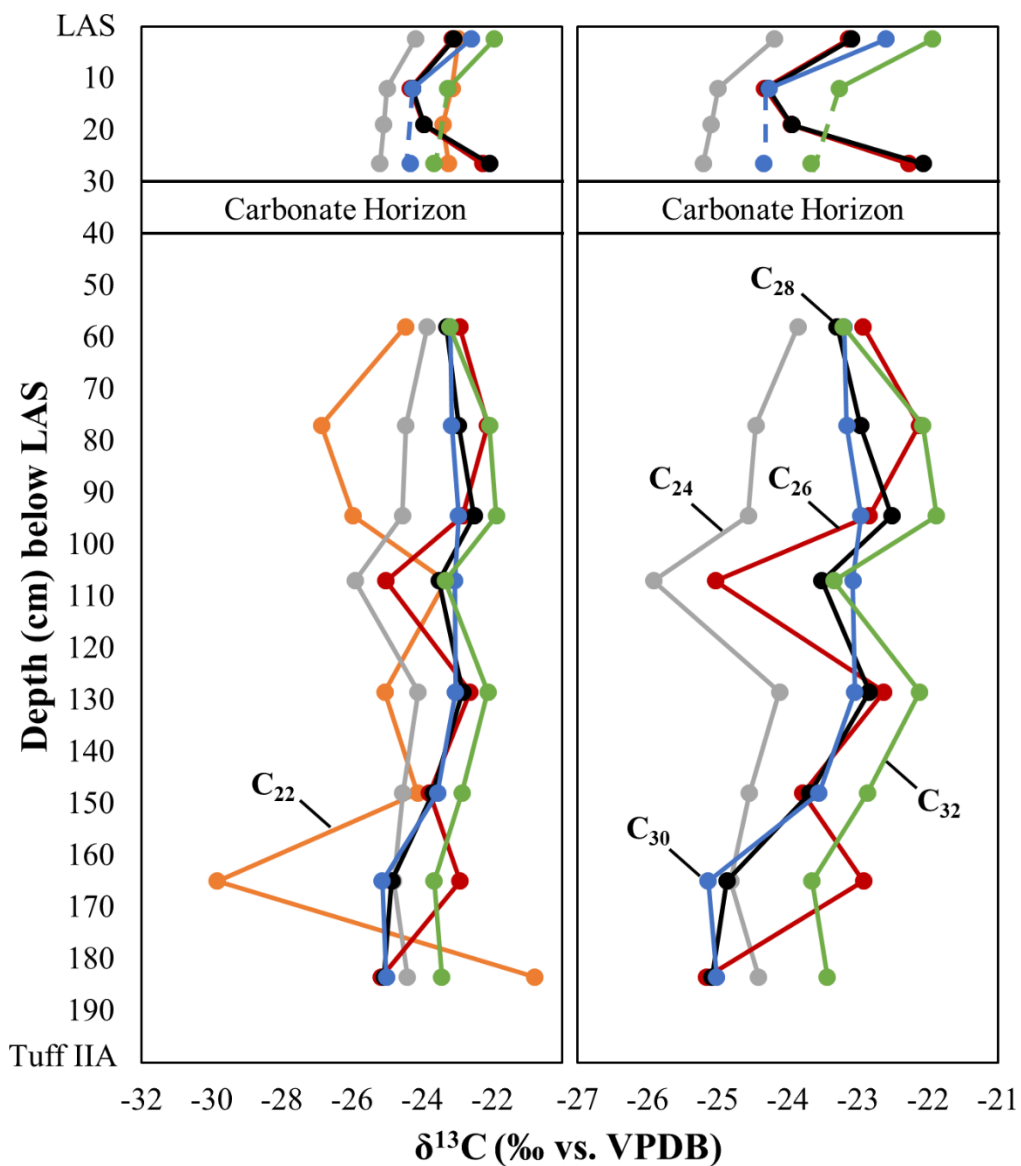


Figure 9-10. Carbon isotope values ($\delta^{13}\text{C}$ VPDB) from the Castle Clays for n -alkanoic acids C_{22} - C_{32} . The left panel shows all compounds while the right side excludes the C_{22} n -acid. Compound C_{22} is anti-phased with the other n -acids, suggesting it was biosynthesized by a non-terrestrial vegetation source; i.e. algae or an emergent plant. Compounds C_{28} - C_{32} , and to a lesser extent C_{24} , have the same general positive-to-negative oscillation trend, suggesting they derive from the same biosynthetic source. C_{26} on the other hand, is anti-phased below 150 cm and possibly derives from multiple organic sources.

Table 9-17. δD (VSMOW) values for the Castle Clays. Isotope values are corrected to account for the isotopic contribution from the methyl group added during methylation.

δD <i>n</i>-Alkanoic Acids							
Sample	Depth (cm)	C₂₂	C₂₄	C₂₆	C₂₈	C₃₀	C₃₂
14	0-5	-147.93	-135.35	-130.06	-137.47	-141.69	-147.09
13	10-13	-138.11	-128.72	-124.90	-130.37	-132.63	-134.86
12	17-21	-138.11	-128.84	-132.54	-134.62	-131.61	-143.28
11	25-28	-168.05	-136.08	-121.31	-115.62	-121.26	-120.09
10	40-46	-149.70	-143.90	-137.09	-139.64	-143.54	-140.20
09	55-61						
08	75-79	-150.95	-144.29	-128.71	-130.24	-130.46	-134.13
07	93-96	-167.48	-157.63	-188.60	-144.09	-134.21	-132.72
06	104-110	-153.22	-143.67	-147.63	-150.37	-150.45	-145.53
05	124-133	-157.38	-140.21	-137.13	-139.15	-137.69	-141.92
04	147-149	-158.10	-145.84	-147.24	-138.03	-138.27	-138.15
03	163-167	-177.34	-147.99	-129.59	-131.82	-130.69	-135.67
02	181-186	-140.60	-138.22	-139.95	-142.38	-144.85	-150.99
01	226-235						

Table 9-18. δD Correlation (r^2) table for the C₂₂-C₃₂ *n*-alkanoic acids from the Castle Clays.

	C₂₂	C₂₄	C₂₆	C₂₈	C₃₀	C₃₂
C₂₂	1.00					
C₂₄	0.47	1.00				
C₂₆	0.07	0.54	1.00			
C₂₈	0.04	0.15	0.40	1.00		
C₃₀	0.13	0.02	0.08	0.78	1.00	
C₃₂	0.32	0.03	0.01	0.56	0.69	1.00

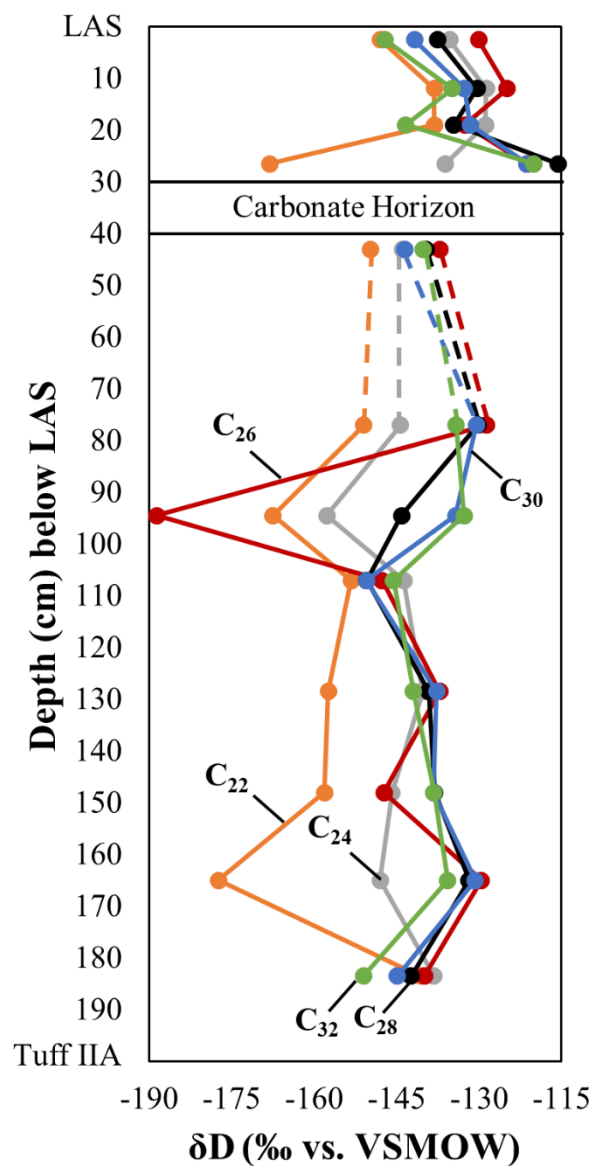


Figure 9-11. Hydrogen isotope values (δD VSMOW) from the Castle Clays for *n*-alkanoic acids C₂₂-C₃₂. The C₂₂ and C₂₄ *n*-acids anti-phase in comparison to the other compounds, suggesting they were biosynthesized by non-terrestrial vegetation sources; between ~100 and 150 cm, C₂₄ does however covary with C₂₈-C₃₂. The C₂₈-C₃₂ compounds have the same positive-to-negative oscillation trend both above and below the carbonate horizon, suggesting they derive from the same biosynthetic source. C₂₆ has large fluctuations in δD between 80 and 110 cm, even though the remainder of the record is comparable to C₂₈-C₃₂. This might suggest that the δD from sample 07, collected at 96-93 cm, records a biogenic isotope signature of mixed origin.

Table 9-19. Results Summary

Sampling Location	Method	Plant Landscape ($\delta^{13}\text{C}$)	Water Availability (δD)
FLK-N	Refined	C ₃ dominated with abundant macrophytes	Abundant freshwater from seeps or surface streams
Clays below Tuff IF	Refined	Mosaic with open grasslands, closed woodlands, and ecotones	Variable throughout the landscape
Castle Clays	Refined	C ₄ grass dominated with a moderate C ₃ bushland component	Dry; precipitation likely the main source
FLK-W	Initial	L6-L4 are C ₃ riparian woodland; L3-L2 are C ₃ /C ₄ mix; L1 is C ₄ dominated	Diatoms suggest abundant freshwater in L6-L4; Stream likely gone by L1
BPT	Initial	Inconclusive	Inconclusive
LAS	Initial	Inconclusive	Inconclusive

Refined: Based on the updated protocol that eluted total lipids over Aminopropyl columns first

Initial: Based on the original protocol that eluted total lipids over silica gel columns first

See Sections 8.4 and 8.5

CHAPTER 10: DISCUSSION

10.1 Leaf Wax Lipid Preservation

One of the major issues with studying plant leaf wax lipid biological markers in terrestrial sediments from Olduvai Gorge is the differential preservation of *n*-alkanes and *n*-alkanoic acids in various sedimentary matrices. Grain size may be one major determinant of biomarker preservation, with clays and silts seemingly having higher concentrations than coarser sands. Samples from Bed I came from fine-grained, silty/waxy clays overlain by Tuff IF. Samples from Bed II on the other hand, were collected in tuffaceous silt, silty clay/claystones, fluvial conglomerates and sands, and unconsolidated sandstones. Overall, there was greater difficulty in processing the Bed II samples for *n*-alkanes and *n*-acids; however, changes to the methodological approach may explain the observed differences between the *clay* and *non-clay* samples, as FLK-W, BPT, and LAS were not eluted over Aminopropyl columns to begin with, nor were they separated using silver nitrate infused silica gel (SiAgNO₃) columns which resulted in GC chromatograms with Unresolved Complex Mixtures (UCMs) (see Section 8.4). Conversely, the Castle Clays, clays below Tuff IF, and FLK-N were first eluted over Aminopropyl, then separated with SiAgNO₃. These were more successful methodologically, as both *n*-alkanes, without UCMs, and *n*-alkanoic acids, without double-bonded fatty acids, were quantifiable with GC-MS and IRMS. It should be noted that Aminopropyl column chromatography does not necessarily need to be conducted first, as *n*-acids were extracted from FLK-W and BPT following the separation of the total lipids into non-polar and polar fractions, where the polar fraction was subsequently eluted of Aminopropyl.

The samples collected in the Lower Augitic Sandstone were the poorest in terms of preservation, as UCMs completely eclipsed the *n*-alkanes while higher molecular weight *n*-

alkanoic acids were not detected with GC-MS. As both the *n*-alkanes and *n*-acids were unquantifiable (unlike those from FLK-W and BPT), it is likely that the preservation of the LAS was dictated by the depositional environment and not due to methodological-related issues. The Lower Augitic Sandstone was deposited along the eastern paleo-lake-margin as a braided stream channel flowing northwest towards the central lake (Uribelarrea et al., 2017), and consists of loosely consolidated or unconsolidated mafic and augitic sands. During deposition, plant life would not have colonized or thrived along the sandy stream channels because of highly erodible banks, an excessive supply of sediment, inconsistent water levels, or low overall nutrients of the sediments. Even if pioneering species established on mid-chain bars within the braided streams, they likely did not contribute significant leaf wax lipids to local sediments. Therefore, higher molecular weight lipids were never biosynthesized by terrestrial plants (as they were nonexistent), and lipids coming from the highlands or plants growing beyond the braided stream channel(s) or within bars would have been transported by the streams and deposited in the silty/clayey sediments in the paleo-lake basin once stream energy lessened. This is attested to by the detection of lower ($\leq C_{24}$) molecular weight *n*-acids in low quantities, which may suggest that algae or aquatic plants grew within or along the braided stream channels even though terrestrial plants did not develop along the banks. Wu et al., (2019) show that soil is the major source of sedimentary and riverine plant waxes, so the fact that lipid compounds were so poorly preserved in the LAS suggests that soils did not developed along the braided stream channels, and if waxes were transported from the highlands, they were likely deposited further downstream. Interestingly, some of the best preservation of *n*-alkanes at FLK-W comes from Levels 5 and 6, which belong to the same fluvial system as the LAS (Uribelarrea et al., 2017). However, at FLK-W, the braided streams likely

converged into a single channel (UribeArrea et al., 2017) allowing for a riparian zone to develop and thus a growing surface for terrestrial vegetation.

There is some contention on the stratigraphic position of FLK-W. McHenry and Stanistreet (2018) propose that the Acheulean site lies within the Middle Augitic Sandstone, a deposit similar in most respects to the LAS (Hay, 1976), but located in middle Bed II above Tuff IIB. Conversely, Diez-Martín et al., (2015) and UribeArrea et al., (2017) situate FLK-W above Tuff IIA in lower Bed II, with the Bird Print Tuff appearing 25 cm above Tuff FLK-Wb. McHenry and Stanistreet (2018) however, position the BPT 3.0 m above Tuff IIB, which is not exposed at FLK-W, and therefore suggest that Tuffs IIA and B and the LAS were eroded before the FLK-W sequence was deposited along with the MAS; this also insinuates that the strata studied by UribeArrea et al., (2017) was in actuality the MAS, not the LAS. Nevertheless, the placement of FLK-W in either lower or middle Bed II is currently arbitrary, as both Tuffs FLK-Wa and FLK-Wb are well dated (whereas there is no firm date for Tuff IIB), and the similarities between the LAS and the MAS would imply that if similar geologic processes were occurring when both sandstones were deposited, then terrestrial plants would have had difficulty growing on either substrate. Consequently, the interpretation of poor lipid preservation in the LAS remains intact for the MAS: the lack of plant growth in the braided stream channel precluded the deposition of lipids into terrestrial sediments.

The preservation of *n*-alkanes, albeit with evidence of (bio)degradation, in FLK-W Levels 5 and 6, believed to be contemporary with the LAS, is surprising when compared to the poor preservation observed in the clayish silt of Level 3. As previously mentioned, the differential preservation between each archaeological level at FLK-W may be due to methodological issues, as silts would seemingly have higher concentrations of lipids than the fine-grained sand and silt of

L1 or the conglomerate of L6. This is not the case however, as the conglomerates of L6, the coarse sand of L5, and sand and silt of L1 had greater total lipid concentrations than L3. (Level 4 also had high concentrations of *n*-alkanes and *n*-acids, but it was within this unit that the UCMs started becoming prevalent.) One hypothesis as to why the archaeological levels with larger grain sizes had greater abundances of lipids involves stream energy and burial speed; higher energy environments allowed for the rapid deposition of sediment thereby burying plant material before it could be extensively (bio)degraded. Archaeological Level 3 on the other hand, may be akin to the modern eolian sediments found in the greater Olduvai area today. That is, samples with extensive UCMs suffered from the multifaceted interactions between microbial activity, alkaline soil chemistry, soil temperature, and the extreme variance in seasonal precipitation that subjected the *n*-alkanes to a high degree of alteration. Therefore, the second major issue with studying plant leaf wax lipid biological markers in terrestrial sediments from Olduvai Gorge is *taphonomy*, or the biological and mechanical alteration of biomarkers upon release into the environment.

10.1.1 Plant Wax Abundances

The contribution of specific *n*-alkanoic acid compounds (i.e. C₂₂ vs. C₂₈,) to the total abundance of sedimentary lipids is used to compare the input and isotopic influence of algae, submerged plants, or terrestrial plants to terrestrial sediments (Liu and Liu, 2017). In the groups of samples that could be confidently measured for the concentration of lipids extracted from terrestrial sediments, Castle Clays sample 06 had the greatest concentration of both the C₂₀-C₃₄ *n*-acids and the C₂₁-C₃₅ *n*-alkanes with 311.37 µg/g and 259.90 µg/g of dry sediment, respectively. This sample is a bit of an anomaly however (Fig. 10-1), as the next most-abundant sample in the set is Castle Clays 02 which has total *n*-acid and *n*-alkane concentrations of 64.27 µg/g and 105.73

$\mu\text{g/g}$, respectively. (This is a difference of $247.1 \mu\text{g/g}$ (*n*-acids) and $154.17 \mu\text{g/g}$ (*n*-alkanes) between Castle Clays 02 and 06.) The clays below Tuff IF sample 15 had the second highest total concentration of *n*-alkanoic acids with $196.94 \mu\text{g/g}$, while sample 20 had the most abundant *n*-alkanes of $70.98 \mu\text{g/g}$. Finally, the most-abundant FLK-N sample is 02, which has a total concentration of $\text{C}_{20}\text{-C}_{32}$ *n*-acids of $78.63 \mu\text{g/g}$ (*n*-alkanes were not calculated).

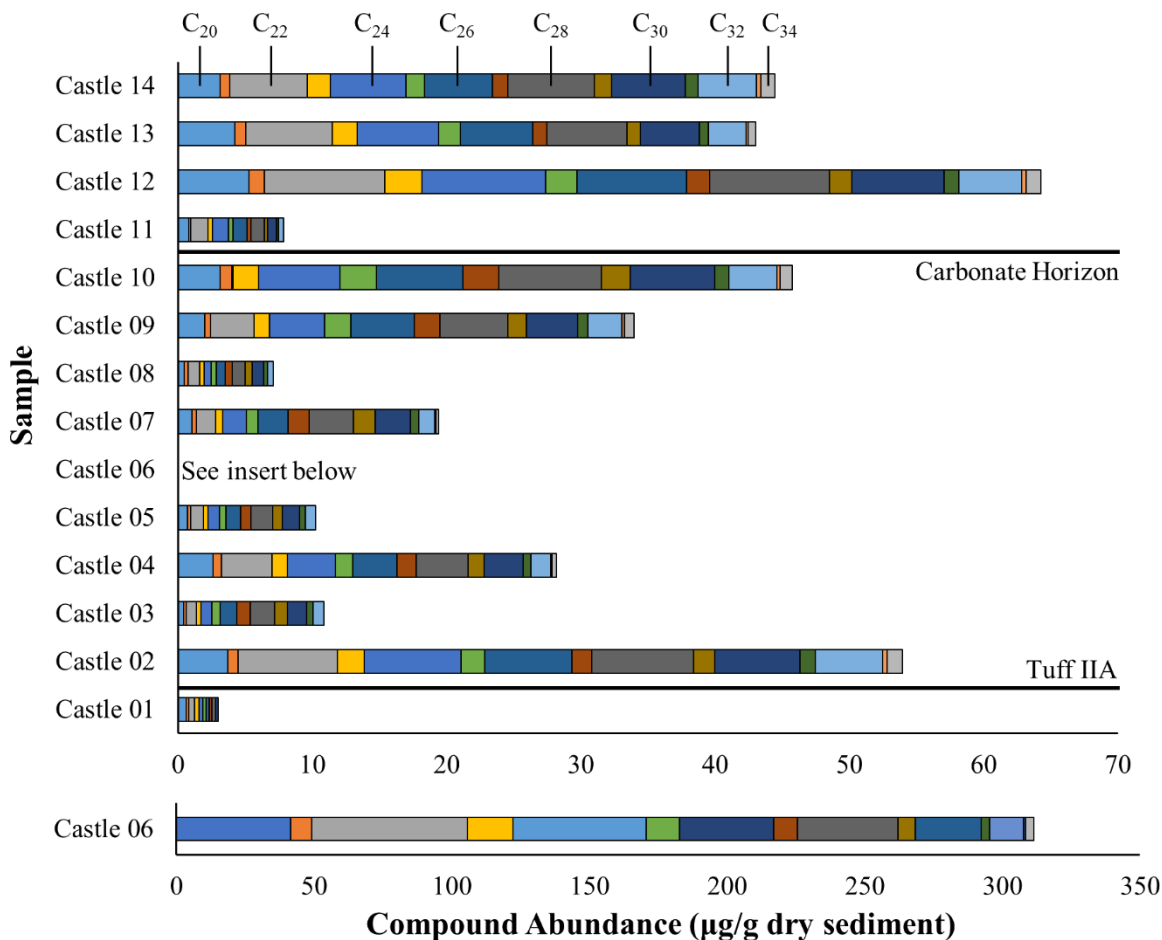


Figure 10-1. Abundances for the C_{20} to C_{34} *n*-alkanoic acids from the Castle Clays. The even numbered compounds are most dominant. Concentrations were not consistent, specifically below the carbonate horizon. Note the concentrations for Sample 06 (insert below) which are much larger than those of the other samples.

Castle Clays

For the Castle Clays, there is no relationship (r^2 0.0028) between depth/age of samples and *n*-alkanoic acid concentrations (Fig. 10-1). Castle Clays 01 has the lowest total *n*-acid abundance, which may be due to its deposition below Tuff IIA whereas all other samples came from above the tuff. Castle Clays 01 was also the only sample that had concentrations too low for IRMS analysis. Sample 11 also has relatively low total *n*-acids (7.85 $\mu\text{g/g}$), which may be related to the carbonate horizon formation; pedogenic carbonates form in soils with a net water deficit, and occur globally in soils where annual rainfall is less than 1,000 mm per year (Retallack, 1990). If a decrease in precipitation occurred, which is attested to by the positive δD shift coinciding with sample 11 (Fig. 10-2), then there was likely a decrease in total plant biomass and total leaf wax lipids in response to dryer conditions. Furthermore, there is a general correlation throughout the Castle column in which *n*-acid abundance directly responds to precipitation amount (Fig. 10-2). Samples that have low relative abundances, Castle Clays 03 (10.88 $\mu\text{g/g}$), 08 (7.08 $\mu\text{g/g}$), and 11, coincide with more-positive isotope shifts indicative of reduced rainfall, while those samples with the greatest total concentrations, 02 (53.95 $\mu\text{g/g}$), 06 (311.37 $\mu\text{g/g}$), 10 (45.76 $\mu\text{g/g}$), 12 (64.27 $\mu\text{g/g}$), and 14 (44.46 $\mu\text{g/g}$), coincide with more-negative δD and increased rainfall (Niedermeyer et al., 2010). Sample 05 seems to go against this trend however, as it has a low total *n*-acid concentration (10.26 $\mu\text{g/g}$) but δD slightly more-negative than sample 04 (28.19 $\mu\text{g/g}$). Sample 05 is only depleted by -1.12‰ compared to 04, which is negligible when comparing δD from two samples. Therefore, there is no significant change in precipitation between samples 04 and 05, so the overall decrease in concentration between the two datapoints is difficult to explain in relation to the other Castle Clay samples.

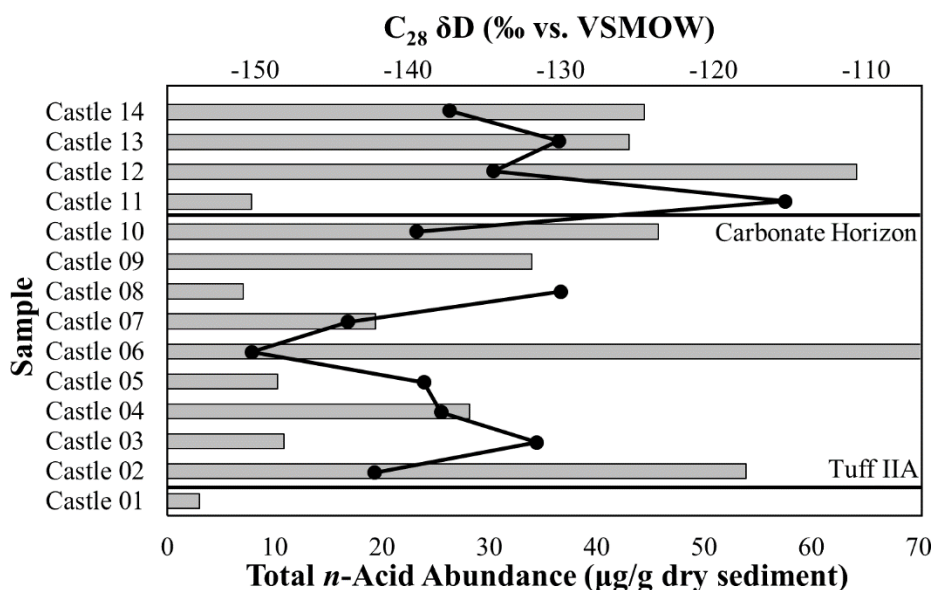


Figure 10-2. Abundances of Castle Clays *n*-alkanoic acids plotted against δD from the C_{28} *n*-acids to show comparison between lipid concentrations and isotope values. Increases in total abundance of *n*-acids coincide with depletions in δD , which signifies an increase in rainfall and correlating plant biomass.

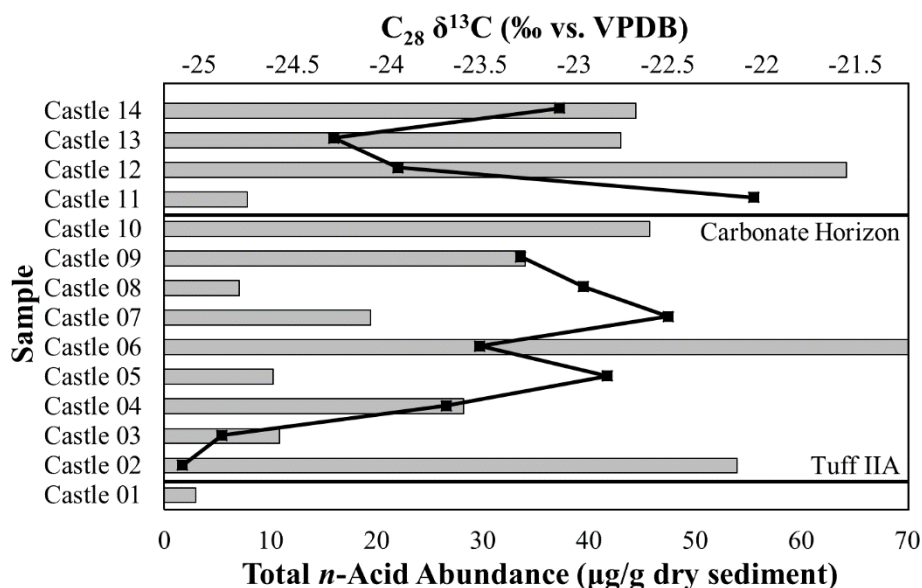


Figure 10-3. Abundances of Castle Clays *n*-alkanoic acids plotted against $\delta^{13}C$ from the C_{28} *n*-acids to show comparison between lipid concentrations and isotope values. This correlation is not as evident however, as not all $\delta^{13}C$ enrichments (suggesting an increase in C_4 grasses) coincide with decreases in total *n*-acid abundance (suggesting less overall biomass).

Plant ecological lifeform (trees vs. shrubs vs. grasses) plays a role in total biomass and lipid production, as trees have higher above-ground biomass relative to grasses (Wu et al., 2019). Consequently, we would expect to see changes in $\delta^{13}\text{C}$ coinciding with *n*-acid concentration (Fig. 10-3), where more-positive values would suggest a greater amount of C_4 grasses while more-negative isotope data would imply increased C_3 vegetation. This relationship is not as apparent as that observed for δD . Some samples, 03, 05, 07, and 11, have lower total *n*-alkanoic acid abundances coinciding with more-positive $\delta^{13}\text{C}$, while 02, 06, 09, and 12 have greater *n*-acid concentrations matching the more-negative $\delta^{13}\text{C}$. This suggests that lipid abundance is directly tied to changes in C_3 vegetation coverage, whereby a depletion in $\delta^{13}\text{C}$, indicative of an increase in C_3 plants, correlates with greater lipid concentrations in terrestrial sediments. On the other hand, samples 04, 08, 13, and 14 counter this trend as concentrations dissociate with $\delta^{13}\text{C}$; that is, higher *n*-acid amounts accompany $\delta^{13}\text{C}$ enrichment which implies greater total C_4 biomass (samples 04 and 14) while lower *n*-acid amounts accompany $\delta^{13}\text{C}$ depletion which implies greater total C_3 biomass (samples 8 and 13) (Fig. 10-3). (This disassociation may be related to the anti-phasing of $\delta^{13}\text{C}$ and δD in these samples (see Section 10.3.2).)

Another noteworthy observation is the large decrease in concentration between Castle Clays 02 (53.95 $\mu\text{g/g}$) and 03 (10.88 $\mu\text{g/g}$) yet only an insignificant $\delta^{13}\text{C}$ enrichment of +0.21‰ for C_{28} and +0.12‰ for C_{30} . Although the change in concentrations between samples would imply a change to the overall plant landscape abundance, $\delta^{13}\text{C}$ suggests that the plant community remained relatively unchanged. This is opposite to the increase in concentration between Castle Clays 03 (10.88 $\mu\text{g/g}$) and 04 (28.19 $\mu\text{g/g}$) in addition to the larger $\delta^{13}\text{C}$ enrichment of +1.18‰ for C_{28} and +1.58‰ for C_{30} that suggests greater C_4 input, assuming C_4 biomass is lower relative to C_3 trees. This then changes again, as there is an enrichment between sample 04 and 05 of

+0.85‰ for C₂₈ and +0.51‰ for C₃₀, yet a decrease in total concentration from 28.19 µg/g to 10.26 µg/g. Thus, between samples 03 and 04, plant type (from δ¹³C) has no apparent impact on *n*-acid abundance (yet precipitation amount might), while between samples 04 and 05, a greater C₄ abundance correlates with lower *n*-alkanoic acid concentration, like other samples in the Castle Clays. These opposing observations are difficult to explain, as an increase in precipitation should result in an increase in C₃ biomass as seen in samples 02, 06, 09, and 12. Because C₄ plants increased in abundance following an increase in precipitation when samples 04 and 14 were deposited, and samples 08 and 13 correspond to a decrease in both biomass and precipitation yet an increase in C₃ vegetation, additional environmental stimuli must have been in effect.

Generally, there is not a considerable difference in δ¹³C throughout the entirety of the Castle Clays. The largest isotopic difference between samples is 3.03‰ for C₂₆, 3.01‰ for C₂₈, and 2.54‰ for C₃₀ (C₂₂ has a difference of 9.05‰, but because this compound likely does not derive from terrestrial/vascular plants, it will be discussed later). This indicates that on the whole, C₄ plants dominated the Castle environment when the sediments were deposited, and total *n*-alkanoic acid concentration is associated with changes in precipitation. However, for those samples (04, 08, 13, 14) in which precipitation dictates biomass, but C₃ increases with reduced rainfall and decreases with amplified rainfall, another mechanism influences δ¹³C of terrestrial plants. One explanation is that changes in CO₂ diminished the effects of precipitation on C₃ plants so that during periods of reduced rainfall (samples 08 and 13), C₃ increased because of higher atmospheric CO₂, whereas during periods of increased rainfall (samples 04 and 14), C₄ dominated due to lower CO₂ concentrations. The more likely explanation though, is that total biomass was shaped by plants with different water-use efficiencies (WUE), whereby plants with greater WUE (as inferred by more-positive δ¹³C values) are negatively correlated with δD values for C₂₆, C₂₈,

and C₃₀ *n*-acids. Plant water-use efficiency is the ratio of the rate of carbon assimilation (photosynthesis) to the rate of water loss (transpiration) (Farquhar et al., 1989; Hou et al., 2007a), and is influenced by temperature, precipitation, sunlight exposure, and other environmental factors, but also by plant-type physiological mechanisms. Accordingly, plants with better WUE transpire less water to produce the same amount of leaf biomass compared to species with lower WUE, and thus, there would be an increase in plant biomass associated with the positive-shifts in δ D. Controls on $\delta^{13}\text{C}$ and δ D will be discussed in length in Section 10.3.2.

FLK North

For FLK-N, there is no relationship (r^2 0.1276) between depth/age of samples and *n*-alkanoic acid concentrations (Fig. 10-4) but overall, the samples had rich abundances of leaf wax lipids. Of the C₂₀-C₃₄ *n*-acids, FLK-N 07 had the smallest total concentration of 51.05 $\mu\text{g/g}$ of dry sediment, while sample 02 had the greatest with 78.63 $\mu\text{g/g}$. Unlike the Castle Clays, there are no large differences in lipid concentrations amongst samples at FLK-N, and the greatest change between any two samples is -23.36 $\mu\text{g/g}$ between FLK-N 01 (55.27 $\mu\text{g/g}$) and 02 (78.63 $\mu\text{g/g}$). Furthermore, the abundances do not correlate with δ D or $\delta^{13}\text{C}$ (Figs. 10-5, 10-6), meaning that precipitation and plant type do not influence the concentrations consistently through the column; for example, the two most $\delta^{13}\text{C}$ depleted samples (02, 07) have both the most and least abundant concentrations of *n*-acids, respectively (Fig. 10-6). This is likely due to the uniform composition of plant type through the deposition period in Level 1 at FLK-N as indicated by the relatively stable values of both $\delta^{13}\text{C}$ and δ D. The largest $\delta^{13}\text{C}$ difference in isotope values between any two consecutive samples is -2.99‰ for C₂₆ (samples 04 and 05), -1.04‰ for C₂₈ (samples 01 and 02),

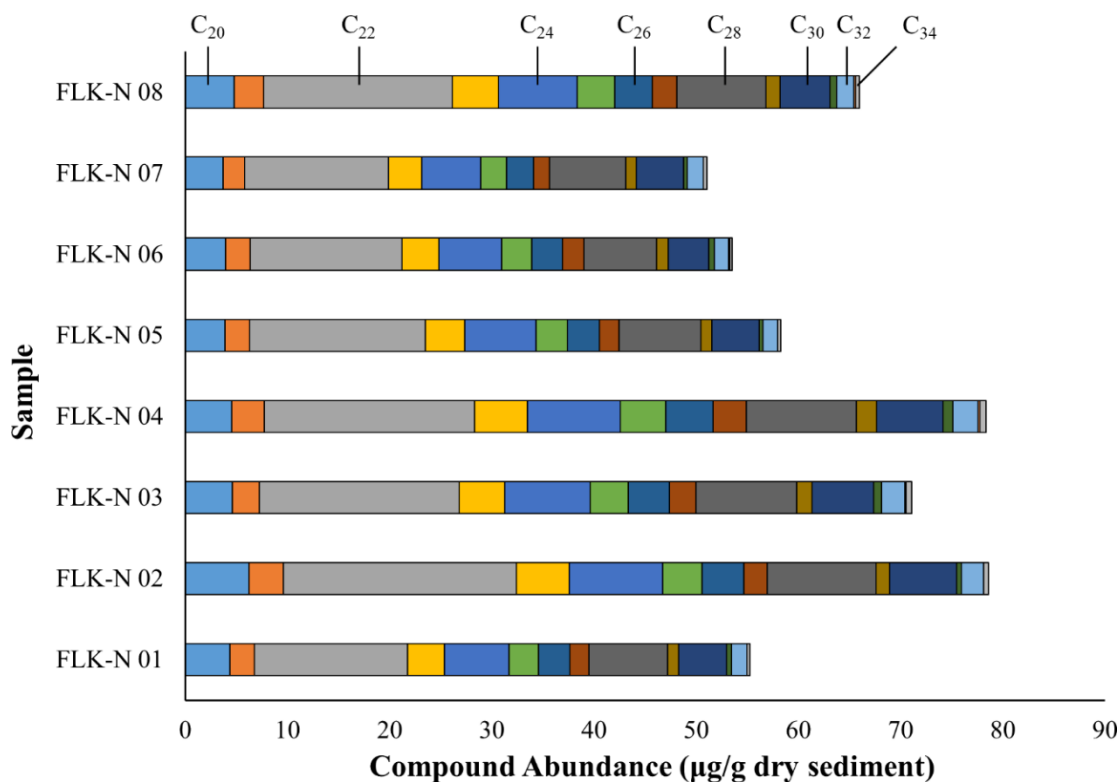


Figure 10-4. Abundances for the C₂₀ to C₃₄ *n*-alkanoic acids from FLK-N Trench 7. The even numbered compounds are most dominant. Concentrations were consistent throughout the sampling column, suggesting no major differences in biomass composition during the deposition of the eight samples. C₂₂ was the most dominant *n*-acid in all samples.

and -1.36‰ for C₃₀ (samples 04 and 05). For δD, the differences are +11.09‰ for C₂₆¹⁷ (samples 07 and 08), -10.35‰ for C₂₈ (samples 01 and 02), and -9.56‰ for C₃₀ (samples 01 and 02). These subtle changes suggest only minor variations in plant community composition over time (the site was dominated by C₃ plants with an average C₂₈ δ¹³C of -33.88 ± 0.19‰) and that source water remained consistent as well. This would also imply that plant ecological lifeform and water-use efficiency remained constant, as indicated by the covarying isotope curves (see Sections 9.2.1 and 10.3.1). In addition, terrestrial plant biomass at FLK-N was rich, likely because plentiful woody vegetation flourished in the presence of a dependable water source, such as an increase in regional precipitation (Hay and Kyser, 2001) or groundwater-fed, freshwater seeps (Ashley et al., 2010a;

¹⁷ The actual largest difference is +35.04‰ between samples 02 and 03, but because of the two extreme deviations of δD in samples below 15 cm compared to the other *n*-acids (see Fig. 9-8), this value was omitted due to its inconsistency with the other *n*-acid compounds (see Section 9.2.1).

Ashley et al., 2009). This plentiful concentration of plants, as indicated by the abundant *n*-alkanoic acids, attracted hominins to the FLK-N site, as evident in the high-density concentration of faunal remains recovered in association with Oldowan stone tools. This is discussed further in Section 10.5.2.

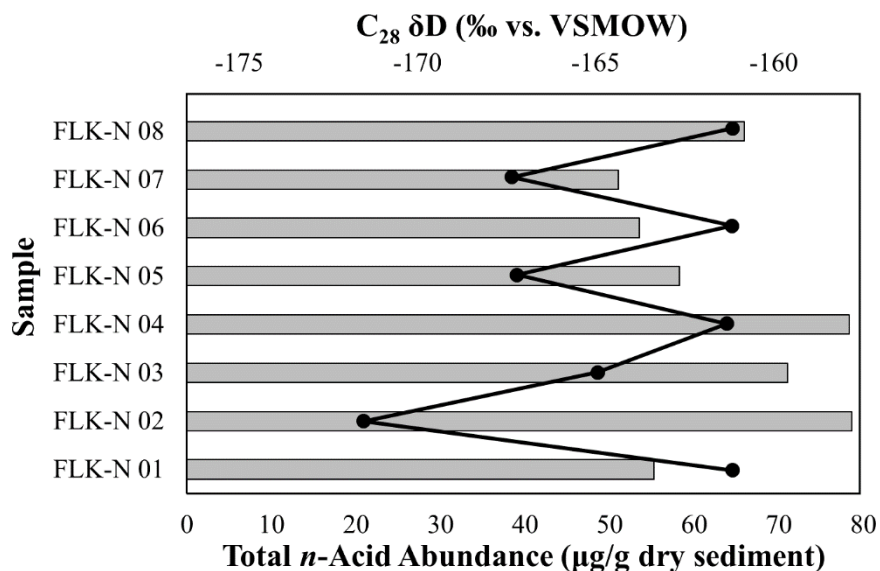


Figure 10-5. Abundances of FLK-N *n*-alkanoic acids plotted against δD from the C_{28} *n*-acids to show comparison between lipid concentrations and isotope values. There is no relationship between the two variables as total biomass is independent of δD value.

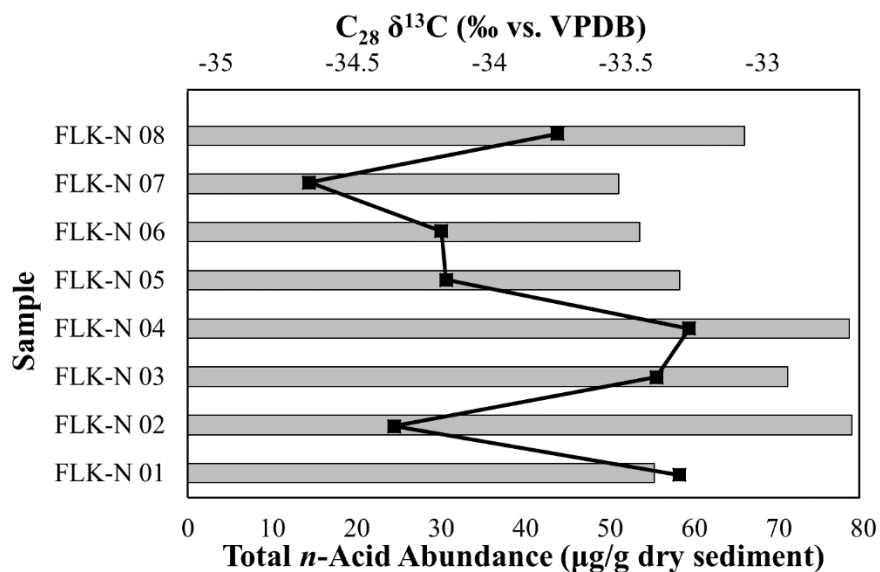


Figure 10-6. Abundances of FLK-N *n*-alkanoic acids plotted against $\delta^{13}C$ from the C_{28} *n*-acids to show comparison between lipid concentrations and isotope values. There is no relationship between the two variables as the two samples with the most $\delta^{13}C$ depleted values (02, 07) have both the most and least abundant concentrations of *n*-acids, while the most enriched sample (04) has the second greatest concentration.

Clays Below Tuff IF

There is great variability in sample preservation and lipid amounts in the clays below Tuff IF¹⁸ (Fig. 10-7). Samples collected on the southern rim of the gorge northeast of the Castle and those from Long Korongo exhibit higher concentrations of *n*-alkanoic acids than those south of the FLK North area and northwest of the Castle for example. Sample 15, east of the Castle, had the highest total concentration of *n*-alkanoic acids with 196.94 µg/g, while samples 25 and 29 from Long Korongo had values too small for GCMS quantification; the smallest sample in terms of total (C₂₀-C₃₄) *n*-acid abundance that could be quantified was 24 from west of the Castle, which had a concentration of 7.55 µg/g. Samples collected in the Side Gorge (19-22) also had abundant *n*-alkanoic acids with quantities between 40 and 90 µg/g.

Five samples were collected in Long Korongo, and of these, samples 26 and 28 had rich total *n*-acid concentrations of 127.67 µg/g and 144.95 µg/g, respectively. However, samples 25 and 29 were poorly preserved even though these samples were collected within 80 meters of 26 and 28 (Fig. 10-7). This is difficult to explain, but the same trend is observed in the concentrations of the *n*-alkanes, meaning that it could be methodological; perhaps these samples were not properly ultrasonically extracted or required additional extraction phases. It is also possible that the poor preservation could be due to differences in erosional processes in this part of the gorge, as these two samples are closer to the confluence with the Main Gorge. The δ¹³C data from the well-preserved samples, however, suggest that Long Korongo was an ecotone when the clays below Tuff IF were deposited; sample 26 has a C₂₈ δ¹³C value of -35.21‰, indicating an increased input of C₃ plants, while sample 28, which has a slightly higher abundance of total *n*-acids, has a C₂₈

¹⁸ For this study, it is assumed that all samples from below Tuff IF were deposited relatively at the same time. This however is unlikely the case, but because there has not been a systematic study on the geology of the clays below Tuff IF, we assume the clays were in place before being capped by the tuff.

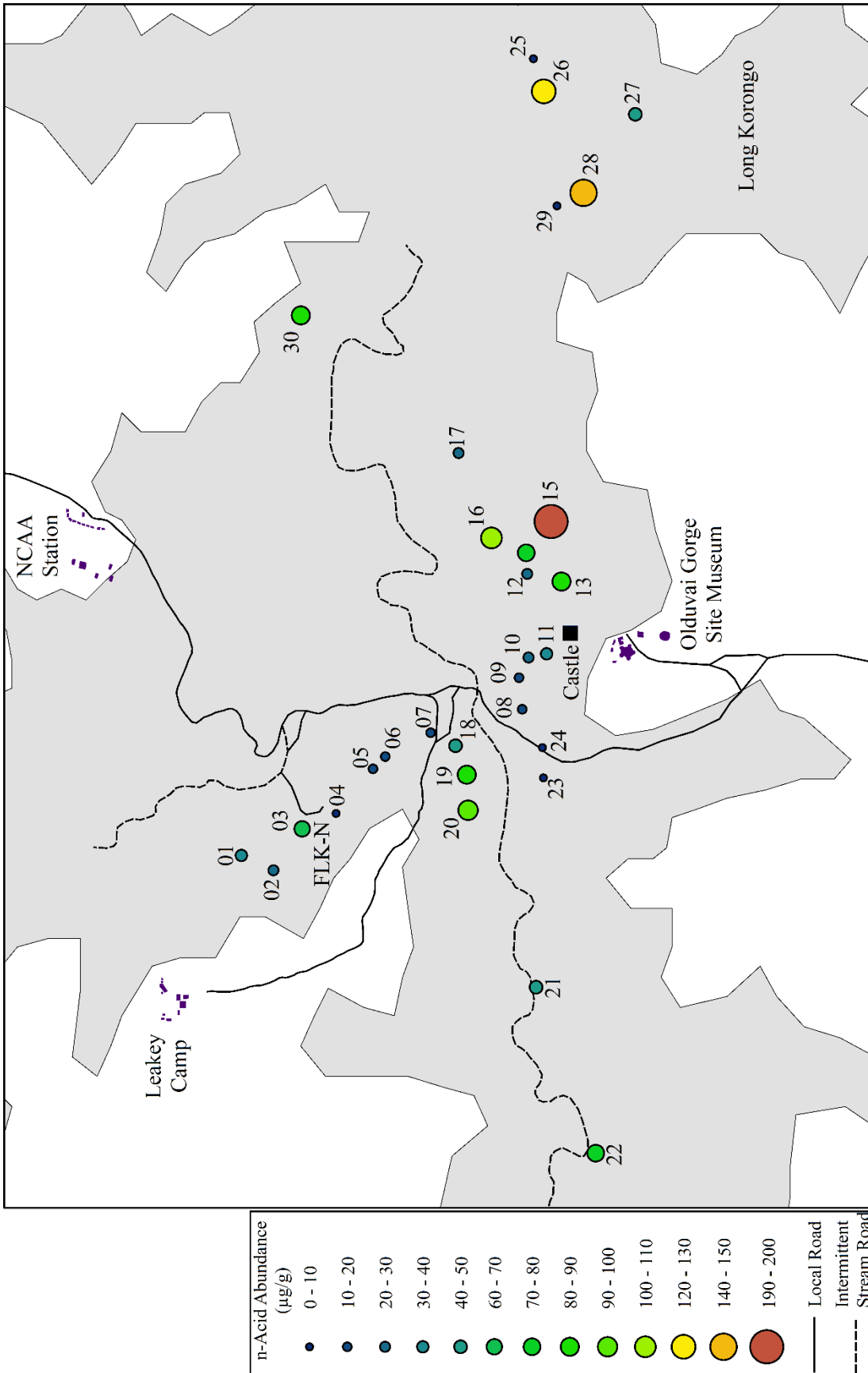


Figure 10-7. Total abundance of *n*-alkanoic (µg/g of dry sediment) from the Clays below Tuff IF.

$\delta^{13}\text{C}$ of -25.29‰, indicating a greater contribution of C_4 plants. Thus, there is a ~10‰ change in $\delta^{13}\text{C}$ across the 270 meters area that separates sample 26 from 28. This evokes an ecological change from a well-wooded area in and around location 26 to a more-open, wooded grassland at sample 28. The clays below Tuff IF sample 27, which is further south yet equidistant to 26 and 28 at ~230 m apiece, also had abundant *n*-alkanoic acids (47.95 $\mu\text{g/g}$) and was ideally situated to test the ecotone transition using $\delta^{13}\text{C}$. Unfortunately, issues with the IRMS precluded successful measurements of carbon isotopes on this sample and therefore, the transition could not be analyzed further.

The highest concentration of *n*-alkanoic acids comes from the area east of the Castle and roughly 450 m west of the Fourth Fault and 60 m west of the KK Fault. For the group of samples in this region (12-17), sample 15 has the highest concentration of *n*-alkanoic acids (196.94 $\mu\text{g/g}$), followed by sample 16 (108.85 $\mu\text{g/g}$), 13 (84.39 $\mu\text{g/g}$), 14 (72.37 $\mu\text{g/g}$), 17 (26.95 $\mu\text{g/g}$), and 12 (22.69 $\mu\text{g/g}$). Of these, only samples 13, 15, and 16 were successfully analyzed for $\delta^{13}\text{C}$, but this was due to issues with the IRMS and not sample preservation. Interestingly, west of the Castle, samples (8-11, 23 and 24) are poorly preserved with sample 11 having the highest *n*-acid abundance of 33.46 $\mu\text{g/g}$ while clays below Tuff IF 24 had the lowest with 7.55 $\mu\text{g/g}$. There is a large difference in total concentrations when comparing the six samples from the east of the Castle to the six from the west; eastern samples have a total concentration of 512.19 $\mu\text{g/g}$, while those on the west have a total abundance of 104.44 $\mu\text{g/g}$. This situation could be the result of methodological issues, but because the samples collected both north of this area (18-20) and further west in the Side Gorge (21 and 22) were both better preserved (in addition to those east of the Castle), it is likely that the low total lipid concentrations are due to differences in preservation in this part of the gorge. This area is heavily traveled, and in fact, samples 23 and 24 were collected

on opposite sides of the main roadway leading into the gorge itself. Furthermore, this road is often accessed by the local Maasai when grazing their livestock as it provides easy movement between the gorge and surrounding plains. Sample 23, which is further removed from the road than 24, also has a UCM in the *n*-alkanes, indicating that (bio)degradation factors into the lower concentration of *n*-acids (sample 09 also has a UCM). Therefore, both natural and anthropogenic physical weathering may explain the reduced lipid concentrations west of the Castle.

There was large variability in $\delta^{13}\text{C}$ between the samples east and west of the Castle that were successfully analyzed with the IRMS (13, 15, 16). Clays below Tuff IF 15 is about 150 m from both sample 13 and 16, while sample 13 is slightly more than 200 m from 16. Sample 15 is also much-more depleted than either 13 or 16, having $\delta^{13}\text{C}$ C₂₈ of -34.71‰ and C₃₀ of -34.86‰ compared to the -22.54‰ (C₂₈) and -22.45‰ (C₃₀) of sample 16 and the -19.35‰ (C₂₈) and -20.17‰ (C₃₀) of sample 13. This may explain the total *n*-acid abundances; sample 15, with $\delta^{13}\text{C}$ representing a C₃ woodland, has greater total biomass (and thus *n*-acids) than either sample 16, which has $\delta^{13}\text{C}$ depicting a C₄ grassland with a small wooded component, or sample 13, which has $\delta^{13}\text{C}$ expressing a C₄ grassland with no input from C₃ vegetation. The dominance of grasses at sample 13, which was collected near the HWK site, is also attested to by numerous and diverse grass phytoliths documented at HWK (Barboni et al., 2010).

As you move further west into the Side Gorge, *n*-alkanoic acid concentration increase, specifically with greater distance from the confluence of the Main Gorge and primary roads. Samples 21 and 22 have total *n*-acid concentrations of 44.49 $\mu\text{g/g}$ and 72.71 $\mu\text{g/g}$, respectively but have a slightly different trend in carbon isotope to biomass correlation; sample 22 has $\delta^{13}\text{C}$ C₂₈ value of -19.91‰ (C₄ grassland), while sample 21 has a $\delta^{13}\text{C}$ C₂₈ value of -22.30‰ (C₄ grassland with a small wooded component). This is opposite to those samples east of the Castle, but because

samples 21 and 22 are ~440 m apart, the differences in *n*-acid amounts is likely the result of variations in depositional history and subsequent preservation over geologic time between the two areas, and not necessarily related to plant landscape. On the northern section of the Side Gorge, opposite to samples 23 and 24, clays below Tuff IF 18, 19, and 20 are well-preserved and have rich *n*-acid abundances. These samples also increased in abundance when moving away from the main confluence, going from 44.90 $\mu\text{g/g}$ (18) to 81.84 $\mu\text{g/g}$ (19) and then 90.98 $\mu\text{g/g}$ (20). Regrettably, only sample 20 was positively analyzed for $\delta^{13}\text{C}$ but only for compounds $\text{C}_{28}\text{-C}_{32}$. These values (average $\delta^{13}\text{C}$ -19.62‰) again suggest a grassland environment in what is now the Side Gorge. Concentrations in the samples to the north (04-07) in the Main Gorge, are not as well preserved and only have *n*-acid abundances between 09 and 18 $\mu\text{g/g}$. (Sample 04 was one of the poorest samples in terms of *n*-acid concentration (9.13 $\mu\text{g/g}$) which is unfortunate because it was the closest sample to the slightly older Bed I FLK Level 22 (*Zinj*) site. This sample was even extracted twice, and on both occasions, few lipids were recovered.) This changes again at FLK-N (clays below Tuff IF 03) where the concentration increases by a factor of seven (65.95 $\mu\text{g/g}$) before decreasing at clays below Tuff IF 02 (20.71 $\mu\text{g/g}$) and then increasing again at sample 01 (39.12 $\mu\text{g/g}$). All three samples returned $\delta^{13}\text{C}$ data, with sample 03 being the most-depleted at -33.75‰ (C_{28}), followed by an enrichment at sample 01 of -21.87‰ and then further enrichment at 02 of -20.19‰; the $\delta^{13}\text{C}$ values correlate with total *n*-alkanoic acid abundance with the more depleted samples having great *n*-acid amounts. Magill et al., (2015) found in the area north of FLK-N (aptly titled FLK North North) a high input of floating or submerged aquatic plants (macrophytes) in standing freshwater. The $\delta^{13}\text{C}$ values from samples 01 and 02, which were sampled in the vicinity of FLK-NN (Fig. 10-7), are enriched and would otherwise suggest a C_4 grassland. However *Typha angustifolia*, a C_3 plant, has $\delta^{13}\text{C}$ values that fall within the C_4 range (-20.1‰) (Vogts et al., 2009),

and thus, *Typha* growing in paleo-wetlands could be falsely interpreted as a C₄ grassland. (It should be highlight that because aquatic plants access a number of sources of carbon beyond atmospheric CO₂ (Katzenberg and Weber, 1999), the assumption that freshwater plants such as *Typha* (photosynthetically) behave like C₃ or C₄ terrestrial plants is simplistic in regard to the complexity of isotopic fractionation in aquatic habitats (Hecky and Hesslein, 1995).) This is likely the situation observed in the clays below Tuff IF samples 01 and 02 collected north of FLK-N; a *Typha* dominated wetland¹⁹ on the outskirts of the heavily wooded area of FLK-N. This is also confirmed by the δD data from the samples collected at FLK-N, which remained relatively consistent through time and suggests a readily available source of freshwater to the local plants.

Finally, sample 30, which is roughly 700 m northwest of Long Korongo and 130 m west of the Fourth Fault, also has good preservation and a total *n*-acid content of 81.80 $\mu\text{g/g}$. This sample, like clays below Tuff IF 28, has $\delta^{13}\text{C}$ values representative of an open C₄ grassland with sparse C₃ trees of a C₂₈ $\delta^{13}\text{C}$ of -21.64‰ and C₃₀ of -21.99‰.

10.1.2 Taphonomy

Samples from the Bird Print Tuff, the Lower Augitic Sandstone, and FLK West could not be quantified confidently. Figure 10-8 shows the relative abundance of the *n*-alkanes across the six archaeological levels at FLK-W. The presence of UCMs in these samples was the major issue in quantifying lipid abundances. This is partly methodological, as FLK-N, clays below Tuff IF, and the Castle Clays were eluted over Aminopropyl columns and silver nitrate infused silica gel and did not have similar issues with UCMs, but it also stems from the degradation of the lipids due

¹⁹ This will have to be confirmed with another plant proxy such as phytoliths, but the abundance of small shorebirds (Prassack et al., 2018) and macrobotanical remains (Blumenschine et al., 2012) at FLK-NN in the vicinity of samples 01 and 02 suggests near shore environments and close proximity to mudflats.

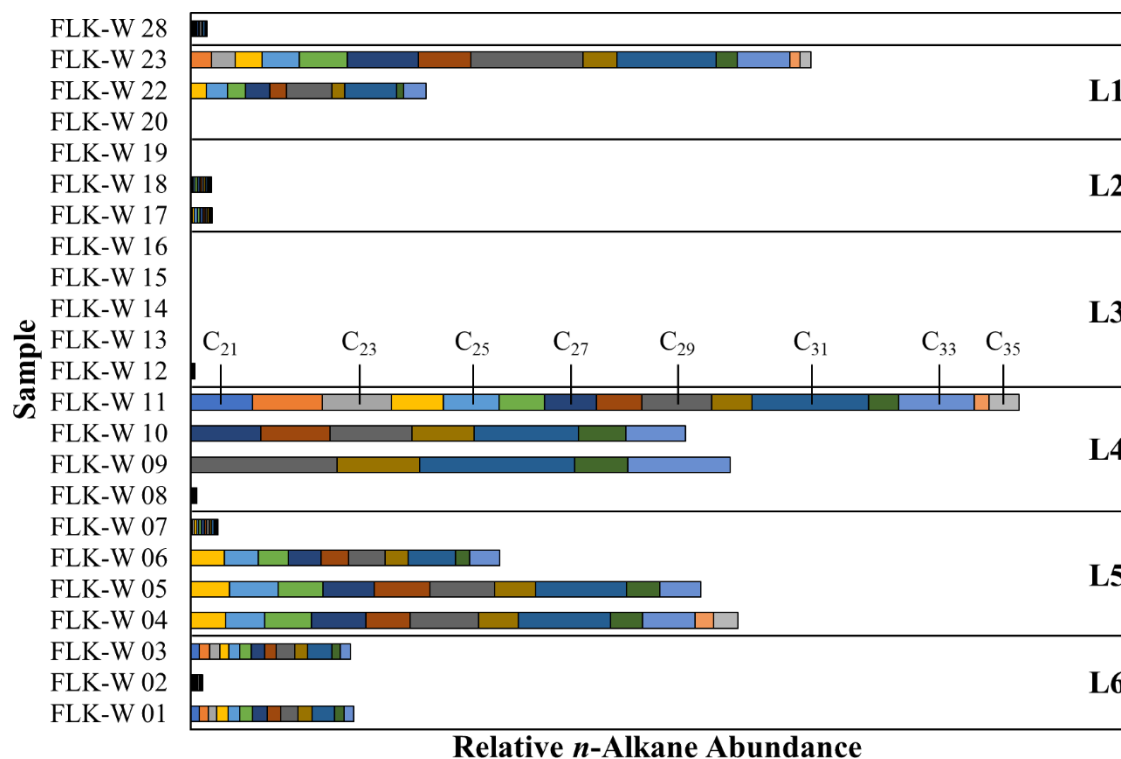


Figure 10-8. Relative abundance of the C₂₁ to C₃₅ *n*-alkanes from FLK-W. Level 3 (massive clayish silt) and L2 (erosive unit of cut-and-fill) were the poorest in terms of preservation and had extensive Unresolved Complex Mixtures. Level 4 (medium-grained Tuffaceous sands), which was relatively abundant, also had issues with UCMs, but the larger compounds ($\geq C_{27}$) were not impacted by it.

to microbial activity and temperature. Taphonomic processes influencing the preservation of lipid compounds in modern African sedimentary environments is not well understood, as no systematic study on the taphonomy of biomarkers has been performed. The preliminary data from Olduvai Gorge and Ngorongoro topsoil (see Section 8.4.3) can help in understanding the degradation of compounds in the region, and studies from outside of East Africa on microbial activity, mesofauna consumption, and soil temperatures (Brittingham et al., 2017; Grimalt et al., 1988; Li et al., 2017; Nguyen Tu et al., 2004; Nguyen Tu et al., 2011; Wu et al., 2019) aid in discerning the mechanisms by which lipid biomarkers preserve over geologic time.

Brittingham et al., (2017) collected two sediment sample sets from the Lusakert Cave archaeological site in Armenia and stored one set at room temperature for three years and froze the other at -20°C after collection and lyophilized it three days later. Samples stored at room

temperature had elevated quantities of medium-chain *n*-alkanes (C₁₈-C₂₆), and a decrease in the abundance of long-chain *n*-alkanes (C₂₇-C₃₃), while C₁₈-C₂₆ were absent from the samples that were immediately frozen. Brittingham et al. also analyzed the DNA of soil microorganisms and found that bacteria containing gene coding for *n*-alkane degrading enzymes flourished in the samples stored for three years. Additionally, they found that δD values of the C₂₉ and C₃₁ *n*-alkanes increased in stored samples by up to +25‰, while $\delta^{13}C$ were found to be depleted by up to -4.2‰.

Alternatively, Wu et al., (2019) did not find any evidence for systematic changes in δD values due to diagenesis in a series of tropical leaf litter-to-soil profiles for both the C₂₉ *n*-alkane and C₃₀ *n*-alkanoic acid, and identified a consistent +4.0‰ to +6.0‰ increase in $\delta^{13}C$ down-profile, which they attribute to a combination of the Suess effect (≤ 2.0 ‰) and diagenetic processes (2.0-4.0‰). Although the 4.0-6.0‰ $\delta^{13}C$ enrichment counters Brittingham et al. long-term storage results, Wu et al., corroborate other leaf-litter-soil studies from different environmental settings (Chikaraishi and Naraoka, 2006; Huang et al., 1996) which documented $\delta^{13}C$ enrichment between leaf and surface soils for C₂₇-C₃₁ *n*-alkanes of 2.0-4.0‰. Therefore, after accounting for the Suess effect over recent decades, Wu et al., (2019) infer a 2.0-4.0‰ $\delta^{13}C$ enrichment in both *n*-alkanes and *n*-alkanoic acids as a result of diagenesis.

Nguyen Tu et al., (2011) provide evidence for microbial contributions to decaying litter for specific alkanes (C₂₅-C₂₉) through litterbag studies. They also note that there is disparity in reported $\delta^{13}C$ values depending on the environment investigated (e.g. oxic vs. anoxic, well-drained vs. stagnant water). In terms of lipid concentrations, Wu et al., (2019) detected a greater loss of *n*-alkanes relative to *n*-acids in litter but noticed that the rate of decay is equivalent with depth. This distinction between lipid concentration in litter and within soil profiles suggest different mechanisms governing the resilience of leaf wax lipids (Wu et al., 2019). Moreover, Grimalt et

al., (1988) show that *n*-alkanes can suffer from biodegradation soon after deposition due to bacterial alteration of hydrocarbons and the reworking of sedimentary lipids, resulting in GC-MS Unresolved Complex Mixtures. Some *modern* topsoil samples at Olduvai, as well as many of the samples from FLK-W and the BPT, suffer from bacterial alteration of hydrocarbons as revealed by the presence of UCMs. At FLK-W, the degree of UCM interference fluctuates throughout the column, but Level 3 had the most-severe instances of microbial degradation of the *n*-alkanes. Furthermore, all but one sample from the BPT had extensive UCMs in the *n*-alkanes, rendering them ineffective for any type of analysis. Because microbial activity is low in buried sediments due to low oxygen and nutrient availability (Leahy and Colwell, 1990), and the litterbag and litter-to-soil studies did not document UCMs as part of the microbial degradation of hydrocarbons, the occurrence of UCMs in FLK-W and the BPT suggests additional taphonomic processes at work. These might include diagenetic processes related to within-sediment chemical imbalances, changes in interstitial water composition, or changes in temperature that altered hydrocarbons after deposition and burial, or the role soil chemistry and soil temperature has in compounding the effects of microbial activity either shortly after lipid deposition or after burial.

Extremes in pH are expected to have a negative influence on the ability of microbial populations to degrade hydrocarbons (Leahy and Colwell, 1990). Soils at Olduvai are alkaline, having a pH between 8.0 and 10.5, and have elevated sodium concentration and low overall moisture content (Jager, 1982). Most heterotrophic bacteria and fungi favor a near-neutral pH, and in experiments where pH was controlled, the rate of microbial biodegradation of hydrocarbons was found to decrease significantly at pH of 8.5 (Verstraete et al., 1976). Moreover, hydrocarbon biodegradation in terrestrial ecosystems is limited by the available water for microbial growth and metabolism. In a study on three California grassland ecosystems (Barnard et al., 2013), soil

bacterial communities paralleled changes in water availability between dry summer months and rainy winter months, regardless of community composition, soil type, and local climate. Metabolic activity significantly increased within hours of saturation, suggesting that changes in precipitation patterns differentially impact microbial communities and the way in which they influence soil nutrients (i.e. hydrocarbons). Conversely, fungal communities were largely unaffected by changes in seasonal precipitation (Barnard et al., 2013), and a study (Grum-Grzhimaylo et al., 2016) on the fungal communities of Lakes Magadi (Kenya) and Natron (Tanzania) showed that soda soils are inhabited by substantial number of filamentous fungal species, which are able to withstand high soil pH. Therefore, fungal communities may be the driving force of leaf wax lipid biodegradation in Olduvai soils.

Temperature on the other hand, influences biodegradation by directly controlling the rate of microorganism hydrocarbon metabolism and the composition of microbial communities (Leahy and Colwell, 1990). For example, higher temperatures increase the rates of hydrocarbon metabolism, and although species type has a large influence on the rate of decomposition in soils (Salinas et al., 2010), temperature is the primary control on the rate of decline of plant wax concentration and decomposition (Wu et al., 2019). Soil temperatures in the greater Serengeti woodlands of Tanzania have a mean annual temperature of 22°C, with mean summer and winter temperatures differing by less than 5°C (Jager, 1982). Therefore, temperatures are likely not a limiting factor in Olduvai microorganism soil communities until burial, as soils are not homogenous in thermal properties and temperature decreases with increasing depth (Jager, 1982).

Annual rainfall at Olduvai Gorge can fluctuate between 331 and 531 mm (Herlocker and Dirschl, 1972), with a dry season that extends from June to October and a wet season lasting from December to April. Rainfall patterns and localized soil conditions influence the vegetation

communities observed in the Serengeti (Anderson and Talbot, 1965), and subsequently, the soil biomass and nutrients available to microorganisms. During the wet season, both bacterial and fungal metabolic activities intensify due to an increase in soil moisture and plant-derived detritus. Thus, the majority of leaf wax lipid degradation would occur during the five-month rainy season before changes in water availability prohibit microbial activity in the dry months.

Olduvai's rainy season is likely the period in which *n*-alkanes are most severely impacted by microbial activity. In the Ngorongoro Crater highlands, samples analyzed for *n*-alkanes did not show evidence of (bio)degradation in the form of Unresolved Complex Mixtures, likely because of cooler average temperatures (20°C, but a minimum average of 6°C) (Anderson and Herlocker, 1973), greater mean annual precipitation (1,037 mm) (Deocampo, 2004), considerable cloud cover during the dry season resulting in less-pronounced differences in seasonal moisture availability, and greater overall plant coverage with a considerable woody component. Although soils are still alkaline (Anderson and Herlocker, 1973) the higher abundance of biomass and greater soil moisture content in the Crater Highlands may have something to do with the lack of UCMs in that there is greater available nutrients for microbial consumption and the higher water content helps preserve alkane integrity. In the sample set from *modern* Olduvai soils, *n*-alkane concentrations were low and suffered from the presence of UCMs (although not nearly as severe as samples from FLK-W or the BPT). During the rainy season, microorganisms, especially bacteria, increase metabolic activity and consume as many nutrients as possible before going dormant again in the dry season; Olduvai today also has limited biomass (during the season in which the samples were collected) and therefore, less overall nutrients available.

Consequently, the extensive UCMs observed in the BPT and Level 3 of FLK-W are likely the result of bacterial and fungal biodegradation of the *n*-alkanes during periods of increased

rainfall in slow-accumulating sediments. Although evidence for this cannot be documented at such a fine (i.e. seasonal) temporal scale in ~1.6 Ma sediments, the clayish silt of FLK-W L3 may corroborate this interpretation. Level 3 is a 30 cm layer of massive clayish silt without flow structures, likely the result of an accumulation of wind-blown dust. This is similar to topsoil around many parts of Olduvai Gorge today that form when wind-borne sediments are stabilized by local vegetation. This process is much more active in the dry season, but during the rainy season when soils are wet, sediment transportation by wind is less intense. However, as soils accumulate in the wetter months, microbial processes also intensify, and biodegradation of lipid compounds commence. Once the dry season returns, the previous soils are buried, and the process begins again. However, because these soils are well drained and aerated, microbial activity can continue for several years, thus continuing the breakdown of previously degraded compounds resulting in more severe UCMs. This could be why L3 of FLK-W had the worst instances of UCMs of levels at the site.

10.2 Plant Landscape Coverage: C₃ and C₄ Proportions

The distinct $\delta^{13}\text{C}$ signature of both C₃ and C₄ plants allow for the estimation of their relative contribution to sedimentary carbon archives, and a common application of carbon isotopic analyses is to estimate the proportion of plants using the C₄ pathway (Cerling et al., 2011; Garcin et al., 2014; Magill et al., 2013a; Schefuß et al., 2003; Uno et al., 2016). Carbon isotope end-member values were used in two different mixing models, a linear and sine-squared model (Section 8.7.3), to estimate changes in plant coverage through time at FLK-N, FLK-W, and the Castle. Several end-member values were used to show the possible range of C₃ or C₄ percent coverage in paleo-landscapes, as Castañeda et al. (2009) noticed a substantial estimation error of up to 20%

for C₄ plants resulting from uncertainty in end-member values used, while Wu et al. (2019) showed that in C₃ tropical forest soils, a 2.0-4.0‰ δ¹³C enrichment in *n*-alkanes or *n*-alkanoic acids due to diagenesis can lead to a 20% overestimation of C₄ coverage depending on end-members used. Only the sine-squared model is discussed here, as the relationship between C₃ and C₄ abundance is nonlinear (Cerling et al., 2011), and this model is used to characterize small variations in % C₃, specifically when nearing minimum or maximum δ¹³C end-member values (Garcin et al., 2014) (C₃ and C₄ percentages using the linear mixing model are presented in Appendix C).

10.2.1 FLK North

The FLK-N Trench 7 site was dominated by C₃ plants regardless of the end-member values or mixing model equation used (Fig. 10-9). Never was there less than 80% C₃ plants (or more than 20% C₄) in the 40 cm directly below Tuff IF in Levels 1 and 2 of FLK-N. Although the total percentage of C₃ vegetation depends on the specific end-member values, they all suggest that the archaeological assemblages at FLK-N were formed within a woodland biome, or even a true, perhaps riparian, forest. Interestingly Model 1 (-35.4‰, -20.7‰) was anti-phased to Models 3 (-32.9‰, -19.0‰) and 4 (-30.0‰, -14.0‰), so that when there is an increase/decrease in C₃ plants in Model 1, there is a decrease/increase in Models 3 and 4. This is the only instance of this occurring, as the proportion models for both the Castle Clays and FLK-W covary throughout the columns. The reason for this is that the recorded δ¹³C isotope values are more-depleted than the end-member values used in Models 3 and 4 and therefore, the sine square model misrepresents the proportion of C₃ and C₄ plants; that is, all values should be at 100% C₃ for Model 4. Focusing on Model 1 and using end-member average values²⁰ of -35.4‰ for C₃ plants and -20.7‰ for C₄, the

²⁰ The end-member values for C₂₈ *n*-acid based on modern plants and correcting for the Suess effect are -34.95‰ for C₃ and -20.54‰ for C₄. while the end-members for C₃₀ are -35.93‰ and -20.93‰ for C₃ and C₄, respectively.

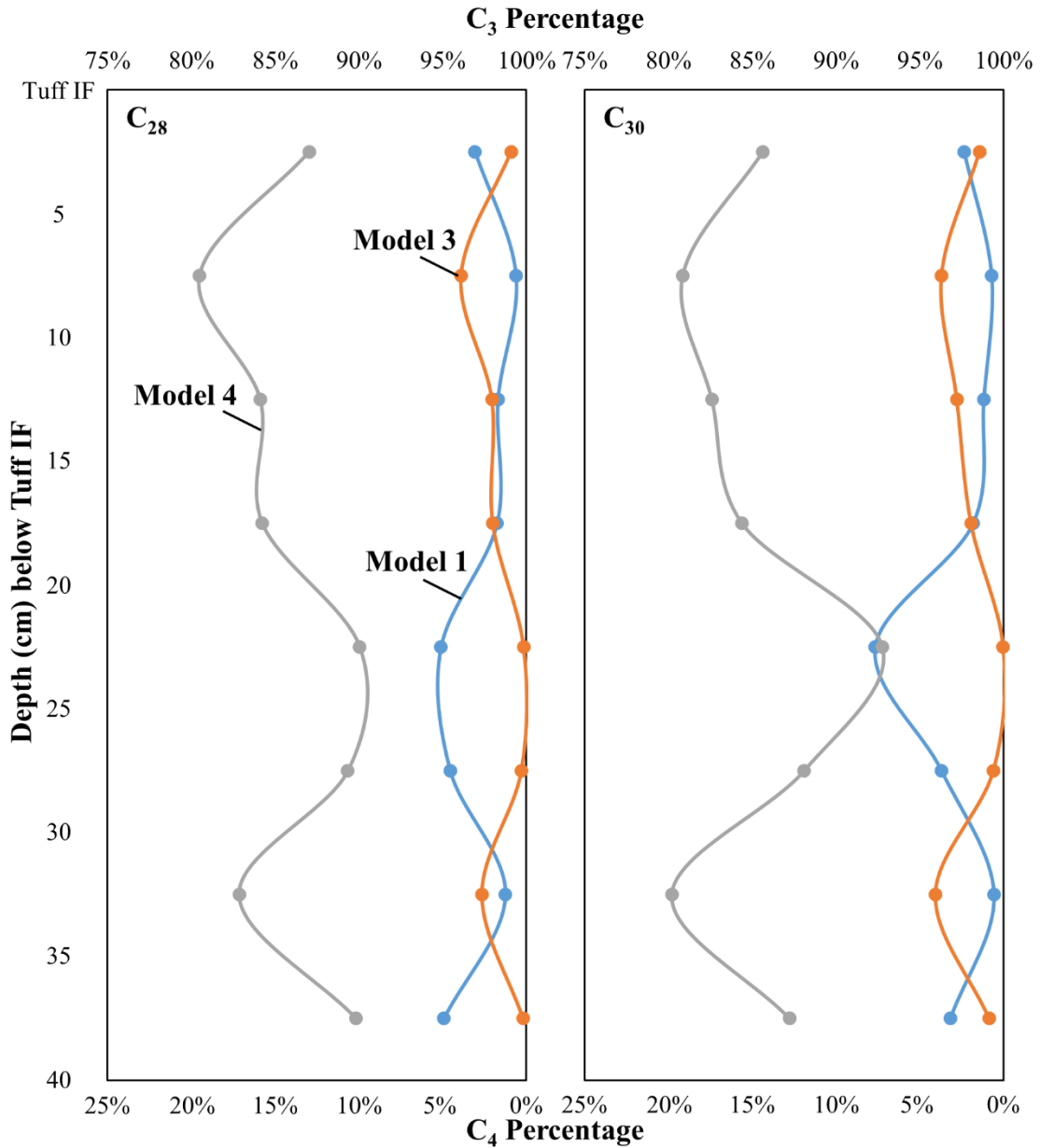


Figure 10-9. Percentage of C₃ and C₄ plants based on *n*-alkanoic acid $\delta^{13}\text{C}$ and specific end-member values (see text) for FLK North Trench 7. Model 1 represents the vegetation at FLK-N best, as end-member values for Models 2 and 3 were smaller than recorded $\delta^{13}\text{C}$ from the FLK-N samples. Model 1 shows that C₃ plants dominated the landscape at FLK-N and that the site was a dense stand of woody vegetation.

maximum proportion of C₄ vegetation at FLK-N only ever reached 5% according to the C₂₈ *n*-alkanoic acid and 8% for the C₃₀ *n*-acid. (These percentages change to 3% and 11%, respectively, when using acid specific end-member values; see Footnote 20.). This suggests that the site was densely covered and that understory C₄ grasses only flourished when the canopy opened and allowed adequate sunlight to reach the ground, such as between 20 and 30 cm, especially for C₃₁ (Fig. 10-9). This also implies that the site was well-watered and plants had continuous access to freshwater in the form of increased regional precipitation (Hay and Kyser, 2001), groundwater-fed seeps (Ashley et al., 2010a; Ashley et al., 2009), or by river systems that flowed from the volcanic highlands (Stanistreet, 2012). Additionally, abundant available water likely diminished any impact that atmospheric CO₂ (*p*CO₂) or high temperatures would have had on promoting the expansion of C₄ plants. The dense vegetation in the FLK North area also acted as a potential “ecological magnet” (Domínguez-Rodrigo et al., 2007b) that attracted both carnivores and hominins to repeatedly use the site as attested to by the large faunal assemblage and Oldowan stone tools. Moreover, the heavy concentration of C₃ plants would have provided access to hard-shelled nuts and fruits (Carvalho et al., 2008; Mercader et al., 2002), a reliable food source for hominins.

The dominance of C₃ vegetation suggests that the FLK-N site may have been similar to the dense evergreen forest that flourishes near freshwater springs percolating out of the rift escarpment on the northwestern shore of Lake Manyara. Here, well-drained alluvial fans support a lush groundwater forest that would not otherwise flourish under the existing Manyara rainfall regime of 650 mm per year. Palms (*Phoenix reclinata*) are frequent in sections of the forest where the canopy is open, while C₄ sedges (Cyperaceae) make up much of the vegetation on the ground

(Barboni, 2014). Ashely et al., (2010b) propose that two localized faults, FLK and FLK Zinj²¹ Faults, provided constant freshwater to the FLK-N area, which would have acted in similar fashion to the freshwater springs northwest of Lake Manyara. On the other hand, Stanistreet (2012) proposes that river systems flowing from the Crater Highlands supplied the freshwater needed to support wetland or riparian zones, similar to the way in which the Munge River feeds wetlands within Ngorongoro Crater today. Phytoliths collected immediately under Tuff IF are attributed to woody plants including trees, shrubs, palms, and sedges, while only a few grass cells were documented in the vicinity of FLK-N (Barboni et al., 2010). This corroborates the $\delta^{13}\text{C}$ isotope interpretation for the site. Furthermore, a few hundred meters beyond the springs at Lake Manyara, the forest is replaced by vegetation more accustomed to the drier conditions found in *Acacia-Commiphora* bushland and woodland. This ecotonal characteristic is also similar to that observed in the $\delta^{13}\text{C}$ plant landscape reconstruction for the clays below Tuff IF (Appendix D).

The abundance of sedges in the freshwater forest near Lake Manyara may preclude its use as a modern referential for the FLK-N site as the $\delta^{13}\text{C}$ data do not record a significant C_4 contribution to the sedimentary archive. However, the 5-8% C_4 vegetation signal recorded in $\delta^{13}\text{C}$ may in fact derive from sedges (Cyperaceae) which are abundant in the phytolith record from FLK-N Geotrench 7 (Itambu, unpublished data). Therefore, modern ecological baselines are needed to obtain a more-definitive answer regarding Lake Manyara as a modern referential.

²¹ The FLK Zinj Fault is a projection of an unnamed fault mapped by Hay (1976). Ashley et al., (2010b) use tufa deposits to project the unnamed fault to the northeast but it has not been physically identified.

10.2.2 Castle Clays

The plant landscape of the Bed II Castle Clays is starkly different than that of the older FLK-N. The Castle was dominated by C₄ plants, but the total proportion of C₄ vegetation can vary by up to 79% depending on the model used (Fig. 10-10). According to Model 1, C₃ plants never account for more than 20% of the total vegetation when the Castle Clays were deposited and average only $9.4 \pm 1.6\%$. However, according to Model 3, C₃ plants reached a maximum of 40% coverage in the lower section of the column but averaged $24 \pm 2.5\%$ across all samples. Model 4 on the other hand, likely overestimates the total contribution of C₃ plants as it suggests that they never make up less than 51% of plant coverage and average $64 \pm 2.4\%$. Model 4 will not be discussed further in this section.

Focusing on end-member values from Model 1, the maximum proportion of C₄ vegetation at the Castle accounts for 90-96% from the carbonate horizon to a depth of 150 cm. The total proportion of C₄ vegetation decreases below 150 cm but continues to account for 80-81% of the total plant biomass documented in the C₂₈ *n*-acid; for the C₃₀ acid, C₄ plants account for 79-94% of the vegetation. Above the carbonate horizon, C₄ plants slightly diminish again to 86% (both C₂₈ and C₃₀) of the total proportion until expanding once again to 95% at the very top of the sampled stratigraphic column. These percentages indicate that at the time of deposition, the Castle area would have been a nearly open grassland with small input of arid-adapted C₃ plants of perhaps bushland and thicket varieties. Because pure grasslands occur on deep sandy soils wherever rainfall is between 100 and 250 mm, in shallow soils, or in valleys where clays become waterlogged (White, 1983), the tuffaceous clays that comprise the sediments at the Castle likely

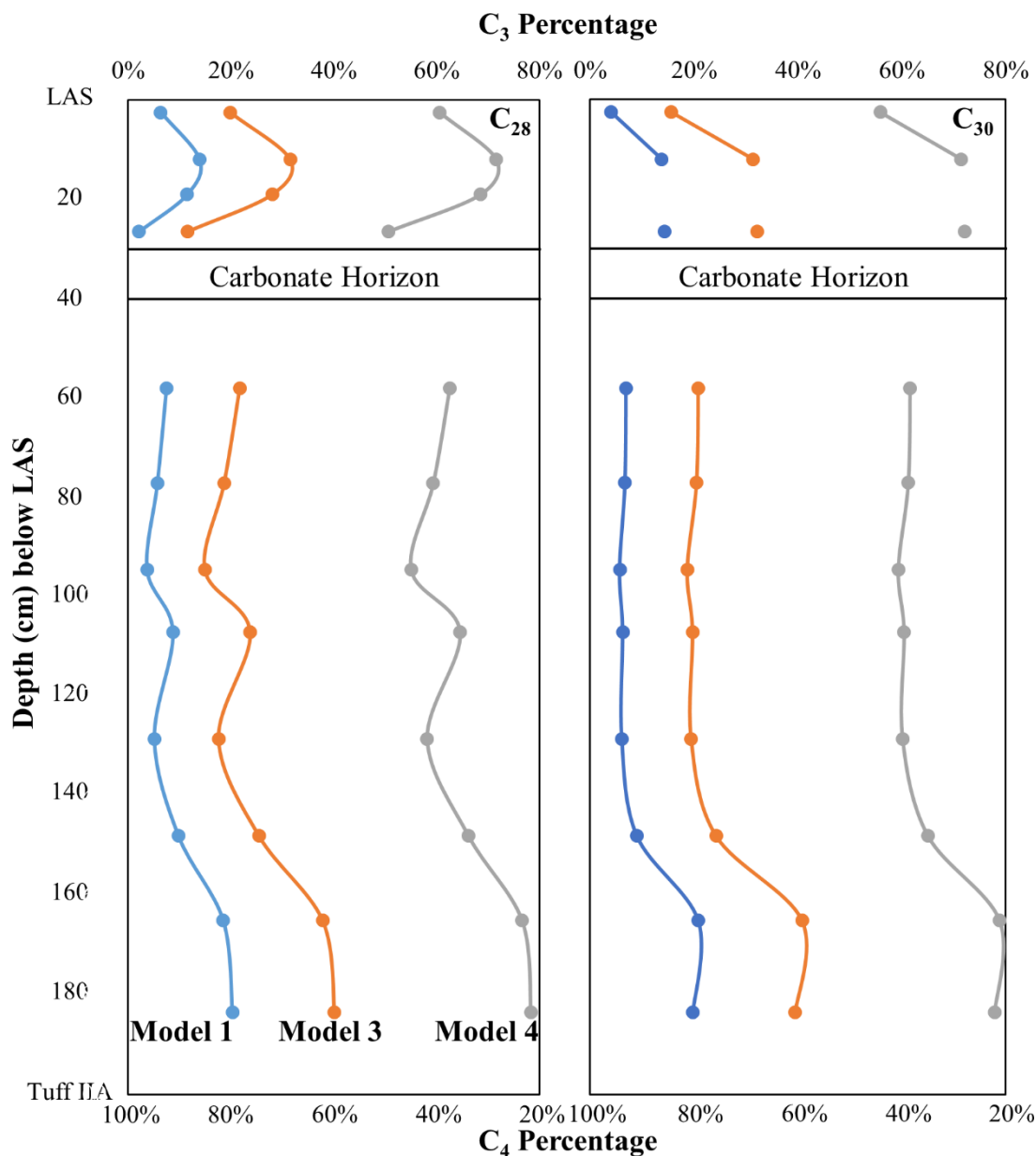


Figure 10-10. Percentage of C₃ and C₄ plants based on *n*-alkanoic acid $\delta^{13}\text{C}$ and specific end-member values (see text) for the Castle Clays. Model 4 likely overestimates the contribution of C₃ vegetation. Model 1 shows that C₄ plants dominated the landscape at the Castle and that the site was an open grassland with only a small wooded component below 150 cm. Model 3 on the other hand, shows that C₄ grasses dominated but woody vegetation still contributed roughly 20-40% of the total plant biomass typical of an *Acacia-Commiphora* mosaic.

supported grassland species like *Sporobolus marginatus* and *Digitaria macroblephara*, which thrive on volcanic ash derived soils (Herlocker and Dirschl, 1972; White, 1983).

When considering end-member values from Model 3, the maximum proportion of C₄ vegetation at the Castle accounts for 74-85% (according to the C₂₈ acid) and 76-81% (C₃₀) from the carbonate horizon to a depth of 150 cm. The total proportion of C₄ vegetation decreases below 150 cm but continues to account for 61% of the total plant biomass documented by the C₂₈ *n*-acid, or 60% of the vegetation using the C₃₀ acid. Directly above the carbonate horizon, as per the C₂₈ *n*-alkanoic acid, C₄ plants increase to 88% of the total proportion until decreasing in accordance with precipitation as recorded in δD to 72% then 68% before increasing once again to 80% at the very top of the sampled stratigraphic column. The C₃₀ *n*-acid suggests a slightly larger percentage of C₄ grasses of 84% at the top of the sampled column (Fig. 10-10). These percentages indicate that at the time of deposition, the Castle area would have been a wooded grassland with C₃ plants covering only 10% and 40% of the surface similar the modern Somalia-Masai floristic region in which *Acacia-Commiphora* deciduous bushland and thicket are the climax vegetation (Kindt et al., 2011). It is also possible that the Castle area was an ecotone between a more-dense woodland to the north closer to paleo-Lake Olduvai and an open grassland to the south away from the paleo-lake; the transitional, ecotonal nature is also characteristic of extant bushland and thick biomes (Mucina and Rutherford, 2006). In wooded grasslands, clayey soils form only in periodically wet hollows which are often covered with edaphic grasses (White, 1983). This would help explain the tuffaceous clays that are now present in the Castle's sedimentological profile. Today, *Acacia-Commiphora* wooded grassland is the most extensive woody vegetation type in the Serengeti National Park representing 88% of all woody vegetation, but over 100 species of grasses occur in the region on soils deriving from volcanic ash. Therefore, the wooded component in the area likely

consisted of Acacia species such as *A. tortilis*, *A. kikkii*, *A. seyal*, and *A. mellifera*, while *Pennisetum mezianum*, *Cynodon plectostachyus*, and *Cynodon dactylon* dominate the grass element.

10.2.3 FLK West

Plant coverage proportions varied the greatest at FLK-W, ranging from a closed woodland in the lowest archaeological levels to an open grassland at the time of Tuff FLK-Wb deposition (Fig. 10-11). The clays below Level 6 and archaeological levels L6, L5, and L4 had the highest concentration of C₃ plants; Model 2 end-member values of -33.6‰ (C₃) and -19.9‰ (C₄) suggest that according to the δ¹³C of the C₂₉ *n*-alkane, C₃ vegetation accounted for 74-94% of the total plant biomass, while using end-member values from Model 3 results in a higher proportion of 81-97% C₃ plants, whereas the end-member values from Model 4 suggest the highest concentration of 98-100% woody vegetation. When using the C₃₁ *n*-alkane, these proportions change to 72-92% and 79-96% for Model 2 and Model 3, respectively, and remain at 98-100% for Model 4. Beginning in L3 and coinciding with the deposition of the massive clayish silt, C₄ grasses begin to become more dominant. According to Model 2 and the C₂₉ *n*-alkane, the base of Level 3 had 20% C₄ grasses, but increased to 36% at the start of L2 (unfortunately there is a large gap in the data between these two points due to abundant UCMs in the L3 samples). Within Level 2, there is a slight increase in the proportion of C₃ vegetation, but then a large ecosystem change follows whereby C₄ grasses flourish and increase to a total proportion of 88%. This phase does not last however, and the total concentration of C₄ plants decreases to 59% right before Tuff FLK-Wb. Above the tuff, the FLK-W area becomes a well mixed mosaic, with C₃ and C₄ vegetation comprising 54% and 46% of the total plant landscape, respectively. Model 3 end-member values suggest a similar composition; the base of Level 3 had 13% C₄ grasses and increased to 28% at the

bottom of L2. Again, there is a slight increase in the proportion of C₃ vegetation within L2, but then the large ecosystem change results in C₄ grasses growing to a total proportion of 81%. Before Tuff FLK-Wb, there was an equal proportion of C₃ and C₄ plants, but then this relationship changes to 63% coverage in favor of C₃ vegetation. The C₃₁ *n*-alkane suggest more gradual fluctuations in the distribution of C₃ and C₄ plants throughout the FLK-W archaeological levels, until middle of L2 when there is a 55% increase in the total concentration of C₄ grasses (Fig. 10-11). Additionally, in relation to the C₃₁ *n*-alkane, the percentage of C₄ grasses does not diminish before the deposition of Tuff FLK-Wb, counter to what is suggested by C₂₉. Finally, C₃₁ δ¹³C suggests that the C₄ component above the tuff is 15% larger than that inferred from the C₂₉ alkane. This is explained by the C₃₁ alkane often being the most-dominant homologue in grasses, while C₂₇ or C₂₉ abound in deciduous trees (Cranwell, 1973; Schwark et al., 2002). (Once more, Model 4 likely overestimates the proportion of C₃ plants and will not be discussed further.)

The number of lithic artifacts and faunal remains from FLK-W decrease in total abundance from archaeological Level 6 to Level 1 (Section 8.1.3 and Table 8.3) in accordance with the total percentage of C₃ plants. Of the 2,120 lithics recovered at the site (Diez-Martín et al., 2015), 90% were excavated in Levels 4, 5, and 6 which also have the highest concentration of C₃ plants according to δ¹³C and end-member values from Models 2 and 3. Interestingly, 501 fewer lithics were recovered in L4 compared to L5 even though the C₂₉ *n*-alkane suggest that the C₃ plant composition was similar in both levels (Fig. 10-11). However, the percentage of plants estimated using the C₃₁ alkane demonstrates that L4 had a ~10% greater input of C₄ grass compared to L5 and that the site was more open than the older archaeological units. Levels 2 and 3 also had similar concentrations of C₃ and C₄ plants, in addition to comparable lithic remains; that is, 89 total lithics were collected in L2 while 97 were retrieved from L3. Finally, the 26 artifacts excavated in L1

were the lowest found at FLK-W, and this layer also had the greatest proportion of C₄ grasses with a C₃₁ estimate between 67-78%.

The FLK West faunal assemblage is dominated by open-habitat taxa, and at least 20 individuals from Bovidae, Suidae, and Equidae were identified in Levels 6 and 5 (Diez-Martín et al., 2015), while the minimum number of individuals in L1, L2, L3, and L4 was 13, three, two, and 12, respectively (Yravedra et al., 2017). Several bones from the recovered assemblage show signs that they had been affected by exposure to water before burial, and UribeArrea et al., (2017) suggest that the FLK-W was located along a sinuous stream that converged into a single channel at the site. Therefore, if water was abundant at FLK-W, specifically during the period when L6 and L5 were deposited, then the higher proportion of C₃ plants in these levels can be explained by the greater availability of freshwater. Moreover, the increase in C₄ grasses in Levels 3, 2, and 1 also implies that overtime, the availability of freshwater declined, thus changing the ecological function of the site.

Because the faunal assemblages of archaeological Levels 6 and 5 are comprised of open-habitat taxa but the $\delta^{13}\text{C}$ suggests a closed woodland with 76-94% C₃ vegetation, the FLK-W and FLK-N sites were similar in that both loci acted as a closed habitat that attracted hominin activity due to the presence of water or the protection of woody vegetation. However, there is a clear distinction in site functionality as the Oldowan FLK-N site was used for the processing of hard-shelled nuts or fruits whereas the Acheulean FLK-W site was utilized for butchering. Both sites were part of a larger mosaic environment that included dense stands of woody vegetation surrounded by more-open wooded grassland or grassland habitats. The further implications of this mosaic environment in regard to human evolution are discussed in detail in Section 10.5.

Due to the possible large error ($\pm 20\%$) in converting $\delta^{13}\text{C}$ values to percent C_3/C_4 , overall trends in the *n*-alkane and *n*-alkanoic acid $\delta^{13}\text{C}$ records are more important than percentage estimates. Therefore, tendencies where enriched (depleted) leaf wax $\delta^{13}\text{C}$ values indicate increased (decreased) inputs from C_4 plants help to provide information on past vegetation shifts at Olduvai Gorge and the environmental stimuli influencing both carbon and hydrogen isotopes.

10.3 Environmental Factors Influencing $\delta^{13}\text{C}$ and δD

When coupled, $\delta^{13}\text{C}$ and δD present a unique opportunity to analyze both paleo-atmospheric and hydrological conditions as well as C_3 vs. C_4 dominated ecosystems. Comparing the two isotope signatures of *n*-alkyl lipids assess changes in plant type, atmospheric CO_2 , plant water-use efficiency, temperature, aridity/humidity (including precipitation), and source water. Hydrogen isotopes of plant biomarkers are primarily influenced by the isotopic composition of precipitation used during photosynthesis, and the isotopic fractionation associated with evapotranspiration (Sachse et al., 2012), but also temperature and successive evaporation-condensation events. Carbon on the other hand is primarily influenced by photosynthetic pathway (C_3 vs. C_4) and the discrimination against the heavy isotope (^{13}C) during photosynthesis. Carbon and hydrogen data were obtained from FLK North and the Castle Clays but unfortunately, not FLK West. Nevertheless, $\delta^{13}\text{C}$ and δD help to infer the environmental context of the FLK-N site at the top of Bed I and that of the Castle in Bed II between Tuff IIA and the LAS. Because the $\text{C}_{28}\text{-C}_{32}$ *n*-alkanoic acids derive from terrestrial vegetation, they will be highlighted in the following sections. However, C_{22} will also briefly be addressed as it is biosynthesized from an alternate source.

10.3.1 FLK North

The carbon and hydrogen isotope signals from the 40 cm below Tuff IF at FLK-N completely covary for the C₂₈ and C₃₀ *n*-acids, except in C₃₀ between 10 and 15 cm (Fig 10-12A-B). Conversely, the C₃₂ acid only mimics C₂₈ and C₃₀ in the trends observed in $\delta^{13}\text{C}$ (Fig. 10-12C), but the δD signature does not fluctuate in accordance with the two shorter compounds. This is likely biological, as the C₃₂ *n*-acid is more enriched in $\delta^{13}\text{C}$ by up to 3.0‰ in some samples compared to C₂₈ and C₃₀, suggesting that this compound is recording isotopic signatures from herbs or shade-adapted grasses. Although grasses have been shown to have more-depleted δD than trees because they absorb surface soil water (Dawson and Ehleringer, 1991; Liu et al., 2006), the δD from C₃₂ is not significantly different than that of either C₂₈ or C₃₀. Therefore, even though the $\delta^{13}\text{C}$ signal from the three *n*-alkanoic acids are documenting differences in ecological lifeform, the δD suggest that they are utilizing the same source water.

For C₂₈ and C₃₀, changes in source water δD coincide with changes in the composition of $\delta^{13}\text{C}$ wherein a depletion or enrichment in hydrogen is mirrored by a depletion or enrichment in carbon (Fig. 10-12A-B). The $\delta^{13}\text{C}$ between samples only suggest slight changes in the composition of the plant landscape at FLK-N as there is only ~1.0‰ difference between individual samples²² (which equates to a ~3-4% change in total C₃ biomass contribution), but because regional meteoric water δD is the primary control on leaf wax signatures (Bi et al., 2005; Garcin et al., 2012; Sachse et al., 2012), the ~10‰ change in δD between samples implies differences in precipitation intensity over time (Dansgaard, 1964), or alternations in the transport history of water vapor deriving from distinct sources (Konecky et al., 2011). Today, changes in vapor source and transport history can

²² However, between samples 05 and 04 there is a depletion of -2.99‰ for C₂₆

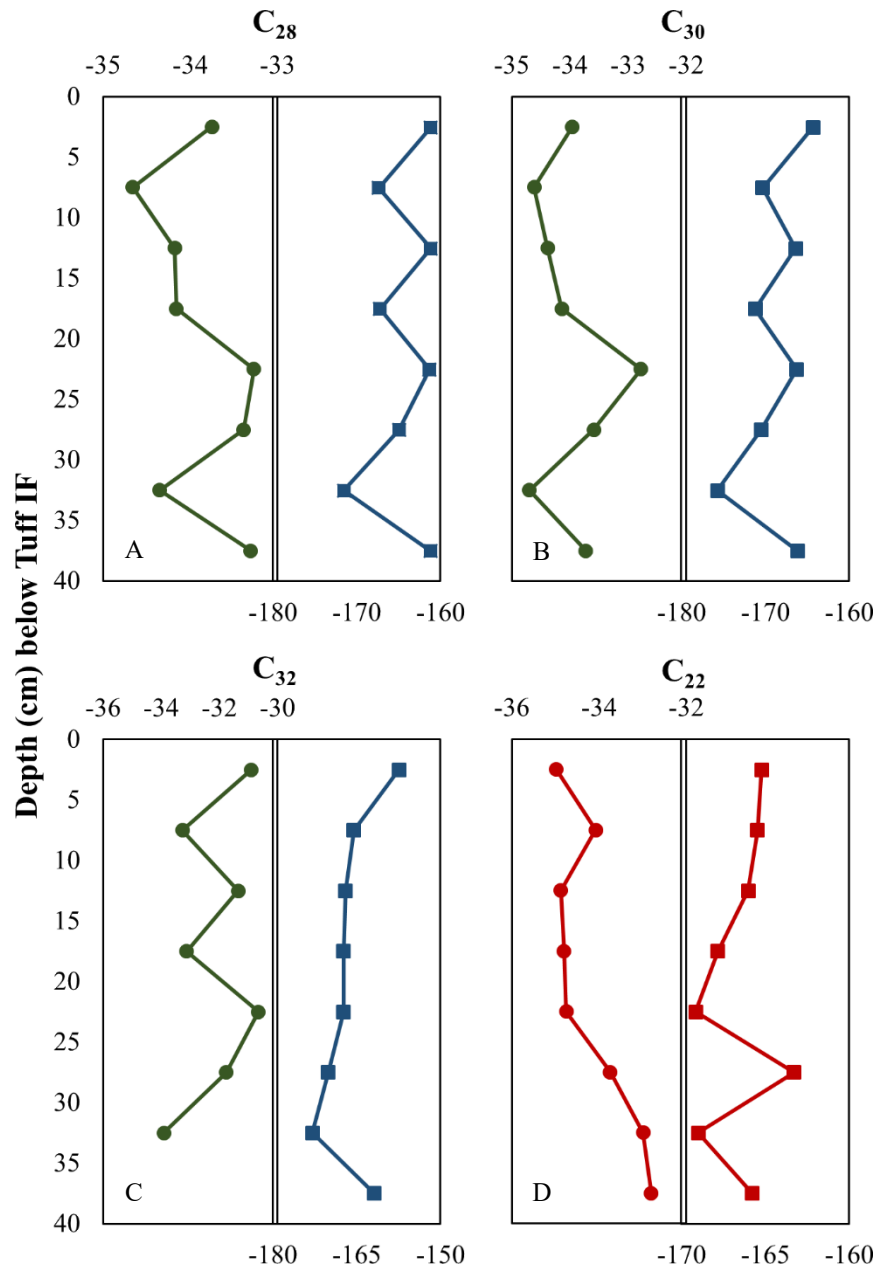


Figure 10-12. Carbon ($\delta^{13}\text{C}$) and hydrogen (δD) isotope fluctuations for *n*-alkanoic acids C_{28} - C_{32} and C_{22} . Left side panels show the changes in $\delta^{13}\text{C}$ while the right-hand panels show δD . For C_{28} and C_{30} , carbon and hydrogen isotopes covary in that an enrichment/depletion in one is mirrored by an enrichment/depletion in the other. Although the $\delta^{13}\text{C}$ of C_{32} covaries with the two shorter compounds, there is very little change in δD between samples; this could be biological in that the plants producing the different *n*-acids are utilizing different source water. As for the C_{22} *n*-acid, the δD covaries with the other compounds but only below 25 cm, while $\delta^{13}\text{C}$ is anti-phased, especially above 10 cm and below 25 cm. This compound is likely being produced by a non-vascular plant organism.

account for up to ~10‰ variability in the δD of precipitation in East Africa (Rozanski et al., 1996), and it is possible we are seeing similar effects influencing the δD of leaf wax lipids from FLK-N. The corresponding enrichments in $\delta^{13}C$ and δD suggest that when precipitation intensity decreases or when there is a change in source water, the plant landscape responds by incorporating plants with more-positive carbon isotope signatures; that is, a greater input of C_4 grasses (Liu et al., 2006), a C_3 cladistic change (Chikaraishi and Naraoka, 2003), or perhaps an increase in the number of palms.

Both the carbon and hydrogen isotope data advocates that the vegetation community of FLK-N was unlike anything found at Olduvai Gorge today. Current annual rainfall at Olduvai averages 550-570 mm (Deocampo, 2004; Hay, 1976), a substantial decrease from that of Bed I times which was estimated to be slightly less than 850 mm (Cerling, 1984; Cerling and Hay, 1986). Moreover, if Olduvai was generally wetter during the Early Pleistocene, then the Crater Highlands, which receives nearly twice as much rainfall as Olduvai, likely received precipitation in excess of the 1,037 mm documented in Ngorongoro today (Deocampo, 2004). Because the Crater Highlands act as a recharge zone for aquifers in the Olduvai region (Ashley et al., 2009), groundwater originating in the highlands likely discharged along faults or impervious beds in and around the FLK area. Additionally, fluvial systems fed by rainfall in the highlands could have provided fresh surface water through incised channels on the paleo-alluvial fan (Stanistreet, 2012). Thus, a constant supply of freshwater resulted in the dense vegetation structure at the FLK-N archaeological site as documented by $\delta^{13}C$ from leaf wax lipid biomarkers. Moreover, the well-watered nature of the site diminished any regional climatic effects such as changes in temperature or atmospheric CO_2 that would otherwise have had an impact on vegetation composition and structure.

The dominance of C₃ vegetation suggests that the FLK-N site may have been similar to the dense evergreen forest on the northwestern shore of Lake Manyara or the Lerai Forest of Ngorongoro Crater. Well-drained alluvial fans north of Lake Manyara support a lush groundwater forest that supports large trees such as the Cape Mahogany (*Trichilia emetica*) which grows to heights of up to 20 meters (Copeland, 2007). The ubiquitous groundwater and the small, spring-fed perennial rivers on the alluvial fans northwest of the lake have a dominant effect on the vegetation community and structure (Copeland, 2007) such that it changes rapidly within a few hundred meters of the freshwater sources. In addition to *Tr. emetica*, which has edible seed pods, other common trees include *Ficus sycomorus* which has both edible figs and leaves, *Croton macrostachyus* that produces fruits eaten by chimpanzees in western Tanzania, and the inedible species *Cordia goetzii* and *Tabernaemontana ventricosa* (Copeland, 2007 and references within). *Acalypha fruticosa* and *Acalypha ornate*, which also produce fruits and leaves eaten by chimpanzees, and *Hibiscus ovalifolius* and *Senna bicapsularis* are additional shrubs commonly found in the groundwater forest. The shade-adapted, inedible C₃ *Oplismenus hirtellus* is one of the rare grasses found on the forest floor.

The Lerai Forest of Ngorongoro Crater was a dense stand of deciduous *Acacia xanthophloea* (fever tree) and the evergreen *Rauvolfia caffra* (quinine tree), species that are associated with abundant groundwater or found along rivers and streams and on floodplains and lake margins (Mills, 2006). Both species are regarded as indicators of water, and dense stands of closed woodlands often form in seasonally flooded areas on alluvial soils. The forest once acted as a refuge for nursing black rhinoceroses and their calves and was a critical habitat for hiding new-born rhinos from predators such as hyenas and lions. Recently however, the extent of the forest has contracted considerably, being replaced by woodland and grassland in many places

(Mills, 2006). Multiple hypotheses have been advanced as to the cause of the contraction such as drought induced reductions in groundwater level and stream flow as well as increases in soil salinity due to flooding from nearby sodic Lake Magadi and the intrusion of saline groundwater into the Lerai area. Similar ecological effects may have eventually led to the opening of the FLK-N area, but the three archaeological horizons above Tuff IF suggests that site was still utilized in Lower Bed II times and that the opening of the landscape did not happen until later in Bed II.

10.3.2 Castle Clays

The three *n*-alkanoic acid compounds, C₂₈-C₃₂, are highly correlated in both $\delta^{13}\text{C}$ and δD , especially below the carbonate horizon, but changes in the carbon isotope values for C₃₀ are not as pronounced as those in C₂₈ or C₃₂ (Fig. 10-13A-C). Nevertheless, similar overall trends are observed in which there are alternating periods of covarying and anti-phasing isotope signatures. The anti-phased sections suggest that alternate controls beyond rainfall amount were acting on both isotope curves. Additionally, both carbon and hydrogen average isotope values from the Castle are enriched by ~10‰ and ~30‰, respectively, compared to those from FLK-N, indicating that the vegetation community is much different at the Castle, as well as differences in plant ecological lifeform, source water, or rates of evapotranspiration; it should be noted that there is about a 65,000-year difference between the two sampling locations so large-scale global climate changes are likely an important factor in both sites' isotope signatures.

The carbon isotope data suggest that the Castle was an open grassland with a small woodland or bushland and thicket component whereby C₄ grasses never comprised less than 60% of the total plant biomass and at times, may have accounted for 99-100% of the vegetation (according to end-member values used). The abundant C₄ biomass easily explains the

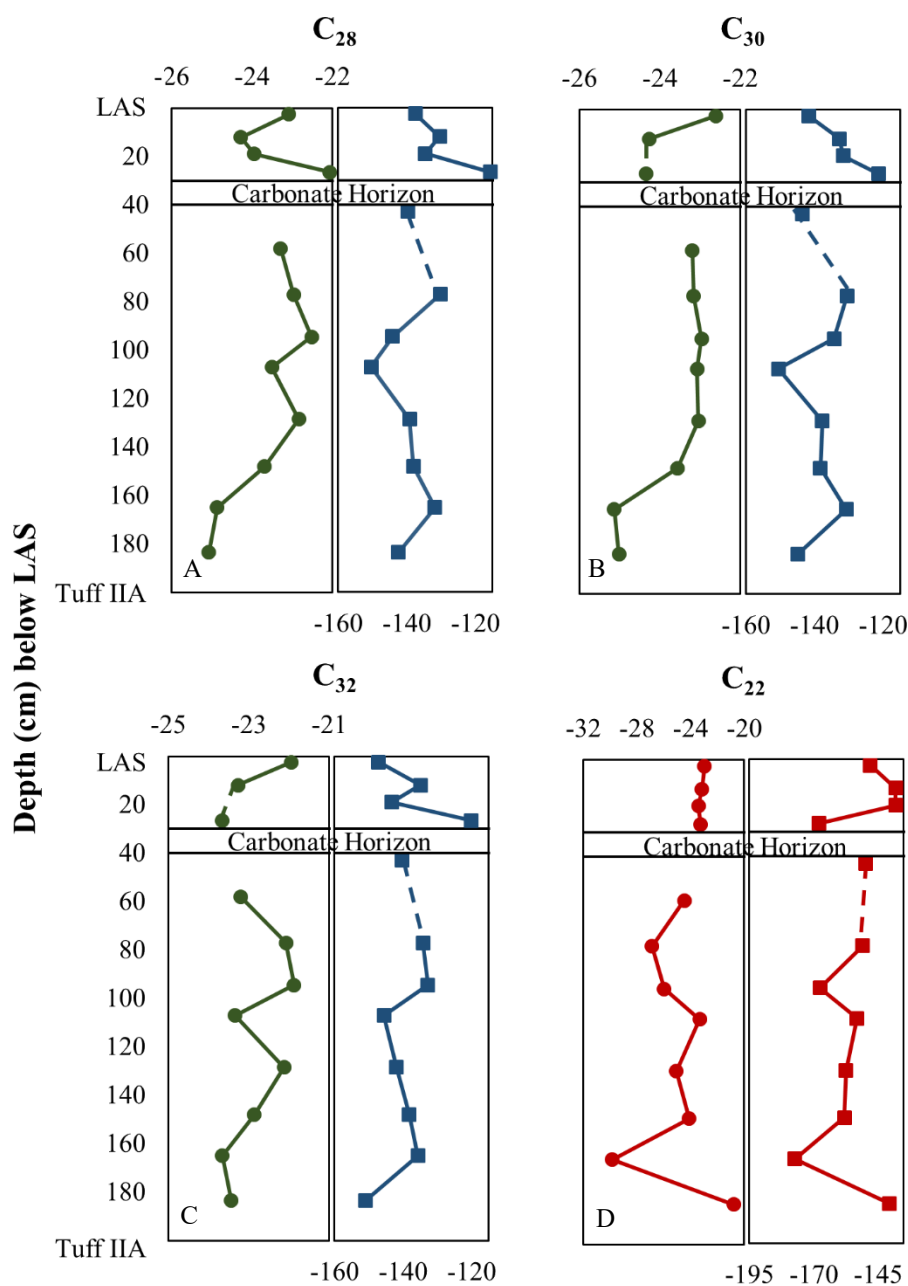


Figure 10-13. Carbon ($\delta^{13}\text{C}$) and hydrogen (δD) isotope fluctuations for *n*-alkanoic acids C_{28} - C_{32} and C_{22} of the Castle Clays. Left side panels show the changes in $\delta^{13}\text{C}$ while the right-hand panels show δD . For C_{28} and C_{32} , carbon isotopes covary in that an enrichment/depletion in one is mirrored by an enrichment/depletion in the other, while for C_{28} and C_{30} , δD are highly synchronized and covary throughout. The C_{30} $\delta^{13}\text{C}$ and C_{32} δD do not fluctuate significantly throughout the sampling column however, specifically below the carbonate horizon. As for the C_{22} *n*-acid, the $\delta^{13}\text{C}$ and δD are anti-phased with the other compounds throughout the column suggesting distinct biological synthesis.

more-enriched $\delta^{13}\text{C}$ values recorded, but the anti-phasing with δD between 0-20, 75-95, and 125-165 cm below the LAS imply that factors beyond water availability influenced plant communities as increases/decreases in $\delta^{13}\text{C}$ do not coincide with increases/decreases in δD (Fig. 10-14). For example, between 0-10 and 125-165 cm, depletions in δD , which would suggest an increase in rainfall, results in an enrichment of $\delta^{13}\text{C}$ or an increase in C_4 grasses, while between 10-20 and 75-95 cm, enrichment in δD results in depleted $\delta^{13}\text{C}$ which would evoke an increase in C_3 plants; opposite to what is expected. For the covarying intervals, C_3 vegetation responds to amplified rainfall, specifically when there are larger ($\sim 10\text{-}20\%$) depletions in δD such as between 95-125 cm and above the carbonate horizon. Hou et al., (2007a) found that trees with greater water-use efficiency (WUE) (as inferred by more-positive $\delta^{13}\text{C}$ values) negatively correlate with δD for C_{26} , C_{28} , and C_{30} *n*-acids. These samples were collected within 50 m of the same pond, so precipitation, temperature, humidity, soil, and source water should be comparable across sampled plants. At the Castle, the isotope data derive from different time intervals, and these factors were likely not consistent through time.

Nevertheless, water-use efficiency is an important factor in the hydrogen isotope ratios of leaf lipids, so observed differences in hydrogen isotopic variation can, at times, be attributed to physiological mechanisms; plants with better WUE transpire less water to produce the same amount of leaf biomass compared to species with lower WUE. Therefore, one explanation for the anti-phased isotope signatures from the two intervals between 0-10 and 125-165 cm is that there was an increase in plants with greater WUE as indicated by the more-positive $\delta^{13}\text{C}$, and the depleted δD is reflecting a change in ecological lifeform to plants that transpire less water, not an increase in precipitation. This interpretation may also be supported by the increase in estimated biomass during these two interludes; as plants with greater WUE increased in abundance, they

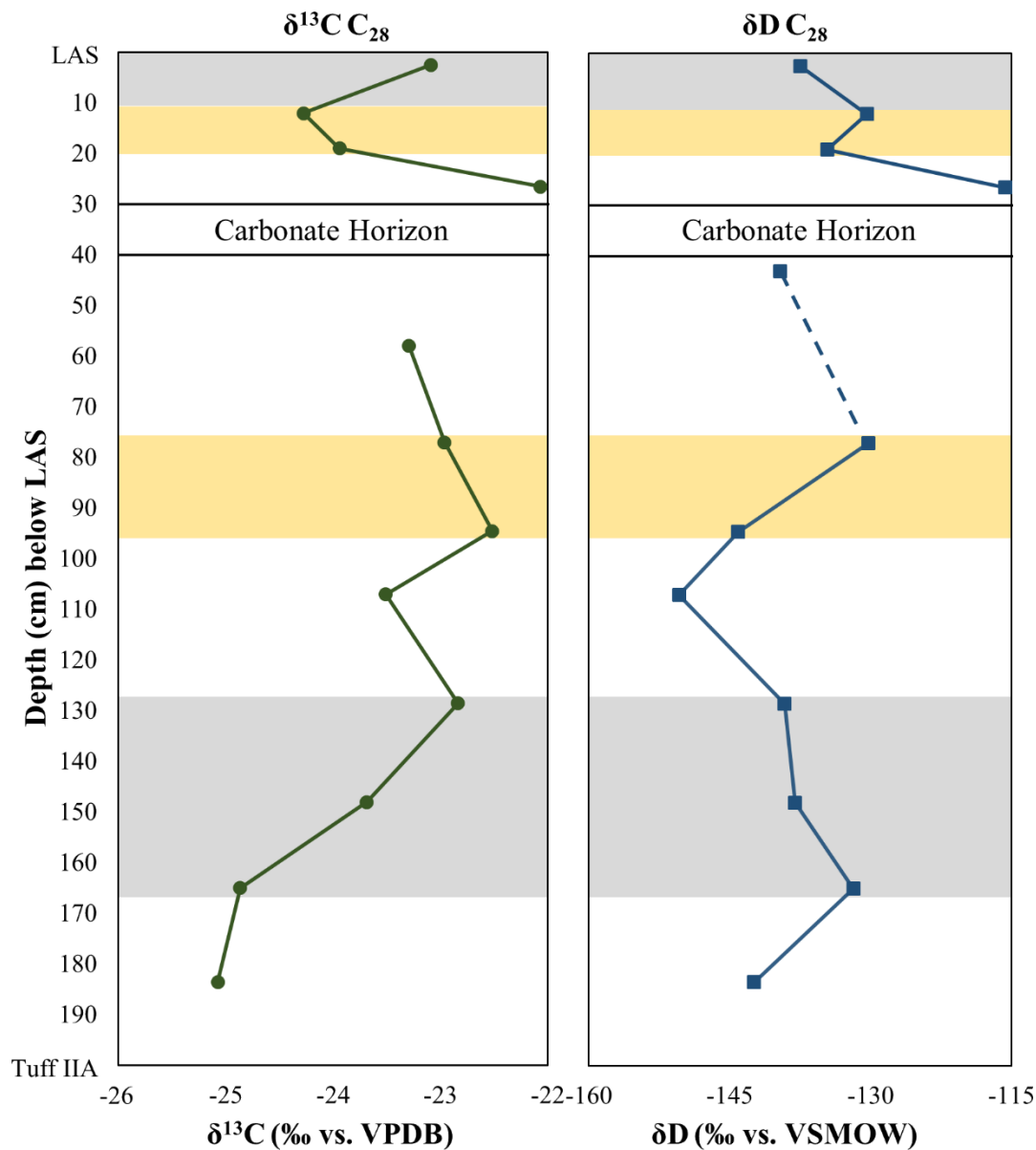


Figure 10-14. Covarying and anti-phasing instance for the C₂₈ *n*-alkanoic acid throughout the Castle Clays. The *white* segments represent covarying $\delta^{13}\text{C}$ and δD in that an enrichment/depletion in one isotope is mirrored by an enrichment/depletion in the other. *Grey* anti-phased segments (0-10 and 125-165 cm below the LAS) represent enrichments in $\delta^{13}\text{C}$ but an inverse depletion in δD suggesting an increase in plants with greater water-use efficiencies. *Yellow* anti-phased segments (10-20 and 75-95 cm below the LAS) represent depletions in $\delta^{13}\text{C}$ but an inverse enrichment in δD suggesting an increase in shrubs or shrub-like trees or changes in global temperatures that resulted in an increase in C₃ biomass but less precipitation being delivered to East Africa.

biosynthesized more total lipids, but overall were not as productive as (C₃) plants that thrived during the stages of increased rainfall (see Section 10.1.1). A second environmental mechanism that may influence the anti-phased isotope trends from these two intervals is that low atmospheric CO₂ prohibited C₃ success even under precipitation levels favorable to their growth, and in fact, influenced plant water-use efficiency as well (Cowling, 2011). However, a reduction in atmospheric CO₂ also promotes increases in stomatal conductance in C₃ plants causing an increase in the rate of water lost to transpiration (Farquhar et al., 1989); this is not supported by the δD data, but if plants with greater water-use efficiencies are thriving under low CO₂, then their ability to reduce transpiration would be reflected in the anti-phased δD. Finally, one other potential mechanism for anti-phased δ¹³C and δD between 0-10 and 125-165 cm involves global temperature changes and varying precipitation response to high latitude ice sheets. Increases in global temperatures and postglacial expansion of East African lakes correlate with depleted δD values in Lake Malawi (Barker et al., 2007), suggesting that elevated global temperatures increased humidity levels and rainfall in the lake basin region. Additionally, cooler global temperatures and increases in Greenland glaciation reduced total precipitation and lake levels (Barker et al., 2007). In C₃ plants, photorespiration increases with light intensity and temperature making them less-metabolically efficient in hot, dry climates (Ehleringer et al., 1986). C₄ plants on the other hand, virtually eliminate photorespiration by concentrating carbon dioxide in the bundle-sheath cells to levels ten time greater than that in the atmosphere (Graham et al., 2006) and have higher net rates of photosynthesis than C₃ plants, specifically under increased light and temperature conditions. Concentrating CO₂ within bundle-sheath cells improves water-use efficiency (Llorens et al., 2009) and prevents photorespiration in high- temperature, light, or salinity environments and in places with limited water supplies or low CO₂ concentrations (Ehleringer et al., 1986; Farquhar et al.,

1989; Sage, 2004). Therefore, increased temperatures may have promoted C₄ expansion even if precipitation increased during the anti-phased intervals. Even though δD suggest increased rainfall in these periods, overall δD values were enriched by ~25-42‰ compared to samples from FLK-N implying that when the Castle was deposited, Olduvai Bed II was generally more arid than the top of Bed I.

The Castle Clays were also marked by two anti-phased intervals whereby a depletion in $\delta^{13}C$ coincided with an enrichment in δD , opposite to the trends described above. Between 10-20 and 75-95 cm below the LAS, carbon isotope data suggest an increase in C₃ plants while hydrogen isotopes denote reduced rainfall. One explanation for this is that reduced global temperatures promoted the expansion of C₃ vegetation but lowered total precipitation in East Africa; although these intervals show an expansion for C₃ plants, they would still only comprise roughly 22-32% of the vegetation according to Model 3, or only ~5.0-15.0% with end-member values from Model 1. If C₃ grasses did expand, and specifically C₃ trees, then it is likely that evapotranspiration was enhanced due to more direct sunlight and greater wind turbulence (Hou et al., 2007b) thus resulting in enriched δD . However, African vegetation models for the last 21,000 years indicate that lower tropical temperatures during glacial periods resulted in reduced evapotranspiration which would have potentially compensated for lessened East African precipitation (Kutzbach et al., 1998). Additionally, it is also possible that shrubs and shrub-like trees became more widespread during these anti-phased hiatuses, as Sachse et al., (2012) found that C₂₉ *n*-alkane δD values in these plant types were the most-enriched compared to trees, forbs, and graminoids, and shrubs and shrub-like trees are common and widespread in seasonally dry, arid environments.

Today, shrubs and shrub-like trees of the genus *Commiphora* (e.g. *C. africana*, *C. habessinica*, *C. madagascariensis*, *C. merkeri*) are common around Olduvai Gorge and were likely

abundant during Bed II deposition. Furthermore, evapotranspiration rates for western Serengeti National Park have been estimated to range between 1.0 and 5.0 mm per day or between 1,100 and 1,900 mm annually (Jager, 1982). Therefore, it is possible to test the effects of evapotranspiration and ecological lifeform on both $\delta^{13}\text{C}$ and δD and whether anti-phased signals are evident in modern vegetation.

10.3.3 FLK West

Although δD was not obtained for the FLK-W samples, diatom counts (Patalano et al., 2017) provide a proxy measure for water availability and the hydrological impact on plant landscape at the Acheulean site (Fig. 10-15). The highest number of diatoms were counted at the base of archaeological Level 6, indicating ample surface or soil water because diatom species distributions are closely linked to water availability and quality (Juggins and Cameron, 2010).

Total abundance steadily declined approaching Level 5 but then remained at a relatively consistent amount throughout the unit before waning again in L4. There was a slight increase in quantity in Level 3, but diatoms are then absent in Levels 2 and 1. The number of diatoms counted is inversely associated with C_4 abundance measured in $\delta^{13}\text{C}$; that is, as diatoms decrease, $\delta^{13}\text{C}$ becomes more-positive demonstrating an increase in C_4 proportions. Therefore, at FLK-W, plant landscape seems to be directly tied to water availability as indicated by diatom abundance.

Today, *Acacia* species (e.g. *A. xanthophloea*, *A. kirkii*, *A. robusta*) are dominant trees within riverine woodlands and bushland of the Serengeti, Ngorongoro, and Manyara regions (Copeland, 2007), while grasses from the species *Sporobolus* are abundant beyond the perimeter of the riparian environment. It is possible that the lower archaeological levels at FLK-W were analogous to the Mbalageti and Sangare River habitats of the modern Serengeti, but as the single stream channel at

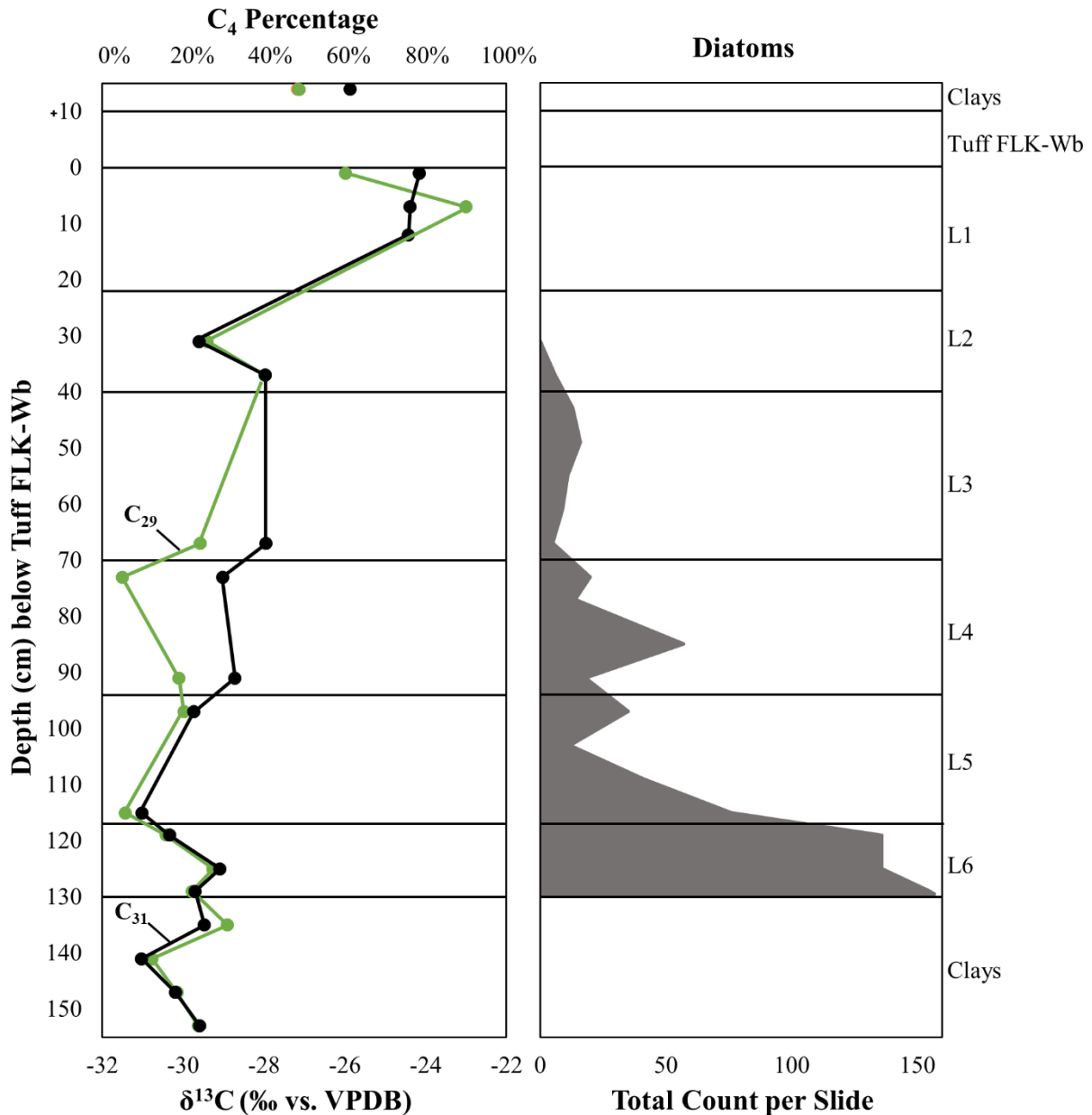


Figure 10-15. Carbon isotope data and corresponding percentage of C₄ grasses according to the C₂₉ and C₃₁ *n*-alkanes plotted against diatom abundance from FLK West. The total amount of diatoms, used as a proxy for water availability, coincide with the total percentage of C₃ plants represented by depleted δ¹³C values, specifically in Levels 6-4. As diatom numbers decrease, the FLK-W landscape opens and develops into a wooded grassland mosaic suggesting that as water availability lessens, C₄ grasses expand while tree coverage becomes sparse. This direct association shows that the FLK-W plant landscape was intimately tied to local hydrological conditions.

the site (Uribelarrea et al., 2017) changed course or dried up to do regional changes in precipitation, *Acacia* dominated woodland reduced and was replaced by dry-adapted grasses such as *Sporobolus consimilis*, *S. ioclados*, and *S. fimbriatus* in the upper archaeological levels.

10.3.4 The C₂₂ n-Acid

For FLK-N Trench 7, the C₂₂ n-acid was the most abundant compound in all samples (Section 9.1.1) but was likely produced by aquatic macrophytes or non-vascular bryophytes (Bakkelund et al., 2018; Liu and Liu, 2017). The C₂₂ n-acid displayed the most-negative (depleted) $\delta^{13}\text{C}$ values for the different carbon compounds in five of the eight samples but had comparable δD to the other n-alkanoic acids with a range between -169.15‰ and -163.29‰ and an average of $-166.47 \pm 0.72\text{‰}$. The stability of isotopes values (Fig. 10-12D) compared to the other acid compounds suggests it was produced from an alternative biosynthetic source; that is, C₂₂ δD and $\delta^{13}\text{C}$ do not exhibit the same oscillations as the other compounds. A similar trend is seen, but with anti-phasing much more evident, in the Castle Clays (Fig. 10-13C), where C₂₂ was the most dominant compound in three samples, had the most-depleted $\delta^{13}\text{C}$ in five samples, but also the most-enriched $\delta^{13}\text{C}$ in one of the 12 samples. Again, the δD is comparable, but generally more-depleted, to the other Castle Clays n-alkanoic acids ranging from -177.34‰ to -138.11‰ with an average of $-153.91 \pm 3.59\text{‰}$. However, the Castle Clays C₂₂ is completely anti-phased with the other n-acids except C₂₄, suggesting that the two compounds share a biosynthesis source; C₂₆ also overlaps with the two smaller compounds and likely is recording a mixture of terrestrial and non-vascular plants.

Mosses and shrubs typically have relatively lower n-alkanoic acid average chain lengths (ACLs) compared to grasses and trees (Bakkelund et al., 2018; Bush and McInerney, 2013), with

values in the 24 to 26 range, respectively. ACL for the C₂₀-C₃₄ *n*-alkanoic acids from FLK-N spans from 24.64-24.97 with an average of 24.77 ± 0.05 , whereas those from C₂₆-C₃₂ (the dominant compounds in woody vegetation and grasses) fall between 28.48 and 28.63 with an average of 28.55 ± 0.02 . This distribution would suggest that mosses contribute significantly to the C₂₂ abundance in the FLK-N terrestrial sediments. The ground layer in many African forests often only consists of bryophytes, while epiphytes varieties of ferns, orchids, and mosses thrive on and amongst woody vegetation (White, 1983). Additionally, tufa deposits, such as those identified at FLK-N, form in areas of persistently high water tables and are extensively covered by macrophytes (Pedley, 1990). If FLK-N was heavily wooded and had an abundant water supply, as implied by $\delta^{13}\text{C}$ and δD , respectively, then mosses likely thrived by utilizing localized humidity for photosynthesis and flourished on both the ground layer and amongst the woody surfaces of terrestrial plants. This is attested to by the abundance of the C₂₂ *n*-acid and the relative consistency of both $\delta^{13}\text{C}$ and δD across the FLK-N samples which show very little change throughout the sampling column (Fig. 10-12D). The one instance of δD enrichment (sample 03) could indicate a period of reduced relative humidity, perhaps due to a reduction in local evapotranspiration, which is potentially mirrored in the other *n*-alkanoic acids.

As for the Castle Clays, ACL spans from 23.80-27.10 with an average of 25.98 ± 0.24 (C₂₀-C₃₄), and 27.81-28.86 with an average of 28.52 ± 0.07 (C₂₆-C₃₂). For the *n*-alkanes, ACL spans 28.36-31.12 with an average of 30.04 ± 0.29 (C₂₁-C₃₅), and 29.75-31.17 with an average of 30.67 ± 0.14 (C₂₇-C₃₃). Therefore, the *n*-alkanoic acids suggest a greater abundance of shrubs contributing to the local biomass when looking at the full range, while the *n*-alkanes imply a greater contribution of both shrubs and grasses, as African species typically have C₃₁ as the most dominant compound (Bush and McInerney, 2013; Vogts et al., 2009). Nevertheless, the C₂₂ *n*-acid was

abundant at the Castle but $\delta^{13}\text{C}$ and δD anti-phase with $\text{C}_{28}\text{-C}_{30}$ (though hydrogen covaries with C_{24} and C_{26} (Section 9.2.5)). However, the $\delta^{13}\text{C}$ and δD covary together suggesting that they fluctuate in response to one another such that a depletion in one isotope results in a depletion in the other. As the δD and $\delta^{13}\text{C}$ data show that the Castle was a relatively dry grassland with a small woodland component, it is currently difficult to determine the biological origin of the C_{22} *n*-alkanoic acid; it does not likely derive from terrestrial vascular plants and emergent macrophytes would not have survived in the drier environment. Lichen on the other hand, may be a potential candidate for the biosynthesis of the C_{22} *n*-alkanoic acid, but more information on lipid production in these organisms is needed. Another candidate could be succulents using crassulacean acid metabolism (CAM), as it has been shown that CAM metabolism modulates hydrogen isotopic fractionation and that CAM plants have leaf waxes with positively correlated $\delta^{13}\text{C}$ and δD values (Feakins and Sessions, 2010b); however, CAM plants tend to produce higher molecular weight *n*-alkane compounds, so further analysis on the C_{22} *n*-alkanoic acid from these plants is needed.

10.4 Using the δD of Rainfall to Infer Paleo-Precipitation

10.4.1 Moisture Dynamics in East Africa

In the tropics, rainfall amount, altitude, distance from coastlines, moisture source, and humidity are the dominant controls on hydrogen (and oxygen) isotopes in precipitation (Dansgaard, 1964). Olduvai Gorge's nearest coastline is around the port city of Tanga, Tanzania, about 490 km away, while the Congo Basin is roughly 1,200 km to the west. Lake Victoria on the other hand, is only about 250 km from Olduvai. There are three stations near Olduvai that are part of the Global Network of Isotopes in Precipitation (GNIP) in East Africa that document δD and $\delta^{18}\text{O}$ values of precipitation; Dar es Salaam (520 km east of Olduvai), Kericho, Kenya (275 km

north), and Muguga/Nairobi, Kenya (240 km northeast) (Fig. 10-16; Table 10-1). Both Dar es Salaam and Muguga receive slightly more than 1,100 mm of rainfall per year, while Kericho is significantly less at around 660 mm annually (IAEA/WMO, 2015). The southeast monsoon system from the Indian Ocean, the westerly/southwesterly humid Congo air stream, and the northeast monsoon that loses much of its moisture over Madagascar are the three major systems controlling precipitation in East Africa (Nicholson, 1996). The Intertropical Convergence Zone (ITCZ) dictates the position of northeast and southeast monsoons and controls the seasonal distribution of precipitation in East Africa, while the Congo Air Boundary (CAB) separates westerly from easterly moisture movement (Levin et al., 2009). The monsoon systems are controlled by Indian Ocean sea surface temperatures (Tierney et al., 2008), but the influence of the Indian Ocean on precipitation variability is mainly limited to coastal and continental Kenya and Tanzania because of the Ethiopian, Kenyan, and Somalia plateau and mountains (Balagizi et al., 2018 and references therein) that block southeast airstreams from penetrating southwest into the continent (Levin et al., 2009).

Precipitation in northern Tanzania peaks in March-April-May with a shorter, less-pronounced season in November-December (Fig. 8-24). Both seasons are governed by the migration of the ITCZ, which is driven by hemispheric solar insolation and temperature gradients. The CAB on the other hand, is a humid, yet uneven air stream at the intersection between the West African Congo Basin (derived from the Atlantic Ocean) and the Indian Ocean monsoon that is seasonally controlled (Nicholson, 1996). It is the movement of these systems that result in the two wet seasons at Olduvai today. However, moisture dynamics in the region are complex because of the East African Rift lakes which add significant water vapor to precipitation during dry periods



Figure 10-16. Moisture dynamics of the major June-August (southeast) and December-February (northeast) monsoons in eastern Africa. The position of the ITCZ and the CAB correlate with the dominant seasonal monsoon. GNIP stations record local δD and $\delta^{18}O$ of rainfall which can be used to track moisture sourcing and transport history.

as they lose more water through evaporation than they receive from precipitation over their surface (Balagizi et al., 2018). The rift lakes play a significant function in the regulation of the East African climate, atmospheric dynamics, and the regional hydrological cycle (Thiery et al., 2015). Furthermore, by being on the boundary of the three moisture systems, wind direction and moisture source is variable from month to month. Over March, April, and May, moisture originates in the east-southeast, and from June to August, winds derive from the southeast. Across September to November on the other hand, moisture source derives exclusively from the northeast, while between December, January, and February, the winds are predominantly from the northeast but vary between all four cardinal directions (Levin et al., 2009). Consequently, isotope values should differ according to month(s) and wind direction. Since Dar es Salaam and Muguga receive comparable amounts of precipitation annually, global trends (Rozanski et al., 1993) would predict depleted oxygen and hydrogen isotope ratios of precipitation in Muguga than in Dar es Salaam due increased fractionation from continental and altitudinal effects. Although this trend is documented in $\delta^{18}\text{O}$ between the two GNIP stations, the δD does not exhibit the same tendency,

specifically during the June-July dry season (Fig. 10-17). Kericho, which receives considerably less rainfall than either of the other stations and is located at a higher altitude, has more-

Table 10-1. Hydrogen isotope values of rainfall recorded at three Global Network of Isotopes in Precipitation stations near Olduvai Gorge.

Month	δD (‰ vs. VSMOW) Avg					
	Dar es Salaam	±	Kericho	±	Muguga	±
January	-6.9	11.0	23.0			
February	-6.3	11.8	0.7	2.4	-2.3	15.6
March	-12.7	12.0	-9.2	4.5	-16.8	7.5
April	-16.9	6.0	-14.1	26.7	-32.1	
May	-6.5	7.4	-14.6	5.7	-26.2	
June	-0.1	10.1	3.4	22.6	10.1	9.0
July	-1.0	14.7	17.5		3.1	
August	-0.6	9.0	7.0		-5.8	
September	2.5	9.4	-11.4		-13.2	
October	-2.7	10.8	-10.7		-35.1	
November	-13.0	13.3	-34.1	22.3	-31.6	
December	-17.7	19.5	-40.2	18.2	-10.1	

depleted $\delta^{18}\text{O}$ values than Dar es Salaam in the March-April-May and October-November-December rainy seasons, but more-enriched $\delta^{18}\text{O}$ in the dry July-August-September months likely due to extensive evaporation (Fig. 10-18). Additionally, Kericho has more-enriched $\delta^{18}\text{O}$ values than Muguga for all months except for November and December even though it is further inland and at a higher elevation; this may be due to enriched water vapor deriving from Lake Victoria. As for δD , Kericho is more-enriched than Dar es Salaam in all months except May and September-to-December and is more-enriched than Muguga in all months except June, November, and December.

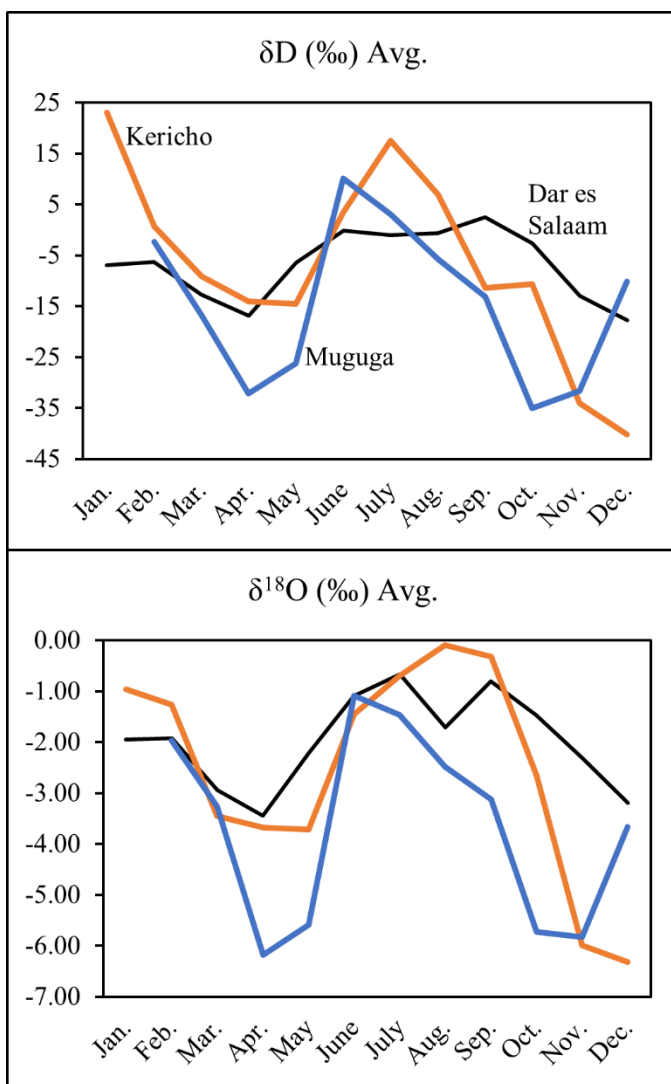


Figure 10-17. Monthly variations in precipitation δD (top) and $\delta^{18}\text{O}$ (bottom) for the three nearest GNIP stations to Olduvai. There is large variability in the Kericho (orange line) δD dataset.

Therefore, neither the continental or altitudinal effect seem to be the dominant control on precipitation isotopes at the Kericho site; instead precipitation-evaporation mechanisms and a shift in the ratio of atmospheric water vapor from different water sources may have a pronounced effect.

Table 10-2. Meteoric Water Line formula for the three nearest Global Network of Isotopes in Precipitation stations to Olduvai Gorge.

GNIP Station	Regression		
	Least-Squares	Reduced Major Axis	Precipitation Weighted
Dar es Salaam	$\delta D = 7.05 \times \delta^{18}O + 6.97$	$\delta D = 7.66 \times \delta^{18}O + 8.19$	$\delta D = 6.88 \times \delta^{18}O + 6.00$
Kericho	$\delta D = 7.69 \times \delta^{18}O + 12.21$	$\delta D = 8.08 \times \delta^{18}O + 13.35$	$\delta D = 7.63 \times \delta^{18}O + 13.06$
Muguga	$\delta D = 8.08 \times \delta^{18}O + 14.87$	$\delta D = 8.35 \times \delta^{18}O + 15.75$	$\delta D = 7.40 \times \delta^{18}O + 11.74$

10.4.2 Meteoric Water Lines

The *Global Meteoric Water Line* (GMWL) is the linear relationship between oxygen and deuterium values of precipitation (Dansgaard, 1964). The GMWL is based on precipitation data from locations around the world, and usually has correlation coefficients reflecting the close association between δD and $\delta^{18}O$ (i.e. $r^2 \geq 95$). However, rainfall or water bodies that have experienced evaporative loss, a continental effect, or an altitude effect deviate from the GMWL, the extent of which can be determined by the deuterium excess (d-excess) of precipitation which reflects the degree of evaporation or the amount of evaporative enrichment in $\delta^{18}O$ after water has condensed (Gat, 1996; Levin et al., 2009). Furthermore, the *Local Meteoric Water Line* (LMWL) is the line derived from precipitation collected from a single site or set of *local* sites and can be significantly different from the GMWL.

The slope of the GMWL was formulated on the $\delta^{18}O$ and δD values of precipitation before evaporation and are linearly related by the equation $\delta D = 8 \times \delta^{18}O + 10$ (Craig, 1961), whereby the “10” is the deuterium excess. The meteoric water line for Africa however, is slightly different; $\delta D = 7.4 \times \delta^{18}O + 10.1$ (Levin et al., 2009; Rozanski et al., 1996). Additionally, Balagizi et al., (2018) developed a MWL for the Virunga Mountain region ($\delta D = 7.6 \times \delta^{18}O + 16.18$), as well as an East African Lakes Evaporation Line ($\delta D = 6.26 \times \delta^{18}O + 1.72$). Finally, each of the GNIP stations have their own MWLs based on the locally recorded δD and $\delta^{18}O$ (Table 10-2).

The $\delta^{18}\text{O}$ and δD values of precipitation for Dar es Salaam, Kericho, and Magugu are plotted in reference to the GMWL, an average of MWLs for Africa (AfMWL), LMWLs based on the precipitation weighted regression from the GNIP, and the East African Lakes Evaporation Line (EALEL) from Balagizi et al., (2018) in Figure 10-18. Rainfall that has experienced evaporative loss or has mixed with evaporated water typically plots below and to the right of meteoric water lines (Levin et al., 2009), such as that of Dar es Salaam against the GMWL and AfMWL, while precipitation condensed from evaporated vapor will plot on a line above and to the left of the MWLs, such as those from Kericho and Magugu. Furthermore, the isotope composition of evaporated moisture is characterized by larger *deuterium-excess* values (Dansgaard, 1964).

Deuterium-excess is calculated with the equation $\delta\text{D} - 8 \times \delta^{18}\text{O}$ for GMWL or $\delta\text{D} - 7.4 \times \delta^{18}\text{O}$ for AfMWL. Table 10-3 lists the d-excess for the three East African GNIP stations using the average monthly δD and $\delta^{18}\text{O}$ values from each location, and the d-excess values for modern Olduvai Gorge and Ngorongoro Crater, determined using the Online Isotope Precipitation Calculator (Table 10-4). Magugu has the greatest number of months with the highest d-excess values, suggesting that the precipitation that falls at the station has the highest degree of evaporation recorded in $\delta^{18}\text{O}$. This also suggests that the precipitation δD and $\delta^{18}\text{O}$ record of Kericho, which is ~200 km further inland than Magugu, is composed of multiple water sources; the Indian Ocean, Lake Victoria, and possible the Congo Basin. Olduvai Gorge, which is nearly 300 km south of Kericho, and on the leeward side of the Crater Highlands also receives moisture from multiple sources but suffers from significant evaporative effects.

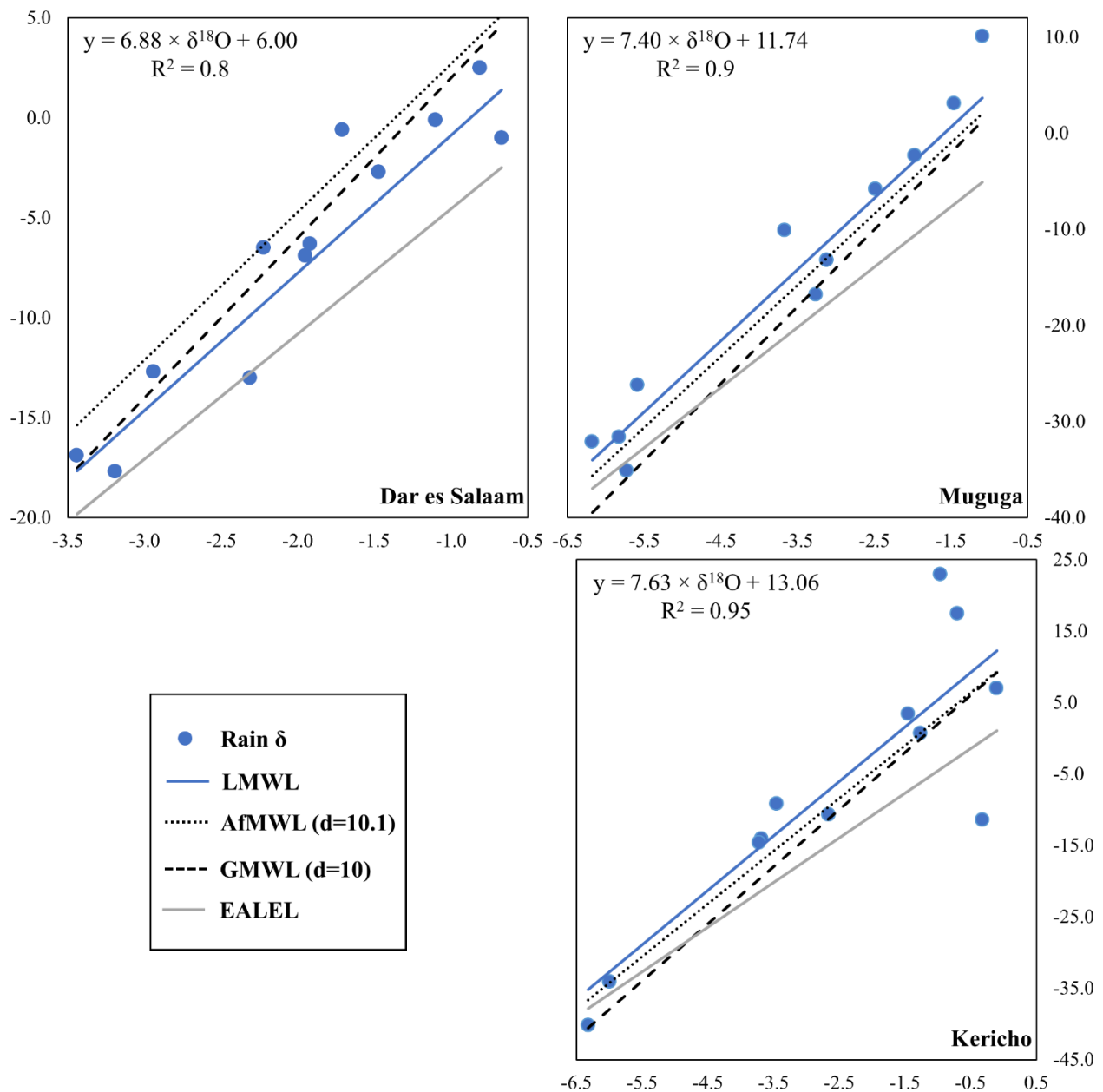


Figure 10-18. Relationship between δD (y-axis) and $\delta^{18}O$ (x-axis) in rainwater recorded at the three GNIP stations near Olduvai. The blue dots are δD and $\delta^{18}O$ monthly averages (not including standard error) and each blue line represents their linear trend. Dashed and dotted lines are the mean water lines (MWL) for Global and African precipitation, respectively. Solid grey line is the East African Lakes Evaporation Line (EALEL) (Balagizi et al., 2018). Local MWLs are based on the Precipitation Weighted Least Squares Regression provided by IAEA/WMO (2015) and do not necessarily represent the slope of the (blue) lines presented as they are means of monthly rainfall from each station.

Table 10-3. Deuterium excess values for the three GNIP stations, Olduvai Gorge, and Ngorongoro.

d-excess (‰) Avg							
Month	Dar es Salaam, Tanzania*	Kericho, Kenya*	Muguga, Kenya*	Olduvai		Ngorongoro	
				GMWL	AfMWL	GWML	AfMWL
January	7.7 ± 5.5	18.2	-	8.2	8.0	11.2	9.5
February	9.1 ± 4.6	15.2 ± 1.9	13.5 ± 1.9	9.0	9.3	11.6	10.3
March	10.8 ± 4.9	16.4 ± 2.8	9.2 ± 4.2	11.4	10.0	15.6	12.8
April	10.5 ± 7.8	14.4 ± 4.1	17.3	11.4	10.0	13.0	10.3
May	11.3 ± 5.8	14.0 ± 3.6	18.5	11.8	9.9	14.6	11.5
June	7.8 ± 3.4	15.0 ± 3.0	18.7 ± 5.3	11.4	10.9	14.0	12.2
July	4.4 ± 4.6	23.1	14.8	9.0	8.7	11.4	10.0
August	11.5 ± 6.2	7.8	14.0	15.2	15.0	13.0	12.1
September	9.0 ± 3.7	-8.8	11.8	11.6	10.6	14.2	12.2
October	9.1 ± 4.5	10.6	10.7	11.2	9.8	13.2	10.6
November	5.5 ± 4.3	13.9 ± 3.4	15.0	7.0	5.8	9.8	7.0
December	7.8 ± 4.5	10.3 ± 0.3	19.3	5.6	5.2	8.2	6.2

* Values from Global Network of Isotopes in Precipitation database (IAEA/WMO, 2015)

GMWL: Global Meteoric Water Line. D-excess = $\delta D - 8 \times \delta^{18}O$

AfMWL: African Meteoric Water Line. D-excess = $\delta D - 7.4 \times \delta^{18}O$

See Table 10-3 for estimated δD and $\delta^{18}O$ of rainfall using the Online Isotopes in Precipitation Calculator

Table 10-4. Monthly δD (left) and $\delta^{18}O$ (right) estimates for Olduvai Gorge (top) and Ngorongoro (bottom) using the Online Isotopes in Precipitation Calculator.

Month $\delta D / \delta^{18}O$	Jan	Feb	Mar	Apr	May	Jun
		5.0 / -0.4	13 / 0.5	-7.0 / -2.3	-7.0 / -2.3	-13 / -3.1
Month $\delta D / \delta^{18}O$	Jul	Aug	Sept	Oct	Nov	Dec
		5.0 / -0.5	12 / -0.4	-2.0 / -1.7	-8.0 / -2.4	-9.0 / -2.0

Estimates for Olduvai at latitude -2.99682°, longitude 35.3519°, altitude 1465 m

Month $\delta D / \delta^{18}O$	Jan	Feb	Mar	Apr	May	Jun
		-12 / -2.9	-6.0 / -2.2	-22 / -4.7	-23 / -4.5	-27 / -5.2
Month $\delta D / \delta^{18}O$	Jul	Aug	Sept	Oct	Nov	Dec
		-7.0 / -2.3	1.0 / -1.5	-13 / -3.4	-22 / -4.4	-27 / -4.6

Estimates for Ngorongoro at latitude -3.24429°, longitude 35.4877°, altitude 2390 m

The Online Isotope Precipitation Calculator (Bowen et al., 2005), estimates the $\delta^{18}\text{O}$ and δD of precipitation at a given site by combining an empirical model for isotope trends related to latitude and altitude with isotope data from stations in the GNIP. Using this calculator, modern isotope data of precipitation in the Olduvai region was computed to compare *n*-alkanoic acid δD values with regional hydrological patterns to help determine source history, evaporative effects, and fractionation factors for FLK North and the Caste Clays. However, in dry and warm regions, δD ratios are strongly affected by evaporation in response to temperature increases that promotes isotopically heavy water molecules to reach the vapor phase, complicating climatic interpretation of leaf wax records (Hou et al., 2008b). Moreover, Balagizi et al., (2018) found that evaporated water from the rift lakes contribute the majority of moisture vapor in the region (i.e. western Tanzania, Uganda, Burundi, and eastern Democratic Republic of the Congo) during the height of the dry season when soil-plant evapotranspiration is minimal.

10.4.3 C₂₈ n-Acid and Paleo-precipitation

The δD values of the C₂₈ *n*-alkanoic acid from the FLK-N samples fall between -161.15‰ and -171.50‰ (average $-164.47 \pm 1.4\text{‰}$) while those from the Castle are between -115.62‰ and -150.37‰ (average $-136.15 \pm 2.5\text{‰}$). The carbon isotope data suggest that the plant landscapes at both sites were completely different, with FLK-N being a dense woodland and the Castle being an open grassland with sparse tree and shrub coverage. An abundance of shrubs or shrub-like trees could explain the +28.32‰ (on average) enrichment in δD at the Castle, as they typically have more enriched leaf wax δD than trees, forbs, or grasses (Sachse et al., 2012), but in the same study, both C₃ and C₄ grasses were found to be the most-depleted δD lifeform; this is not supported by the FLK-N or Castle data however, most likely because there was a regional change in moisture

availability and all plants experienced an enrichment in δD . (It should be noted that the Sachse et al., (2012) study did not include a single African plant species and used *n*-alkane δD , but other studies (e.g. Chikaraishi and Naraoka (2003), Liu et al., (2006)) found similar D-depletion in grasses.) If δD were an artefact of vegetation changes, a shift to a C_4 grass-dominated environment, such as that at the Castle of Bed II, would increase the apparent fractionation, shifting to more D-depleted values, assuming the same water source. Thus, the primary control on the variability in δD between the two sites is not likely plant landscape controlled, but rather precipitation and evaporative-enrichment dominated.

Hou et al., (2008) found that plants growing in relatively dry and warm regions of the United States use precipitation directly as source water for biosynthesis in order to maximize water-use efficiencies and that the effect of evapotranspiration on soil and leaf water is enhanced in such environments. Additionally, the authors found that the δD of river water sourced at colder temperatures and higher elevation is isotopically depleted, which is reflected in both precipitation and leaf wax δD . Wirth and Sessions identified an altitude effect of $-3.7\text{‰}/100\text{ m}$ for δD in the southern European Alps over an altitudinal range from 440 to 1,130 m a.s.l. This gradient is due to the δD of precipitation, which is dependent on altitude and becomes sequentially more-depleted with increasing elevation because of the rainout of heavy hydrogen (Dansgaard, 1964). Jaeschke et al., (2018) noted an altitude effect on δD of $-1.7\text{‰}/100\text{ m}$ in forest soil *n*-alkanes from the southwest Ethiopian highlands over an altitudinal range from 1,600 to 2,700 m a.s.l. Balagizi et al., (2018) found a smaller altitude effect of only $-0.9\text{‰}/100\text{ m}$ on Mount Nyiragongo over a range of 1,460 to 3,460 m a.s.l. Progressive cooling of air masses leads to precipitation of water depleted in δD , specifically when air masses are transported to high latitudes with lower temperatures (Alley and Cuffey, 2001; Dansgaard, 1964), as colder climates have depleted δD precipitation values,

with nearly a 5‰ change of δD per degree Celsius (Alley and Cuffey, 2001). Today, the elevation difference between Ngorongoro and Olduvai Gorge is ~700 m, while that of Mount Loolmalasin, the highest peak in the Highlands (3,682 m.a.s.l) and the Olbalbal Depression is nearly 2,400 m. If the vegetation at FLK-N utilized groundwater originating in the Crater Highlands that discharged along faults or impervious geologic beds, then this source water would have been δD depleted due to a combination of altitude and temperature effects, and thus could explain the significant (~25-42‰) difference in C_{28} *n*-alkanoic acids between FLK-N and the Castle Clays. This groundwater would also not suffer from evaporative isotope enrichment typical of surface waters.

The δD of plant leaf waxes from low lying areas are affected by multiple factors such as hybrid water sources (i.e. precipitation vs. groundwater), seasonality of rainfall, and the diversity of vegetation coverage. There is extreme seasonality in rainfall at Olduvai today and vegetation coverage responds directly to available water. The ground and soil water in the Olduvai region are mainly recharged in March-April-May and again in November-December with extensive arid months of extreme evaporation in between. However, during the height of the dry season (July), soil-plant evapotranspiration is reduced as most leaf and soil water has already evaporated and the lack of rainfall prohibits recharge of the soil-leaf reservoir. The impact of evapotranspiration on both soil water and leaf water is enhanced with low relative humidity, and plants growing in arid environments produce leaf wax lipids that are isotopically enriched relative to precipitation due to strong evaporation (Hou et al., 2008). Because such plants are thought to use water directly from precipitation for biosynthesis, the δD of *n*-alkanoic acids of these plants may be a better proxy for rainfall isotope composition. Thus, the isotope data from the Castle Clays are likely a better indicator of paleo-precipitation for Olduvai Gorge.

The Olduvai mean modeled δD of precipitation (δD_p) from the Online Isotopes in Precipitation Calculator is -9.0‰ for March-April-May and -4.5‰ for November-December (the two rainy seasons) but -0.6‰ for the entire year. Because plants take advantage of seasonal water availability and produce the majority of leaf waxes during rainy seasons (Garcin et al., 2012), a value of -7.2‰ (average of the two rainy seasons) was used for modeled δD_p . Furthermore, measurements on bulk leaf water approximates a total biosynthetic fraction between precipitation and C_{28} δD of -150‰, but D-enrichment associated with transpiration yields a net fractionation of around -95‰, specifically in arid regions (Feakins and Sessions, 2010a; Hou et al., 2008a). The modern isotopic composition of precipitation at Olduvai (approximately -7.2‰) should yield $\delta D_{C_{28}}$ values around -102.2‰ using the net fractionation value of -95‰. Assuming this apparent fractionation was similar during the deposition of the Caste Clays, $\delta D_{C_{28}}$ should generally fall between -100‰ and -120‰ when tracking an Indian Monsoon signal as recorded at the Dar es Salaam GNIP (δD_p , -7.0‰ to -18‰), or between -110‰ and -140‰ when tracking southeasterly source (δD_p , -15‰ to -45‰). Table 10-5 present the range of potential C_{28} δD using a fractionation factor of -95‰ for the three GNIP stations near Olduvai, but also two stations on the western shore of Lake Victoria (Entebbe and Masaka, Uganda), Ndola, Zambia (which tracks a southeasterly/westerly mixed signal, but may be too distant to be representative of Olduvai),

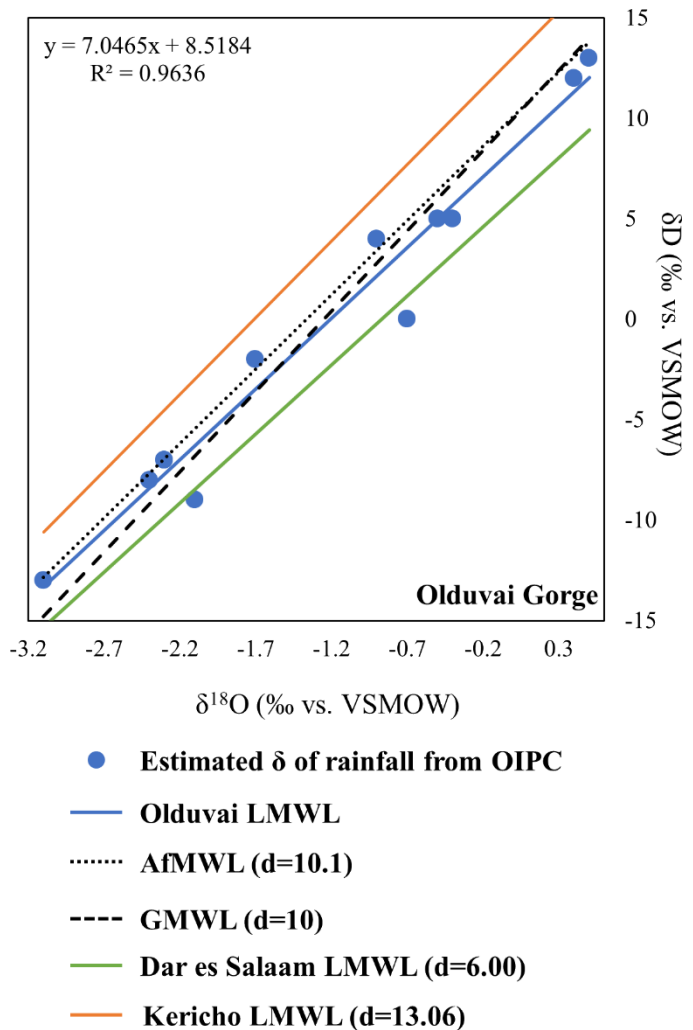
Table 10-5. Estimated C_{28} δD values (assuming a fractionation of -95‰) from eastern African GNIP stations and the Virunga Mountains for comparison with the Castle Clays.

Month	Dar es Salaam	Kericho	Muguga	Entebbe	Masaka	Ndola	Antananarivo	Virunga*
March	-108	-104	-112	-102	-106	-131	-139	-119
April	-112	-109	-127	-109	-106	-126	-111	-126
May	-102	-110	-121	-105	-102	-111	-125	-125
November	-108	-129	-127	-110	-106	-113	-114	-111
December	-113	-135	-105	-93	-98	-132	-117	-101
Max	-102	-104	-105	-93	-98	-111	-111	-101
Min	-113	-135	-127	-110	-106	-132	-139	-126

*Virunga values are based on the minimum δD_p recorded at various elevations on Mt. Nyiragongo and may not be representative of the full range of values recorded. Data from Balagizi et al., (2018).

Antananarivo, Madagascar (which tracks a southeasterly signal), and minimum values recorded at different elevations in the Virunga Mountains, values which are closer to East Africa in terms of precipitation-evaporation dynamics (Balagizi et al., 2018). Interestingly, Ndola and Antananarivo plot closest to the Castle Clays values with isotope fractionation ranges between -110‰ and -140‰ (Ndola δD_p -16‰ to -37‰; Antananarivo δD_p -16‰ to -44‰) (Table 10-5). Virunga also coincides with the Castle Clay δD values, but only in certain months (April-May) or at elevations above 2,000 m, which is not representative of Olduvai Gorge. Plus, the variability of δD_p at Mount Nyiragongo ranges between -32.53‰ and +58.89‰ depending on month and altitude, complicating comparisons between Olduvai and the Virunga Mountains. Kericho, on the other hand, overlaps with the Castle Clay values as well, but only in November-December. Although Kericho and Olduvai receive comparable annual rainfall (550-600 mm), δD and $\delta^{18}O$ estimates for all months from the Olduvai OIPC plot well below and to the right of the Kericho MWL (Fig. 10-19). Additionally, Olduvai estimated δD and $\delta^{18}O$ for November-December plot below and to the right of the Dar es Salaam MWL (Fig. 10-19), but this demonstrates how the shorter rainy season derives moisture from an alternate source (i.e. a predominant northeasterly wind from the Indian Ocean). If variations in Olduvai δD are largely driven by changes in the amalgamation of precipitation from northeasterly and southeasterly/westerly moisture sources, then variations in the δD of C_{28} should be on the order of ~10‰ to 40‰. Many of the Castle Clays C_{28} δD falls between -130‰ and -140‰ (with two outliers at -115 and -150‰), reflecting a predominant moisture source from a southeasterly/westerly mixture, assuming δD_p recorded at the Ndola and Antananarivo GNIP stations today. A high amplitude variation in the C_{28} δD between samples 10 and 11 of +24‰ therefore suggest a replacement of the southeasterly source with a northeast Indian Ocean monsoon source.

Without high-resolution dating, it is impossible to know whether the enrichment recorded in Castle Clays sample 11 is due to a seasonal change (such as the November-December rainy season) or a long-term trend of significant drying in East Africa dictated by large-scale global changes. One other complicating factor is the East African lakes which contribute significant water vapor to precipitation during the dry seasons (Balagizi et al., 2018) but are strongly enriched in δD due to extensive evaporation, whereas precipitation is typically depleted compared to lake water. Atmospheric moisture is thus a mixture of comparatively enriched water vapor from lakes evaporation and depleted water vapor from soil-plants evapotranspiration. Therefore, the complicated dynamics of moisture transport history and sourcing makes paleo-precipitation interpretations difficult. Nevertheless, it appears that the C_{28} *n*-acid is a potential tool for tracking paleo-precipitation dynamics for Pleistocene Olduvai Gorge and how moisture availability changed through time.



10.5 Implications for Human Evolution

10.5.1 Stone Tools and Woody Plant

Abundance

Based on the isotope content of paleosol carbonates from Upper Bed I and

Figure 10-19. Monthly δD and $\delta^{18}O$ estimates from the OIPC for Olduvai Gorge. For the most part, values plot along the African and Global MWLs, but only months November and December plot to the right and below the Dar es Salaam MWL.

Lower Bed II, Cerling (1984) proposed that the percentage of C₄ plants varied from less than 40% at 1.74 Ma to as high as 60% at 1.695 Ma, but there was a drastic increase of C₄ biomass to 80% at ~1.65 Ma, coinciding with bovid faunal remains indicative of savannah grassland with scrub and bush (Hay, 1976). Bibi et al., (2018) propose that tree cover from 1.7 to 1.4 Ma must have been low and true woodlands practically absent from the Olduvai landscape. The authors also suggest that the transition toward drier, more open conditions occurred earlier in Upper Bed I, prior to the appearance of the Acheulean, as they did not identify any observable species turnover between the two beds. Prassack et al., (2018) on the other hand, advocate that the lowermost portion of Bed II was predominantly comprised of a mosaic of wetland, lacustrine, and riverine habitats based on fossil avifaunal communities, and the shift to more-open dry and wet grasslands and open woodlands occurred in Middle and Upper Bed II. Additionally, Kovarovic et al., (2013) using mammalian fossil assemblages situate Lower Bed II (older than 1.74 ± 0.03 Ma) within a mosaic environment of Miombo woodlands interspersed with seasonal floodplains adjoining major rivers and tributaries. For Upper Bed II (younger than 1.74 ± 0.03 Ma) however, abundant terrestrial, grazing, and carnivorous species imply that open environments prevailed, but wooded coverage was still an important component of the landscape.

The $\delta^{13}\text{C}$ data from FLK North and the Clays below Tuff IF indicate that at the top of Bed I (1.803 ± 0.002 Ma), Olduvai's landscape was a mosaic with areas of dense vegetation and abundant fresh water (e.g. FLK-N), *Typha* dominated wetlands (Clays below Tuff IF samples 01 and 02), open grassland, and ecotones. Isotopes from FLK West and the limited data from the Bird Print Tuff suggest that at ~1.7 Ma, woodlands were still an important component of the landscape but by ~1.6 Ma, changes in hydrology led to a reduction in woody coverage but not a total replacement by C₄ grasses. Stone tool use, whether Oldowan or Acheulean, was apparently

concentrated in areas of dense tree coverage. At the FLK-N site, Oldowan tools were used in a lush groundwater forest likely to process hard-shelled fruits and nuts, even though carnivores (leopards or *Dinofelis*) occupied the same habitat. At FLK-W, Acheulean tools in the lower archaeological levels were used in a riparian forest to butcher open-habitat animals that were brought to the site from nearby grassland environments, but also to process plant matter. Because both Oldowan and Acheulean tools have been shown to be multipurpose (Blumenschine, 1995; Domínguez-Rodrigo et al., 2001; Goren-Inbar et al., 2002), and multiple paleoenvironmental proxies, including $\delta^{13}\text{C}$, propose a mosaic environment at Olduvai for Beds I and II, then dense woody plant coverage likely acted as “ecological magnets” (Domínguez-Rodrigo et al., 2007b) and provided refugia for Pleistocene hominins (Shea, 2008), especially if drier conditions in Africa prevailed after ~ 1.7 Ma as evident in marine (Feakins et al., 2007; Schefuß et al., 2003), soil carbonate (Levin et al., 2004; Quade and Levin, 2013), and wind-borne dust (deMenocal, 2004) records.

10.5.2 FLK North Advantage

Felids, such as leopards or extinct saber-toothed cats (e.g. *Dinofelis*), were likely responsible for the majority of fauna accumulation in Levels 1 and 2 of FLK-N (Domínguez-Rodrigo and Barba, 2007), while percussion activity is seemingly the dominant form of hominin behavior recognized at the site (Diez-Martín et al., 2010), even though hominins were not actively involved in breaking long-bones or butchering carcasses. Therefore, FLK North encouraged hominins to continuously visit the site, although it was frequented by felids, by offering an advantage in the form of plant food resources, exploited through battering activities, and protection from larger cursorial carnivores that hunted on the more-open grasslands. Both the $\delta^{13}\text{C}$ and δD

data show that FLK-N was a dense, groundwater woodland analogous to the evergreen forest northwest of Lake Manyara or the *Acacia-Rauvolfia* Lerai Forest of Ngorongoro Crater. Edible plant parts (figs, fruits, leaves, seed pods) would have been abundant if *Ficus*, *Trichilia*, *Acalypha*, and other tree species were present as they are today in well-watered areas of East Africa, so the battering activity involved in hard-shelled fruit and nut cracking was probably not too different from that observed in West African chimpanzee stone accumulations sites (Mercader et al., 2007; Mercader et al., 2002), whereby stones were transported to focal points on the landscape and used for accessing hard plant foodstuffs. Hominins (i.e. *Homo habilis*) specifically selected volcanic raw material based on their dimension, shape, and ergonomic suitability for hammering (Diez-Martín et al., 2010), and transported such stones from off-site to the FLK-N focal point to be used in food processing as the locality offered not only abundant plant material, but also freshwater and safety from predators.

Apart from the FLK *Zinj* Level 22 and David's Site (DS) assemblages, no other Bed I site provides evidence for primary access and the direct consumption of carcasses by hominins (Domínguez-Rodrigo et al., 2017; Domínguez-Rodrigo et al., 2007c); that is, all other sites seemingly involved the use of Oldowan tools for plant processing (cf. Blumenschine, 1995). An abundance of woody vegetation may have been the incentive that enticed hominins to use the FLK *Zinj* and DS sites as focal points on the landscape for butchery. Therefore, this would imply that regardless of sustenance being consumed, woody vegetation was the ecological element that influenced hominin activity during Bed I times. This behavior of using tree coverage for concentrated activity continued into Bed II and across the Oldowan-Acheulean transition.

10.5.3 The Environmental Context of the Earliest Acheulean at Olduvai Gorge

Although evidence suggests that East Africa was becoming drier throughout Bed II and Olduvai shifted from a lake-dominated to a riverine-dominated ecosystem by Bed III ~1.33 Ma (Hay, 1976), woodland habitats remained an important component of the ecological landscape. At the FLK-W site, hominin (i.e. *Homo erectus* though no remains have yet been found) activity again was concentrated within a dense stand of trees, according to $\delta^{13}\text{C}$, but as the landscape opened in the upper archaeological levels (L3-1), human occupation diminished, as evident in both the archaeological and faunal accumulations (Fig. 10-20). Even though FLK-W was not as closed as FLK-N, C_3 plants comprised 70-95% of the plant biomass in Levels 4-6; these levels also contained the greatest concentration of lithics (Diez-Martín et al., 2015), faunal remains (Yravedra et al., 2017), and in Levels 5 and 6, human modified bones (Yravedra et al., 2017). As grasses started expanding in Level 3, likely in response to localized drying, indicated by fewer diatoms (Fig. 10-15) in association with a reduction in streamflow, both the number of lithics and fauna brought to the site fell considerably and the importance of FLK-W as a focal point diminished. Moreover, while faunal remains increased again in the grassland environment of L1, lithics were a minor component of the archaeological record and no human modified bone was identified, suggesting that the greater amount of remains was due to non-anthropogenic factors. Thus, hominin behavior at the site was seemingly tied directly to the presence of woody vegetation, as they were bringing in the remnants of animals adapted to open areas for butchering, attesting to the ecotonal nature of the surrounding landscape, specifically in archaeological Levels 5 and 6. Additionally, as C_3 trees became less abundant, so too did hominin activity, showing that a reduction in both tree coverage and water supply downgraded the appeal of FLK-W around 1.6 Ma.

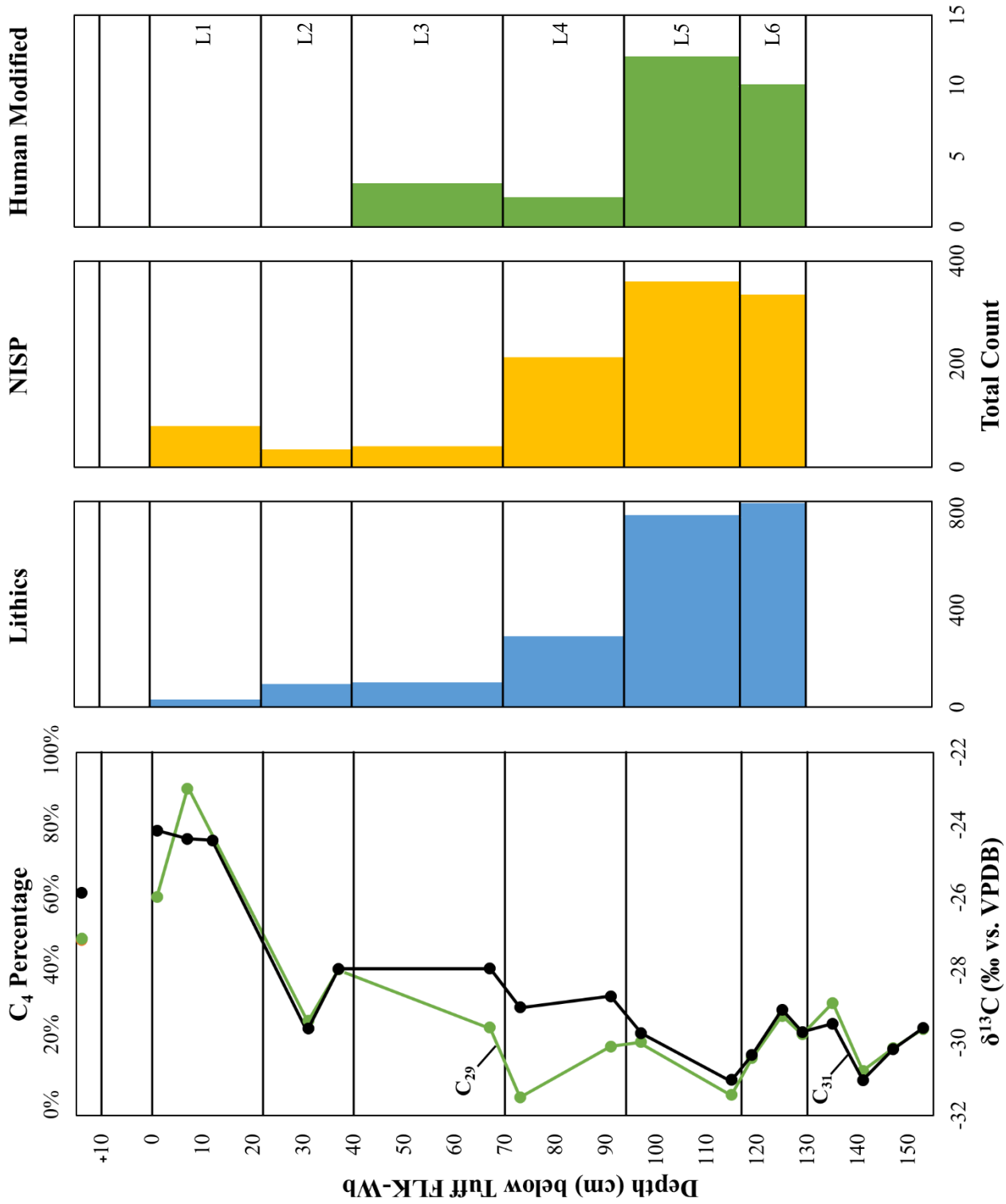


Figure 10-20. FLK-W $\delta^{13}\text{C}$ data plotted against total number of recovered lithics, number of identifiable specimens (NISP), and bones with identifiable cut or percussion marks. The total number of lithics and bones correlates with woody vegetation cover as indicated by $\delta^{13}\text{C}$; that is, the greatest number of archaeological remains coincides with the greatest percentage of C_3 plants (L5 and L6). As the landscape becomes more open (L1-3), the number of lithics and bones drops significantly. The increase in NISP in L1 is non-anthropogenic. Lithic data from Diez-Martin et al., 2015. Faunal data from Yravedra et al., 2017.

Interestingly, both Oldowan percussive elements and Large Cutting Tools were uncovered at FLK-W (Diez-Martín et al., 2015), insinuating that an ecological continuity of sorts exists between the two industries and the behavioral characteristics of the predominant users. Moreover, because the FLK-W handaxes do not seem to be related to the defleshing and disarticulation of carcasses (this was most likely conducted using quartzite flakes) (Yravedra et al., 2017), handaxes were conceivably used for alternative pursuits such as bone breaking or even digging. This would further insinuate some form of technological continuity between Oldowan percussion tools and Acheulean handaxes, and that within well-wooded areas, both industries were primarily associated with exploiting plant resources (e.g. Goren-Inbar et al., 2002), or in the case of handaxes, underground storage organs/tubers (Mercader, 2017; Mercader et al., 2017). Nevertheless, woodlands still would have offered an advantage to Acheulean hominins in that they not only provided sustenance in the form of plant foodstuffs, but also would have provided them protection from large carnivores or scavengers when defleshing or disarticulating animal remains. Therefore, the multipurpose nature of handaxes and other LCTs would have allowed early *Homo* to expand their ecological niche to incorporate more diverse, energy-rich foods procured within both grassland and woodland biomes.

The $\delta^{13}\text{C}$ data from *n*-alkane leaf wax lipid biological markers shows that for the earliest Acheulean at Olduvai Gorge, riparian woodland habitats acted as concentration zones for hominin activity, and that although paleobiological studies (Leonard and Robertson, 1997) suggest that *Homo erectus* occupied a more intensified ecological niche than earlier *Homo*, the emergence of the Acheulean was tied to a reliance on closed stands of trees similar to Bed I sites. It is probable that around ~1.7-1.6 Ma, changes in regional climate and the opening of the landscape fragmented Olduvai vegetation communities, pushing Acheulean toolmakers to become evermore reliant on

the ecotonal setting of their environment. FLK-W provides both a paleoecological background and information on the subsistence strategies of early Acheulean hominins at Olduvai Gorge, and can help to understand how a technological shift may relate to the way in which habitats and their resources were configured. The site specific, *n*-alkane $\delta^{13}\text{C}$ data from terrestrial sedimentary archives, shows that vegetations structure, dictated by localized hydrology, was a dominant control on early human behavior, and that when the site's ecology changed from a closed woodland to a more-open grassland or wooded grassland over a 34,000-year period, activity shifted away from FLK-W as it no longer provided an ecological advantage. Perhaps as FLK-W became less sustainable, Acheulean hominins settled ecologically more-productive locations such as at EF-HR, SHK, BK, or TK. Furthermore, Acheulean hominins likely used waterways and riparian woodlands as dispersal routes to move out of, across, or into East Africa.

CHAPTER 11: CONCLUSIONS

11.1 Leaf Wax Preservation

In order to reconstruct paleoenvironments using leaf wax lipids, the *n*-alkanes and *n*-alkanoic acids must preserve over geologic time and withstand substantial (bio)degradation. There was greater difficulty in interpreting the Bed II samples (FLK-W, LAS, BPT) for $\delta^{13}\text{C}$ and δD than those from Bed I (FLK-N and Clays below Tuff IF). This may be explained by changes to the methodological approach, as FLK-W, BPT, and LAS were not eluted over aminopropyl columns to begin with, nor were they separated using silver nitrate infused silica gel (SiAgNO_3) columns. The Bed I samples and the Bed II Castle Clays were extracted with Aminopropyl first and then SiAgNO_3 and both *n*-alkanes, without UCMs, and *n*-alkanoic acids, without double-bonded fatty acids, were quantifiable with GC-MS and IRMS. Beyond the methodological approach however, the clay sediments from FLK-N, Clays below Tuff IF, and the Castle Clays were likely a better matrix for preserving lipids long term than the sandy or sandstone sediments found in the LAS and FLK-W. On the other hand, the samples from the BPT, which were collected in the waxy, silty clays that underline the tuff, were poorly preserved regardless of the methodological approach; a subset of these samples were reprocessed using Aminopropyl and SiAgNO_3 columns first, yet only small quantities of lipids were recovered, similar to when only silica gel was used.

The samples collected in the Lower Augitic Sandstone were the poorest in terms of preservation, while the BPT also had poor preservation and Unresolved Complex Mixture (UCM) interference. For FLK-W, preservation was likely tied to the sedimentary matrix of each archaeological level, as Level 3 (for example), had to poorest preservation, potentially due to the it being a massive clayish silt without flow structures, likely deposited of an accumulation of wind-

blown dust. Furthermore, microbial (i.e. fungal) biodegradation is a significant factor in the taphonomy of leaf wax lipids, and samples from FLK-W, LAS, and BPT suffered substantially from the effects of microbial activity. As for the Castle Clays and FLK-N, both were well-preserved and had high concentrations of *n*-alkanes and *n*-alkanoic acids. At the Castle, leaf wax abundances seem to be tied to water availability and the resulting total plant biomass; increases in water led to increases in non-grass biomass and thus leaf wax lipids. Conversely, at FLK-N abundances are not tied to water availability or biomass, as changes in one or the other do not influence the total concentration of lipids. This may be due to the uniform composition of the vegetation through time and the constant supply of freshwater.

11.2 Water Availability and Plant Landscapes

The $\delta^{13}\text{C}$ data from FLK North suggest that it was a groundwater fed forest dominated by C_3 plants with a significant macrophyte component. Even though variations in the $\delta^{13}\text{C}$ signal from different *n*-alkanoic acid compounds (C_{22} - C_{32}) suggest different ecological lifeforms (tree vs. grass vs. macrophyte) thrived at the site, the δD data shows that the plant types were all utilizing the same source water. Furthermore, the $\delta^{13}\text{C}$ between samples only suggest slight changes in the composition of the plant landscape as there is only $\sim 1.0\text{‰}$ difference between individual samples, but because regional meteoric water δD is the primary control on leaf wax signatures, the observed $\sim 10\text{‰}$ change in δD between samples implies differences in precipitation intensity over time (Dansgaard, 1964), or alternations in the transport history of water vapor deriving from distinct sources (Konecky et al., 2011). Therefore, with the abundant freshwater available at FLK-N, either sourced from Crater Highland-recharged groundwater aquifers or surface streams draining the

highlands, both the carbon and hydrogen isotope data advocates that the vegetation community of FLK-N was unlike anything found at Olduvai Gorge today.

Alternating instances of covarying and anti-phasing $\delta^{13}\text{C}$ and δD were observed in the Castle Clays; this suggest that alternate controls beyond rainfall amount were acting on both isotope curves. Additionally, both carbon and hydrogen average isotope values from the Castle are enriched by $\sim 10\text{‰}$ and $\sim 30\text{‰}$, respectively, compared to those from FLK-N, indicating that the vegetation community was much different at the Castle, in addition to differences in plant ecological lifeform, source water, and rates of evapotranspiration. The carbon isotope data suggest that the Castle was an open grassland with a small woodland or bushland and thicket component whereby C_4 grasses never comprised less than 60% of the total plant biomass.

The anti-phased subsections, whereby increases/decreases in $\delta^{13}\text{C}$ do not coincide with increases/decreases in δD , suggest that changes in precipitation did not directly influence plant community structure, but rather plant ecological lifeform dictated the isotopic signatures. For example, trees with greater water-use efficiency (WUE) (as inferred by more-positive $\delta^{13}\text{C}$ values) negatively correlate with δD ; this would help explain why some samples had enriched $\delta^{13}\text{C}$ but depleted δD . Moreover, it is possible that shrubs and shrub-like trees became more widespread during anti-phased periods where $\delta^{13}\text{C}$ became more-depleted while δD became enriched. Another factor that may have influenced the isotope record may be that a reduction in global temperatures would have favored the expansion of C_3 plants (and a depletion in $\delta^{13}\text{C}$) but would have resulted in decreases in East African precipitation (and thus more-enriched δD).

Although δD data was not obtained from FLK-W, the correlation between diatom abundance and $\delta^{13}\text{C}$ values shows that the total amount of C_3 or C_4 plants was directly tied to the availability of moisture. The archaeological levels with the greatest concentration of diatoms (L6

and L5) also had the most-depleted $\delta^{13}\text{C}$ indicating an increase in C_3 plants. Levels 1 and 2 however, had very few, if any, diatoms and the most-enriched $\delta^{13}\text{C}$ values indicating an increase in C_4 plants. Once again, this shows that vegetation structure at the FLK-W site was directly tied to the availability of water.

11.3 Plant Ecosystems in Upper Bed I and Lower to Middle Bed II, Olduvai Gorge

The dominance of C_3 vegetation suggests that the FLK-N site may have been similar to the dense evergreen forest on the northwestern shore of Lake Manyara where trees with edible plant parts, such as the Cape Mahogany (*Trichilia emetica*), Sycamore Fig (*Ficus sycomorus*), and the Broad-Leaved Croton (*Croton macrostachyus*), are found. *Acalypha fruticosa* and *Acalypha ornate*, which also produce fruits and leaves eaten by chimpanzees, and *Hibiscus ovalifolius* and *Senna bicapsularis* are shrubs commonly found in the groundwater forest. The shade-adapted, inedible C_3 *Oplismenus hirtellus* is one of the rare grasses found on the forest floor. The ubiquitous groundwater and the small, spring-fed perennial rivers on the alluvial fans northwest of the lake have a dominant effect on the vegetation community and structure such that it changes rapidly within a few hundred meters of the freshwater sources. The $\delta^{13}\text{C}$ data from FLK-N and the Clays below Tuff IF show that similar effects existed at the top of Bed I whereby forests (e.g. FLK-N) grew in areas of abundant freshwater, while a few hundred meters away (e.g. Clays below Tuff IF samples 01, 02, and 20) had a dominant grass component (or in the case of samples 01 and 02, *Typha*).

The landscape around the Castle would have been a wooded grassland with C_3 plants covering only 10% and 40% of the surface similar the modern Somalia-Masai floristic region in which *Acacia-Commiphora* deciduous bushland and thicket are the climax vegetation (Kindt et

al., 2011). It is also possible that the Castle area was an ecotone between a more-dense woodland to the north closer to paleo-Lake Olduvai and an open grassland to the south away from the paleo-lake; the transitional, ecotonal nature is also characteristic of extant bushland and thick biomes (Mucina and Rutherford, 2006). Today, *Acacia-Commiphora* wooded grassland is the most extensive woody vegetation type in the Serengeti National Park representing 88% of all woody vegetation, but over 100 species of grasses occur in the region on soils deriving from volcanic ash. Therefore, the wooded component at the Castle likely consisted of *Acacia* species such as *A. tortilis*, *A. kirkii*, *A. seyal*, and *A. mellifera*, while *Pennisetum mezianum*, *Cynodon plectostachyus*, and *Cynodon dactylon* dominate the grass element. Additionally, shrubs and shrub-like trees of the genus *Commiphora* (e.g. *C. africana*, *C. habessinica*, *C. madagascariensis*, *C. merkeri*) are common around Olduvai Gorge and were likely also abundant on the Castle landscape.

Today, *Acacia* species (e.g. *A. xanthophloea*, *A. kirkii*, *A. robusta*) are dominant trees within riverine woodlands and bushland of the Serengeti, Ngorongoro, and Manyara regions (Copeland, 2007), while grasses from the species *Sporobolus* are abundant beyond the perimeter of the riparian environment. It is possible that the lower archaeological levels at FLK-W were analogous to the Mbalageti and Sangare River habitats of the modern Serengeti, but as the single stream channel at the site changed course or dried up to do regional changes in precipitation, *Acacia* dominated woodland reduced and was replaced by dry-adapted grasses such as *Sporobolus consimilis*, *S. ioclados*, and *S. fimbriatus* in the upper archaeological levels.

11.4 Environments and Stone Tool Technology

One central question in human evolution research asks whether the adoption of the Acheulean in favor of the Oldowan was environmentally driven. On the other hand, the emergence of the Acheulean has been linked to the appearance of *Homo erectus*, a species which predates the stone tool industry by roughly 150,000. Furthermore, because meat or underground storage organs may have been an important component of diet once East Africa became more arid after 2.0 Ma (Peters and O'Brien, 1981; Sponheimer and Lee-Thorp, 1999), the advent of the Acheulean may have facilitated an expanded human dietary niche that included foods from across an ecotonal spectrum.

Although it is difficult to answer whether the Acheulean emerged as a response to the opening of African landscapes with this limited dataset, the $\delta^{13}\text{C}$ and δD isotope records from Olduvai Gorge provide new information on the environmental context of the archaeological transition from the Oldowan to the Acheulean between Olduvai Beds I and II. Leaf wax lipid biomarkers show that the earliest Acheulean site at Olduvai Gorge, FLK West, was a riverine woodland and bushland with a dense component of *Acacia* species (e.g. *A. xanthophloea*, *A. kirkii*, *A. robusta*), that was used as a focal point to process open-habitat taxa and exploit underground storage organs. This differs from the older, Oldowan FLK North site, which was a dense groundwater forest where only hard-shelled nuts and fruits were consumed. (However, at the Bed I FLK *Zinj* and DS sites, hominins had primary access to carcasses; thus, we know meat was already a dietary component of Olduvai species before the transition to the Acheulean.) Nevertheless, because both archaeological assemblages were formed in habitats that were dominated by C_3 vegetation surrounded by open grasslands, marshlands, and ecotones, a form of ecological continuity existed between the two stone tool industries. This also suggest that although

large-scale, global or regional (East Africa) changes in climate may have dictated water availability (i.e. precipitation) at Olduvai Gorge, localized hydrology superseded the large-scale changes and determined plant landscapes and therefore, hominin land-use patterns. This is evident in the decreasing number of artifacts at FLK-W coinciding with a reduction in C₃ plant coverage that follow a reduction in water availability at the site. Therefore, hominins continued to use dense stands of trees as focal points of activity even after the Acheulean was adopted but consumed a larger breadth of food resources than earlier Oldowan individuals. Quartzite flakes were used to deflesh and disarticulate carcasses, while handaxes were used for bone breaking, hard-shelled nut and fruit processing, and digging for tubers and other underground storage organs.

Therefore, the emergence of the Acheulean was tied to closed woodland environments, likely used as focal points on the landscape to avoid cursorial predators and direct sun and wind exposure, but also for access to freshwater and plant food resources. Moreover, Acheulean hominins would have used waterways and riparian woodlands as dispersal routes across and out of East Africa.

11.5 Recommendations for Future Biomarker Research at Olduvai Gorge

Leaf wax lipid biologically specific marker molecules are powerful tools for understanding paleoenvironmental processes and the climatic context in which they originated, and for reconstructing ancient plant type, atmospheric CO₂, plant water-use efficiency, temperature, aridity/humidity (including precipitation), and source water. The research makes significant contributions to the science of human ecology and evolution studies through its integration of environmental disciplines with archaeology to assess the interaction between water accessibility, mosaic ecosystems, and dietary behavior in the various habitats that existed at Olduvai Gorge during Upper Bed I and Lower and Middle Bed II. However, the (bio)degradation of leaf waxes,

especially *n*-alkanes, can lead to difficulties in analyzing and interpreting the isotopic signal of terrestrial archives. As more research is conducted at Olduvai using lipids recovered in a wider range of sedimentary context, *best practice* techniques and protocols should be adopted to ensure optimal results are achieved. The following recommendations are designed to increase proficiency and systematize biomarker analyses for future research at Olduvai Gorge or other early human archaeological sites:

- Extract and analyze multiple biomarker compounds, such as both *n*-alkanes and *n*-alkanoic acids, as issues with taphonomy may preclude the use of certain molecules.
- Use multiple stationary phase compound isolation techniques. That is, Aminopropyl, silver nitrate infused silica gel (SiAgNO₃), and silica gel columns. These different techniques are beneficial in separating specific lipid components and will help reduce interference from such things as Unresolved Complex Mixtures.
- Using isotope values from multiple biosynthesized compounds can provide a broader picture of paleoenvironments than focusing on compounds synthesized only by terrestrial plants (e.g. *n*-acids C₂₈-C₃₄). Short, mid, and long-chain compounds when available, should all be characterized isotopically.
- Modern correlates are important for our understanding of past environments. More research is needed on existing ecosystems and how lipid compounds synthesized in specific habitats (open grassland vs. closed woodland) influence the environmental signal recovered in terrestrial archives.
- Do not rush into things, start small, and always collect more sample in the field than you intend to use. Many unforeseen issues arise when conducting laboratory research and

samples can easily become contaminated or mishandled. Problems with instrumentation are common (and frustrating), so try not to “waste” samples by running and rerunning them if machines are not cooperating.

REFERENCES

- Abell, P.I., Margolis, M.J., 1982. *n*-Paraffins in the sediments and in situ fossils of the Lake Turkana Basin, Kenya. *Geochimica et Cosmochimica Acta* 46, 1505-1511.
- Aichner, B., Herzsuh, U., Wilkes, H., 2010a. Influence of aquatic macrophytes on stable carbon isotope signatures of sedimentary organic matter in lakes on the Tibetan Plateau. *Organic Geochemistry* 41, 706-718.
- Aichner, B., Herzsuh, U., Wilkes, H., Vieth, A., Böhner, J., 2010b. δD values of *n*-alkanes in Tibetan lake sediments and aquatic macrophytes – A surface sediment study and application to a 16 ka record from Lake Koucha. *Organic Geochemistry* 41, 779-790.
- Albert, R., Bamford, D.B., 2012. Vegetation during UMBI and deposition of Tuff IF at Olduvai Gorge, Tanzania (ca. 1.8Ma) based on phytoliths and plant remains. *Journal of Human Evolution* 63, 342-350.
- Albert, R.M., Bamford, M., Cabanes, D., 2009. Palaeoecological significance of palms at Olduvai Gorge, Tanzania, based on phytolith remains. *Quaternary International* 193, 41-48.
- Albert, R.M., Bamford, M., Stanistreet, I.G., Stollhofen, H., Rivera-Rondón, C., Njau, J., Blumenschine, R.J., 2018. River-fed wetland palaeovegetation and palaeoecology at the HWK W site, Bed I, Olduvai Gorge. *Review of Palaeobotany and Palynology* 259, 223-241.
- Albert, R.M., Bamford, M.K., Cabanes, D., 2006. Taphonomy of phytoliths and macroplants in different soils from Olduvai Gorge (Tanzania) and the application to Plio-Pleistocene palaeoanthropological samples. *Quaternary International* 148, 78-94.
- Alley, R.B., Cuffey, K.M., 2001. Oxygen- and Hydrogen-Isotopic Ratios of Water in Precipitation: Beyond Paleothermometry, in: Valley, J.W., Cole, D. (Eds.), *Stable Isotope Geochemistry*. Mineralogical Society of America, Chantilly, VA, pp. 527-553.
- Andersen, N., Paul, H.A., Bernasconi, S.M., McKenzie, J.A., Behrens, A., Schaeffer, P., Albrecht, P., 2001. Large and rapid climate variability during the Messinian salinity crisis: evidence from deuterium concentrations of individual biomarkers. *Geology* 29, 799-802.
- Anderson, G.D., Herlocker, D., 1973. Soil Factors Affecting the Distribution of the Vegetation Types and Their Utilization by Wild Animals in Ngorongoro Crater, Tanzania. *Journal of Ecology* 61, 627-651.
- Anderson, G.D., Talbot, L.M., 1965. Soil Factors Affecting the Distribution of the Grassland Types and their Utilization by Wild Animals on the Serengeti Plains, Tanganyika. *Journal of Ecology* 53, 33-56.

- Andrews, P.J., 1989. Paleoeecology of Laetoli. *Journal of Human Evolution* 18, 173-181.
- Ashley, G.M., 2007. Orbital rhythms, monsoons, and playa lake response, Olduvai Basin, equatorial East Africa (ca. 1.85-1.74 Ma). *Geology* 35, 1091-1094.
- Ashley, G.M., Barboni, D., Domínguez-Rodrigo, M., Bunn, H., Mabulla, A., Diez Martin, F., Barba, R., Baquedano, E., 2010a. A spring and wooded habitat at FLK Zinj and their relevance to origins of human behavior. *Quaternary Research* 74, 304-314.
- Ashley, G.M., Bunn, H.T., Delaney, J.S., Barboni, D., Domínguez Rodrigo, M., Mabulla, A., Gurtov, A.N., Baluyot, R., Beverly, E.J., Baquedano, E., 2014. Paleoclimatic and paleoenvironmental framework of FLK North archaeological site, Olduvai Gorge, Tanzania. *Quaternary International* 322-323, 54-65.
- Ashley, G.M., Domínguez-Rodrigo, M., Bunn, H., Mabulla, A., Diez-Martín, F., Barba, R., Baquedano, E., 2010b. Paleoenvironmental and paleoecological reconstruction of a freshwater oasis in savannah grassland at FLK North, Olduvai Gorge, Tanzania. *Quaternary Research* 74, 333-343.
- Ashley, G.M., Tactikos, J.C., Owen, R.B., 2009. Hominin use of springs and wetlands: paleoclimate and archaeological records from Olduvai Gorge. *Palaeogeography, Palaeoclimatology, Palaeoecology* 272, 1-16.
- Bakkellund, A., Porter, T.J., Froese, D., Feakins, S.J., 2018. Net fractionation of hydrogen isotopes in *n*-alkanoic acids from soils in the northern boreal forest. *Organic Geochemistry* 125, 1-13.
- Balagizi, C.M., Kasereka, M.M., Cuoco, E., Liotta, M., 2018. Influence of moisture source dynamics and weather patterns on stable isotopes ratios of precipitation in Central-Eastern Africa. *Science of the Total Environment* 628-629, 1058-1078.
- Ballentine, D.C., Macko, S.A., Turekian, V.C., 1998. Variability of stable carbon isotopic compositions in individual fatty acids from combustion of C₄ and C₃ plants: implications for biomass burning. *Chemical Geology* 152, 151-161.
- Bamford, M., 2012. Fossil sedges, macroplants, and roots from Olduvai Gorge, Tanzania. *Journal of Human Evolution* 63, 351-363.
- Bamford, M.K., Albert, R.M., Cabanes, D., 2006. Plio-Pleistocene macroplant fossil remains and phytoliths from overmost Bed II in the eastern palaeolake margin of Olduvai Gorge, Tanzania. *Quaternary International* 148, 95-112.
- Bamford, M.K., Stanistreet, I.G., Stollhofen, H., Albert, R.M., 2008. Late Pliocene grassland from Olduvai Gorge, Tanzania. *Palaeogeography, Palaeoclimatology, Palaeoecology* 257, 280-293.

Bar-Yosef, O., 1994. The lower paleolithic of the Near East. *Journal of World Prehistory* 8, 211-265.

Bar-Yosef, O., Goren-Inbar, N., 1993. The lithic assemblages of 'Ubeidiya. A lower Palaeolithic site in the Jordan Valley. Quedum, Jerusalem.

Barboni, D., 2014. Vegetation of Northern Tanzania during the Plio-Pleistocene: A synthesis of the paleobotanical evidences from Laetoli, Olduvai, and Peninj hominin sites. *Quaternary International* in press.

Barboni, D., Ashley, G.M., Domínguez-Rodrigo, M., Bunn, H., Mabulla, A., Baquedano, E., 2010. Phytoliths infer locally dense and heterogeneous paleovegetation at FLK North and surrounding localities during upper Bed I time, Olduvai Gorge, Tanzania. *Quaternary Research* 74, 344-354.

Barboni, D., Bonnefille, R., Alexandre, A., Meunier, J.D., 1999. Phytoliths as palaeoenvironmental indicators, West Side Middle Awash Valley, Ethiopia. *Palaeogeography, Palaeoclimatology, Palaeoecology* 152, 87-100.

Barboni, D., Bremond, L., Bonnefille, R., 2007. Comparative study of modern phytolith assemblages from inter-tropical Africa. *Palaeogeography, Palaeoclimatology, Palaeoecology* 246, 454-470.

Barbour, M.M., Farquhar, G.D., 2000. Relative humidity- and ABA-induced variation in carbon and oxygen isotope ratios of cotton leaves. *Plant Cell and Environment* 23, 473-485.

Barker, P.A., Leng, M.J., Gasse, F., Huang, Y., 2007. Century-to-millennial scale climatic variability in Lake Malawi revealed by isotope records. *Earth and Planetary Science Letters* 261, 93-103.

Barnard, R.L., Osborne, C.A., Firestone, M.K., 2013. Responses of soil bacterial and fungal communities to extreme desiccation and rewetting. *Multidisciplinary Journal of Microbial Ecology* 7, 2229-2241.

Barnes, M.A., Barnes, W.C., 1978. Organic compounds in lake sediments, in: Lerman, A. (Ed.), *Lakes: Chemistry, Geology, Physics*. Springer-Verlag, Berlin, pp. 127-152.

Berger, W.H., Jansen, E., 1994. Mid-Pleistocene climate shift: the Nansen connection, in: Johannessen, O.M., Muench, R.D., Overland, J.E. (Eds.), *The Polar Oceans and their Role in Shaping the Global Environment*. American Geophysical Union, Washington, D. C. , pp. 295-311.

Bernard, A., Domergue, F., Pascal, S., Jetter, R., Renne, C., Faure, J.-D., Haslam, R.P., Napier, J.A., Lessire, R., Joubès, J., 2012. Reconstitution of Plant Alkane Biosynthesis in Yeast

Demonstrates That *Arabidopsis* ECERIFERUM1 and ECERIFERUM3 Are Core Components of a Very-Long-Chain Alkane Synthesis Complex. *The Plant Cell* 24, 3106-3118.

Berry, P.A., 2012. Lake Cycles and Sediments: Locality 80, Olduvai Gorge, Tanzania, Department of Geosciences. Georgia State University, Atlanta, GA, p. 73.

Beyene, Y., 2003. The Emergence and Development of the Acheulean at Konso. *Anthropological Science* 111, 58.

Beyene, Y., Katoh, S., WoldeGabriel, G., Hart, W.K., Uto, K., Sudo, M., Kondo, M., Hyodo, M., Renne, P.R., Suwa, G., Asfaw, B., 2013. The characteristics and chronology of the earliest Acheulean at Konso, Ethiopia. *Proceedings of the National Academy of Science* 110, 1584-1591.

Bi, X., Sheng, G., Liu, X., Li, C., Fu, J., 2005. Molecular and carbon and hydrogen isotopic composition of *n*-alkanes in plant leaf waxes. *Organic Geochemistry* 36, 1405-1417.

Biberson, P., 1963. Human Evolution in Morocco, In The Framework of the Paleoclimatic Variation of the Atlantic Pleistocene, in: Howell, F.C., Bourlière, F. (Eds.), *African Ecology and Human Evolution*. Aldine, Chicago, pp. 417-447.

Bibi, F., Kiessling, W., 2015. Continuous evolutionary change in Plio-Pleistocene mammals of eastern Africa. *Proceedings of the National Academy of Science* 112, 10623-10628.

Bibi, F., Pante, M., Souron, A., Stewart, K., Varela, S., Werdelin, L., Boisserie, J.R., Fortelius, M., Hlusko, L., Njau, J., de la Torre, I., 2018. Paleoecology of the Serengeti during the Oldowan-Acheulean transition at Olduvai Gorge, Tanzania: The mammal and fish evidence. *Journal of Human Evolution* 120, 48-75.

Bishop, W.W., 1976. Pliocene problems relating to human evolution, in: Isaac, G.L., McCown, E.R. (Eds.), *Human Origins: Perspectives on Human Evolution*. WA Benjamin, Menlo Park, CA, pp. 139-153.

Bishop, W.W., 1978. *Geological Background to Fossil Man: Recent Research in the Gregory Rift Valley, East Africa*. Scottish Academic Press, Edinburgh.

Blumenschine, R.J., 1995. Percussion marks, tooth marks, and experimental determinations of the timing of hominid and carnivore access to long bones at FLK Zinjanthropus, Olduvai Gorge, Tanzania. *Journal of Human Evolution* 29, 21-51.

Blumenschine, R.J., Masao, F.T., 1991. Living site at Olduvai Gorge, Tanzania? Preliminary landscape archaeology results in the basal Bed II lake margin zone. *Journal of Human Evolution* 21, 451-462.

Blumenschine, R.J., Stanistreet, I.G., Njau, J.K., Bamford, M., Masao, F.T., Albert, R.M., Stollhofen, H., Andrews, P., Prassack, K.A., McHenry, L.J., Fernández, J.Y., Camilli, E.L., Ebert, J.I., 2012. Environments and hominin activities across the FLK Peninsula during *Zinjanthropus* time (1.84 Ma), Olduvai Gorge, Tanzania. *Journal of Human Evolution* 63, 364-383.

Bobe, R., Behrensmeyer, A.K., 2004. The expansion of grassland ecosystems in Africa in relation to mammalian evolution and the origin of the genus *Homo*. *Palaeogeography, Palaeoclimatology, Palaeoecology* 207, 399-420.

Bobe, R., Eck, G., 2001. Responses of African bovids to Pliocene climatic change. *Paleobiology* 27, 1-47.

Boesch-Achermann, H., Boesch, C., 1994. Hominization in the rainforest: the chimpanzee's piece of the puzzle. *Evolutionary Anthropology* 3, 9-16.

Boesch, C., Boesch, H., 1990. Tool Use and Tool Making in Wild Chimpanzees. *Folia Primatol* 54, 86-99.

Boesch, C., Boesch, H., 2000. *The Chimpanzees of the Taï Forest: Behavioural Ecology and Evolution*. Max Planck Institute of Evolutionary Anthropology, Leipzig.

Bognar, A.L., Paliyath, G., Rogers, L., Kolattukudy, P.E., 1984. Biosynthesis of alkanes by particulate and solubilized enzyme preparations from pea leaves (*Pisum sativum*). *Archives of Biochemistry and Biophysics* 235, 8-17.

Boisserie, J.R., Brunet, M., Andossa, L., Vignaud, P., 2003. Hippopotamids from the Djurab Pliocene faunas, Chad, Central Africa. *Journal of African Earth Sciences* 36, 15-27.

Boisserie, J.R., Zazzo, A., Merceron, G., Blondel, C., Vignaud, P., Likius, A., Mackaye, H.T., Brunet, M., 2005. Diets of modern and late Miocene hippopotamids: Evidence from carbon isotope composition and micro-wear of tooth enamel. *Palaeogeography, Palaeoclimatology, Palaeoecology* 221, 153-174.

Boivin, N.L., Zeder, M.A., Fuller, D.Q., Crowther, A., Larson, G., Erlandson, J.M., Denham, T., Petraglia, M.D., 2016. Ecological consequences of human niche construction: Examining long-term anthropogenic shaping of global species distributions. *Proceedings of the National Academy of Science* 113, 6388-6396.

Bonnefille, B., 1995. A reassessment of the Plio-Pleistocene pollen record of East Africa, in: Vrba, E., Denton, G., Partridge, T., Burckle, L. (Eds.), *Paleoclimate and Evolution, with emphasis on human origins*. Yale University Press, New Haven, pp. 299-310.

Bonnefille, R., 1984. Palynological Research at Olduvai Gorge. National Geographic Society Research Reports, pp. 227-242.

Bouloubassi, I., Saliot, A., 1993. Investigation of anthropogenic and natural organic inputs in estuarine sediments using hydrocarbon markers (NAH, LAB, PAH). *Oceanologica Acta* 16, 145-161.

Bowen, G.J., Wassenaar, L.I., Hobson, K.A., 2005. Global application of stable hydrogen and oxygen isotopes to wildlife forensics. *Oecologia* 14, 337-348.

Bray, E.E., Evans, E.D., 1961. Distribution of normal-paraffins as a clue to recognition of source beds. *Geochimica et Cosmochimica Acta* 22, 2-15.

Brittingham, A., Hren, M.T., Hartman, G., 2017. Microbial alteration of the hydrogen and carbon isotopic composition of *n*-alkanes in sediments. *Organic Geochemistry* 107, 1-8.

Broman, D., Colmsjö, A., Ganning, B., Näf, C., Zebühr, Y., Östman, C., 1987. 'Fingerprinting' Petroleum Hydrocarbons in Bottom Sediment, Plankton, and Sediment Trap Collected Seston. *Marine Pollution Bulletin* 18, 380-388.

Bruggemann, J.H., Buffler, R.T., Guillaume, M.M.M., Walter, R.C., von Cosel, R., Ghebretensae, B.N., Berhe, S.M., 2004. Stratigraphy, palaeoenvironments and model for the deposition of the Abdur Reef Limestone: context for an important archaeological site from the last interglacial on the Red Sea coast of Eritrea. *Palaeogeography, Palaeoclimatology, Palaeoecology* 23, 179-206.

Brunet, M., Guy, F., Pilbeam, D., Mackaye, H.T., Likius, A., Ahounta, D., Beauvilain, A., Blondel, C., Bocherens, H., Boisserie, J.R., De Bonis, L., Coppens, Y., Dejax, J., Denys, C., Druinger, P., Eisenmann, V.R., Fanone, G., Fronty, P., Geraads, D., Lehmann, T., Lihoreau, F., Louchart, A., Mahamat, A., Merceron, G., Mouchelin, G., Otero, O., Campomanes, P.P., De Leon, M.P., Rage, J.C., Sapanet, M., Schuster, M., Sudre, J., Tassy, P., Valentin, X., Vignaud, P., Viriot, L., Zazzo, A., Zollikofer, C., 2002. A new hominid from the Upper Miocene of Chad, central Africa. *Nature* 418, 145-151.

Bunn, H., Mabulla, A., Domínguez-Rodrigo, M., Ashley, G.M., Barba, R., Diez-Martín, F., Remer, K., Yravedra, J., Baquedano, E., 2010. Was FLK North levels 1–2 a classic “living floor” of Oldowan hominins or a taphonomically complex palimpsest dominated by large carnivore feeding behavior? *Quaternary Research* 74, 355–362.

Bunn, H.T., 1986. Patterns on skeletal representation and hominid subsistence activities at Olduvai Gorge, Tanzania, and Koobi Fora, Kenya. *Journal of Human Evolution* 15, 673-690.

Bunn, H.T., Kroll, E.M., 1986. Systematic Butchery by Plio-Pleistocene Hominids at Olduvai Gorge, Tanzania. *Current Anthropology* 27, 431-452.

Burgoyne, T.W., Hayes, J.M., 1998. Quantitative production of H₂ by pyrolysis of gas chromatographic effluents. *Analytical Chemistry* 70, 5136-5140.

Bush, R.T., McInerney, F.A., 2013. Leaf wax *n*-alkane distributions in and across modern plants: Implications for paleoecology and chemotaxonomy. *Geochimica et Cosmochimica Acta* 117, 161-179.

Bush, R.T., McInerney, F.A., 2015. Influence of temperature and C₄ abundance on *n*-alkane chain length distributions across the central USA. *Organic Geochemistry* 79, 65-73.

Butzer, K.W., Isaac, G.L., 1975. *After the Australopithecines: Stratigraphy, Ecology and Culture Change in the Middle Pleistocene*. De Gruyter Mouton, The Hague.

Calvin, M., Benson, A.A., 1948. *The Path of Carbon in Photosynthesis, The Path of Carbon in Photosynthesis*. Ernest Orlando Lawrence Berkeley National Laboratory, Berkeley, CA; University of California Radiation Laboratory, Berkeley, CA, Berkely, CA.

Carter, J.F., Barwick, V.J., 2011. *Good practice guide for isotope ratio mass spectrometry*. FIRMS. ISBN 978-0-948926-31-0.

Carvalho, S., Cunho, E., Sousa, C., Matsuzawa, T., 2008. Chaînes opératoires and resource-exploitation strategies in chimpanzee (*Pan troglodytes*) nut cracking. *Journal of Human Evolution* 55, 148-163.

Castañeda, I.S., Mulitza, S., Schefuß, E., Lopes dos Santos, R.A., Sinninghe Damste, J.S., Schouten, S., 2009. Wet phases in the Sahara/Sahel region and human migration patterns in North Africa. *Proceedings of the National Academy of Sciences* 106, 20159–20163.

Castañeda, I.S., Schouten, S., 2011. A review of molecular organic proxies for examining modern and ancient lacustrine environments. *Quaternary Science Reviews* 30, 2845-2891.

Castañeda, I.S., Werne, J.P., Johnson, T.C., 2007. Wet and arid phases in the southeast African tropics since the Last Glacial Maximum. *Geoarchaeology* 35, 823-826.

Cavallo, J.A., Blumenschine, R.J., 1989. Tree-stored leopard kills: Expanding the hominid scavenging niche. *Journal of Human Evolution* 18, 393-399.

Cerling, T., 1984. The stable isotopic composition of modern soil carbonate and its relationship to climate. *Earth and Planetary Science Letters* 71, 229-240.

Cerling, T., 1991. On the isotopic composition of carbon in soil carbon dioxide. *Geochimica et Cosmochimica Acta* 55, 3403-3405.

Cerling, T., 1992. Development of grasslands and savannas in East Africa during the Neogene. *Palaeogeography, Palaeoclimatology, Palaeoecology* 97, 241-247.

Cerling, T., Harris, J.M., Ambrose, S.H., Leakey, M.G., Solounias, N., 1997a. Dietary and environmental reconstruction with stable isotope analysis of herbivore tooth enamel from the Miocene locality of Fort Ternan, Kenya. *Journal of Human Evolution* 33, 635-650.

Cerling, T., Harris, J.M., MacFadden, B.J., Ehleringer, J.R., Leakey, M.G., Quade, J., Eisenmann, V.R., 1997b. Global Vegetation Change through the Miocene/Pliocene Boundary. *Nature* 389, 153-158.

Cerling, T., Hay, R., 1986. An isotopic study of paleosol carbonates from Olduvai Gorge. *Quaternary Research* 25, 63-78.

Cerling, T., Levin, N.E., Quade, J., Wynn, J.G., Fox, D.L., Kingston, J.D., Klein, R.G., Brown, F.H., 2010. Comment on the Paleoenvironment of *Ardipithecus ramidus*. *Science* 328, 1105.

Cerling, T., Quade, J., 1993. Stable carbon and oxygen isotopes in soil carbonates, in: Swart, P.K., Lohmann, K.C., McKenzie, J.A., Savin, S. (Eds.), *Climate Change in Continental Records. Geophysical Monograph* 78. American Geophysical Union, pp. 217-231.

Cerling, T., R., B.J., O'Neill, J.R., 1988. An isotopic study of a fluvial-lacustrine sequence: the Plio-Pleistocene Koobi Fora sequence, East Africa. *Palaeogeography, Palaeoclimatology, Palaeoecology* 63, 335-356.

Cerling, T., Wang, Y., Quade, J., 1993. Global ecological change in the late Miocene: expansion of C4 ecosystems. *Nature* 361, 344-345.

Cerling, T., Wynn, J., Andanje, S., Bird, M., Korir, D., Levin, N.E., Mace, W., Macharia, A., Quade, J., Remien, C., 2011. Woody cover and hominin environments in the past 6 million years. *Nature* 476, 51-56.

Cerling, T.E., Harris, J.M., Ambrose, S.H., Leakey, M.H., Solounias, N., 1997c. Dietary and environmental reconstruction with stable isotope analyses of herbivore tooth enamel from the Miocene locality of Fort Ternan, Kenya. *Journal of Human Evolution* 33, 635-650.

Chazan, M., Ron, H., Matmon, A., Porat, N., Goldberg, P., Yates, R., Avery, M., Summer, A., Horwitz, L., 2008. Radiometric dating of the Earlier Stone Age sequence in Excavation I at Wonderwerk cave, South Africa: preliminary results. *Journal of Human Evolution* 55, 1-11.

Chikaraishi, Y., Naraoka, H., 2001. Organic hydrogen-carbon isotope signatures of terrestrial higher plants during biosynthesis for distinctive photosynthetic pathways. *Geochemical Journal* 35, 451-458.

Chikaraishi, Y., Naraoka, H., 2003. Compound-specific δD -delta $\delta^{13}C$ analyses of *n*-alkanes extracted from terrestrial and aquatic plants. *Phytochemistry* 63, 361-371.

Chikaraishi, Y., Naraoka, H., 2006. Carbon and hydrogen isotope variation of plant biomarkers in a plant–soil system. *Chemical Geology* 231, 190-202.

Chikaraishi, Y., Naraoka, H., 2007. $\delta^{13}C$ and δD relationships among three *n*-alkyl compound classes (*n*-alkanoic acid, *n*-alkane and *n*-alkanol) of terrestrial higher plants. *Organic Geochemistry* 38, 198-215.

Chikaraishi, Y., Naraoka, H., Poulson, S.R., 2004. Hydrogen and carbon isotopic fractionations of lipid biosynthesis among terrestrial (C3, C4 and CAM) and aquatic plants. *Phytochemistry* 65, 1369-1381.

Chorowicz, J., 2005. The East African rift system. *Journal of African Earth Sciences* 43, 379-410.

Clark, J.D., 1975. A comparison of the late Acheulian industries of Africa and the Middle East, in: Butzer, K.W., Isaac, G. (Eds.), *After the Australopithecines: Stratigraphy, Ecology, and Culture Change in the Middle Pleistocene*. The Hague, Mouton, pp. 605-660.

Clark, J.D., 1987. Transitions: *Homo erectus* and the Acheulian: the Ethiopian sites of Gadeb and the Middle Awash. *Journal of Human Evolution* 16, 809-826.

Clark, J.D., 2001. *Kalambo Falls Prehistoric Site, Volume III: The Earlier Cultures: Middle and Earlier Stone Age*. Cambridge University Press, Cambridge.

Collister, J.W., Rieley, G., Stern, B., Eglinton, G., Fry, B., 1994. Compound-specific $\delta^{13}C$ analyses of leaf lipids from plants with differing carbon dioxide metabolisms. *Organic Geochemistry* 21, 619-627.

Committee on the Earth System Context for Hominin Evolution, 2010. *Understanding Climate's Influence on Human Evolution*. National Research Council, Washington, DC, p. 116.

Conte, M.H., Weber, J.C., 2002. Plant biomarkers in aerosols record isotopic discrimination of terrestrial photosynthesis. *Nature* 417, 639-641.

Conte, M.H., Weber, J.C., Carlson, P.J., Flanagan, L.B., 2003. Molecular and carbon isotopic composition of leaf wax in vegetation and aerosols in a northern prairie ecosystem. *Oecologia* 135, 67-77.

Copeland, S.R., 2007. Vegetation and Plant Food Reconstruction of Lowermost Bed II, Olduvai Gorge, Using Modern Analogs. *Journal of Human Evolution* 53, 146-175.

Coppens, Y., 1994. East Side Story: The Origin of Humankind. *Scientific American* 270, 88-95.

Cowling, S.A., 2011. Ecophysiological response of lowland tropical plants to Pleistocene climate, in: Bush, M., Flenley, J., Gosling, W. (Eds.), *Tropical Rainforest Responses to Climatic Change*. Springer Berlin Heidelberg, Berlin, pp. 359-380.

Craig, H., 1961. Isotopic variations in meteoric waters. *Science* 133, 1702-1703.

Cranwell, P.A., 1973. Chain-length distribution of *n*-alkanes from lake sediments in relation to post-glacial environmental change. *Freshwater Biology* 3, 259-265.

Cranwell, P.A., 1984. Lipid geochemistry of sediments from Upton Broad, a small productive lake. *Organic Geochemistry* 7, 25-37.

Cranwell, P.A., Eglinton, G., Robinson, N., 1987. Lipids of aquatic organisms as potential contributors to lacustrine sediments. *Organic Geochemistry* 11, 513-527.

Dansgaard, W., 1964. Stable isotopes in precipitation. *Tellus* 16, 436-468.

Dart, R.A., 1925. *Australopithecus africanus*: The Man-Ape of South Africa. *Nature* 115, 195-199.

Dawson, A.G., 1996. Pleistocene, in: Fagan, B.M. (Ed.), *The Oxford Companion to Archaeology*. Oxford University Press, New York, pp. 570-573.

Dawson, T.E., Ehleringer, J.R., 1991. Streamside trees that do not use stream water. *Nature* 350, 335-337.

de la Torre, I., 2016. The origins of the Acheulean: past and present perspectives on a major transition in human evolution. *Philosophical Transactions of the Royal Society B* 371, 20150245.

de la Torre, I., Albert, R.M., Macphail, R., McHenry, L.J., Pante, M., Rodríguez-Cintas, A., Stanistreet, I.G., Stollhofen, H., 2017. The contexts and early Acheulean archaeology of the EF-HR paleo-landscape (Olduvai Gorge, Tanzania). *Journal of Human Evolution* 120, 274-297.

de la Torre, I., Mora, R., 2005. *Technological Strategies in the Lower Pleistocene at Olduvai Beds I and II*. University of Liège Press.

de la Torre, I., Mora, R., 2014. The Transition to the Acheulean in East Africa: an Assessment of Paradigms and Evidence from Olduvai Gorge (Tanzania). *Journal of Archaeological Method and Theory* 21, 781-823.

de la Torre, I., Mora, R., 2018. Technological behaviour in the early Acheulean of EF-HR (Olduvai Gorge, Tanzania). *Journal of Human Evolution* 120, 329-377.

de la Torre, I., Mora, R., Martínez-Moreno, J., 2008. The early Acheulean in Peninj (Lake Natron, Tanzania). *Journal of Anthropological Archaeology* 27, 244-264.

de la Torre, I., Wehr, K., 2018. Site formation processes of the early Acheulean assemblage at EF-HR (Olduvai Gorge, Tanzania). *Journal of Human Evolution* 120, 298-328.

Deino, A.L., 2012. $^{40}\text{Ar}/^{39}\text{Ar}$ dating of Bed I, Olduvai Gorge, Tanzania, and the chronology of early Pleistocene climate change. *Journal of Human Evolution* 63, 251-273.

deMenocal, P.B., 1995. Plio-Pleistocene African climate. *Science* 270, 53-59.

deMenocal, P.B., 2004. African climate change and faunal evolution during the Pliocene-Pleistocene. *Earth and Planetary Science Letters* 220, 3-24.

deMenocal, P.B., 2011. Climate and Human Evolution. *Science* 331, 540-542.

Deocampo, D.M., 2004. Hydrogeochemistry in the Ngorongoro Crater, Tanzania, and implications for land use in a World Heritage Site. *Applied Geochemistry* 19, 755-767.

Diefendorf, A.F., Freeman, C.L., Wing, S.L., Graham, J.M., 2011. Production of *n*-alkyl lipids in living plants and implications for the geologic past. *Geochimica et Cosmochimica Acta* 75, 7472-7485.

Diefendorf, A.F., Freimuth, E.J., 2017. Extracting the most from terrestrial plant-derived *n*-alkyl lipids and their carbon isotopes from the sedimentary record: A review. *Organic Geochemistry* 103, 1-21.

Diez-Martín, F., Sánchez-Yustos, P., Uribelarrea, D., Domínguez-Rodrigo, M., Fraile-Márquez, C., Obregón, R.-A., Díaz-Muñoz, I., Mabulla, A., Baquedano, E., Pérez-González, A., Bunn, H.T., 2014. New archaeological and geological research at SHK main site (Bed II, Olduvai Gorge, Tanzania). *Quaternary International* 322-323, 107-128.

Diez-Martín, F., Sánchez, P., Domínguez-Rodrigo, M., Mabulla, A., Barba, R., 2009. Were Olduvai Hominins making butchering tools or battering tools? Analysis of a recently excavated lithic assemblage from BK (Bed II, Olduvai Gorge, Tanzania). *Journal of Anthropological Archaeology* 28, 274-289.

Diez-Martín, F., Sánchez Yustos, P., Uribelarrea, D., Baquedano, E., Mark, D.F., Mabulla, A., Fraile, C., Duque, J., Díaz, I., Pérez-González, A., Yravedra, J., Egeland, C.P., Organista, E.,

Domínguez-Rodrigo, M., 2015. The Origin of The Acheulean: The 1.7 Million-Year-Old Site of FLK West, Olduvai Gorge (Tanzania). *Nature Scientific Reports* 5, 1-9.

Diez-Martín, F., Yustos, P.S., Domínguez-Rodrigo, M., Mabulla, A., Bunn, H., Ashley, G.M., Barba, R., Baquedano, E., 2010. New insights into hominin lithic activities at FLK North Bed I, Olduvai Gorge, Tanzania. *Quaternary Research* 74, 376-387.

Domínguez-Rodrigo, M., 2014. Is the “Savanna Hypothesis” a Dead Concept for Explaining the Emergence of the Earliest Hominins? *Current Anthropology* 55, 59-81.

Domínguez-Rodrigo, M., Barba, R., 2007. A palimpsest at FLK North 1–2: independent carnivore- and hominid-made bone accumulations, in: Domínguez-Rodrigo, M., Barba, R., Egeland, C.P. (Eds.), *Deconstructing Olduvai: A Taphonomic Study of Bed I Sites*. Springer, Dordrecht, The Netherlands, pp. 127-164.

Domínguez-Rodrigo, M., Barba, R., de la Torre, I., Mora, R., 2007a. A cautionary tale about early archaeological sites: a reanalysis of FLK North 6, in: Domínguez-Rodrigo, M., Barba, R., Egeland, A.G. (Eds.), *Deconstructing Olduvai: A Taphonomic Study of the Bed I Sites*. Springer, Dordrecht, The Netherlands, pp. 101-126.

Domínguez-Rodrigo, M., Barba, R., Organista, E., 2007b. A taphonomic study of FLK North 3 and 4: a felid–hyaenid and hominid palimpsest, in: Domínguez-Rodrigo, M., Barba, R., Egeland, C.P. (Eds.), *Deconstructing Olduvai: A Taphonomic Study of the Bed I Sites*. Springer, Dordrecht, The Netherlands, pp. 165-190.

Domínguez-Rodrigo, M., Bunn, H., Mabulla, A., Baquedano, E., Uribelarrea, D., Pérez-González, A., Gidna, A., Yravedra, J., Diez-Martín, F., Egeland, C.P., Barba, R., Arriaza, M.C., Organista, E., Ansón, M., 2014a. On meat eating and human evolution: A taphonomic analysis of BK4b (Upper Bed II, Olduvai Gorge, Tanzania), and its bearing on hominin megafaunal consumption. *Quaternary International* 322-323, 129-152.

Domínguez-Rodrigo, M., Cobo-Sánchez, L., Uribelarrea, D., Arriaza, M.C., Yravedra, J., Gidna, A., Organista, E., Sistiaga, A., Martín Perea, D.M., Baquedano, E., Aramendi, J., Mabulla, A., 2017. Spatial simulation and modelling of the early Pleistocene site of DS (Bed I, Olduvai Gorge, Tanzania): a powerful tool for predicting potential archaeological information from unexcavated areas. *Boreas* 46, 805-815.

Domínguez-Rodrigo, M., Diez-Martín, F., Yravedra, J., Barba, R., Mabulla, A., Baquedano, E., Uribelarrea, D., Sánchez, P., Eren, M.I., 2014b. Study of the SHK Main Site faunal assemblage, Olduvai Gorge, Tanzania: implications for Bed II taphonomy, paleoecology, and hominin utilization of megafauna. *Quaternary International* 322-323, 153-166.

Domínguez-Rodrigo, M., Egido, R.B., Egeland, C.P., 2007c. *Deconstructing Olduvai: A Taphonomic Study of the Bed I Sites*. Springer.

Domínguez-Rodrigo, M., Mabulla, A., Bunn, H., Diez Martin, F., Baquedano, E., Barboni, D., Barba, R., Dominguez Solera, S., Sanchez, P., Ashley, G.M., Yravedra, J., 2010. Disentangling hominin and carnivore activities near a spring at FLK North (Olduvai Gorge, Tanzania). *Quaternary Research* 74, 363-375.

Domínguez-Rodrigo, M., Mabulla, A., Bunn, H.T., Barba, R., Diez-Martín, F., Egeland, C.P., Espílez, E., Egeland, A.G., Yravedra, J., Sánchez, P., 2009. Unraveling hominid behavior at another anthropogenic site from Olduvai Gorge (Tanzania): new archaeological, taphonomic and technological research at BK, Bed II. *Journal of Human Evolution* 57, 260-283.

Domínguez-Rodrigo, M., Pickering, T.R., Baquedano, E., Mabulla, A., Mark, D.F., Musiba, C., Bunn, H.T., Uribelarrea, D., Smith, V., Diez-Martín, F., Pérez-González, A., Sánchez, P., Santonja, M., Barboni, D., Gidna, A., Ashley, G.M., Yravedra, J., Heaton, J.L., Arriaza, M.C., 2013. First partial skeleton of a 1.34-million-year-old *Paranthropus boisei* from Bed II, Olduvai Gorge, Tanzania. *PLOS One* 8, e80347.

Domínguez-Rodrigo, M., Serrallonga, J., Juan-Tresseras, J., Alcalá, L., Luque, L., 2001. Woodworking activities by early humans: a plant residue analysis on Acheulean stone tools from Peninj (Tanzania). *Journal of Human Evolution* 40, 289-299.

Duan, Y., Xu, L., 2012. Distributions of *n*-alkanes and their hydrogen isotopic composition in plants from Lake Qinghai (China) and the surrounding area. *Applied Geochemistry* 27, 806-814.

Duplessy, J.-C., Shackleton, N.J., 1985. Response of global deep-water circulation to Earth's climatic change 135,000–107,000 years ago. *Nature* 316, 500-507.

Ebinger, C.J., Deino, A.L., Tesha, A.L., Becker, T., Ring, U., 1993. Tectonic Controls on Rift Basin Morphology: Evolution of the Northern Malawi (Nyasa) Rift *Journal of Geophysical Research* 98, 17821-17836.

Eglinton, G., Hamilton, R.J., 1967. Leaf epicuticular waxes. *Science* 156, 1322-1335.

Eglinton, T.I., Eglinton, G., 2008. Molecular Proxies for Paleoclimatology. *Earth and Planetary Science Letters* 275, 1-16.

Ehleringer, J.R., 1989. Carbon Isotope Ratios and Physiological Processes in Aridland Plants, in: Rundel, P.W., Ehleringer, J.R., Nagy, K.A. (Eds.), *Stable Isotopes in Ecological Research*. Springer-Verlag, New York, New York, p. 525.

Ehleringer, J.R., Field, C.B., Lin, Z.-f., Kuo, C.-y., 1986. Leaf Carbon Isotope and Mineral Composition in Subtropical Plants along an Irradiance Cline. *Oecologia* 70, 520-526.

Ehleringer, J.R., Rundel, P.W., 1989. Stable Isotopes: History, Units, and Instrumentation, in: Rundel, P.W., Ehleringer, J.R., Nagy, K.A. (Eds.), *Stable Isotopes in Ecological Research*. Springer-Verlag, New York, New York, p. 535.

Ellsworth, P.Z., Williams, D.G., 2007. Hydrogen isotope fractionation during water uptake by woody xerophytes. *Plant and Soil* 291, 93-107.

Epstein, S., Thompson, P., Yapp, C.J., 1977. Oxygen and hydrogen isotopic ratios in plant cellulose. *Science* 198, 1209-1215.

Estep, M.F., Hoering, T.C., 1980. Biochemistry of the stable hydrogen isotopes. *Geochim Cosmochim Acta* 44, 1197-1206.

Falguères, C., Bahain, J.J., Saleki, H., 1997. U-series and ESR dating of teeth from Acheulean and Mousterian levels at La Micoques (Dordogne, France). *Journal of Archaeological Science* 24, 537-545.

Farquhar, G.D., Hubick, K.T., Condon, A.G., Richards, R.A., 1989. Carbon isotope fractionation and plant water use efficiency, in: Rundel, P.W., Ehleringer, J.R., Nagy, K.A. (Eds.), *Stable Isotopes in Ecological Research*. Springer-Verlag, New York, p. 525.

Farrington, J.W., Quinn, J.G., 2015. ‘‘Unresolved Complex Mixture’’ (UCM): A brief history of the term and moving beyond it. *Marine Pollution Bulletin* 96, 29-31.

Feakins, S.J., deMenocal, P.B., Eglinton, T.I., 2005. Biomarker records of late Neogene changes in northeast African vegetation. *Geology* 33, 977-980.

Feakins, S.J., Eglinton, T.I., deMenocal, P.B., 2007. A comparison of biomarker records of northeast African vegetation from lacustrine and marine sediments (ca. 3.40 Ma). *Organic Geochemistry* 38, 1607-1624.

Feakins, S.J., Levin, N.E., Liddy, H.M., Sieracki, A., Eglinton, T.I., Bonnefille, R., 2013. Northeast African vegetation change over 12 m.y. *Geology* 41, 295-298.

Feakins, S.J., Sessions, A.L., 2010a. Controls on the D/H ratios of plant leaf waxes in an arid ecosystem. *Geochimica et Cosmochimica Acta* 74, 2128–2141.

Feakins, S.J., Sessions, A.L., 2010b. Crassulacean acid metabolism influences D/H ratio of leaf wax in succulent plants. *Organic Geochemistry* 41, 1269-1276.

Feibel, C., Brown, F., McDougall, I., 1989. Stratigraphic context of fossil hominids from the Omo group deposits: Northern Turkana Basin, Kenya and Ethiopia. *American Journal of Physical Anthropology* 78, 595-622.

Feng, X.H., Epstein, S., 1994. Climatic implications of an 800-year hydrogen isotope time series from bristlecone pine trees. *Science* 265, 1079-1081.

Ficken, K.J., Li, B., Swain, D.L., Eglinton, G., 2000. An *n*-alkane proxy for the sedimentary input of submerged/floating freshwater aquatic macrophytes. *Organic Geochemistry* 31, 745-749.

Ficken, K.J., Street-Perrott, F.A., Perrott, R.A., Swain, D.L., Olago, D.O., Eglinton, G., 1998. Glacial/interglacial variations in carbon cycling revealed by molecular and isotope stratigraphy of Lake Nkunga, Mt. Kenya, East Africa. *Organic Geochemistry* 29, 1701-1719.

Fitzhugh, B., 2001. Risk and invention in human technological evolution. *Journal of Anthropological Archaeology* 20, 125-167.

Foster, A., Ebinger, C., Mbede, E., Rex, D., 1997. Tectonic development of the northern Tanzanian sector of the East African Rift system. *Journal of the Geological Society, London* 154, 689-700.

Freier, K., Glaser, B., Zech, W., 2010. Mathematical modeling of soil carbon turnover in natural *Podocarpus* forest and *Eucalyptus* plantation in Ethiopia using compound specific $\delta^{13}\text{C}$ analysis. *Global Change Biology* 16.

Fry, B., 2006. Isotope Notation and Measurement, in: Fry, B. (Ed.), *Stable Isotope Ecology*. Springer Science+Business Media, New York, NY, p. 308.

Frysjer, G.S., Gaines, R.B., Xu, L., Reddy, C.M., 2003. Resolving the Unresolved Complex Mixture in Petroleum-Contaminated Sediments. *Environmental Science & Technology* 37, 1653-1662.

Gallotti, R., Mussi, M., 2018a. Before, During, and After the Early Acheulean at Melka Kunture (Upper Awash, Ethiopia): A Techno-economic Comparative Analysis, in: Gallotti, R., Mussi, M. (Eds.), *The Emergence of the Acheulean in East Africa and Beyond: Contributions in Honor of Jean Chavaillon*. Springer International Publishing, New York, NY, pp. 53-92.

Gallotti, R., Mussi, M., 2018b. The Emergence of the Acheulean in East Africa: Historical Perspectives and Current Issues, in: Gallotti, R., Mussi, M. (Eds.), *The Emergence of the Acheulean in East Africa and Beyond: Contributions in Honor of Jean Chavaillon*. Springer International Publishing, New York, NY, p. 242.

Gamble, C., Gowlett, J., Dunbar, R., 2011. The social brain and the shape of the Palaeolithic. *Cambridge Archaeological Journal* 21, 111-135.

Gao, L., Guimond, J., Thomas, E., Huang, Y., 2015. Major trends in leaf wax abundance, $\delta^2\text{H}$ and $\delta^{13}\text{C}$ values along leaf venation in five species of C_3 plants: Physiological and geochemical implications. *Organic Geochemistry* 78, 144-152.

Gao, L., Hou, J., Toney, J., MacDonald, D., Huang, Y., 2011. Mathematical modeling of the aquatic macrophyte inputs of mid-chain n-alkyl lipids to lake sediments: implications for interpreting compound specific hydrogen isotopic records. *Geochimica et Cosmochimica Acta* 75, 3781-3791.

Garcin, Y., Junginger, A., Melnick, D., Olago, D.O., Strecker, M.R., Trauth, M.H., 2009. Late Pleistocene-Holocene rise and collapse of Lake Suguta, northern Kenya Rift. *Quaternary Science Reviews* 28, 911-925.

Garcin, Y., Schefuß, E., Schwab, V.F., Garreta, V., Gleixner, G., Vincens, A., Todou, G., Sene, O., Onana, J.M., Achoundong, G., Sachse, D., 2014. Reconstructing C₃ and C₄ vegetation cover using n-alkane carbon isotope ratios in recent lake sediments from Cameroon, Western Central Africa. *Geochimica et Cosmochimica Acta* 142, 482–500.

Garcin, Y., Schwab, V.F., Gleixner, G., Kahmen, A., Todou, G., Sene, O., Onana, J.M., Achoundong, G., Sachse, D., 2012. Hydrogen isotope ratios of lacustrine sedimentary n-alkanes as proxies of tropical African hydrology: insights from a calibration transect across Cameroon. *Geochim. Geochimica et Cosmochimica Acta* 79, 106-126.

Garcin, Y., Vincens, A., Williamson, D., Guiot, J., 2006. Wet phases in tropical southern Africa during the last glacial period. *Geophysical Research Letters* 33, L07703-07706.

Garrett, N.D., Fox, D.L., McNulty, K.P., Faith, J.T., Peppe, D.J., Van Platinga, A., Tryon, C.A., 2015. Stable isotope paleoecology of Late Pleistocene Middle Stone Age humans from the Lake Victoria basin, Kenya. *Journal of Human Evolution* 82, 1-14.

Gat, J.R., 1996. Oxygen and hydrogen isotopes in the hydrologic cycle. *Annual Review of Earth and Planetary Sciences* 24, 225-262.

Gathogo, P.N., Brown, F., 2006. Revised stratigraphy of Area 123, Koobi Fora, Kenya, and new age estimates of its fossil mammals, including hominins. *Journal of Human Evolution* 51, 471-479.

Geldenhuis, C.J., 1992. Richness, composition and relationships of the floras of selected forests in southern Africa. *Bothalia* 22.

Gibbard, P.L., Head, M.J., 2009. IUGS ratification of the Quaternary System/Period and the Pleistocene Series/Epoch with a base at 2.58 Ma. *Quaternaire* 20, 411-412.

Gibbard, P.L., Head, M.J., 2010. The newly-ratified definition of the Quaternary System/Period and redefinition of the Pleistocene Series/Epoch, and comparison of proposals advanced prior to formal ratification. *Episodes* 33, 152-158.

Gibbon, R., Granger, D., Kuman, K., Partridge, T., 2009. Early Acheulean technology in the Rieputs formation, South Africa, dated with cosmogenic nuclides. *Journal of Human Evolution* 56, 152-160.

Gibbons, A., 2006. *The First Human*. Anchor Books, New York.

Goren-Inbar, N., Sharon, G., Melamed, Y., Kislev, M., 2002. Nuts, nut-cracking, and pitted stones at Gesher Benot Ya'aqov, Israel. *Proceedings of the National Academy of Sciences* 99, 2455-2460.

Gough, M.A., Rowland, S.J., 1990. Characterization of unresolved complex mixtures of hydrocarbons in petroleum. *Nature* 344, 648-650.

Graham, L.E., Graham, J.M., Wilcox, L.W., 2006. *Plant Biology*. Pearson Prentice Hall, Upper Saddle River, NJ.

Grimalt, J.O., Alsaad, H.T., Douabul, A.A.Z., Albaigés, J., 1985. *n*-alkane distributions in surface sediments from the Arabian Gulf. *Naturwissenschaften* 72.

Grimalt, J.O., Torras, E., Albaigés, J., 1988. Bacterial reworking of sedimentary lipids during sample storage. *Advances in Organic Geochemistry* 13, 741-746.

Grum-Grzhimaylo, A.A., Georgieva, M.L., Bondarenko, S.A., Debets, A.J.M., Bilanenko, E.N., 2016. On the diversity of fungi from soda soils. *Fungal Diversity* 76, 27-74.

Hadley, J.L., Smith, W.K., 1989. Wind erosion of leaf surface wax in alpine timberline conifers. *Arctic Alpine Research* 21, 392-398.

Haile-Selassie, Y., Suwa, G., White, T.D., 2004. Late Miocene teeth from Middle Awash, Ethiopia, and early hominid dental evolution. *Science* 303, 1503-1505.

Hardt, T., Menke, P.R., Hardt, B., 2015. Paleoecology: An Adequate Window on the Past?, in: Henke, W., Tattersall, I. (Eds.), *Handbook of Paleoanthropology*, 2nd ed. Springer-Verlag, Berlin, pp. 571-622.

Hardy, K., Brand-Miller, J., Brown, K.D., Thomas, M.G., Copeland, L., 2015. The Importance of Dietary Carbohydrate in Human Evolution. *The Quarterly Review of Biology* 90, 251-268.

Harris, J.W.K., Isaac, G.L., 1997. Sites in the Upper KBS, Okote, and Chari Members: reports, in: Isaac, G.L. (Ed.), *Koobi Fora Research Project: Plio-Pleistocene Archaeology*. Cambridge University Press, Cambridge, pp. 115-236.

Harvey, H.R., Macko, S.A., 1997. Catalysts or contributors tracking bacterial mediation of early diagenesis in the marine water column. *Organic Geochemistry* 26, 531-544.

Hatch, M.D., 1987. C₄ photosynthesis: a unique blend of modified biochemistry, anatomy and ultrastructure. *Biochemica et Biophysica Acta (BBA) - Reviews on Bioenergetics* 895, 81-106.

Haug, G.H., Tiedemann, R., 1998. Effect of the formation of the Isthmus of Panama on Atlantic Ocean thermohaline circulation. *Nature* 393, 673-676.

Hay, R., 1976. *Geology of the Olduvai Gorge: A Study of Sedimentation in a Semiarid Basin*. University of California Press, London, England.

Hay, R., Kyser, T.K., 2001. Chemical sedimentology and paleoenvironmental history of Lake Olduvai, a Pleistocene lake in northern Tanzania. *Geological Society of America Bulletin* 113, 1505-1521.

Hays, J.D., Imbrie, J., Shackleton, N.J., 1976. Variations in the Earth's Orbit: Pacemaker of the Ice Ages. *Science* 194, 1121-1132.

Hecky, R.E., Hesslein, R.H., 1995. Contributions of benthic algae to lake food webs as revealed by stable isotope analysis. *Journal of the North American Benthological Society* 14, 631-653.

Hedberg, O., 1965. Afroalpine flora elements. *Webbia* 19, 519-529.

Herlocker, D.J., Dirschl, H.J., 1972. *Vegetation of the Ngorongoro Conservation Area, Tanzania*, Canadian Wildlife Service Report.

Hernandez-Aguilar, A., 2009. Chimpanzee nest distribution and site reuse in a dry habitat: implications for early hominin ranging. *Journal of Human Evolution* 57, 350-364.

Hilgen, F.J., Lourens, L.J., Van Dam, J.A., Beu, A.G., Boyes, A.F., Cooper, R.A., Krijgsman, W., Ogg, J.G., Piller, W.E., Wilson, D.S., 2012. The neogene Period, in: Gradstein, F.M., Ogg, J.G., Schmitz, M.D., Ogg, G.M. (Eds.), *The Geologic Time Scale*. Elsevier, pp. 923-978.

Hilkert, A.W., Douthitt, C.B., Schluter, H.J., 1999. Isotope ratio monitoring gas chromatography/mass spectrometry of D/H by high temperature conversion isotope ratio mass spectrometry. *Communications in Mass Spectrometry* 13, 1226-1230.

Hitchcock, C., Nichols, B.W., 1971. *Plant lipid biochemistry : the biochemistry of fatty acids and acyl lipids with particular reference to higher plants and algae*. Academic Press, New York, NY.

Hobbie, E.A., Werner, R.A., 2004. Intramolecular, compound-specific, and bulk carbon isotope patterns in C³ and C₄ plants: a review and synthesis. *New Phytologist* 161, 371-385.

Hoefs, J., 2009. *Stable Isotope Geochemistry*, 6 ed. Springer-Verlag, Berlin.

Hou, J., D'Andrea, W.J., Huang, Y.S., 2008a. Can sedimentary leaf waxes record D/H ratios of continental precipitation? Field, model, and experimental assessments. *Geochimica et Cosmochimica Acta* 72, 3503-3517.

Hou, J., D'Andrea, W.J., Huang, Y.S., 2008b. Can sedimentary leaf waxes record D/H ratios of continental precipitation? Field, model, and experimental assessments. *Geochimica et Cosmochimica Acta* 72, 3503–3517.

Hou, J., D'Andrea, W.J., MacDonald, D., Huang, Y., 2007a. Evidence for water use efficiency as an important factor in determining the δD values of tree leaf waxes. *Organic Geochemistry* 38, 1251-1255.

Hou, J., D'Andrea, W.J., MacDonald, D., Huang, Y., 2007b. Hydrogen isotopic variability in leaf waxes among terrestrial and aquatic plants around Blood Pond, Massachusetts (USA). *Organic Geochemistry* 38, 977-984.

Hou, Y., Potts, R., Yuan, B., Guo, Z., Deino, A., Wang, W., Clark, J., Xie, G., Huang, W., 2000. Mid-Pleistocene Acheulean-like stone technology of the Bose basin, South China. *Science* 287, 1622-1626.

Howell, F.C., Clark, J.D., 1963. Acheulean Hunter-Gatherers of Sub-Saharan Africa, in: Howell, F.C., Bourlière, F. (Eds.), *African Ecology and Human Evolution*. Aldine, Chicago, pp. 458-533.

Huang, Y., Bol, R., Harkness, D.D., Ineson, P., Eglinton, G., 1996. Post-glacial variations in distributions, ^{13}C and ^{14}C contents of aliphatic hydrocarbons and bulk organic matter in three types of British acid upland soils. *Organic Geochemistry* 24, 273-287.

Huang, Y., Clemens, S.C., Liu, W., Wang, Y., Prell, W.L., 2007. Large-scale hydrological change drove the late Miocene C₄ plant expansion in the Himalayan foreland and Arabian Peninsula. *Geology* 35, 531-534.

Huang, Y., Eglinton, G., Ineson, P., Latter, P.M., Bol, R., Harkness, D.D., 1997. Absence of carbon isotope fractionation of individual *n*-alkanes in a 23-year field decomposition experiment with *Calluna vulgaris*. *Organic Geochemistry* 26, 497-501.

Huang, Y., Shuman, B., Wang, Y., III, W.T., 2004. Hydrogen isotope ratios of individual lipids in lake sediments as novel tracers of climatic and environmental change: a surface sediment test. *Journal of Paleoclimatology* 31, 363-375.

Huang, Y., Shuman, B., Wang, Y., Webb III, T., 2002. Hydrogen isotope ratios of palmitic acid in lacustrine sediments record late Quaternary climate variations. *Geology* 30, 1103-1106.

Huang, Y., Shuman, B., Wang, Y., Webb III, T., Grimm, E.C., Jacobson, G.L., 2006. Climatic and environmental controls on the variation of C₃ and C₄ plant abundances in central Florida for the past 62,000 years. *Palaeogeography, Palaeoclimatology, Palaeoecology* 237, 428-435.

Huang, Y., Street-Perrott, F.A., Metcalfe, S.E., Brenner, M., Moreland, M., Freeman, K.H., 2001. Climate Change as the Dominant Control on Glacial-Interglacial Variations in C₃ and C₄ Plant Abundance. *Science* 293, 1647-1651.

Huang, Y., Street-Perrott, F.A., Perrott, R.A., Metzger, P., Eglinton, G., 1999. Glacial–interglacial environmental changes inferred from molecular and compound-specific $\delta^{13}\text{C}$ analyses of sediments from Sacred Lake, Mt. Kenya. *Geochimica et Cosmochimica Acta* 63, 1383-1404.

Hughen, K.A., Eglinton, T.I., Xu, L., Makou, M., 2004. Abrupt Tropical Vegetation Response to Rapid Climate Changes. *Science* 304, 1955-1959.

Huybers, P., 2006. Early Pleistocene Glacial Cycles and the Integrated Summer Insolation Forcing. *Science* 313, 508-511.

IAEA/WMO, 2015. Global Network of Isotopes in Precipitation. The GNIP Database. Accessible at: <https://nucleus.iaea.org/wiser>.

Isaac, G.L., 1971. The Diet of Early Man: Aspects of Archaeological Evidence from Lower and Middle Pleistocene Sites in Africa. *World Archaeology* 2, 278-299.

Isaac, G.L., 1976. East Africa as a source of fossil evidence for human evolution, in: Isaac, G.L., McCown, E.R. (Eds.), *Human Origins: Perspectives on Human Evolution*. WA Benjamin, Menlo Park, CA, pp. 121-137.

Isaac, G.L., McCown, E.R., 1976. *Human Origins: Perspectives on Human Evolution*. WA Benjamin, Menlo Park, CA.

Jaeschke, A., Rethemeyer, J., Lappé, M., Schouten, S., Boeckx, P., Schefuß, E., 2018. Influence of land use on distribution of soil *n*-alkane δD and brGDGTs along an altitudinal transect in Ethiopia: Implications for (paleo)environmental studies. *Organic Geochemistry* 124, 77-87.

Jager, T., 1982. *Soils of the Serengeti Woodlands, Tanzania*. Centre for Agricultural Publishing and Documentation, Wageningen, Netherlands.

Jetter, R., Kunst, L., 2008. Plant surface lipid biosynthetic pathways and their utility for metabolic engineering of waxes and hydrocarbon biofuels. *The Plant Journal* 54, 670-683.

Johanson, D.C., Lovejoy, O., Kimbel, W.H., White, T.D., Ward, S.C., Bush, M.E., Latimer, B., Coppens, Y., 1982. Morphology of the Pliocene partial hominid skeleton (A.L. 288-1) from the Hadar formation, Ethiopia. *American Journal of Physical Anthropology* 51, 403-451.

Jolly, C.J., 1978. *Early Hominids of Africa*. St. Martin's Press, New York, NY.

Jones, P.R., 1995. Results of experimental work in relation to the stone industries of Olduvai Gorge, in: Leakey, M.D., Roe, D.A. (Eds.), *Olduvai Gorge: Volume 5, Excavations in Beds III, IV and the Masek Beds*. Cambridge University Press, Cambridge.

Joordens, J.C.A., Dupont-Nivet, G., Feibel, C., Spoor, F., Sier, M.J., van der Lubbe, J.H.J.L., Nielson, T.K., Knul, M.V., Davies, G.R., Vonhof, H., 2013. Improved age control on early Homo fossils from the upper Burgi Member at Koobi Fora, Kenya. *Journal of Human Evolution* 65, 731-745.

Juggins, S., Cameron, N.G., 2010. Diatoms and Archeology, in: Smol, J.P., Stoermer, E.F. (Eds.), *The Diatoms: Applications for the Environmental and Earth Sciences*, 2nd ed. Cambridge University Press, Cambridge, pp. 514-522.

Katzenberg, M.A., Weber, A., 1999. Stable Isotope Ecology and Palaeodiet in the Lake Baikal Region of Siberia. *Journal of Archaeological Science* 26, 651-659.

Kavembe, G.D., Meyer, A., Wood, C.M., 2016. Fish Populations in East African Saline Lakes, in: Schagerl, M. (Ed.), *Soda Lakes of East Africa*. Springer, Switzerland, p. 408.

Khan, A., Kolattukudy, P.E., 1994. Decarboxylation of long chain fatty acids to alkanes by cell free preparations of pea leaves (*Pisum sativum*). *Biochemical and Biophysical Research Communications* 61, 1379-1386.

Killops, S.D., Killops, V.J., 2005. *Introduction to Organic Geochemistry*, 2nd ed. Blackwell Publishing, Malden, MA.

Kindt, R., Van Breugel, P., Lillesø, J.B., Bingham, M., Demissew, S., Dudley, C., Friis, I., Gachathi, F., Kalema, J., Mbago, F., Minani, V., Moshi, H., Mulumba, J., Namaganda, M., Ndangalasi, H., Ruffo, C., Jamnadass, R., Graudal, L.O.V., 2011. *Potential Natural Vegetation of Eastern Africa (Ethiopia, Kenya, Malawi, Rwanda, Tanzania, Uganda and Zambia)*. University of Copenhagen, Department of Geosciences and Natural Resource Management, Copenhagen, Denmark.

Kingston, J.D., Deino, A., Edgar, R.K., Hill, A., 2007. Astronomically forced climate change in the Kenyan Rift Valley 2.7-2.55 Ma: implications for the evolution of early hominin ecosystems. *Journal of Human Evolution* 53, 487-503.

Klein, R.G., 2009. *The Human Career: Human Biological and Cultural Origins.*, 3 ed. University of Chicago Press, Chicago.

Kleindienst, M.R., 1961. Variability within the Late Acheulian assemblage in East Africa. *The South African Archaeological Bulletin* XV, 35-52.

Koch, P.L., Clyde, W.C., Hepple, R.P., Fogel, M.L., Wing, S.L., Zachos, J.C., 2003. Carbon and oxygen isotope records from paleosol spanning the Paleocene-Eocene boundary, Bighorn Basin, Wyoming. *Geological Society of America Special Paper* 369, 49-64.

Kohn, M.J., 2010. Carbon isotope compositions of terrestrial C₃ plants as indicators of (paleo)ecology and (paleo)climate. *Proceedings of the National Academy of Science* 107, 19691-19696.

Kolattukudy, P.E., Buckner, J.S., Brown, L., 1972. Direct evidence for a decarboxylation mechanism in the biosynthesis of alkanes in *B. oleracea*. *Biochemical and Biophysical Research Communications* 47, 1306-1313.

Konecky, B.L., Russell, J.M., Johnson, T.C., Brown, E.T., Berke, M.A., Werne, J.P., Huang, Y., 2011. Atmospheric circulation patterns during late Pleistocene climate changes at Lake Malawi, Africa. *Earth and Planetary Science Letters* 312, 318-326.

Körner, C., Farquhar, G.D., Roksandic, Z., 1988. A global survey of carbon isotope discrimination in plants from high altitude. *Oecologia* 74, 623-632.

Kovarovic, K., Slepko, R., McNulty, K.P., 2013. Ecological continuity between Lower and Upper Bed II, Olduvai Gorge, Tanzania. *Journal of Human Evolution* 64, 538-555.

Kristen, I., Wilkes, H., Vieth, A., Zink, K.G., Plessen, B., Thorpe, J., Partridge, T.C., Oberhansli, H., 2010. Biomarker and stable carbon isotope analyses of sedimentary organic matter from Lake Tswaing: evidence for deglacial wetness and early Holocene drought from South Africa. *Journal of Paleolimnology* 44, 143-160.

Kuhn, S.L., 2004. Evolutionary perspectives on technology and technological change. *World Archaeology* 36, 561-570.

Kuman, K., 2007. The earlier Stone Age in South Africa: site context and the influence of cave studies, in: Pickering, T., Schick, K., Toth, N. (Eds.), *Breathing Life into Fossils: Taphonomic Studies in Honor of C. K. (Bob) Brain*. Stone Age Institute Press, Bloomington, IN.

Kuman, K., Clarke, R.J., 2000. Stratigraphy, artefact industries, and hominid associations for Sterkfontein, Member 5. *Journal of Human Evolution* 38, 827-847.

Kuman, K., Li, C., Li, H., 2014. Large cutting tools in the Danjiangkou Reservoir Region, central China. *Journal of Human Evolution* 76, 129-153.

Kunst, L., Samuels, A.L., 2003. Biosynthesis and secretion of plant cuticular wax. *Progress in Lipid Research* 42, 51-80.

Kutzbach, J.E., Gallimore, R., Harrison, S., Behling, P., Selin, R., Laarif, F., 1998. Climate and Biome Simulations for the Past 21,000 Years. *Quaternary Science Reviews* 17, 473-506.

Laporte, L.F., Zihlman, A., 1983. Plates, climate and hominoid evolution. *South African Journal of Science* 79, 96-110.

Larick, R., Ciochon, R.L., 1996. The African Emergence and Early Asian Dispersals of the Genus *Homo*. *American Scientist* 84, 538-551.

Larrasoana, J.C., Roberts, A.P., Rohling, E.J., Winkhofer, M., Wekhausen, R., 2003. Three million years of monsoon variability over the northern Sahara. *Climate Dynamics* 21, 689-698.

Lattuati, A., Metzger, P., Acquaviva, M., Bertrand, J.C., Largeau, C., 2002. *n*-alkane degradation by *Marinobacter hydrocarbonoclasticus* strain SP 17: long chain beta-hydroxy acids as indicators of bacterial activity. *Organic Geochemistry* 33, 37-45.

Le Fur, S., Fara, E., Mackaye, H.T., Vignaud, P., Brunet, M., 2009. The mammal assemblage of the hominid site TM266 (Late Miocene, Chad Basin): ecological structure and paleoenvironmental implications. *Naturwissenschaften* 96, 565-574.

Le Fur, S., Fara, E., Mackaye, H.T., Vignaud, P., Brunet, M., 2014. Toros-Menalla (Chad, 7 Ma), the earliest hominin-bearing area: How many mammal paleocommunities? . *Journal of Human Evolution* 69, 79-90.

Leahy, J.G., Colwell, R.R., 1990. Microbial degradation of hydrocarbons in the environment. *Microbiological Reviews* 54, 305-315.

Leakey, L.S.B., 1951. Olduvai Gorge. A report on the evolution of the hand-axe culture in Beds I-IV. Cambridge University Press, Cambridge, UK.

Leakey, L.S.B., 1959. A new fossil from Olduvai. *Nature* 184, 491-494.

Leakey, L.S.B., 1965. Olduvai Gorge 1951-1961: A Preliminary Report on the Geology and Fauna. Cambridge University Press, Cambridge.

Leakey, L.S.B., 1974. By the evidence: memoirs, 1932-1951. Harcourt Brace Jovanovich, Inc., New York.

- Leakey, M., 1984. *Disclosing the Past*. Rainbird Publishing Group Limited, London.
- Leakey, M., Hay, R., Thurber, D., Protsch, R., Berger, R., 1972. Stratigraphy, archaeology and age of the Ndutu and Naisiusu Beds, Olduvai Gorge, Tanzania. *World Archaeology* 3, 328-341.
- Leakey, M.D., 1967. Preliminary Survey of the Cultural Material from Beds I and II, Olduvai Gorge, Tanzania, in: Bishop, W.W., Clark, J.D. (Eds.), *Background to evolution in Africa*. University of Chicago Press, Chicago, pp. 417-446.
- Leakey, M.D., 1971. *Olduvai Gorge Vol. 3: Excavations in Beds I and II, 1960 - 1963*. Cambridge University Press, Cambridge.
- Leakey, M.G., Feibel, C.S., McDougall, I., Walker, A., 1995. New four-million-year-old hominid species from Kanapoi and Allia Bay, Kenya. *Nature* 376, 565-571.
- Lebreton, L., Desclaux, E., Hanquet, C., Moigne, A.-M., Perrenoud, C., 2016. Environmental context of the Caune de l'Arago Acheulean occupations (Tautavel, France), new insights from microvertebrates in Q-R levels. *Quaternary International* 411, 182-192.
- Lee-Thorp, J.A., Sponheimer, M., 2007. Contribution of Stable Light Isotopes to Paleoenvironmental Reconstruction, in: Henke, W., Tattersall, I. (Eds.), *Handbook of Paleoanthropology*. Springer, New York, NY, p. 299.
- Leng, Q., Langlois, G., Yang, H., 2010. Paleogene Arctic terrestrial ecosystems affected by the change of polar hydrology under global warming: Implications for modern climate change at high latitudes. *Science China* 53, 933-944.
- Leonard, W., Robertson, M., 1997. Comparative primate energetics and hominid evolution. *American Journal of Physical Anthropology* 102, 265-281.
- Lepre, C.J., Kent, D.V., 2015. Chronostratigraphy of KNM-ER 3733 and other Area 104 hominins from Koobi Fora. *Journal of Human Evolution* 86, 99-111.
- Lepre, C.J., Quinn, R.L., Joordens, J.C.A., Swisher III, C.C., Feibel, C.S., 2007. Plio-Pleistocene facies environments from the KBS Member, Koobi Fora Formation: implications for climate controls on the development of lake-margin hominin habitats in the northeast Turkana Basin (northwest Kenya). *Journal of Human Evolution* 53, 504-514.
- Lepre, C.J., Roche, H., Kent, D.V., Harmand, S., Quinn, R.L., Brugal, J.-P., Texier, P.-J., Lenoble, A., Feibel, C., 2011. An earlier origin for the Acheulean. *Nature* 477, 85-85.

Levin, N.E., Brown, F.H., Behrensmeyer, A.K., Bobe, R., Cerling, T., 2011. Paleosol carbonates from the Omo Group: Isotopic records of local and regional environmental change in East Africa. *Palaeogeography, Palaeoclimatology, Palaeoecology* 307, 75-89.

Levin, N.E., Quade, J., Simpson, S., Semaw, S., Rogers, M., 2004. Isotopic Evidence for Plio-Pleistocene Environmental Change at Gona, Ethiopia. *Earth and Planetary Science Letters* 219, 93-110.

Levin, N.E., Simpson, S.W., Quade, J., Cerling, T.E., Frost, S.R., 2008. Herbivore enamel carbon isotopic composition and the environmental context of *Ardipithecus* at Gona, Ethiopia. *Geological Society of America Special Paper* 446, 215-234.

Levin, N.E., Zipser, E.J., Cerling, T.E., 2009. Isotopic composition of waters from Ethiopia and Kenya: Insights into moisture sources for eastern Africa. *Journal of Geophysical Research* 114, 1-13.

Li, R., Fan, J., Xue, J., Meyers, P.A., 2017. Effects of early diagenesis on molecular distributions and carbon isotopic compositions of leaf wax long chain biomarker *n*-alkanes: comparison of two one-year-long burial experiments. *Organic Geochemistry* 104, 8-18.

Li, T.-S., Li, J.-T., Li, H.-Z., 1995. Modified and convenient preparation of silica impregnated with silver nitrate and its application to the separation of steroids and triterpenes. *Journal of Chromatography A* 715, 372-375.

Lisiecki, L.E., Raymo, M.E., 2005. A Pliocene-Pleistocene stack of 57 globally distributed benthic $\delta^{18}\text{O}$ records. *Paleoceanography* 20, 1-17.

Liu, H., Liu, W., 2017. Concentration and distributions of fatty acids in algae, submerged plants and terrestrial plants from the northeastern Tibetan Plateau. *Organic Geochemistry* 113, 17-26.

Liu, H., Yang, H., Cao, Y., Leng, Q., Liu, W., 2018. Inter-molecular variations of fatty acid dD in algae and submerged plants from the north-eastern Tibetan Plateau. *Organic Geochemistry* 122, 17-28.

Liu, W., Huang, Y., 2005. Compound specific *D/H* ratios and molecular distributions of higher plant leaf waxes as novel paleoenvironmental indicators in the Chinese Loess Plateau. *Organic Geochemistry* 36, 851-860.

Liu, W., Liu, Z., An, Z., Wang, X., Chang, H., 2011. Wet climate during the 'Little Ice Age' in the arid Tarim Basin, northwestern China. *The Holocene* 21, 409-416.

Liu, W., Yang, H., 2008. Multiple controls for the variability of hydrogen isotopic compositions in higher plant *n*-alkanes from modern ecosystems. *Global Change Biology*, 2166-2177.

Liu, W., Yang, H., Li, L., 2006. Hydrogen isotopic compositions of *n*-alkanes from terrestrial plants correlate with their ecological life forms. *Oecologia* 150, 330-338.

Liutkus, C.M., Wright, J.D., Ashley, G.M., Sikes, N.E., 2005. Paleoenvironmental interpretation of lake-margin deposits using $\delta^{13}\text{C}$ and $\delta^{18}\text{O}$ results from Early Pleistocene carbonate rhizoliths, Olduvai Gorge, Tanzania. *Geology* 33, 377-380.

Llorens, L., Osborne, C.P., Beerling, D.J., 2009. Water-use responses of 'living fossil' conifers to CO_2 enrichment in a simulated Cretaceous polar environment. *Annals of Botany* 104, 179-188.

Lockheart, M.J., van Bergen, P.F., Evershed, R.P., 1997. Variations in the stable carbon isotope compositions of individual lipids from the leaves of modern angiosperms: implications for the study of higher land plant-derived sedimentary organic matter. *Organic Geochemistry* 26, 137-153.

Louchart, A., Mourer-Chauviré, C., Vignaud, P., Mackaye, H.T., Brunet, M., 2005. A finfoot from the Late Miocene of Toros Menalla (Chad, Africa): Palaeobiogeographical and palaeoecological implications. *Palaeogeography, Palaeoclimatology, Palaeoecology* 222, 1-9.

Lupien, R.L., Russell, J.M., Feibel, C., Beck, C., Castañeda, I.S., Deino, A., Cohen, A., 2018. A leaf wax biomarker record of early Pleistocene hydroclimate from West Turkana, Kenya. *Quaternary Science Reviews* 186, 225-235.

Lutgens, F.K., Tarbuck, E.J., 2012. *Essentials of Geology*, 11th ed. Pearson Education, Inc., Upper Saddle River, New Jersey.

Maffei, M., Mucciarelli, M., Scannerini, S., 1993. Environmental factors affecting the lipid-metabolism in *Rosmarinus-officinalis* l. *Biochemical Systematics and Ecology* 21, 765-784.

Magill, C.R., Ashley, G.M., Domínguez-Rodrigo, M., Freeman, K., 2015. Dietary options and behavior suggested by plant biomarker evidence in an early human habitat. *Proceedings of the National Academy of Science* 113, 2874-2879.

Magill, C.R., Ashley, G.M., Freeman, K.H., 2013a. Ecosystem variability and early human habitats in eastern Africa. *Proceedings of the National Academy of Science* 110, 1167-1174.

Magill, C.R., Ashley, G.M., Freeman, K.H., 2013b. Water, plants, and early human habitats in eastern Africa. *Proceedings of the National Academy of Science* 110, 1175-1180.

Manega, P., 1993. Geochronology, geochemistry and isotopic study of the PlioPleistocene hominid sites and the Ngorongoro Volcanic Highland in Northern Tanzania. University of Colorado, Boulder, CO.

Marlow, J.R., Lange, C.B., Wefer, G., Rosell-Melé, A., 2000. Upwelling Intensification as part of the Pliocene-Pleistocene Climate Transition. *Science* 290, 2288-2291.

Marshall, F., Reid, R.E.B., Goldstein, S., Storozum, M., Wreschnig, A., Hu, L., Kiura, P., Shahack-Gross, R., Ambrose, S.H., 2018. Ancient herders enriched and restructured African grasslands. *Nature* 561, 387-390.

Maslin, M.A., Christensen, M., 2007. Tectonics, orbital forcing, global climate change, and human evolution in Africa: introduction to the African paleoclimate special volume. *Journal of Human Evolution* 53, 443-464.

Maslin, M.A., Christensen, M., Wilson, K.E., 2013. Tectonics, Orbital Forcing, Global Climate Change, and Human Evolution, in: Sponheimer, M., Lee-Thorp, J.A., Reed, K.E., Ungar, P. (Eds.), *Early Hominin Paleoecology*. University of Colorado Press, Boulder, CO, pp. 103-160.

Maslin, M.A., Ridgwell, A.J., 2005. Mid-Pleistocene revolution and the 'eccentricity myth', in: Head, M.J., Gibbard, P.L. (Eds.), *Early–Middle Pleistocene Transitions: The Land–Ocean Evidence*. Geological Society of London, London, pp. 19-34.

Maslin, M.A., Trauth, M.H., 2009. Plio-Pleistocene East African Pulsed Climate Variability and Its Influence on Early Human Evolution, in: Grine, F.E., Fleagle, J.G., Leakey, R.E. (Eds.), *The First Humans - Origin and Early Evolution of the Genus *Homo**. Springer Netherlands, pp. 151-158.

Mauseth, J.D., 2009. *Botany: an introduction to plant biology*. Jones and Bartlett Publishers, Sudbury, MA.

McDougall, I., Brown, F.H., Fleagle, J.G., 2008. Spropels and the age of hominins Omo I and II, Kibish, Ethiopia. *Journal of Human Evolution* 55, 409-420.

McHenry, L.J., Njau, J.K., de la Torre, I., Pante, M., 2016. Geochemical “fingerprints” for Olduvai Gorge Bed II tuffs and implications for the Oldowan–Acheulean transition. *Quaternary Research* 85, 147-158.

McHenry, L.J., Stanistreet, I.G., 2018. Tephrochronology of Bed II, Olduvai Gorge, Tanzania, and placement of the Oldowan-Acheulean transition. *Journal of Human Evolution* 120, 7-18.

McPherron, S.P., 2000. Handaxes as a Measure of the Mental Capabilities of Early Hominids. *Journal of Archaeological Science* 27, 655-663.

McWilliams, K.M., Angelici, R.J., 2016. Batchwise extraction of methyl linolenate (18:3, ALA) from fatty acid methyl esters derived from soybean and canola oils using silver nitrate/silica gel. *European Journal of Lipid Science and Technology* 118, 252-261.

Mercader, J., 2017. Acheulean Hominin Ecology: Organic Residue on Lithics as Evidence of Plant Processing, Society for American Archaeology 82nd Annual Meeting. Society of American Archaeology, Vancouver, BC.

Mercader, J., Abtosway, M., Clarke, S., DeBuhr, C., Diez-Martín, F., Domínguez-Rodrigo, M., Favreau, J., Itambu, M., Krause, F., Lee, P., Mabulla, A., Patalano, R., Tucker, L., Uribelarrea, D., Walde, D., 2017. Fossilized starch shows Acheulean harvesting of yams 1.7 million years ago at Olduvai Gorge, The East African Association for Paleoanthropology and Paleontology (EAAPP) 6th Biennial Meeting. The East African Association for Paleoanthropology and Paleontology (EAAPP) Addis Ababa, Ethiopia.

Mercader, J., Astudillo, F., Barkworth, M., Bennett, T., Esselmont, C., Kinyanjui, R., Laskin Grossman, D., Simpson, S., Walde, D., 2010. Poaceae phytoliths from the Niassa Rift, Mozambique. *Journal of Archaeological Science* 37, 1953-1967.

Mercader, J., Barton, H., Gillespie, J., Harris, J., Kuhn, S., Tyler, R., Boesch, C., 2007. 4,300-year-old chimpanzee sites and the origins of percussive stone technology. *Proceedings of the National Academy of Science* 104, 3043-3048.

Mercader, J., Bennett, T., Esselmont, C., Simpson, S., Walde, D., 2009. Phytoliths in woody plants from the Miombo woodlands of Mozambique. *Annals of Botany* 104, 91-113.

Mercader, J., Panger, M., Boesch, C., 2002. Excavation of a Chimpanzee Stone Tool site in the African Rainforest. *Science* 296, 1452-1455.

Mills, A.J., 2006. The role of salinity and sodicity in the dieback of *Acacia xanthophloea* in Ngorongoro Caldera, Tanzania. *African Journal of Ecology* 44, 61-71.

Monroe, J.S., Wicander, R., Hazlett, R., 2007. *Physical Geology: Exploring the Earth*, 6th ed. Thomson Brooks/Cole, Belmont, CA.

Mucina, L., Rutherford, M., 2006. The vegetation of South Africa, Lesotho, and Swaziland, Strelitzia. Sanbi, Pretoria.

Naraoka, H., Ishiwarati, R., 1999. Carbon isotope compositions of individual long-chain *n*-fatty acids and *n*-alkanes in sediments from river to open ocean: Multiple origins for their occurrence. *Geochemical Journal* 33, 215-235.

Naraoka, H., Ishiwarati, R., 2000. Molecular and isotopic abundances of long chain *n*-fatty acids in open marine sediments of the western North Pacific. *Chemical Geology* 165, 23-36.

Newell, R.E., 1974. Changes in the Poleward Energy Flux by the Atmosphere and Ocean as a Possible Cause for Ice Ages. *Quaternary Research* 4, 117-127.

Nguyen Tu, T.T., Derenne, S., Largeau, C., Bardoux, G., Mariotti, A., 2004. Diagenesis effects on specific carbon isotope composition of plant *n*-alkanes. *Organic Geochemistry* 35, 317-329.

Nguyen Tu, T.T., Egasse, C., Zeller, B., Bardoux, G., Biron, P., Ponge, J.F., David, B., Derenne, S., 2011. Early degradation of plant alkanes in soils: a litterbag experiment using ¹³C labelled leaves. *Soil Biology and Biochemistry* 43, 2222-2228.

Nicholson, S.E., 1993. An overview of African Rainfall Fluctuations of the Last Decade. *Journal of Climate* 6, 1463-1466.

Nicholson, S.E., 1996. A review of climate dynamics and climate variability in eastern Africa, in: Johnson, T.C., Odada, E.O. (Eds.), *The Limnology, Climatology, and Paleoclimatology of the East African Rift Lakes*. Gordon and Breach, Amsterdam, pp. 25-56.

Niedermeyer, E.M., Schefuß, E., Sessions, A.L., Mulitza, S., Mollenhauer, G., Schulz, M., Wefer, G., 2010. Orbital- and millennial-scale changes in the hydrologic cycle and vegetation in the western African Sahel: insights from individual plant wax δ D and δ^{13} C. *Quaternary Science Reviews* 29, 2996-3005.

Nikolova-Damyanova, B., 2009. Retention of lipids in silver ion high-performance liquid chromatography: Facts and assumptions. *Journal of Chromatography A* 1216, 1815-1824.

O'Leary, M., 1981. Carbon Isotope Fractionation in Plants. *Phytochemistry* 20, 553-567.

Ohlrogge, J., Browse, J., 1995. Lipid Biosynthesis. *The Plant Cell* 7, 957-970.

Paddayya, K., Blackwell, B.A.B., Jhaldiyal, R., Petraglia, M.D., Fevrier, S., Chaderton, D.A., Blickstein, J.I.B., R., S.A., 2002. Recent findings on the Acheulian of the Hunsgi and Baichabl valleys, Karnataka, with special reference to the Isampur excavation and its dating. *Current Science* 83, 641-647.

Pagani, M., Arthur, M.A., Freeman, K.H., 1999a. Miocene evolution of atmospheric carbon dioxide. *Paleoceanography* 14, 273-292.

Pagani, M., Freeman, K.H., Arthur, M.A., 1999b. Late Miocene Atmospheric CO₂ Concentrations and the Expansion of C₄ Grasses. *Science* 285, 876-879.

Pagani, M., Pedentchouk, N., Huber, M., Sluijs, A., Schouten, S., Brinkhuis, H., Sinninghe Damste, J.S., Dickens, G.R., Scientists, E., 2006. Arctic hydrology during global warming at the Palaeocene/Eocene thermal maximum. *Nature* 442, 671-675.

Pante, M., de la Torre, I., 2018. A hidden treasure of the Lower Pleistocene at Olduvai Gorge, Tanzania: The Leakey HWK EE assemblage. *Journal of Human Evolution* 120, 114-139.

Pante, M., Njau, J.K., Hensley-Marschand, B., Keevil, T.L., Martín-Ramos, C., Peters, R.F., de la Torre, I., 2018. The carnivorous feeding behavior of early *Homo* at HWK EE, Bed II, Olduvai Gorge, Tanzania. *Journal of Human Evolution* 120, 215-235.

Pappu, S., Gunnell, Y., Akhilesh, K., Braucher, R., Taieb, M., Demory, F., Thouveny, N., 2011. Early Pleistocene presence of Acheulian hominins in south India. *Science* 331, 1596-1599.

Patalano, R., Diez-Martín, F., Domínguez-Rodrigo, M., Favreau, J., Itambu, M., P., L., Mabulla, A., Martín Perea, D.M., Tucker, L., Uribelarrea, D., Mercader, J., 2017. Molecular Isotopic Analysis Reveals Details on the Environmental Context of the Earliest Acheulean at Olduvai Gorge, Annual Meeting of the Paleoanthropology Society. Paleoanthropology Society, Vancouver, BC.

Patalano, R., Wang, Z., Leng, Q., Liu, W., Zheng, Y.F., Sun, G.P., Yang, H., 2015. Hydrological changes facilitated early rice farming in the lower Yangtze River Valley in China: A molecular isotope analysis. *Geology* 43, 639-642.

Pedley, H.M., 1990. Classification and environmental models of cool freshwater tufas. *Sedimentary Geology* 68, 143-154.

Perelman, P., Johnson, W.E., Roos, C., Seuánez, H.N., Horvath, J.E., Moreira, M.A.M., Kessing, B., Pontius, J., Roelke, M., Rumpler, Y., Schneider, M.P.C., Silva, A., O'Brien, S.J., Pecon-Slattery, J., 2011. A Molecular Phylogeny of Living Primates. *PLOS Genetics* 7, 1-17.

Peters, C., O'Brien, E., 1981. The Early Hominid Plant-Food Niche: Insights from an Analysis of Plant Food Exploitation by *Homo*, *Pan*, and *Papio* in Eastern and Southern Africa. *Current Anthropology* 22, 127-140.

Peters, C.R., Blumenshine, R.J., 1995. Landscape perspectives on possible land use patterns for Early Pleistocene hominids in the Olduvai Basin, Tanzania. *Journal of Human Evolution* 29, 321-362.

Peters, K., Walters, C., Moldovan, J., 1993. *The Biomarker guide*. Cambridge Univ Press, Cambridge.

Petraglia, M., LaPorta, P., Paddayya, K., 1999. First Acheulian quarry in India: stone tool manufacture, biface morphology and behaviors. *Journal of Anthropological Research* 55, 39-70.

Pickering, R.J., 1960. Geological survey of Tanganyika: A preliminary note on the quaternary geology of Tanganyika. Endulen Geological Survey, Leopoldville.

Pickford, M., 1975. Late Miocene sediments and fossils from the northern Kenya Rift Valley. *Nature* 256, 279-284.

Pickford, M., Senut, B., 2001a. The geological and faunal context of Late Miocene hominid remains from Lukeino, Kenya. *Earth and Planetary Sciences* 332, 145-152.

Pickford, M., Senut, B., 2001b. 'Millennium Ancestor', a 6-million-year-old bipedal hominid from Kenya - Recent discoveries push back human origins by 1.5 million years. *South African Journal of Science* 97, 22.

Piperno, M., 2001. The prehistory of Melka Kunture (Ethiopia). *Bulletin du Centre de Recherche Français de Jérusalem* 8, 135-145.

Plass, G.N., 1956. The Carbon Dioxide Theory of Climatic Change. *Tellus* 8.

Polissar, P.J., Freeman, K.H., 2010. Effects of aridity and vegetation on plant-wax δD in modern lake sediments. *Geochimica et Cosmochimica Acta* 74, 5785-5797.

Potts, R., 1988. *Early Hominids Activities at Olduvai Aldine Gruyter*, New York.

Potts, R., 1996. Evolution and Climate Variability. *Science* 273, 922-923.

Potts, R., 1998a. Environmental hypotheses of Hominin evolution. *Yearbook of Physical Anthropology* 41, 93-136.

Potts, R., 1998b. Variability Selection in Hominid Evolution. *Evolutionary Anthropology* 7, 81-96.

Potts, R., 2012a. Environmental and Behavioral Evidence Pertaining to the Evolution of Early *Homo*. *Current Anthropology* 53, S299-S317.

Potts, R., 2012b. Evolution and Environmental Change in Early Human Prehistory. *Annual Review of Anthropology* 41, 151-167.

Potts, R., 2013. Hominin evolution in settings of strong environmental variability. *Quaternary Science Reviews* 73, 1-13.

Potts, R., Behrensmeier, A.K., Faith, J.T., Tryon, C.A., Brooks, A., Yellen, J.E., Deino, A.L., Kinyanjui, R., Clark, J.B., Haradon, C., Levin, N., Meijer, H.J.M., Veatch, E.G., Owen, R.B., Renaut, R.W., 2018. Environmental dynamics during the onset of the Middle Stone Age in eastern Africa. *Science* 360, 86-90.

Powers, L.A., Johnson, T.C., Werne, J.P., Castañeda, I.S., Hopmans, E.C., Sinninghe Damste, J.S., Schouten, S., 2005. Large temperature variability in the southern African tropics since the Last Glacial Maximum. *Geophysical Research Letters* 32, 1-4.

Prassack, K.A., 2010. Late Pliocene Avifauna from the Hominid Bearing *Zinjanthropus* Land Surface at Olduvai Gorge, Tanzania. *Records of the Australian Museum* 62, 185-192.

Prassack, K.A., Pante, M., Njau, J.K., de la Torre, I., 2018. The paleoecology of Pleistocene birds from Middle Bed II, at Olduvai Gorge, Tanzania, and the environmental context of the Oldowan-Acheulean transition. *Journal of Human Evolution* 120, 32-47.

Pzadur, A., Dobrowoski, R., Durakiewicz, T., Piotrowska, N., Mohanti, M., Das, S., 2002. $\delta^{13}\text{C}$ and $\delta^{18}\text{O}$ time record and palaeoclimatic implications of the Holocene calcareous tufa from South Eastern Poland and Eastern India (Orissa). *Geochronometria* 21, 97-108.

Quade, J., Levin, N.E., 2013. East African Human Paleoecology: Isotopic Evidence from Paleosols, in: Sponheimer, M., Lee-Thorp, J.A., Reed, K.E., Ungar, P. (Eds.), *Early Hominin Paleoecology*. University Press of Colorado, Boulder, CO, pp. 59-102.

Quinn, R.L., Lepre, C.J., Feibel, C., Wright, J.D., Mortlock, R.A., Harmand, S., Brugal, J.P., Roche, H., 2013. Pedogenic carbonate stable isotopic evidence for wooded habitat preference of early Pleistocene tool makers in the Turkana Basin. *Journal of Human Evolution* 65, 65-78.

Quinn, R.L., Lepre, C.J., Wright, J.D., Feibel, C., 2007. Paleogeographic variations of pedogenic carbonate $\delta^{13}\text{C}$ values from Koobi Fora, Kenya: implications for floral compositions of Plio-Pleistocene hominin environments. *Journal of Human Evolution* 53, 560-573.

Ravelo, A.C., Andreasen, D.H., Lyle, M., Lyle, A.O., Wara, M.W., 2004. Regional climate shifts caused by gradual global cooling in the Pliocene epoch. *Nature* 429, 263-267.

Raymo, M.E., Nisancioglu, K., 2003. The 41 kyr world: Milankovitch's other unsolved mystery. *Paleoceanography* 18, 11-11 - 11-16.

Raynard, L.M., Hedges, R.E.M., 2007. Stable hydrogen isotopes of bone collagen in palaeodietary and palaeoenvironmental reconstruction. *Journal of Archaeological Sciences* 35, 1934-1942.

Rayner, R.J., Moon, B.P., Masters, J.C., 1993. The Makapansgat australopithecine environment. *Journal of Human Evolution* 24, 219-231.

Reed, K.E., 1997. Early Hominid Evolution and Ecological Change Through the African Plio-Pleistocene. *Journal of Human Evolution* 32, 289-322.

Reed, K.E., Spencer, L.M., Rector, A.L., 2013. Faunal Approaches in Early Hominin Paleoecology, in: Sponheimer, M., Lee-Thorp, J.A., Reed, K.E., Ungar, P. (Eds.), *Early Human Paleoecology*. University Press of Colorado, Boulder, CO.

Retallack, C.J., 1990. *Soils of the Past: An Introduction to Paleopedology*. Unwin Hyman, London.

Roche, H., Brugal, J.-P., Delagnes, A., Feibel, C., Harmand, S., Kibunjia, M., Texier, P.-J., 2003. Les sites archéologiques plio-pléistocènes de la formation de Nachukui, Ouest-Turkana, Kenya: bilan synthétique. *Comptes Rendus Palevol* 2, 663-673.

Roe, D.A., 1996. Acheulean Tradition, in: Fagan, B.M. (Ed.), *The Oxford Companion to Archaeology*. Oxford University Press, Oxford, pp. 1-3.

Roebroeks, W., 2011. Hominid behaviour and the earliest occupation of Europe: an exploration. *Journal of Human Evolution* 41, 437-461.

Rogers, M.J., Semaw, S., 2008. From Nothing to Something: The Appearance and Context of the Earliest Archaeological Record, in: Camps, M., Chauhan, P. (Eds.), *Sourcebook of Paleolithic Transitions*. Springer, New York, pp. 155-171.

Rogge, W.F., Hildemann, L.M., Mazurek, M.A., Cass, G.R., Simoneit, B.R.T., 1993. Sources of fine organic aerosol. 4. Particles shed from leaf surface of higher plants. *Environmental Science & Technology* 28, 1375-1388.

Rohling, E.J., 1994. Review and new aspects concerning the formation of eastern Mediterranean sapropels. *Marine Geology* 122, 1-28.

Rommerskirchen, F., Plader, A., Eglinton, G., Chikaraishi, Y., Rullkötter, J., 2006. Chemotaxonomic significance of distribution and stable carbon isotopic composition of long-chain alkanes and alkan-1-ols in C₄ grass waxes. *Organic Geochemistry* 37, 1303-1332.

Rossignol-Strick, M., Nesteroff, W., Olive, P., Vergnaud-Grazzini, C., 1982. After the deluge: Mediterranean stagnation and sapropel formation. *Nature* 295, 105-110.

Rozanski, K., Araguás-Araguás, L., Gonfiantini, R., 1993. Isotopic Patterns in Modern Global Precipitation, in: Swart, P.K., McKenzie, J.A., Lohmann, K.C. (Eds.), *Continental Indicators of Climate, Proceedings of Chapman Conference*. American Geophysical Union, Jackson Hole, WY, pp. 1-36.

Rozanski, K., Araguás-Araguás, L., Gonfiantini, R., 1996. Isotope patterns of precipitation in the East African region, in: Johnson, T., Odada, E.O. (Eds.), *The Limnology, Climatology and Paleoclimatology of the East African Lakes*. Gordon and Breach, Amsterdam, pp. 79-94.

Ruddiman, W.F., Kutzbach, J.E., 1991. Plateau uplift and climatic change. *Scientific American* 264, 66-75.

Sachse, D., Billault, I., Bowen, G.J., Chikaraishi, Y., Dawson, T.E., Feakins, S.J., Freeman, K.H., McGill, C.R., McInerney, F.A., van der Meer, M.T.J., Pollisar, P., Robins, R.J., Sachs, J.P., Schmidt, H.L., Sessions, A.L., White, J.W., West, J.B., Kahmen, A., 2012. Molecular

Paleohydrology, Interpreting the Hydrogen-Isotopic Composition of Lipid Biomarkers from Photosynthesizing Organisms. *Annual Review of Earth and Planetary Sciences* 40, 221-249.

Sachse, D., Radke, J., Gleixner, G., 2004. Hydrogen isotope ratios of recent lacustrine sedimentary *n*-alkanes record modern climate variability. *Geochim Cosmochim Acta* 68, 4877-4889.

Sachse, D., Radke, J., Gleixner, G., 2006. δD values of individual *n*-alkanes from terrestrial plants along a climatic gradient – Implications for the sedimentary biomarker record. *Organic Geochemistry* 37, 469-483.

Sage, R.F., 2004. The evolution of C₄ photosynthesis. *New Phytologist* 161, 341-370.

Salinas, N., Malhi, Y., Meir, P., Silman, M., R., R.C., Huaman, J., Salinas, D., Huaman, V., Gibaja, A., Mamani, M., Farfan, F., 2010. The sensitivity of tropical leaf litter decomposition to temperature: results from a large-scale leaf translocation experiment along an elevation gradient in Peruvian forests. *New Phytologist* 189, 967-977.

Samuels, A.L., Kunst, L., Jetter, R., 2008. Sealing plant surfaces: cuticular wax formation by epidermal cells. *Annual Review of Plant Biology* 59, 683-707.

Santonja, M., Panera, J., Rubio-Jara, S., Pérez-González, A., Uribelarrea, D., Domínguez-Rodrigo, M., Mabulla, A., Bunn, H., Baquedano, E., 2014. Technological strategies and the economy of raw materials in the TK (Thiongo Korongo) lower occupation, Bed II, Olduvai Gorge, Tanzania. *Quaternary International* 322-323, 181-208.

Santonja, M., Villa, P., 2006. The Acheulian of Western Europe, in: Goren-Inbar, N., Sharon, G. (Eds.), *Axe Age. Acheulian Tool-making from Quarry to Discard*. Equinox, London, pp. 429-478.

Sauer, P., Eglinton, T.I., Hayes, J.M., Schimmelmann, A., Sessions, A.L., 2001. Compound-specific D/H ratios of lipid biomarkers from sediments as a proxy for environmental and climatic conditions. *Geochim Cosmochim Acta* 65, 213-222.

Schefuß, E., Schouten, S., Fred Jansen, J.H., Sinninghe Damste, J.S., 2003. African vegetation controlled by tropical sea surface temperatures in the mid-Pleistocene period. *Nature* 422, 418-421.

Schick, K., Toth, N., 1993. *Making silent stones speak. Human evolution and the dawn of technology*. Simon and Schuster, New York.

Scholz, C.A., Johnson, T.C., Cohen, A.S., King, J.W., Peck, J.A., Overpeck, J.T., Talbot, M.R., Brown, E.T., Kalindekaffe, L., Amoako, P.Y.O., Lyons, R.P., Shanahan, T.M., Castañeda, I.S., Heil, C.W., Forman, S.L., McHargue, L.R., Beuning, K.R., Gomez, J., Pierson, J., 2007. East

African megadroughts between 135 and 75 thousand years ago and bearing on early-modern human origins. *Proceedings of the National Academy of Science* 104, 16416-16421.

Schubert, B.A., Jahren, A.H., 2012. The effect of atmospheric CO₂ concentration on carbon isotope fractionation in C₃ land plants. *Geochimica et Cosmochimica Acta* 96, 29-43.

Schwark, L., Zink, K., Lechterbeck, J., 2002. Reconstruction of postglacial to early Holocene vegetation history in terrestrial Central Europe via cuticular lipid biomarkers and pollen records from lake sediments. *Geology* 30, 463-466.

Scrimgeour, C.M., Begley, I.S., Thomason, M.L., 1999. Measurement of deuterium incorporation into fatty acids by gas chromatography/isotope ratio mass spectrometry. *Rapid Commun Mass Spectrom* 13, 271-274.

Sealy, J., 1986. Stable carbon isotopes and prehistoric diets in the southwestern Cape Province, South Africa. *BAR International Series* 293, Oxford.

Semaw, S., Rogers, M., Stout, D., 2008. The Oldowan-Acheulian Transition: Is there a “Developed Oldowan” Artifact Tradition?, in: Camps, M., Chauhan, P. (Eds.), *Sourcebook of Paleolithic Transitions*. Springer, New York, pp. 173-192.

Semaw, S., Rogers, M. J., Quade, J., Renne, P. R., Butler, R. F., Dominguez-Rodrigo, M., Stout, D., Hart, W. S., Pickering, T., and Simpson, S. W., 2003. 2.6-Million-year-old stone tools and associated bones from OGS-6 and OGS-7, Gona, Afar, Ethiopia. *Journal of Human Evolution* 45, 169-177.

Sept, J.M., 2013. Plants and Protopeople: Paleobotanical Reconstruction and Early Hominin Ecology, in: Sponheimer, M., Lee-Thorp, J.A., Reed, K.E., Ungar, P. (Eds.), *Early Hominin Paleoecology*. University Press of Colorado, Boulder, CO.

Sepulchre, P., Ramstein, G., Fluteau, F., Schuster, M., Tiercelin, J.-J., Brunet, M., 2006. Tectonic Uplift and East African Aridification. *Science* 313, 1419-1423.

Sessions, A.L., 2006. Seasonal changes in D/H fractionation accompanying lipid biosynthesis in *Spartina alterniflora*. *Geochimica et Cosmochimica Acta* 70, 2153-2162.

Sessions, A.L., Burgoyne, T.W., Schimmelmann, A., Hayes, J.M., 1999. Fractionation of hydrogen isotopes in lipid biosynthesis. *Organic Geochemistry* 30, 1193-1200.

Sessions, A.L., Sylva, S.P., Summons, R.E., Hayes, J.M., 2004. Isotopic exchange of carbon-bound hydrogen over geologic timescales. *Geochimica et Cosmochimica Acta* 68, 1545-1559.

Shackleton, N.J., 1987. Oxygen Isotopes, Ice Volume and Sea Level. *Quaternary Science Reviews* 6, 183-190.

Shea, J.J., 2008. The Middle Stone Age archaeology of the Lower Omo Valley Kibish Formation: Excavations, lithic assemblages, and inferred patterns of early *Homo sapiens* behavior. *Journal of Human Evolution* 55, 448-485.

Shennan, S., 2011. Descent with modification and the archaeological record. *Philosophical Transactions of the Royal Society B* 366, 1070-1079.

Sikes, E.L., Medeiros, P.M., Augustinus, P., Wilmshurst, J.M., Freeman, K.R., 2013. Seasonal variations in aridity and temperature characterize changing climate during the last deglaciation in New Zealand. *Quaternary Science Reviews* 74, 245-256.

Sikes, N., 1994. Early hominid habitat preferences in East Africa: paleosol carbon isotopic evidence. *Journal of Human Evolution* 27, 25-45.

Sikes, N.E., Ashley, G.M., 2007. Stable isotopes of pedogenic carbonates as indicators of paleoecology in the Plio-Pleistocene (upper Bed I), western margin of the Olduvai Basin, Tanzania. *Journal of Human Evolution* 53, 574-594.

Sillen, A., Balter, V., 2018. Strontium isotopic aspects of *Paranthropus robustus* teeth; implications for habitat, residence, and growth. *Journal of Human Evolution* 114, 118-130.

Simanjuntak, T., Semah, F., Gaillard, C., 2010. The palaeolithic in Indonesia: nature and chronology. *Quaternary International* 223, 418-421.

Slack, C.R., Hatch, M.D., 1967. Comparative studies on the activity of carboxylases and other enzymes in relation to the new pathway of photosynthetic carbon dioxide fixation in tropical grasses. *Biochemical Journal* 103, 660-665.

Smith, F.A., Freeman, K.H., 2006. Influence of physiology and climate on δD of leaf wax *n*-alkanes from C₃ and C₄ grasses. *Geochimica et Cosmochimica Acta* 70, 1172-1187.

Soreng, R.J., Peterson, P.M., Romaschenko, K., Davidse, G., Teisher, J.K., Clark, L.G., Barbera, P., Gillespie, L.J., Zuloaga, F.O., 2017. A worldwide phylogenetic classification of the Poaceae (Gramineae) II: An update and a comparison of two 2015 classifications. *Journal of Systematics and Evolution* 55, 259-290.

Sparkman, O.D., Penton, Z.E., Kitson, F.G., 2011. *Gas Chromatography and Mass Spectrometry: A Practical Guide*, Second ed. Elsevier Science & Technology, Burlington, MA.

Sponheimer, M., Lee-Thorp, J.A., 1999. Isotopic Evidence for the Diet of an Early Hominid, *Australopithecus africanus* Science 283, 368-370.

Sponheimer, M., Passey, B.H., de Ruiter, D.J., Guatelli-Steinberg, D., Cerling, T.E., Lee-Thorp, J.A., 2006. Isotopic Evidence for Dietary Variability in the Early Hominin *Paranthropus robustus*. Science 314.

Stanistreet, I.G., 2012. Fine resolution of early hominin time, Beds I and II, Olduvai Gorge, Tanzania. Journal of Human Evolution 63, 300-308.

Stanley, S., 1992. An ecological theory for the origin of *Homo*. Paleobiology 18, 237-257.

Sternberg, L.S.L., 1988. D/H ratios of environmental water recorded by D/H ratios of plant lipids. Nature 333, 59-61.

Still, C.J., Berry, J.A., Collatz, G.J., DeFries, R.S., 2003. Global distribution of C₃ and C₄ vegetation: carbon cycle implications. Global Biogeochemistry Cycles 17, 6-1-6-14.

Styring, A.K., Sealy, J., Evershed, R.P., 2010. Resolving the bulk $\delta^{15}\text{N}$ values of ancient human and animal bone collagen via compound-specific nitrogen isotope analysis of constituent amino acids. Geochimica et Cosmochimica Acta 74, 241-251.

Suwa, G., Nakaya, H., Asfaw, B., Saegusa, H., Amzaye, A., Kono, R.T., Beyene, Y., Katoh, S., 2003. Plio-Pleistocene Terrestrial Mammal Assemblage from Konso, Southern Ethiopia. Journal of Vertebrate Paleontology 23, 901-916.

Tcherkez, G., Mahé, A., Hodges, M., 2011. $^{12}\text{C}/^{13}\text{C}$ fractionations in plant primary metabolism. Trends in Plant Science 16, 499-506.

Texier, P.-J., Roche, H., Harmand, S., 2006. Kokiselei 5, Formation de Nachukui, West Turkana (Kenya): Un témoignage de la variabilité ou de l'évolution des comportements techniques au Pléistocène Ancien?, in: Congrès, L.S.d. (Ed.), 14th International Congress of Prehistoric and Protohistoric Sciences: Préhistoire en Afrique: sessions générales et posters. BAR International Series, Université de Liège, pp. 11-22.

Thiery, W., Davin, E., Panitz, H., Demuzere, M., Lhermitte, S., Van Lipzig, N., 2015. The impact of the African Great Lakes on the regional climate. Journal of Climate 28, 4061-4085.

Thomas, E.K., McGrane, S., Briner, J.P., Huang, Y., 2012. Leaf wax $\delta^2\text{H}$ and varve-thickness climate proxies from proglacial lake sediments, Baffin Island, Arctic Canada. Journal of Paleolimnology 48, 193-207.

Tierney, J.E., Russell, J.M., Huang, Y., Sinninghe Damste, J.S., Hopmans, E.C., Cohen, A.S., 2008. Northern Hemisphere Controls on Tropical Southeast African Climate During the Past 60,000 Years. *Science* 322, 252-255.

Tipple, B.J., Berke, M.A., Doman, C.E., Khachatryan, S., Ehleringer, J.R., 2013. Leaf-wax *n*-alkanes record the plant-water environment at leaf flush. *PNAS* 110, 2659-2664.

Tipple, B.J., Meyers, S.R., Pagani, M., 2010. Carbon isotope ratio of Cenozoic CO₂: A comparative evaluation of available geochemical proxies. *Paleoceanography* 25, 1-11.

Tipple, B.J., Pagani, M., 2007. The Early Origins of Terrestrial C₄ Photosynthesis. *Annual Review of Earth and Planetary Sciences* 35, 435-461.

Tipple, B.J., Pagani, M., 2010. A 35 Myr North American leaf-wax compound-specific carbon and hydrogen isotope record: Implications for C₄ grasslands and hydrologic cycle dynamics. *Earth and Planetary Science Letters* 299, 250-262.

Tobias, P.V., 2003. Louis Leakey, self-styled White African: Appreciation and some personal recollections. *Transactions of the Royal Society of South Africa* 58, 41-50.

Trauth, M., Larrasoana, J., Mudelsee, M., 2009. Trends, rhythms and events in Plio-Pleistocene African climate. *Quaternary Science Reviews* 28, 399-411.

Trauth, M., Maslin, M., Deino, A., Strecker, M., Bergner, A., Dühnforth, M., 2007. High- and low-latitude forcing of Plio-Pleistocene East African climate and human evolution. *Journal of Human Evolution* 53, 475-486.

Trauth, M.H., Deino, A., Bergner, A.G.N., Strecker, M.R., 2003. East African climate change and orbital forcing during the last 175 kyr BP. *Earth and Planetary Science Letters* 206, 297-313.

Trauth, M.H., Maslin, M.A., Deino, A.L., Junginger, A., Lesoloyia, M., Odada, E.O., Olago, D.O., Olaka, L.A., Strecker, M.R., Tiedmann, R., 2010. Human evolution in a variable environment: the amplifier lakes of Eastern Africa. *Quaternary Science Reviews* 29, 2981-2988.

Trauth, M.H., Maslin, M.A., Deino, A.L., Strecker, M.R., 2005. Late Cenozoic moisture history of East Africa. *Science* 309, 2051-2035.

Trauth, M.H., Maslin, M.A., Deino, A.L., Strecker, M.R., Bergner, A.G.N., Duhnforth, M., 2006. High- and low-latitude forcing of Plio-Pleistocene East African climate and human evolution. *Journal of Human Evolution* 53, 475-486.

Turner, I.M., 2004. *The Ecology of Trees in Tropical Rain Forest*. Cambridge University Press, Cambridge, UK.

Uno, K.T., Polissar, P.J., Kahle, E., Feibel, C., Harmand, S., Roche, H., deMenocal, P.B., 2016. A Pleistocene palaeovegetation record from plant wax biomarkers from the Nachukui Formation, West Turkana, Kenya. *Philosophical Transactions of the Royal Society B* 371, 1-10.

UribeArrea, D., Martín-Perea, D., Díez-Martín, F., Sánchez Yustos, P., Domínguez-Rodrigo, M., Baquedano, E., Mabulla, A., 2017. A reconstruction of the paleolandscape during the earliest Acheulian of FLK West: The co-existence of Oldowan and Acheulian industries during lowermost Bed II (Olduvai Gorge, Tanzania). *Palaeogeography, Palaeoclimatology, Palaeoecology* 488, 50-58.

Van Wyk, A., Smith, G., 2001. *Regions of Floristic Endemism in Southern Africa*. CTP Book Printers, Cape Town.

Venkatesan, M.I., Kaplan, I.R., 1982. Distribution and transport of hydrocarbons in surface sediments of the Alaskan Outer Continental Shelf. *Geochimica et Cosmochimica Acta* 46, 2135-2149.

Verstraete, W., Vanlooche, R., DeBorger, R., Verlinde, A., 1976. Modelling of the breakdown and the mobilization of hydrocarbons in unsaturated soil layers, in: Sharpley, J.M., Kaplan, A.M. (Eds.), 3rd International Biodegradation Symposium. Applied Science Publishers, London, pp. 99-112.

Vignaud, P., Durringer, P., Mackaye, H.T., Likius, A., Blondel, C., Boisserie, J.R., de Bonis, L., Eisenmann, V.R., Etienne, M.-E., Geraads, D., Guy, F., Lehmann, T., Lihoreau, F., Lopez-Martinez, N., Mourer-Chauvire, C., Otero, O., Rage, J.C., Schuster, M., Viriot, L., Zazzo, A., Brunet, M., 2002. Geology and palaeontology of the upper Miocene Toros-Menalla hominin locality, Chad. *Nature* 418, 152-155.

Villmoare, B., Kimbel, W.H., Seyoum, C., Campisano, C., DiMaggio, E.N., Rowan, J., Braun, D., Arrowsmith, R., Reed, K.E., 2015. Early *Homo* at 2.8 Ma from Ledi-Geraru, Afar, Ethiopia. *Science* 347, 1352-1355.

Vogts, A., Moossen, H., Rommerskirchen, F., Rullkötter, J., 2009. Distribution patterns and stable carbon isotopic composition of alkanes and alkan-1-ols from plant waxes of African rain forest and savanna C₃ species. *Organic Geochemistry* 40, 1037-1054.

Vrba, E., 1995a. On the connection between paleoclimate and evolution, in: Vrba, E., Denton, G., Partridge, L., Burckle, L. (Eds.), *Paleoclimate and Evolution, with emphasis on human origins*. Yale University Press, New Haven, pp. 24-45.

Vrba, E.S., 1980. Evolution, Species and Fossils: How Does Life Evolve? *South African Journal of Science* 76, 61-84.

Vrba, E.S., 1985. Environment and evolution: alternative causes of the temporal distribution of evolutionary events. *South African Journal of Science* 81, 229-236.

Vrba, E.S., 1995b. The fossil record of African antelopes (Mammalia, Bovidae) in relation to human evolution and paleoclimate, in: Vrba, E.S., Denton, G.H., Partridge, T.C., Burckle, L.H. (Eds.), *Paleoclimate and Evolution, With Emphasis on Human Origins*. Yale University Press, New Haven, CT, pp. 385-424.

Vrba, E.S., 1995c. On the connection between paleoclimate and evolution, in: Vrba, E.S., Denton, G.H., Partridge, T.C., Burckle, L.H. (Eds.), *Paleoclimate and Evolution, With Emphasis on Human Origins*. Yale University Press, New Haven, CT, pp. 24-45.

Vrba, E.S., 2007. Role of Environmental Stimuli in Hominid Origins, in: Henke, W., Tattersall, I. (Eds.), *Handbook of Paleoanthropology*. Springer, New York, NY, p. 1462.

Vrba, E.S., Denton, G.H., Prentice, M.L., 1989. Climatic influences on early hominid behavior. *Ossa* 14, 127-156.

Walter, R.C., Buffler, R.T., Bruggemann, J.H., Guillaume, M.M.M., Berhe, S.M., Negassi, B., Libsekal, Y., Cheng, H., Edwards, R.L., von Cosel, R., Néraudeau, D., Gagnon, M., 2000. Early human occupation of the Red Sea coast of Eritrea during the last interglacial. *Nature* 405, 65-69.

Wang, L., Okin, G.S., Caylor, K.K., Macko, S.A., 2009. Spatial heterogeneity and source of soil carbon in southern African savannas. *Geoderma* 149, 402-408.

Wang, N., Zong, Y., Brodie, C.R., Zheng, Z., 2014. An examination of the fidelity of *n*-alkanes as a palaeoclimate proxy from sediments of Palaeolake Tianyang, South China. *Quaternary International* 333, 100-109.

Wang, Y.L., Fang, X.M., Zhang, T.W., Li, Y.M., Wu, Y.Q., He, D.X., Wang, Y.X., 2010. Predominance of even carbon-numbered *n*-alkanes from lacustrine sediments in Linxia Basin, NE Tibetan Plateau: implications for climate change. *Applied Geochemistry* 25, 1478-1486.

Wang, Z., Liu, W., 2012. Carbon chain length distribution in *n*-alkyl lipids: a process for evaluating source inputs to Lake Qinghai. *Organic Geochemistry* 50, 36-43.

Washburn, S.L., 1960. Tools and human evolution. *Scientific American* 203, 63-75.

Wasser, S.K., Lovett, J.C., 1993. Introduction to the biogeography and ecology of the rain forests of eastern Africa, in: Lovett, J.C., Wasser, S.K. (Eds.), *Biogeography and ecology of the rain forests of eastern Africa*. Cambridge University Press, Cambridge, UK.

Wei, K., Jia, G., 2009. Soil *n*-alkane $\delta^{13}\text{C}$ along a mountain slope as an integrator of altitude effect on plant species $\delta^{13}\text{C}$. *Geophysical Research Letters* 36, 1-5.

Wells, J.C.K., 2012. Ecological volatility and human evolution: a novel perspective on life history and reproductive strategy. *Evolutionary Anthropology* 21, 277-288.

Werger, M.J.A., 1978. *Biogeography and ecology of Southern Africa*. W. Junk, The Hague, Neatherlands.

Wesselman, H., 1995. Of mice and almost-men: regional paleoecology and human evolution in the Turkana basin, in: Vrba, E., Denton, G., Partridge, T., Burckle, L. (Eds.), *Paleoclimate and Evolution, with emphasis on human origins*. Yale University Press, New Haven, pp. 356-368.

White, F., 1979. The Guineo-Congolian Region and its relationships to other phytochoria. *Bulletin du Jardin Botanique National de Belgique* 49, 11-55.

White, F., 1983. *The Vegetation of Africa: A descriptive memoir to accompany the UNESCO/AETFAT/UNSO vegetation map of Africa*, Natural Resources Research. Unesco, Paris, p. 336.

White, J.W., 1989. Stable Hydrogen Isotope Ratios in Plants: A Review of Current Theory and Some Potential Applications, in: Rundel, P.W., Ehleringer, J.R., Nagy, K.A. (Eds.), *Stable Isotopes in Ecological Research*. Springer-Verlag, New York, NY, p. 525.

White, J.W., Cook, E.R., Lawrence, J.R., Broecker, W.S., 1985. The D/H ratios of sap in trees: implications for water sources and tree ring D/H ratios. *Geochim Cosmochim Acta* 49.

White, T.D., Ambrose, S.H., Suwa, G., Su, D.F., DeGusta, D., Bernor, R.L., Boisserie, J.R., Brunet, M., Delson, E., Frost, S., Garcia, N., Giaourtsakis, I.X., Haile-Selassie, Y., Clark Howell, F., Lehmann, T., Likius, A., Pehlevan, C., Saegusa, H., Semprebon, G., Teaford, M.F., Vrba, E.S., 2009a. Macrovertebrate Paleontology and the Pliocene Habitat of *Ardipithecus ramidus*. *Science* 326, 87-93.

White, T.D., Ambrose, S.H., Suwa, G., WoldeGabriel, G., 2010. Response to comment on the paleoenvironment of *Ardipithecus ramidus*. *Science* 328, 1105.

White, T.D., Asfaw, B., Beyene, Y., Haile-Selassie, Y., Lovejoy, O., Suwa, G., WoldeGabriel, G., 2009b. *Ardipithecus ramidus* and the paleobiology of early hominins. *Science* 326, 75-86.

White, T.D., Suwa, G., Asfaw, B., 1994. *Australopithecus ramidus*, a new species of early hominid from Aramis, Ethiopia. *Nature* 371, 306-312.

Wilson, E.O., 1979. *On Human Nature*. Harvard University Press, Cambridge, MA.

Wirth, S.B., Sessions, A.L., 2016. Plant-wax D/H ratios in the southern European Alps record multiple aspects of climate variability. *Quaternary Science Reviews* 148, 176-191.

WoldeGabriel, G., Ambrose, S.H., Barboni, D., Bonnefille, R., Bremond, L., Currie, B., DeGusta, D., Hart, W.K., Murray, A.M., Renne, P.R., Jolly-Saad, M.C., Stewart, K.M., White, T.D., 2009. The Geological, Isotopic, Botanical, Invertebrate, and Lower Vertebrate Surroundings of *Ardipithecus ramidus*. *Science* 326, 65e61-65e65.

WoldeGabriel, G., Haile-Selassie, Y., Renne, P., Hart, W., Ambrose, S., Asfaw, B., Heiken, G., White, T., 2001. Geology and paleontology of the late Miocene Middle Awash valley, Afar rift, Ethiopia. *Nature* 412, 175-178.

WoldeGabriel, G., White, T., Suwa, G., Renne, P., Heinzelin, J.d., Hart, W., Heiken, G., 1994. Ecological and temporal placement of early Pliocene hominids at Aramis, Ethiopia. *Nature* 371, 330-333.

Wolfenden, E., C., E., G., Y., Deino, A., Ayalew, D., 2004. Evolution of the northern main Ethiopian rift: birth of a triple junction. *Earth and Planetary Science Letters* 224, 213-228.

Wolpoff, M.H., 1980. *Paleoanthropology*. McGraw-Hill, Knopf, New York.

Wood, B., Harrison, T., 2011. The evolutionary context of the first hominins. *Nature* 470, 347-352.

Wu, M.S., West, A.J., Feakins, S.J., 2019. Tropical soil profiles reveal the fate of plant wax biomarkers during soil storage. *Organic Geochemistry* 128, 1-15.

Wynn, J.G., 2000. Paleosols, stable carbon isotopes, and paleoenvironmental interpretation of Kanapoi, Northern Kenya. *Journal of Human Evolution* 39, 411-432.

Wynn, J.G., 2001. Paleosols, stable carbon isotopes, and paleoenvironments of hominid evolution in the Neogene Turkana Basin, Northern Kenya, Department of Geological Sciences. University of Oregon, Ann Arbor, MI, p. 170.

Wynn, J.G., 2004. Influence of Plio-Pleistocene Aridification on Human Evolution: Evidence From Paleosols of the Turkana Basin, Kenya. *American Journal of Physical Anthropology* 123, 106-118.

Wynn, T., Tierson, F., 1990. Regional comparison of the shapes of later Acheulian handaxes. *American Anthropologist* 92, 73-84.

Xie, S.C., Nott, C.J., Avsejs, L.A., Volders, F., Maddy, D., Chambers, F.M., Gledhill, A., Carter, J.F., Evershed, R.P., 2000. Paleoclimate records in compound-specific δD values of a lipid biomarker in ombrotrophic peat. *Organic Geochemistry* 31, 1053-1057.

Yamei, H., Potts, R., Baoyin, Y., Zhengtang, G., Deino, A., Wei, W., Clark, J., Guangmao, X., Weiwen, H., 2000. Mid-Pleistocene Acheulean-like stone technology of the Bose Basin, South China. *Science* 287, 1622-1626.

Yang, H., Huang, Y.S., 2003. Preservation of lipid hydrogen isotope ratios in Miocene lacustrine sediments and plant fossils at Clarkia, northern Idaho, USA. *Organic Geochemistry*, 413-423.

Yang, H., Leng, Q., 2009. Molecular hydrogen isotope analysis of living and fossil plants - *Metasquoia* as an example. *Progress in Natural Science* 19, 901-912.

Yang, H., Pagani, M., Briggs, D.E.G., Equiza, M.A., Jagels, R., Leng, Q., LePage, B.A., 2009. Carbon and hydrogen isotope fractionation under continuous light: implications for paleoenvironmental interpretations of the High Arctic during Paleogene warming. *Oecologia* 160, 461-470.

Yapp, C.J., Epstein, S., 1982. A re-examination of cellulose carbon bound hydrogen D measurement and some factors affecting plant-water D/H relationships. *Geochim Cosmochim Acta* 49, 955-965.

Yravedra, J., Diez-Martín, F., Egeland, C.P., Maté-González, M., Palomeque-González, J.F., Arriaza, M.C., Aramendi, J., Vargas, E.G., Estaca-Gómez, V., Sánchez, P., Fraile, C., Duque, J., de Francisco Rodríguez, S., González-Aguilera, D., Uribe Larrea, D., Mabulla, A., Baquedano, E., Domínguez-Rodrigo, M., 2017. FLK West (Lower Bed II, Olduvai Gorge, Tanzania): a new early Acheulean site with evidence for human exploitation of fauna. *Boreas* 46, 816-830.

Yravedra, J., Domínguez-Rodrigo, M., Santonja, M., Rubio-Jara, S., Panera, J., Pérez-González, A., Uribe Larrea, D., Egeland, C.P., Mabulla, A., Baquedano, E., 2016. The larger mammal palimpsest from TK (Thiongo Korongo), Bed II, Olduvai Gorge, Tanzania. *Quaternary International* 417, 3-15.

Zafiriou, O.C., Gagosian, R.B., Peltzer, E.T., Almond, J.B., 1985. Air-to-sea fluxes of lipids at Enewetak Atoll. *Journal of Geophysical Research* 90, 2409-2423.

Zazzo, A., Bocherens, H., Brunet, M., Beuvilain, A., Billou, D., Mackaye, H.T., Vignaud, P., Mariotti, A., 2000. Herbivore Paleodiet and Paleoenvironmental Changes in Chad during the Pliocene Using Stable Isotope Ratios of Tooth Enamel Carbonate. *Paleobiology* 26, 294-309.

Zhang, J., Marshall, J.D., 1994. Population differences in water use efficiency of well-watered and water-stressed western larch seedlings. *Canadian Journal of Forest Research* 24, 92-99.

Zhu, R.X., Potts, R., Xie, F., Hoffman, K.A., Deng, C.L., Shi, C.D., Pan, Y.X., Wang, H.Q., Shi, R.P., Wu, N.Q., 2004. New evidence on the earliest human presence at high northern latitudes in northeast Asia. *Nature* 431, 559-562.

Ziegler, H., 1989. Hydrogen Isotope Fractionation in Plant Tissues, in: Rundel, P.W., Ehleringer, J.R., Nagy, K.A. (Eds.), *Stable Isotopes in Ecological Research*. Springer-Verlag, New York, NY, p. 525.

APPENDIX A

Concentrations for individual *n*-alkanoic acids - µg/g of dry sediment

FLK North µg/gdw <i>n</i> -alkanoic acids		C ₂₀	C ₂₁	C ₂₂	C ₂₃	C ₂₄	C ₂₅	C ₂₆	C ₂₇	C ₂₈	C ₂₉	C ₃₀	C ₃₁	C ₃₂	C ₃₃	C ₃₄
Sample	Amount	C ₂₀	C ₂₁	C ₂₂	C ₂₃	C ₂₄	C ₂₅	C ₂₆	C ₂₇	C ₂₈	C ₂₉	C ₃₀	C ₃₁	C ₃₂	C ₃₃	C ₃₄
FLK-N 01	40.1	4.36	2.44	14.93	3.61	6.32	2.90	3.10	1.82	7.73	1.09	4.68	0.46	1.52	0.00	0.29
FLK-N 02	40.5	6.24	3.34	22.83	5.16	9.13	3.90	4.04	2.30	10.64	1.34	6.59	0.48	2.17	0.00	0.48
FLK-N 03	40.1	4.59	2.69	19.54	4.45	8.38	3.71	4.03	2.59	9.85	1.52	6.04	0.76	2.27	0.15	0.52
FLK-N 04	41.1	4.53	3.19	20.60	5.17	9.07	4.48	4.60	3.25	10.78	1.99	6.52	0.93	2.48	0.20	0.56
FLK-N 05	41.1	3.87	2.43	17.21	3.87	6.94	3.07	3.15	1.90	8.01	1.11	4.60	0.40	1.43	0.00	0.28
FLK-N 06	42.0	3.95	2.42	14.87	3.58	6.17	2.92	3.02	2.08	7.11	1.13	3.99	0.55	1.37	0.11	0.26
FLK-N 07	41.7	3.69	2.10	14.12	3.24	5.80	2.50	2.64	1.57	7.43	1.07	4.58	0.41	1.57	0.00	0.33
FLK-N 08	39.4	4.78	2.88	18.52	4.48	7.73	3.64	3.69	2.40	8.69	1.43	4.86	0.66	1.70	0.14	0.36

Clays below Tuff IF $\mu\text{g/gdw}$ *n*-alkanoic acids

Sample	Amount	C ₂₀	C ₂₁	C ₂₂	C ₂₃	C ₂₄	C ₂₅	C ₂₆	C ₂₇	C ₂₈	C ₂₉	C ₃₀	C ₃₁	C ₃₂	C ₃₃	C ₃₄
01	10.44	1.71	0.00	1.89	0.64	2.67	1.20	4.72	1.57	8.58	1.94	5.06	1.84	5.53	0.53	1.24
02	10.35	0.53	0.00	0.48	0.41	1.25	1.47	2.02	2.27	3.14	2.19	2.05	1.67	2.39	0.41	0.45
03	10.80	0.47	0.00	0.30	0.00	0.43	0.44	1.05	1.56	3.94	3.04	3.63	2.36	3.80	0.47	0.56
04	10.47	0.99	0.00	0.29	0.00	0.32	0.00	0.30	0.00	0.46	0.00	0.00	0.00	0.00	0.00	0.00
05	11.00	0.80	0.00	0.59	0.52	1.39	0.63	2.55	0.86	4.00	0.92	2.46	0.80	2.27	0.00	0.42
06	10.96	0.75	0.00	1.01	0.42	1.83	0.62	2.82	0.65	3.42	0.79	2.78	0.56	2.07	0.00	0.00
07	10.40	0.91	0.00	0.93	0.58	0.94	0.62	0.95	0.92	1.70	1.08	1.48	0.89	1.69	0.00	0.00
08	10.34	0.99	0.00	1.04	0.61	1.47	0.70	1.11	0.76	1.75	0.90	1.47	0.61	1.57	0.00	0.00
09	11.16	1.06	0.00	1.56	0.53	1.71	0.86	1.83	1.26	2.65	1.36	2.07	1.02	2.00	1.04	0.00
10	11.02	0.49	0.00	0.38	0.00	0.62	0.85	1.40	2.01	3.42	2.84	3.06	2.64	3.86	0.82	0.88
11	10.24	0.98	0.00	1.18	1.04	2.85	1.69	4.11	2.09	5.91	1.90	4.99	1.48	3.79	0.53	0.93
12	10.90	1.03	0.00	1.29	0.78	2.37	1.12	2.63	1.23	3.49	1.12	2.76	1.07	2.74	0.43	0.62
13	10.46	1.03	0.00	1.33	0.82	2.84	2.50	4.51	5.83	11.69	9.07	12.05	9.58	16.21	2.87	4.07
14	10.02	1.17	0.00	1.67	1.02	3.48	3.32	5.55	6.16	10.23	7.40	9.19	7.00	10.94	2.10	3.14
15	14.90	15.27	7.95	55.79	11.86	22.40	8.82	10.13	5.78	28.04	4.05	17.07	1.76	6.22	0.37	1.43
16	10.19	2.77	0.40	3.36	1.18	4.48	1.76	7.69	2.79	12.02	4.75	12.16	6.01	16.15	2.06	4.09
17	10.28	0.83	0.00	0.66	0.00	1.07	0.72	1.21	1.33	2.92	2.19	3.39	3.38	6.37	1.24	1.63
18	10.30	1.85	0.00	2.28	0.68	2.33	0.90	3.77	1.64	7.43	2.43	7.46	2.74	8.50	0.90	2.00
19	10.86	3.11	0.57	5.36	1.94	7.81	2.09	9.79	2.44	14.01	3.29	12.29	3.26	12.25	1.24	2.38
20	10.19	1.31	0.00	1.30	0.67	1.75	1.45	5.21	4.31	16.65	6.80	21.61	6.83	17.42	1.96	3.73
21	11.60	1.15	0.38	2.34	1.99	4.58	2.93	4.65	3.58	6.09	3.27	5.01	2.38	4.21	0.87	1.05
22	10.23	1.75	0.61	1.63	2.77	5.33	4.76	7.30	6.29	10.31	6.09	8.58	5.41	8.23	1.50	2.14
23	11.34	1.03	0.00	0.50	0.00	0.79	0.35	0.99	0.41	1.34	0.41	1.14	0.37	0.91	0.00	0.00
24	10.21	1.67	0.00	0.42	0.00	0.62	0.49	0.60	0.63	0.87	0.54	0.60	0.46	0.65	0.00	0.00
25	10.13	0.00	0.00	0.00	0.00	0.00	0.00	0.00	0.00	0.00	0.00	0.00	0.00	0.00	0.00	0.00
26	17.30	9.50	5.81	40.04	8.58	15.08	6.53	6.41	3.42	16.80	1.96	9.94	0.60	2.99	0.00	0.00
27	10.74	2.08	0.00	2.24	0.71	2.48	1.11	3.87	2.15	8.52	3.22	9.51	2.67	7.11	0.76	1.51
28	10.33	2.10	0.35	3.84	1.27	7.57	2.79	16.47	5.47	28.61	8.03	34.14	7.31	20.53	2.22	4.28
29	10.31	0.00	0.00	0.00	0.00	0.00	0.00	0.00	0.00	0.00	0.00	0.00	0.00	0.00	0.00	0.00
30	10.11	2.02	0.35	2.69	1.42	5.00	2.49	8.96	3.41	15.20	4.37	17.52	3.52	10.77	1.28	2.81

Clays below Tuff IF $\mu\text{g/gdw}$ *n*-alkanes

Sample	Amount	C ₂₁	C ₂₂	C ₂₃	C ₂₄	C ₂₅	C ₂₆	C ₂₇	C ₂₈	C ₂₉	C ₃₀	C ₃₁	C ₃₂	C ₃₃	C ₃₄	C ₃₅
01	10.44	0.00	0.00	0.00	0.00	1.43	0.65	1.84	0.70	1.86	0.00	6.24	0.00	5.95	0.00	0.00
02	10.35	0.00	0.00	0.00	0.00	0.48	0.55	1.07	0.68	2.24	0.83	6.45	0.00	4.97	0.00	0.72
03	10.80	0.00	0.00	0.00	0.53	0.71	0.69	1.44	0.86	3.12	1.20	9.83	0.50	3.26	0.00	0.00
04	10.47	0.00	0.00	0.00	0.00	0.00	0.00	0.00	0.00	0.00	0.00	0.00	0.00	0.00	0.00	0.00
05	11.00	0.00	0.00	0.00	0.00	1.57	0.43	1.14	0.00	0.93	0.00	2.49	0.00	1.77	0.00	0.00
06	10.96	0.00	0.00	0.00	0.00	0.52	0.00	0.91	0.00	1.79	0.00	3.79	0.00	2.63	0.00	0.00
07	10.40	0.00	0.00	0.00	0.00	0.00	0.00	0.57	0.00	4.29	0.77	7.76	0.51	4.50	0.00	0.00
08	10.34	0.00	0.00	0.00	0.00	0.00	0.00	0.49	0.00	3.61	0.64	7.14	0.00	4.18	0.00	0.00
09	11.16	0.00	0.00	0.00	0.00	0.00	0.00	0.80	0.00	1.07	0.00	3.99	0.00	4.10	0.00	1.20
10	11.02	0.00	0.00	0.00	0.00	0.00	0.00	0.50	0.00	0.76	0.53	4.02	0.00	4.82	0.00	1.09
11	10.24	0.00	0.00	0.00	0.00	0.58	0.00	1.07	0.00	2.84	0.00	5.16	0.00	2.90	0.00	0.00
12	10.90	0.00	0.00	0.00	0.00	0.49	0.00	0.63	0.00	2.64	0.55	5.70	0.00	3.52	0.00	0.00
13	10.46	0.56	0.93	1.52	0.90	1.49	1.09	2.52	1.42	2.55	1.49	7.81	0.89	7.78	0.00	1.49
14	10.02	0.00	0.00	0.00	0.00	1.79	1.08	2.47	1.89	2.45	1.45	7.16	0.83	6.90	0.00	1.58
15	10.15	0.00	1.25	3.95	9.94	21.11	29.27	34.09	30.42	27.11	19.81	22.27	9.99	13.20	2.36	2.06
16	10.19	0.00	0.00	1.12	0.75	2.44	1.32	3.98	1.35	4.59	2.08	15.88	1.66	13.79	0.00	1.81
17	10.28	0.00	0.00	0.00	0.00	0.00	0.49	0.87	0.52	0.81	0.51	2.64	0.00	2.59	0.00	0.00
18	10.30	0.00	0.00	0.00	0.00	1.08	0.00	1.66	0.41	3.29	0.69	14.01	0.98	10.21	0.00	1.36
19	10.86	0.00	0.00	0.00	0.00	0.00	0.00	0.00	0.00	0.00	0.00	0.00	0.00	0.00	0.00	0.00
20	10.19	0.00	0.00	0.00	0.00	1.32	0.65	4.34	1.28	22.00	1.64	24.61	1.33	12.48	0.00	1.34
21	11.60	0.00	0.00	0.00	0.00	0.00	0.00	0.50	0.00	0.84	0.00	2.66	0.00	2.11	0.00	0.00
22	10.23	0.00	0.00	0.59	0.54	0.68	0.70	1.96	1.08	4.35	1.80	18.57	1.64	16.25	0.00	0.00
23	11.34	0.00	0.00	0.00	0.00	0.51	0.00	0.80	0.00	0.60	0.00	1.56	0.00	0.75	0.00	0.00
24	10.21	0.00	0.00	0.00	0.00	0.00	0.00	0.00	0.00	0.00	0.00	0.00	0.00	0.00	0.00	0.00
25	10.13	0.00	0.00	0.00	0.00	0.00	0.00	0.00	0.00	0.00	0.00	0.00	0.00	0.00	0.00	0.00
26	10.16	0.00	0.00	0.00	0.00	0.00	0.00	0.00	0.00	0.00	0.00	0.00	0.00	0.00	0.00	0.00
27	10.74	0.00	0.00	0.00	0.47	0.88	0.53	1.64	0.67	6.07	0.72	12.28	0.71	6.50	0.00	0.67
28	10.33	0.00	0.00	0.94	0.59	2.56	0.79	3.51	1.00	7.44	1.40	18.08	1.62	14.13	0.00	1.41
29	10.31	0.00	0.00	0.00	0.00	0.00	0.00	0.00	0.00	0.00	0.00	0.00	0.00	0.00	0.00	0.00
30	10.11	0.00	0.00	0.00	0.00	0.00	0.56	2.49	0.71	11.20	1.13	18.38	1.06	13.00	0.00	1.68

Bird Print Tuff $\mu\text{g/gdw}$ *n* -alkanoic acids

Sample	C ₂₀	C ₂₁	C ₂₂	C ₂₃	C ₂₄	C ₂₅	C ₂₆	C ₂₇	C ₂₈	C ₂₉	C ₃₀	C ₃₁	C ₃₂	C ₃₃	C ₃₄
BPT1	0.37	0.00	0.00	0.00	0.32	0.31	0.48	0.40	0.51	0.00	0.00	0.00	0.00	0.00	0.00
BPT2	2.81	0.00	2.42	1.22	2.73	0.74	3.03	0.93	3.83	0.75	2.89	0.40	1.44	0.00	0.00
BPT3	5.36	0.65	8.83	2.64	11.93	2.99	16.19	3.03	20.45	3.36	16.98	3.02	13.15	0.77	2.48
BPT4	1.50	0.00	0.53	0.00	0.58	0.00	0.58	0.00	0.70	0.00	0.39	0.00	0.00	0.00	0.00
BPT5															
BPT6															
BPT7	3.36	0.41	4.28	1.45	4.71	1.18	4.91	0.91	5.20	0.72	3.44	0.00	1.15	0.00	0.00
BPT8															
BPT9															
BPT10															
BPT11	3.20	0.72	8.75	2.90	15.65	5.71	24.46	5.38	14.96	1.22	1.55	0.00	0.00	0.00	0.00

Castle Clays µg/gdw *n* -alkanoic acids

Sample	Amount	C ₂₀	C ₂₁	C ₂₂	C ₂₃	C ₂₄	C ₂₅	C ₂₆	C ₂₇	C ₂₈	C ₂₉	C ₃₀	C ₃₁	C ₃₂	C ₃₃	C ₃₄
01	39.60	0.80	0.17	1.25	0.34	1.20	0.33	1.05	0.27	1.04	0.20	0.69	0.13	0.39	0.00	0.00
02	40.10	5.29	1.12	9.00	2.75	9.24	2.34	8.12	1.72	8.94	1.68	6.83	1.12	4.67	0.34	1.11
03	40.70	4.25	0.80	6.44	1.84	6.08	1.60	5.41	1.05	5.94	1.01	4.40	0.66	2.82	0.16	0.55
04	38.30	3.15	0.72	5.78	1.67	5.68	1.37	5.05	1.14	6.44	1.30	5.47	0.97	4.36	0.32	1.05
05	42.50	3.15	0.83	0.09	1.93	6.05	2.70	6.48	2.64	7.66	2.15	6.27	1.08	3.55	0.26	0.91
06	44.40	2.01	0.42	3.22	1.16	4.08	1.98	4.70	1.89	5.06	1.41	3.82	0.73	2.55	0.20	0.72
07	30.40	0.48	0.26	0.85	0.34	0.56	0.38	0.66	0.53	0.94	0.54	0.86	0.26	0.42	0.00	0.00
08	37.40	1.05	0.30	1.44	0.56	1.72	0.88	2.23	1.59	3.31	1.60	2.64	0.61	1.20	0.10	0.20
09	40.00	41.42	7.71	56.64	16.40	48.47	12.10	34.24	8.56	36.57	6.32	23.77	3.09	12.27	0.75	3.07
10	40.00	0.71	0.24	0.92	0.36	0.86	0.49	1.10	0.76	1.58	0.75	1.29	0.41	0.78	0.00	0.00
11	41.10	2.60	0.61	3.79	1.16	3.59	1.28	3.30	1.40	3.89	1.21	2.87	0.57	1.48	0.13	0.32
12	32.40	0.43	0.18	0.75	0.36	0.79	0.62	1.25	0.98	1.85	0.93	1.45	0.48	0.81	0.00	0.00
13	34.00	3.69	0.80	7.38	2.01	7.20	1.76	6.52	1.45	7.58	1.57	6.38	1.13	5.03	0.32	1.13
14	22.10	0.63	0.19	0.41	0.32	0.32	0.22	0.26	0.15	0.31	0.00	0.19	0.00	0.00	0.00	0.00

Castle Clays µg/gdw *n* -alkanes

Sample	Amount	C ₂₁	C ₂₂	C ₂₃	C ₂₄	C ₂₅	C ₂₆	C ₂₇	C ₂₈	C ₂₉	C ₃₀	C ₃₁	C ₃₂	C ₃₃	C ₃₄	C ₃₅
01	39.60	0.33	0.52	0.91	1.01	2.57	1.71	4.18	1.72	11.44	2.04	25.68	1.92	21.24	0.77	2.20
02	40.10	0.28	0.52	0.94	0.95	3.22	1.59	4.95	1.92	14.67	2.36	35.80	2.66	31.16	1.22	3.49
03	40.70	0.25	0.47	0.94	0.91	3.37	1.50	5.27	1.79	14.16	1.91	27.55	1.90	21.69	0.74	1.99
04	38.30	0.20	0.27	0.58	0.31	1.43	0.56	2.98	1.20	11.21	1.56	24.36	1.64	19.13	0.65	1.84
05	42.50	0.55	0.82	0.90	0.76	1.15	0.56	1.63	0.59	4.31	0.50	6.88	0.40	4.56	0.13	0.41
06	44.40	0.18	0.26	0.31	0.24	0.55	0.29	0.96	0.39	2.67	0.43	6.25	0.41	4.96	0.15	0.48
07	30.40	0.00	0.32	0.44	0.34	0.54	0.39	0.69	0.35	0.78	0.18	1.22	0.00	0.30	0.00	0.00
08	37.40	0.00	0.00	0.00	0.00	0.00	0.00	0.00	0.00	0.00	0.00	0.00	0.00	0.00	0.00	0.00
09	40.00	0.56	0.72	2.52	1.57	10.57	3.70	23.48	6.18	65.78	6.47	81.33	4.69	46.01	1.64	4.66
10	40.00	0.26	0.42	0.41	0.31	0.51	0.33	0.72	0.32	0.81	0.20	1.61	0.00	0.44	0.00	0.00
11	41.10	0.00	0.00	0.00	0.00	0.00	0.00	0.00	0.00	0.00	0.00	0.00	0.00	0.00	0.00	0.00
12	32.40	0.00	0.96	0.63	0.33	0.56	0.32	0.77	0.34	0.97	0.27	2.29	0.00	1.13	0.00	0.00
13	34.00	0.00	0.00	0.00	0.00	1.68	1.32	3.16	1.38	10.21	1.23	23.59	1.68	21.47	0.68	1.86
14	22.10	0.00	0.16	0.29	0.29	0.58	0.40	0.85	0.42	0.77	0.31	2.43	0.00	0.91	0.00	0.00

APPENDIX B

Raw and Corrected $\delta^{13}\text{C}$ and δD Isotope Values

Clays Below Tuff IF

Raw $\delta^{13}\text{C}$ *n*-Alkanoic Acids

Sample	C ₂₂	C ₂₄	C ₂₆	C ₂₈	C ₃₀	C ₃₂
1			-20.56	-22.00	-20.30	
2			-19.34	-20.37	-21.13	-20.21
3	-34.56	-31.85	-30.47	-33.47	-33.69	-30.74
4						
5						
6						
7						
8						
9						
10						
11						
12						
13		-22.21	-18.43	-19.56	-20.34	-19.21
14						-19.60
15	-34.05	-32.95	-33.21	-34.40	-34.56	-31.32
16	-23.12	-23.05	-21.26	-22.64	-22.55	-20.90
17						
18						
19						
20				-19.73	-20.24	-19.45
21	-26.12	-22.46	-21.06	-22.41	-23.36	-21.30
22		-19.86	-20.55	-20.10	-20.43	-19.98
23						
24						
25						
26	-34.11	-33.88		-34.88	-34.84	-34.07
27						
28	-26.95	-26.35	-25.20	-25.30	-23.50	-22.36
29						
30	-23.59	-22.27	-21.69	-21.77	-22.11	-21.72

Clays Below Tuff IF

Corrected $\delta^{13}\text{C}$ *n*-Alkanoic Acids

Sample	C ₂₂	C ₂₄	C ₂₆	C ₂₈	C ₃₀	C ₃₂
1			-20.37	-21.87	-20.13	
2			-19.11	-20.19	-20.99	-20.05
3	-34.97	-32.11	-30.66	-33.75	-33.96	-30.90
4						
5						
6						
7						
8						
9						
10						
11						
12						
13		-22.07	-18.16	-19.35	-20.17	-19.01
14						-19.42
15	-34.44	-33.26	-33.50	-34.71	-34.86	-31.50
16	-23.01	-22.94	-21.10	-22.54	-22.45	-20.76
17						
18						
19						
20				-19.52	-20.07	-19.26
21	-26.15	-22.34	-20.89	-22.30	-23.29	-21.17
22		-19.63	-20.36	-19.91	-20.27	-19.80
23						
24						
25						
26	-34.50	-34.22		-35.21	-35.15	-34.34
27						
28	-27.02	-26.39	-25.19	-25.29	-23.43	-22.26
29						
30	-23.50	-22.13	-21.54	-21.64	-21.99	-21.60

FLK North

Raw $\delta^{13}\text{C}$ *n* -Alkanoic Acids

Sample	C ₂₂	C ₂₄	C ₂₆	C ₂₈	C ₃₀	C ₃₂
8	-34.56	-31.85	-30.47	-33.47	-33.69	-30.74
7	-33.70	-32.97	-32.40	-34.34	-34.32	-33.03
6	-34.46	-32.01	-31.12	-33.88	-34.10	-31.17
5	-34.40		-32.93	-33.86	-33.86	-32.89
4	-34.35	-31.95	-30.04	-33.00	-32.54	-30.49
3	-33.38	-31.90	-31.04	-33.12	-33.33	-31.57
2	-32.66	-33.21		-34.04	-34.40	-33.65
1	-32.48	-32.23		-33.04	-33.46	

Raw δD *n* -Alkanoic Acids

Sample	C ₂₂	C ₂₄	C ₂₆	C ₂₈	C ₃₀	C ₃₂
8	-161.13	-152.28	-158.20	-158.11	-161.31	-154.90
7	-161.36	-158.03	-168.67	-163.98	-167.01	-162.64
6	-161.87	-153.55	-163.94	-158.13	-163.29	-164.02
5	-163.57	-156.10	-174.16	-163.85	-167.86	-164.38
4	-164.80	-154.20	-171.87	-158.27	-163.16	-164.40
3	-159.33	-154.65	-140.66	-161.71	-167.22	-166.97
2	-164.66	-160.34	-173.76	-167.93	-172.15	-169.68
1	-161.64	-154.17	-204.42	-158.12	-163.05	-159.09

Corrected $\delta^{13}\text{C}$ *n* -Alkanoic Acids

Sample	C ₂₂	C ₂₄	C ₂₆	C ₂₈	C ₃₀	C ₃₂
8	-34.97	-32.11	-30.66	-33.75	-33.96	-30.90
7	-34.07	-33.28	-32.66	-34.66	-34.61	-33.26
6	-34.87	-32.28	-31.34	-34.18	-34.38	-31.35
5	-34.80		-33.21	-34.16	-34.14	-33.12
4	-34.75	-32.22	-30.22	-33.27	-32.78	-30.65
3	-33.74	-32.17	-31.26	-33.39	-33.59	-31.76
2	-32.98	-33.54		-34.35	-34.69	-33.90
1	-32.80	-32.51		-33.31	-33.72	

Corrected δD *n* -Alkanoic Acids

Sample	C ₂₂	C ₂₄	C ₂₆	C ₂₈	C ₃₀	C ₃₂
8	-165.22	-155.45	-161.48	-161.15	-164.30	-157.40
7	-165.47	-161.57	-172.56	-167.34	-170.29	-165.50
6	-166.02	-156.81	-167.56	-161.16	-166.38	-166.95
5	-167.83	-159.52	-178.37	-167.20	-171.18	-167.32
4	-169.15	-157.50	-175.96	-161.31	-166.25	-167.34
3	-163.29	-157.98	-142.91	-164.94	-170.51	-170.04
2	-169.00	-164.03	-177.95	-171.50	-175.69	-172.88
1	-165.77	-157.46	-210.41	-161.15	-166.13	-161.78

FLK West

			$\delta^{13}\text{C } n\text{-Alkanes}$				
Level	Sample	Depth (cm)	C ₂₅	C ₂₇	C ₂₉	C ₃₁	C ₃₃
Above FLK-Wb	28	-	-27.73	-27.17	-27.14	-25.86	-24.60
L1	23	0-2	-28.53	-28.19	-25.98	-24.16	-24.69
	22	6-8	-27.87	-24.27	-23.00	-24.38	-24.64
	21	12-14	-26.72	-25.63		-24.43	
	20	18-20					
L2	19	24-26					
	18	30-32	-28.69	-28.84	-29.40	-29.61	-28.85
	17	36-38	-27.81	-27.81	-27.97	-27.96	-27.04
L3	16	42-44					
	15	48-50					
	14	54-56					
	13	60-62					
	12	66-68	-28.40	-27.78	-29.58	-27.95	-26.21
L4	11	72-74	-27.34	-27.73	-31.49	-29.03	
	10	78-80					
	09	84-86					
	08	90-92	-29.65	-28.96	-30.10	-28.72	-26.24
L5	07	96-98	-29.50	-29.44	-29.98	-29.73	-27.40
	06	102-104					
	05	108-110					
	04	114-116	-27.59	-28.52	-31.43	-31.02	
L6	03	118-120	-28.08	-28.39	-30.42	-30.33	
	02	124-126	-27.46	-28.07	-29.26	-29.09	
	01	128-130	-28.47	-28.45	-29.77	-29.70	
Clays below L6	27	134-136	-28.16	-28.50	-28.90	-29.47	-28.69
	26	140-142	-29.27	-29.58	-30.77	-31.03	-29.11
	25	146-148	-28.33	-28.79	-30.15	-30.18	-28.92
	24	152-154	-28.59	-28.23	-29.62	-29.58	-28.28

Castle Clays

Raw $\delta^{13}\text{C}$ *n* -Alkanoic Acids

Sample	C₂₂	C₂₄	C₂₆	C₂₈	C₃₀	C₃₂
14	-23.07	-24.24	-23.22	-23.17	-22.69	-22.04
13	-23.25	-25.01	-24.37	-24.32	-24.30	-23.33
12	-23.49	-25.11	-24.01	-23.99		
11	-23.34	-25.21	-22.39	-22.18	-24.37	-23.72
10						
09	-24.51	-23.92	-23.02	-23.37	-23.27	-23.27
08	-26.81	-24.49	-22.25	-23.05	-23.23	-22.18
07	-25.95	-24.60	-22.93	-22.62	-23.04	-21.99
06	-23.42	-25.89	-25.04	-23.58	-23.15	-23.41
05	-25.07	-24.17	-22.74	-22.93	-23.12	-22.22
04	-24.18	-24.58	-23.84	-23.75	-23.62	-22.94
03	-29.65	-24.84	-23.01	-24.89	-25.14	-23.71
02	-20.99	-24.45	-25.17	-25.09	-25.03	-23.50
01						

Corrected $\delta^{13}\text{C}$ *n* -Alkanoic Acids

Sample	C₂₂	C₂₄	C₂₆	C₂₈	C₃₀	C₃₂
14	-22.96	-24.19	-23.13	-23.09	-22.60	-21.93
13	-23.15	-24.99	-24.33	-24.28	-24.26	-23.27
12	-23.40	-25.09	-23.95	-23.94		
11	-23.24	-25.20	-22.27	-22.07	-24.34	-23.66
10						
09	-24.47	-23.85	-22.92	-23.29	-23.19	-23.20
08	-26.87	-24.45	-22.12	-22.96	-23.16	-22.07
07	-25.97	-24.56	-22.83	-22.52	-22.96	-21.88
06	-23.32	-25.91	-25.03	-23.51	-23.07	-23.34
05	-25.06	-24.11	-22.63	-22.84	-23.04	-22.12
04	-24.12	-24.54	-23.78	-23.68	-23.56	-22.86
03	-29.84	-24.81	-22.92	-24.87	-25.13	-23.65
02	-20.79	-24.41	-25.15	-25.08	-25.01	-23.43
01						

Castle Clays

Raw δD *n*-Alkanoic Acids

Sample	C₂₂	C₂₄	C₂₆	C₂₈	C₃₀	C₃₂
14	-144.97	-133.38	-128.53	-135.66	-139.79	-145.07
13	-135.79	-127.15	-123.65	-128.93	-131.17	-133.39
12	-135.79	-127.26	-130.87	-132.96	-130.20	-141.43
11	-163.77	-134.07	-120.27	-114.94	-120.36	-119.29
10	-146.62	-141.42	-135.17	-137.72	-141.55	-138.49
09						
08	-147.79	-141.78	-127.25	-128.80	-129.11	-132.69
07	-163.24	-154.32	-183.82	-141.94	-132.68	-131.35
06	-149.91	-141.20	-145.12	-147.90	-148.13	-143.57
05	-153.80	-137.94	-135.20	-137.26	-135.98	-140.13
04	-154.48	-143.24	-144.76	-136.20	-136.54	-136.53
03	-172.46	-145.26	-128.09	-130.30	-129.33	-134.16
02	-138.11	-136.07	-137.87	-140.32	-142.80	-148.78
01						

Corrected δD *n*-Alkanoic Acids

Sample	C₂₂	C₂₄	C₂₆	C₂₈	C₃₀	C₃₂
14	-147.93	-135.35	-130.06	-137.47	-141.69	-147.09
13	-138.11	-128.72	-124.90	-130.37	-132.63	-134.86
12	-138.11	-128.84	-132.54	-134.62	-131.61	-143.28
11	-168.05	-136.08	-121.31	-115.62	-121.26	-120.09
10	-149.70	-143.90	-137.09	-139.64	-143.54	-140.20
09						
08	-150.95	-144.29	-128.71	-130.24	-130.46	-134.13
07	-167.48	-157.63	-188.60	-144.09	-134.21	-132.72
06	-153.22	-143.67	-147.63	-150.37	-150.45	-145.53
05	-157.38	-140.21	-137.13	-139.15	-137.69	-141.92
04	-158.10	-145.84	-147.24	-138.03	-138.27	-138.15
03	-177.34	-147.99	-129.59	-131.82	-130.69	-135.67
02	-140.60	-138.22	-139.95	-142.38	-144.85	-150.99
01						

APPENDIX C

C₃ percentages modeled using linear and sine-squared equations

FLK North

% C₃ Linear						
Sample	Model 1		Model 3		Model 4	
	C₂₈	C₃₀	C₂₈	C₃₀	C₂₈	C₃₀
8	89%	90%	106%	108%	123%	125%
7	95%	95%	113%	112%	129%	129%
6	92%	93%	109%	111%	126%	127%
5	92%	91%	109%	109%	126%	126%
4	86%	82%	103%	99%	120%	117%
3	86%	88%	104%	105%	121%	122%
2	93%	95%	110%	113%	127%	129%
1	86%	89%	103%	106%	121%	123%

% C₃ Sine-Squared						
Sample	Model 1		Model 3		Model 4	
	C₂₈	C₃₀	C₂₈	C₃₀	C₂₈	C₃₀
8	97%	98%	99%	99%	87%	86%
7	99%	99%	96%	96%	81%	81%
6	98%	99%	98%	97%	84%	83%
5	98%	98%	98%	98%	84%	84%
4	95%	92%	100%	100%	90%	93%
3	95%	96%	100%	99%	89%	88%
2	99%	99%	97%	96%	83%	80%
1	95%	97%	100%	99%	90%	87%

Castle Clays

% C₃ Linear						
Sample	Model 1		Model 3		Model 4	
	C₂₈	C₃₀	C₂₈	C₃₀	C₂₈	C₃₀
14	16%	13%	29%	26%	37%	33%
13	24%	24%	38%	38%	48%	48%
12	22%	-141%	36%		45%	
11	9%	25%	22%	38%	28%	49%
10						
09	18%	17%	31%	30%	39%	38%
08	15%	17%	28%	30%	36%	38%
07	12%	15%	25%	28%	32%	36%
06	19%	16%	32%	29%	41%	37%
05	15%	16%	28%	29%	35%	37%
04	20%	19%	34%	33%	43%	41%
03	28%	30%	42%	44%	53%	56%
02	30%	29%	44%	43%	55%	55%
01						

% C₃ Sine-Squared						
Sample	Model 1		Model 3		Model 4	
	C₂₈	C₃₀	C₂₈	C₃₀	C₂₈	C₃₀
14	6%	4%	20%	16%	61%	56%
13	14%	14%	32%	31%	72%	71%
12	12%		28%		69%	
11	2%	14%	12%	32%	51%	72%
10						
09	7%	7%	22%	21%	63%	62%
08	6%	7%	19%	21%	59%	61%
07	4%	6%	15%	19%	55%	59%
06	9%	6%	24%	20%	65%	60%
05	5%	6%	18%	19%	58%	60%
04	10%	9%	26%	24%	66%	65%
03	19%	21%	38%	41%	77%	79%
02	20%	20%	40%	40%	78%	78%
01						

FLK West

Sample	% C ₃ Sine-Squared							
	Model 2		Model 3		Model 4			
	C ₂₉	C ₃₁	C ₂₉	C ₃₁	C ₂₉	C ₃₁	C ₂₉	C ₃₁
28	54%	40%	63%	49%	92%	84%	92%	84%
23	41%	22%	50%	30%	85%	71%	85%	71%
22	12%	24%	19%	33%	60%	73%	60%	73%
21		25%		33%		73%		73%
18	79%	80%	85%	87%	100%	100%	100%	100%
17	64%	64%	72%	72%	96%	96%	96%	96%
12	80%	64%	87%	72%	100%	96%	100%	96%
11	94%	75%	97%	82%	98%	99%	98%	99%
08	85%	72%	90%	79%	100%	98%	100%	98%
07	84%	82%	89%	88%	100%	100%	100%	100%
04	94%	91%	97%	96%	98%	99%	98%	99%
03	87%	87%	92%	92%	100%	100%	100%	100%
02	77%	76%	84%	83%	99%	99%	99%	99%
01	82%	81%	88%	87%	100%	100%	100%	100%
27	74%	79%	81%	86%	99%	100%	99%	100%
26	90%	92%	94%	96%	99%	99%	99%	99%
25	85%	85%	91%	91%	100%	100%	100%	100%
24	81%	80%	87%	87%	100%	100%	100%	100%

FLK West

Sample	% C ₃ Linear							
	Model 2		Model 3		Model 4			
	C ₂₉	C ₃₁	C ₂₉	C ₃₁	C ₂₉	C ₃₁	C ₂₉	C ₃₁
28	53%	44%	59%	49%	74%	62%	74%	62%
23	44%	31%	50%	37%	63%	47%	63%	47%
22	23%	33%	29%	39%	36%	49%	36%	49%
21		33%		39%		49%		49%
18	69%	71%	75%	76%	95%	96%	95%	96%
17	59%	59%	65%	64%	82%	81%	82%	81%
12	71%	59%	76%	64%	96%	81%	96%	81%
11	85%	67%	90%	72%	114%	91%	114%	91%
08	74%	64%	80%	70%	101%	88%	101%	88%
07	74%	72%	79%	77%	100%	98%	100%	98%
04	84%	81%	89%	86%	113%	109%	113%	109%
03	77%	76%	82%	82%	104%	103%	104%	103%
02	68%	67%	74%	73%	93%	92%	93%	92%
01	72%	72%	77%	77%	98%	97%	98%	97%
27	66%	70%	71%	75%	90%	95%	90%	95%
26	79%	81%	85%	87%	107%	109%	107%	109%
25	75%	75%	80%	80%	101%	102%	101%	102%
24	71%	71%	76%	76%	97%	96%	97%	96%

APPENDIX D

Clays Below Tuff IF

Only 12 Clays Below Tuff IF samples were successfully analyzed for $\delta^{13}\text{C}$ and used for C_3 - or C_4 -dominated plant landscape reconstruction (Fig. D-1). Samples with a larger woodland component ($\delta^{13}\text{C} \leq -30\text{‰}$, dark green circles) appear to be located along or nearby fault lines, while those consisting of predominantly grass ($\delta^{13}\text{C} \geq -20\text{‰}$, orange circles) are further from the faults. However, more $\delta^{13}\text{C}$ data are needed to determine whether there is an actual relationship between faults and plant communities or if this is entirely coincidental. Samples 01 and 02, which have $\delta^{13}\text{C}$ values of $\sim -19\text{‰}$ but located only 40-50 m from the FLK Fault may have actually been a *Typha* dominated wetland (Section 10.1.1) which would explain the enriched $\delta^{13}\text{C}$ values. Some samples ($\delta^{13}\text{C}$ between -20‰ and -30‰ , light green circles) were likely ecotones between the woodlands and grasslands. Note that the *Zinj Fault* is a projection by Ashley et al., (2010b) of an unnamed fault mapped by Hay (1976), but this fault has not been physically identified.

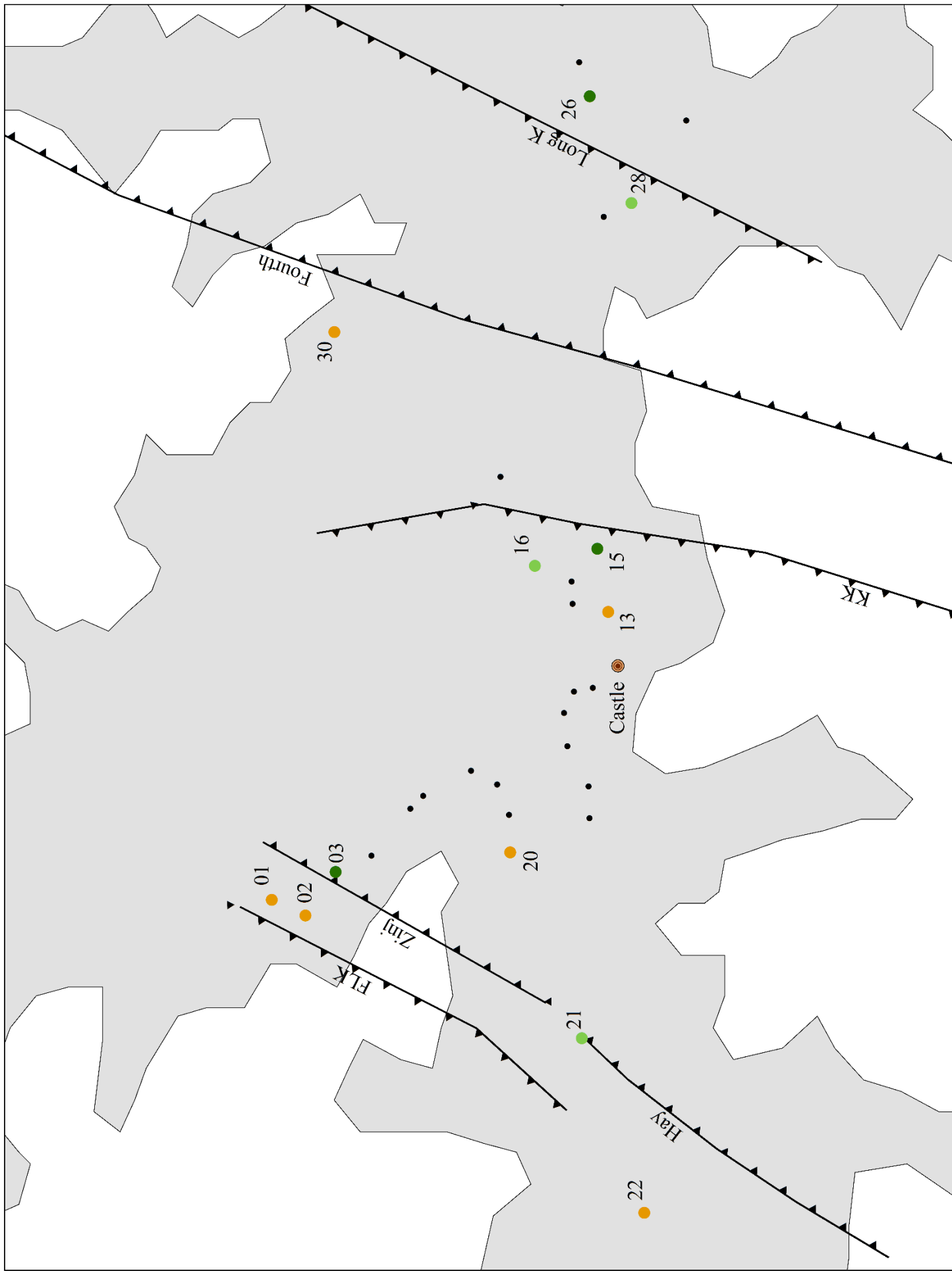


Figure D-1. $\delta^{13}\text{C}$ values for 12 Clays below Tuff IF samples attesting to the mosaic environment at the top of Bed I. Dark green circles $\delta^{13}\text{C} \geq -20\text{‰}$; light green circles $\delta^{13}\text{C}$ between -30‰ and -20‰ ; orange circles $\delta^{13}\text{C} \leq -30\text{‰}$;